



## Durham E-Theses

---

*An assessment of tropical dryland forest ecosystem biomass and climate change impacts in the Kavango-Zambezi (KAZA) region of Southern Africa*

DAVID, RUUSA-MAGANO

### How to cite:

---

DAVID, RUUSA-MAGANO (2022) *An assessment of tropical dryland forest ecosystem biomass and climate change impacts in the Kavango-Zambezi (KAZA) region of Southern Africa*, Durham theses, Durham University. Available at Durham E-Theses Online: <http://etheses.dur.ac.uk/14741/>

### Use policy

---

The full-text may be used and/or reproduced, and given to third parties in any format or medium, without prior permission or charge, for personal research or study, educational, or not-for-profit purposes provided that:

- a full bibliographic reference is made to the original source
- a [link](#) is made to the metadata record in Durham E-Theses
- the full-text is not changed in any way

The full-text must not be sold in any format or medium without the formal permission of the copyright holders.

Please consult the [full Durham E-Theses policy](#) for further details.

---

Academic Support Office, Durham University, University Office, Old Elvet, Durham DH1 3HP  
e-mail: [e-theses.admin@dur.ac.uk](mailto:e-theses.admin@dur.ac.uk) Tel: +44 0191 334 6107  
<http://etheses.dur.ac.uk>

An assessment of tropical dryland forest  
ecosystem biomass and climate change  
impacts in the Kavango-Zambezi (KAZA)  
region of Southern Africa.

Ruusa-Magano David

Thesis submitted for the degree of Doctor of Philosophy

Department of Geography

Durham University

2021



# Abstract

---

The dryland forests of the Kavango-Zambezi (KAZA) region in Southern Africa are highly susceptible to disturbances from an increase in human population, wildlife pressures and the impacts of climate change. In this environment, reliable forest extent and structure estimates are difficult to obtain because of the size and remoteness of KAZA (519,912 km<sup>2</sup>). Whilst satellite remote sensing is generally well-suited to monitoring forest characteristics, there remain large uncertainties about its application for assessing changes at a regional scale to quantify forest structure and biomass in dry forest environments. This thesis presents research that combines Synthetic Aperture Radar, multispectral satellite imagery and climatological data with an inventory from a ground survey of woodland in Botswana and Namibia in 2019. The research utilised a multi-method approach including parametric and non-parametric algorithms and change detection models to address the following objectives: (1) To assess the feasibility of using openly accessible remote sensing data to estimate the dryland forest above ground biomass (2) to quantify the detail of vegetation dynamics using extensive archives of time series satellite data; (3) to investigate the relationship between fire, soil moisture, and drought on dryland vegetation as a means of characterising spatiotemporal changes in aridity. The results establish that a combination of radar and multispectral imagery produced the best fit to the ground observations for estimating forest above ground biomass. Modelling of the time-series shows that it is possible to identify abrupt changes, longer-term trends and seasonality in forest dynamics. The time series analysis of fire shows that about 75% of the study area burned at least once within the 17-year monitoring period, with the national parks more frequently affected than other protected areas. The results presented show a significant increase in dryness over the past 2 decades, with arid and semi-arid regions encroaching at the expense of dry sub-humid, particularly in the south of the region, notably between 2011-2019.

**Keywords:** Above ground biomass, Remote sensing, Synthetic Aperture Radar (SAR), Multispectral data, Climate change, Dryland forest change, Burned area mapping, Biodiversity

# DECLARATION

---

I confirm that no part of the material presented in this thesis has previously been submitted for a degree in this or any other university. In all cases the words of others, where relevant, have been fully acknowledged.

Ruusa-Magano David

Durham University – 2021

copyright © 2021 David Ruusa

*The copyright of this thesis rests with the author. No quotation from it should be published without the author's prior written consent and information derived from it should be acknowledged."*

## ACKNOWLEDGEMENT

---

I have received a great deal of support during my PhD from many people that I would like to thank. Firstly, I would like to thank my supervisors, Prof. Danny Donoghue and Prof. Nick Rosser for their continued support, assistance and guidance throughout my PhD. Without my supervisor's valuable scientific zeal, intellectual input, encouragement and most importantly their patience, the completion of this research would not have been possible. It has been an amazing privilege to work with you both.

My PhD was funded by the *Commonwealth Scholarship Commission (CSC)*, for which I am most grateful. I would also like to thank the *Royal Geographical Society (with IBG) - Monica Cole Research Grant* and *WWF Namibia Mike Knight* for the fieldwork travel and financial support for my project. I received additional support during my PhD from the *NERC*, which provided me with a loan and training for the Field Spectroscopy equipment (FSF). I would like to thank the *Durham Research Trust* who kindly funded my attendance at 8th European space agency (ESA) advanced training course on land remote sensing, Leicester University, UK, *Geography department Postgraduate Conference Fund at Durham University* for funding my attendance to Google Earth Engine Summit training in Dublin, Ireland and *Funds for Women Graduates (FFWG)* for the support grant to in my writing year.

I am thankful to WWF KAZA Secretariat Dr. Nyambe Nyambe, Chobe National Park Authority Dr. Michael Flyman, and University of Namibia (Katima Branch) Dr. Ekkehard Klingelhoefter, for their friendliness and the huge amount of logistical advice they have given me during fieldwork, which made the research experience so enjoyable. Additionally, my thanks go to Dr. Jonathan Kamwi, Morgan Kamwi, Nawa Kamwi, for helping me with data collection during the fieldwork. I would like to thank fellow PhD students, and support staff across the Geography Department for their encouragement, friendship and support throughout my time in Durham University. I will never forget your kindness.

My sincere thanks are once again due to my supervisor Prof. Danny for joining me on fieldwork and providing me with financial assistance for my field visits. Finally, I would like to thank my Dad David Joseph, and my family for their encouragement,

support and prayer over the last four years. Above all, I am grateful to the Lord Almighty who is my source of strength.

*Dedicate to my parents Mrs Helena Johannes and Mr David Joseph*

*“Let the b-pressure go up, it will surely come down”*



## Publications arising from the thesis

This thesis is presented as a collection of papers and chapters. The Supplementary information is presented at the end of each paper/chapter. The reference list and appendices are presented at the end of the thesis. The analytical codes of the thesis have been written in R and Google Earth Engine (Appendix B), and the substantial codes will be uploaded to GitHub. Details and the current status of each paper are shown below:

### **Remote sensing for monitoring tropical dryland forests: A review of current research, knowledge gaps and future directions for Southern Africa**

Chapter 2 is published by *Environment Research Communications*, DOI:

<https://doi.org/10.1088/2515-7620/ac5b84>

Chapter 2 is also published as a policy brief by *n8agrifood for policy makers*,

<https://policyhub.n8agrifood.ac.uk/activity/rapid-evidence-synthesis-training/>, DOI:  
10.5281/ZENODO.5566492

### **The estimation of above ground biomass is improved by combining Sentinel-1 SAR and Sentinel-2 multispectral imagery in the dryland forests of Southern Africa.**

Chapter 3 is published in *Remote Sensing of Environment*: DOI:

<https://doi.org/10.1016/j.rse.2022.113232>

### **Identifying and understanding dryland forest changes and disturbances in Southern Africa using Landsat and MODIS time series and field vegetation data**

In progress: Intended for submission to *International Journal of Applied Earth Observation and Geoinformation*.

**A spatio-temporal drought and fire analysis for semi-arid dryland ecosystems in southern Africa using moderate resolution satellite imagery.**

In progress: Intended for submission to *Remote Sensing in Ecology and Conservation*.

# TABLE OF CONTENTS

---

<b>Abstract</b> .....	<b>i</b>
<b>Declaration</b> .....	<b>ii</b>
<b>Acknowledgement</b> .....	<b>iii</b>
<b>1 Introduction and Research Context</b> .....	<b>25</b>
1.1 Background and Motivation.....	25
1.2 Conceptual frameworks .....	26
1.3 Importance of dryland forests .....	29
1.4 Threats to tropical dryland forests .....	29
1.4.1 Degradation/Deforestation .....	29
1.4.2 Climate and drought.....	32
1.5 Application of remote sensing .....	35
1.5.1 Optical and Synthetic-Aperture Radar (SAR) remote sensing in dryland forests .....	35
1.5.2 Vegetation Indices .....	37
1.5.3 Forest biomass and structural parameters.....	40
1.5.4 The benefits and challenges of remote sensing in dryland forests .....	43
1.5.5 Google Earth Engine platform .....	45
1.6 The world’s largest conservation park .....	46
1.6.1 Rationale of the study .....	47
1.7 Aims and Objectives .....	50
1.8 Thesis Structure.....	52
<b>2 Remote sensing for monitoring tropical dryland forests: A review of current research, knowledge gaps and future directions for Southern Africa</b> .....	<b>54</b>
Abstract .....	56
2.1 Introduction .....	57
2.1.1 Tropical dryland forest.....	57
2.1.2 Recent research trends on tropical dry forests.....	59
2.1.3 Review focus justification.....	65
2.2 Remote sensing applications in dryland forest.....	67
2.2.1 Optical data.....	67
2.2.2 Synthetic Aperture Radar (SAR).....	71
2.2.3 Limitations of optical and radar, and benefits of combining sensors .....	72

2.3	Methodology .....	74
2.4	Results .....	78
2.4.1	Temporal development of publications and author affiliations.....	78
2.4.2	Spatial coverage, spatial extent, and investigated protected areas .....	80
2.4.3	Research topics.....	85
2.5	Discussion .....	93
2.5.1	Temporal extent.....	93
2.5.2	Spatial scale.....	93
2.5.3	Accuracy assessment.....	94
2.5.4	Research topics and geographical focus.....	95
2.5.5	Vegetation indices, optical, SAR, and fusion of optical and SAR sensors.....	96
2.5.6	Remote sensing platforms and cloud-based computing.....	97
2.6	Conclusion .....	98
2.7	Acknowledgments.....	100
<b>3</b>	<b>Improving above ground biomass estimates of Southern Africa dryland forests by combining Sentinel-1 SAR and Sentinel-2 multispectral imagery.....</b>	<b>101</b>
	Abstract .....	103
3.1	Introduction .....	104
3.2	Materials and methods .....	110
3.2.1	Study area .....	110
3.2.2	Fieldwork and sampling design.....	112
3.2.3	Satellite image data collection.....	115
3.2.4	Methods and modelling.....	118
3.3	Results.....	125
3.3.1	Land cover classification.....	125
3.3.2	Simple linear regression (SLR) .....	125
3.3.3	Multivariate linear (ML) regression models.....	126
3.3.4	Comparing parametric and non-parametric machine learning for estimating stand parameters.....	129
3.3.5	Spatial distribution of AGB.....	131
3.4	Discussion .....	138
3.4.1	Relationship between S1 SAR, S2, and LC8 with AGB.....	138
3.4.2	Selection of suitable algorithms and methods.....	140
3.4.3	Comparing regional AGB estimates with pan-tropical maps.....	141
3.4.4	Suitability of different models for land and wildlife management.....	144
3.5	Conclusion .....	147
3.6	Acknowledgments.....	148
3.7	Supplementary Information 1 .....	149

<b>4</b>	<b>Identifying and understanding dryland forest changes and disturbances in Southern Africa using Landsat and MODIS time series and field vegetation data .....</b>	<b>153</b>
	Abstract .....	155
4.1	Introduction .....	156
4.2	Materials and methods .....	159
4.2.1	Study area .....	159
4.2.2	Fieldwork and sampling design.....	163
4.2.3	CHIRPS precipitation data.....	164
4.2.4	Vegetation indices from remote sensing imagery.....	165
4.2.5	Landsat Imagery.....	167
4.2.6	Validating data .....	167
4.3	Methods.....	168
4.3.1	Preparation of high-quality MODIS datasets.....	169
4.3.2	Vegetation and precipitation time series anomaly.....	171
4.3.3	Change detection algorithms .....	172
4.3.4	Land cover classification.....	174
4.3.5	Accuracy assessment.....	175
4.3.6	Validation of estimated forest changes and disturbance .....	176
4.4	Results.....	178
4.4.1	Spatial pattern of vegetation and drought stress in KAZA TFCA.....	178
4.4.2	Comparison of the sensitivity of BFAST and BEAST algorithms.....	180
4.4.3	Robustness of predicting forest dynamics using breakpoints and change magnitude .....	191
4.4.4	Spatial pattern of predicted forest changes using breakpoints and magnitude .....	193
4.4.5	Validation of spatial pattern of predicted forest changes and disturbances..	195
4.4.6	Land cover classification.....	198
4.4.7	Land cover change detection .....	201
4.5	Discussion .....	202
4.5.1	Effectiveness of BFAST and BEAST algorithms for characterising change in dryland forests.....	202
4.5.2	Spectral index sensitivity in dryland forests .....	205
4.5.3	Land cover classification and spatial pattern of forest changes using breakpoints and magnitude .....	207
4.6	Conclusion .....	210
4.7	Acknowledgments.....	212
4.8	Supplementary Information 2 .....	213

<b>5</b>	<b>A spatio-temporal drought and fire analysis for semi-arid dryland ecosystems in southern Africa using moderate resolution satellite imagery. ....</b>	<b>222</b>
	Abstract .....	224
5.1	Introduction .....	225
5.1.1	Drought stress on dryland vegetating.....	225
5.1.2	Fire impacts on dryland vegetation .....	227
5.2	Aims and Objectives .....	231
5.3	Materials and methods .....	232
5.3.1	Study Area.....	232
5.3.2	Fieldwork and Sampling Design .....	234
5.3.3	Ground-based Climate Data.....	234
5.3.4	Remote sensing based rainfall - Climate Hazards Group Infrared Precipitation with Station Data (CHIRPS) .....	237
5.3.5	Root Soil Moisture (GLEAM) .....	238
5.3.6	Vegetation Indices from Remote Sensing Imagery .....	238
5.3.7	Product of burnt area MODIS MCD64A1 .....	239
5.3.8	MODIS MCD14ML Active Fire Product.....	240
5.4	Methods.....	243
5.4.1	Calculating the standardised precipitation evapotranspiration index (SPEI) from ground observation.....	243
5.4.2	Calculation of the satellite-based aridity index (AI).....	245
5.4.3	Evaluation Criteria .....	246
5.5	Results .....	248
5.5.1	Temporal analyses drought and water stress.....	248
5.5.2	Spatial analyses of drought and water stress on vegetation.....	252
5.5.3	Temporal analyses of fire .....	257
5.5.4	Spatial analyses of fire seasonality and extent.....	259
5.5.5	Fire frequency index.....	261
5.5.6	Spatiotemporal changes in the Aridity Index.....	265
5.6	Discussion .....	267
5.6.1	Drought impacts on vegetation.....	267
5.6.2	Fire.....	268
5.6.3	Changes in aridity .....	272
5.7	Conclusion .....	274
5.8	Supplementary Information 3 .....	275
<b>6</b>	<b>Discussion .....</b>	<b>280</b>
6.1	Introduction .....	281
6.2	Suitability of remote sensing data .....	283

6.2.1	Combining sensors .....	283
6.2.2	Spatial scale.....	286
6.2.3	Temporal scale.....	288
6.2.4	Ecological relevance of mapping changes .....	290
6.3	Recommendation for policy and practice .....	292
6.4	Future work .....	294
6.5	Conclusion .....	297
	<b>References</b> .....	299
	<b>Appendix A</b> .....	346
	<b>Appendix B</b> .....	349

# LIST OF FIGURES

## Chapter 1

- Fig. 1. 1 The graphic illustration shows the relative distribution of tropical dry forests.  
Source: FAO, (1999). Reproduced with permission..... 28
- Fig. 1. 2 Illustration of the degradation thresholds within forest and non-forest typically  
caused by disturbances which vary in terms of the extent, severity, quality,  
origin, and frequency (Simula, 2009)..... 32
- Fig. 1. 3 Conceptual framework depicting the key abiotic factors (disturbance and soil  
resource availability) and biotic factors (vegetation/forest structure, diversity,  
and trait composition) controlling temporal and spatial heterogeneity of  
demographic processes (biomass growth, and degradation). Physical damage  
by wildfire, mega-herbivores, e.g., elephants, and deforestation e.g.,  
logging/coppicing are one of the main disruptions to the ecosystems. Forest  
structure (e.g., plot basal area, tree density) is based on all alive trees in the  
selected plots, while diversity and trait composition are based on the  
individuals of that demographic group (i.e., vegetation recruits). The dryland  
forests ecosystem has an option of closed woodland form and open grass form  
depending on the soil resource availability, climate, disturbances, and  
anthropogenic disruption e.g., fire. (Reproduced from Van-der-Sande et al.,  
2017). ..... 35
- Fig. 1. 4 Spectral signatures as functions of wavelength for vegetation, soil and water. .... 38
- Fig. 1. 5 Map of the study area showing KAZA region in Southern Africa and the and  
land management classes as designated by the World Database on Protected  
Areas (WDPA)..... 47
- Fig. 1. 6 Example of ground data captured during a field campaign in February to May  
2019; (A) deforestation in Zambezi state forest in Namibia; (B) forest  
degradation in Chobe National Park in Botswana; (C) Burned forest for  
cultivation near the protected area of Mudumu NP, Namibia; (D) elephant  
browsing; (E) Sampling diameter at breast height of all tree per plot; (F)  
Meeting and interviews with community members concerning dryland forests.... 49

## Chapter 2



Fig. 2. 1 (a) Projected biome change from the periods 1961–1990 to 2071–2100 using the MC1 Dynamic Vegetation Model. (b) Vulnerability of ecosystems to biome shifts based on historical climate (1901–2002) and projected vegetation (2071–2100) (source: IPCC, 2014).....	67
Fig. 2. 2 Interaction mechanisms for dryland forest canopies and source of variability and challenges related to each stage of remote sensing monitoring tropical dryland forest extents. Adapted from Barbosa et al., 2014. ....	70
Fig. 2. 3 PRISMA follow diagram (Moher et al., 2009) showing the flow of information through the different phases of the systematic review .....	76
Fig. 2. 4. Number of papers included in the review integrating remote sensing and dryland forests in Southern Africa published annually between 1997 and 2020...	78
Fig. 2. 5. Number of papers by research institutions.....	80
Fig. 2. 6. Spatial extent of investigated studies.....	81
Fig. 2. 7. Number of studies per country and National Park in Southern Africa. (Note: The data are not scaled to the proportion of dryland forest area of countries, and National Parks with fewer or no publications are not shown. Source: FAO, (1999). Reproduced with permission).....	83
Fig. 2. 8. Temporal duration of studies included in the review integrating remote sensing and dryland forests in Southern Africa between 1997 and 2020.....	85
Fig. 2. 9. Research topic categories of reviewed articles between 1997 and 2020. Note that some studies cover different topics, which may result in multiple entries. ....	86
Fig. 2. 10. Number of studies based upon platform and sensor type. Note that studies investigating forest change with multiple platforms were counted multiple times.....	88
Fig. 2. 11. Research topic by country. Note that the order of the mentioned topics has changed when compared to Fig. 2.9 as some studies were conducted in several countries.....	91

## Chapter 3

Fig. 3. 1. Location of the study area highlighting the countries (Botswana, Namibia, Angola, Zambia and Angola) and Chobe National Park where the field work was conducted. The coloured polygons around the sampled points indicate the type of vegetation structural formation and a range of land cover types that field sites represent (e.g., green-coloured circle: closed forests, purple-coloured square: open forests, orange-coloured square: shrubs, red-coloured square: grassland).	112
Fig. 3. 2. Examples of collected ground truth captured during a field campaign in Chobe National Park in 2019. The photos represent typical forest cover types and recent degradation activities resulting from A: drought impacts, B: Trees toppled by elephants causing mortality, C and D: Trees destroyed by wildfire, and E and F: elephant and herbivory browsing.	115
Fig. 3. 3. Overview of methodological approach.	119
Fig. 3. 4. Optimal AGB model. A: Observed and predicted AGB using ML regression. B: ML regression standardised residuals. C: Observed and predicted AGB using MRF regression. D: MRF regression standardised residuals.	130
Fig. 3. 5. Modelled AGB maps of a dryland forest landscape of the study area and the RGB 432 S2 image (10 m).	132
Fig. 3. 6. Examples of dryland forest types and their respective ground pictures across Chobe National Park. A: closed canopy forest. B: open canopy woodland. C: scattered trees with low herbaceous cover. D: non-forest land cover.	132
Fig. 3. 7. A: AGB maps and histograms with the A: S1S2 model. B: S1 VV model. C: Modelled AGB map with NDRE1 model. D: Modelled AGB map with the NDVI model (the NDVI model saturates at values >80 Mg/ha).	135
Fig. 3. 8. Comparison between A: This Study AGB estimates and the AGB estimates from Bouvet et al. (2018). B: This Study AGB estimates and the AGB estimates from Baccini et al. (2017). C: This Study AGB estimates and the AGB estimates from Avitabile et al. (2016).	137
Fig. 3. 9. Comparison of AGB distribution (Mg/ha) among the different AGB estimates from this study, Avitabile et al. (2016), Baccini et al. (2017), and Bouvet et al. (2018). The models are arranged from the highest median AGB to the lowest. The horizontal line of the box plot for each model represents the median and	

the width of violin plot represents the proportion of the data using a kernel probability density.....138

Fig. 3. 10. Biomass map in a subset of forests in the (I) northern part of the study area and (II) Shimwanza valley. A: estimated AGB map by this study. B: estimated AGB map by Bouvet et al. (2018). C: estimated AGB map by Baccini et al. (2017). D: estimated AGB map by Avitabile et al. (2016). E: RGB 432 S2 image. ....143

Fig. 3. 11. A: RGB 432 S2 image. B: S2 a difference map between this study and Bouvet et al., 2018 (This study –Bouvet et al., (2018), C: This study AGB map. D: Bouvet et al., 2018 AGB map. ....146

## Chapter 4

Fig. 4. 1. Location of the study area in KAZA TFCA. The yellow circles show sampling sites in Zambezi ST, and Mudumu NP Namibia (top), and Chobe NP (bottom). Examples of sample plots representing disturbance types and recent degradation activities captured during a field campaign in 2019 are shown, A) clear-cut deforestation of forest area in Zambezi ST Namibia, B) Burned forest for cultivation near protected area of Mudumu NP, Namibia, C) the visible forest loss, especially the woodland along the Chobe riverfront, D) high population of elephants destructive influence on vegetation. ....162

Fig. 4. 2. Flow chart of data and methods.....169

Fig. 4. 3. Time series representing forest, grassland, altered forest, and agricultural land.....171

Fig. 4. 4. Spatial pattern of ndvi and gndvi and precipitation anomalies for the 21st century from 2010 through 2019.....179

Fig. 4. 5. Example of the corresponding BFAST algorithm output for NDVI and GNDVI extracted from a forest stand that underwent conversion from clear-cut to non-forest vegetation. The vertical dotted lines represent the dates of detected breakpoints, while the red horizontal bars represent the associated confidential intervals. The raw time series (Yt), the seasonal component (St), the trend component (Tt), and the noise (et) component, are also shown. The location of the corresponding pixels, field photo taken in Namibia in 2019 and Landsat time series images illustrating changes are shown in the supplementary information (see: Fig. B. 1 and B. 2). ....183

Fig. 4. 6. Example of the decomposition generated by the application of BEAST algorithm for the NDVI and GNDVI time series extracted from a forest stand that underwent conversion from clear-cut to non-forest vegetation. Seasonal and Trend represent the best fitted seasonal and trend signals (red line), respectively. The vertical dotted lines represent the dates of detected breakpoints in the trend/seasonal components, while the black lines at the bottom panels represent the probabilities of the changepoint in the seasonal/trend components. The location of the corresponding pixels, field photo taken in Namibia in 2019 and Landsat time series images illustrating changes are shown in the supplementary information (see: Fig. B. 1 and B. 2).....185

Fig. 4. 7. Example of the corresponding BFAST for NDVI and GNDVI extracted from a forest stand of a degraded forest. The vertical dotted lines represent the dates of detected breakpoints, while the red horizontal bars represent the associated confidential intervals. The raw time series ( $Y_t$ ), the seasonal component ( $S_t$ ), the trend component ( $T_t$ ), and the noise ( $\epsilon_t$ ) component, are also shown. The location of the corresponding pixels, field photo taken in Botswana in 2019 and Landsat time series images illustrating changes are shown in the supplementary information (see: Fig. B. 3 and B. 4).....186

Fig. 4. 8. Example of the decomposition generated by the application of BEAST algorithm for the NDVI and GNDVI time series extracted from a forest stand of a degraded forest. Seasonal and Trend represent the best fitted seasonal and trend signals (red line), respectively. The vertical dotted lines represent the dates of detected breakpoints in the trend/seasonal components, while the black lines at the bottom panels represent the probabilities of the changepoint in the seasonal/trend components. The location of the corresponding pixels, field photo taken in Botswana in 2019 and Landsat time series images illustrating changes are shown in the supplementary information (see: Fig. B. 3 and B. 4).....188

Fig. 4. 9. Example of the corresponding BFAST algorithm output for NDVI and GNDVI extracted from a forest stand that considered stable. The vertical dotted lines represent the dates of detected breakpoints, while the red horizontal bars represent the associated confidential intervals. The raw time series ( $Y_t$ ), the seasonal component ( $S_t$ ), the trend component ( $T_t$ ), and the noise ( $\epsilon_t$ ) component, are also shown. The location of the corresponding pixels, field

photo taken in Namibia in 2019 and Landsat time series images illustrating changes are shown in the supplementary information (see: Fig. B. 5 and 4. 6).....189

Fig. 4. 10. Example of the decomposition generated by the application of BEAST algorithm for the NDVI and GNDVI time series extracted from a forest stand that considered stable. Seasonal and Trend represent the best fitted seasonal and trend signals (red line), respectively. The vertical dotted lines represent the dates of detected breakpoints in the trend/seasonal components, while the black lines at the bottom panels represent the probabilities of the changepoint in the seasonal/trend components. The location of the corresponding pixels, field photo taken in Namibia in 2019 and Landsat time series images illustrating changes are shown in the supplementary information (see: Fig. B. 5 and B. 6).....191

Fig. 4. 11. A: 2002 LC5 ETM, 2019 LC8 OLI image and a map of the magnitude of change in the trend component from 01/01/2010 to 01/12/2019 generated by BFAST algorithm in and around the Zambezi ST and Mudumu NP; the colour scale represents the magnitude and direction of change. The circles here represent abrupt changes with a negative magnitude; a square represents a vegetation regrowth with a positive magnitude, and the arrow shows a forest stand plot for a forest disturbed by drought and subsequent forest canopy clearing. Fig.4.11. B: MODIS time series from 01/01/2002 to 31/12/2019 for a plot shown by an arrow in Fig. 4.11. A. Fig. 4.11. C: Shows the photograph of the selected plot (location coordinate is 17.49°S, 24.21°E) in Fig. 4.11. A, with logged for timbers photographed during a field campaign in Zambezi ST near the border of Namibia and Zambia in 2019.....193

Fig. 4. 12. A. shows the magnitude of change in the trend component and the predicted time of change generated by BFAST; red colour represents negative breakpoint typically associated with vegetation loss. Green colour represents positive breakpoint associated with vegetation gain. The turquoise polygon shows Zambezi ST, and the black polygon shows Mudumu NP. B: shows the estimated year of change from 2010 to 2019. ....195

Fig. 4. 13. Land cover classification in 2004 and 2019; panel A1 and A2 are zoom in of land cover in 2004 and 2019. ....199

Fig. 4. 14. Changed areas for the epoch (2004–2019) in the study area .....202

## Chapter 5

- Fig. 5. 1. Conceptual model depicting theoretical relationships among moisture availability, temperature, plant growing conditions, and disturbance (fire frequency), water scarcity (droughts) and their effects on dryland vegetation cover directly or indirectly as it characterises desertification.....229
- Fig. 5. 2. Location of the study area in KAZA Conservation Area Southern Africa, showing the yellow circles representing the sampling sites, protected areas and land management classes as designated by the World Database on Protected Areas (WDPA). Examples of sample plots representing degradation from fire captured during a field campaign in 2019 are shown, A) Burned Forest for cultivation near the protected area of Mudumu NP, Namibia, B) Forest scorched by wildfire with dead trees that could not recover in the Zambezi state forests (ST) C) forest or woodland burned down to create a field.....233
- Fig. 5. 3. Monthly (top) and annual (bottom) precipitation (mm) for the period 1983 to 2019 using data obtained from Kasane meteorological station in Botswana.....235
- Fig. 5. 4. Climograph of average monthly precipitation and temperature from 1983 to 2019 using data obtained from Kasane meteorological station in Botswana.....236
- Fig. 5. 5. SPEI for 37 years calculated from ground precipitation and temperature at different timescales. SPEI index scale is given as, extreme drought ( $\leq -2$ ), severe drought ( $-2$  to  $-1.5$ ) and moderate drought ( $-1.5$  to  $-1$ )......249
- Fig. 5. 6. Number of drought events for the years that experienced droughts in the period of 1983 to 2019 using a 3-month time scale, ranked by number of drought months.....250
- Fig. 5. 7. Top: SPEI from 2002 through 2019 calculated from ground precipitation and temperature at 3 months timescales. SPEI index scale is given as, extreme drought ( $\leq -2$ ), severe drought ( $-2$  to  $-1.5$ ), and moderate drought ( $-1.5$  to  $-1$ ). The different vertical line colours represent the drought scale (yellow colour shows mild drought and red colour shows extreme drought). Bottom: Temporal variation of the NDVI (black circles) and inverted monthly precipitation from ground station data (red squares) from 2002 through 2019. ....251
- Fig. 5. 8. Spatial distribution of PRECIPITATION, NDVI, SPEI and RSM anomalies expressed as numbers of standard deviations sampled from the monthly data in

the growing season from 2010 to 2019. Extreme droughts ( $\leq -2$ ), severe drought ( $-2$  to  $-1.5$ ) and moderate drought ( $-1.5$  to  $-1$ ), mild droughts ( $-1$  to  $-0.5$ ) and no drought ( $-0.5$  to  $0.5$ ). The map shows the whole of KAZA region as represented by the study area in Fig. 5.2. ....254

Fig. 5. 9. Association between climate variables and NDVI from the Kavango Zambezi region. The average daily mean, maximum temperatures, precipitation, SPEI and Root Soil Moisture were calculated from the monthly data in the growing season from 2010 to 2019. ....256

Fig. 5. 10. Pearson’s correlation of the NDVI, precipitation, SPEI, root soil moisture, minimum temperature and maximum temperature. ....257

Fig. 5. 11. Total area burnt annually for each country of KAZA from 2002 to 2019 in km<sup>2</sup> based on the MODIS Burnt Area product data. ....258

Fig. 5. 12. Cumulative monthly fire incidences for the whole of KAZA from 2002 to 2019 using FIRMS fire activity data. ....259

Fig. 5. 13. Burnt area derived from the September month of MODIS MCD64A1 product for selected drought years (2002, 2005, 2015 and 2019) and wet years (2004, 2006, 2008 and 2017) based on SPEI data. ....261

Fig. 5. 14. The area affected by fire determined from monthly using MODIS Burnt Area data from 2002 to 2019 for different land categories in the region. Colours indicate the number of times pixels were classified as burnt. White areas represent pixels that were classified as unburnt over the time period. ....263

Fig. 5. 15. Areas where the fire frequency is under varying degrees of climatic condition (precipitation, potential evapotranspiration, root soil moisture), and NDVI sampled from the averaged monthly-mean of the growing season of 2002 to 2019. ....265

Fig. 5. 16. Spatial distribution of averaged aridity over KAZA region for 2002-2010 and 2011-2019. ....266

## Supplementary Figures

Fig. A. 1. Density and histogram plots A: Aboveground biomass (AGB); B: Carbon stock (Mg/ha) of each field plot with woodland trees. ....213

Fig. A. 2. Relationships of S1 polarisations and S2 spectral bands with stand forest parameters in the study area. A: S1 VV polarisation vs AGB. B: S1 VH polarisation vs AGB. C: S2 B3 vs AGB. D: S2 B5 vs AGB.....2130

Fig. A. 3. Dispersion diagram of the observed versus predicted biomass at each fold on a log scale using 70% of the training data... ..2130

Fig. A. 4. Linear and Bootstrap regression of Sentinel 2 Band 3 on a standardised scale....2131

Fig. A.5. Land cover classification map of Zambezi region in Namibia and Chobe District in Botswana for 2019.....2131

**No table of figures entries found.**

## LIST OF TABLES

### Chapter 2

Table 2. 1 Parameters used to extract relevant information for this review ..... 77

### Chapter 3

Table 3. 1. Summary statistics for field sample data in Chobe National Park.....114

Table 3. 2. Description of predictor variables for the AGB estimation.....117

Table 3.3. Simple linear relationship of satellite-based predictors with AGB. The backscatter polarisation, spectral bands, and indices with a strong linear relationship with AGB are highlighted in bold. The  $R^2 > 0.5$  is considered to indicate relatively a strong relationship between the variable (Silvy et al., 2020). .....125

Table 3.4. Multivariate linear relationship and validation results of 19 experiments/models conducted for AGB modelling (label a-k represents S1 and S2) and (label l-p represents LC8). The best model is highlighted in grey.....128

Table 3. 5. Summary statistics and coefficients of linear and bootstrap regression for AGB.....128

Table 3. 6. Confidence intervals (95 %) of linear and bootstrap regression for AGB.....129



Table 3. 7. Summary diagnostics for the AGB models developed by ML and RFR regression methods using the S1S2 model. In this study, the best model throughout the study was the RF regression model, highlighted in grey.....	130
--	-----

## **Chapter 4**

Table 4. 1. Characteristics of the main datasets used in this study .....	166
Table 4. 2. Dates of trend and seasonal breakpoint detection relative to BFAST and BEAST algorithms. The Bold date represents the seasonal shift with the highest probability with a vertical dotted line. ....	180
Table 4. 3. Analysis of area estimates for each class changes .....	197
Table 4. 4. Mean negative break and non-disturbance per hectare (ha).....	198
Table 4. 5. Confusion matrix of land cover classification in 2004 and 2019 using Random Forest. ....	200

## **Chapter 5**

Table 5. 1. Weather stations in the study area.....	236
Table 5. 2. Characteristics of the main datasets used in this study.....	241
Table 5. 3. Categories of dry and wet conditions indicated by SPEI values.....	245
Table 5. 4. UNESCO (1979) aridity classification and bioclimatic index thresholds.....	246

## **Supplementary Tables**

Table A 1. Image acquisition date and scene ID.....	149
Table A 2. Area statistics of the Land cover classes. ....	152
Table A 3. Accuracy assessment of the Land cover classification .....	152
Table B 1. Land cover areas in the study area per year (2004 and 2019) in km <sup>2</sup> and hectares. ....	217
Table B 2. Area changes of BFAST (2002-2019) using sample-based estimates and the observed disturbance change rates in hectares. ....	217

Table B 3. Area changes for the Random Forest classification in the Zambezi region in hectares. ....	218
Table B 4. Area-based transition among land cover categories for the Random Forest classification for the period 2004–2019 in the Zambezi region in hectares. ....	220
Table C 1. Estimates of the total area of burnt and unburnt areas in km <sup>2</sup> and their % from 2002 to 2017 in KAZA region.....	276
Table C 2. Recorded areal fire frequencies of burnt and unburnt areas in km <sup>2</sup> and their % from 2002 to 2017 in KAZA region.....	277
Table C 3. KAZA shifts of AI per class from 2001-2010 to 2011-2020.....	278
Table C 4 Drought years and drought categories of SPEI at different time scales .....	278

# 1 INTRODUCTION AND RESEARCH CONTEXT

---

## 1.1 Background and Motivation

Tropical forests play an important role in global carbon storage and are therefore an important natural component of climate change mitigation (Baccini et al., 2017). Tropical dryland forests (TDFs) make up ca. 40% of all tropical forest region, however, they are facing threats both from human-induced and natural factors (Murphy et al., 1986). During the 20th century, substantial change in TDFs through land-cover conversion and modification has been unprecedented throughout Sub-Saharan Africa, resulting in loss of forest biodiversity and land degradation (Eva et al., 2006; Petheram et al., 2006). Brink et al. (2009) noted that the greatest amount of deforestation in Africa is taking place in dryland forests, accounting for about 70% of forest loss between 1975 and 2000 compared to moist tropical forest loss which accounted for 16% of forest loss. Deforestation in Southern Africa is a major concern, with ca. 1.4 million ha of net forest loss annually, contributing to increased land degradation and the ensuing impacts on the balance of ecosystem function (Lesolle, 2012). According to Intergovernmental Panel on Climate Change (IPCC), these changes have impacts on carbon emissions to the atmosphere and forest biodiversity loss, reducing the region's adaptive capacity and resilience to the impact of high temperatures and varying precipitation (IPCC, 2014).

Tropical countries are beginning to develop policies and initiate projects to reduce greenhouse-gas emissions from deforestation and forest degradation (e.g., REDD+), seeing forests both as environmental resources and carbon sinks (Gibbs et al., 2007; UNCCD, 2015). For these, resource managers, stakeholders, governments, and United Nations (UN) agencies need high-quality reliable information on biomass carbon stocks, forest structure, and the REDD+ -related research in TDFs monitoring (Gizachew et al., 2017; UNCCD, 2009). Recently, the UN called for all to mobilise to deliver 17 Sustainable Development Goals (SDGs) by 2030, including the aim to ensure the conservation, restoration, and sustainable

30 use of forests (SDG 15; UN, 2015). These objectives require the ability to localise,  
31 measure, and monitor forest change at both community and regional levels.

32 The UN argues that to mitigate climate change and biodiversity loss, and to stop  
33 degradation and deforestation processes, action must be taken at all levels: people,  
34 local, regional, global, and by all countries: poor, middle-income, and rich (UN,  
35 2011). Recently, ecologists have embraced remote sensing to study forest change  
36 and biodiversity and have used this to prepare conservation responses to potential  
37 threats (Schulte to Bühne & Pettorelli 2018; Dawson et al., 2016). However, remote  
38 sensing in tropical forests faces challenges including accessibility to and/or the  
39 suitability of different remote sensing data; methods for relating vegetation  
40 structural changes to remotely sensed proxies across different ecosystem types;  
41 and access to suitable data for validating the estimates of forest changes to detect  
42 trends in dryland forests (Lehmann et al., 2015; Privette et al., 2005).

43 This study was designed and undertaken to further understand the large-spatial  
44 and temporal-scale variation of dryland forests dynamics, focussing on the  
45 development of an integrated assessment method for use in the context of climate  
46 change. In line with the multiple threats forced by climate change and  
47 anthropogenic activities, and the challenges of using remote sensing in these  
48 landscapes, this research examined these issues in Kavango Zambezi Conservation  
49 Area (KAZA) in Southern Africa. This focus constitutes the research gap that this  
50 study addresses, by assessing and estimating forest biomass and structural  
51 parameters, fire, and climatic impacts at a regional scale using novel application of  
52 remote sensing.

53 This chapter introduces with fundamental aspects of the research problem and  
54 aims to demonstrate the appropriateness of remote sensing as the best tool to  
55 address fundamental questions about changes in dryland forests.

## 56 1.2 Conceptual frameworks

57 Many of the unique properties of TDFs relate to their rainfall regimes. TDFs are  
58 characterised by prolonged dry seasons of six months or more, with rainfall less  
59 than 100 mm, which in turn determines the distinctive phenology of the forest

60 (Murphy et al., 1986). The definition of “dryland forest” remains debatable and  
61 controversial, which contributes to be difficulty in accurately assessing and  
62 measuring its distribution patterns and status (Blackie et al., 2014). The lack of a  
63 clear and comprehensive understanding of general terms including “drylands” and  
64 “forests” makes it a challenge to explicitly define dryland forests (Charles-D et al.,  
65 2015). Given the fact that dryland forests progressively grade into other vegetation  
66 types such as wet forests, woodlands and savannas, also makes clear definitions  
67 complex (Putz et al., 2010). Walter et al. (1971) noted that the accuracy of  
68 estimates of all tropical forest areas is constrained by uncertainty in the  
69 distribution of open woodlands in dryland areas, which are extensive in Africa,  
70 Australia, and Latin America.

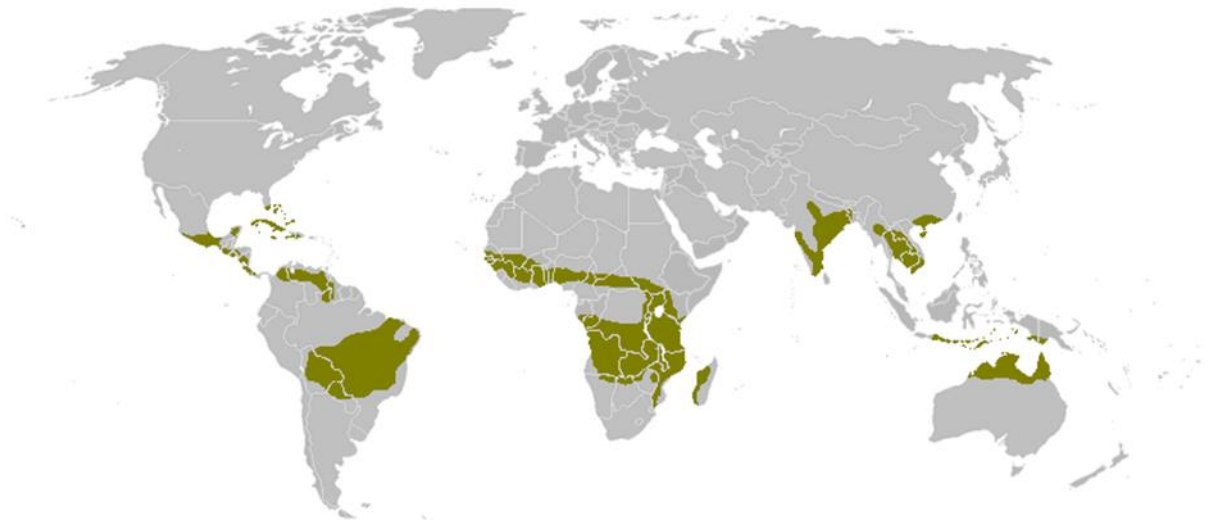
71 In the general literature, many different names have been applied to TDFs,  
72 including savanna forests, Sudanian woodland and miombo woodland in Africa,  
73 monsoon forest in Asia, neotropical dry forests in South America (Chidumayo,  
74 2013; Linares-Palomino et al., 2011; Suresh et al., 2011). The neotropical dry  
75 forests in South America have a plethora of names from “caatinga” in northeast  
76 Brazil, to “bosque tropical caducifolio” in Mexico, and “cuabal” in Cuba, which in  
77 part hinders comparisons (Mayes et al., 2017; Sánchez-Azofeifa et al., 2005). For  
78 example, Dexter et al. (2015) identified dry deciduous forest in India (Suresh et al.,  
79 2011), miombo woodland in southern Africa (Chidumayo, 2013), and deciduous  
80 dipterocarp forest in continental Asia (Bunyavejchewin et al., 2011) as a form of  
81 savanna, and not TDFs, despite the formal classification as TDFs by these studies,  
82 and the FAO (FAO, 2001).

83 There are several definitions currently available for TDFs, but there is still a lack of  
84 consensus in developing a common understanding. Mooney et al. (1995) defined  
85 TDFs as forests occurring in the tropical regions characterised by pronounced  
86 seasonality in rainfall, where there are several months of severe, or even absolute  
87 drought. A widely accepted definition is that of the FAO, that has identified TDFs as  
88 a Global Ecological Zone (GEZ), which includes the drier type of miombo and  
89 Sudanian woodlands, savannah (Africa), caatinga and chaco (South America), and  
90 dry deciduous dipterocarp forest and woodlands (Asia) (FAO, 2001).  
91 Sánchez-Azofeifa et al. (2005) broadly defined TDFs as a vegetation type typically

92 dominated by deciduous trees (at least 50% of trees present are drought  
93 deciduous), where the mean annual temperature is  $\geq 25$  °C, total annual  
94 precipitation ranges between 700 and 2000 mm, and there are three or more dry  
95 months every year (precipitation < 100 mm per month).

96 For the scope of this present study, TDFs are defined as forests occurring in  
97 tropical regions which include the drier type of miombo and Sudanian woodlands,  
98 savanna forests (Africa), caatinga and chaco (South America), and dry deciduous  
99 dipterocarp forest and woodlands as defined by FAO (see: Fig. 1.1). The thesis  
100 adopted the definition of FAO because it recognises forests occurring in the dry  
101 tropical climate globally, then those based entirely on climate definitions. The  
102 current climate does not define the biogeography of TDFs, particularly in the  
103 context of future unprecedented climate change (IPCC, 2007). If climates become  
104 sufficiently warmer and drier in the tropics, dry forests may expand into areas that  
105 are currently dominated by rain forests (Putz et al., 2010). The research however  
106 acknowledges the diverse definitions and views of different researchers on the  
107 topic, such as those pointed out by Dexter et al. (2015) and Murphy et al. (1986).

108



109

110 Fig. 1. 1 The graphic illustration shows the relative distribution of tropical dry forests.  
111 Source: FAO, (1999). Reproduced with permission.

112

113

## 114 1.3 Importance of dryland forests

115 TDFs provide ecosystem services to more than two billion people, including  
116 providing habitat for numerous rare and endemic organisms, supporting  
117 significant crop production, and forage for wildlife and domestic livestock  
118 (Petheram et al., 2006). The dryland ecosystem (including dry forests) harbors  
119 considerable biodiversity in terms of species richness, endemism, and functional  
120 diversity of plants and animals that sometimes even exceeds that of moist forests  
121 (Pennington et al., 2018). Furthermore, TDFs are known to play an important role  
122 in supporting the agricultural systems on which millions of rural subsistence  
123 farmers depend, and so TDFs are central to achieving broader food security  
124 (Chidumayo et al., 2010; Sunderland et al., 2015).

125 Beyond subsistence farming, TDFs contribute to the direct and indirect provision  
126 of various products, including timber and non-timber products to their inhabitants  
127 (Petheram et al., 2006). Other ecosystem services provided include flood control,  
128 tourism revenue, pollination, local diets with wild fruits, bushmeat, and medicinal  
129 plants (Djouidi et al., 2015; Safriel et al., 2006). In dry forested regions, majority of  
130 people use firewood and charcoal from TDFs as a source of energy (Sunderland et  
131 al., 2015). Drylands have major global climate benefits; their carbon storage  
132 (including soil carbon) accounts for more than one-third of global stocks (Durant  
133 et al., 2012; Pennington et al., 2018). The capacity to store carbon depends on  
134 many factors including climate, past land use, and opportunity for management  
135 change (UN, 2011). Growing pressure on dryland forests to meet human and  
136 socioeconomic development needs means that TDFs are increasingly being utilised  
137 unsustainably, and so the degradation of these resources poses a serious problem  
138 (Petheram et al., 2006).

## 139 1.4 Threats to tropical dryland forests

### 140 1.4.1 Degradation/Deforestation

141 For more than 20 years, TDFs have been recognised among the world's most  
142 threatened ecosystems when compared across all major tropical forest types

143 (Janzen, 1988). These activities may take place either abruptly (land cover  
144 conversion) or gradually (land cover modification) (Hayward et al., 2001; Lambin  
145 et al., 2003). Land cover conversion is defined as a shift from one land cover class  
146 to another, whilst modification is subtle changes in continuous properties within  
147 classes (e.g., plant biomass, canopy cover, leaf area) (Hansen et al., 2012). Human  
148 activity causes deforestation through logging of timber and clearing of the forest  
149 where extraction exceeds regeneration.

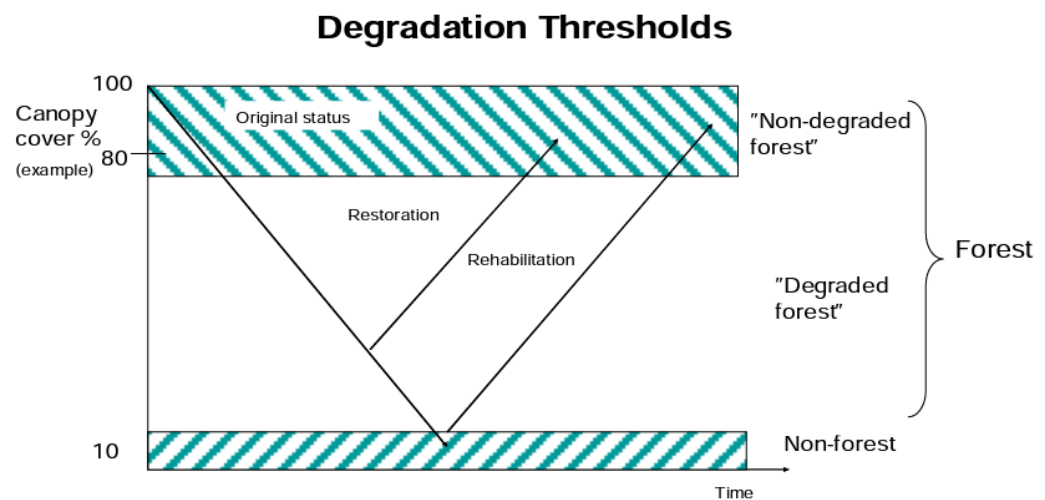
150 Land degradation, which is sometimes used synonymously with desertification in  
151 dryland areas, is a term that refers to the many processes that drive the decline or  
152 loss in biodiversity, ecosystem functions or productivity (Scholes et al., 2018).  
153 Land degradation includes the degradation of all terrestrial ecosystems (e.g., dry  
154 land, semi-arid land, rain-soiled areas in sub-humid areas or grassland, rangeland,  
155 forest, and wetland) (Xie et al., 2020). Forest degradation is land degradation that  
156 occurs within forest land and is most often loosely defined as a loss of particular  
157 forest attributes that negatively affect the structure or function of the stand or site  
158 (IPCC, 2003; ITTO, 2003; Scholes et al., 2018; Simula, 2009). Lund, (2009) provides  
159 a detailed review of more than 50 definitions of forest degradation. FAO, (2011)  
160 defines forest degradation as the change process caused by natural disturbance,  
161 and human-induced that leads to the reduction of the capacity of a forest to  
162 provide goods and services. Services might include biomass, carbon sequestration,  
163 water regulation, soil protection, and biodiversity conservation. According to  
164 Simula, (2009) land degradation acts synergistically with forest degradation.  
165 Figure 1.2 shows degradation thresholds which shows that degradation can  
166 usually be reversible through restoration and management interventions. On the  
167 other hand, degradation is sometimes long-term or permanent leading to the  
168 irreversible loss of forest (Lund 2009). As shown in Fig. 1.2, it's considered forest  
169 degradation when there is a reduction of the canopy cover or carbon stock within a  
170 forest, provided that the canopy cover stays above 10% (FAO, 2000). The status of  
171 degraded areas is distinguished in terms of the degree of degradation (e.g.,  
172 slightly/moderately/severely degraded), as it could help identify priority areas for  
173 preventive or corrective action when monitoring changes. The ability to identify a  
174 degraded forest is essential to help develop techniques to establish systems for  
175 monitoring forest degradation and practical approaches to restore forest cover and



176 structure, species composition and forest regeneration as well as rehabilitation  
177 (see: Fig. 1.2 and 1.3) (Chazdon et al., 2016;). In this study, land degradation and  
178 vegetation degradation are used to describe degradation taking place in forests  
179 and non-forests, while forest degradation was used to refer to degradation largely  
180 taking place in forested areas.

181 Biggs et al. (2008) reported that degradation of dryland landscapes in Southern  
182 Africa happen through alteration of intact ecosystems, for example, the  
183 fragmentation of habitats, the modifications of forests to pasture, and conversion  
184 of extensive land uses to intensive ones, causes a severe loss in biodiversity. Forest  
185 degradation has been described using variables such as changes in canopy cover,  
186 understory tree density, plant or animal species richness, biomass loss from  
187 extensive standing forests, and changes in vegetation attributes as measured  
188 against a baseline undisturbed condition (Thompson et al., 2013; Washington-  
189 Allen et al., 2008). These changes can be caused by natural disturbance such as  
190 wildfire, storms or drought, and also can be human-induced such as via harvesting,  
191 road construction, poor agricultural practices, or grazing, which may each vary in  
192 extent, severity, and frequency. While deforestation is the rapid transformation  
193 from forest to the non-forest area, forest degradation is usually a gradual process  
194 though it may be induced by quick, single events such as hurricanes, and it is  
195 typically more difficult to discern and quantify than deforestation (Thompson et  
196 al., 2013).

197 These alterations in land-cover/land-use could also impact global and regional  
198 climate through alterations in the length of the growing seasons, changes in the  
199 climatic regimes, including extreme high temperatures or rainfall, and increases in  
200 perturbation regimes such as fires, which in turn impact the structure and function  
201 of the dryland forest (Le Houérou, 1996; Naik, 2015). Along with deforestation,  
202 forest degradation contributes to global carbon emissions, and reporting on both is  
203 required by the United Nations Framework Convention on Climate Change  
204 (UNFCCC) through incentives for developing countries through the REDD+  
205 programme (UNFCCC, 2009).



206

207 Fig. 1. 2 Illustration of the degradation thresholds within forest and non-forest typically  
 208 caused by disturbances which vary in terms of the extent, severity, quality, origin, and  
 209 frequency (Simula, 2009).

## 210 1.4.2 Climate and drought

211 TDFs are known to be extremely vulnerable to predicted changes in climate  
 212 (Huang et al., 2017), and the effects of these changes are already being experienced  
 213 in biodiversity showing significant shifts in species ranges in Africa (McClellan et al.,  
 214 2005). There is now abundant evidence from models and observations that  
 215 suggest rainfall regimes in the seasonal tropics are changing to hotter and drier  
 216 conditions, with predicted elevated temperatures (Chadwick et al., 2016; Dai,  
 217 2013), likely exacerbating the risk of further land degradation (Huang et al., 2016).  
 218 Dryland CO<sub>2</sub> uptake is strongly associated with variations of both precipitation  
 219 and temperature, and changes in aridity. The effectiveness of each is impacted by  
 220 deforestation, widespread increases in plant disturbances, and declines in  
 221 ecosystem function (Williams et al., 2013). Dryland vegetation responses to  
 222 environmental perturbations depends upon the frequency and magnitude of  
 223 disturbances (e.g., temperature, precipitation, fire, land use), and the resilience of  
 224 the ecosystem concerned (see: Fig. 1.2) (Lambin et al., 2010).

225 African dryland forests are identified as the most threatened and least protected  
 226 ecosystem on the continent, largely as a result of population growth, climate  
 227 change, and poor environmental governance and policy frameworks (Brink et al.,

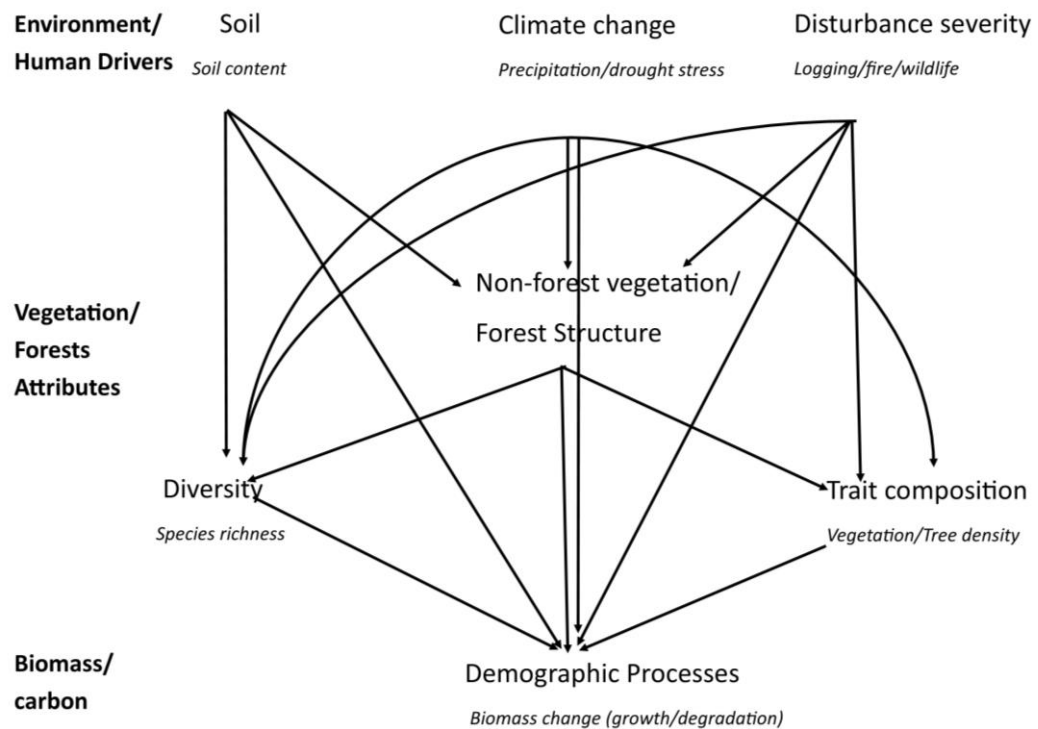
228 2009). The IPCC reported that when climate threats are coupled with a growing  
229 population and future changes in land use could lead to severe dry forest biome  
230 shifts and biomass degradation, particularly in Southern Africa (King, 2014; Niang  
231 et al., 2014). The role of climatic variation, land-use practices, and disturbance  
232 regimes, such as herbivory, has been identified by several studies to be among the  
233 main drivers of ongoing changes in dryland ecosystems leading to forest  
234 degradation and land cover change in Southern Africa (Fig. 1.3) (Anyamba et al.,  
235 2002; Prince, 2012; Privette et al., 2005; Shackleton et al., 2010). Biodiversity in  
236 the region has responded with significant recorded shifts in species ranges,  
237 impacting species composition and productivity (IPCC, 2014; King, 2014). Given  
238 that the availability of water is a determinant of forest resources in drylands, these  
239 types of change affect forest tree cover, demographic processes, biological  
240 diversity, trait composition, habitat quality, and in turn movements of wildlife  
241 (Naidoo et al., 2016). Fig. 1.3 provide a schematic representation of factors  
242 controlling temporal and spatial heterogeneity of biomass plants. This schematic is  
243 not exhaustive but provides a framework of changes in vegetation land cover and  
244 main dryland forest attributes, i.e., composition, structure and function, which is  
245 addressed in this research. This thesis report on the development of open access  
246 codes to map forest structural parameters such as biomass and monitor changes in  
247 dryland forests because of climate change and other disturbances such as  
248 fire/logging. The changes are mapped using a combination of ground and Earth  
249 observation data including multispectral and synthetic aperture radar (SAR)  
250 satellite imagery at a regional scale of Kavango Zambezi region.

251 On a regional level, few studies have evaluated the forest structural parameters  
252 and changes in dryland forests of Southern Africa (David et al., 2022a). Majority of  
253 these studies are done in Republic of South Africa, for example, Mathieu et al. 2013  
254 and Naidoo et al. (2015) found in dryland forests in Kruger National Park that  
255 Woody vegetation cover is accurately mapped with Synthetic Aperture Radar  
256 (SAR) data, however these studies observe an overestimation of woody cover  
257 below 20% as a results of surface contributions to the signal, such as roughness in  
258 radar retrievals (Mathieu et al. 2013; Santoro et al. 2011). There is, however, very  
259 limited spatial information on structural parameters such as above ground  
260 biomass distribution and forest changes in other part of Southern Africa. To date in

261 most of Southern Africa, most quantitative spatial data on forests are available  
262 from products developed globally, such as the pantropical African savanna  
263 biomass map (Bouvet et al., 2018), tree density map (Glick et al., 2016), global  
264 forest height map (Simard et al., 2011), Global Land Cover Map (Arino et al., 2012),  
265 and global tree cover maps (Hansen et al., 2013; Sexton et al. 2013). However,  
266 there is unreliability regarding the accuracies of these maps at regional scales,  
267 particularly in open forest ecosystems such as savannas and dry forests, because  
268 these products were developed primarily to track tropical forest losses (Bastin et  
269 al., 2017). Underestimation for the woody cover above 60% has been observed  
270 likewise in other studies (Bouvet et al. 2018) because of saturation in dense  
271 canopies.

272 To identify changes to dryland forest, and their drivers, and to separate these from  
273 long- and short-term trends, it is essential to select remote sensing data with good  
274 temporal coverage (time series data) but also with a sufficiently frequent revisit  
275 period and spatial resolution. This is however not an easy task, since the  
276 availability of remote sensing data for long-term monitoring purposes is  
277 constrained by sensor characteristics (e.g., revisit time) and then the data utility  
278 can be significantly influenced by environmental factors (e.g., cloud cover)  
279 (Donoghue, 2000; Kuplich et al., 2013).

280



281

282 Fig. 1. 3 Conceptual framework depicting the key abiotic factors (disturbance and soil  
 283 resource availability) and biotic factors (vegetation/forest structure, diversity, and  
 284 trait composition) controlling temporal and spatial heterogeneity of demographic processes  
 285 (biomass growth, and degradation). Physical damage by wildfire, mega-herbivores, e.g.,  
 286 elephants, and deforestation e.g., logging/coppicing are one of the main disruptions to the  
 287 ecosystems. Forest structure (e.g., plot basal area, tree density) is based on all alive trees  
 288 in the selected plots, while diversity and trait composition are based on the individuals of  
 289 that demographic group (i.e., vegetation recruits). The dryland forests ecosystem has an  
 290 option of closed woodland form and open grass form depending on the soil resource  
 291 availability, climate, disturbances, and anthropogenic disruption e.g., fire. (Reproduced  
 292 from Van-der-Sande et al., 2017).

## 293 1.5 Application of remote sensing

### 294 1.5.1 Optical and Synthetic-Aperture Radar (SAR) remote 295 sensing in dryland forests

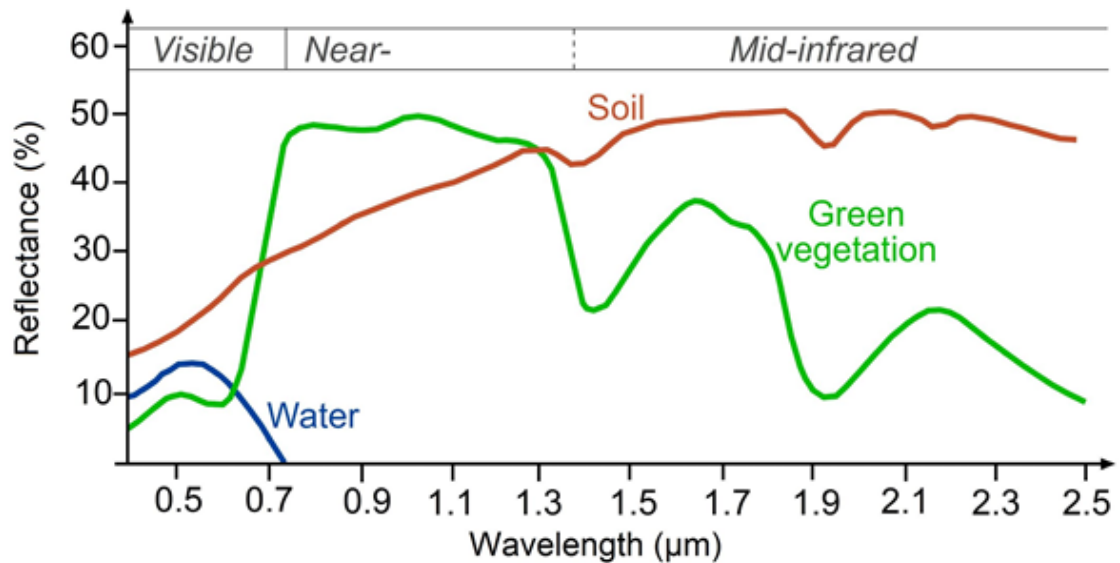
296 Remote sensing has contributed greatly to the mapping and understanding of the  
 297 tropical forest ecosystems in relation to local and global environmental change

298 (Foody, 2003). Advances in the remote detection of burned areas (Zhang et al.,  
299 2011), land-use and land-cover (De Oliveira et al., 2019), forest structure (Hyde et  
300 al., 2006), biomass (Cutler et al., 2012) and biodiversity (Rampheri et al., 2020)  
301 have also changed the understanding with regards to forest functioning. From the  
302 TDF resources perspective, satellite remote sensing has been used to provide three  
303 levels of information. The first is information on the spatial extent of forest cover  
304 and forest change patterns; the second level comprises information on forest type;  
305 and the third provides information on the biophysical and biochemical properties  
306 of forests (Boggs, 2010; Higginbottom et al., 2018; Wood et al., 2012). Several  
307 studies have established the many advantages of remote sensing over traditional  
308 field investigation methods for measuring and monitoring tropical forests (Hyde et  
309 al., 2006; Puhr et al., 2000). The most obvious advantages include the potential to  
310 survey large areas rapidly or over longer periods at low cost, especially in remote,  
311 inaccessible, and sometimes dangerous environments (Rumiano et al., 2020).

312 In general terms, Earth Observation (EO) platforms have carried two types of  
313 sensor: optical and active SAR. The optical systems measure reflected radiation of  
314 one or more discrete wavelengths located in the spectral range 400–3000 nm,  
315 wherein the wavelengths are notably several orders of magnitude smaller than the  
316 leaves, needles, and branches that make up a forest canopy, and so these  
317 components absorb and scatter radiation (Boyd et al., 2005). Synthetic-Aperture  
318 Radar (SAR) systems measure backscattered microwave radiation at wavelengths  
319 between 1 cm and 1000 cm, characterising scattering from leaves, branches, stems  
320 trunks and the ground (Mitchard et al., 2009). Optical remote sensing systems may  
321 provide information on the amount of foliage and its biochemical properties, while  
322 SAR (microwave) systems provide information on woody biomass and forest  
323 structure (Armston et al., 2009; Higginbottom et al., 2018). Many SAR sensors can  
324 both transmit and receive microwaves with two different polarisations, which  
325 enhances the information provided, particularly that which describes surface  
326 roughness and geometric regularities in the forest stand (Kasischke et al., 1997).  
327 Therefore, satellite remote sensing signals provide additional proxy information  
328 that can be linked to forest parameters and health indicators, as well as  
329 disturbance factors when using vegetation indices.

## 330 1.5.2 Vegetation Indices

331 In satellite remote sensing for forests, vegetation indices, biophysical variables,  
332 and data transformations are often used for data analyses (Morley et al., 2019;  
333 Yengoh et al., 2015). The various materials of the earth's surface absorb and reflect  
334 different amounts of energy at different wavelengths. The magnitude of energy  
335 that an object reflects or emits across a range of wavelengths is called its spectral  
336 response pattern (Aggarwal, 2004). The graph below illustrates the spectral  
337 response patterns of soils, water, and vegetation (Fig. 1.4). The healthy vegetation  
338 has a unique spectral reflectance signature that is dictated by various plant  
339 attributes. The visible reflectance of plants is mainly characterised by absorption  
340 of the leaf pigments like chlorophyll, carotenoids and xanthophylls (Gibson et al.,  
341 2013). Stressed vegetation will give off a different spectral  
342 signature corresponding to the effect of the stress on the various leaf pigments.  
343 Knowing the typical spectral response characteristics makes it possible to  
344 distinguish forests, crops, and soils, and to evaluate their condition (e.g., stressed  
345 plants) using remotely sensed images (Ranjan et al., 2012). In the case of  
346 vegetation, the measured spectral reflectance values from two or more  
347 wavelengths are usually used to estimate vegetation indices. NDVI is one of such  
348 indices, commonly used to distinguish live green plant canopies, calculated as a  
349 ratio of near-infrared to red vegetation reflectance (Rouse, 1974; Tucker, 1979).  
350 NDVI has been used as a proxy of vegetation greenness and has been shown to  
351 relate closely to leaf area index (LAI), biomass, and the fraction of  
352 photosynthetically active radiation absorbed by vegetation (fAPAR) (Curran,  
353 1980).



354

355 Fig. 1. 4 Spectral signatures as functions of wavelength for vegetation, soil and water.

356 Source: <https://seos-project.eu/classification/classification-c01-p05.html/> (accessed 02  
357 May 2021).

358 Ringrose et al. (1994) and Turner et al. (1999) indicate that the strength of the  
359 relationships between forest LAI and vegetation indices, such as the NDVI, is site-,  
360 time- and species-specific and that above a LAI of about 5 or 6, NDVI may not be  
361 sensitive to LAI variation. Several well-known limitations of NDVI for robust  
362 estimation of biomass in drylands exist. NDVI is sensitive to green components and  
363 insensitive to woody components where the majority of carbon is stored (Tucker,  
364 1979). Also, Above Ground Biomass (AGB) production is not always uniformly  
365 linked to either greenness or plant structure (herbaceous and woody  
366 compositions), as moisture content and vegetation species composition have been  
367 shown to impact the biomass-NDVI relationship (Asner et al., 2009; Wessels et al.,  
368 2006). These observations may help explain reportedly weak relationships  
369 between NDVI and tropical forest canopies, particularly for areas with complex  
370 and high vegetation amounts as in TDFs (Foody et al., 2001; Sader et al., 1989). For  
371 example, Madonsela et al. (2018) investigated the interactions between seasonal  
372 NDVI and woody canopy cover in the savanna of the Kruger National Park (NP) to  
373 model tree species diversity using a factorial model and found that the interaction  
374 between NDVI and woody canopy cover was insignificant. It is also widely  
375 reported that the NDVI signal is influenced by woody canopy foliage, underlying  
376 canopy background, and soil moisture in sparse vegetative areas (LAI <3), which



377 reduces the apparent NDVI signal and seasonal variations in vegetation phenology  
378 (Pettorelli et al., 2005; Wagenseil et al., 2006).

379 These challenges have led to the development of alternative formulations which  
380 include correction factors or constants introduced to account for or minimise, the  
381 varying background reflectance (Gitelson et al., 1996; Huete et al., 1999). The  
382 Enhanced Vegetation Index (EVI) is a modification of NDVI that provides  
383 complementary information about the spatial and temporal variations of  
384 vegetation while minimising many of the contamination problems present in the  
385 NDVI, such as those associated with canopy background and atmospheric  
386 influences (Huete et al., 2002). Other closely related indices include the Simple  
387 Ratio (SR), the Green Normalised Difference Vegetation Index (GNDVI), Soil-  
388 Adjusted Vegetation Index (SAVI) amongst others. Xue et al. (2017) provides a  
389 detailed review of vegetation indices. Critically, an increase in availability of EO  
390 data with improved spatial, spectral, and radiometric resolution combined with  
391 the machine or deep learning techniques and development in computational  
392 resources would enhance the potential dryland forest information to be exploited  
393 (Ali et al., 2015). The constraint in spectral, spatial, and radiometric resolutions of  
394 remote sensing data may result in different saturation values of AGB depending on  
395 vegetation characteristics (Zhao et al., 2016). The spatial resolution of images such  
396 as NOAA AVHRR, SPOT Vegetation, and MODIS imagery data particularly at 1-8 km  
397 spatial resolution has been reported to result in poor spectral purity and limited  
398 identification of broad forest types such as coniferous and lack sufficient spatial  
399 details, particularly for less abundant species broad-leafed forests (Immitzer et al.,  
400 2018; Xu et al., 2021). Stratoulis et al. (2015) showed that the 10 m spatial  
401 resolution of Sentinel 2 allows for detecting fragmented patches in the lakeshore  
402 ecosystems but argued that enhanced spectral and spatial capabilities provide  
403 further potential in habitat monitoring and classification of environmentally  
404 complex areas. Other studies such as Wulder et al. (2004) and Xu et al. (2021)  
405 concluded that medium-high resolution Earth observation satellites can be used to  
406 produce more accurate results of forest species composition and land cover use  
407 classification by providing detailed spectral features of the canopy of tree species  
408 (Salajanu and Olson, 2001). Dube et al. (2014) have concluded that fine spatial  
409 resolution data with improved spectral bands (e.g., red edge) contains more

410 spectral information critical for accurately predicting forest metrics such as  
411 biomass in South Africa. Other remotely sensed studies estimated forest biomass  
412 at different scales and concluded that coarse spatial resolution optical sensors are  
413 useful for biomass mapping at continental and global scales rather than at local  
414 scales because the limited spatial detail of these coarse-resolution images misses  
415 the biomass variability in heterogeneous forests (Avitabile et al., 2012; Dube et al.,  
416 2014; van der Wer et al., 2006; Zhang and Kondragunta, 2006; Zhu and Liu, 2015).  
417 Lu (2006) demonstrated that the use of coarse spatial resolution sensors (i.e.,  
418 Landsat, MODIS etc.) for AGB estimation resulted in poor prediction accuracy due  
419 to the presence of mixed pixels together with a mismatch between the size of field  
420 measurements and the pixel (Avitabile et al., 2012). Various statistical methods,  
421 vegetation indices and textures have been explored to reduce the impacts of data  
422 saturation in Landsat imagery on AGB estimation accuracy (Lu et al., 2016).  
423 Studies such as Basuki et al. (2013) and Kajisa et al. (2009) observed that the  
424 application of statistical methods, spectral mixture analysis and integrating radar  
425 data with Landsat images improves forest AGB estimation accuracy significantly.  
426 Time series of Landsat imagery is another alternative explored that can result in  
427 more accurate AGB estimation and reduce saturation effects compared to the use  
428 of a single NDVI (Gasparri et al., 2010; Zhu and Liu, 2015).

429

### 430 1.5.3 Forest biomass and structural parameters

#### 431 1.5.3.1 Forest biomass estimation in dryland forests

432 Biomass, in general, includes the above-ground and below-ground living mass, and  
433 is usually expressed as dry weight (Lu, 2006). AGB includes all living biomass  
434 above the soil surface that includes the stem, stump, branches, bark, seeds, and  
435 foliage. Measuring forest biomass and its change acts as an indicator of climate  
436 change and forest health (Pause et al., 2016), however, the majority of studies on  
437 biomass have focused on boreal and temperate forests (Dong et al., 2003; Naidoo  
438 et al., 2006). Studies on TDFs are limited because they are dynamic with complex  
439 species composition and structure, coupled with environmental conditions which  
440 are difficult to assess and model (McElhinny et al., 2005). AGB estimation requires

441 field measurements as a prerequisite for developing estimation models, but field  
442 measurements are often difficult to implement, especially in remote areas (Lu,  
443 2006; Wingate et al., 2018), and they cannot provide the spatial distribution of  
444 biomass across large areas. Thus, remote sensing techniques offer the most  
445 practical approach to estimating dryland forest biomass and monitoring changes in  
446 forest structure, overcoming the limitations of sample size, timeliness, expense,  
447 and access (Lu, 2006; Lucas et al., 2015).

448 With increasing concern regarding greenhouse gas emissions, there is a need to  
449 better quantify the biomass of forests associated with regeneration and clearance  
450 (FAO, 2011; UN, 2011). Such information needs to be obtained at scales ranging  
451 from entire regions to individual forest stands (e.g., for carbon accounting  
452 purposes). However, assessments of biomass are typically obtained by applying  
453 species-specific allometric equations to forest inventory data (Chave et al., 2005).  
454 Although many studies have investigated the ability to estimate the biomass of  
455 forests, including tropical moist forests (Asner et al., 2009), dryland forests  
456 (Gizachew et al., 2016), temperate forests, and boreal forests (Dong et al., 2003)  
457 from remotely sensed data, a number of problems have been encountered. Of key  
458 concern is the generalisation of relationships derived for the accurate prediction of  
459 biomass at a specific location or time period (e.g., generalisation between images  
460 of one location acquired over a period of time to estimate characteristics at  
461 another location) (Woodcock et al., 2001). This problem is common in less well  
462 studied ecosystems such as dryland forests and can substantially limit the  
463 contribution remote sensing can make to environmental studies. Overall, regional  
464 variations in forest biomass arise as a result of differences in tree stem density,  
465 growth and disturbances rates, and other species-specific attributes, such as wood  
466 density (Asner et al., 2009).

### 467 1.5.3.2 Application of optical and SAR sensor in forest biomass

468 Different remote sensing sensors have been successful in forest biomass studies  
469 (Gizachew et al., 2016; Powell et al., 2010). However, in the tropics, where the  
470 cloud cover is common, optical data could not be used over large areas. Optical  
471 sensors are also less sensitive to variations within dense forests, and can only

472 provide spectral and horizontal distribution and not the vertical distribution (e.g.  
473 tree height or difference between single-story and multi-story vertical structural  
474 classes) of canopy elements in forests (Joshi et al., 2016). Under these conditions,  
475 radar remote sensing provides an alternative (Michelakis et al., 2014; Paradzayi et  
476 al., 2013). SAR has the advantage that it includes: the ability to collect data in all  
477 weathers, and during day and night; the sensor penetrates cloud, vegetation, dry  
478 soil, sand, dry snow; the data is sensitive to surface roughness, dielectric  
479 properties and moisture content; and the reflected signal is sensitive to  
480 polarisation and frequency (HH, VV, HV, and VH), and can be used for volumetric  
481 analysis (Balzter, 2001; Mitchard et al., 2009). However, radar remote sensing also  
482 has limitations including uncertainties in estimation, expensive datasets,  
483 difficulties in data processing, and data saturation problems (Balzter, 2001;  
484 Mitchard et al., 2009). Furthermore, Light Detection and Ranging (LiDAR) has  
485 become popular for deriving tree height variables closely related to the AGB  
486 (Unger et al., 2014), and a few studies have combined optical and LiDAR for AGB  
487 mapping (Lu et al., 2012). However, the applicability of this technique is limited to  
488 local regions because of its high economic costs and labour-intensive collection  
489 (Gibbs et al., 2007). Alternatively, other authors have explored the combination of  
490 optical and SAR (e.g., Cutler et al., 2012; Wingate et al., 2018). Combining  
491 frequently available SAR observations with less frequent (due to cloud cover)  
492 optical remote-sensing data may provide a sound information source in the  
493 tropics, but there remain few studies of this nature in tropical dryland forests.

494 Accurate delineation of biomass distribution at scales from local (ca.  $1 \times 10^{-1}$  km)  
495 to pantropical is significant in reducing the uncertainty of carbon emissions and  
496 sequestration, understanding their roles in influencing land degradation, and  
497 wider environmental processes (Foody, 2003). However, the lack of spatially  
498 explicit maps of biomass and forest structural parameters over dryland forests  
499 areas in Southern Africa is one of the largest sources of uncertainty in estimates of  
500 carbon emissions (Midgley et al., 2011; Timothy et al., 2016). With regards to  
501 tropical forests, forest biomass and structure are often relatively well studied in  
502 the tropical rainforests as compared to dryland forests, but rainforests are  
503 progressively shifting to TDFs, especially in South America and Africa, often

504 irreversibly because of fire events (Zhao et al., 2021). This phenomenon justifies  
505 the importance of studying TDF carbon stocks.

506

#### 507 1.5.4 The benefits and challenges of remote sensing in 508 dryland forests

509 The development of the Earth observation satellites during the past decades has  
510 enhanced our ability to assess the status and dynamics of vegetation change as  
511 well as impacts of climate change at a large scale (Nicholson, 2011). In forest  
512 ecosystems, identifying changes in canopy cover with remote sensing generally re-  
513 quires data at frequent intervals because the spectral signature changes rapidly  
514 with regrowth. Optical sensors provide the best alternative for vegetation change  
515 mapping and biomass estimation to field sampling due to global coverage and  
516 repeatability, given the ability to estimate characteristics such as forest type and  
517 leaf area index (LAI) (Lu, 2006; Symeonakis et al., 2018). Such sensors are  
518 however limited in the degree to which they can generate structural information  
519 and are restricted by cloud occlusion which is particularly problematic in tropical  
520 regions (Herold, 2007; Symeonakis et al., 2018). Light Detection Ranging (LIDAR)  
521 and Hyperspatial data can observe tree crowns, basal area, tree height and  
522 biomass but cannot cover large areas (Falkowski et al., 2008, Blackburn, 2007).  
523 The selection of suitable satellite data depends on the ecological characteristics of  
524 the ecosystems, spatial and temporal scales of interest (Estes et al., 2018). As the  
525 region of interest and temporal extent increases, the volume of data, and the  
526 complexity of image-processing becomes significant and an obstacle to many  
527 researchers and operational users with limited access to high-performance  
528 computing infrastructures (Smith et al., 2019).

529 Due to the inherent trade-offs between spatial and temporal resolution in EO data,  
530 and geographic coverage, the vegetation patterns on both spatial and temporal  
531 domains have been revealed by various technological advances resulted in the  
532 growing availability of remote sensing data and methods (Toth and Józków, 2016;  
533 Zhou et al., 2020). The application of non-parametric machine learning regression

534 algorithms, such as decision trees, random forests (RF), support vector machines  
535 (SVMs), and k-nearest neighbour have become more predominant and  
536 demonstrate the ability to outperform widely used parametric approaches, such as  
537 polynomial and multiple linear regression variables used with remotely sensed  
538 data in a forest environment (Breiman, 2001; Latifi et al., 2010). Non-parametric  
539 machine and deep learning models are sufficiently versatile to uncover  
540 complicated nonlinear relationships and able to extract combinations of the input  
541 data that are difficult to describe explicitly by humans, particularly, in areas with  
542 high structural variability such as dryland forests (Hastie et al., 2009; Shao et al.,  
543 2017). Machine and deep learning have been used by many remote sensing studies  
544 to provide in-depth forest investigation from the perspectives of hyperspectral  
545 image analysis, interpretation of SAR/ LiDAR images, interpretation of high-  
546 resolution satellite images and classification, and multimodal data fusion (e.g., the  
547 fusion of Hyperspectral, SAR, LiDAR and optical data (Guirado et al., 2020; Shao et  
548 al., 2017; Trier et al., 2018). Improved techniques in remote sensing such as  
549 Vegetation Indices, VOD, and machine and deep learning have been utilised to  
550 estimate dryland forest attributes globally and other dryland ecosystems,  
551 however, very few of these focused on the local and regional scale of Southern  
552 Africa (e.g., Symeonakis et al., 2020).

553 The uncertainties reported in many dryland forests studies relating to remote  
554 sensing (Bastin et al. 2017), could be decreased following further development,  
555 application, and comparison of these improved approaches in future works at  
556 local, regional, and continental studies in dryland forest ecosystems. It has been  
557 discovered that there is plausible trade-off between spatial resolution, image  
558 coverage and frequency in data acquisition, and many studies has shown that  
559 coarse spatial resolution optical sensors are useful for biomass mapping at  
560 national and global scale rather than at local scale (Wulder et al. 2004; Lu, 2006).  
561 For example, Dube et al., (2014) used spaceborne multispectral RapidEye sensor  
562 with a fine spatial resolution have the potential to satisfactorily predict intra-and-  
563 inter species predicting forest metrics, such as biomass in areas of closed and  
564 dense vegetation. The RapiEye have the capability to provide a better prediction  
565 for biomass because they contain more spectral information critical for vegetation  
566 mapping in comparison to the existing broadband multispectral images (Dube et

567 al., 2014). The rise of innovative and high-performance computing facilities and  
568 web-based software tools such as Google Earth Engine (GEE) platform and  
569 growing use of machine learning algorithms helps to overcome many barriers,  
570 enabling large volumes of data to be integrated, processed, and analysed for large  
571 areas and over long time periods (Warren et al., 2015). For a detailed review of  
572 machine learning and deep learning for remote sensing and Sustainable  
573 Development Goals, see Zhu et al. (2017) and Holloway and Mengersen (2018).  
574 Also, more information on research trends, benefits, and challenges of remote  
575 sensing in dryland forests are provided in David et al., 2002a, (Chapter 2). Using  
576 the new advances in data management and cloud computing capabilities of Google  
577 Earth Engine led to a recent discovery that forests in drylands exceeds previous  
578 estimates by over 40% (Bastin et al., 2017).

### 579 1.5.5 Google Earth Engine platform

580 The Google Earth Engine (GEE) platform provides pre-processed satellite imagery,  
581 enabling large volumes of data to be integrated, processed, and analysed for large  
582 areas and over long time periods (Warren et al., 2015). The platform provides  
583 online access to extensive imagery including the entire Landsat archive, complete  
584 archives of data from MODIS, Sentinel-1 and Sentinel-2. GEE also co-locates climate  
585 forecast data, land cover data, and many other environmental and socioeconomic  
586 data covering much of the planet. All processing and computations are done on-  
587 the-fly in the cloud which allows the user to process data in close to real-time  
588 (Hansen et al., 2013). The catalogue is continuously updated, and users can request  
589 the addition of new datasets to the public catalogue, or they can upload their  
590 private data via a REST (representational state transfer) interface using either  
591 browser-based or command-line tools (Gorelick et al., 2017).

592 GEE's functionality affords a unique opportunity to overcome the limitations  
593 imposed by the volume of data and the scale of analysis that would otherwise  
594 prevent analysis in many organisations in tropical dryland regions (Hansen et al.,  
595 2013; Shelestov et al., 2017). Although GEE has removed many computational and  
596 analysis barriers, the technology is not yet comprehensive. The approach is still  
597 evolving and there are shortcomings around the challenges of completing analysis

598 that would normally be better suited to a GIS environment, such as the intersection  
599 of raster- and vector-based datasets. This thesis has, therefore, utilised other  
600 analytical software such as R and ArcGIS since GEE allows files and data to be  
601 imported and exported for use elsewhere.

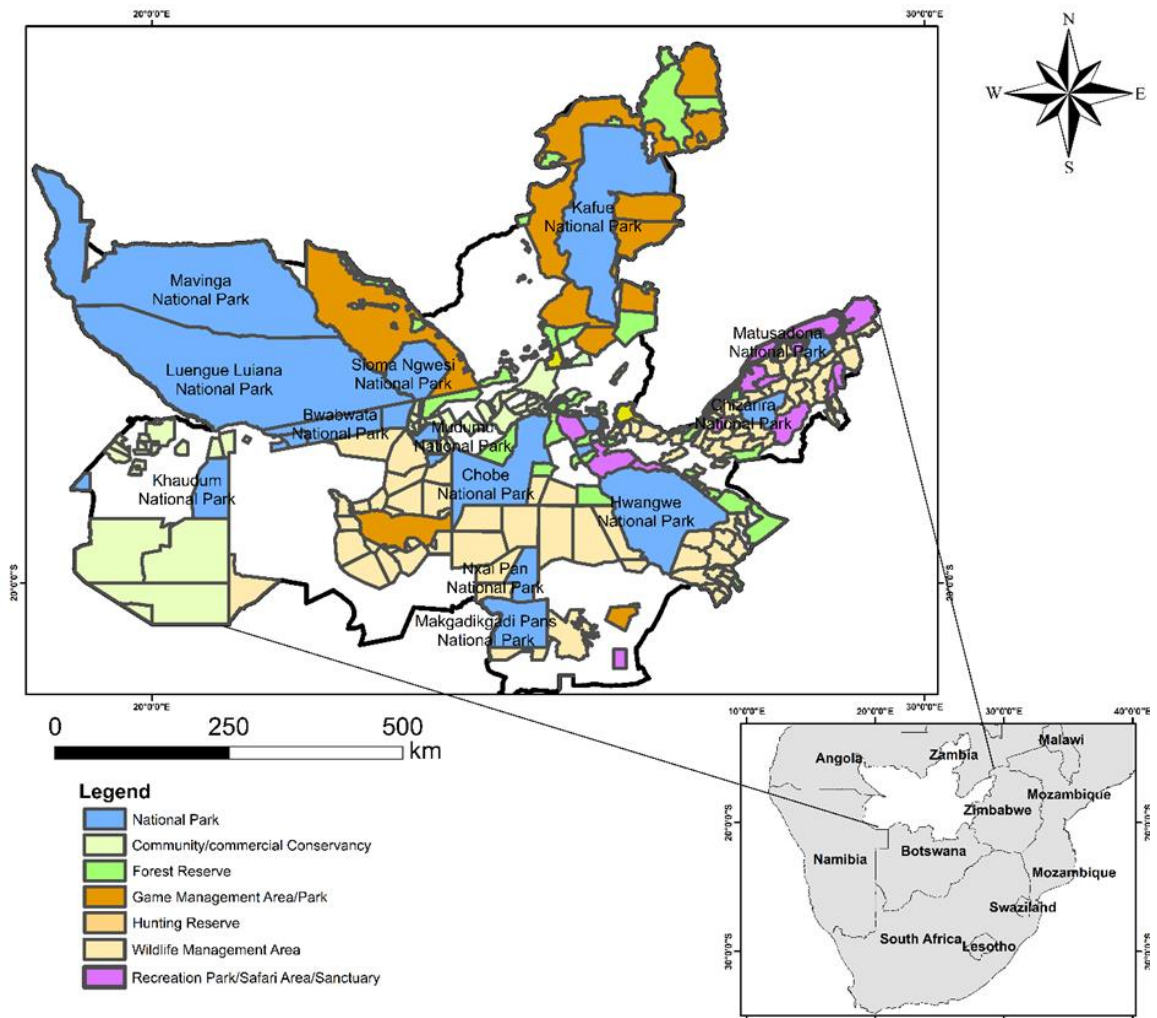
602

## 603 1.6 The world's largest conservation park

604 The Kavango-Zambezi Transfrontier Conservation Area (KAZA TFCA) was  
605 established in 2011 by its member states of Angola, Botswana, Namibia, Zambia,  
606 and Zimbabwe, with support from World Wide Fund for Nature (WWF) and the  
607 Peace Parks Foundation (WWF, 2016). KAZA TFCA is the World's largest  
608 transfrontier conservation area covering a land area of 519,912 km<sup>2</sup> (200,739 sq.  
609 mi, equivalent to the area of Spain or Thailand) (Murphy, 2008). About 71% of  
610 KAZA is protected to create economic development and conserve the unique  
611 biodiversity within the region, and only 29% of the land is not protected.

612 One key aim of KAZA is to connect and coordinate efforts across protected areas  
613 and create free movement for wildlife within its borders, without political  
614 boundaries hampering the ability to meet conservation objectives (Cumming,  
615 2008). KAZA links several conservation areas including 20 protected national  
616 parks, 103 wildlife management areas, 85 forest reserves, 11 game management  
617 areas, 11 sanctuaries, and communal lands (Fig. 1.5) (Karidozo et al., 2016). The  
618 area hosts the largest population (ca. 250,000) of the African elephant, one quarter  
619 (25%) of the African wild dog population, amongst other wildlife, and a human  
620 population of 2,677,086 (Karidozo et al., 2016). The growing human population  
621 and increasing wildlife population in KAZA have given rise to human  
622 encroachment and increased human-wildlife conflict (Stoldt et al., 2020).





623

624 Fig. 1. 5 Map of the study area showing KAZA region in Southern Africa and the and land  
 625 management classes as designated by the World Database on Protected Areas (Wdpa).

### 626 1.6.1 Rationale of the study

627 It is important to acknowledge the inherent pressure on dryland resources from  
 628 the perspective of the local population that depends on these ecosystems for  
 629 livelihoods, even in the remote and protected areas of the KAZA region. The  
 630 vegetation structure of KAZA consists of desert shrubs in the southwest, and  
 631 dryland forest in the northeast, with Baikiaea, miombo, mopane, and acacia  
 632 woodland species occupying by far the greatest portion of the area (Cumming,  
 633 2008). Within this region, forest loss and degradation are a major concern because  
 634 TDFs are already severely degraded as a result of competing land use, and from  
 635 overuse (Kamwi et al., 2020; Shackleton et al., 2010), as shown by field photos  
 636 collected in 2019, from Namibia and Botswana (Fig. 1.6).

637 These changes do not only directly impact wildlife species distribution, but can  
638 also undermine efforts to maintain, expand and link wildlife populations and  
639 economic sustainability (Naidoo et al., 2016). Dryland vegetation in arid, semi-arid,  
640 and dry sub-humid areas of Southern Africa are highly sensitive because  
641 precipitation is scarce and typically more or less unpredictable, temperatures are  
642 high, humidity is low and soils generally contain small amounts of organic material  
643 (King, 2014; Meadows, 2006; Niang et al., 2014).

644 For KAZA, no large-scale study exists that provides spatially explicit and up-to-date  
645 information on both the protected areas and forests throughout the region, that  
646 also includes detailed information on forest biomass, vegetation density, fire and  
647 drought impact, and land degradation (Cumming, 2008). This hampers efforts to  
648 mitigate the threats against KAZA. For example, many species (flora and fauna) are  
649 identified as endangered or threatened and would almost certainly merit Alliance  
650 for Zero Extinction (AZE) ranking (IUCN, 2020). For example, the *Baikiaea*  
651 *plurijuga* (Zambezi Teak) is on the International Union for Conservation of Nature  
652 (IUCN) red list due to overexploitation through logging and fire damage in Zambia  
653 and Namibia. The Zambezi and Kavango East regions within KAZA have low levels  
654 of income and high levels of poverty and are the most heavily forested regions in  
655 Namibia (USAID, 2010). A large part of the Zambezi region's land surface is state-  
656 run protected areas, where there is an ongoing land-use pressure, agricultural  
657 expansion, and conversion of closed woodland into secondary woods and shrubs  
658 (Kamwi et al., 2015). Due to the remoteness of the area, wildlife dangers, and the  
659 fact that KAZA extends across international borders, continuous and in-situ field  
660 sampling to measure and assess vegetation characteristics is an effectively  
661 impossible and expensive task. With a view on time and expense, satellite remote  
662 sensing is therefore here considered as an appropriate methodology for measuring  
663 changes in the dryland of KAZA, building on a limited number of localised previous  
664 studies (e.g., Schultz et al., 2018). This study provides an initiative for a significant  
665 advancement in mapping the dryland forests using remote sensing technology.



666

667 Fig. 1. 6 Example of ground data captured during a field campaign in February to May 2019; (A)  
 668 deforestation in Zambezi state forest in Namibia; (B) forest degradation in Chobe National Park in  
 669 Botswana; (C) Burned forest for cultivation near the protected area of Mudumu NP, Namibia; (D)  
 670 elephant browsing; (E) Sampling diameter at breast height of all tree per plot; (F) Meeting and  
 671 interviews with community members concerning dryland forests.

672

673

674

## 675 1.7 Aims and Objectives

### 676 Aims

677 The fundamental aim of this thesis is to estimate and characterise forest  
678 parameters, disturbance, and land cover change in the context of climate change in  
679 the KAZA region of Southern Africa. Throughout the thesis, the goal is to explore  
680 the use of novel application of remote sensing approaches and the fusion of  
681 multiple remote sensing data from optical and SAR sensors. The research seeks to  
682 consider their combination to ascertain the potential insights into the spatial and  
683 temporal change of dryland forests that remote sensing is able to provide. To  
684 address the aim, the thesis will tackle the following objectives:

### 685 Objectives

686 **Objective 1:** Provide a systematic review of the scientific literature related to the  
687 use of remotely sensed data within the context of dryland forests, with a focus on  
688 Southern Africa.

- 689 ○ Provide a detailed overview of the current approaches and limitations for  
690 monitoring dryland forests using optical and radar remote sensing data.
- 691 ○ Quantify general trends in remote sensing data studies focusing on  
692 monitoring dryland forests in Southern Africa.
- 693 ○ Identify research gaps and make recommendations for monitoring dryland  
694 forests using remote sensing data.

695

696 **Objective 2:** To assess the feasibility of using remote sensing data derived from  
697 SAR, multispectral, and ground measurements to estimate dryland forest above  
698 ground biomass.

- 699 ○ Develop empirical models to determine the relationship between field-  
700 measured AGB and Sentinel-1 SAR backscatter coefficients, S Sentinel-2,  
701 and Landsat-8 multispectral reflectance in the dryland forest environment.

702 The focus will be on the contribution and prediction potential of SAR data,  
703 multispectral bands, and their spectral indices, both individually and in  
704 combination.

705 ○ Develop parametric and non-parametric models for estimating and testing  
706 the accuracy of AGB estimation and mapping.

707 ○ To compare these models to different published biomass estimates in the  
708 dryland forest environment.

709 ○ To discuss the suitability of different models for land and wildlife  
710 management at different spatial scales (regional to global).

711 **Objective 3:** Investigate the evidence for water stress conditions across KAZA and  
712 to test the utility of structural breaks for detecting dryland forest changes using  
713 two methods: (1) BFAST and (2) BEAST change detection in the dryland forests of  
714 KAZA.

715 ○ Spatial characterisation of climatic data with vegetation indices as a proxy  
716 indicator of climate variability to improve understanding of vegetation  
717 response to drought.

718 ○ Compare the common vegetation index NDVI with GNDVI to evaluate their  
719 respective sensitivities and performance in detecting changes.

720 ○ To characterise changes in trends and phenological patterns using Breaks  
721 for Additive Seasonal and Trend (BFAST), and Bayesian Estimator of Abrupt  
722 change, Seasonality, and Trend (BEAST).

723 **Objective 4:** Investigate the relationship between fire and different climate effects  
724 on vegetation spectral characteristics at the regional scale of KAZA.

725 ○ To characterise drought conditions using climatic data (SPEI, root soil  
726 moisture, temperature, and precipitation) and explore the variability of  
727 drought using monitoring indicators (i.e., the drought duration, severity,  
728 and magnitude)

- 729       ○ To characterise the frequency, seasonality, and extent of fires through time  
730           on different land use management in the KAZA region
- 731       ○ To investigate the spatiotemporal changes in aridity in the KAZA region  
732           from 2002 to 2010 and 2011 to 2019

## 733   1.8 Thesis Structure

734   The thesis comprises six chapters structured as follows.

735   **Chapter 1** has introduced the general background, motivation and critically  
736   examines concepts and remote sensing of TDFs.

737   **Chapter 2** presents a detailed review of the scientific literature related to the use  
738   of remotely sensed data including synthetic aperture radar (SAR) and optical  
739   sensors within the context of dryland forests, with a focus on Southern Africa. The  
740   research presents examples of the literature from 1997 to 2020 that summarises  
741   past achievements, current efforts, and geoinformation knowledge gaps.

742   **Chapter 3** assesses the combination of synthetic-aperture radar (SAR) and  
743   multispectral data to estimate in dryland forests. Different parametric and non-  
744   parametric models for estimating parameters are developed and resulting maps  
745   accuracy is tested with ground measurements and different published biomass  
746   models in the dryland forest environment.

747   **Chapter 4** examines water stress conditions on vegetation and changes in dryland  
748   forests using multiple data streams for time series assessment over National parks  
749   and surrounding communal areas within KAZA. BFAST and BEAST algorithms  
750   were applied to evaluate their sensitivity to detect changes in trend and  
751   seasonality in tropical dryland forests. Different vegetation indices suitability in  
752   drylands were tested.

753   **Chapter 5** seeks to investigate the relationship between fire and different climate  
754   effects on vegetation spectral characteristics at the regional scale of KAZA. The  
755   chapter investigating the impacts, severity, and characteristics of drought a  
756   conditions in drylands. The fire dynamics are also investigated at the regional scale

757 of KAZA. The purpose is to expand the understanding from Chapter 4, linking it to  
758 climate and fire.

759 **Chapter 6** draws together the key findings presented in Chapters 2-5, addressing  
760 the research aim, bringing the findings into the wider research context, and  
761 contains the primary recommendations and conclusions of the research presented  
762 in the thesis.

763

764

765

766 **2 REMOTE SENSING FOR MONITORING TROPICAL**  
 767 **DRYLAND FORESTS: A REVIEW OF CURRENT**  
 768 **RESEARCH, KNOWLEDGE GAPS AND FUTURE**  
 769 **DIRECTIONS FOR SOUTHERN AFRICA**

---

770

771 Chapter 2 is published by *Environment Research Communications*, DOI:  
 772 <https://doi.org/10.1088/2515-7620/ac5b84>

773 Chapter 2 is also published as a policy brief by n8agrifood for policy makers,  
 774 <https://policyhub.n8agrifood.ac.uk/activity/rapid-evidence-synthesis-training/>, DOI:  
 775 10.5281/ZENODO.5566492

776

777 **Title:** Remote sensing for monitoring tropical dryland forests: A review of current  
 778 research, knowledge gaps and future directions for Southern Africa

779

780

781 Authors: Ruusa M. David, Nick J. Rosser, Daniel N.M. Donoghue

782

783

784 Department of Geography, Durham University, Science Laboratories, DH1 3LE  
 785 Durham, UK

786

787

788 **Author Contribution**

789

790 David Ruusa- Design the research, perform the data analysis, interpret the results,  
 791 wrote the manuscript, and revised the manuscript. Nick Rosser- Contributed to the  
 792 research design, manuscript editing and supervision. Daniel Donoghue-  
 793 Contributed to the research design, manuscript editing and supervision.

794

795

796



797

798

799

800

801 **Abstract**

802 Climate change, manifest via rising temperatures, extreme drought, and associated  
803 anthropogenic activities, has a negative impact on the health and development of  
804 tropical dryland forests. Southern Africa encompasses significant areas of dryland  
805 forests that are important to local communities but are facing rapid deforestation  
806 and are highly vulnerable to biome degradation from land uses and extreme  
807 climate events. Appropriate integration of remote sensing technologies helps to  
808 assess and monitor forest ecosystems and provide spatially explicit, operational,  
809 and long-term data to assist the sustainable use of tropical environment  
810 landscapes. The period from 2010 onwards has seen the rapid development of  
811 remote sensing research on tropical forests, which has led to a significant increase  
812 in the number of scientific publications. This review aims to analyse and synthesise  
813 the evidence published in peer review studies with a focus on optical and radar  
814 remote sensing of dryland forests in Southern Africa from 1997-2020. For this  
815 study, 137 citation indexed research publications have been analysed with respect  
816 to publication timing, study location, spatial and temporal scale of applied remote  
817 sensing data, satellite sensors or platforms employed, research topics considered,  
818 and overall outcomes of the studies. This enabled us to provide a comprehensive  
819 overview of past achievements, current efforts, major research topics studies, EO  
820 product gaps/challenges, and to propose ways in which challenges may be  
821 overcome. It is hoped that this review will motivate discussion and encourage  
822 uptake of new remote sensing tools (e.g., Google Earth Engine (GEE)), data (e.g.,  
823 the Sentinel satellites), improved vegetation parameters (e.g., red-edge related  
824 indices, vegetation optical depth (VOD)) and methodologies (e.g., data fusion or  
825 deep learning, etc.), where these have potential applications in monitoring dryland  
826 forests.

827 **Keywords:** Remote sensing, Dryland forests, Southern Africa, Forest monitoring,  
828 SAR, Optical, Systematic review

829

## 830 2.1 Introduction

### 831 2.1.1 Tropical dryland forest

832 Approximately 40% of the Earth's tropical and subtropical land surface is covered  
833 by open or closed forests. Of this, tropical dryland forests account for the largest  
834 share at 42%; the remaining 33% is moist forest, and only 25% is rain forest  
835 (Murphy et al., 1986; Janzen, 1988). The largest proportion of dryland forests  
836 ecosystems are found in Africa, accounting for 60 - 80% of the total biome area  
837 (three times the area covered by African rain forest) (Bodart et al., 2013; Bullock et  
838 al., 1995). Dryland forests hold a significant amount of terrestrial organic carbon  
839 that may contribute more to climate mitigation and adaptation than previously  
840 appreciated (Valentini et al., 2014). Dryland forests also provide diverse ecosystem  
841 services, including water regulation and erosion control, the provision of food, fuel,  
842 and tourism opportunities (Djouidi et al., 2015; Schröder et al., 2021). On the other  
843 hand, dryland forests are subject to prolonged dry seasons and their rate of  
844 conversion to secondary forests has historically been higher than other tropical  
845 forest types (Pennington et al., 2018). According to the Intergovernmental Panel  
846 on Climate Change (IPCC), these changes have impacts on carbon emissions to the  
847 atmosphere and forest biodiversity loss that reduce adaptive capacity and  
848 resilience to the impact of high temperatures and varying precipitation (IPCC,  
849 2014).

850 The definition of “dryland forest” remains debatable and controversial, which  
851 contributes to the difficulty in accurately assessing and measuring its distribution  
852 patterns and status (Blackie et al., 2014). The lack of a clear and comprehensive  
853 understanding of general terms including “drylands” and “forests” makes it a  
854 challenge to explicitly define dryland forests (Charles-D et al., 2015). Given the fact  
855 that dryland forests progressively grade into other vegetation types such as moist  
856 tropical forests, woodlands, and savannas, also makes clear definitions complex  
857 (Putz et al., 2010). Walter et al. (1971) noted that the accuracy of estimates of all  
858 tropical forest areas is constrained by uncertainty in the distribution of open  
859 woodlands in dryland areas, which are extensive in Africa, Australia, and Latin  
860 America.

861 In the scientific literature, many different names have been applied to tropical  
862 dryland forests, including savanna forests, Sudanian woodland and miombo  
863 woodland in Africa, monsoon forest in Asia, neotropical dry forests in South  
864 America (Chidumayo, 2013; Linares-Palomino et al., 2011; Suresh et al., 2011). The  
865 neotropical dry forests in South America have a plethora of names from “caatinga”  
866 in northeast Brazil, to “bosque tropical caducifolio” in Mexico, and “cuabal” in  
867 Cuba, which in part hinders comparisons (Mayes et al., 2017; Sánchez-Azofeifa et  
868 al., 2005). For example, Dexter et al. (2015) identified dry deciduous forest in India  
869 (Suresh et al., 2011), miombo woodland in southern Africa (Chidumayo, 2013),  
870 and deciduous dipterocarp forest in continental Asia (Bunyavejchewin et al., 2011)  
871 as a form of savanna, and not TDFs, despite the formal classification as TDFs by  
872 these studies, and the FAO (FAO, 2001). The Caatinga and Chaco vegetation in  
873 Latin America is also considered by some authors as part of the dry forests  
874 (Gasparri and Grau, 2009; Pennington and Ratter, 2006), although Olson et al.,  
875 (2001) classifies these regions as a shrubland ecosystem.

876 There are several definitions currently available for TDFs, but there is still a lack of  
877 consensus in developing a common understanding. Mooney et al. (1995) defined  
878 TDFs as forests occurring in the tropical regions characterised by pronounced  
879 seasonality in rainfall, where there are several months of severe, or even absolute  
880 drought. Sánchez-Azofeifa et al. (2005) broadly defined TDFs as a vegetation type  
881 typically dominated by deciduous trees (at least 50% of trees present are drought  
882 deciduous), where the mean annual temperature is  $\geq 25$  °C, total annual  
883 precipitation ranges between 700 and 2000 mm, and there are three or more dry  
884 months every year (precipitation < 100 mm per month). A widely accepted  
885 definition is that of the FAO, which has identified TDFs as a Global Ecological Zone  
886 (GEZ), experiencing a tropical climate, with a dry period of 5 to 8 months and  
887 annual rainfall ranges from 500 to 1500 mm; GEZ includes the drier type mbo and  
888 Sudanian woodlands, savannah (Africa), caatinga and chaco (South America), and  
889 dry deciduous dipterocarp forest and woodlands (Asia) (FAO, 2001). For the scope  
890 of this review, the FAO. (2001) definition of TDFs was followed because it  
891 recognises forests occurring in the dry tropical climate globally including areas  
892 with relatively open canopies such as woodlands, and woody stands, then those  
893 based entirely on climate definitions. The growing body of evidence suggests that

894 the current climate does not define the biogeography of TDFs or determine biome  
895 distributions (Staver et al., 2011; Sunderland et al., 2015), particularly in the  
896 context of future unprecedented climate change (IPCC, 2007). If climates become  
897 sufficiently warmer and drier in the tropics, dry forests may expand into areas that  
898 are currently dominated by moist tropical forests (Putz et al., 2010).

899

## 900 2.1.2 Recent research trends on tropical dry forests

### 901 2.1.2.1 Geographical research trends on tropical dry forests

902 Studies have pointed out that dryland forests generally receive a lower number of  
903 scientific publications and are under-represented in research in comparison with  
904 tropical moist forests (Miles et al., 2006; Quesada et al., 2009). Global reviews on  
905 dryland forests addressed the imbalance in the geographical coverage of dryland  
906 forest publications using remote sensing with certain tropical countries such as  
907 Latin America receiving the highest publications on dryland forests in comparison  
908 to most places in Africa (Blackie et al., 2014; Schröder et al., 2021). To investigate  
909 the geographical distribution of tropical dry forest studies, the study initially  
910 searched for publications in ISI web of knowledge and Scopus on tropical dryland  
911 forests from Asia, Africa, America, and Australia. This search was conducted by  
912 using the keywords 'Dry Forest', 'Dryland Forest' 'Savan\* Woodland', 'Savan\* Tree',  
913 'Dryland Vegetation', 'Dry Vegetation' 'Satellite', 'Remote Sensing', 'Optical', 'Radar',  
914 'Image', 'SAR', 'Earth Observation', 'country/continent e.g., Africa'. In the search  
915 period from 1997 to 2020, the study identified 1662 papers for Africa, 1639 for  
916 Australia, 1338 for America, and 1134 for Asia. In Africa, when the search was  
917 narrowed to individual countries, the results showed that about 743 publications  
918 are from the Republic of South Africa (RSA) while 355 publications were from the  
919 Sahel region of Nigeria. The study also investigated scientific publications from  
920 other Southern African countries with dryland forest and 369 publications were  
921 identified, including from Botswana (87), Zimbabwe (69), Mozambique (60),  
922 Namibia (68), Zambia (49), Angola (24), Lesotho (6), Swaziland (5). When the  
923 review combined the scientific publications from the above 8 Southern African  
924 countries, the results were 369 publications, indicating that publications on

925 dryland forests for the Republic of South Africa were 2.01 times higher than all 8  
926 Southern African countries combined. These results confirm that much less  
927 progress has been made in developing objective methods for assessing the rates of  
928 deforestation/conservation and threats to dryland forests ecosystems in most  
929 Southern African countries except for the Republic of South Africa.

930 The dryland forests in other parts of the world like Latin America are increasingly  
931 well studied at local, regional, national and continental scale, particularly with  
932 regards to carbon/biomass (Chazdon et al., 2016; Marín-Spiotta et al., 2008), fire  
933 (Campos-Vargas et al., 2021; White, 2019; Pereira et al., 2014), climate change  
934 (Mendivelso et al., 2014; Castro et al., 2018; González-M et al., 2021), floristic and  
935 diversity composition (Alvarez-Añorve et al., 2012; Gillespie et al., 2000),  
936 ecosystem services (Castillo et al., 2005; Paruelo et al., 2016), Payment for  
937 Environmental Services (PES) (Alcañiz and Gutierrez, 2020; Corbera et al., 2009),  
938 novel conservation approaches (e.g., sustainable intensification for  
939 protected/conservation areas) (Méndez et al., 2007; Reynolds et al., 2016) and has  
940 the most comprehensive forest change/deforestation and biophysical aspects  
941 including species population changes, with extensive use of remote sensing (do  
942 Espírito-Santo et al., 2020; Gasparri and Grau, 2009; Stan and Sanchez-Azofeifa,  
943 2019; Trejo and Dirzo, 2000; Portillo-Quintero et al., 2012). In terms of reviews,  
944 many remote sensing reviews are providing valuable information on TDF's  
945 biophysical, ecological and socioeconomic at a regional level of Latin America  
946 (Castro et al., 2003; Metternicht et al., 2010; Portillo, 2010; Sanchez-Azofeifa et  
947 al., 2003; Sánchez-Azofeifa et al., 2005; Sánchez-Azofeifa et al., 2013; Stan and  
948 Sanchez-Azofeifa, 2019; Quijas et al. 2019), and Australia (Lawley et al., 2016;  
949 Moore et al., 2016; Fensham et al., 2002). Also, reviews of current progress on  
950 dryland forests in individual countries can be found in many neotropics countries  
951 such as Mexico (Castillo et al., 2005; Curry, 2020), Venezuela (Fajardo et al., 2005;  
952 Rodríguez et al., 2008), and Costa Rica (Frankie et al., 2004; Stoner et al., 2004)  
953 enabling the identification of knowledge gaps and aiding in the development of a  
954 policy-relevant approach to conservation of these forests (Miles et al., 2006).

955 Latin America is one of the best-represented areas for remote sensing research in  
956 dryland forests, for example, Portillo-Quintero and Sánchez-Azofeifa. (2010)

957 utilised remote sensing data at continental America, dryland forests ecoregion, and  
958 neotropics countries to show that 66% of tropical dry forest in the region has  
959 already been converted and that in some countries the conversion rate is as high as  
960 86% and 95%, respectively. Aide et al. (2012) using Moderate Resolution Imaging  
961 Spectroradiometer (MODIS) satellite data estimated that 200,000 km<sup>2</sup> of woody  
962 vegetation of Latin American and the Caribbean region were lost due to  
963 deforestation between 2001 and 2010. Nanni et al. (2019) utilised MODIS satellite  
964 data at 250 m spatial resolution to assess reforestation at the regional level and  
965 reported that the reforestation hotspots cover 167,667.7 km<sup>2</sup> (7.6 %) of Latin  
966 America between 2001 and 2014. While there are continental studies in Africa  
967 utilising remote sensing on biophysical parameters such as biomass/deforestation  
968 (Bouvet et al., 2018; Bodart et al., 2013), as compared to Latin America, these  
969 studies may not consider the empirical observations of dryland forests  
970 extent/change per region or country level. In addition, most continental studies in  
971 Africa rather focus the attention on tropical rainforest in Central Africa (e.g., core  
972 Congolese forest) which may under-represent dryland forest (e.g., Aleman et al.,  
973 2018). Global applications often report general land use/cover change which  
974 results in inaccurate or poor estimates of dryland forest (Smith et al., 2019;  
975 Aleman et al., 2018).

976 Several studies using optical and passive microwave instruments in the African  
977 Sahel (Horion et al., 2014; Brandt et al., 2016; Olsson et al., 2005; Tian et al., 2017)  
978 has reported that the density/size of woody vegetation stands have increased, with  
979 few areas in northern Nigeria reported to experience logging and agricultural  
980 expansion into forest reserves. Deforestation in Southern Africa is a major concern,  
981 with ca. 1.4 million ha of net forest loss annually, contributing to increased land  
982 degradation and the ensuing impacts on the balance of ecosystem function  
983 (Lesolle, 2012). A global study by Tian et al. (2017) utilising the optical Normalised  
984 Difference Vegetation (NDVI) index and passive microwave VOD across tropical  
985 drylands has reported a decreasing trend in woody vegetation in Southern African  
986 countries such as Botswana and Zimbabwe. Mitchard and Flintrop. (2013)  
987 conducted a coarse-scale analysis of changes in woody vegetation from 1982 to  
988 2006 using NDVI time series from the Global Inventory Modeling and Mapping  
989 Studies (GIMMS) dataset and found that significant woody encroachment is

990 occurring in most west African countries, but, in contrast, in Southern Africa, a  
991 rapid reduction in woody vegetation (deforestation) is occurring. Bodart et al.  
992 (2013) used Landsat satellite imagery between 1990 and 2000 to estimate forest  
993 cover and forest cover changes in the African continent and found that 84% of the  
994 total deforested area occurred in the dry ecosystems of the Southern African  
995 region, with large spatially concentrated areas of forest loss found in Angola,  
996 Mozambique, Tanzania, Zambia and Zimbabwe, and isolated hotspots found in  
997 Nigeria and the border of the humid forest in Ghana. While such global and  
998 continental level studies are useful to highlight and reinforce the need to direct  
999 more attention and resources to these threatened/poorly studied ecosystems,  
1000 research efforts on forest change/deforestation and climate change impacts of  
1001 dryland forests at the regional level of Southern Africa are much harder to come by  
1002 (Blackie et al., 2014).

#### 1003 2.1.2.2 Remote Sensing approaches research trends in tropical dry 1004 forests

1005 In recent decades, satellite remote sensing or Earth observation (EO) has proved a  
1006 valuable tool in forest ecology, owing to its capability to perform systematic,  
1007 frequent, and synoptic observation of the Earth, resulting in large data volumes  
1008 and multiple datasets at varying spatial and temporal scales (Donoghue, 2002; Zhu,  
1009 2017). There are several sensors including multi-spectral scanners, laser scanners  
1010 (LiDAR), hyper-spectral scanners as well as satellite-borne Synthetic Aperture  
1011 Radar (SAR), that provide information on the colour and structure of forest  
1012 environments (Donoghue, 2002). EO has been applied to mapping the distribution,  
1013 changes in cover and condition including deforestation, desertification, fire  
1014 damage, and climate impact (Dogru et al., 2020; Smith et al., 2019). Additionally,  
1015 these data have been used to estimate biophysical characteristics such as total  
1016 above ground biomass (AGB), leaf area index (LAI), woody area index, tree  
1017 diameter, and canopy height which are key inputs into a variety of ecological  
1018 models, as well as calculations of carbon balance and primary production (Barbosa  
1019 et al., 2014; Donoghue, 2000). The continuous forest metrics obtained using EO  
1020 data can be extracted at leaf and crown level to evaluate spectral elements of leaf  
1021 or species properties and at stand-level and plot-level, or beyond to understand



1022 the variation between and among species, and through time (Muraoka et al., 2009).  
1023 Monitoring of dryland forest cover and forest metrics using EO data also helps to  
1024 improve the understanding of the ecological drivers behind land cover change  
1025 dynamics (Chambers et al., 2007; Veldkamp et al., 2001).

1026 Biomass has extensively been estimated based on the spectral reflectance values  
1027 from two or more wavelengths, and the sensitivity of optical and near-infrared  
1028 wavelengths to photosynthetic canopy cover has long been used for vegetation  
1029 analyses (Rouse, 1974; Tucker, 1979). Spectral vegetation indices (VIs), including  
1030 the NDVI index, are commonly used as a proxy of vegetation cover and have been  
1031 shown to relate closely to LAI, biomass, and the fraction of photosynthetically  
1032 active radiation absorbed by vegetation (fAPAR) (Curran, 1980). Several well-  
1033 known limitations of NDVI for robust estimation of biomass in drylands exist. NDVI  
1034 is sensitive to green components and insensitive to woody components where the  
1035 majority of carbon is stored (Tucker, 1979). Also, AGB production is not always  
1036 uniformly linked to either greenness or plant structure (herbaceous and woody  
1037 compositions), as moisture content and vegetation species composition have been  
1038 shown to impact the biomass-NDVI relationship (Asner et al., 2009; Wessels et al.,  
1039 2006). These observations may help explain reportedly weak relationships  
1040 between NDVI and tropical forest canopies, particularly for areas with complex  
1041 and high vegetation amounts as in TDFs (Foody et al., 2001; Sader et al., 1989). For  
1042 example, Madonsela et al. (2018) investigated the interactions between seasonal  
1043 NDVI and woody canopy cover in the savanna of the Kruger National Park (NP) to  
1044 model tree species diversity using a factorial model and found that the interaction  
1045 between NDVI and woody canopy cover was insignificant. These challenges have  
1046 led to the development of alternative formulations which include correction  
1047 factors or constants introduced to account for or minimise, the varying  
1048 background reflectance (Gitelson et al., 1996; Huete et al., 1999). The Enhanced  
1049 Vegetation Index (EVI) is a modification of NDVI that provides complementary  
1050 information about the spatial and temporal variations of vegetation while  
1051 minimising many of the contamination problems present in the NDVI, such as  
1052 those associated with canopy background and atmospheric influences (Huete et al.,  
1053 2002). Other closely related indices include the Simple Ratio (SR), the Green  
1054 Normalised Difference Vegetation Index (GNDVI), Soil-Adjusted Vegetation Index

1055 (SAVI) amongst others. Xue et al. (2017) provides a detailed review of vegetation  
1056 indices.

1057 Although vegetation monitoring has been largely based on the multispectral  
1058 “greenness” indices, which have proven invaluable for monitoring biophysical and  
1059 biogeochemical parameters, it has been widely reported in the literature that they  
1060 suffer from several weaknesses in dryland ecosystems (Tian et al., 2016; Shi et al.,  
1061 2008). Other remote sensing systems such as the passive microwave-based  
1062 satellite systems capture the biomass signal in the parameter termed vegetation  
1063 optical depth (VOD) which has been used to monitor changes in vegetation  
1064 dynamics (Andela et al., 2013; Brandt et al., 2018a; Brandt et al., 2018b). Unlike the  
1065 optical remote sensing-based vegetation indices that are sensitive to chlorophyll  
1066 abundance and photosynthetically active biomass of the leaves, the vegetation  
1067 information (e.g., VOD) deriving from passive microwave instruments is sensitive  
1068 to the water content in the total aboveground vegetation, including both the  
1069 canopy (e.g. woody plant foliage) and non-green woody (e.g. plant stems and  
1070 branches) components due to greater penetration and sensitivity (Liu et al., 2011;  
1071 Shi et al., 2008). The passive microwave observations VOD is relatively insensitive  
1072 to signal degradation from solar illumination and atmospheric effects and provide  
1073 a valuable alternative tool for rapid monitoring of carbon stocks and their changes  
1074 (Jones et al., 2011). One of the advantages of passive microwave-derived VOD is  
1075 that it continues to distinguish biomass variations at a relatively high biomass  
1076 density, as compared to optical-based vegetation indices which are likely to  
1077 become saturated over dense canopies (Jones et al., 2011; Liu et al., 2015). The  
1078 main disadvantage of passive microwave observations is the relatively coarse  
1079 spatial resolution (>10km), as compared to satellite data in the visible and near-  
1080 infrared parts of the spectrum; however, these data still have highly useful  
1081 applications at regional and global scales (Liu et al., 2015; Rahmoune et al., 2013;  
1082 Owe et al., 2001). Some recent global and local studies from Latin America and  
1083 Africa in the dryland ecosystems found VOD to be more robust against the NDVI  
1084 drawbacks of saturation effect and continues to distinguish structural differences  
1085 for vegetation with a near-closed canopy when used as a proxy for vegetation  
1086 productivity (van Marle et al., 2015; Cui et al., 2015; Liu et al., 2011; Tian et al.,  
1087 2016). Apart from the VOD and NDVI, an intercomparison between several

1088 vegetation indices including other passive microwave-based vegetation indices,  
1089 such as the Microwave Polarisation Difference Index (MPDI) (Becker & Choudhury,  
1090 1988), and the Microwave Vegetation Indices (MVIS) (Shi et al., 2008) would be of  
1091 benefit in monitoring dryland biomes.

### 1092 2.1.3 Review focus justification

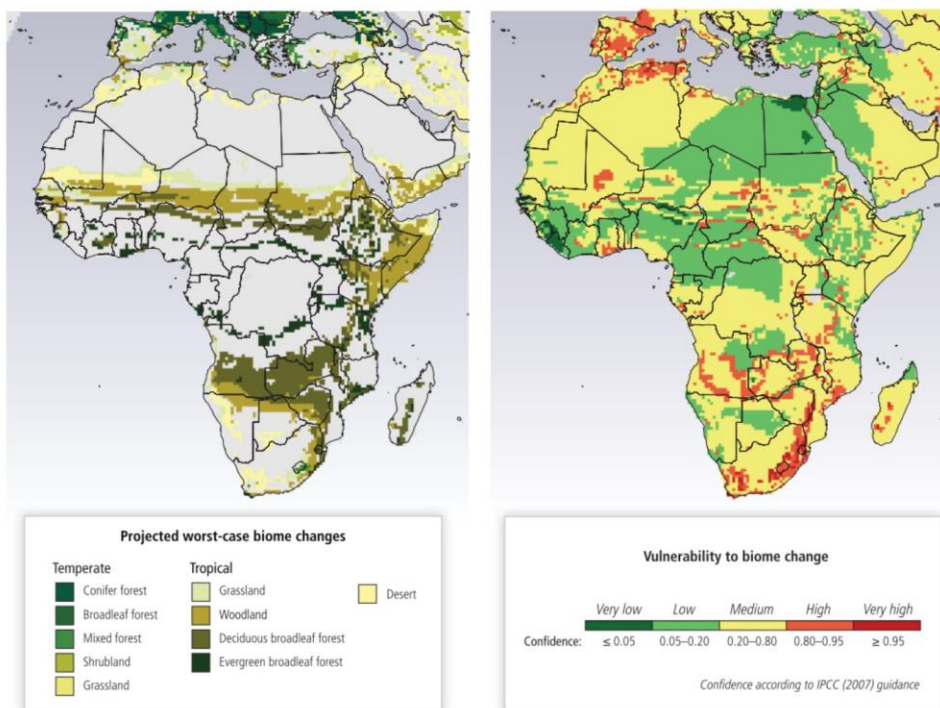
1093 The majority of the residents of Southern Africa are poor and about 75% of them  
1094 live in rural areas with high reliance on dryland forests (Bond 2010). Additionally,  
1095 these dryland areas display a high susceptibility to bush encroachment (O'Connor  
1096 et al., 2014) and economic reliance on tourism (Ferreira 2004) and forest products  
1097 (Kamwi et al., 2020), which means that both agriculture and tourism development  
1098 encroach on the dryland forests, resulting in loss of forest biodiversity and land  
1099 degradation (Eva et al., 2006; Petheram et al., 2006). Across Southern Africa,  
1100 sustainable management of dryland ecosystems is hindered by complex land  
1101 tenure due to historical legacy, weak links between policy and woodland use and  
1102 management, and cultural drivers (Balint and Mashinya, 2006; Dewees, 1994).  
1103 Also, the dryland ecosystems of Southern Africa are dominated by private land  
1104 ownership, a high concentration of wildlife and human populations, and  
1105 agriculture where TDFs occur (Child et al. 2012). This review focuses on Southern  
1106 Africa because there is a gap in knowledge on carbon storage, biomass, and the  
1107 long-term trend of forest distribution and degradation in dryland forests. Much of  
1108 the research on dryland forests in Southern African has concentrated on  
1109 livelihoods, community forest management, and conservation/development trade-  
1110 offs (Chidumayo et al., 2010; Chidumayo and Gumbo, 2010; Chidumayo, 2019;  
1111 Djoudi et al., 2015, Dewees 1994; Du Preez, 2014; Ryan et al., 2016), leaving forests  
1112 highly vulnerable to deforestation and degradation (Keenan et al., 2015). The  
1113 social and economic aspects are important given the large numbers of African  
1114 people that rely on dry forests for their livelihoods and a range of goods and  
1115 services. However, the gap in biophysical aspects, threats status, and adaptation to  
1116 climate change identified for Southern African TDFs at the regional and national  
1117 level (Blackie et al., 2014; Sunderland et al., 2015), presents an urgent need for an  
1118 assessment of the effectiveness of the EO scientific foundation on current  
1119 understanding of TDFs in Southern Africa; this can aid in the development of

1120 policy-relevant approaches and long-term, regional perspective for planning and  
1121 conservation of the TDFs.

1122 With the prospects of multiple free datasets from optical and SAR sensors being  
1123 available; combining information from optical sensors on photosynthetic activity  
1124 (e.g., through various vegetation indices) with SAR-derived information on forest  
1125 structure and volume brings the benefits of higher spectral resolution and  
1126 compensating for the shortcomings of using single data products alone. Based on  
1127 this hypothesis, this review focuses on examining the studies using optical and SAR  
1128 sensors, both individually and the combination of the two types of EO data in  
1129 monitoring tropical forests. While forest distribution, carbon storage, and reducing  
1130 emissions from deforestation and forest degradation (REDD+) related research  
1131 exists in African dryland forests, the geographical focus has tended to be confined  
1132 to several West/Central African countries, whereas Southern Africa is relatively  
1133 poorly analysed (Lewis et al., 2013; Sunderland et al., 2015). Although numerous  
1134 reviews have been conducted discussing the application of optical and radar  
1135 remote sensing, they are either concentrated on mangroves forests (Kuenzer et al.,  
1136 2011; Wang et al., 2019), rain forests (Dupuis et al., 2020), or ecosystem services  
1137 (Barbosa et al., 2015). To date, reviews on remote sensing and EO in Southern  
1138 Africa have focused on research conducted in the Republic of South Africa (RSA)  
1139 (Hoffman et al., 2000; Mutanga et al., 2016; Mutanga et al., 2009).

1140 As shown in Fig. 2.1, the climate threats coupled with a growing human population  
1141 and future anticipated changes in land use are predicted to lead to severe dry  
1142 forest biome shifts and degradation across the whole of Southern Africa, hence the  
1143 need to expand the geographical scope of this review from previous work (IPCC,  
1144 2014; King, 2014). This paper provides a systematic review of the scientific  
1145 literatures related to the use of Earth observation data including SAR and optical  
1146 sensors used to study dryland forests, with a focus on Southern Africa. To achieve  
1147 this, examples from the literature that summarise past achievements, current  
1148 efforts, and knowledge gaps are presented. The objectives of this review are to (i)  
1149 to provide a detailed overview of the current approaches and limitations for  
1150 monitoring dryland forests using optical and radar remote sensing data. (ii) to  
1151 provide a critical evaluation and synthesis of the literature monitoring dryland

1152 forests using remote sensing data and discuss how EO data can contribute to  
 1153 dryland forest monitoring and forest conservation in Southern Africa. (iii) to  
 1154 identify knowledge gaps and make recommendations for research that will  
 1155 enhance monitoring of dryland forests using remote sensing data.



1156

1157 Fig. 2. 1 (a) Projected biome change from the periods 1961–1990 to 2071–2100 using the  
 1158 MC1 Dynamic Vegetation Model. (b) Vulnerability of ecosystems to biome shifts based on  
 1159 historical climate (1901–2002) and projected vegetation (2071–2100) (source: IPCC,  
 1160 2014).

1161

## 1162 2.2 Remote sensing applications in dryland forest

### 1163 2.2.1 Optical data

1164 In broad terms, the satellite platforms developed over the past 40 years (since  
 1165 1972) have carried two broad types of sensor systems; passive optical and active  
 1166 synthetic aperture radar (SAR). Successful change detection and parameter  
 1167 estimation over tropical dryland forests require: (a) correct selection and  
 1168 application of sensor type; (b) coupling with field observation data for calibration

1169 and validation, and (c) data integration and appropriate techniques for modelling  
1170 (Fig. 2.2). Optical sensors have been widely used for land cover and forest resource  
1171 mapping, providing access to long-term data dating back to the launch of Landsat  
1172 ERTS (Earth Resources Technology Satellite) satellites in 1972. Landsat and  
1173 several other coarse/medium spatial resolution optical sensor missions (National  
1174 Oceanic and Atmospheric Administration (NOAA) - Advanced Very High-  
1175 Resolution Radiometer (AVHRR); the National Aeronautics and Space  
1176 Administration (NASA) -Aqua/Terra- Moderate Resolution Imaging  
1177 Spectroradiometer (MODIS); Indian Remote Sensing Satellites-1C/1D (ISRO-IRS-  
1178 1C/D), Sentinel-2) provide well-calibrated, nadir-viewing, near-global systematic  
1179 coverage which have built up a valuable archive of image data that can be used to  
1180 analyse ecosystem dynamics (Congalton, 2018; Donoghue, 2000). In 2014, ESA  
1181 launched the Multispectral Instrument (MSI) onboard Sentinel-2 as part of its  
1182 Copernicus EO mission. Sentinel-2 MSI uses two identical satellite sensors to  
1183 measure the Earth's reflected radiance with a revisit time of 5 days and a fine  
1184 spatial resolution of 10 - 20 m pixel size. The length of the Sentinel-2 archive is  
1185 short (from 2015), compared to the Landsat mission from 1972-present, NOAA-  
1186 AVHRR 1979-present; Satellite Pour l'Observation de la Terre VEGETATION  
1187 (SPOT/VGT) (1998-present), IRS-1C/1D (ISRO-IRS-1C/D) (1995-2010), ENVISAT -  
1188 Medium Resolution Imaging Spectrometer (MERIS) (2002-2010) and the NASA -  
1189 MODIS (2000-present) and the French Space Agency (CNES-Centre national  
1190 d'études spatiales) high-resolution SPOT satellite constellation (6 m - 20 m pixel  
1191 size) - SPOT-1 in 1986-1990, SPOT-2 in 1990-2009, SPOT-3 in 1993-2009; SPOT-4  
1192 in 1990-2013; SPOT-5 in 2002-present; SPOT-6 in 2012-present; SPOT-7 in 2014-  
1193 present. The VEGETATION 1 (VGT 1) (1998-2012) and VEGETATION 2 (VGT 2)  
1194 (2002-2014) instrument on the SPOT 4 and SPOT 5 (SPOT/VGT) satellites  
1195 provided global daily monitoring of vegetation cover, and it is successor the  
1196 European PROBA-V satellite (2013-present), with a pixel size of 1 km, 300 m and  
1197 100 m are supplied by the VEGETATION image Processing Centre (CTIV) of VITO  
1198 (Belgium), which can be accessed through the internet site <http://free.vgt.vito.be>.  
1199 Although a large number of satellite sensors have been launched that are capable  
1200 of observing land dynamics, and their pixel size has decreased from 80 m of the  
1201 Landsat-1 to 0.41-1.65 m of the GeoEye-1 satellites (Aguilar et al., 2013), very few

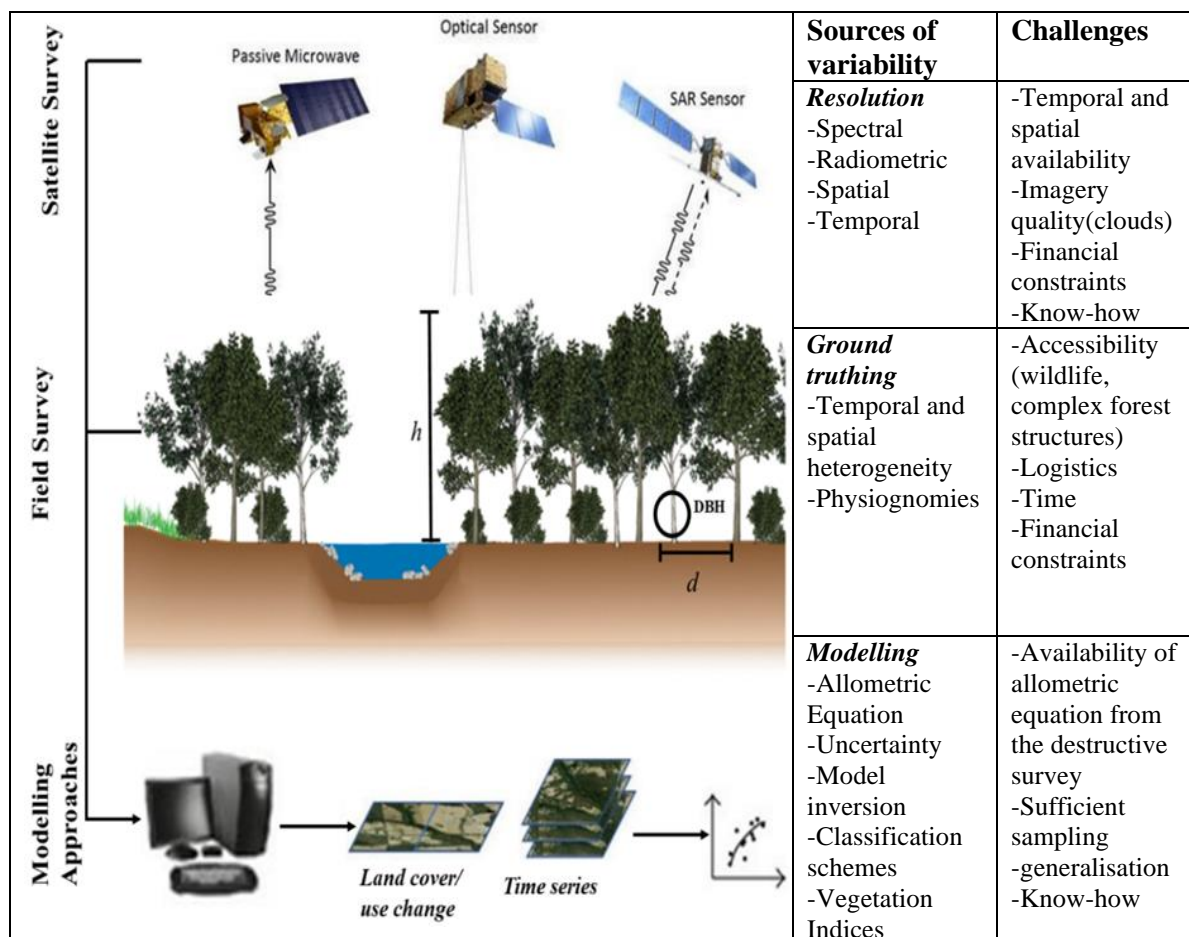
1202 sensors provide well-calibrated multispectral, nadir-viewing observations and  
1203 even fewer systematically capture all global data and provide a long-term archive  
1204 of data free of charge to the public. Except for AVHRR and Landsat, no other sensor  
1205 or sensor line offers the chance of long-term monitoring of an area to be monitored  
1206 back in time to the 1970s, covering about four decades.

1207 There are several non-systematic commercial high-resolution satellites that allow  
1208 the detection of individual trees or populations. Maxar Technologies Inc. launched  
1209 4 very fine resolution satellites - WorldView-1 in 2007, WorldView-2 in 2009,  
1210 WorldView-3 in 2010, and WorldView-4 in 2019 that acquire images with spatial  
1211 resolution of 0.5, 0.41, and 0.31 m, respectively. From 2009 onward, Planet labs  
1212 launched a swarm of micro-satellites including PlanetScope (PS), RapidEye (RE),  
1213 and SkySat (SS) Earth-imaging constellations with multispectral imaging capability  
1214 with the aim of acquiring daily image capture for any part of the world at a spatial  
1215 resolution of 3.125 m to 6.5 m (Marta, 2018). In 2011 and 2012, the Space Agency  
1216 of France (CNES) launched the Pléiades – fine resolution optical imaging satellite  
1217 constellation (Pléiades-1A and Pléiades-1B), with a fine spatial resolution of 0.7 –  
1218 2.8 m. Other very fine-resolution commercial space imaging satellites include  
1219 Earlybird (1997), GeoEye (2008), EROS-A (1998), IKONOS (1999), QuickBird  
1220 (2001), OrbView (2001) (Maglione, 2016). In Africa, South Africa started satellite  
1221 developments in the 1990s, with the successful launch of SunSat-1 with a spatial  
1222 resolution of 15 m in 1999 and SumbandilaSat low orbit satellite with a high fine  
1223 resolution of 6.25 m in 2009 (Cho et al., 2012; Mutanga et al., 2016). While the first  
1224 Nigerian satellite, a microsatellite called NigeriaSat-1, was successfully launched  
1225 into low earth orbit in 2003, followed by Nigeriasat-2 with a higher spatial  
1226 resolution of 2.5 – 5 m, built by Surrey Satellite Technology Limited (SSTL) of UK  
1227 (Agbaje, 2010).

1228 Nevertheless, the use of data acquired by higher spatial resolution optical sensors,  
1229 particularly at regional and global scales, can be limited by their relatively high  
1230 cost, huge data volumes, and low frequency of data acquisition compounded  
1231 further in tropical regions where cloud cover is prevalent (Lehmann et al., 2015;  
1232 Zhu et al., 2012). The temporal resolution of sensors has also increased from, for  
1233 example, 16 days for Landsat to nearly 1 day for the NOAA-AVHRR, NASA-

1234 Aqua/Terra-MODIS, NOAA-AVHRR, SPOT, SPOT/VGT (PROBA-V), and/or  
 1235 ENVISAT-MERIS data, but with a coarse spatial resolution of 250 m to 1 km (Arino  
 1236 et al., 2007; Herold et al., 2008). Although lacking fine spatial detail, the daily  
 1237 temporal resolution of such sensors enables frequent estimation of deforestation,  
 1238 detection of disturbances using dense time series data, and enables gaps due to  
 1239 cloud cover to be overcome (Mbow et al., 2015). It is important to mention that the  
 1240 acquisitions of some satellites such as NOAA-AVHRR, IRS-1C/1D, and MERIS  
 1241 ceased operations, however, the Sentinel, MODIS, SPOT-VGT, and Landsat series  
 1242 continue to operate, with ongoing continuity of data collection ensured with the  
 1243 recent launch of Landsat-9 in September 2021.

1244



1245 Fig. 2. 2 Interaction mechanisms for dryland forest canopies and source of variability and  
 1246 challenges related to each stage of remote sensing monitoring tropical dryland forest  
 1247 extents. Adapted from Barbosa et al., 2014.

1248



1249

## 1250           2.2.2 Synthetic Aperture Radar (SAR)

1251 SAR sensors for civilian applications first appeared in 1978 with NASA's SeaSat but  
1252 have grown in importance as a tool for forest studies. SAR sensors can operate at  
1253 different frequencies and polarisations; these system parameters provide  
1254 information on the roughness and scattering properties of forest canopies and data  
1255 can be captured day and night independent of weather conditions (Durden et al.,  
1256 1989). Since SAR can penetrate cloud, rain, smoke, and haze, and it is a valuable  
1257 source of data when atmospheric conditions hamper optical data capture,  
1258 particularly in the tropical dryland forest such as Southern Africa where the cloud  
1259 and smoke from forest fires are prominent features (Le Canut et al., 1996). Radar  
1260 signals are sensitive to moisture, variations, surface roughness, and vegetation  
1261 structure properties, whereas data from optical systems use characteristics related  
1262 to reflected solar illumination or surface temperature (for thermal infrared  
1263 sensors) as a basis for discrimination of the land cover (Kasischke et al., 1997;  
1264 Mitchard et al., 2009). Cloud cover-free SAR images have great potential in the  
1265 dryland tropical areas but have been used less often for forest monitoring  
1266 applications compared to optical imagery, partly because of the scarcity of data  
1267 (Castro et al., 2003). Since the launch of the Sentinel-1A and B, dense SAR time-  
1268 series data are now available over tropical forest areas freely and openly, with  
1269 systematic acquisitions at a 10 m spatial resolution and a 6 - 12 day revisit time  
1270 (dependent on the location) in all weather conditions.

1271 Over the last 30 years, several satellite-borne SAR has been launched, including the  
1272 United State Spaceborne Imaging Radar-Synthetic Aperture Radar (SIR-C/X-SAR),  
1273 European Remote Sensing (ERS-1/-2), Advanced Synthetic Aperture Radar (ASAR),  
1274 Japanese Earth Resources Satellite (JERS-1), Advanced Land Observation Satellite  
1275 (ALOS/PALSAR-1/-2), German TerraSAR-X, and the Canadian RADARSAT-1/-2  
1276 (Shimada, 2018). Depending on the sensor configuration, a single channel  
1277 (wavelength/frequency) or multiple channels may be recorded in either single or  
1278 multiple polarisations. Generally, studies have reported that the longer the  
1279 wavelength (e.g. P (30–100 cm) and L (15–30 cm)), the further is its penetration

1280 into the forest and the greater the importance of scattering beyond the upper  
1281 canopy (Huang et al., 2015). Besides the greater sensitivity of longer radar  
1282 wavelengths to forest structure, different studies indicate that cross-polarised  
1283 backscatter (HV-horizontally transmitted, and vertically received, VH-vertically  
1284 transmitted and horizontally received) often exhibits greater sensitivity to forest  
1285 biomass than like-polarised backscatter (co-polarised bands: HH-horizontally  
1286 transmitted and horizontally received, VV-vertically transmitted and vertically  
1287 received) (Kasischke et al., 1997).

### 1288 2.2.3 Limitations of optical and radar, and benefits of 1289 combining sensors

1290 Despite the different generations and types of satellite sensors, no one sensor  
1291 currently meets fully the requirements of a comprehensive forest resource  
1292 assessment EO system. The selection of an appropriate source of data requires first  
1293 the identification of the ecological question being asked, identification of the  
1294 limitations and advantages of each sensor. The varying temporal, spatial, spectral,  
1295 and radiometric resolutions unique to the individual sensor system, result in  
1296 different advantages and disadvantages to the monitoring of dryland ecosystems  
1297 (Lu, 2006). Optical data are limited in the monitoring of this forest type. For  
1298 example (1) cloud and smoke severely limit the use of optical products (Le Canut  
1299 et al., 1996); (2) Dramatic seasonal changes in the dryland forests conditions  
1300 including droughts and leaf shedding make it unsuitable for systematic all-season  
1301 monitoring of this forest type (Boggs, 2010). One of the reasons for this is  
1302 associated with the seasonality of the tropical vegetation: during the wet season,  
1303 cloud-free satellite imagery is difficult to acquire, while during the dry season  
1304 when the imagery is more available, the leaf-off configuration of the forest causes  
1305 misclassification with savanna shrubland or grassland; (3) Optical data is sensitive  
1306 at the early stages of growth but as forest canopies close, reflected radiation is no  
1307 longer sensitive to biomass as the reflectance signal saturates at higher biomass  
1308 values (Lu, 2006); (4) Passive optical sensors only detect the surface top layer,  
1309 meaning that forest canopy obscures the understory, and similarly grasses/crops  
1310 obscure soil; (5) Changes in the spectral properties of the soil and atmosphere can

1311 also hinder the inference of forest cover properties (Santos et al., 2002; Wang et al.,  
1312 1998).

1313 Similarly, there are a number of challenges to analysing and interpreting radar  
1314 images for tropical forest applications, which include: (1) Difficulty in interpreting  
1315 radar backscatter, including, for example, speckle, which is unwanted random  
1316 noise inherent in all SAR images, which may increase measurement uncertainty  
1317 and make interpretation difficult (Klogo et al., 2013); (2) Topography is a major  
1318 limitation in mountainous regions due to geometric and radiometric effects such as  
1319 radar shadowing caused by foreshortening and layover when the satellite is not  
1320 able to illuminate the whole ground surface (Mitchard et al., 2009); (3) SAR  
1321 observations often lack a long-term and dense time series because they demand a  
1322 relatively high energy provision on satellite platforms. Until recently, satellite-  
1323 based SAR data for multi-temporal assessments over large areas were constrained  
1324 by coarse spatial and temporal coverage at medium resolution, although this now  
1325 may be overcome with acquisitions from the recently launched C-band Sentinel-1  
1326 and L-band ALOS-2 satellite missions (Reiche et al., 2016).

1327 Rather than using EO data from a single satellite sensor, the synergy of remotely  
1328 sensed data from multiple sensors, particularly SAR systems with those acquired  
1329 by optical sensors, has been shown to be beneficial for forest resource assessment  
1330 (Lehmann et al., 2015). Because optical data is capable of measuring the  
1331 reflectance of the topmost layer of the forest canopy and SAR data deliver useful  
1332 within-canopy biophysical parameters without being affected by cloud cover and  
1333 weather conditions, one dataset may compensate for the shortcomings of the other  
1334 (Reiche et al., 2016). Previous research indicated that integration of optical and  
1335 radar can improve land and forest cover characterisation (Symeonakis et al.,  
1336 2018). For example, the fusion of optical and radar sensor data has the potential to  
1337 improve AGB estimation because it may compensate for the mixed pixels in a  
1338 tropical forest area. In addition to the spectral synergy afforded, the cloud  
1339 penetrating capability of microwave radar sensors allows areas that have missing  
1340 optical data to be included in analyses, particularly if multi-temporal methods are  
1341 being employed (Reiche et al., 2016).

## 1342 2.3 Methodology

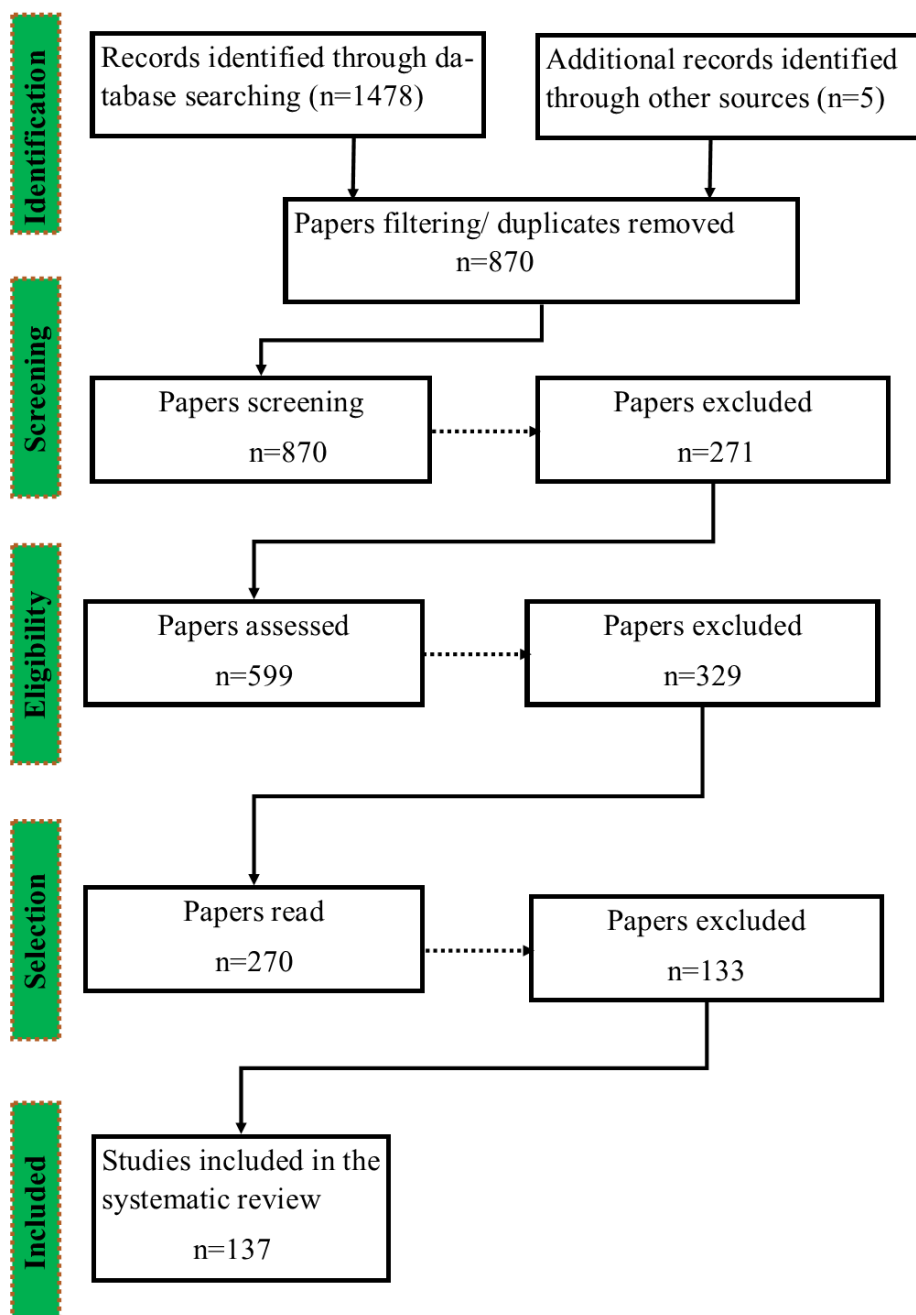
1343 This review focused on scientific papers studying tropical dryland forests  
1344 and made use of remote sensing data to monitor and estimate changes in dryland  
1345 forests. Airborne remote sensing studies were excluded from this review process,  
1346 since the review's major focus lies on satellite Earth observation of dryland forests  
1347 and because the acquisition of airborne sensors have low area coverage and high  
1348 cost per unit area of ground coverage (e.g., the airborne hyperspectral images),  
1349 making them spatially and temporally limited in most African countries. The  
1350 systematic search approach taken to querying the literature was carried out by  
1351 making use of selective keyword searches in the form of structured queries using  
1352 field tags and Boolean operators through the Web of Science  
1353 (<http://apps.webofknowledge.com>) and Scopus (<http://www.scopus.com>)  
1354 databases. At each query, terms and keywords such as '*Dryland forests*', '*Savan\**',  
1355 '*Woodland*', '*Tree*', '*Vegetation*', '*Satellite*', '*Remote Sensing*', '*Optical*', '*Radar*',  
1356 '*Image*', '*SAR*', and '*Earth Observation*' were used to produce an extensive list of  
1357 articles, where \* is a wildcard search. The results were further refined with  
1358 keywords such as '*Forest change*', '*Degradation*', '*Deforestation*', '*Trend*',  
1359 '*Biodiversity*', '*Phenology*', '*Biomass*', '*Structural parameter*', and also keywords  
1360 representing the countries in Southern Africa, such as '*Botswana*', '*Namibia*',  
1361 '*Mozambique*', '*South Africa*', to provide a comparison in terms of the numbers of  
1362 studies undertaken across the region. Within the context of this review, all  
1363 research articles were categorised into eight categories, including: 'Land-use/land-  
1364 cover', 'Forest cover/types', 'Biomass', 'Forest structure', 'Biodiversity/habitats',  
1365 'Phenology', 'Plant traits', and 'Disturbances'. Articles with a publication date  
1366 between 1997 and 2020 were considered, capturing a period of two decades  
1367 within the review, based on a broad set of inclusion criteria:

- 1368 1. The paper should address dryland forests and remote sensing as either  
1369 main or secondary subjects.
- 1370 2. The selection terms and keywords should exist as a whole in at least one of  
1371 the fields: title, keywords, and abstract.
- 1372 3. The paper should be published in a peer-reviewed scientific journal.

1373 4. The paper should be written in the English language.

1374 During the data extraction process and literature search, the research aimed to  
1375 find studies meeting the criteria for peer-reviewed publications, available through  
1376 the chosen indexed bibliographic databases. For this reason, the literature search  
1377 did not include general non-scientific reports, books, grey literature, thesis  
1378 documents or dissertations, extended abstracts, or presentations. The initial steps  
1379 of the search process returned 1,478 published articles. Additional publications  
1380 were added to the total set of studies by identifying relevant literature found in the  
1381 reference lists of these selected papers that conform to the inclusion criteria. The  
1382 review methodology was guided by the Guidelines for Systematic Review and  
1383 Evidence Synthesis in Environmental Management (Collaboration for  
1384 Environmental Evidence, 2013). A systematic review and meta-analysis were  
1385 undertaken and framed based on the PICO (population, intervention, comparison,  
1386 outcomes) model (McKenzie et al., 2019) and reported using PRISMA (Preferred  
1387 Reporting Items for Systematic reviews and Meta-Analyses) flow diagram (Moher  
1388 et al., 2009). The 1,478 articles were reduced to 870 articles as only the studies  
1389 that had a full text available in English, papers published in peer-reviewed journals  
1390 were selected for inclusion in the review, and all repetitions across databases were  
1391 removed. Initially, the titles and abstracts were screened to assess eligibility, by  
1392 searching for predefined keywords and terms of the abstract or summary,  
1393 identifying terms 'dry or dryland forests and the country or countries where the  
1394 research took place. In this way, studies not conducted in Southern Africa or  
1395 dryland forests were filtered out, which reduced papers from 870 to 599 papers.  
1396 The screening was followed by a full-text assessment that reduced the papers to  
1397 270 by excluding studies that, for example, mentioned the term 'dryland forest'  
1398 once in the abstract but did not investigate dryland forests, as outlined in the  
1399 PRISMA flow diagram in Fig. 3.3. The search was subsequently refined by assigning  
1400 the papers to each of the study aims they addressed and to each category for the  
1401 variables identified in the search protocol, reviewing the methodologies of each  
1402 publication, excluding them from further analysis if they did not meet the inclusion  
1403 criteria on review. These steps reduced the total number of entries to 137  
1404 scientific publications. The selected literature was reviewed systematically,  
1405 searching for specific information regarding the publication temporal

1406 development, study location, remote sensing sensor/platform used, spatial and  
 1407 temporal coverage, remote sensing product (e.g., biophysical indices) used, and  
 1408 application areas of the study (e.g., land cover, forest biomass). The parameters  
 1409 used to extract relevant information from the remaining 137 identified scientific  
 1410 publications are in Table 2.1. Fig. 3.3 is a PRISMA schematic representation of the  
 1411 methodology used and the derivation of the final number of articles selected.



1412

1413 Fig. 2. 3 PRISMA follow diagram (Moher et al., 2009) showing the flow of information  
 1414 through the different phases of the systematic review

1415

1416

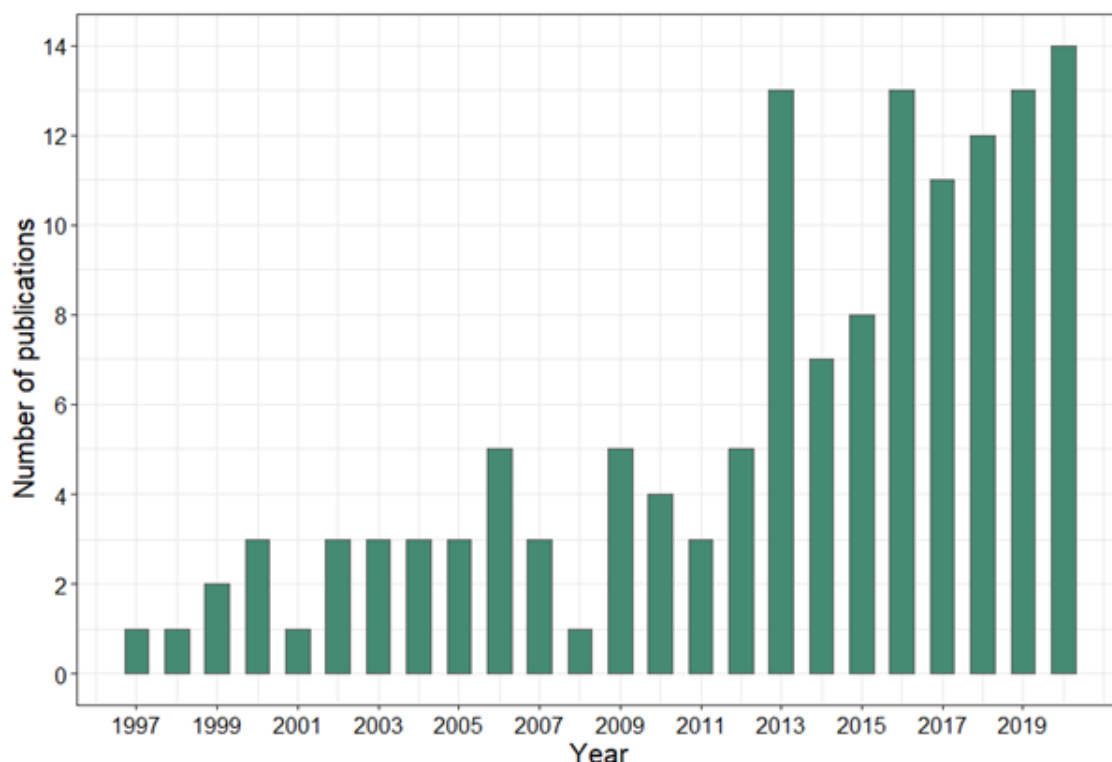
1417 Table 2. 1 Parameters used to extract relevant information for this review

<b>General information</b>
Paper Id
1st author's institution
Research institute city
Publication year
Publishing Journal
Journal category
No of Citation
Study type
<b>Site specific information</b>
Location of the study area
Study country
Forest management area
Predominant forest type
<b>Information on remote sensing data</b>
Sensor Type
Instrument name
Image resolution
Time period observed
Temporal resolution of EO data
Database used
<b>Information on research</b>
Research topic considered: Forest cover/type, disturbance, phenology, biodiversity/habitats, plant traits, land cover/land use
Parameters examined in the study
Examined object scale
Applied methodology
Information on validation and accuracy of results
Database used

## 1418 2.4 Results

### 1419 2.4.1 Temporal development of publications and author 1420 affiliations

1421 From the literature search, the cumulative number of published research papers  
1422 integrating remote sensing data in dryland forests of Southern Africa grew  
1423 exponentially from 2 in 1997 to 155 in 2020. The temporal development of the 137  
1424 investigated research articles is illustrated in Fig. 2.4. The graphic shows that the  
1425 number of studies has increased significantly over the last 23 years, with the  
1426 majority of the studies published from 2013. More than 105 (80%) of articles were  
1427 published from 2009 to 2020 and only 4 (3%) of articles were published before  
1428 2000. The growth in number is also related to the increased availability of remote  
1429 sensing platforms, sensors, data, for example, Landsat 8 in 2013 and Sentinel  
1430 satellite in 2014, respectively.



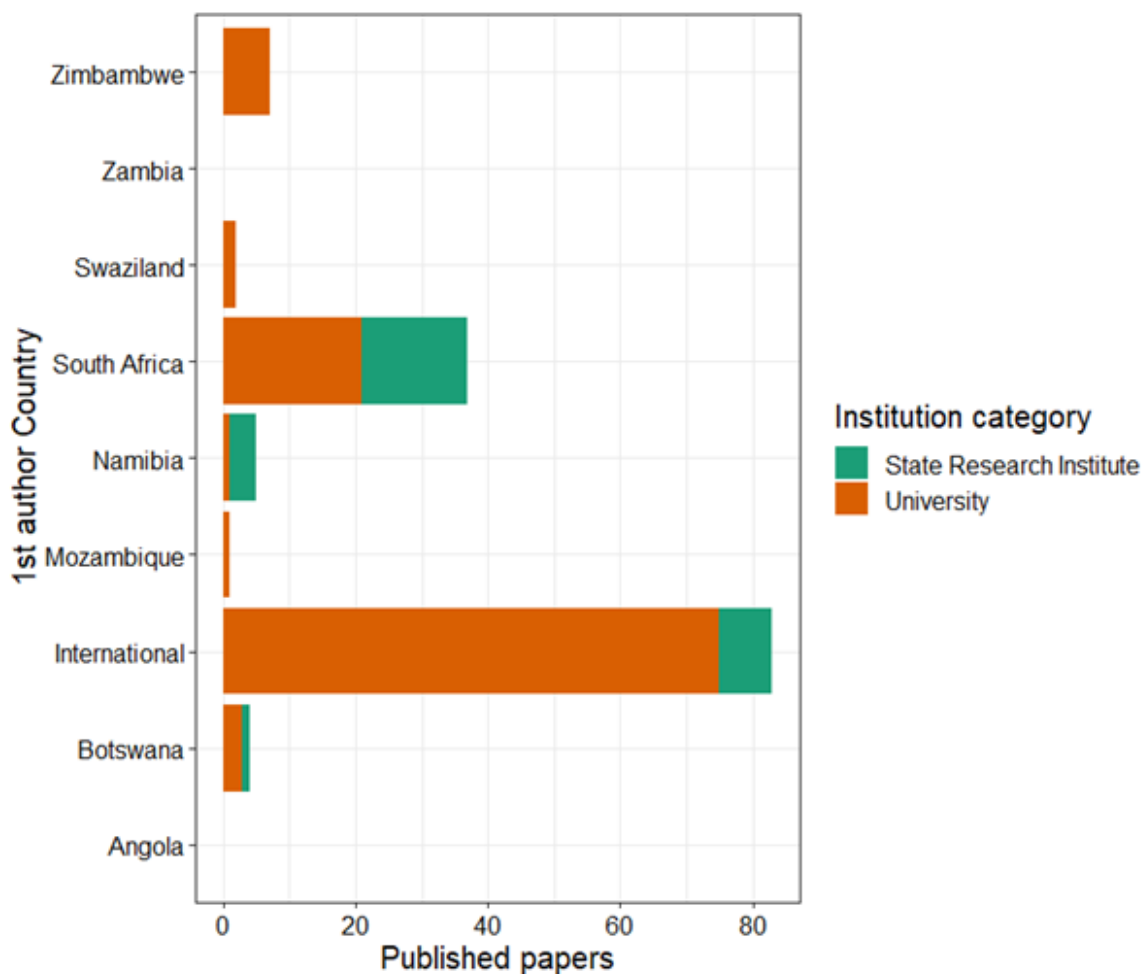
1431

1432 Fig. 2. 4. Number of papers included in the review integrating remote sensing and dryland  
1433 forests in Southern Africa published annually between 1997 and 2020.

1434



1435 In the review, only studies within Southern Africa were considered; however, the  
1436 majority of first authors, 83 (61%) of 137 investigated papers, are mainly  
1437 scientists from international research institutions outside of the focus region,  
1438 mainly the USA, UK, Portugal, Germany, and The Netherlands (Fig. 2.5). Conversely,  
1439 the majority of first author institutions from Africa, 37 (27%) of published papers,  
1440 were from RSA research institutions. The state funded research institutions in  
1441 Southern Africa shown in Fig. 2.5 include South African Council for Scientific and  
1442 Industrial Research (CSIR), South African National Space Agency (SANSA), Water  
1443 Resource Commission of South Africa, South Africa Agricultural Research Council,  
1444 Range and Forage Institute, Botswanan Harry Oppenheimer Okavango Research  
1445 Centre, Desert Research Foundation of Namibia, and Namibia Ministry of  
1446 Environment and Tourism. Considering the 137 studies conducted, about 120  
1447 (90%) of the first authors are affiliated with either International and RSA  
1448 institutions, but no first authors were from Zambia, Lesotho, or Angola.



1449

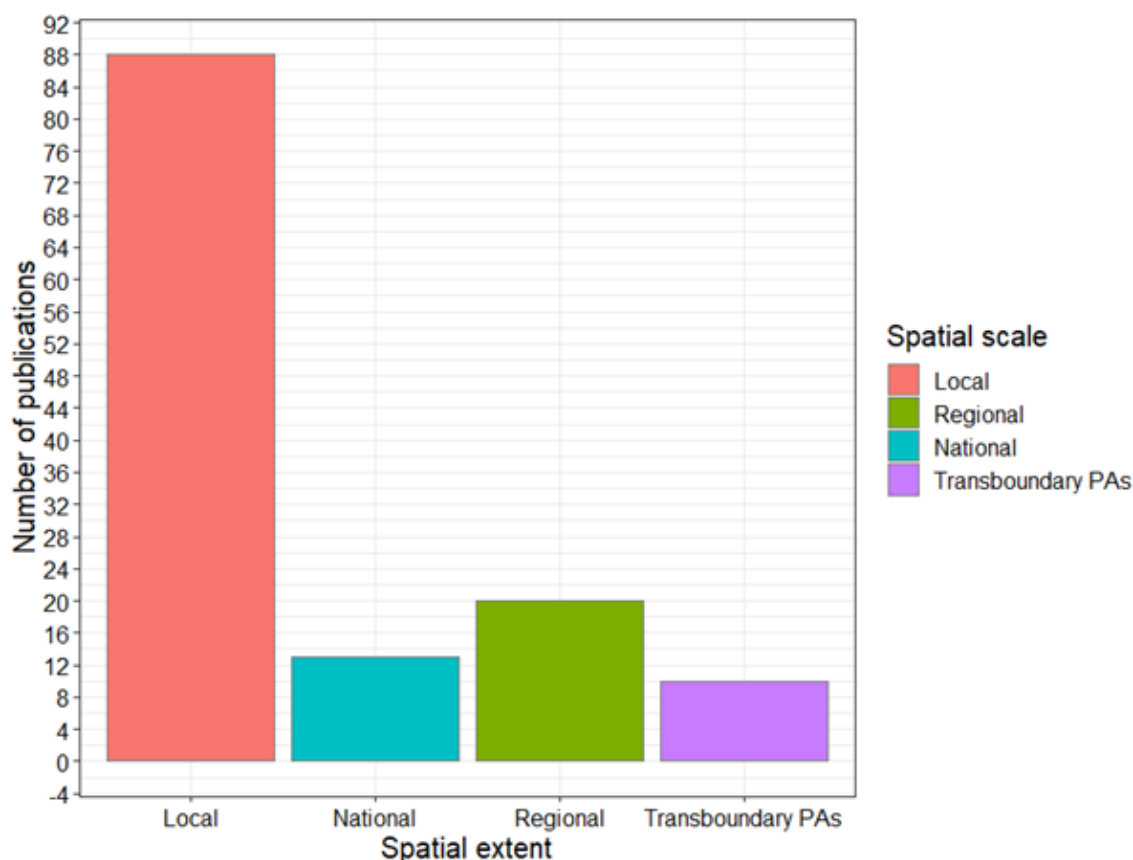
1450 Fig. 2. 5. Number of papers by research institutions.

1451

## 1452 2.4.2 Spatial coverage, spatial extent, and investigated 1453 protected areas

1454 Looking at the spatial scale of the study areas, the research distinguished between  
1455 studies done at a local community level in a single country, termed local scale, and  
1456 studies done at more than one local community or province termed regional scale.  
1457 Also studies done at the national level and the whole of Southern Africa were  
1458 considered. If a study covered more than three countries, it was counted as an  
1459 analysis of Southern Africa. The spatial extent of the studies in the review is shown  
1460 in Fig. 2.6. The majority 88 (64%) of the investigated studies focused on a local  
1461 scale, despite the need for regional scale information on dryland forest  
1462 distribution. From Fig. 2.6, out of 137 investigated research papers, 20 (15%) and

1463 13 (9%) research papers covered regional and national scales, respectively. Only  
 1464 10 (7%) out of 137 research papers dealt with transboundary protected areas,  
 1465 while 6 (4%) of research papers were covering Southern African, considering the  
 1466 region as a whole, using mainly multispectral data of large spatial resolution of  
 1467 1km to 8km (MODIS, SPOT, and AVHRR) to generate information on phenology,  
 1468 and vegetation condition (fire or drought), as shown in Fig. 2.8.



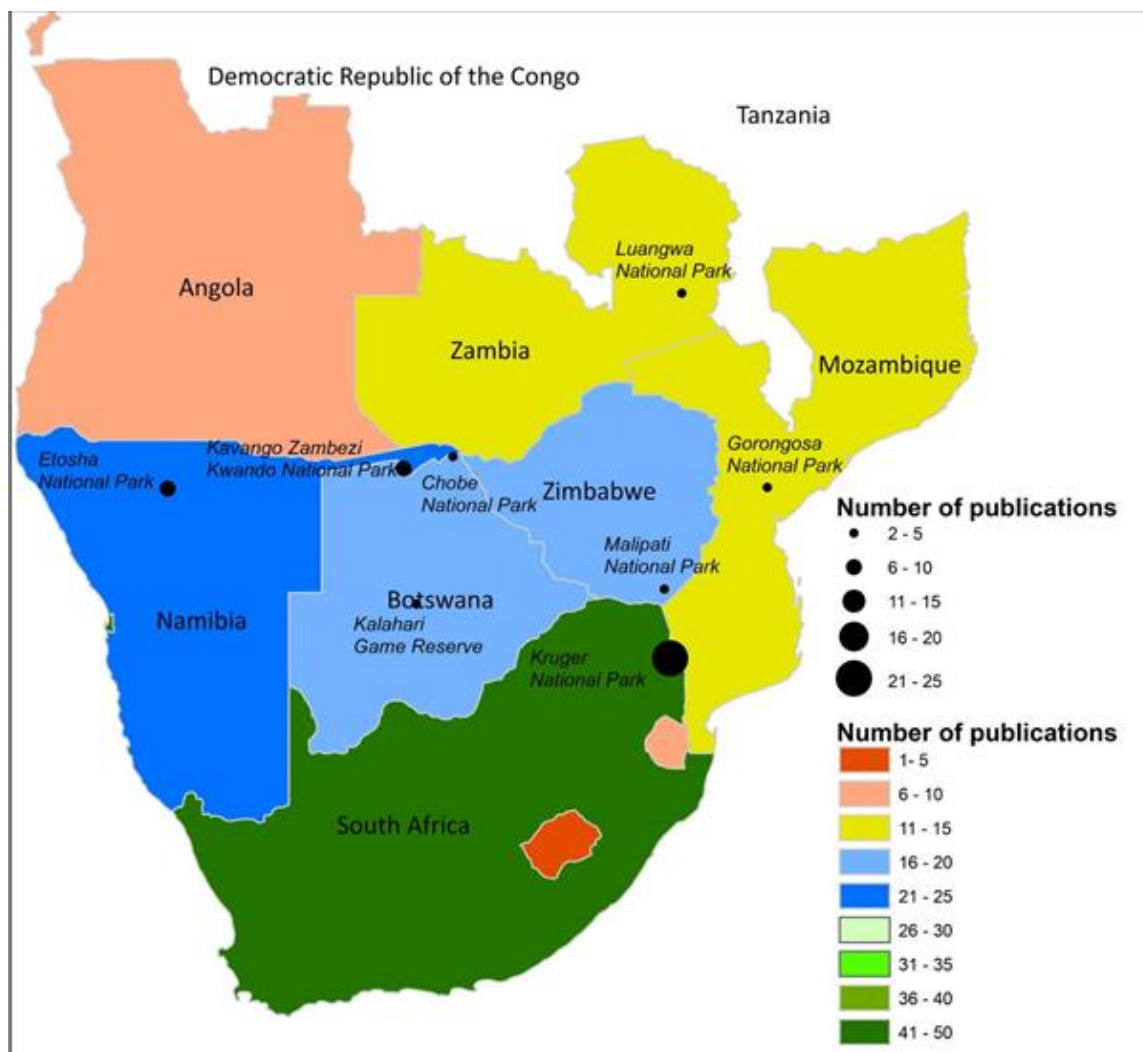
1469

1470 Fig. 2. 6. Spatial extent of investigated studies.

1471

1472 From Fig. 2.7, it is evident that considerable gaps in geographical focus of research  
 1473 on tropical dryland forests mapping still exist in Southern Africa. With respect to  
 1474 spatial coverage of the research, most studies, 50 (36%) of research papers were  
 1475 carried out in RSA, followed by Namibia and Botswana, with 22 (16%) and 18  
 1476 (13%) of research papers, respectively. Swaziland, Angola, and Lesotho were the  
 1477 least frequently investigated, each with < 10 papers. Angolan dryland forests are  
 1478 even less well studied with 4 (6%) of research papers, despite being found

1479 extensively in that country. Fig. 2.7 also shows the location of the most frequently  
1480 studied protected areas. By far, the most studied was the Kruger National Park  
1481 (NP) in RSA, involving research by local and foreign researchers from as far afield  
1482 as the USA, the UK, and beyond. With this interest in the Kruger NP, there is,  
1483 unfortunately, a lack of attention on other conservation areas and parks in  
1484 Southern Africa. Kruger NP was the only subject of more than one-third, 23 (37%)  
1485 of the 61 of all reviewed papers on protected areas. The second most frequently  
1486 studied protected areas are the Etosha NP in Namibia with 6 (8%) of papers,  
1487 Chobe NP with 4 (7%) of papers, and Kwando, Kavango and Zambezi  
1488 transboundary NP with 8 (13%) of papers). Malipati Safari Area, South Luangwa  
1489 NP, Gorongosa NP, and Central Kalahari Game Reserve were each studied 3 (5%)  
1490 and 2 (3%) times.



1491

1492 Fig. 2. 7. Number of studies per country and National Park in Southern Africa. (Note: The  
 1493 data are not scaled to the proportion of dryland forest area of countries, and National  
 1494 Parks with fewer or no publications are not shown. Source: FAO, (1999). Reproduced with  
 1495 permission).

1496 To identify land surface changes and the drivers behind these, as well as short- and  
 1497 long-term trends, it is essential that EO temporal coverage has sufficiently frequent  
 1498 revisit periods and resolutions. Nonetheless, this is not an easy task since the  
 1499 availability of remote sensing data for long-term monitoring is constrained by  
 1500 sensor characteristics (e.g., revisit time) and environmental factors (e.g., cloud  
 1501 cover). Looking at the temporal resolution of the EO datasets used, the research  
 1502 distinguished between data acquired at a single point in time on a monthly basis,  
 1503 termed mono-temporal analyses, and on a single annual basis, termed mono-  
 1504 annual analyses. In addition, multi-temporal and multi-annual to separate monthly

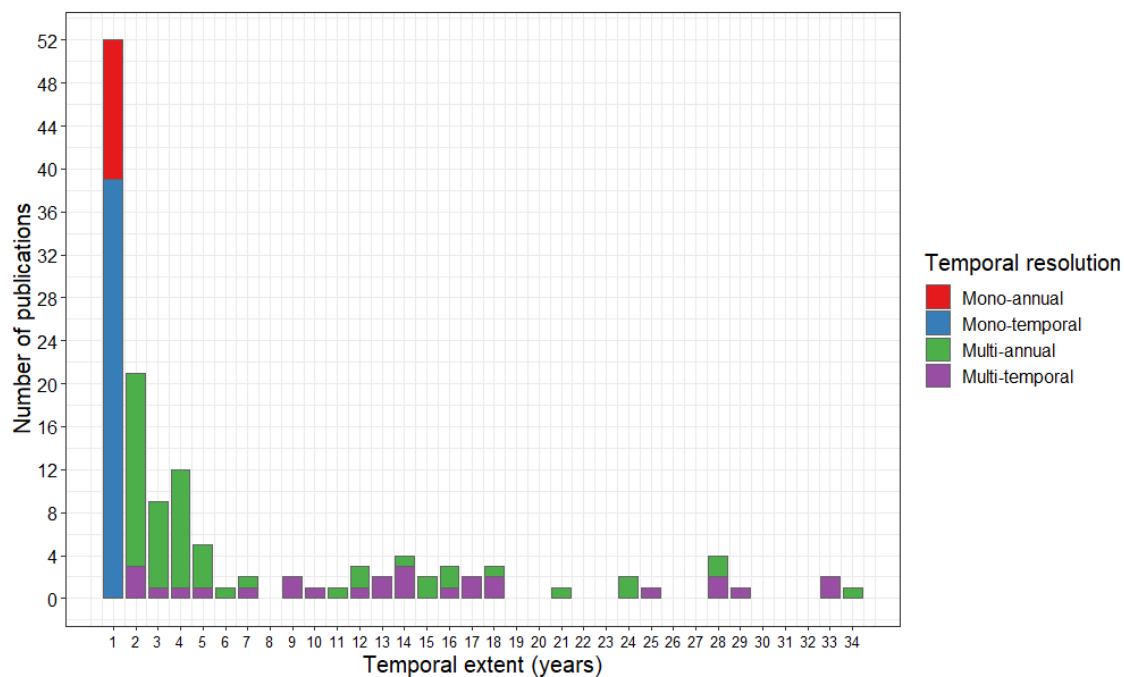
1505 and yearly analyses studies were considered. From Fig. 2.8 it is seen that the  
1506 majority of published material has focused on a single temporal period. The  
1507 majority of studies involved mapping over two or more years (multi-  
1508 temporal/multi-annual) comparing images at two or more different times, with a  
1509 bi-temporal approach based on discrete classification (e.g., Chiteculo et al., 2018;  
1510 Coetzer-Hanack et al., 2016; Matavire et al., 2015). Although the bi-temporal  
1511 approach is mathematically simple and does not require large data storage, it is  
1512 less useful compared to the time series approach that can provide a more  
1513 comprehensive understanding of the complexity of the Earth's land surface  
1514 dynamics. Very few studies feature time series analysis, which is required to  
1515 perform continuous long-term monitoring of changes in a tropical forest  
1516 ecosystem. The majority of articles on time series analysed multi-annual data,  
1517 which masks within-year variations, as compared to the detail provided at a  
1518 monthly temporal scale (e.g., Akinyemi et al., 2019; Venter et al., 2020; Verlinden et  
1519 al., 2006a; Wessels et al., 2006). Only 22 (16%) out of the 137 studies analysed  
1520 more than 15 years and only 11 (8%) studies covered more than 20 years using  
1521 monthly time series (e.g., Bunting et al., 2018; Schultz et al., 2018).

1522

1523

1524

1525



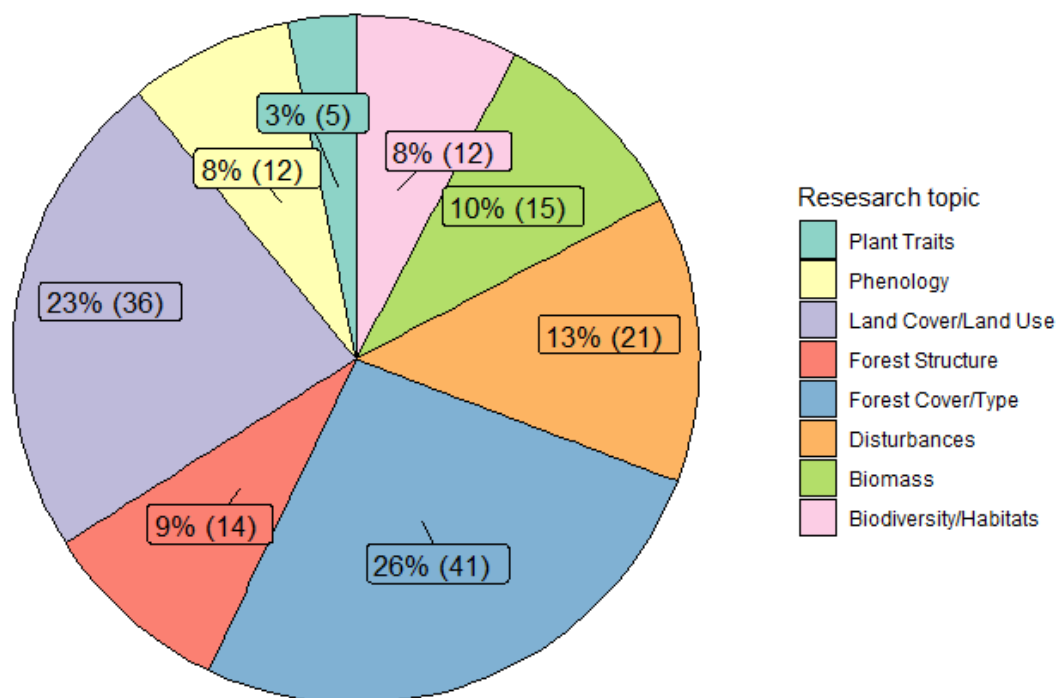
1526

1527 Fig. 2. 8. Temporal duration of studies included in the review integrating remote sensing  
 1528 and dryland forests in Southern Africa between 1997 and 2020.

1529

### 1530 2.4.3 Research topics

1531 The study classified the large number of research topics into eight broad  
 1532 categories that cover the diversity of research into dryland forests. The eight  
 1533 categories, and the number of studies belonging to each of them, are shown in Fig.  
 1534 2.9.



1535

1536 Fig. 2. 9. Research topic categories of reviewed articles between 1997 and 2020. Note that  
 1537 some studies cover different topics, which may result in multiple entries.

1538

### 1539 2.4.3.1 Land cover/land use

1540 Land-cover change is one of the most researched areas using EO in Southern  
 1541 Africa, with 36 (23%) publications making it the second most common topic. Land-  
 1542 use/cover describing land surface classification, typically represented in thematic  
 1543 maps of different dryland vegetation were considered. Land-use/cover changes  
 1544 with a specific focus on other dryland vegetation such as rangelands, grassland,  
 1545 coastal vegetation, or plantation forests without covering dryland forests were  
 1546 excluded. The majority of publications on land-use/land-cover used optical data.  
 1547 For example, Landsat data have been used by more than 90% of publications,  
 1548 except Daskin et al. (2016) and Hüttich et al. (2011) which used RapidEye and  
 1549 MODIS data. Only one publication used a combination of Radar and optical data  
 1550 (Symeonakis et al., 2018). Sentinel data have not been utilised for land cover and  
 1551 land use study in the reviewed papers, probably due to the relatively recent  
 1552 availability of these data. Looking at scale, the majority of papers on land-cover  
 1553 change focused on the local scale in Southern Africa, but there is still a general lack

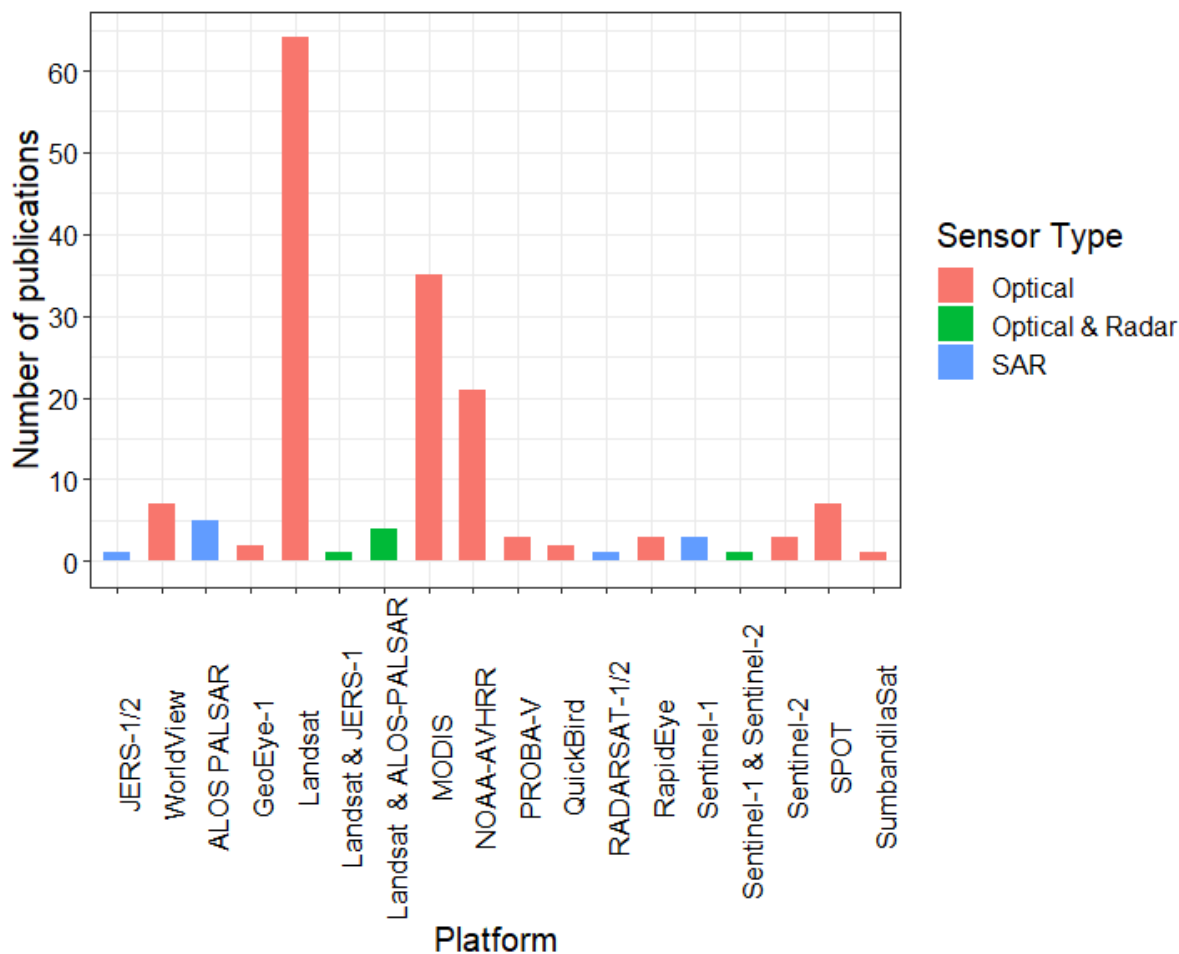


1554 of synthesis of land-use /cover change assessment at the regional, national or  
1555 subcontinental scale (Fig. 2.6).

### 1556 2.4.3.2 Forest cover/type

1557 The majority of publications, 46 (31%) of studies cover the topic “Forest  
1558 cover/type”. The forest cover/type comprises the generation of a forest/non-forest  
1559 mask (Dlamini, 2017; Heckel et al., 2020), forest cover change estimation (Erkkilä  
1560 et al., 1999; Ringrose et al., 2002), forest type discrimination between dryland  
1561 forests (McCarthy et al., 2005), forest health assessment (Herrero et al., 2020),  
1562 woody cover (Boggs, 2010; Ibrahim et al., 2018), and tree species classification  
1563 (Adelabu et al., 2013; Hüttich et al., 2009). The majority of forest type/cover  
1564 mapping was undertaken with optical multi-spectral data including Landsat,  
1565 MODIS, and AVHRR and a few studies used high-resolution data such as RapidEye,  
1566 GeoEye, and WorldView. On the other hand, a few studies on forest cover/type  
1567 mapping used a combination of multispectral and spaceborne SAR data (X-band, C-  
1568 band, and L-band) such as Landsat and JERS-1 (Bucini et al., 2009), Landsat and  
1569 ALOS PALSAR (Higginbottom et al., 2018; Naidoo et al., 2016) and Sentinel-1 and -  
1570 2 (Heckel et al., 2020) (Fig. 2.10).

1571 A few studies on forest cover/type mapping relied on field data (Bucini et al., 2009;  
1572 Ibrahim et al., 2018; Schultz et al., 2018) or forest inventory plots (Heckel et al.,  
1573 2020). Most studies did not include detailed field measurements (species  
1574 composition, density, frequency, dominance, and basal area, percentage soil cover,  
1575 total height) and had very few field samples (Gessner et al., 2013). Other studies  
1576 relied on fine resolution EO data (Dlamini, 2017; Higginbottom et al., 2018), and  
1577 published maps (Westinga et al., 2020) as reference data to validate their results.  
1578 The majority of studies did not perform any form of accuracy assessment or  
1579 validation of quantitative estimates (e.g., Campo-Bescós et al., 2013; Harris et al.,  
1580 2014). Forest cover and species mapping is essential for many forestry-related  
1581 tasks and play a key role in sustainable forest management; the importance of  
1582 these topics can be seen in the fact that they are addressed across all countries in  
1583 Southern Africa, with the majority of studies conducted in RSA, followed by  
1584 Namibia and Botswana (Fig. 2.11).



1585

1586 Fig. 2. 10. Number of studies based upon platform and sensor type. Note that studies  
 1587 investigating forest change with multiple platforms were counted multiple times.

1588

### 1589 2.4.3.3 Forest biomass and structures

1590 Fifteen research papers (10%) studied forest biomass, and fourteen publications  
 1591 (10%) assessed “forest structure”. Studies on biomass included the estimation of  
 1592 AGB (Dube et al., 2018; Mutanga et al., 2006), and changes in carbon stock (Gara et  
 1593 al., 2017). Some of the publications used National Forest Inventory (NFI) data  
 1594 (Halperin et al., 2016; Verbesselt et al., 2007), and field-based samples (Mareya et  
 1595 al., 2018; Tsalyuk et al., 2017) to estimate biomass in Southern Africa.

1596 Forest structure in the review includes research on stand structure (Mathieu et al.,  
 1597 2013), canopy cover (Erkkilä et al., 1999; Huemrich et al., 2005), canopy gaps  
 1598 (Cho et al., 2015), and stand density (Adjorlolo et al., 2013). The majority of studies

1599 on “forest structure” in Southern Africa dealt with canopy cover (e.g., Adjorlolo et  
1600 al., 2014; Yang et al., 2000). Very few studies considered vertical forest structure  
1601 including tree height and tree crown diameter (e.g., Verlinden et al., 2006b).  
1602 Mareya et al. (2018) utilised freely available fine resolution Google satellite  
1603 imagery in combination with object-based image analysis (OBIA) to estimate tree  
1604 crown areas in miombo forests and found the overall accuracy to be low and  
1605 unsuitable when high accuracy is required. Some of the “forest structure”  
1606 publications are also assigned to the research topic “biomass”, which discusses the  
1607 relevance of forest structure for biomass (Meyer et al., 2014). Forest structure is  
1608 also a very important parameter when it comes to habitat suitability, species  
1609 diversity, biodiversity estimation, and conservation studies and thus some  
1610 publications cover both topics (e.g., Akinyemi et al., 2019).

1611 The methods applied in the biomass and forest structure publications are diverse.  
1612 Most studies employed some sort of regression analysis between in-situ field data  
1613 and EO data, with the most popular methods being random forests, support vector  
1614 machines, kriging, linear and generalised linear models (Berger et al., 2019;  
1615 Carreiras et al., 2013; Halperin et al., 2016; Mutanga et al., 2006; Wingate et al.,  
1616 2018). Williams et al. (2013) utilised the simple ensemble model to analyse  
1617 biomass dynamics and found that biomass distributions can diagnose disturbance  
1618 processes in miombo woodlands. Most studies utilised the normalised difference  
1619 vegetation index (NDVI) in dryland forest mapping to correlate with biomass  
1620 (Gizachew et al., 2016; Wessels et al., 2006), but very few studies considered other  
1621 vegetation indices such as red-edge (RE)-computed indices (e.g., Dube et al., 2018;  
1622 Gara et al., 2016). For the most part, optical sensors were used to derive forest  
1623 biomass and structures, only four papers utilised radar data, and one paper used a  
1624 combination of radar and optical data to estimate biomass (Wingate et al., 2018).  
1625 More research is needed to explore the improvement of forest AGB and forest  
1626 structure estimation through multi-sensor (optical and radar) data fusion.

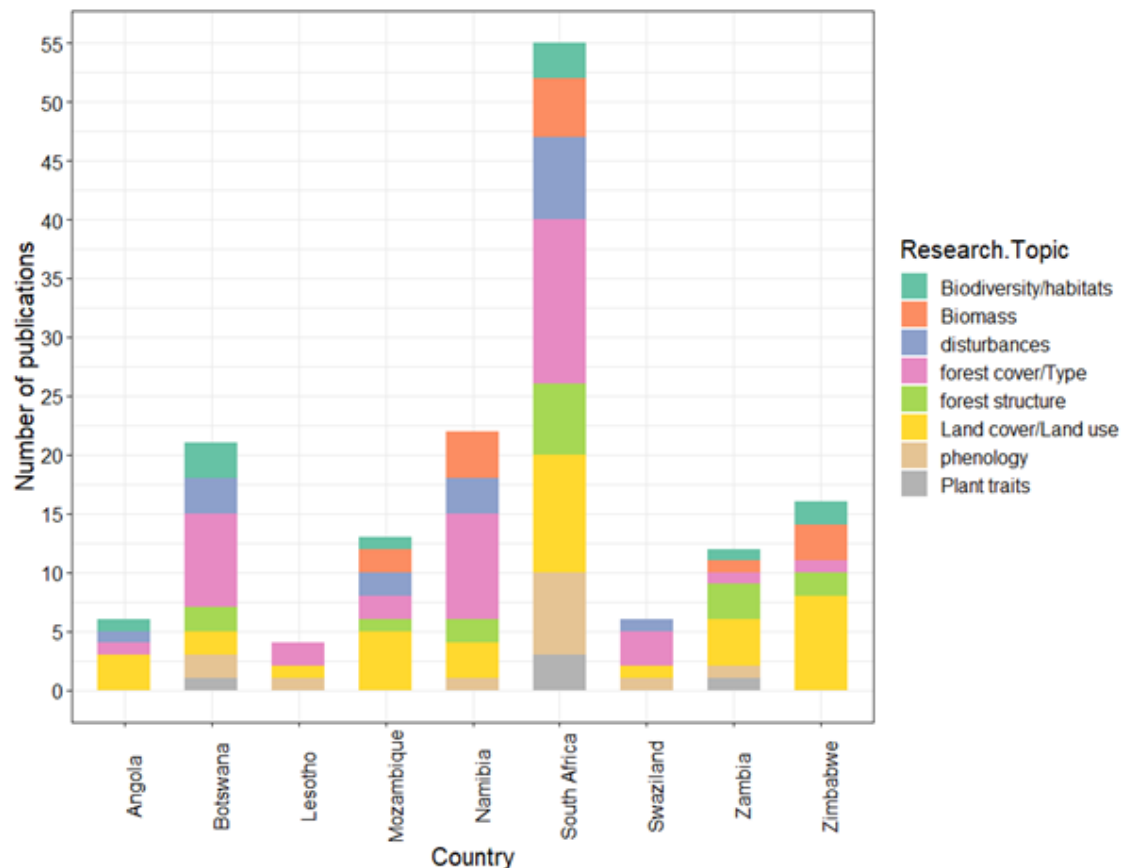
#### 1627 2.4.3.4 Climate change and disturbances

1628 Here the study refer to dryland forests stress monitoring e.g., damage due to fire,  
1629 climate/weather-related hazards including drought events, floods, extreme

1630 temperatures as part of climate change and disturbances. Twenty-one papers  
1631 (13%) investigated disturbances to forest cover. Among the different forms of  
1632 disturbance, fire damage was the most commonly studied (Mayr et al., 2018;  
1633 Pricope et al., 2012; Roy et al., 2019; Silva et al., 2003). In the context of threats of  
1634 climate change, other disturbances included drought (Lawal et al., 2019;  
1635 Marumbwa et al., 2021; Urban et al., 2018) and floods (Pricope et al., 2015). A  
1636 regional studies Lawal et al. (2019) used gridded climate data from the Climate  
1637 Research Unit and GMMS NDVI to characterise the impact of drought to vegetation  
1638 in southern Africa from 1981 to 2005; They found that the responses of vegetation  
1639 varied according to season and biome, and showed that droughts had extensive  
1640 impacts over the central parts of South Africa and Namibia, and the southern  
1641 border of Botswana and the western parts of Zambia. In this review, only studies  
1642 that investigated climate change in terms of temperature/drought in dryland  
1643 forests where satellite data are a primary or secondary source of data were  
1644 considered. Although there are a number of studies on climate change modelling in  
1645 Southern Africa, the results show that there is a striking lack of studies  
1646 investigating climate change into dryland forest change and stress monitoring.

1647 The sensors used to detect disturbances differs, with most studies using MODIS  
1648 (Alleaume et al., 2005; Archibald et al., 2009; Chongo et al., 2007; Giglio et al.,  
1649 2009), two publications used SPOT-VGT (Silva et al., 2003; Verbesselt et al., 2006),  
1650 and one Landsat and Sentinel-2 (Roy et al., 2019). Only two publications utilised  
1651 SAR data. Mathieu et al. (2019) investigated SAR Sentinel-1A C-band images for  
1652 detecting surface fires in the Kruger NP, while Williams et al. (2013) used ALOS  
1653 PALSAR to analyse known disturbance agents in tropical woodlands in  
1654 Mozambique. The research by Urban et al. (2018) used Sentinel-1 SAR time series  
1655 NDVI from Sentinel-2 and Landsat-8 to derive surface moisture for drought  
1656 monitoring in the Kruger NP between 2015 and 2017. A combination/fusion of  
1657 SAR and Optical data for detecting disturbances is not tested by any study. Only  
1658 one study used field data as input data for validation (Alleaume et al., 2005), while  
1659 two studies used forest inventory data (Verbesselt et al., 2006; Verlinden et al.,  
1660 2006a).

## 1661 2.4.3.5 Biodiversity, plant traits, and phenology



1662

1663 Fig. 2. 11. Research topic by country. Note that the order of the mentioned topics has  
 1664 changed when compared to Fig. 2.9 as some studies were conducted in several countries.

1665

1666 Twelve (8%) of the reviewed publications dealt with research questions in the  
 1667 context of forest biodiversity. Almost half of the papers on forest biodiversity  
 1668 examined plant species diversity (Adjorlolo et al., 2014; Chapungu et al., 2020;  
 1669 Mapfumo et al., 2016). Others looked at animal species and habitat suitability (e.g.,  
 1670 Cáceres et al. (2015) for birds, Ducheyne et al. (2009) for tsetse flies, impala (Van  
 1671 Bommel et al., 2006), and elephants (Marston et al., 2020). Forest biodiversity is  
 1672 often related to structural canopy parameters. Most studies, nine (75%) of twelve  
 1673 used Landsat to derive parameters such as plant canopy height, species  
 1674 occurrence, richness, and diversity. Three (25%) of the studies used MODIS data  
 1675 (e.g., Fullman et al. (2014) used MODIS at 250 m pixel resolution and a Moving  
 1676 Standard Deviation Index (MSDI) to detect elephant-modified vegetation along the  
 1677 Chobe riverfront in Botswana; Akinyemi et al. (2019) utilised 1 km spatial

1678 resolution of SPOT - VGT and PROBA-V annual time series of 18 years to  
1679 understand species diversity and richness assessment based on the Vegetation  
1680 Degradation Index in Palapye Botswana.; Adjorlolo et al. (2014) investigated the  
1681 utility of SPOT-5 multispectral data to assess tree equivalents and total leaf mass to  
1682 model grazing and browsing capacity in KwaZul-Natal province in RSA.

1683 Five papers (3%) dealt with different plant characteristics, known as plant  
1684 functional traits. These include canopy chlorophyll content (Cho et al., 2012), leaf  
1685 nitrogen concentration (Cho et al., 2013), and vegetation water content (Verbesselt  
1686 et al., 2006), and Leaf Area Index (LAI) (Scholes et al., 2004). Plant functional traits  
1687 including vegetation biophysical and biochemical properties (e.g., pigment levels,  
1688 nitrogen content) are often related to patterns of biodiversity. Huemmrich et al.  
1689 (2005) explored monthly MODIS data at 1 km spatial resolution over two years to  
1690 estimate LAI and the fraction of absorbed photosynthetically active radiation  
1691 (FAPAR) and found that ground-measured LAI values correspond well with MODIS  
1692 LAI, and showed a discrepancy with FAPAR. Cho et al. (2012) utilised variogram  
1693 analysis and the red edge shift from SumbandilaSat and SPOT 5 to estimate canopy  
1694 chlorophyll content in Dukuduku forest in Southern Africa and found that  
1695 SumbandilaSat provides additional information for quantifying stress in vegetation  
1696 as compared to SPOT image data. All studies on plant traits were undertaken at the  
1697 local scale.

1698 Looking at research categories per country, biodiversity/habitat publications were  
1699 mainly undertaken in Botswana and RSA (Fig. 2.11). All studies in the context of  
1700 forest biodiversity and plant traits covered only mono-temporal and multi-annual  
1701 classifications. Only two studies utilised multi-annual time series (Akinyemi et al.,  
1702 2019; Verbesselt et al., 2006), and one study used MODIS multi-temporal time  
1703 series over two years (Huemmrich et al., 2005). All of these studies focused on a  
1704 coarse resolution of 1 km.

1705 Phenology is also strongly linked to plant traits, but analysis puts more emphasis  
1706 on the seasonal variations including growing season (green-up date) (Archibald et  
1707 al., 2007; Whitecross et al., 2017), end of the season, and length of the season  
1708 (Davis et al., 2017). To date, phenological research in Southern African dryland  
1709 forests is limited, and more than half of the published papers on phenology focused

1710 only on examples from RSA. In the few studies that have analysed phenology, most  
1711 studies dealt with estimating leaf flush and early-greening dates (Chidumayo,  
1712 2001; Higgins et al., 2011). For example, Archibald et al. (2007) developed an  
1713 intricate algorithm that used MODIS NDVI products and field-based parameter  
1714 estimates to predict green-up dates for grass and tree components at a site in the  
1715 Kruger NP in RSA. Jolly et al. (2004) compared a water balance model to a 3-year  
1716 NDVI time series and found the deviation between the onset of leaf flush predicted  
1717 by the model and empirical data was between 10 and 40 days.

## 1718 2.5 Discussion

### 1719 2.5.1 Temporal extent

1720 In this article, the current research with EO on dryland forests, with a particular  
1721 focus on Southern Africa were synthesised. Although the volume of scientific  
1722 literature has demonstrated a sharp increase, the use of remote sensing is still  
1723 limited, and up until 2013, the number of publications on this topic was relatively  
1724 small. Substantial research on the dryland forests of Southern African is mainly  
1725 based on single-date observations, and comparing classified images at two or more  
1726 different times. Maps that relate successive land cover change between two dates  
1727 typically lack information regarding underlying processes and do not enable  
1728 insights on the nature of the transformations present, such as the rate or  
1729 persistence of change (Lambin et al., 2003). Time series analysis on dryland  
1730 forests, which enables tracking changes is scarce, only 22 (16%) out of 137 studies  
1731 feature time series lengths that exceed 15 years and only 11 (8%) studies that  
1732 cover more than 20 years. Longer time series of remote sensing data afford the  
1733 ability to assess the dynamics of forest structures, biodiversity, degradation,  
1734 disturbance from climatic extremes, and change in phenology, in which a gap still  
1735 exists.

### 1736 2.5.2 Spatial scale

1737 Another finding that stands out from the analyses is that there are very few studies  
1738 at the national and regional levels. Despite new sensor and EO data availability, it

1739 is clear that a systematic and consistent regional monitoring of dryland forests is  
1740 not yet fully exploited and is still in its infancy in Southern Africa. In fact, the  
1741 majority of publications 88 (64%) concentrated their research efforts on local  
1742 scale investigations (Fig. 2.6). Desanker et al. (2001) and Geist (2002) also  
1743 emphasised that Southern Africa is limited to local-scale studies, thereby lacking a  
1744 simultaneous analysis of the impacts of these changes at a larger scale. To fully  
1745 assess regional and long-term implications for tropical dryland forest change  
1746 studies, analyses on large(r) scales are needed, ideally with higher spatial  
1747 resolutions and longer temporal duration.

### 1748 2.5.3 Accuracy assessment

1749 Through evaluation of the literature, the review identified that the assessment of  
1750 accuracy for thematic/classified maps and statistical data to be another important  
1751 issue, with only 54 (39%) of the studies appearing to have performed some form of  
1752 accuracy assessment. The results show there is limited information on sources of  
1753 error and uncertainty levels of the estimates provided by most studies. The review  
1754 found that most forest and vegetation-related scientific outputs in Southern Africa  
1755 are not yet strongly linked to field measurements and forest inventory data.  
1756 Among the reviewed studies, very few studies utilised field test sites/ ground-  
1757 based independent datasets for accuracy assessment, while other studies  
1758 estimated uncertainties using other procedures e.g., using a sample of finer spatial  
1759 resolution remote sensing data, or did not report the map uncertainty. Some  
1760 studies employed root-mean-square error to assess model accuracy (RMSE) (e.g.,  
1761 Adjorlolo and Mutanga, 2013; Higginbottom et al., 2018), while many studies used  
1762 an error matrix to assess map uncertainties, which was employed for instance (e.g.,  
1763 Adelabu et al., 2013; Hüttich et al., 2011). However, some studies used sample  
1764 points below the desirable target number of validation points per class (e.g., Cabral  
1765 et al., 2011), while studies briefly mentioned that a confusion matrix was  
1766 calculated but did not report how many sample points were used for validation  
1767 (e.g., Chagumaira et al., 2016). Congalton. (1988) suggests planning to collect a  
1768 minimum of 50 samples for each map class for maps of less than 1 million acres in  
1769 size with less than 12 classes. It has been empirically confirmed that a good  
1770 balance between statistical validity and practicality for larger area maps or more



1771 complex maps can be achieved with about 75 to 100 sample sites per class  
1772 (Congalton & Green, 2009).

1773 Globally, owing to TDFs low commercial importance in comparison to other  
1774 tropical forests such as moist forest, they are often not assessed by field surveys, or  
1775 surveyed regularly by governments (Keenan et al., 2015). Independent validation  
1776 data for dryland forest estimations are rarely available because acquiring  
1777 appropriate field survey data is a time-consuming and expensive task. In Southern  
1778 Africa, these areas are often remote and dangerous to visit in the field, due to the  
1779 hazard posed by wildlife and if present, unexploded landmines, almost  
1780 impracticable to obtain independent validation data for large(r) area studies,  
1781 especially for many protected areas. Despite challenges to obtain ground-based  
1782 observation, effective integration of these data and remote sensing methods will be  
1783 key to accurately mapping and monitoring dryland forest across a range of spatial  
1784 scales and in reporting the accuracy of models. However, the applicability of  
1785 remotely measured geospatial data is reliant on quality and translating remote  
1786 sensing data into accurate and meaningful information is often a challenge prone  
1787 to errors (Congalton et al., 2009; Donoghue, 2002). In this context, it is critical to  
1788 ensure the validity of these data and their suitability for each particular  
1789 application, particularly where coarse spatial maps can be misleading. In addition,  
1790 characterising dryland forest for large areas of Africa cannot entirely rely on global  
1791 and pantropical monitoring studies for dry forest estimation because global forest  
1792 monitoring generally underestimates, and in some instances overestimates,  
1793 dryland biomes (Bastin et al., 2017).

#### 1794 2.5.4 Research topics and geographical focus

1795 The classification of studies into eight broad subject categories revealed forest  
1796 cover/types 41 (26%) and land cover/land use 36 (23%) to be the most commonly  
1797 researched topics. Topics receiving less attention included phenology, plant traits,  
1798 and biodiversity/habitats, and disturbances with regards to climate change (Fig.  
1799 2.9). With regards to disturbances, fire damage was the most commonly studied  
1800 but there is a missing body of literature on the climate change impact on the  
1801 composition, biodiversity, and ecological health of dry forest ecosystems in most

1802 countries of Southern Africa. The thesis also found an interesting, non-uniform  
1803 spatial distribution of dryland vegetation and forest studies using spaceborne  
1804 remote sensing, particularly when considering disparities among countries and  
1805 across protected areas. The distribution of research categories by country reveals  
1806 that RSA is, by far the most studied nation across all categories in Southern Africa  
1807 (Fig. 2.7). It should be noted that care should be taken here not to assume that the  
1808 number of studies equates to research quality, which remains difficult to articulate  
1809 from a review of this nature. However, the dryland forests of Mozambique,  
1810 Lesotho, Swaziland, and Zambia are noticeably very poorly studied. Studies on the  
1811 dryland forests of Angola are even less frequent, receiving relatively little global  
1812 attention, and the few studies conducted on its forests were mostly conducted by  
1813 researchers from Portuguese Universities (Catarino et al., 2020; Leite et al., 2018).  
1814 The focus of publications tended to be biased towards conservation and national  
1815 parks, particularly as a large proportion of studies were undertaken in the Kruger  
1816 NP, leaving many other private and international protected areas relatively  
1817 understudied. Transboundary conservation areas, such as Kavango-Zambezi  
1818 (KAZA), have received relatively little attention but merit further research in terms  
1819 of the vast dryland forests extent, biodiversity, species abundance and diversity,  
1820 and the potential for this area to form important corridor areas for wildlife  
1821 animals. There is a further concern as a result of such gaps because some of the  
1822 dryland forests, and species to which they are home, notably in countries like  
1823 Angola and Zambia, are listed on the IUCN red list and would almost certainly  
1824 merit Alliance for Zero Extinction (AZE) ranking (Cumming, 2008). Furthermore,  
1825 future efforts to estimate important variables such as forest cover and biomass  
1826 need not be restricted by country boundaries. Future studies, based on medium-  
1827 fine resolution EO and validated with field data, will provide information to  
1828 improve the understanding of African dryland vegetation and its management.

### 1829           2.5.5 Vegetation indices, optical, SAR, and fusion of optical 1830 and SAR sensors

1831 The most commonly used vegetation index was the NDVI, with more than half of  
1832 the studies, 84 (54%) of papers utilising this index, but only 13 (8%) of papers  
1833 used Enhanced Vegetation Index (EVI) and soil-adjusted vegetation index (SAVI).

1834 Other vegetation indices such as the Green Normalised Difference Vegetation Index  
1835 (GNDVI) and Sentinel red-edge related indices and passive microwave  
1836 observations such as Vegetation Optical Depth were not utilised in studies  
1837 considered in this review. One major problem commonly encountered in the less  
1838 studied ecosystems, such as dryland forests, is that of generalising or transferring  
1839 knowledge and methods derived from remotely sensed imagery over both space  
1840 and time (Foody et al., 2003). For example, commonly used vegetation indices and  
1841 classification schemes are in general mainly been calibrated on other, better-  
1842 studied ecosystems, such as temperate or rain forests, and this has led to poor  
1843 accuracy results when extrapolated, to for example, tropical dryland forests. This  
1844 phenomenon justifies the importance of utilising a range of vegetation indices  
1845 when studying dryland forests using EO data. Imagery from optical sensors is most  
1846 commonly used, out of all sensor types, providing the data used in 90% of papers  
1847 reviewed, followed by SAR data with 6%. The fusion of optical and radar data was  
1848 rarely used, with only 4% of publications exploring this. The most frequently used  
1849 platforms are Landsat, followed by MODIS and AVHRR. Imagery taken by the  
1850 Sentinel-1/2 satellites only makes up a small portion of the remote sensing data on  
1851 dryland forests. For example, Sentinel-2 was only used by 2% of investigated  
1852 studies, but this may reflect the relatively short period (since 2015) when these  
1853 data have been available.

## 1854 2.5.6 Remote sensing platforms and cloud-based computing

1855 Most of the EO data used in the publications reviewed were downloaded, and are  
1856 available at no cost from a number of online portals, including the Oak Ridge  
1857 National Laboratory (ORNL), the United States Geological Survey (USGS)  
1858 Distributed Active Archive System (DAAC) and Earth Explorer (EE) tool. The lack  
1859 of remote sensing research centres in most Southern African research institutions  
1860 may contribute to limit the number of African Scientists engaged in monitoring  
1861 forests resources. For example, most studies in RSA made use of remote sensing  
1862 data through the University of the Witwatersrand, Satellite Application Centre  
1863 (SAC), the South African National Space Agency (SANSA), and the Council of  
1864 Science and Industrial Research (CSIR). The development of remote sensing  
1865 capacity at local universities has inevitably contributed to RSA universities and

1866 research institutions conducting the majority of studies in Southern Africa (Fig.  
1867 2.5). To improve EO data access, and the skills to handle and interpret this across  
1868 Southern Africa, there is a need to increase the number of local institutions that  
1869 distribute the remote sensing data, and who have the capacity to access and use  
1870 innovative web-based platforms such as the Google Earth Engine (GEE) and  
1871 Amazon Web Services to overcome some of the logistical and financial constraints  
1872 of this type of research.

1873 Southern African countries face considerable technical challenges with remote  
1874 sensing, particularly in respect to REDD+-related research on dryland forests  
1875 monitoring. Freely available tools, for example, the cloud-based geospatial analysis  
1876 platform Google Earth Engine (GEE), make it easier to access powerful computing  
1877 resources for processing and analysing pre-processed large-scale datasets  
1878 (Shelestov et al., 2017). However, only nine papers (6%) out of 137 used GEE to  
1879 access or analyse remote sensing data. The “near real-time” remote sensing data  
1880 offered by GEE is of particular interest for monitoring changes and automating the  
1881 analysis of time-series, when detecting and tracking trends in surface reflectance  
1882 properties. With increasing spatio-temporal coverage of satellite data and  
1883 computational platforms that reduce the need for costly local infrastructure (e.g.,  
1884 GEE), there is an opportunity to overcome the limitations previously enforced by  
1885 large volumes of data and the scale of analysis, whereby the knowledge of dryland  
1886 forest dynamics can be improved in the upcoming years.

## 1887 2.6 Conclusion

1888 This review summarises research progress towards the use and integration of  
1889 remote sensing data within the context of monitoring dryland forests in Southern  
1890 Africa, using a systematic review methodology that focused on 137 most relevant  
1891 research articles. The study has systematically reviewed the temporal and spatial  
1892 coverage of these studies, their application area, and the remote sensing platforms  
1893 and sensors used. Based on the results, the following conclusions can be drawn.  
1894 There is a broad range of topics covered by research on dryland forests, from  
1895 which land-use/land-cover and forest cover and disturbances from the fire were  
1896 the most frequently studied. However, there is still a relative lack of studies

1897 assessing dryland forest structure, phenology, biodiversity/habitats, plant traits,  
1898 and disturbance from climatic extremes, suggesting additional research is  
1899 required. The majority of studies relied on single-date or annual data and bi-  
1900 temporal discrete classification; only a very few studies employed time series  
1901 analysis.

1902 The thesis considers some of the limitations of the research reviewed, which  
1903 indicates a need for more frequent use of field and inventory data, a greater use of  
1904 validation/accuracy assessments, and testing other vegetation indices beyond  
1905 NDVI and EVI such as the Vegetation Optical Depth and Sentinel-2 red-edge related  
1906 indices. In addition, further improvements should focus on for extensive  
1907 combination and fusion of SAR and optical data in order to have a temporally and  
1908 spatially consistent data set necessary for several applications in dryland forests.  
1909 Given the state of decline of woody vegetation condition in Southern Africa, long-  
1910 term monitoring of monthly time series of EO data at regional and transboundary  
1911 scale clearly hold potential to capture dryland forests dynamics and to understand  
1912 their current status and future trends. A significant move from EO predictions that  
1913 are extremely site-dependent to large(r) ecoregional level monitoring approach  
1914 that integrates a range of remotely-sensed data of sufficiently fine spatial and  
1915 temporal resolution with field measurements and using machine/deep learning  
1916 models could provide a sound basis for assessing dryland forest-related changes  
1917 and dynamics. Information inferred from these kinds of models would be  
1918 extremely useful for the current knowledge, management and conservation of the  
1919 dryland forests as well as for understanding their responses to disturbance  
1920 (natural or anthropogenic) and climatic change at regional to sub-continental level.  
1921 Finally, there is significant geographical heterogeneity in study coverage; whilst  
1922 there is substantial research on the forests in the Kruger NP and across RSA, the  
1923 same cannot be said for other areas of Southern Africa. The EO interventions not  
1924 only assess deforestation rate, but also support other forest related REDD+  
1925 activities such as sustainable forest management which reduce forest degradation  
1926 and enhance forest carbon stocks at a range of scales, transcending both provincial  
1927 and national boundaries e.g., Kavango-Zambezi Transfrontier Conservation Area  
1928 (KAZA TFCA). Nevertheless, REDD+-related research on dryland forests in most  
1929 Southern African countries and protected areas has been limited, with clear gaps

1930 across Angola, Mozambique, Zambia, and Zimbabwe. Finally, Africa has the  
1931 potential to emulate other continents, such as Latin America, that have made  
1932 notable progress in employing freely available remote sensing data to monitor  
1933 tropical dryland forest area change and biomass on a large scale.

## 1934 2.7 Acknowledgments

1935 This work was supported by the Commonwealth Scholarship Commission Ph.D  
1936 grant number: NACS-2017-409 from 2017–2020, Geography doctoral program at  
1937 Durham University. The authors would like to acknowledge the support provided  
1938 through the Rapid Evidence Synthesis Training (REST) programme. REST was  
1939 organised and delivered through a collaboration between the University of Leeds,  
1940 The University of Newcastle, and the N8 AgriFood Programme and supported by  
1941 Research England QR-SPF funds from The University of Leeds and University of  
1942 York.

1943

1944 **3 IMPROVING ABOVE GROUND BIOMASS ESTIMATES OF**  
1945 **SOUTHERN AFRICA DRYLAND FORESTS BY**  
1946 **COMBINING SENTINEL-1 SAR AND SENTINEL-2**  
1947 **MULTISPECTRAL IMAGERY.**

---

1948

1949

1950

1951

1952

1953

1954

1955

1956

1957

1958

1959

1960

1961

1962

1963

1964

1965 Chapter 3 is published in *Remote Sensing of Environment*: DOI:

1966 <https://doi.org/10.1016/j.rse.2022.113232>

1967

1968 **Title:** Improving above ground biomass estimates of Southern Africa dryland  
1969 forests by combining Sentinel-1 SAR and Sentinel-2 multispectral imagery.

1970

1971

1972 Authors: Ruusa M. David, Daniel N.M. Donoghue, Nick J. Rosser

1973

1974

1975 Department of Geography, Durham University, Science Laboratories, DH1 3LE  
1976 Durham, UK

1977

1978

1979

1980 **Author Contribution**

1981

1982 David Ruusa- Design the research, perform the data analysis, interpret the results,  
1983 wrote the manuscript, and revised the manuscript. Nick Rosser- Contributed to the  
1984 research design, manuscript editing and supervision. Daniel Donoghue-  
1985 Contributed to the research design, conducting fieldwork, manuscript editing and  
1986 supervision.

1987

1988

1989

1990

1991

1992

1993

1994

1995

1996



1997 **Abstract**

1998 Having the ability to make accurate assessments of above ground biomass (AGB) at  
1999 fine spatial resolution is invaluable for the management of dryland forest  
2000 resources in areas at risk from deforestation, forest degradation pressure and  
2001 climate change impacts. This study reports on the use of satellite-based synthetic-  
2002 aperture radar (SAR) and multispectral imagery for estimating AGB by correlating  
2003 satellite observations with ground truth data collected on forest stands from  
2004 dryland forests in the Chobe National Park, Botswana. The study undertooks  
2005 nineteen quantitative experiments with Sentinel-1 (S1), Sentinel-2 (S2) and  
2006 Landsat 8 OLI (LC8) and tested simple and multivariate regression including  
2007 parametric (linear) and non-parametric (random forests) algorithms, to explore  
2008 the optimal approaches for AGB estimation. The largest AGB value of 145 Mg/ha  
2009 was found in northern Chobe while a large part of the study area (85%) is  
2010 characterised by low AGB values ( $< 80$  Mg/ha), with an average estimated at 51  
2011 Mg/ha. The results show that the AGB estimated using SAR backscatter values  
2012 from vertical transmit receive (VV) polarisation is more accurate than that based  
2013 on horizontal receive (VH) polarisation, accounting for 58% of the variance  
2014 compared to 32%. Nevertheless, the combination of S1 SAR and S2 multispectral  
2015 image data produced the best fit to the ground observations for dryland forests  
2016 explaining 83% of the variance with an accuracy of 89%. Furthermore, the optimal  
2017 AGB model performance was achieved with a multivariate random forest (MRF)  
2018 regression trees algorithm using S1 (SAR) and S2 (multispectral) image data ( $R^2 =$   
2019  $0.95$ ;  $RMSE = 0.25$  Mg/ha). From the 11 vegetation indices tested, GNDVI,  
2020 Normalised Difference Red Edge (NDRE1), and NDVI obtained the highest linear  
2021 relationship with AGB ( $R^2 = 0.71$  and  $R^2 = 0.56$ ,  $p < 0.001$ ), however, GNDVI and  
2022 NDRE1 improved the AGB estimation at medium to high-density forests compared  
2023 to NDVI. The GRVI and EVI were the least correlated with AGB ( $R^2 = 0.09$  and  $R^2 =$   
2024  $0.31$ ) at a significance level of  $p < 0.001$ , respectively. The thesis shows that NDVI  
2025 saturates in areas with  $>80$  Mg/ha AGB, whereas the inclusion of SAR backscatter  
2026 and optical red edge bands (B5) significantly reduces saturation effects in areas of  
2027 high biomass. GNDVI and red edge (B5) derived vegetation indices have more  
2028 potential for estimating AGB in dryland forests than NDVI. This study results  
2029 demonstrate that dryland AGB can be estimated with a reasonable level of

2030 precision from open access Earth observation data using multivariate random  
2031 forest regression.

2032 **Keywords:** Dryland forests, Above ground biomass, Random forest, Linear  
2033 regression, Sentinel, SAR, Southern Africa, Chobe, Conservation

## 2034 3.1 Introduction

2035 Dryland forests in Southern Africa are currently experiencing high rates of forest  
2036 loss as a result of overexploitation, wildfire, and herbivory, and are projected to  
2037 experience the impacts of climate change (Miles et al., 2006). Although large  
2038 uncertainties surround the contribution of tropical savanna forests and open  
2039 woodland (hereafter referred to as dryland forests) to the global carbon budget,  
2040 recent studies have shown that dryland above ground biomass (AGB) is a more  
2041 dominant driver of variations in the global carbon cycles when compared with  
2042 moist tropical forests (Ahlström et al., 2015; Poulter et al., 2014). However,  
2043 wildfires and a high density of mega-herbivores in most protected/conservation  
2044 areas (particularly elephants, *Loxodonta africana*) can have a significant impact on  
2045 tree cover and structural diversity by modifying vegetation structure through  
2046 grazing and physical damage thereby making trees less tolerant to fire (Ben-  
2047 Shahr, 1996; Shannon et al., 2011). With these pressures degrading the dryland  
2048 forests, techniques are urgently needed to measure, map, and monitor the forest  
2049 stand parameters reliably and to produce this information at appropriate scales to  
2050 support conservation and management actions. AGB estimates from sub-tropical  
2051 dryland forests have received less attention than many other biomes and so  
2052 estimates of AGB remain highly uncertain, despite the importance of these areas as  
2053 carbon stores and for ecosystem services (Pennington et al., 2018; Olson and  
2054 Dinerstein, 2002). For instance, studies of tropical moist forests are well  
2055 represented in the scientific literature (Salis et al., 2006; Williams et al., 2008),  
2056 primarily because they have the highest carbon (C) uptake of the World's forests  
2057 (Olson and Dinerstein, 2002). The largest proportion of dryland forests ecosystems  
2058 are found in Africa, accounting for 60 - 80% of the total biome area (three times  
2059 the area covered by African rain forest) (Bodart et al., 2013; Bullock et al., 1995),  
2060 which provides a significant carbon stock for the African continent.

2061

2062 AGB is recognised as an essential terrestrial climate variable (ECV) by the Global  
2063 Climate Observing System (GCOS) led by the UN Framework Convention on  
2064 Climate Change (UNFCCC) (Bojinski et al., 2014). In addition, having information  
2065 on AGB, and other biophysical structural parameters such as canopy height and  
2066 habitat density in dryland forests can feed into a wide range of activities related to  
2067 carbon accounting and conservation purposes (Wulder et al., 2012). Information  
2068 about the distribution of biomass at local, regional, and global scales can also  
2069 detect land changes due to factors such as deforestation (a reduction in a  
2070 woodland area) and forest degradation (Harris et al., 2012; Saatchi et al., 2011).  
2071 However, at the same time, dryland forests experience an increase in woody  
2072 carbon stock, including widespread regrowth following shifting cultivation, bush  
2073 encroachment, and a reduction in browsing megaherbivores (McNicol et al., 2018).  
2074 Southern Africa, particularly the KAZA region, is experiencing large-scale shifts in  
2075 vegetation cover, biomass degradation, and increased vulnerability to climate  
2076 change which hold significant implications for forest ecosystem function  
2077 (Cumming, 2008; King, 2014; Niang et al., 2014). Yet, the location and rates of the  
2078 AGB and biomass loss and regrowth, and the above ground woody carbon stocks  
2079 are largely unknown (David et al., 2022a).

2080 Estimates of biomass using conventional techniques based on field measurements  
2081 are the most accurate ways of collecting biomass data. However, extensive  
2082 fieldwork is not feasible due to the inaccessibility, and logistical challenges of such  
2083 field surveys which limit the number of plots that can reasonably be surveyed  
2084 which impact AGB characterisation over large areas (Næsset et al. 2016). Biomass  
2085 measurements based on Earth observation measurements are obtained through  
2086 statistically-based integration of tree-level allometric equations with biophysical  
2087 or structural information derived from satellite data (Boisvenue & White, 2019).  
2088 The shortcoming of utilising satellite imagery for AGB estimation is related to  
2089 selecting suitable models and data availability (Houghton et al., 2009; Lu, 2006). In  
2090 terms of optical sensors, Landsat is one of the most utilised datasets because it  
2091 provides freely accessible imagery, at a high temporal coverage with a medium  
2092 spatial resolution (Dogru et al., 2020). In their study within miombo forests,  
2093 Gizachew et al. (2016) identified a linear relationship between AGB and Landsat 8

2094 derived spectral variables, concluding that the approach was suitable for  
2095 monitoring and reporting of biomass baselines in low-biomass, open-canopy  
2096 woodlands for REDD+ projects. The launch of the Sentinel-2 series satellites  
2097 through the EU Copernicus program provides new opportunities to enhance forest  
2098 monitoring in tropical countries on a large scale (ESA, 2020). Compared to  
2099 Landsat, the Sentinel-2 data provides four additional spectral bands strategically  
2100 positioned in the red-edge region that are expected to contribute to improved AGB  
2101 estimation and mapping (Li et al., 2021; Mutanga et al., 2012). Previous studies  
2102 that compared Sentinel 2 to Landsat 8 found Sentinel 2 to have spatial and spectral  
2103 capabilities that improved the estimation of AGB in different vegetations (Sibanda  
2104 et al., 2016; Forkuor et al., 2018). Such optical sensors are however limited in the  
2105 degree to which they can generate structural information because they have  
2106 difficulty penetrating beyond upper canopy layers and optical data can be  
2107 obscured by frequent cloud cover (Hyde et al., 2006). Certain limitations related to  
2108 data saturation also exist, particularly at sites with high woody cover, or those  
2109 areas with complex vegetation structures such as dryland vegetation, as so many  
2110 satellite sensors can be insensitive to large AGB variations (Lu et al., 2012; Powell  
2111 et al., 2010). Optical sensors are also limited in their ability to estimate higher  
2112 biomass levels as they are more sensitive to canopy density/cover rather than  
2113 canopy height (Joshi et al., 2016). Biomass saturation for low and medium spatial  
2114 resolution passive optical sensors such as the Moderate Resolution Imaging  
2115 Spectroradiometer (MODIS) or Landsat is a well-recognised problem (Steininger,  
2116 2000; Zhao et al., 2016).

2117 Space-borne Synthetic Aperture Radar (SAR) sensors such as Sentinel 1, TerraSAR-  
2118 X, ALOS PALSAR can be used to estimate AGB through cloud, as well as provide  
2119 detailed vegetation structural information from backscatter (Berninger et al.,  
2120 2019; Lucas et al., 2008). SAR data has the advantage that it includes the ability to  
2121 collect data in all weathers, during both day and night; the sensor has the  
2122 capability to penetrate through cloud and forest canopy; data are sensitive to  
2123 surface roughness, dielectric properties, and moisture content (Balzter, 2001;  
2124 Santos et al., 2002). The radar backscatter and the reflected signal is sensitive to  
2125 polarisation and frequency (HH, VV, HV, and VH), and can be used for volumetric  
2126 analysis rather than just the colour and density of leaves and so has the potential

2127 to be more sensitive to AGB in the woodlands of savanna (Balzter, 2001; Mitchard  
2128 et al., 2011). Recent research has shown that SAR data are suitable for classifying  
2129 vegetation types and assessing biomass at regional scales (Omar et al., 2017). Minh  
2130 et al. (2016) used SAR tomography to model tropical forest biomass and height in  
2131 central French Guiana and found a high correlation between the backscatter signal  
2132 and AGB in the high-biomass forest areas. In Africa, Bouvet et al. (2018) created an  
2133 ALOS PALSAR map at 25-m spatial resolution using an L-band PALSAR mosaic  
2134 produced by JAXA and in situ data, to estimate AGB over the whole of Africa.  
2135 Conversely, the saturation problem is also common in radar data at the middle to  
2136 high biomass levels, depending on wavelength and forest type, as documented by  
2137 Balzter (2001) and Lucas et al. (2008). The saturation level has been found to vary  
2138 as a function of the wavelength and polarisation of the incident radiation and  
2139 studies have reported saturation at approximately 30 - 50 Mg/ha, 60–100 Mg ha  
2140 and 100–150 Mg ha for C-, L- and P-band respectively (Lucas et al., 2006; Lucas et  
2141 al., 2015). Water content, forest spatial structure, and surface geometry (terrain  
2142 slope) derive errors and can cause saturation (Balzter, 2001). Studies have  
2143 successfully demonstrated the capabilities of Light Detection And Ranging (LiDAR)  
2144 for measuring vegetation distribution and estimating associated biophysical  
2145 parameters (Popescu, 2007). LiDAR can be used to directly estimate a spatially  
2146 explicit 3D canopy structure as a laser pulse emitted from the LiDAR sensor can  
2147 penetrate the multi-layered tree canopies reaching the ground, which has great  
2148 potential for improving the estimates of vegetation parameters (Pearse et al.,  
2149 2019). This leads to more accurate estimations of basal area, tree height and stem  
2150 volumes (Pirotti, 2011), but such approaches remain intensive and unsuited to  
2151 regional or global coverage (Gibbs et al., 2007). For the direct derivation of  
2152 biomass from optical, radar and LiDAR data, no single data type can fulfil all  
2153 requirements with each limited by either weather, saturation, and other bio-  
2154 physical conditions (Kellndorfer et al., 2010). Given these limitations, research  
2155 exploring the fusion of different data types is crucial to develop accurate AGB maps  
2156 (Koch, 2010).

2157 To assess and monitor forest structural parameters, various approaches to reduce  
2158 the impacts of data saturation in optical imagery in AGB estimation have also been  
2159 explored. Vegetation indices and textures generated from optical and airborne

2160 LiDAR data are often used as an alternative (Zhao et al., 2016). Many factors  
2161 influence data saturation, ranging from spectral, spatial, and radiometric  
2162 resolutions, vegetation type, or topographic features, which may lead to different  
2163 saturation values of AGB (Lu et al., 2016). For example, Lu et al. (2004) compared  
2164 different vegetation indices in the moist tropical region of the Brazilian Amazon  
2165 and found that vegetation indices including near-infrared (NIR) improved  
2166 correlations with AGB in relatively simple forest stand structures. Gizachew et al.  
2167 (2016) used Landsat 8 derived NDVI to estimate total living biomass (TLB) in the  
2168 miombo woodlands of Liwale district, south-eastern Tanzania. Despite its wide  
2169 application, NDVI has major limitations for modelling the spatial variability of  
2170 biomass including its instability. The NDVI signal is influenced by the underlying  
2171 canopy background, varying with soil colour, canopy structure, leaf optical  
2172 properties, and atmospheric conditions (Tucker, 1979; Pettorelli et al., 2005).  
2173 Madonsela et al. (2018) investigated the interactions between seasonal NDVI and  
2174 woody canopy cover in the savanna of the Kruger National Park (KNP) to model  
2175 tree species diversity using a factorial model and found that the interaction  
2176 between NDVI and woody canopy cover was insignificant. NDVI is known to give  
2177 poor estimates in the growing seasons and in estimates of areas with high-density  
2178 wood cover. These challenges have led to the development of alternative  
2179 formulations which include correction factors or constants introduced to account  
2180 for or to minimise the varying background reflectance, such as the Enhanced  
2181 Vegetation Index (EVI) (Huete et al., 1999). Xue et al. (2017) reviews other closely  
2182 related indices that include the Normalised Burn Ratio (NBR), the Green  
2183 Normalised Difference Vegetation Index (GNDVI), Soil-Adjusted Vegetation Index  
2184 (SAVI), the Transformed Soil Adjusted Vegetation Index (TSAVI) and the Green Red  
2185 Vegetation Index (GRVI) amongst others. Some studies have demonstrated that the  
2186 use of vegetation indices derived from the NIR narrow and red-edge bands  
2187 situated between red and near-infrared at wavelengths 680–780 nm can yield a  
2188 higher accuracy of AGB estimation as compared to conventional NDVI (Cho et al.,  
2189 2007; Laurin et al., 2016). Ramoelo et al. (2015) and Li et al. (2021) found a strong  
2190 correlation between biomass and the red edge position for a rangeland and  
2191 grassland ecosystem in South Africa and China, respectively. Comparable research  
2192 in dryland forested regions remains extremely limited (Michelakis et al., 2014;  
2193 Forkuor et al., 2020),

2194 thus this study has tested vegetation indices derived from the NIR narrow and red-  
2195 edge bands, GNDVI, EVI, NDVI, NBR, NBR2, SAVI, MSAVI in dryland forest of  
2196 Southern Africa. In this study vegetation indices such as NDVI, GNDVI, NBR, and  
2197 NDRE (Table 3.2) were selected because they all use a NIR band but differ in terms  
2198 of the second band, e.g., NDVI utilised the red band, GNDVI the green band, NBR  
2199 the SWIR2 and NDRE the red-edge band. Furthermore, it is important to choose a  
2200 suitable method to estimate forest AGB. The linear and multiple regression (LR and  
2201 MLR) method has been the most commonly utilised statistical algorithm for AGB  
2202 estimation in past research (Propastin, 2012). However, it is documented that the  
2203 linear regression method does not effectively explain the complex nonlinear  
2204 relationship between biomass and Earth observation data and has been known to  
2205 be unreliable at values beyond a saturation point of the canopy reflectance (Lu,  
2206 2006; Puhr and Donoghue, 2000). Also, identifying suitable variables for  
2207 developing a multiple regression model is critical because some variables are  
2208 weakly correlated with AGB or are likely to suffer from multicollinearity (Jong et  
2209 al., 2003). Thus, understanding the performance and contribution of multiple  
2210 sources of data and methods for forest biomass estimation has the potential to  
2211 exploit the strengths of each and can help minimise the limitations of single  
2212 sensors.

2213 Several assessments have indicated that global forest cover datasets based on  
2214 satellite data have clear limitations for characterising forest structural parameters  
2215 in areas where the tree canopy is open, such as in savannas (McElhinny et al.,  
2216 2005). Approaches that integrate forest structural parameters and remote sensing  
2217 need to be replicated and tested across different regions, and geographic scales  
2218 (Lehmann et al., 2015; Mitchard et al., 2013). Furthermore, Foody et al. (2003) and  
2219 Woodcock et al. (2001) have pointed out concerns of generalising or transferring  
2220 methods and results derived from remotely sensed imagery over both space and  
2221 time. Many studies lack field data to build and validate AGB models, particularly in  
2222 tropical dryland forests where national forest inventory data is not available  
2223 (Grainger, 1999; Schimel et al. 2015). To the best of the author's knowledge, there  
2224 are very few studies that have tested the combination of synthetic-aperture radar  
2225 (SAR) and multispectral data to map AGB in Southern African dryland forests. Such  
2226 structural diversity maps are an invaluable data source for monitoring and

2227 managing biodiversity of forests and conservations of wildlife habitats and  
2228 corridors reducing the isolation of wildlife populations. Such maps also contribute  
2229 to the ecological functioning and health of savanna ecosystems. This study aims to  
2230 assess the feasibility of using remote sensing data derived from SAR, multispectral,  
2231 and ground measurements to estimate AGB in an area of typical African dryland  
2232 forests. The study developed parametric and non-parametric models for  
2233 estimating and testing the accuracy of AGB estimation and mapping. The models  
2234 developed by this thesis are compared to different published biomass models in  
2235 the dryland forest environment (Avitabile et al., 2016; Baccini et al., 2017; Bouvet  
2236 et al., 2018). The study presents a novel remote-sensing approach of dataset  
2237 combination and methodology, that can, in principle, be applied to the estimation  
2238 and mapping of AGB in dryland forest sites worldwide.

## 2239 3.2 Materials and methods

### 2240 3.2.1 Study area

2241 This study area is situated in Chobe National Park, in the north-east of Botswana  
2242 covering an area of around 10,589 km<sup>2</sup> (18.7°S and 24.5°E) (see: Fig. 3.1) within  
2243 the Kavango Zambezi Transfrontier Conservation Area (KAZA) of Southern Africa.  
2244 KAZA is the World's largest conservation area with an enclosed area of 519,912  
2245 km<sup>2</sup>. KAZA is shared by Angola, Botswana, Namibia, Zambia, and Zimbabwe and  
2246 links together over 36 proclaimed protected areas including national parks, forest  
2247 reserves, and wildlife management areas. Chobe National Park was chosen as the  
2248 field site because it is one of the largest protected areas in Botswana featuring an  
2249 impressive population of large mammals and several endemic plant species,  
2250 including large areas of the dryland forests and globally significant wetlands.  
2251 Within these habitats, there is a broad range of vegetation types ranging from low  
2252 herbaceous to high-density woody cover (McIntyre, 2010). The largest population  
2253 of African elephants (>150,000) is in northern Botswana drawn by the Chobe River  
2254 basin which serves as a source of surface water in the dry season when animals  
2255 converge on this stretch of water (Fullman, 2009).

2256 Chobe NP is a relatively flat area with an average elevation of 980 m. The climate is  
2257 semiarid with a highly variable mean annual rainfall of about 600 - 700 mm,

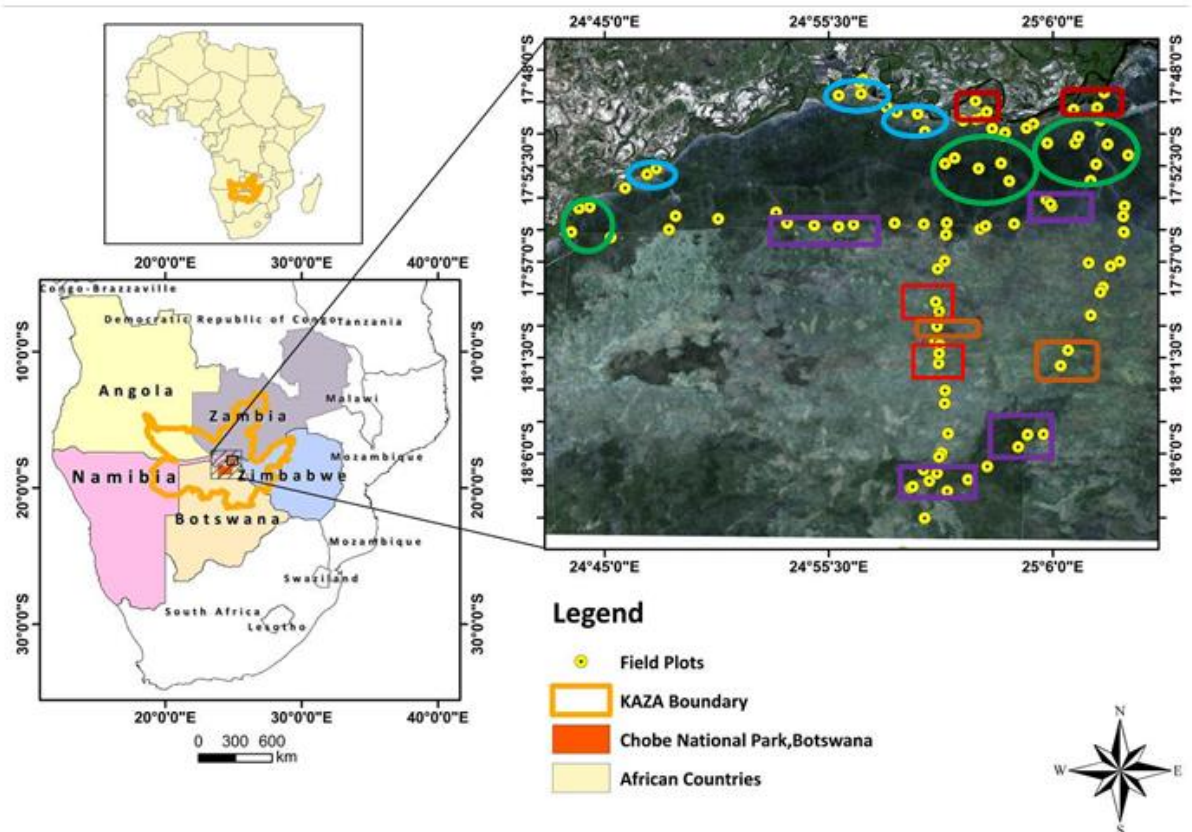


2258 mainly falling between November and March and a mean annual temperature of  
2259 21.8 °C (Fullman and Child, 2013). There is a general absence of rainfall in the dry  
2260 season (April–October). The nearest permanent water source is the Chobe River  
2261 forming the northern boundary of the park and the political border between  
2262 Botswana and Namibia. A high concentrations of large mammalian herbivores  
2263 including elephant, giraffe (*Giraffa camelopardalis* (L.)), impala (*Aepyceros*  
2264 *melampus*), and buffalo (*Syncerus caffer*) are found along the Chobe River front  
2265 during the dry season when seasonal pans are dry (Melton, 1985). Vegetation in  
2266 Chobe National Park is dominated by savanna grassland and low-density  
2267 woodland. Within these habitats, there is a broad array of vegetation types from  
2268 low herbaceous to high-density woody cover (McIntyre, 2010). The vegetation  
2269 found on the banks of the river is riparian woodland including *Capparis tomentosa*,  
2270 *Trichilia emetica*, *Acacia nigrescens*, and *Croton megalobotrys*. Because of the  
2271 intense pressure from elephants, vegetation along the Chobe riverfront has been  
2272 heavily impacted and is now dominated by low shrubs and very few large trees  
2273 (Fullman and Child, 2013). Often, the remains of dead trees suggest they have been  
2274 ring-barked, heavily browsed and toppled by elephants causing mortality. In the  
2275 south of the Chobe River, the most dominant woodland species are *Baikiaea*  
2276 *plurijuga*, *Burkea africana*, *Ochna pulchra* (Mosugelo et al., 2002).

2277 The high population of elephants has a wider destructive influence on vegetation,  
2278 especially within the Chobe River basin as they migrate to neighbouring countries  
2279 including Angola, Zambia, and Namibia. According to the United Nations  
2280 Framework Convention on Climate Change (UNFCCC) many of the countries of  
2281 southern Africa, including Botswana, Zambia, and Namibia, has been classified as  
2282 highly vulnerable to climate change and its effects (McGann, 2004). The visible  
2283 forest loss, especially that along the Chobe River frontage, has caused concerns  
2284 among stakeholders regarding dryland forest degradation pressure and  
2285 accompanying loss of biodiversity (see: Fig. 3.2A-F) (Nichols et al., 2017). In  
2286 addition to climate change and wildlife damage, it is estimated that 55% of year-  
2287 old saplings across all woodland species are killed by fire in Chobe National Park  
2288 (Fidzani, 2014). The KAZA region has been identified as biodiversity hot spot and  
2289 estimates of dryland forest cover and distribution not only are important tools to  
2290 help conservation and sustainable management of forests but also because of the

2291 risk to dryland forest areas from several potential threats: climate change, forest  
 2292 fragmentation, fire, conversion to agriculture, and increasing wildlife population  
 2293 density (Cumming, 2008).

2294



2295

2296 Fig. 3. 1. Location of the study area highlighting the countries (Botswana, Namibia, Angola,  
 2297 Zambia and Angola) and Chobe National Park where the field work was conducted. The  
 2298 coloured polygons around the sampled points indicate the type of vegetation structural  
 2299 formation and a range of land cover types that field sites represent (e.g., green-coloured  
 2300 circle: closed forests, purple-coloured square: open forests, orange-coloured square:  
 2301 shrubs, red-coloured square: grassland).

2302

### 2303 3.2.2 Fieldwork and sampling design

2304 Fieldwork was carried out during March 2019, which is the growing season, when  
 2305 the vegetation photosynthetic activity is still high. Sentinel-2 (S2) and Landsat 8  
 2306 OLI (LC8) wet season images (February - April) were acquired then classified into

2307 four classes (forests, open woodland, shrubs, and grassland) as these classes  
2308 represent the main land cover types in the study area of Chobe NP. The allocation  
2309 of field plots followed a stratified random sampling approach based on the four  
2310 strata (forest, open woodland, scattered trees with low herbaceous cover, and non-  
2311 forest) that represent broad vegetation types, and capture change between key  
2312 land cover types well. Measurements were collected from a total of 101 individual  
2313 sample plots throughout the savanna landscape of Chobe National Park. The  
2314 sample plots were widely distributed across Chobe NP (Fig. 3.1) and encompassed  
2315 relatively homogeneous tracts across a range of typical ecosystems (e.g., savanna  
2316 grasslands, shrubs) and structural formations (open woodland to closed forest).  
2317 Data from 61 of the 101 plots surveyed represented forest, and 40 samples  
2318 described represented non-forest land cover types. Examples of the collected  
2319 ground truth of typical forest cover types and recent vegetation degradation  
2320 activities through herbivory, drought, and burning captured during the field  
2321 campaign in 2019 are shown in Fig. 3.2. Within the 61 sample plots, a total of 4337  
2322 individual trees were measured. Table 3.1 presents stand parameters statistics  
2323 based upon this survey for dryland forests. Fig. A. 1 shows the density and  
2324 histogram plots of Aboveground biomass (AGB) and Carbon stock (Mg/ha) of each  
2325 field plot within savanna forest.

2326 Prior to fieldwork, the size of field sampling plots was defined based on S2 with 10,  
2327 20 m and LC8 multi-temporal data with 30 m pixel resolution, respectively. Hence,  
2328 plot sizes of (20 m × 20 m, 0.04 ha) and (10 m × 10 m, 0.01 ha) were considered  
2329 adequate in this study to ensure correspondence between field-measurement and  
2330 pixel size in the image. This area was large enough to contain almost the complete  
2331 diversity of the known plant community. 0.04 ha plots have been widely applied in  
2332 the National Forest Monitoring Plan in Botswana (Manatsha and Malebang, 2016)  
2333 and in different forests elsewhere (Baker et al., 2004; Carreiras et al., 2013) as it  
2334 normally encompasses a representative sample of trees within a single stand and  
2335 allows detection of changes in vegetation structure.

2336 The field measurements of stand characteristics included: mean height, diameter  
2337 at breast height (DHB), tree density, canopy closure, and tree species. Sample plots  
2338 were circular and the UTM coordinates at the centre of each plot were recorded in  
2339 the field with a hand-held Garmin GPS 64S. Tree height of each individual tree was

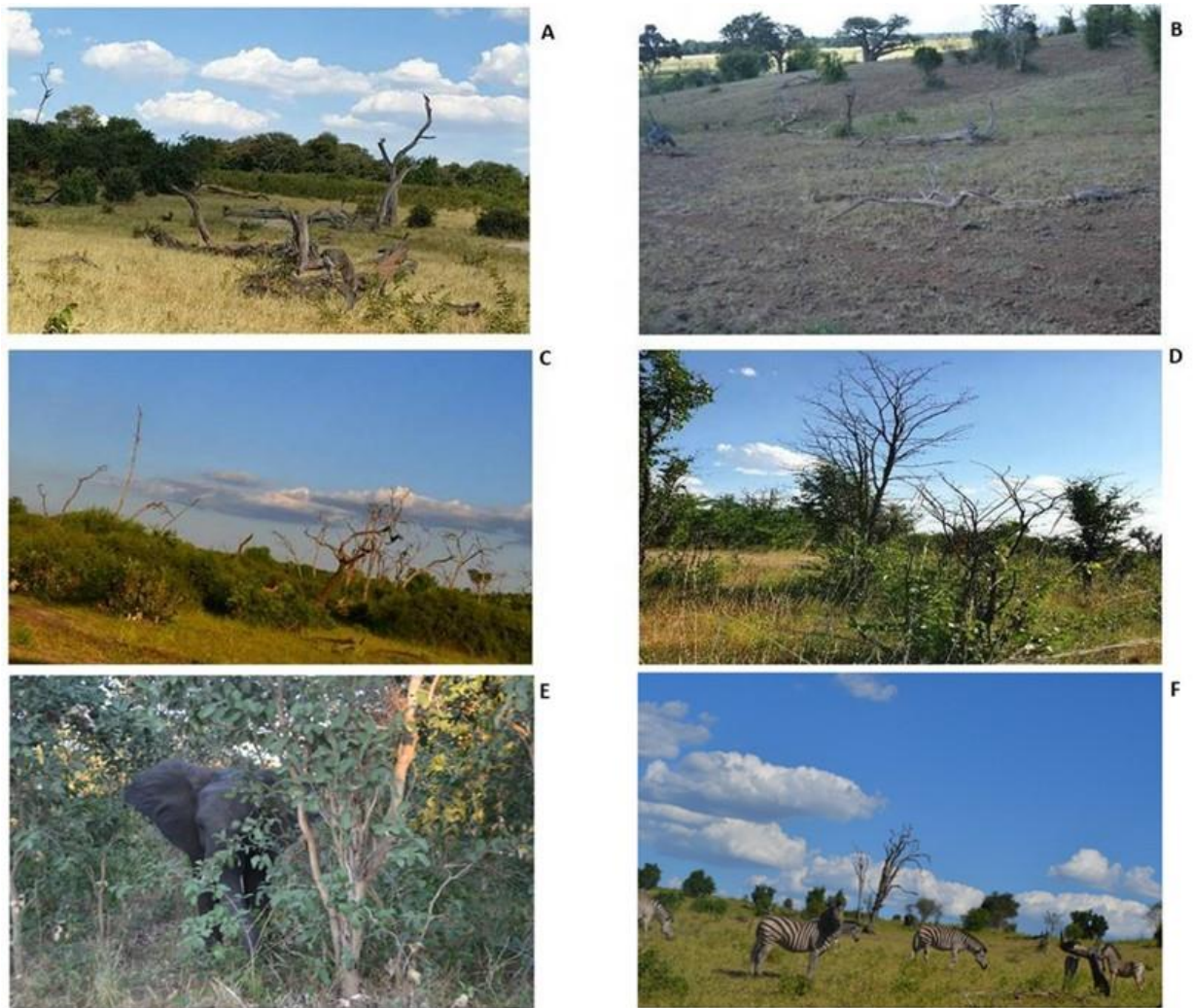
2340 measured using an ultrasonic Vertex III hypsometer which requires finding a  
 2341 suitable position to observe each tree tip (Božić et al., 2005), while stem diameter  
 2342 was measured using a Diameter above Breast Height (DBH) tape. All trees with a  
 2343 stem diameter of >3 m and >1.5 m height were recorded. Fractional vegetation  
 2344 cover (FVC) of shrubs between 1 and 6 m in height was estimated visually within  
 2345 all plots in the field. In the case of multi-stemmed species, such as *Burkea Africana*,  
 2346 *Compretum collinum* and *Baikiaea plurijuga*, individual stems are recorded as an  
 2347 individual.

2348

2349 Table 3. 1. Summary statistics for field sample data in Chobe National Park.

Variables	AGB (Mg/ha)	Carbon Stock (Mg/ha)	BA (m <sup>2</sup> /ha)	MDBH (cm)	MH (m)	TD (no. trees/ha)
Minimum	2.07	1.03	0.62	4.73	3.14	103.50
Maximum	166.98	83.49	35.42	30.07	15.23	4297.20
Mean	54.99	26.93	11.18	8.78	5.58	1183.40
S.D.	44.27	22.34	8.80	4.69	1.87	1019.68

2350 \*AGB= above ground biomass, MDBH=mean diameter at breast height, BA=basal area,  
 2351 MH= mean height, TD= tree density, S.D. =standard deviation.



2352

2353 Fig. 3. 2. Examples of collected ground truth captured during a field campaign in Chobe  
 2354 National Park in 2019. The photos represent typical forest cover types and recent  
 2355 degradation activities resulting from A: drought impacts, B: Trees toppled by elephants  
 2356 causing mortality, C and D: Trees destroyed by wildfire, and E and F: elephant and  
 2357 herbivory browsing.

### 2358 3.2.3 Satellite image data collection

2359 The imagery included Sentinel-1 Synthetic Aperture RADAR (S1-SAR), Sentinel-2  
 2360 Multispectral Instrument (MSI) data, and Landsat 8 - Operational Land Imager  
 2361 (OLI) were all accessed via Goggle Earth Engine (GEE) (Table 3.2). The GEE  
 2362 platform provides pre-processed top and bottom-of-atmosphere reflectance data,  
 2363 enabling large volumes to be integrated, processed, and analysed for extensive  
 2364 areas over long time periods (Warren et al., 2015). The Sentinel 1 and 2 data were  
 2365 acquired as close in time to the fieldwork as shown in Table A 1.

### 2366 3.2.3.1 Sentinel-1 image pre-processing

2367 S1 is a C-band SAR remote sensing satellite launched into orbit on 03.04.2014.  
2368 There are four imaging modes (Stripmap [SM], Interferometric Wide swath [IW],  
2369 Extra Wide swath [EW], and Wave [WV]), but the level-1 Interferometric Wide  
2370 (IW) Ground Range Detection (GRD) were also used in the study. Radar data were  
2371 analysed using the single co-polarisation with vertical transmit/receive and dual-  
2372 band co-polarisation, with vertical transmit and horizontal receive (VV + VH) from  
2373 Sentinel-1A and 1B C-band SAR. Within GEE, S1 images are pre-processed using  
2374 the S1 Toolbox (ESA, 2020) to an analysis-ready format using border and thermal  
2375 noise removal, radiometric calibration, and orthorectification (Google, 2020).  
2376 Radar data is not significantly affected by cloud cover, so a considerable number of  
2377 complete images can be obtained each month. However, radar data can be affected  
2378 by recent rainfall or wind and so an image from a period of good weather  
2379 (14.3.19), close to the field data collection date, was selected for analysis. The date  
2380 closest to the date of field collection (February-March 2019) was selected because  
2381 2019 was an extreme drought year in Southern Africa including Chobe NP, and  
2382 there was minimal recorded rainfall or soil moisture in the area during the time  
2383 period, hence soil moisture will have a minimal influence on the backscatter  
2384 (Chikoore and Jury, 2021; Lucas et al., 2006; Liu and Zhou, 2021).

### 2385 3.2.3.2 Sentinel-2 image pre-processing

2386 S2 MSI data, processed to level-2A were used. These data have been orthorectified  
2387 and radiometrically corrected providing Bottom-Of-Atmosphere (BOA) corrected  
2388 reflectance values (ESA, 2013). S2 images were further pre-processed with an  
2389 automatic cloud masking procedure using QA bands provided for the S2 2A  
2390 product, masking both opaque and cirrus cloud cover. Ten of the thirteen bands  
2391 from S2 (4 visible, 4 red edge, 2 short-wavelength infrared (SWIR)), were  
2392 extracted for pre-processing and analysis. The 20 m bands of S2 (SWIR and red  
2393 edge bands) were resampled to 10 m using the cubic convolution algorithm. S2  
2394 spectral indices, (see: Table 3.2 for all indices and their derivation) were used to  
2395 create the “indices” datasets. Previous studies suggested that numerous spectral  
2396 vegetation indices provided more information than the individual spectral bands  
2397 for retrieval of forest structure (Lu et al., 2012). Eleven spectral vegetation indices

2398 from S2 previously shown useful for biomass modelling and estimation were  
2399 computed (Hawryło et al., 2018).

### 2400 3.2.3.3 Landsat 8 image pre-processing

2401 LC8 was launched on 11.03.13 and provides multispectral images at 30 m  
2402 resolution with a 16-day return cycle. The study used LC8 Level 2 Tier 1 ortho-  
2403 rectified collections from 15.03.19. These data are derived from L8's OLI/TIRS  
2404 sensors and have been orthorectified and atmospherically corrected to obtain  
2405 surface reflectance. The LC8 reflectance orthorectified product was used because  
2406 GEE has already converted digital number (DN) values into surface reflectance  
2407 data as a result of standardising across image products to a common radiometric  
2408 scale (Chander et al., 2009). A cloud masking procedure was applied using the  
2409 Function of Mask (FMask) band included with the Landsat data (Zhu and  
2410 Woodcock, 2012). Eight spectral indices from LC8 were computed as "indices"  
2411 datasets. As shown in Table 3.2, a total of 39 initial variables were used for the  
2412 statistical analysis of the forest parameter estimation in this study.

### 2413 3.2.3.4 Land Cover Classification

2414 In order to allocate field plots throughout landscape using a stratified random  
2415 sampling approach, the sentinel 2 images in 2019 were independently classified  
2416 into four main land cover classes in GEE using a RF classifier because of its  
2417 robustness (Belgiu et al., 2016; Breiman, 2001). Based on the prior knowledge of  
2418 the study area, spectral clusters from the classification were assigned to four  
2419 general land cover classes: Forests, open forests, grassland, and shrubs. A total of  
2420 367 ground points were randomly distributed on the study area, and they were  
2421 split equally into 50% of points as reference points for image classification and the  
2422 remaining 50% of points used for accuracy assessment.

2423

2424 Table 3. 2. Description of predictor variables for the AGB estimation.

<i>Satellite</i>	<i>Band</i>	<i>Description, wavelength, spatial resolution)</i>
<b>S1 GRD</b> ( 14.03.2019)	<i>VV - Vertical transmit-vertical channel</i>	<i>5.6 cm (10 m)</i>
	<i>VH - Vertical transmit-horizontal</i>	<i>5.6 cm (10 m)</i>

	<i>channel</i>	
	<i>Band 1 – Coastal aerosol</i>	<i>0.443nm - (60 m)</i>
	<i>Band 2 – Blue</i>	<i>0.490nm -(10 m)</i>
	<i>Band 3 – Green</i>	<i>0.560nm - (10 m)</i>
	<i>Band 4 – Red</i>	<i>0.665nm -(10 m)</i>
<b>S2 SR (14.03.2019)</b>	<i>Band 5 – Vegetation red edge</i>	<i>0.705 nm -(20 m)</i>
	<i>Band 6 – Vegetation red edge</i>	<i>0.740 nm - (20 m)</i>
	<i>Band 7 – Vegetation red edge</i>	<i>0.783 nm - (20 m)</i>
	<i>Band 8 – NIR</i>	<i>0.842 nm - (20 m)</i>
	<i>Band 8A – Narrow NIR</i>	<i>0.865 nm - (20 m)</i>
	<i>Band 11 – SWIR</i>	<i>1.61 nm - (20 m)</i>
	<i>Band 12 – SWIR</i>	<i>2.19 nm - (20 m)</i>
<b>LC8 OLI TOA (15.03.2019)</b>	<i>Band 1 Coastal</i>	<i>0.43 - 0.45 nm (30 m)</i>
	<i>Band 2 Blue</i>	<i>0.45 - 0.51 nm (30 m)</i>
	<i>Band 3 Green</i>	<i>0.53 - 0.59 nm (30 m)</i>
	<i>Band 4 Red</i>	<i>0.63 - 0.67 nm (30 m)</i>
	<i>Band 5 NIR</i>	<i>0.85 - 0.88 nm (30 m)</i>
	<i>Band 6 SWIR 1</i>	<i>1.57 - 1.65 nm (30 m)</i>
	<i>Band 7 SWIR 2</i>	<i>2.11 - 2.29 nm (30 m)</i>
<b>Vegetation Indices</b>	<i>Normalised vegetation index (NDVI)</i>	<i>(NIR -R)/(NIR + R)</i>
	<i>Green red vegetation Index (GRVI)</i>	<i>(G-R)/(G + R)</i>
	<i>Enhanced Vegetation Index (EVI)</i>	<i>2.5NIR-RED(NIR+6RED-7.5 BLUE)+1</i>
	<i>Green NDVI (GNDVI)</i>	<i>(NIR - G)/(NIR + G)</i>
	<i>Normalised Difference NIR/SWIR2 (NBR)</i>	<i>NIR-SWIR/NIR+SWIR</i>
	<i>Normalised Difference SWIR1/SWIR2 (NBR2)</i>	<i>(SWIR1 - SWIR2) / (SWIR1 + SWIR2)</i>
	<i>Soil-adjusted vegetation index (SAVI)</i>	<i>(NIR - R)/(NIR + R + L)*1.5</i>
	<i>Modified Soil-adjusted vegetation index (MSAVI2)</i>	<i>(2 * NIR + 1 - sqrt ((2 * NIR + 1)<sup>2</sup> - 8 * (NIR - R))) / 2.</i>
	<i>Normalised Difference Index 45 (NDI45)</i>	<i>B5-B4/B5+B4</i>
	<i>Inverted red-edge chlorophyll index (IRECI)</i>	<i>RE3 -R/(RE1/RE2)</i>
	<i>Normalised difference red edge index (NDRE1)</i>	<i>(NIR -RE1)/(NIR + RE1)</i>

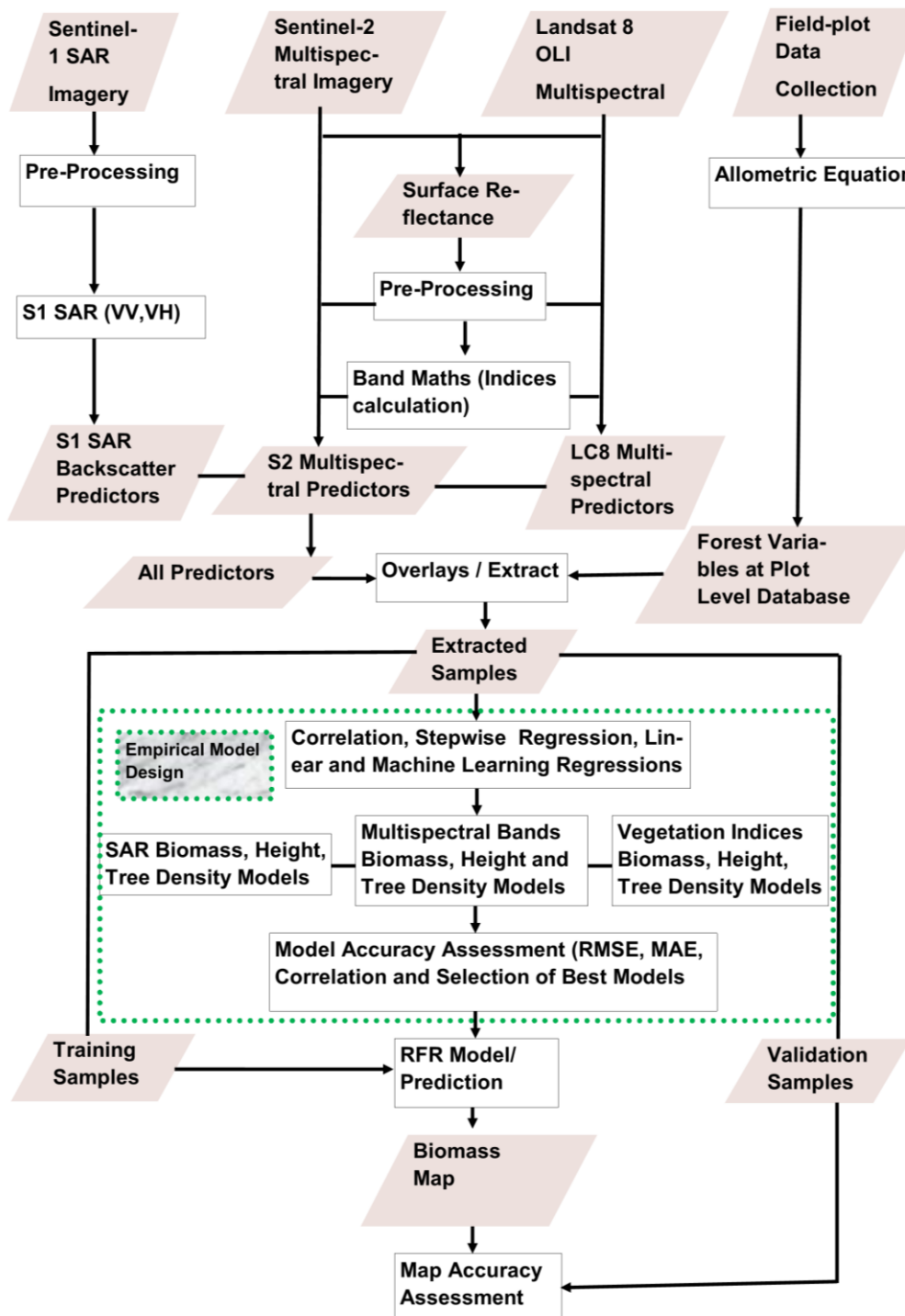
2425 \*RE: Red-edge; NIR: Near infra-red; SWIR1: Short-wave infra-red 1; SWIR2: Short-wave  
2426 infra-red 2.

### 2427 3.2.4 Methods and modelling

2428 A full overview of the methodological approach for AGB is shown in Fig. 3.3. For all  
2429 forest parameters, analysis was undertaken using S1 backscatter values (VV and  
2430 VH polarisations) the reflectance values from individual spectral bands (B2-12),



2431 and spectral vegetation indices from S2 and LC8 OLI (NDVI, GRVI, EVI, GNDVI,  
 2432 NBR, NBR2, SAVI, MSAVI2, NDI45, IRECI, and NDRE1) as shown in Table 3.2. All  
 2433 models and their combinations are shown in Table 3.3 and 3.4.



2434

2435 Fig. 3. 3. Overview of methodological approach

## 2436 3.2.4.1 Calculation of AGB at the tree level

2437 Locally defined allometric equations are not available for most of the species in the  
 2438 study area; AGB in kilograms per tree was estimated using the following  
 2439 generalised biomass estimation model (Eq. 3.1) developed for tropical dry forests  
 2440 (Chave et al., 2005).

$$\begin{aligned}
 AGB_{est} &= \exp(-2.187 + 0.916 \times \ln(\rho D^2 H)) \\
 &\equiv 0.112 \times (\rho D^2 H)^{0.916}
 \end{aligned}
 \tag{Eq.3.1}$$

2441 Where AGB is the above ground biomass in kg per tree;  $H$  = height (m);  
 2442  $D$  = diameter at breast height;  $\rho$  = wood density ( $\text{g cm}^{-3}$ ).

2443 The AGB of each individual tree was first calculated based on wood density, and  
 2444 then the total AGB per plot was summed based on the number of trees and the  
 2445 proportion between species. The wood density for species was obtained from the  
 2446 World Agroforestry Database (worldagroforestry, 2019). The biomass values were  
 2447 produced using the allometric equation developed by Chave et al. (2005) using  
 2448 Statistical Package R software (version 4.1.1) (R Core Team, 2013). Three tree-  
 2449 specific variables (tree wood density, DBH, height) were then generated and  
 2450 normalised by the area of the plots to estimates AGB in Mg/ha. The allometric  
 2451 model accounts for uncertainty and error in the estimation due to both data  
 2452 measurement and model uncertainty by averaging out the tree-level uncertainties  
 2453 at the stand scale, which is typically less than 10% of the mean as detailed in Chave  
 2454 et al., 2014. According to Baker et al. (2004) and Chave et al. (2005) excluding  
 2455 wood density and height would result in a poor overall AGB prediction and  
 2456 overestimation of the forest AGB. Rahman et al., 2021 showed that the generic  
 2457 allometric models overestimated AGB between 22% and 167% compared to the  
 2458 species-specific models and AGB was overestimated by up to 20% when using plot  
 2459 top height and underestimated by 8% using plot average height data from  
 2460 databases rather than individual tree heights in the mangroves (Rahman et al.,  
 2461 2021).

2462 The allometric equation used in the study was specifically developed for tropical  
 2463 dryland forests and already includes the uncertainty and correction factor. The

2464 dryland forest model typically achieves 90% accuracy in AGB stock estimation and  
2465 the standard error in estimating stand biomass was 12.5% if height is available,  
2466 and 19.5% if height is not available for dryland forests (Chave et al., 2005).  
2467 Therefore, this research used species-specific models and individual tree  
2468 measurements including DBH, tree height and wood density as independent  
2469 variables in the allometric equation to reduce uncertainty and improved the  
2470 quality of the AGB prediction. This study didn't calculate the allometric equation  
2471 uncertainty since the error due to the DBH, height, and wood density  
2472 measurements are already calculated and factored in one error term of the  
2473 allometric equation (Chave et al., 2004). The average and total AGB and carbon  
2474 stocks per land cover class (i.e., closed forest, open forest) were estimated, as well  
2475 as the total AGB and carbon stock in the forests of Chobe NP. The amount of carbon  
2476 in biomass was determined by multiplying by a factor of 0.5 to obtain the amount  
2477 of carbon existing in dry wood biomass, assuming biomass is approximately 50%  
2478 of dry weight (Brown and Lugo, 1982; Chave et al., 2005). Table 3.1 presents plot  
2479 summary statistics (minimum, maximum, mean, and standard deviation) for the  
2480 variables of interest. The density and histogram plots of AGB and carbon stock  
2481 (Mg/ha) of each field plot with woodland trees are presented in the supplementary  
2482 materials as Fig. A3.

#### 2483 3.2.4.2 Extraction of remote sensing data at field plot location

2484 Each circular field plot had a radius of 10 and 20 m, and for each plot location, the  
2485 coordinates of each plot centre were established with GPS. Field plot location data  
2486 were then overlaid on the SAR and S2 images to create a vegetation plot region-of-  
2487 interest (ROI) map, based upon plot centre GPS position. Although the coordinates  
2488 of each plot centre were collected with a high-quality device with GPS and  
2489 GLONASS sensors, there may be small positional errors, especially when  
2490 differential corrections are unavailable (errors up to 8–10 m are common). To  
2491 compensate for possible positional errors, a 20 m radius buffer was created  
2492 around the plot centre. This buffer was used to collect biomass image spectra. All  
2493 pixels inside each 20 m buffer were extracted, with several metrics computed  
2494 (mean, minimum, maximum, and standard deviation) (see Table 3.1), and these  
2495 data were used to establish relationships with the AGB at plot level. As the original  
2496 Sentinel data mosaic had a 10 m resolution and the buffer around each plot centre

2497 was set to 20 m, the extracted values per plot were those located approximately on  
2498 a  $4 \times 4$ -pixel window size, thus extracting from a  $40 \times 40$  m area.

#### 2499 3.2.4.3 Selection of relevant predictors

2500 The selection of suitable variables is critical for developing biomass estimation  
2501 models, as some variables are weakly correlated with AGB, or the variables can be  
2502 co-dependent. Selected variables should be significantly correlated with AGB, but  
2503 independent (Lu, 2006). In order to obtain valid predictor variables, correlation  
2504 analysis was first used for candidate variable selection. Pearson correlation  
2505 coefficients ( $p$ ) and scatterplots were used to examine the nature of the AGB  
2506 correlation, then variables were accepted for further analysis based on their  
2507 significance ( $P < 0.05$ ). In addition to the  $p$ -value, the variation inflation factor  
2508 (VIF) generated for each predictor variable was used to minimise multicollinearity  
2509 in the model. The VIF measures the increase in the variance of an estimated  
2510 regression coefficient due to collinearity, indicating how much larger the variance  
2511 is compared to when the independent variables are not linearly related in the  
2512 model (Fox, 2015). A VIF of 1, indicates no collinearity and several studies have  
2513 used a  $VIF < 10$  to avoid serious multicollinearity between the chosen predictor  
2514 variables. Generally, a VIF greater than 10 indicates high collinearity with other  
2515 predictor variables in the model and interpreting the regression estimates  
2516 associated with a high VIF predictor variable can lead to unstable estimates (James  
2517 et al., 2013; O'Brien, 2007). VIF has been used in the field of remote sensing to  
2518 check multicollinearity in a model with independent predictors (Tu et al., 2018;  
2519 Yang et al., 2012). To test for collinearity between the selected variables, a  
2520 variance inflation factor (VIF) threshold of 10 was applied.

#### 2521 3.2.4.4 Model development and selection

2522 Different statistical models were developed including parametric linear regression  
2523 and non-parametric machine learning using random forest regression in the R  
2524 programming platform. The dataset was first subjected to linear regression  
2525 (Simple linear (SL) regression, Multivariate linear (ML) regression, and STEPWISE-  
2526 AIC regression) to determine the optimum model (Bozdogan, 1987). Since biomass  
2527 is usually nonlinearly related to remotely sensed variables, to improve the

2528 nonlinear estimation of the biomass model, non-parametric random forest (RF)  
2529 models are widely used in satellite-based estimation of the forest AGB (Nandy et  
2530 al., 2017; Wu et al., 2014). RF does not make a priori assumptions regarding the  
2531 probability distribution of variables, and thus offers a significant advantage over  
2532 parametric statistical models which assume a Gaussian distribution. Ensemble  
2533 learning methods like RF (Breiman, 2001) play a significant role in remote sensing  
2534 and forest mapping because of their robustness, processing ability for high-  
2535 dimensional features, and ability to handle complex relationships between  
2536 independent variables in biomass estimation modelling (Belgiu et al., 2016; Adam  
2537 et al., 2014).

2538 A challenge is to select the fewest number of predictors that offer the best  
2539 predictive power and help in the interpretation of the final model. 12 experiments  
2540 were conducted to explore the suitability of different datasets (SAR, optical  
2541 spectral bands, and indices) and their combinations, in estimating AGB. To  
2542 overcome the challenge of selecting the fewest number of predictors that offer the  
2543 best predictive power and to help in the interpretation of the final model, the RF  
2544 was used to rank the predictor variables. This was followed by a backward feature  
2545 elimination method (BFE) as part of the evaluation process for the final model  
2546 selection (Guyon and Elisseeff, 2003). The BFE starts with all the possible  
2547 predictors and progressively drops the least promising variable, in this case, the  
2548 SAR, optical spectral bands, and indices. The model optimisation and comparison  
2549 was based on absolute and relative measures of fit: by calculating the accuracy  
2550 assessment (Acc%) and error statistics for the models including Root Mean  
2551 Squared Error (RMSE), Mean Absolute Error (MAE), Mean Absolute Percentage  
2552 Error (MAPE), coefficient of determination ( $R^2$ ), adjusted  $R^2$  ( $R^2_{adj}$ ), and Akaike  
2553 information criterion (AIC) and VIF. The concordance index was adopted to rank  
2554 the effectiveness of the ML and RF models (Gerds et al., 2012). The smallest subset  
2555 of variables with the highest coefficient of determination ( $R^2$ ), accuracy, adjusted  
2556  $R^2$  ( $R^2_{adj}$ ), and lowest RMSE, VIF, and AIC were then selected to predict the AGB.  
2557 Table 3.4 details the 19 multivariate models and the datasets used for estimating  
2558 AGB.

2559 The RF regression tree algorithm was selected to model forest parameters after  
2560 analyses showed that it performed better than ML regression algorithms. The

2561 decision tree-based models such as random forests, make no assumptions  
2562 regarding the distribution of the input data and can capture non-linear  
2563 relationships between the response and predictor variables (Breiman, 2001; Liaw  
2564 and Wiener, 2002). It is essential to optimise the model with the best combination  
2565 of parameters. For RF, only two parameters need to be tuned: *ntree* (with a default  
2566 value of 500 trees) that controls the number of trees to grow ( $k$ ), and *mtry* (with a  
2567 default value is 1/3 of the total number of the predictors) that controls the number  
2568 of variables randomly sampled at each split ( $m$ ). The study identified the number of  
2569 trees ( $k = 1000$ ) and *mtry* (the default was accepted) because it minimised the  
2570 error rate and produced the best results for AGB estimation in this study.

#### 2571 3.2.4.5 Model Validation

2572 The field dataset ( $n = 101$ ) was randomly split 70/30 for training and validation,  
2573 respectively (Ismail et al., 2006). The training dataset was used to optimise the  
2574 random forest regression and train the prediction model, and to assess the  
2575 goodness of fit of each model, the accuracy and the reliability of the prediction  
2576 model were assessed using the 30% validation sample. A regression equation  
2577 developed from the training data set ( $n = 71$ ) was then used to predict AGB on the  
2578 independent test data set ( $n = 30$ ). Validation techniques such as leave one out for  
2579 cross-validation and k-fold cross-validation are widely used in previous studies to  
2580 assess the model performance using reference data (Fassnacht et al., 2014). Cross-  
2581 validation is very similar to the out-of-bag (OOB) estimate, which is a formal  
2582 approach to quantify the predictive performance of a model, automatically  
2583 accounting for model complexity (Hastie et al., 2009). The sensitivity of the model  
2584 to the selection of the training and validation datasets was evaluated using a  
2585 repeated k-fold cross-validation and bootstrapping where the data are randomly  
2586 divided and spatially independent. The k-fold cross-validation procedure was used  
2587 to test for overfitting by partitioning the data  $K$  times ( $K=5$ ), using the shuffle  
2588 option of three repetitions ( $S=3$ ) when splitting the samples into 5 folds. In  
2589 addition, to assess the model uncertainty, a 1000 runs of bootstrapping was used.  
2590 The random forest regression performance in estimating AGB was compared with  
2591 the commonly utilised multiple linear regression. The correlation between  
2592 measured and predicted AGB from the independent validation plots was examined.

## 2593 3.3 Results

### 2594 3.3.1 Land cover classification

2595 The results of the land cover classification are presented in Fig. A. 5. Open forests  
 2596 were the dominant form of land-cover occupying 43%, followed by grassland with  
 2597 25%, forests with 23% and shrubs with a total of 9% of the land total area (see  
 2598 Table A 2). The difficulty was experienced in the separation of forests and open  
 2599 woodland due to difficulty in interpreting them. As shown in Table A 3, the overall  
 2600 classification accuracy was 97% and the Kappa statistic of 60% which denotes a  
 2601 good agreement between classes indicating generally low misclassification error,  
 2602 with the highest confusion arising between forests and open woodland. The  
 2603 validation overall accuracy was 67% which is reasonable for the random  
 2604 stratification purpose. A total of 101 ground plots were surveyed in Chobe NP. A  
 2605 total of 61 of the 101 plots surveyed represented forest, and 40 samples  
 2606 represented non-forest land cover types as shown in Fig. 3.2.

### 2607 3.3.2 Simple linear regression (SLR)

2608 Table 3.3 summarises the strength of the linear relationship between all variables  
 2609 derived from S1, S2, and LC8 data. S1 VV polarisation is substantially more  
 2610 sensitive to AGB ( $R^2 = 0.58$  and  $RMSE = 0.70$  Mg/ha) as compared to VH  
 2611 polarisation ( $R^2 = 0.32$  with  $RMSE = 0.89$  Mg/ha) at 99% confidence level. Among  
 2612 the S2 spectral bands, the highest coefficient of determination for AGB was  
 2613 obtained using spectral bands blue (B2), green (B3), red edge 1 (B5) ( $R^2=0.73$ ,  
 2614  $R^2=0.73$ , and  $R^2=65$  at p-value 0.001, respectively). The relationships of S1  
 2615 polarisations and selected S2 spectral bands (B3 and B5) with AGB are shown in  
 2616 Fig. A. 4A-D. S2 spectral indices Green Normalised Difference Vegetation Index  
 2617 (GNDVI) and Normalised Difference Red Edge (NDRE1) and Normalised Difference  
 2618 Vegetation Index (NDVI) obtained the highest linear relationship with AGB ( $R^2 =$   
 2619  $0.71$  and  $R^2 = 0.56$ ) at 99% confidence level, respectively.

2620

2621 Table 3.3. Simple linear relationship of satellite-based predictors with AGB. The  
 2622 backscatter polarisation, spectral bands, and indices with a strong linear relationship with

2623 AGB are highlighted in bold. The  $R^2 > 0.5$  is considered to indicate relatively a strong  
 2624 relationship between the variable (Silvy et al., 2020).

<i>Modelling Group</i>	<i>Response</i>	<i>Bands/Predictors</i>	<i>Intercept</i>	<i>Slope</i>	$R^2$	<i>RMSE error Mg/ha</i>	<i>AIC</i>
<b>S1</b>	<b>AGB</b>	<b>VV</b>	<b>9.35</b>	<b>0.51</b>	<b>0.58***</b>	<b>0.70</b>	<b>104.06</b>
		VH	39.04	-0.04	0.32***	0.89	125.95
<b>S2</b>	<b>AGB</b>	<b>B2</b>	<b>6.69</b>	<b>-72.99</b>	<b>0.73***</b>	<b>0.56</b>	<b>83.15</b>
		<b>B3</b>	<b>6.98</b>	<b>-47.73</b>	<b>0.73***</b>	<b>0.56</b>	<b>83.23</b>
		B4	6.15	-36.09	0.63***	0.66	98.48
		<b>B5</b>	<b>7.37</b>	<b>-31.21</b>	<b>0.65***</b>	<b>0.64</b>	<b>95.61</b>
		B6	10.84	-30.22	0.41***	0.83	119.68
		B7	8.76	-18.05	0.15*	1.0	136.30
		B8	7.65	-13.86	0.09*	1.03	139.47
		B8A	8.12	-14.32	0.09*	1.03	139.50
		<b>B11</b>	<b>9.97</b>	<b>-24.19</b>	<b>0.57***</b>	<b>0.71</b>	<b>104.50</b>
		<b>B12</b>	<b>7.079</b>	<b>-20.75</b>	<b>0.57***</b>	<b>0.71</b>	<b>104.89</b>
		<b>NDVI</b>	<b>-1.70</b>	<b>8.52</b>	<b>0.56***</b>	<b>0.72</b>	<b>106.40</b>
		GRVI	3.48	5.93	0.09*	1.03	139.29
		EVI	-0.73	10.44	0.31***	0.90	126.56
		<b>GNDVI</b>	<b>-4.09</b>	<b>12.43</b>	<b>0.71***</b>	<b>0.59</b>	<b>87.38</b>
		SAVI	-1.72	13.53	0.39***	0.84	121.01
MSAVI	-0.82	11.82	0.36***	0.87	123.34		
NBR	1.52	7.29	0.46***	0.80	115.79		
NBR2	-0.05	15.86	0.52***	0.75	109.86		
NDI45	0.80	10.04	0.33***	0.89	125.54		
IRECI	1.18	5.24	0.35***	0.87	123.96		
<b>NDRE1</b>	<b>-0.52</b>	<b>9.67</b>	<b>0.56***</b>	<b>0.72</b>	<b>105.92</b>		
NDRE2	0.59	28.63	0.46***	0.80	115.71		
<b>LC8</b>	<b>AGB</b>	<b>B2</b>	<b>10.62</b>	<b>-78.30</b>	<b>0.52***</b>	<b>0.75</b>	<b>109.72</b>
		<b>B3</b>	<b>7.77</b>	<b>-49.61</b>	<b>0.54***</b>	<b>0.73</b>	<b>108.16</b>
		B4	6.27	-34.78	0.48***	0.78	113.80
		B5	7.25	-12.48	0.07	1.05	140.65
		B6	8.27	-21.99	0.41***	0.83	119.50
		B7	6.29	-22.15	0.43***	0.81	117.58
		<b>NDVI</b>	<b>-2.59</b>	<b>10.42</b>	<b>0.52***</b>	<b>0.75</b>	<b>110.38</b>
		GRVI	2.98	11.42	0.26***	0.93	130.16
		EVI	-2.40	11.77	0.43***	0.82	118.29
		<b>GNDVI</b>	<b>-5.89</b>	<b>16.90</b>	<b>0.62***</b>	<b>0.67</b>	<b>99.53</b>
		NBR	-0.27	13.80	0.44***	0.81	117.44
		NBR2	0.24	7.89	0.44***	0.81	116.71
		SAVI	-3.95	19.95	0.45***	0.80	116.47
MSAVI	-2.98	18.43	0.42***	0.82	118.37		

2625 Significance codes: '\*\*\*' 0.001 '\*\*' 0.01 '\*' 0.05 '.' 0.1 ' ' 1

### 2626 3.3.3 Multivariate linear (ML) regression models

2627 Table 3.4 presents the multivariate relationships and validation results of the 19  
 2628 experiments conducted with S1 SAR signals, S2, and LC8 spectral bands, and  
 2629 indices for AGB. The results show that the relationship strength with AGB, and



2630 associated errors, are improved when the polarisation variables are combined.  
2631 Further improvements were attained when predictors are combined, from either a  
2632 single sensor or by integrating both sensors. Taking the linear relationship from S1  
2633 VV and VH polarisation, with  $R^2$  of 0.58 and 0.32 respectively, the  $R^2$  increased to  
2634 0.61 when combined. On the other hand, a combination of both S1 and S2 bands  
2635 generated a higher  $R^2$  of 0.85 and reduced the RMSE to 0.42 Mg/ha with an  
2636 increased estimation accuracy of 90%. A step-wise regression obtained the highest  
2637  $R^2$  of 0.95, a very low RMSE of 0.25 Mg/ha, and the highest accuracy of 94% for S1  
2638 backscatter and S2 spectral variables.

2639

2640 However, although the models with all S2 and LC8 spectral variables and stepwise-  
2641 regression models have high  $R^2$  values and low errors, they were excluded from  
2642 estimation because of high co-dependence between spectral bands and indices,  
2643 resulting in a high VIF (Table 3.4). A backward stepwise approach is useful to  
2644 reduce the number of parameters within the model in a systematic way. Based on  
2645  $R^2$ , MAE, and RMSE, the most suitable predictive model was obtained with S1 SAR  
2646 VV polarisation, the green (B-3) and red edge spectral band (B-5) of S2, explaining  
2647 82% of the variance but with a VIF of less than 10 for AGB (Table 3.4). The  
2648 inclusion of SAR data with optical data strengthens the relationship between  
2649 biomass and remote sensing variables, and consequently improves the model  
2650 performance as shown in Table 3.4. The results of the repeated k-fold cross-  
2651 validation shown in Supplementary materials in Fig A 3, show that the model fit is  
2652 not sensitive to the selection of training and validation sampling. The results of the  
2653 bootstrap validation in Fig A. 4 indicate that the model performance was stable  
2654 across bootstrap replicates. The bootstrap distribution, errors, and intercepts  
2655 correspond very closely to the linear model estimates, see Table 3.5 and 3.6 for  
2656 parameter values. If the predicted bootstrapping  $R^2$  was found to be significantly  
2657 smaller than the original multiple linear model  $R^2$ , that would indicate that the  
2658 model was over-fitted which is not the case with the linear model. The lower = .025  
2659 and upper = .975 of the 95-percent confidence interval for the coefficients of the  
2660 multiple linear and the bootstrap regression are shown in Table 3.6. The bootstrap  
2661 approach yields a similar estimation for AGB without relying on assumptions, and  
2662 this helps to confirm the stability of the model coefficients for the multiple linear  
2663 regression used in this study.

2664 Table 3.4. Multivariate linear relationship and validation results of 19  
 2665 experiments/models conducted for AGB modelling (label a-k represents S1 and S2) and  
 2666 (label l-p represents LC8). The best model is highlighted in grey.

AGB Model Label	Variables	$R^2$	RMSE (Mg/ha)	MAE	MAPE	ACC %	AIC	VIF
a	<b>S1 bands all</b>	0.61	0.68	0.55	0.21	0.84	102.8	1.46
b	<b>S2 bands all</b>	0.79	0.50	0.41	0.14	0.88	88.48	67.70
c	<b>S2 bands &amp; S1 bands all</b>	0.85	0.42	0.35	0.12	0.90	77.25	77.17
d	<b>S2 indices all</b>	0.85	0.42	0.35	0.12	0.89	83.39	19063.24
e	<b>Step regression S1 bands, S2 bands &amp; indices all</b>	0.95	0.25	0.19	0.06	0.94	47.79	11600.7
f	<b>Step backward selection with selected S1 &amp; S2 B3, B5, S1 VH, S1 VV, GRVI, GNDVI, NDRE1, NDI45</b>	0.88	0.38	0.31	0.10	0.90	61.92	2927.90
g	<b>Step backward selection with selected S2 Bands &amp; indices B3, B5, GRVI, GNDVI, NDRE1, NDI45</b>	0.82	0.46	0.36	0.13	0.89	74.34	2493.00
h	<b>Step Backward Selection with selected S1 &amp; S2 B3, B5, S1 VV, S1 VH, GNDVI, NDRE1</b>	0.84	0.43	0.37	0.13	0.89	69.13	1143.50
i	<b>Step Backward Selection with selected S1 Bands &amp; S2 indices GNDVI, NDRE1, S1 VV, S1 VH</b>	0.82	0.45	0.38	0.14	0.88	69.98	9.8
j	<b>Step Backward Selection with selected S1 &amp; S2 Bands B3, B5, S1 VV, S1 VH</b>	0.83	0.45	0.37	0.13	0.89	69.15	10.1
<b>k</b>	<b>Selected AGB model B3, B5, S1 VV</b>	<b>0.82</b>	<b>0.45</b>	<b>0.36</b>	<b>0.13</b>	<b>0.90</b>	<b>67.92</b>	<b>9.9</b>
l	<b>LC8 bands all</b>	0.68	0.62	0.47	0.18	0.87	102.00	75.28
m	<b>LC8 Indices all</b>	0.69	0.60	0.45	0.18	0.87	104.28	9408.0
N	<b>Step regression LC8 bands and indices</b>	0.72	0.57	0.42	0.17	0.88	99.23	11926.0
o	<b>Step backward selection with selected LC8 bands &amp; indices B3, B4, B7, GNDVI, NBR2</b>	0.68	0.61	0.45	0.18	0.87	98.97	282.24
p	<b>Step backward with selected LC8 indices GNDVI, NBR2</b>	0.67	0.62	0.47	0.19	0.86	94.94	9.1

2667

2668 Table 3. 5. Summary statistics and coefficients of linear and bootstrap regression for AGB

	Linear Regression	Bootstrap
--	-------------------	-----------

<b><i>R</i><sup>2</sup></b>	0.82	0.80
<b><i>RMSE</i></b>	0.45	0.42
<b><i>MSE</i></b>	0.36	0.32
<b><i>Intercept</i></b>	8.65	8.54
<b><i>B3</i></b>	-52.46	-56.11
<b><i>B5</i></b>	13.15	13.66
<b><i>SI-VV</i></b>	0.26	0.23

2669

2670 Table 3. 6. Confidence intervals (95 %) of linear and bootstrap regression for AGB

	<b>2.5%</b>	<b>97.5%</b>	<b>2.5%</b>	<b>97.5%</b>
	<b>Linear Regression</b>	<b>Linear Regression</b>	<b>Bootstrap</b>	<b>Bootstrap</b>
<b><i>Intercept</i></b>	7.58	9.72	7.47	9.65
<b><i>B3</i></b>	-78.68	-26.23	-74.88	-37.35
<b><i>B5</i></b>	-5.12	31.42	0.13	26.83
<b><i>SI-VV</i></b>	0.15	0.38	0.11	0.36

2671

### 2672 3.3.4 Comparing parametric and non-parametric machine 2673 learning for estimating stand parameters

2674

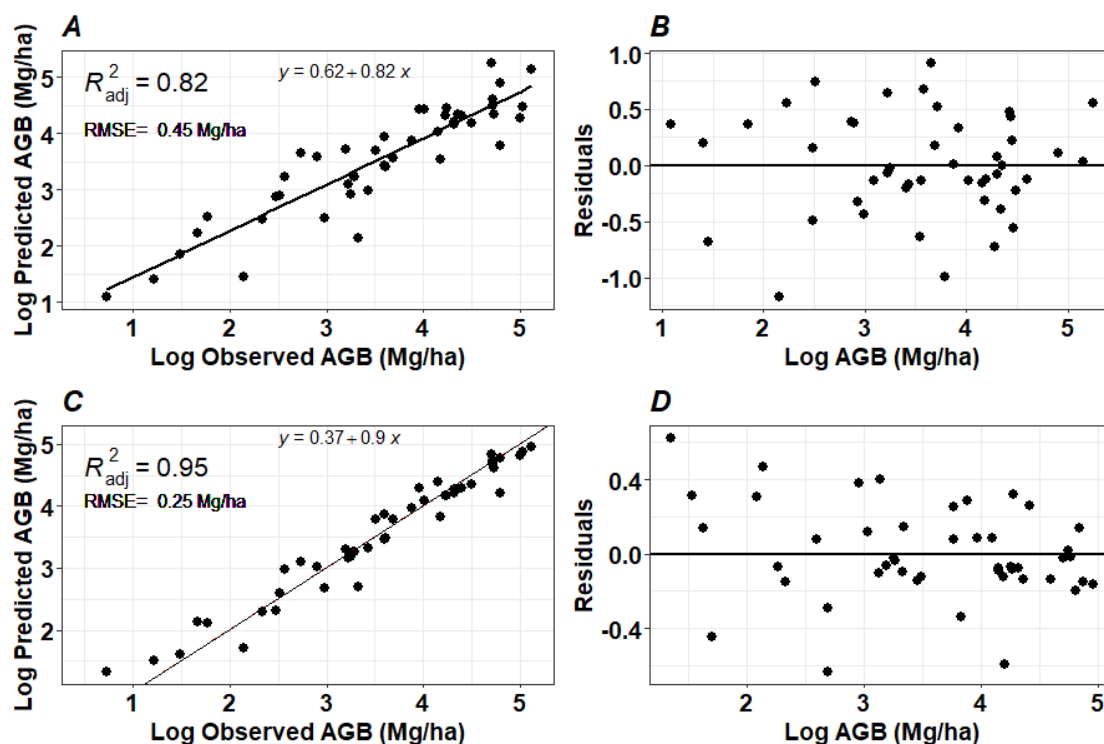
2675 Table 3.7 shows the summary statistics for the ML and RF regression models for  
2676 AGB using the three optimum predictor variables (S1 VV polarisation, S2 green  
2677 (B3), and red edge (B5)) hereafter referred to as S1S2), from the final models. It  
2678 can be seen that features derived from the MRF regression model offer the most  
2679 accurate estimates for all forest parameters compared to the ML regression model.  
2680 Graphical illustrations for the performance of the AGB models are presented in Fig.  
2681 3.4 that show the ML and RF fitted regression models for AGB and the associated  
2682 residuals. The plots of observed vs predicted AGB and residuals, indicate that the  
2683 RF residuals were rather stable across medium and high AGB values and had an

2684 average around zero compared to ML that under predicted AGB across the same  
 2685 data range. It can also be seen that low AGB values are not estimated well by any of  
 2686 the regression methods, although RF still had a more accurate estimation than the  
 2687 ML regression model. For AGB, the RF regression has the highest  $R^2$  of 0.95 and an  
 2688 RMSE of 0.25 Mg/ha compared to ML regression model with an  $R^2$  of 0.82 and  
 2689 RMSE of 0.45 Mg/ha. Based on  $R^2$ , RMSE, MSE, and concordance between predicted  
 2690 and observed value, the MRF regression performed better than the ML and so the  
 2691 MRF regression model was used for estimating forest stand parameters. Graphical  
 2692 illustrations for the performance of the AGB models are presented in Fig. 3.4.

2693 Table 3. 7. Summary diagnostics for the AGB models developed by ML and RFR regression  
 2694 methods using the S1S2 model. In this study, the best model throughout the study was the  
 2695 RF regression model, highlighted in grey.

<i>Model Type</i>	$R^2$	<i>RMSE</i>	<i>MSE</i>	<i>Concordance</i>
<i>ML Regression AGB</i>	0.82	0.45	0.21	0.88
<i>RF Regression AGB</i>	0.95	0.25	0.06	0.95

2696



2697

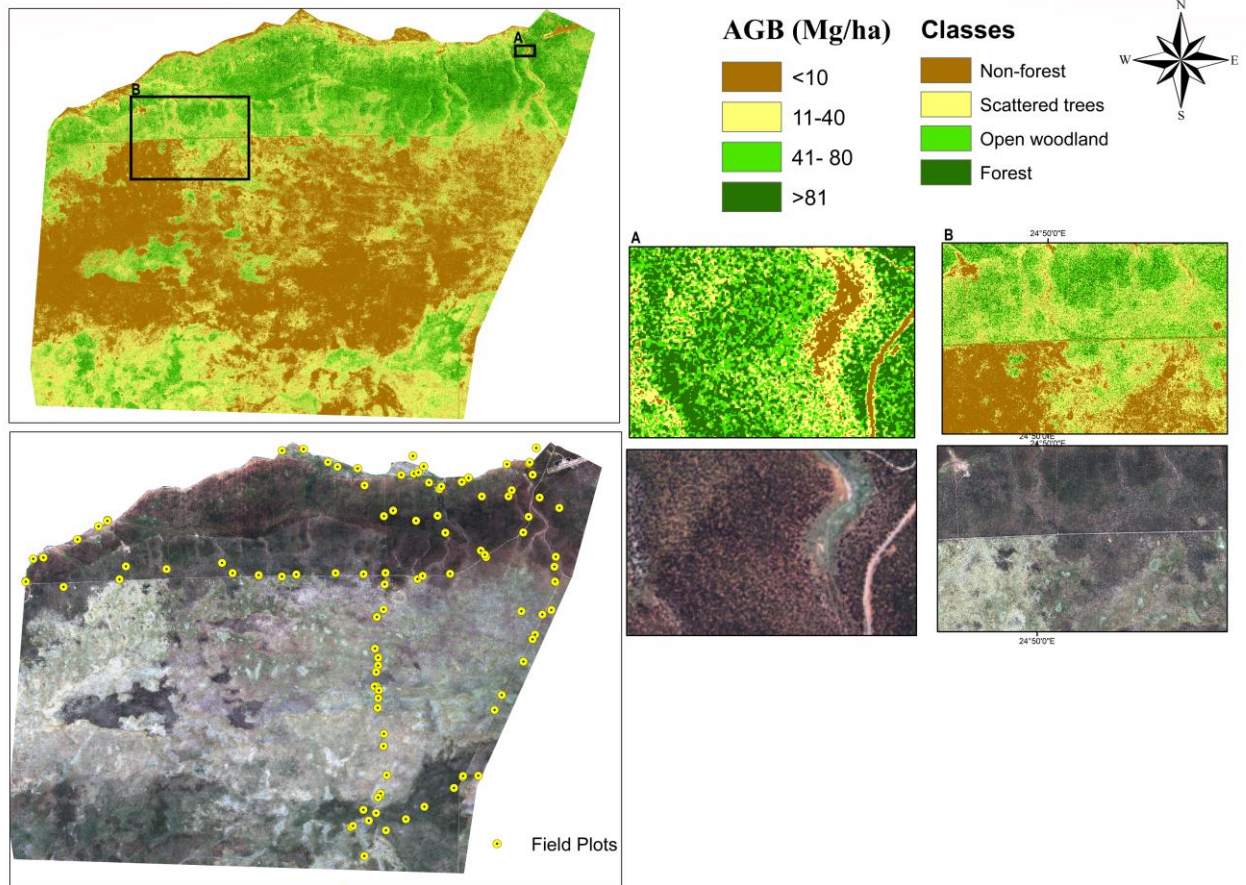
2698 Fig. 3. 4. Optimal AGB model. A: Observed and predicted AGB using ML regression. B: ML  
 2699 regression standardised residuals. C: Observed and predicted AGB using MRF regression.  
 2700 D: MRF regression standardised residuals.

2701

2702

### 3.3.5 Spatial distribution of AGB

2703 Fig. 3.5 maps the spatial distribution of the AGB estimations across the study area using  
2704 the RF regression-based model and S1 SAR and S2 spectral bands (S1S2). The  
2705 distribution of AGB ranges from 4.0 Mg/ha to 145 Mg/ha, which closely corresponds to  
2706 the range of values measured in the field where the highest AGB values were 167  
2707 Mg/ha. The estimated AGB map revealed that the highest AGB values range from 80 to  
2708 145 Mg/ha in northern Chobe, while a large part of the study area (80%) is characterised  
2709 by low AGB values < 80 Mg/ha, with an average AGB estimated at 51 Mg/ha. In the  
2710 southern part of the study area, there is a mixture of high and low-density forests, as  
2711 shown in both the modelled maps and S2 imagery. Similarly, the lowest AGB estimates  
2712 were found in the central part of the study area, which is consistent with field conditions  
2713 where grassland, shrubs, and scattered trees are found, as a result of degradation  
2714 associated with overgrazing and wildfire. The field photos corresponding to the mapped  
2715 land cover types are shown in Fig. 3.6A, which shows an example of a typical forest  
2716 plot where AGB ranges from 80 Mg/ha to 145 Mg/ha, as shown in dark green colour in  
2717 Fig. 3.5A. Fig. 3.6B represents an open woodland with AGB ranging from 41 Mg/ha to  
2718 80 Mg/ha, shown in light green colour in Fig. 3.5. The field photo in Fig. 3.6C shows an  
2719 example of scattered trees with herbaceous cover, corresponding to AGB ranges  
2720 between 11 Mg/ha and 40 Mg/ha, as shown in yellow colour in Fig. 3.5. Fig. 3.6D  
2721 represents non-forest land cover with occasional scattered trees and/or shrubs which  
2722 matches AGB values of <10 Mg/ha.



2723

2724 Fig. 3. 5. Modelled AGB maps of a dryland forest landscape of the study area and the RGB  
 2725 432 S2 image (10 m).

2726



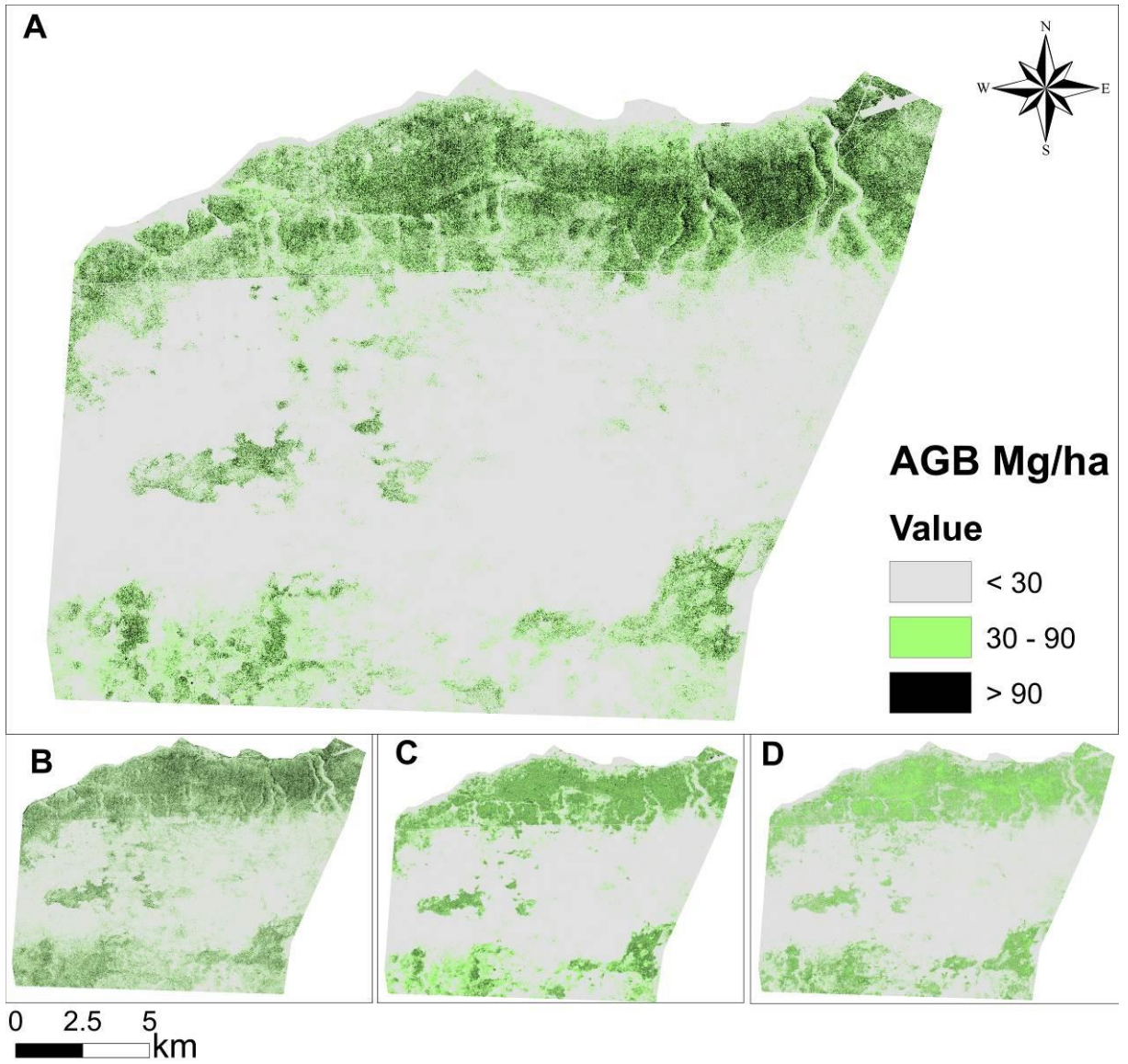
2727  
 2728

Fig. 3. 6. Examples of dryland forest types and their respective ground pictures across

2729 Chobe National Park. A: closed canopy forest. B: open canopy woodland. C: scattered trees  
2730 with low herbaceous cover. D: non-forest land cover.

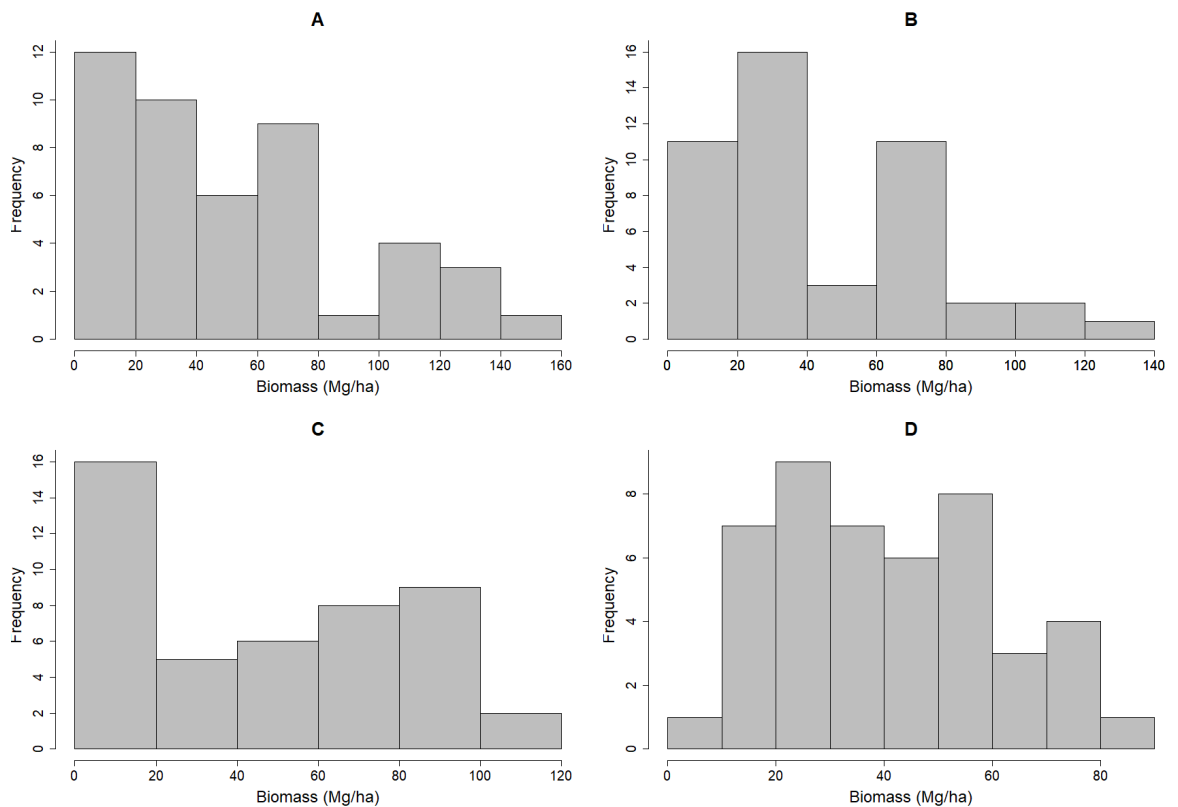
2731

2732 This study selected and compared the combination of S1 C-band SAR, LC8 and S2  
2733 optical data (S1S2), S1 polarisations and vegetation indices (NDRE1 and NDVI)  
2734 that were suitable for forest structural parameter estimation. The results in Fig. 3.7  
2735 show that the combination of S1 C-band SAR and S2 optical data estimated  
2736 medium to high biomass density with a higher level of accuracy as compared to  
2737 either sensor alone. A saturation effect for the S2 NDVI (S2NDVI) model was  
2738 observed, wherein the sensitivity to biomass variability declines when biomass  
2739 density exceeds 80 Mg/ha (see Fig. 3.7A). The saturation points for S1 polarisation  
2740 (Fig. 3.7B) and NDRE1 (Fig. 3.7C) models were higher in comparison to NDVI. The  
2741 combination of S1 backscatter values and S2 red edge position bands (S1S2) are  
2742 capable of estimating biomass > 80 Mg/ha (black colours) and did reduce the  
2743 saturation effect in high-density forest areas as shown in Fig. 3.7B. The maps in Fig.  
2744 3.7 confirm that the S1S2 model produced the best fit with the ground  
2745 observations for dryland forests, while reducing the under-estimation of large AGB  
2746 values estimated by the S2NDVI model. The study observed a small but noticeable  
2747 over-estimation for low values of biomass areas in the S2-NDVI model, although  
2748 this was more prevalent in the degraded and fragmented vegetation areas e.g.,  
2749 along the Chobe River frontage (see: Fig 3.7).



2750





2751

2752 Fig. 3. 7. A: AGB maps and histograms with the A: S1S2 model. B: S1 VV model. C: Modelled  
 2753 AGB map with NDRE1 model. D: Modelled AGB map with the NDVI model (the NDVI model  
 2754 saturates at values >80 Mg/ha).

2755

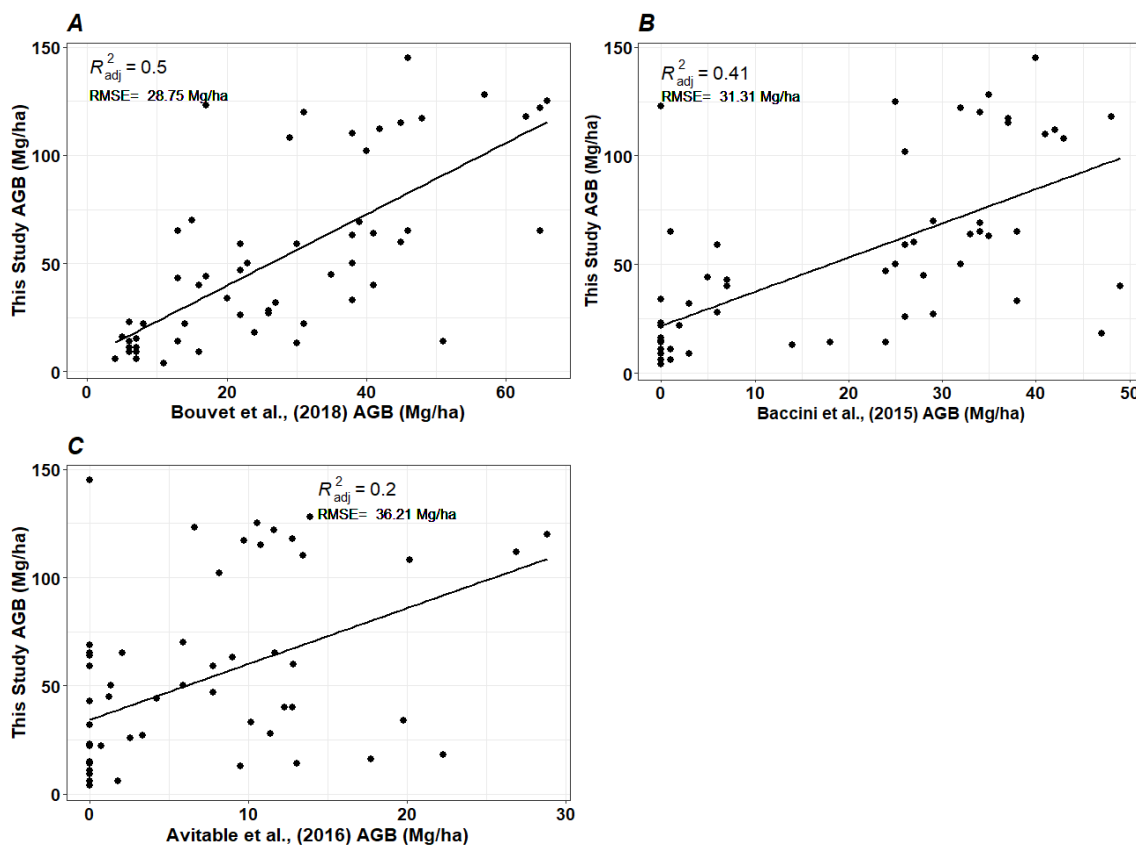
2756 In addition to cross-validation, the AGB map was evaluated by comparison with  
 2757 the most recent published pan-tropical AGB datasets (Avitabile et al., 2016; Baccini  
 2758 et al., 2017; Bouvet et al., 2018). The differences between models were analysed as  
 2759 displayed in Fig. 3.8, 9, and 10. Avitabile et al. (2016) integrated two existing global  
 2760 datasets of AGB from Saatchi et al., (2011) and Baccini et al. (2012) to create an  
 2761 improved pan-tropical AGB map at 1 km resolution, using an independent  
 2762 reference dataset of field observations to reduce bias and improve the accuracy.  
 2763 Baccini et al. (2017) used Landsat data to produce an AGB map at 30 m resolution,  
 2764 while Bouvet et al. (2018) used an ALOS PALSAR mosaic produced by JAXA in  
 2765 2010 to produce an AGB map at 25 m resolution for continental Africa.

2766 Fig. 3.8 shows a comparison between this study AGB estimates with these three  
 2767 published pan-tropical AGB datasets. A comparison with Avitabile et al. (2016)  
 2768 predicts low AGB values in the 0 to 30 Mg/ha range with a very low  $R^2$  of 0.20 and

2769 a precision of 36.21 Mg/ha. The result from Bouvet et al. (2018) using ALOS  
2770 PALSAR shows the highest agreement with this study with a coefficient of  
2771 determination  $R^2$  of 0.50, compared to Baccini et al. (2017) which reported  
2772 precision for the AGB estimates of 31.31 Mg/ha and an  $R^2$  of 0.41. The pan-tropical  
2773 maps all exhibited a high RMSE and a low  $R^2$  when compared with this study,  
2774 which has AGB estimates with  $R^2$  of 0.95 and RMSE of 0.25.

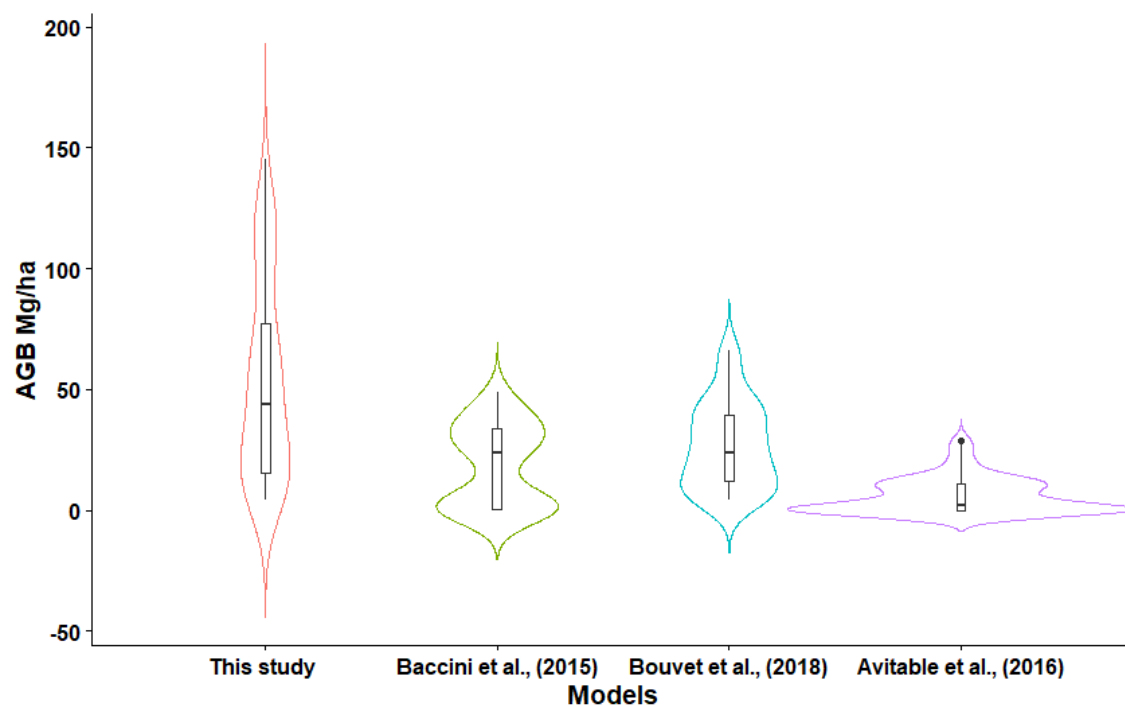
2775 Fig. 3.9 shows the spread, and distribution of the AGB from this study and three  
2776 published pan-tropical AGB datasets. The mean AGB varied from 5.92 Mg/ha with  
2777 the Avitabile et al. (2016), 18.5 Mg ha<sup>-1</sup> for Baccini et al., (2015), 26.7 Mg/ha for  
2778 Bouvet et al., (2018) to the highest 51 Mg/ha for this study (Fig. 3.9). The lowest  
2779 median is observed in Avitabile et al. (2016) and a relatively high variance is  
2780 observed in this study. Some bimodality is suggested by Avitabile et al. (2016) and  
2781 Baccini et al., (2015). This study and Bouvet et al., (2018) have a similar AGB  
2782 spread and the highest mean AGB estimation, with this study estimating a AGB of  
2783 145 Mg ha compared to 66 Mg/ha from Bouvet et al., (2018), 49 Mg/ha from  
2784 Baccini et al., (2015) and 28.8 Mg/ha from Avitabile et al. (2016). Bouvet et al.  
2785 (2018) was derived by limiting the model-based inversion method in predicting  
2786 AGB of forest plots to not exceed 85 Mg/ha for dryland ecosystem, and this could  
2787 explain the low AGB estimation in the high-density forest of the study area.

2788



2789

2790 Fig. 3. 8. Comparison between A: This Study AGB estimates and the AGB estimates from  
 2791 Bouvet et al. (2018). B: This Study AGB estimates and the AGB estimates from Baccini et al.  
 2792 (2017). C: This Study AGB estimates and the AGB estimates from Avitabile et al. (2016).



2793

2794 Fig. 3. 9. Comparison of AGB distribution (Mg/ha) among the different AGB estimates from  
2795 this study, Avitabile et al. (2016), Baccini et al. (2017), and Bouvet et al. (2018). The  
2796 models are arranged from the highest median AGB to the lowest. The horizontal line of the  
2797 box plot for each model represents the median and the width of violin plot represents the  
2798 proportion of the data using a kernel probability density.

2799

## 2800 3.4 Discussion

### 2801 3.4.1 Relationship between S1 SAR, S2, and LC8 with AGB

2802 In this study, simple linear regression models from S1 backscatter, S2, and LC8  
2803 spectral coefficients were statistically significant ( $p < 0.001$ ). However, the simple  
2804 models estimating the AGB from all sensors provided low  $R^2$  values and high RMSE  
2805 that are considered unreliable for estimating forest structure parameters for  
2806 practical forest management and habitat mapping. The RMSE observed in this  
2807 study is lower than other AGB studies reported in the region, but it is similar to  
2808 Mutanga et al. (2012) who predicted biomass using a similar sized plot from  
2809 homogeneous areas (20 m × 20 m) to compute 3 NDVIs from the WorldView-2 red  
2810 edge and NIR bands and yielded an RMSE of 0.441 kg/m<sup>2</sup>. The highest  $R^2$  was  
2811 generated using multivariate models that employed both SAR and optical data  
2812 (S1S2) highlighted in grey in Table 3.4, indicating the responsiveness of SAR to  
2813 forest parameters particularly when sensors are used in combination for  
2814 monitoring structural parameters in dryland forests, as reported by Townsend  
2815 (2002).

2816 In terms of the radar polarimetric parameters, VV polarisation showed a better  
2817 correlation and relationship with AGB and is shown to be more useful for the AGB  
2818 estimations as compared to VH. However, the combination of VV and VH  
2819 polarisation improves the  $R^2$  and lowers the RMSE. This result is not consistent  
2820 with the results obtained by Liu et al. (2019) but it is similar to the results of Omar  
2821 et al. (2017) and (Pham et al. (2020) who found VV polarisation to perform better  
2822 in estimating AGB and sensitive to the increase in AGB as compared to VH.  
2823 Nizalapur and Madugundu, (2010) used backscatter intensities obtained in X, C, L  
2824 and P- bands from DLR-ESAR data in Indian tropical forests, in which VV was

2825 found to correlate with biomass when compared to HH, HV and VH polarisations.  
2826 The selection of VV polarisation and their strong correlation with AGB and forest  
2827 parameters estimation also aligns with the studies by Ouaadi et al. (2020) and  
2828 Wijaya et al. (2015).

2829 Further, it could be observed that the SAR data was better at detecting  
2830 aggregations of individual trees in the savanna landscape than its optical  
2831 counterpart, while overestimating AGB and tree density cover in this area. This  
2832 effect was also shown in a study that was conducted in the Sahel dryland  
2833 ecosystems using S1/2 data (Zhang et al., 2019). The overestimation of AGB was  
2834 reduced from the combined use of S1 and S2 as compared to the single use of any  
2835 of the sensors.

2836 For optical data, although NDVI and EVI remain two of the most widely used  
2837 vegetation indices, they were outperformed by the NDRE1 and GNDVI in  
2838 estimating AGB, for dryland forests. The results are in agreement with the study by  
2839 Wang et al. (2007) that tested the capabilities of GNDVI for estimating the Leaf  
2840 Area Index (LAI), which were tested under different circumstances, and found that  
2841 GNDVI performed better than the conventional NDVI in both circumstances. The  
2842 results also align with the study by Otsu et al. (2019) who found that GNDVI  
2843 performed best in distinguishing broad leaf from needle leaf forests as compared  
2844 to NDVI. Another study by Yoder et al. (1994) used the green channel in a  
2845 vegetation index and found that it had a better correlation with the photosynthetic  
2846 activity of the tree canopy in miniature Douglas-firs as compared to the red  
2847 channel. The main reason for the difference in the performance of NDVI and GNDVI  
2848 is likely because the former is more sensitive to low chlorophyll concentrations,  
2849 while GNDVI is more sensitive to high chlorophyll concentrations and so is more  
2850 accurate for assessing chlorophyll content at the tree crown level (Gitelson et al.,  
2851 1996). Besides the use of the green channel in a vegetation index, the red edge  
2852 band is found to be more effective in estimating AGB at high canopy density as  
2853 compared to conventional vegetation indices because it covers chlorophyll  
2854 absorption and leaf cell structure reflection (Mutanga and Cho., 2012, Eitel et al.,  
2855 2011).

2856 The study found that a combination of S1 polarisation, S2 green, and red edge  
2857 bands, have led to the mitigation of data saturation in high-density biomass, when  
2858 compared to S2 NDVI models that saturate at biomass levels above 80 Mg/ha. The  
2859 saturation of the relationship between biomass and the NDVI due to strong  
2860 absorption in the red wavelength is a well-recognised problem (Zhao et al., 2016).  
2861 SAR acquired across the range of frequencies (namely C-, L- and P-band) has a  
2862 demonstrated capacity to quantify biomass up to a saturation level after which  
2863 sensitivity is lost, depending on the frequency used. For example, it is reported that  
2864 the C-band radar backscatter response saturates at biomass values of 30 Mg/ha to  
2865 50 Mg/ha, and the L-band backscatter is generally reported to occur between 70  
2866 Mg/ha and 150 Mg/ha and P-band backscatter can measure from 100 Mg/ha  
2867 up to 200 Mg/ha (Lucas et al., 2015). For this study, the synergy between the two  
2868 data sources, particularly the inclusion of SAR backscatter values from VV  
2869 polarisation and the red-edge (B5) spectral bands have reduced saturation effects  
2870 typical in optical and radar backscatter remote sensing data for the dense or  
2871 mature forest with complex stand structures in dryland forest (Liu et al., 2019).

### 2872 3.4.2 Selection of suitable algorithms and methods

2873 The estimations derived from the machine learning algorithm showed the ability  
2874 for improved the estimation of all forest parameters including AGB. Although the  
2875 results from ML regression models exhibited a strong linear relationship, this  
2876 study found that the RF regression algorithm performed better than ML  
2877 regression, reducing the RMSE for the estimation models by almost 50% in all  
2878 instances. In this study, ML regression derived relationships between observed  
2879 and estimated AGB and residuals show some linearity, that is, overestimations and  
2880 underestimations for the low and high biomass observations, respectively. This  
2881 demonstrates the problem of using linear regression models, as identified by Zhao  
2882 et al. (2016) who used Landsat and linear regression to estimate biomass  
2883 saturation values in the Zhejiang Province of Eastern China.

2884 Even though MRF regression models reduce the overestimation and  
2885 underestimation of biomass compared to ML regression models in this study, there  
2886 remains room for improvement. Specifically, the RF regression model estimated  
2887 medium and high-density forests with good accuracy but showed variation in low-

2888 density forests <30 Mg/ha. Most of these low-density forest plots include  
2889 understoreys and low herbaceous cover such as grassland, open forest, and burned  
2890 woodlands, often with relatively low canopy density. Therefore, soil and moisture  
2891 conditions under the canopy would have a significant impact on surface  
2892 reflectance and considerably influence AGB estimation. These results are similar to  
2893 numerous studies that assessed dryland forests using radar backscatter signals  
2894 and decision tree models (Baccini et al., 2004; Santos et al., 2002; Wang et al.,  
2895 1998) which all found that variations in understorey and ground conditions had an  
2896 impact on the interaction of microwave radiation with vegetation cover. Using  
2897 Radar C- and L-band, Wang et al. (1998) noted that the sensitivity of SAR to surface  
2898 parameters is most pronounced for co-polarisation signals C-VV and C-HH angles  
2899 at low biomass levels, with a sensitivity decrease for high biomass stands. This was  
2900 also an issue in this study because data were acquired during the wet season  
2901 where errors associated with moisture are likely (Mitchard et al., 2013).

2902

### 2903 3.4.3 Comparing regional AGB estimates with pan-tropical 2904 maps

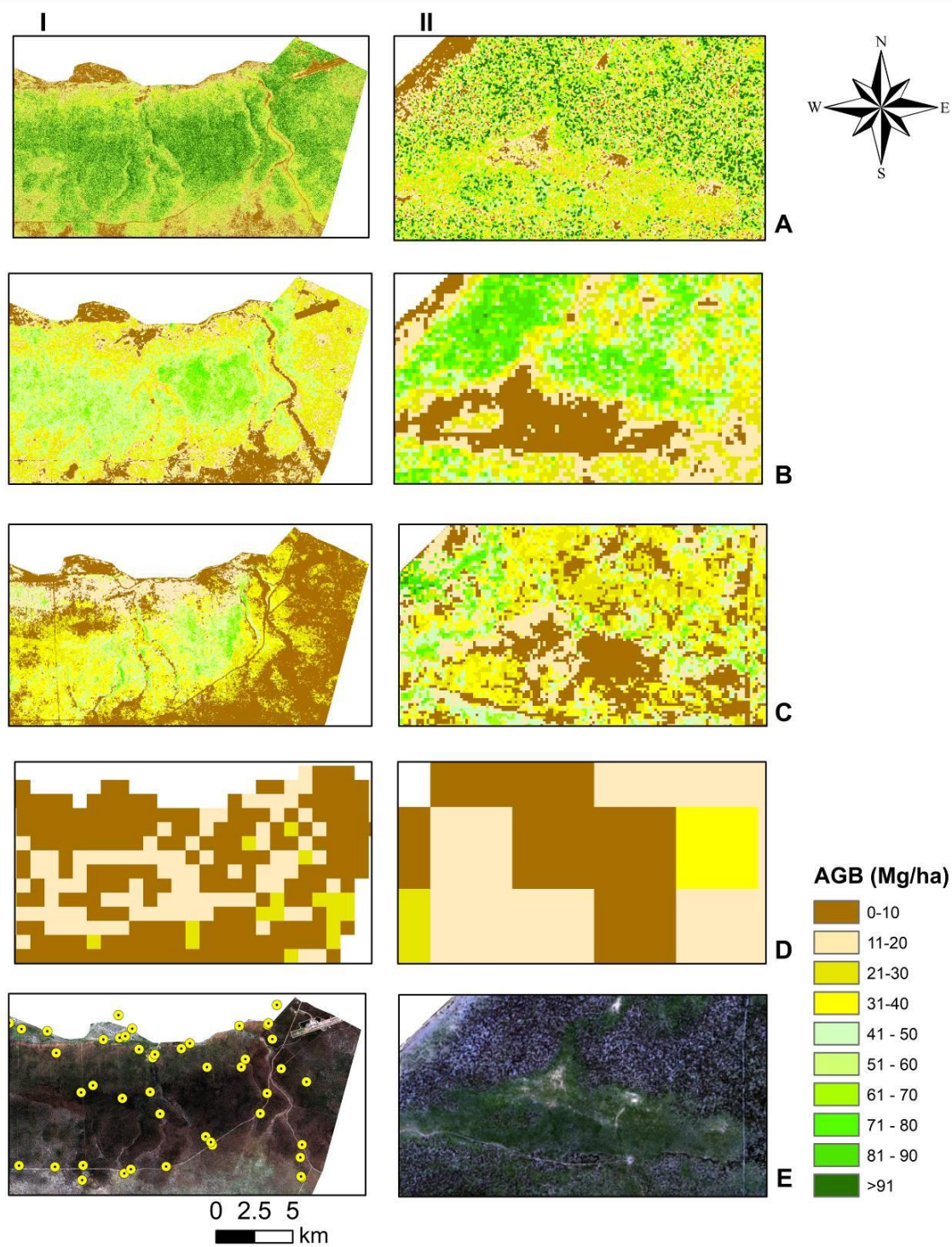
2905 The spatial distribution of high values of AGB (>145 Mg/ha) closely corresponds to  
2906 field measurements, with the forests in the northern part of Chobe National Park  
2907 found to have the highest AGB values. This can be attributed to the predominance  
2908 of species with large DBH such as Zambezi teak (*Baikaea Pluijuga*). Also, the  
2909 impacts of fire on the northern part of Chobe Park are better controlled than the  
2910 southern areas, as they commonly experience a higher burning frequency (Dube,  
2911 2013).

2912 Fig. 3.10 (I) shows a detailed view of a subset of forests in the northern part of the  
2913 study area, dominated by high density forests. The inability to estimate AGB  
2914 heterogeneity and a large under-estimation of biomass in dryland forests can be  
2915 clearly seen in the AGB map of Avitabile et al. (2016) when compared to all the  
2916 other AGB datasets. In contrast, Baccini et al. (2017) using Landsat imagery  
2917 underestimate AGB in the area of high-density forest around the airport situated to  
2918 the northeast of the study area (0-10 Mg/ha). Bouvet et al. (2018), using ALOS

2919 PALSAR, predict higher levels of biomass than Baccini et al. (2017) around the  
2920 airport area (10-30 Mg/ha), but these estimates are lower than this study  
2921 estimates of >80 Mg/ha. This study estimates higher biomass stocks in large areas  
2922 of northern Chobe > 80 Mg/ha particularly when compared to Bouvet et al. (2018)  
2923 and Baccini et al. (2017).

2924 The area shown in Fig. 3.10(II) is along the Shimwanza Valley, characterised by  
2925 bare ground, gullies, tall shrub savanna, and open woodland with a mixture of  
2926 medium and large trees. Results showed very large discrepancies from the pan-  
2927 tropical map in this area. For example, it can be seen that Bouvet et al. (2018)  
2928 underestimated a large portion of large and mature individual trees and were not  
2929 able to characterise the variability in dryland forests or the patterns of open  
2930 woodland. In addition, Bouvet et al., (2018) estimated high biomass of 50 Mg/ha to  
2931 70 Mg/ha in the degrading forest along the Chobe River frontage (see: Fig. 3.9B).  
2932 The S2 image reveals that there are actually fewer trees in this area with more  
2933 bare ground in between. The S1S2 model from this study was able to clearly show  
2934 the fine details of trees in different AGB ranges, with a mix of very low biomass  
2935 (due to different degrees of degradation) to intermediate biomass for certain areas  
2936 with very large but scattered trees, as shown in S2 imagery (see: Fig. 3.10E).  
2937 Baccini et al. (2017) shows a broad range of AGB (low to intermediate) similar to  
2938 this study AGB estimates in the Chobe River frontage; although their study  
2939 estimated lower biomass in high-density forest areas (see: Fig. 3.10C).





2940

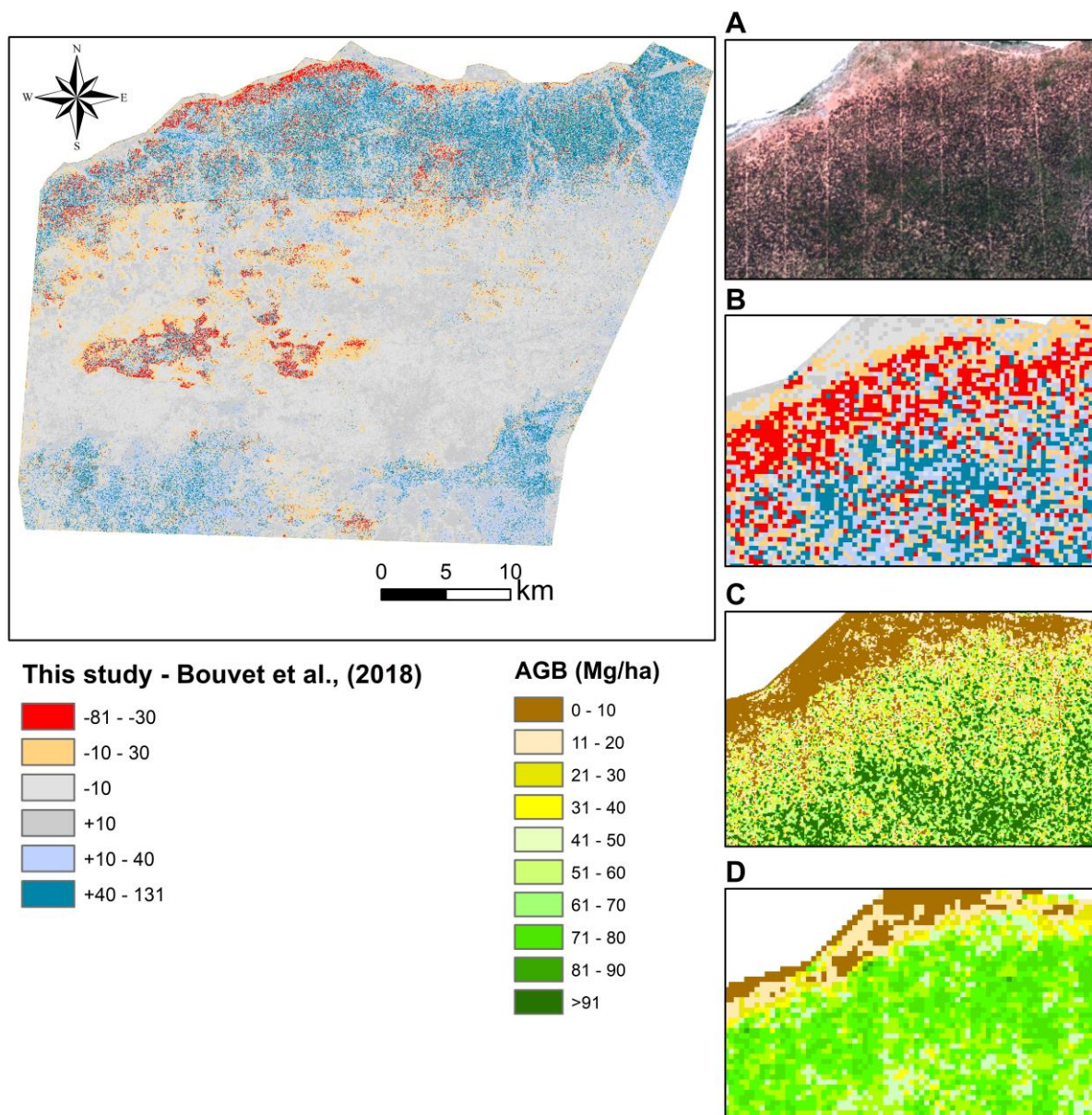
2941 Fig. 3. 10. Biomass map in a subset of forests in the (I) northern part of the study area and  
 2942 (II) Shimwanza valley. A: estimated AGB map by this study. B: estimated AGB map by  
 2943 Bouvet et al. (2018). C: estimated AGB map by Baccini et al. (2017). D: estimated AGB map  
 2944 by Avitabile et al. (2016). E: RGB 432 S2 image.

### 2945 3.4.4 Suitability of different models for land and wildlife 2946 management

2947 Optical Landsat imagery utilised by Baccini et al. (2017) was able to capture broad-  
2948 scale information on forest biomass but was less able to describe fine-scale  
2949 disturbance. Where it captured the patterns of biomass fragmentation, it mostly  
2950 overly overestimated AGB (Baccini et al., 2017). While Bouvet et al. (2018), using  
2951 ALOS PALSAR L-band, was effective in mapping biomass structural density, but it  
2952 was less capable at distinguishing biomass from degraded habitat areas, and  
2953 largely failed to capture biomass variability and relatively small-scale changes  
2954 associated with features such as roads, which were captured by this study and to a  
2955 larger extend by Baccini et al. (2017) (see: Fig. 3.11). The large discrepancies in  
2956 biomass distribution from Pan-tropical datasets can also be attributed to forest  
2957 masks derived from different land cover maps which excluded certain  
2958 woodland/vegetation types from their estimation. For example, Avitabile et al.  
2959 (2016) used the GLC2000 map from Bartholomé & Belward. (2005) as a forest  
2960 mask, while Bouvet et al. (2018) masked out forest classes (broadleaf evergreen  
2961 closed to open forest) using the ESA CCI Land Cover 2010 map from ESA (2014),  
2962 which can have a large impact on the estimation of biomass and carbon stocks in  
2963 dryland forests. The AGB map generated by this study is the most accurate and  
2964 detailed published for the study area and complements the global products,  
2965 therefore facilitating regional to international reporting of biomass and carbon  
2966 dynamics. This is in agreement with (Lucas et al., 2008) who utilised ALOS PALSAR  
2967 data and the Landsat-derived Foliage Projected Cover (FPC) in Queensland,  
2968 Australia, and reported that the combination of radar and optical data has the  
2969 ability to allow better assessment of deforestation patterns, regeneration and  
2970 woody thickening, tree death from climate change, and biomass change. In  
2971 addition, the AGB model from this study showed that biomass for dryland forests  
2972 exceeds estimates derived from pan-tropical products which underestimate  
2973 biomass and forests in dryland ecosystems of less-studied areas such as the KAZA  
2974 region, which are often neglected in this type of analysis (David et al., 2022a). The  
2975 sensor fusion explored here complements this study and encouragingly suggests a  
2976 high potential for separating biomass in dryland cover types that are structurally  
2977 distinct but spectrally similar, which are notably those areas that are challenging

2978 to distinguish through optical remote sensing alone (Buhne and Pettoirelli, 2018;  
2979 Treuhaft et al., 2004).

2980 In addition to sensor integration, issues of scale are critical for biomass and habitat  
2981 mapping, where the adequacy of spatial resolution is key (Buhne and Pettoirelli,  
2982 2018). For example, biomass mapping at a regional scale utilising the fusion of  
2983 optical and radar data in this study reduced the saturation effect at high AGB  
2984 values above 80 Mg/ha, allowing the identification of habitat fragmentation, and  
2985 small-scale degradation patterns of biomass compared to broader scale maps.  
2986 Maps of AGB, if sufficiently detailed, can assist conservation managers,  
2987 practitioners, and policymakers to formulate specific practices (e.g., corridor  
2988 planning, tree thinning, fire control, biodiversity surveys, etc.) that are appropriate  
2989 to support the conservation of forest habitats and their management. Many  
2990 countries presently lack the capacity to produce their own local maps of forest  
2991 biomass and so must rely on existing biomass maps founded upon broader pan-  
2992 tropical and global datasets. Whilst the AGB maps produced by Baccini et al.  
2993 (2017) and Bouvet et al. (2018) may be used to meet national-scale emissions  
2994 reporting requirements when no finer scale information is available, these maps  
2995 need to be validated against local forest stock surveys or local/regional AGB maps  
2996 from higher resolution satellite imagery. Given the decision-making on  
2997 sustainability at national and subnational levels, this study contends that the pan-  
2998 tropical and global data sets are unable to provide finer scale mapping of aspects  
2999 that are relevant to wildlife habitat and biodiversity in dryland forests. These  
3000 results support the assertion that countries should not rely on pan-tropical  
3001 datasets but should rather estimate biomass and carbon stocks at the regional and  
3002 local level, which in turn feeds into meeting the United Nations' Sustainable  
3003 Development Goals (SDGs), as suggested by Mitchard et al. (2013). This is essential  
3004 for land and forest management in these areas, particularly in protected zones,  
3005 given the vulnerability to anthropogenic pressure, disturbance from wildlife, and  
3006 climatic fluctuations.



3007

3008 Fig. 3. 11. A: RGB 432 S2 image. B: S2 a difference map between this study and Bouvet et  
 3009 al., 2018 (This study -Bouvet et al., (2018), C: This study AGB map. D: Bouvet et al., 2018  
 3010 AGB map.

3011

3012

3013

3014

### 3015 3.5 Conclusion

3016 This study combined satellite-based synthetic-aperture radar (SAR) and  
3017 multispectral imagery with ground truth data to map above ground biomass  
3018 throughout the dryland forests in the Chobe region of Botswana. The main finding  
3019 from the results is that using a combination of data types (SAR and multispectral  
3020 sensors) it is possible to estimate above ground biomass in dryland forests with a  
3021 good level of precision. The estimations of AGB reveal that the highest biomass  
3022 values of 80-145 Mg/ha were found in northern Chobe where the dominant tree  
3023 species are *Baikiaea plurijuga*, *Burkea africana*, and *Pterocarpus angolensis*. A large  
3024 part of the study area (85%) is characterised by low AGB values (< 80 Mg/ha). In  
3025 Southern Chobe and along the Chobe River frontage area, a high burning frequency  
3026 and degradation associated with overgrazing and elephant damage may have  
3027 contributed to the generally low AGB values observed. Three main conclusions can  
3028 be drawn from this study:

3029 First, combining freely available SAR and multispectral imagery (S1 and S2) has  
3030 the potential to estimate biomass at local and regional levels with a good level of  
3031 precision compared to using single sensors alone. The research observed that the  
3032 relatively fine resolution of Sentinel (10 m pixels) reduced the mixed pixel  
3033 problem observed in medium spatial resolution data (30 m pixels; e.g. Landsat 8),  
3034 which led to an increase in the precision of biomass estimation. The results  
3035 demonstrated that SAR backscatter in conjunction with the strategically positioned  
3036 optical bands (red edge wavebands) significantly improved forest stand parameter  
3037 estimations and the reduced saturation effect in areas of high biomass in dryland  
3038 forests. The NDRE1 and GNDVI yielded a higher linear relationship than NDVI,  
3039 while GRVI and EVI yielded the lowest correlation with AGB.

3040 Secondly, dryland forest ecosystems and conservation organisations can use global  
3041 and continental datasets as sources of information that could provide early  
3042 warnings of regional-scale ecological change. However, regional and local studies  
3043 are critical and serve to provide useful information in evidence-based decision  
3044 making for improved estimation of carbon stocks, monitoring the impacts of  
3045 climate change, and the conservation of dryland forest habitats under pressure.

3046 Finally, after comparing and analysing the effects of the various empirical models  
3047 using ML and RF regression approaches, this study found that the decision tree  
3048 model (RF regression algorithm) is the most robust for estimating AGB in dryland  
3049 forests, as compared to linear analysis. The precise and timely quantification of  
3050 AGB can help improve the understanding of dryland forest habitats and to plan and  
3051 monitor land and forest resources in conservation areas, which are critical for  
3052 wildlife function and sustainable land management at present and into the future.

### 3053 3.6 Acknowledgments

3054 This work was supported by Commonwealth Scholarship Commission PhD grant  
3055 number: NACS-2017-409 from the 2017–2020, Geography doctoral program at  
3056 Durham University. The authors acknowledge financial support from the Royal  
3057 Geographical Society (with IBG) - Monica Cole Research Grant (grant number: MC  
3058 08/19) and WWF Namibia Mike Knight for travel support grant number: T225. I  
3059 thank WWF KAZA TFCA Secretariat Dr Nyambe Nyambe, Chobe National Park  
3060 Authority Michael Flyman, and University of Namibia (Katima Branch) Dr.  
3061 Ekkehard Klingelhoefter for the support during the field. I also thank Morgan  
3062 Kamwi who helped with data collection.

3063

3064

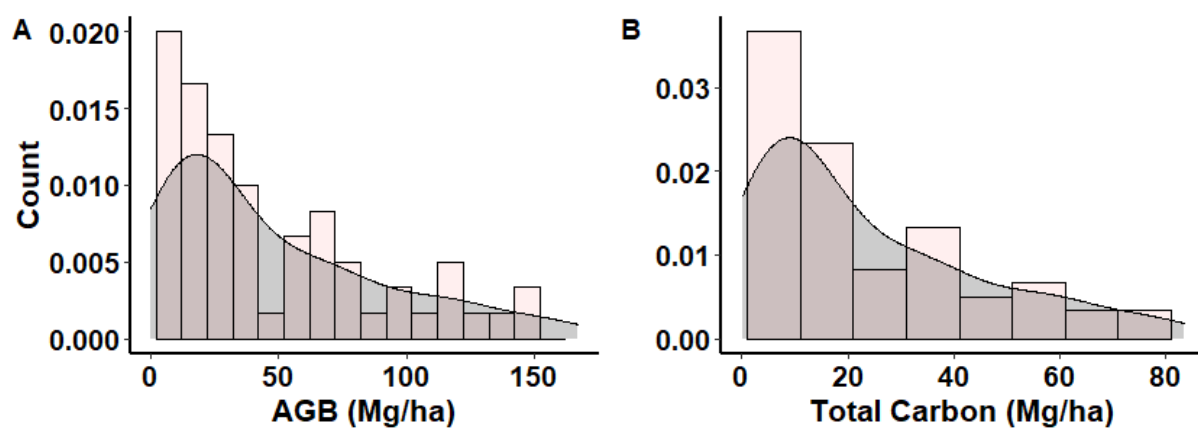
3065

## 3066 3.7 Supplementary Information 1

3067 Table A. 1. Image acquisition date and scene ID.

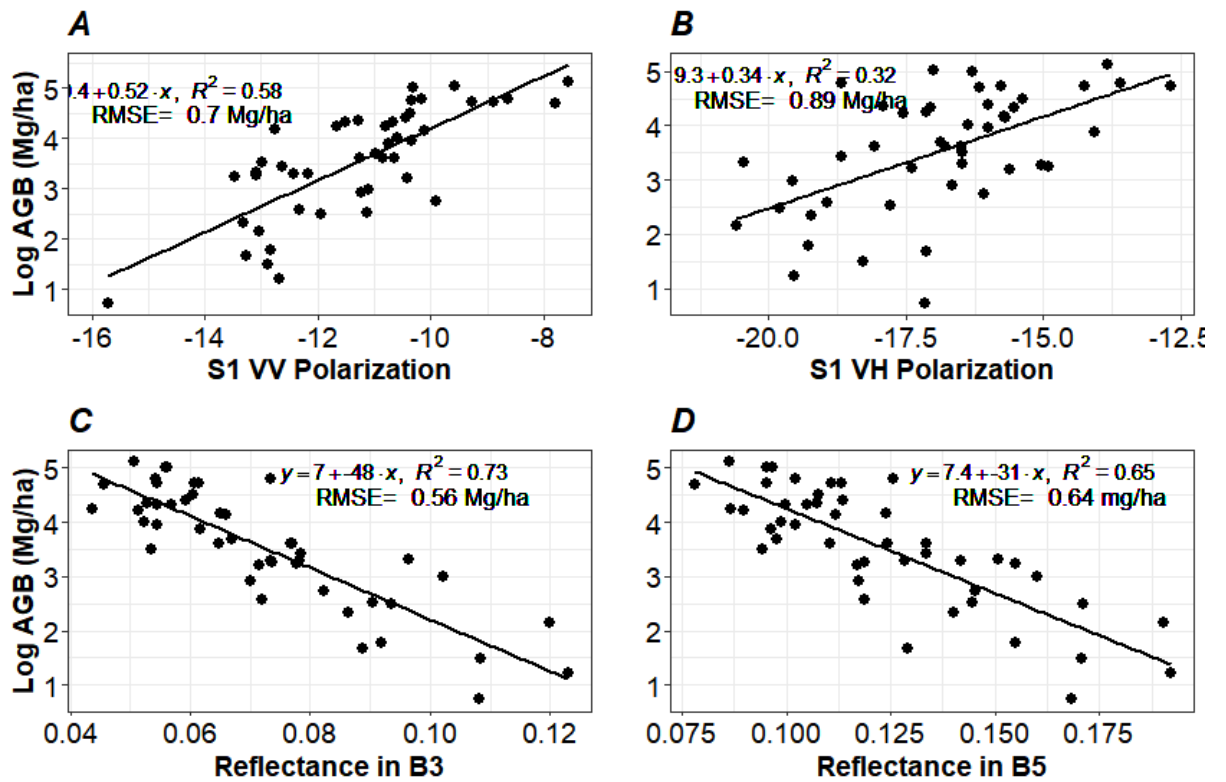
<i>Satellite</i>	<i>Cloud cover</i>	<i>Acquisition Date</i>	<i>Satellite Name</i>
S1	0	15/03/2019	COPERNICUS/S1_GRD
S2	0	14/03/2019	COPERNICUS/S2_SR/20190314T080709_20190314T083245_T35KKA
LC08	0	15/03/2019	LANDSAT/LC08/C01/T1_SR/LC08_174072_20190315

3068



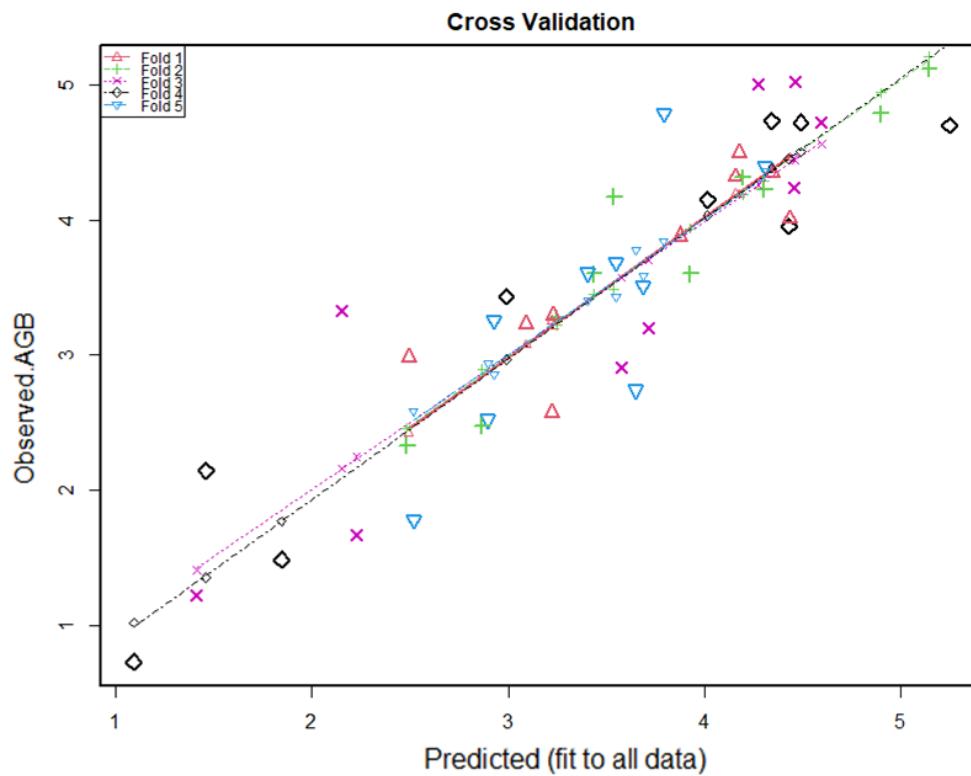
3069

3070 Fig A. 1. Density and histogram plots A: Aboveground biomass (AGB); B: Carbon stock  
 3071 (Mg/ha) of each field plot with woodland trees.



3072

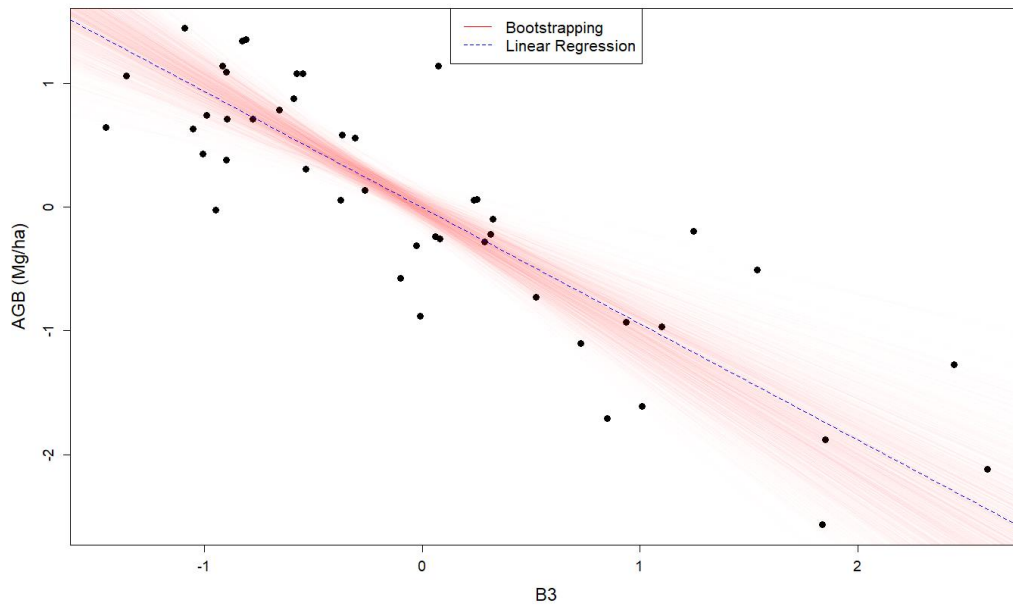
3073 Fig A. 2. Relationships of S1 polarisations and S2 spectral bands with stand forest  
 3074 parameters in the study area. A: S1 VV polarisation vs AGB. B: S1 VH polarisation vs AGB.  
 3075 C: S2 B3 vs AGB. D: S2 B5 vs AGB.



3076

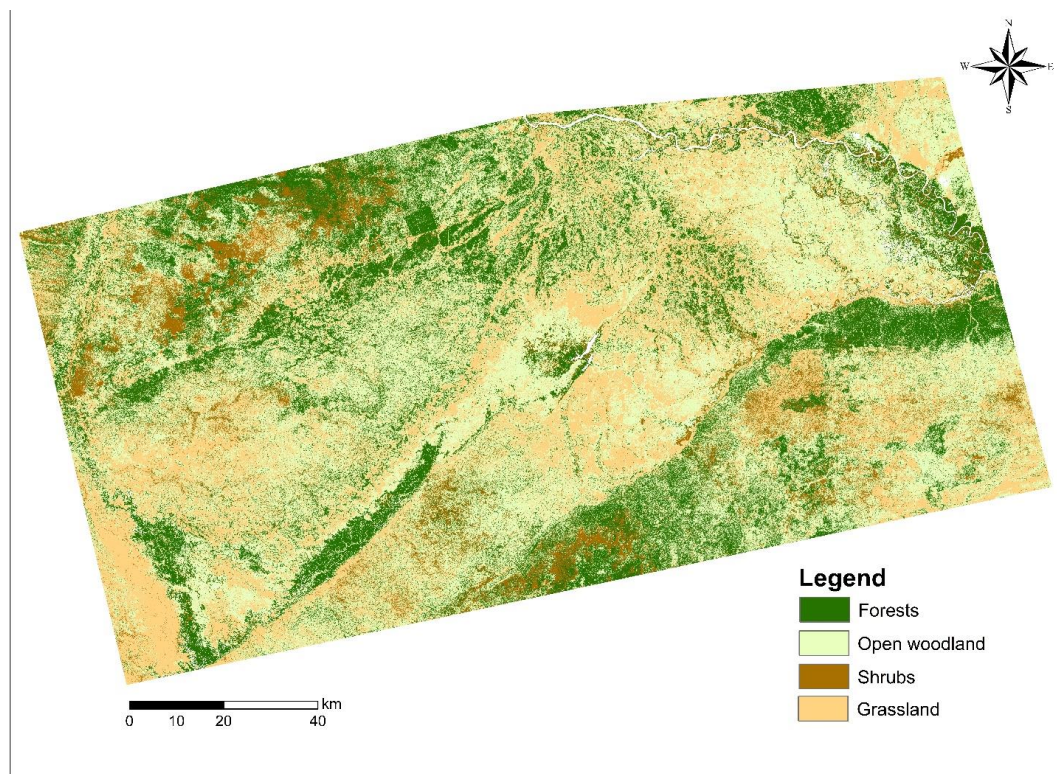
3077 Fig A. 3. Dispersion diagram of the observed versus predicted biomass at each fold on a log  
 3078 scale using 70% of the training data.





3079

3080 Fig A. 4. Linear and Bootstrap regression of Sentinel 2 Band 3 on a standardised scale.



3081

3082 Fig A. 5. Land cover classification map of Zambezi region in Namibia and Chobe District in  
3083 Botswana for 2019

3084

3085

3086 Table A. 2. Area statistics of the land cover classes.

<b>Land cover classes</b>	<b>Total Area (km<sup>2</sup>)</b>	<b>Percentage (%)</b>
Forests	4,475	23
Open woodland	8,216	43
Grassland	4,910	25
Shrubs	1,719	9
Sum	19,321	100%

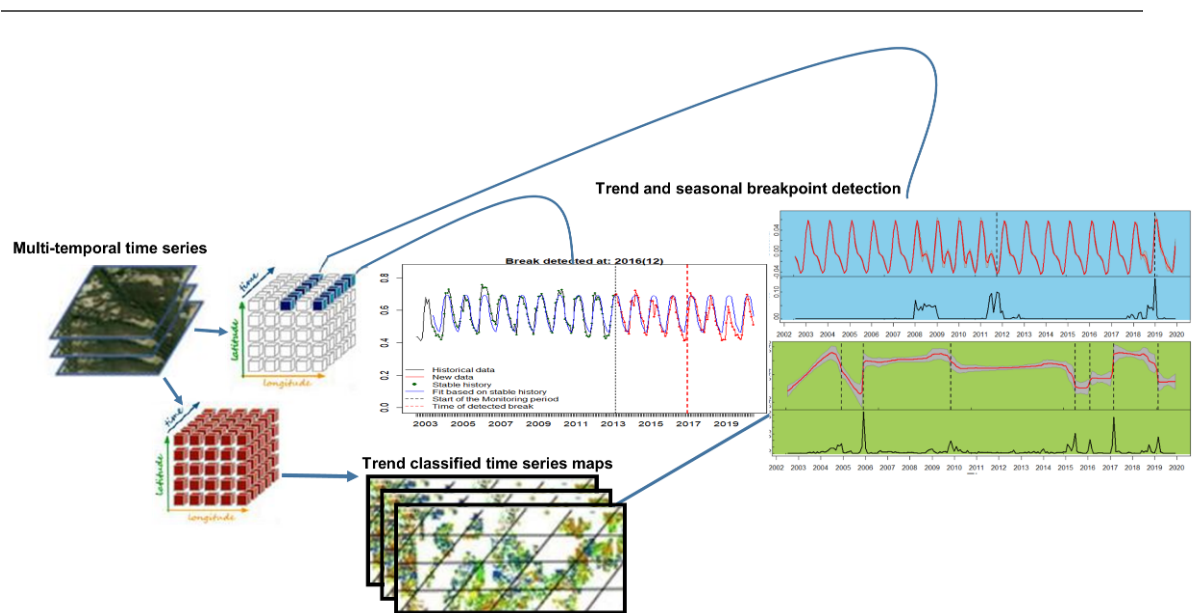
3087

3088 Table A. 3. Accuracy assessment of the land cover classification

<b>Accuracy</b>	<b>Percentage (%)</b>
Overall Accuracy	97%
Validation Overall Accuracy	67%
Kappa coefficient	60%

3089

3090 **4 IDENTIFYING AND UNDERSTANDING DRYLAND**  
 3091 **FOREST CHANGES AND DISTURBANCES IN SOUTHERN**  
 3092 **AFRICA USING LANDSAT AND MODIS TIME SERIES**  
 3093 **AND FIELD VEGETATION DATA**



3094

3095

3096

3097

3098 Chapter 4 Manuscript in progress: Intended for submission to *International Journal of*  
3099 *Applied Earth Observation and Geoinformation*.

3100

3101 **Title:** Identifying and understanding dryland forest changes and disturbances in  
3102 Southern Africa using Landsat and MODIS time series and field vegetation data.

3103

3104 **Author contributions**

3105

3106 David Ruusa- Design the research, perform the data analysis, interpret the results,  
3107 wrote the manuscript, and revised the manuscript. Nick Rosser- Contributed to the  
3108 research design, manuscript editing and supervision. Daniel Donoghue-  
3109 Contributed to the research design, conducting fieldwork, manuscript editing and  
3110 supervision.

3111

3112

3113

3114

3115

3116

3117 **Abstract**

3118 The Kavango Zambezi (KAZA) Transfrontier Conservation Area is sensitive to  
3119 water availability, and drought, in addition to anthropogenic disturbances, impacts  
3120 vegetation cover in the region. An effective method for change detection to  
3121 examine vegetation response across KAZA needs to account for seasonal as well as  
3122 abrupt changes over at fine temporal resolutions (e.g., monthly) rather than yearly  
3123 basis. In this study, an approach that quantifies dryland forest change by  
3124 combining Landsat and MODIS imagery with climate data, validated against  
3125 ground-based measurements collected from Namibia and Botswana was  
3126 presented. The Breaks for Additive Seasonal and Trend (BFAST), and Bayesian  
3127 Estimator of Abrupt change, Seasonality and Trend (BEAST) algorithms were  
3128 applied to evaluate their ability to detect changes in both long-term trend and  
3129 seasonality based upon the MODIS normalised difference vegetation (NDVI) and  
3130 Green normalised difference vegetation (GNDVI) time series. The results  
3131 demonstrate that there is a close relationship between the ground survey data and  
3132 the estimated changepoints. The Bayesian analysis (BEAST) was found to give the  
3133 best performance in identifying abrupt changes associated with fire, drought, and  
3134 seasonal changes driven by climate and clear-cutting events as compared to  
3135 BFAST. BFAST failed to detect seasonal shifts in the entire study period. GNDVI  
3136 was an effective dataset for detecting both small and large magnitude changes (e.g.,  
3137 deforestation, fire, and drought), while the NDVI was most effective in detecting  
3138 large magnitude changes, particularly those that resulted in complete land-cover  
3139 class changes (e.g., deforestation). The study found that the NDVI was more  
3140 influenced by canopy background variations and herbaceous layers when  
3141 detecting changes with regrowth of herbaceous layers than the GNDVI. Tropical  
3142 dryland forests in KAZA are highly dynamic and water-sensitive with high rates of  
3143 deforestation and widespread degradation, which mainly result in abrupt  
3144 vegetation changes, continuous vegetation recovery and regrowth. The approach  
3145 presented can accurately identify the vegetation changes, phenological variations  
3146 and time of disturbance in both the spatial and temporal domains. Therefore, it can  
3147 contribute to the understanding of forest decline and habitat changes and their

3148 vulnerability in the context of land cover change, climate change and sustainable  
3149 development policies in tropical dryland forests.

3150 **Keywords:** Change detection, Time-series decomposition algorithm, Forest  
3151 disturbance, Bayesian estimators, BFAST, Abrupt change, Southern Africa

## 3152 4.1 Introduction

3153 Tropical dryland forests experience a high degree of pressure from human activity  
3154 but monitoring forest degradation in these systems is challenging due to high  
3155 canopy complexity, phenology, climatic variability, and diverse degradation  
3156 drivers (Grainger, 1999, McElhinny et al., 2005, McNicol et al., 2018). Protected  
3157 Areas (PAs) underpin global efforts to preserve the Earth's biodiversity and  
3158 maintain functional terrestrial and aquatic ecosystems (Wiens et al., 2009). The  
3159 Kavango Zambezi Transfrontier Conservation Area (KAZA TFCA) is the largest  
3160 "hyper" hotspot for endemism and conservation support. However, the tropical  
3161 savanna forests and woodlands (hereafter referred to as "dryland forest") face an  
3162 increasing number of threats, ranging from those originating from climate,  
3163 disturbance by large mammalian herbivores, to those associated with the  
3164 increasingly invasive competition for diminishing resources. These multiple  
3165 threats have led to deforestation and degradation of protected landscapes, which  
3166 directly impacts wildlife species distributions (Cumming, 2008). Changes in  
3167 climate regimes and competition for the available natural habitats have  
3168 contributed to the escalation of human-wildlife conflict (HWC) in the KAZA region,  
3169 especially in Namibia and Botswana (FAO, 2009). Furthermore, climate modelling  
3170 of Africa has shown that dryland forest in and around KAZA TFCA is among the  
3171 world's most vulnerable at warming levels of 1.5–2.0° (IPCC, 2014).

3172 Monitoring long-term ecological processes in these PAs is therefore crucial to  
3173 ecological conservation and biodiversity (FAO, 2009). The possibility that arises  
3174 when changes are not monitored routinely is that the adverse impacts may have  
3175 already occurred and it may be too late to reverse the change or even adapt to it  
3176 (Sheffield et al., 2008). This will lead to large-scale destruction of important  
3177 habitats for many species and a dramatic decrease in wildlife habitats. Thus, for  
3178 conservation goals to be met, it is essential to detect whether vegetation changes

3179 and degradation are occurring within the forests of PAs and their causes.  
3180 Assessment of the regional impacts of land use and land cover (LULC) change are  
3181 fundamental for determining the appropriate policy responses to forest decline,  
3182 increased human-wildlife conflicts, and managing of animal movement patterns  
3183 and wildlife corridors in KAZA TFCA (Stoldt et al., 2020). Such efforts are equally  
3184 important for enhancing forest carbon sequestration and avoiding deforestation  
3185 for developing nations, as encouraged by Reducing Emissions from Deforestation  
3186 and forest Degradation (REDD+) schemes.

3187 In Africa, almost all remaining dryland forests in PAs are threatened by  
3188 deforestation and degradation and so should be given high conservation priority  
3189 (Clark et al., 2008). Although the focus in detecting forest cover loss using different  
3190 indices soon after they occur overwhelmingly remains in humid forests (Janzen,  
3191 1988; Masiello et al., 2020), dryland forests are beginning to receive more  
3192 attention. However, published studies on dryland forests in Africa are generally  
3193 concentrated on the Sahel in West Africa (Liu et al., 2017), while most studies in  
3194 Southern Africa have been confined to Kruger NP (Bucini et al., 2010).  
3195 Unfortunately, the forests in PAs of other parts of Southern Africa such as KAZA  
3196 TFCA have received far less attention. An additional challenge is understanding the  
3197 sensitivity and therefore suitability of conventional satellite-based NDVI  
3198 measurements in detecting large and small-scale forest disturbances and seasonal  
3199 change in highly heterogeneous forest environments such as drylands (Blackie et  
3200 al., 2014). The lack of historical disturbance events in KAZA TFCA constitutes a  
3201 challenge for in-depth temporal and spatial analysis which is crucial to ecological  
3202 conservation and biodiversity. This is raising concerns that disturbances within  
3203 the dryland, natural resources and wildlife habitat management areas might  
3204 increasingly interfere with continuous and sustainable provisioning of ecosystem  
3205 services to society and wildlife.

3206 The availability of MODIS satellite data and new automated data processing  
3207 techniques that provide high-quality continuous time-series data represent a  
3208 major advancement for the automated monitoring at monthly rather than annual  
3209 intervals which potentially masks considerable within-year variations. The daily  
3210 temporal resolution of the MODIS NDVI has a significant advantage over Landsat  
3211 data for monitoring the disturbance and recovery state. The limitation of MODIS

3212 based Vegetation Indices (VIs) for change detection is associated with the  
3213 moderate spatial resolution. With the advancement of cloud computing,  
3214 particularly the Google Earth Engine (GEE) platform, which provides an archive of  
3215 data including MODIS and Landsat with associated data processing capacity at no  
3216 cost (Gorelick et al., 2017), has become a valuable tool for change monitoring in  
3217 tropical environments. Access to such temporally rich time series has also led to an  
3218 increase in methods that aim to track the occurrence of disturbance events at  
3219 regional scale. It is reported that disturbance rates in dryland forests have  
3220 increased in recent decades, and there is evidence that climate change and past  
3221 land use both have contributed to the disturbance increasing rate (Wilcox, et al.,  
3222 2011). Continuous disturbances in an area consisting of natural habitats result in  
3223 habitat fragmentation and reduce its ability to support the ecosystems and  
3224 surroundings that are essential for their sustainability (Visscher, 2006). The  
3225 accurate reconstruction of past forest disturbance dynamics at spatial, temporal,  
3226 and thematic scales offered by time series will allow ecological analyses to help  
3227 provide a better understanding of disturbance regimes (Senf et al., 2017). The  
3228 dense time series information enables the quantification and characterisation of  
3229 disturbances in terms of disturbance magnitude, duration, and attribution of  
3230 recent disturbance activities (Kennedy et al., 2012). Before the availability of time  
3231 series analysis, forest change detection mapping was done using bi-temporal  
3232 differences or supervised image classifications (David et al., 2022a). Bi-temporal  
3233 image classifications were able to detect large-scale deforestation, but they are less  
3234 useful for assessing small-scale deforestation, degradation, and regrowth because  
3235 they fail to capture the dynamic behaviour of vegetation during the year and over  
3236 longer time periods (Hamunyela et al., 2020; Zhu and Woodcock, 2014). Moving  
3237 from a relatively static, bi-temporal view of change toward a more continuous view  
3238 of ecosystem dynamics can improve understanding regarding the disturbance's  
3239 spatiotemporal patterns, their causes, and consequences (Kennedy et al. 2014).  
3240 Effective change detection ideally identifies variations at the seasonal scale while  
3241 simultaneously detecting abrupt, and subtle changes in any long-term trends.  
3242 Breaks For Additive Seasonal and Trend (BFAST), BFAST Seasonal and Bayesian  
3243 Estimator of Abrupt change, Seasonality and Trend (BEAST) algorithms have been  
3244 developed to do this (Verbesselt et al., 2012; Zhao et al., 2019). However, their



3245 effectiveness in tropical dryland forests, where vegetation response is typically  
3246 aseasonal, has yet to be assessed.

3247 This paper aims to provide a systematic assessment of vegetation dynamics and  
3248 spatially detailed patterns of change in the dryland forests. To do this, the research  
3249 employs multiple data streams for the time series assessment of forest change over  
3250 parks and surrounding areas within KAZA TFCA from 2002–2019. The premise is  
3251 that by taking advantage of the different characteristics of vegetation indices and  
3252 different change detection model, change detection results could be improved in  
3253 dryland forests. The general objective was to investigate the evidence of water  
3254 stress conditions and assess the suitability of the change detection model on  
3255 MODIS time series data for mapping forest disturbances (e.g., clear-cutting,  
3256 drought) in dynamic and diverse tropical dryland forests. Specifically, this paper  
3257 reports three steps: (1) spatial characterisation of climatic data with vegetation  
3258 indices as a proxy indicator of climate variability to improve understanding of  
3259 vegetation response to drought; (2) Compare the commonly used NDVI vegetation  
3260 index with GNDVI and evaluate their sensitivities and performances in detecting  
3261 changes; and (3) Characterise changes in trends and phenological patterns using  
3262 BFAST and BEAST algorithms. (4) Quantify and identify the LULC change,  
3263 locations, types, and trends of the land cover during the 19-year period in  
3264 communal and protected areas of Zambezi region. Ideally, such an analysis will  
3265 provide conservation efforts with frequently updated information for monitoring  
3266 disturbances and potentially deforested areas, allowing targeted mitigation actions  
3267 to be taken.

3268

## 3269 4.2 Materials and methods

### 3270 4.2.1 Study area

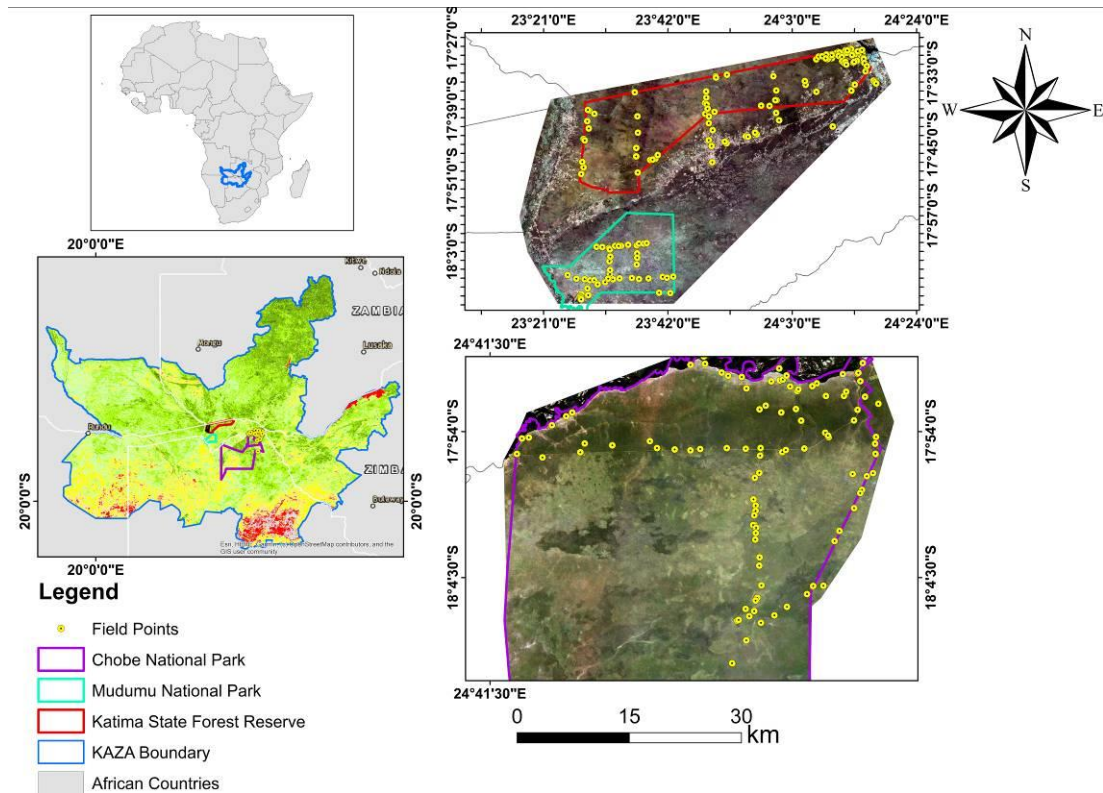
3271 The KAZA TFCA (18.00°S, 23.00°E) in Southern Africa, is an iconic PA that inhabits  
3272 a rich ecology and enormous wildlife. KAZA TFCA is established in March 2013  
3273 with an enclosed area equivalent to the size of France at 519,912 km<sup>2</sup> (Cumming,  
3274 2008), and is situated in the Kavango and Zambezi River basins- and is shared by

3275 Angola, Botswana, Namibia, Zambia, and Zimbabwe. Within this area, 371,394 km<sup>2</sup>  
3276 are under conservation and the remaining 148,520 km<sup>2</sup> are mainly used for  
3277 agricultural activities including rangeland.

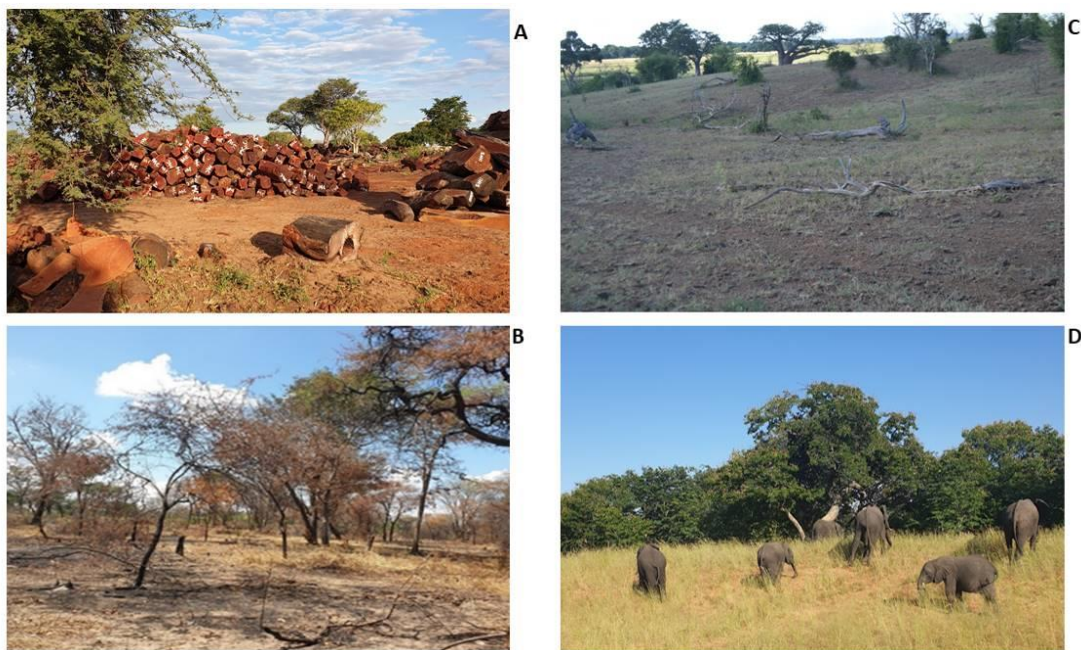
3278 This conservation area is considered to be an important means to create economic  
3279 development and conserve the unique biodiversity by establishing links between  
3280 fragmented habitats with a particular focus on large-scale migrations of wildlife  
3281 (WWF, 2016). KAZA links together over 36 proclaimed PAs including national  
3282 parks (NPs), forest reserves, community conservancies, and wildlife management  
3283 areas. PAs carry substantial populations of large mammals and several plant  
3284 endemic plant species, including large areas of the dryland forests, and globally  
3285 significant wetlands. The dryland vegetation domain in KAZA ranges from forest  
3286 formations with a dense canopy cover to shrubs and grasslands ranges, which are  
3287 also considered a biodiversity hotspot. However, these areas are under severe  
3288 pressure from agricultural expansion and settlement, wildlife, large-scale burning,  
3289 and timber harvesting (NACSO, 2014) (see: Fig. 4.1). This study focuses on the  
3290 Namibian and Botswanan components of the KAZA TFCA. In particular, the study  
3291 was conducted in three protected areas situated in the Okavango Zambezi region:  
3292 (a) Chobe NP in Botswana, (b) Zambezi state forest (ST) in Namibia, and (c)  
3293 Mudumu NP in Namibia. The selection of study sites depended on the ecological  
3294 importance and the land conservation practices implemented within the region.  
3295 The selection of sites in Namibia included state-run protected areas such as  
3296 Zambezi state forest (red-coloured polygon), a conserved forest area which was  
3297 traditionally protected by the government and residents in the area (see: Fig. 4.1).  
3298 Zambezi state forest is designed to be only used sustainably used for timber and other  
3299 forest products but has now been pushed back by human settlement (Bollig and  
3300 Vehrs, 2021). The Mudumu National Park (Aqua-coloured polygon) is one of the  
3301 largest protected areas in the Zambezi region established as a core wildlife area  
3302 with animals migrating from the park to surrounding communal conservancies,  
3303 where they can be used for quota hunting or through tourism (O'Connell et al.,  
3304 2000). The unprotected surrounding communal area including the communal  
3305 conservancies that depend on agriculture and tourism development and both  
3306 encroach on the dryland forests (Hank, 2003).

3307 The Chobe NP, in the north-east of Botswana (18.7°S, 24.5°E), features the largest  
3308 number of elephants in KAZA; the number of elephants in northern Botswana  
3309 alone is estimated at more than 156,000 (Junker, 2009). The Chobe River basin  
3310 serves as a source of surface water for the Chobe District and in the dry season,  
3311 animals converge on this stretch of water from Northern Botswana (Hanks, 2003).  
3312 Chobe NP contrasts with the Namibian component of KAZA TFCA. The Zambezi  
3313 Region (17.8° S, 23.9° E), in the heart of KAZA, is a long strip of land with multiple  
3314 land uses, containing several national parks much smaller by comparison to Chobe  
3315 NP. The Mudumu NP, in north-eastern Namibia, and is bordered by the Kwando  
3316 River. The park is in the centre of KAZA TFCA and as there is no boundary fence, it  
3317 acts as a corridor for large game species such as African elephants, as migrating  
3318 between Botswana, Zambia, Angola, and Zimbabwe. The Zambezi ST area is  
3319 surrounded by conservancies and communally governed areas. The Zambezi ST  
3320 generally features very high population densities with consequent overgrazing and  
3321 widespread unsustainable wood harvesting with many areas considered now  
3322 degraded.

3323 Topography in both parks is relatively flat characterised by low elevations ranging  
3324 from 910 to 1100 m above sea level (Omphile et al., 2002). Climatically, the sites  
3325 have similar rainfall patterns throughout the year, and so the KAZA region has a  
3326 subtropical dry climate characterised by highly variable rainfall. The annual  
3327 average rainfall is approximately 650 mm, with almost all falling between  
3328 November to March, followed by a dry season from April to October. Daytime  
3329 temperatures increase towards the end of the dry season, when the heat soars and  
3330 the expectation of rain is high. Average temperatures range between 15.2°C -  
3331 30.2°C.



3332



3333

3334 Fig. 4. 1. Location of the study area in KAZA TFCA. The yellow circles show sampling sites  
 3335 in Zambezi ST, and Mudumu NP Namibia (top), and Chobe NP (bottom). Examples of  
 3336 sample plots representing disturbance types and recent degradation activities captured  
 3337 during a field campaign in 2019 are shown, A) clear-cut deforestation of forest area in  
 3338 Zambezi ST Namibia, B) Burned forest for cultivation near protected area of Mudumu NP,  
 3339 Namibia, C) the visible forest loss, especially the woodland along the Chobe riverfront, D)  
 3340 high population of elephants destructive influence on vegetation.

## 3341           4.2.2 Fieldwork and sampling design

3342 Survey fieldwork was undertaken to record forest tree stands and observe the  
3343 different land cover types present in the study area during the growing season (1st  
3344 February - 30th April 2019). The field samples of the five main land cover classes  
3345 (forests, open woodland, shrubs, grassland, and bare land) were collected at three  
3346 sites in the KAZA TFCA region; one park was located in Botswana, the Chobe NP.  
3347 The other two sites are located in Namibia - the Mudumu NP, and Zambezi ST (see:  
3348 Fig. 4.1). These sites were chosen because dryland forests within and around the  
3349 PAs are particularly susceptible to disturbance and drought, warranting particular  
3350 attention (Feng et al., 2013). However, these areas are often remote and dangerous  
3351 to visit in the field, due to the hazard posed by wildlife and if present, unexploded  
3352 landmines (see: Fig. 4.1). Another challenge is there are very little plot data in the  
3353 dryland forests, which are more sensitive to inter-annual variations in climate than  
3354 humid forests (Grainger, 1999). This is particularly true for the forest in the KAZA  
3355 region that experienced several extreme droughts in recent.

3356 The allocation of plots followed a stratified random sampling approach based on  
3357 the four strata (forest, open woodland, scattered trees with low herbaceous cover,  
3358 and non-forests). The plot sizes of (20 m × 20 m) and (10 m × 10 m) were  
3359 considered adequate to enable sampling a good number of trees in each plot.  
3360 Smaller plot sizes of (10 m × 10 m) were adopted only in areas of very high tree  
3361 density that were dangerous to visit due to the hazard posed by wildlife. In total,  
3362 measurements were collected from 271 individual sample plots randomly  
3363 distributed throughout the dryland landscape. A total of 101 plots in Chobe NP,  
3364 115 plots in Zambezi ST, and 50 plots in Mudumu NP were visited. In Botswana, 61  
3365 sample plots represent woody vegetation, 40 sample plots represented non-  
3366 woodland cover, while in Namibia 95 sample plots represent woody vegetation,  
3367 and 75 represented non-woodland cover. The total number of individual trees  
3368 measured was 4337 in Botswana, 2400 trees in Zambezi ST, and 1600 trees in  
3369 Mudumu NP. For each tree inside the plot, mean height, diameter at breast height  
3370 (DHB), tree density, canopy closure, and tree species were recorded. The UTM  
3371 coordinates at the centre of each plot were taken with the hand-held GPS. Although  
3372 the coordinates of each plot centre were collected with a high-quality device with

3373 GPS and GLONASS sensors, there may be small positional errors, especially when  
3374 differential corrections are unavailable (errors up to 8–10 m are common). The  
3375 images used in this chapter have a spatial resolution of 30 m for Landsat and 500m  
3376 for MODIS data which have a coarser pixel size which compensated for the  
3377 possible positional error of the GPS used. Heights of individual trees were  
3378 measured using an ultrasonic Vertex III hypsometer which requires finding a  
3379 suitable position to observe each tree tip (Božić et al., 2005), while stem diameter  
3380 was measured using a Diameter above Breast Height (DBH) tape. The diameters of  
3381 all the trees in each plot were measured at breast height, which is at 1.37 m above  
3382 the ground surface. All trees with a stem diameter >3 cm and 1.5 m height were  
3383 recorded. Field surveys of woody plants were conducted on sites where damage to  
3384 plants was specifically observed to identify where drought had an obvious impact.

#### 3385 4.2.3 CHIRPS precipitation data

3386 Climate data were selected under the assumption that plant growth in the region is  
3387 limited by water availability, temperature, and/or incident radiation (Field et al.,  
3388 1995). Changes in either of these parameters might induce changes in vegetation  
3389 productivity and the proxy NDVI signal. For this region, water availability is  
3390 determined by the amount of precipitation, and so the study confined this  
3391 parameter to precipitation as productivity here is water rather than temperature  
3392 limited (Nemani et al., 2003). However, for most parts of Africa, and especially the  
3393 semi-arid lands, the network of climatological stations is not dense enough to  
3394 provide a coherent spatial picture of climate variability. As a result, the spatial  
3395 characterisation of the effects of drought events on the land surface is not well  
3396 defined. The study used satellite-based monthly precipitation estimates from the  
3397 Climate Hazards Group InfraRed Precipitation with Station data (CHIRPS) product  
3398 ( $0.05^\circ \times 0.05^\circ$ ). CHIRPS data span from 1981 to the present. CHIRPS incorporates  
3399 in-situ station data and CHPclim,  $0.05^\circ$  resolution satellite imagery to represent  
3400 sparsely gauged locations such as Southern Africa (Funk et al., 2015a). To be  
3401 consistent with MODIS VIs, the CHIRPS rainfall data from 2002 to 2019 was used.

#### 3402 4.2.4 Vegetation indices from remote sensing imagery

3403 The vegetation datasets used in this study include NDVI and GNDVI greenness  
3404 vegetation indices derived from the MODIS sensors. The vegetation indices use the  
3405 wavelength and intensity of the reflected light within the visible and near-infrared  
3406 wavelengths to measure the density of green leaf vegetation, acting as proxies for  
3407 leaf area index (LAI), fractional vegetation cover, and photosynthetic capacity  
3408 (Broge et al., 2001). Generally, the plant is under stress when there is a change in  
3409 the health condition of the plant foliage, reflected by a corresponding decrease of  
3410 LAI. Under stress conditions, plants increase their reflectance in the green and red  
3411 portions as leaves become yellowish or chlorotic. This has led to the suggestion  
3412 that the VIS portion is the most consistent leaf reflectance indicator of plant stress  
3413 (Carter, 1993).

3414 The Normalised Difference Vegetation Index (NDVI) is a commonly used  
3415 vegetation index that measures green healthy vegetation as it utilises the regions  
3416 of the electromagnetic spectrum most associated with high absorption of  
3417 chlorophyll in the red band, and high reflectance of NIR by mesophyll layers in  
3418 green leaf biomass (Rouse, 1974). It is calculated as a normalised ratio between  
3419 Red and NIR reflectance values (Eq. 4.1). Higher NDVI values suggest higher  
3420 amounts of photosynthetic active biomass. The NDVI was used in this study  
3421 because it is a biophysical parameter that correlates with the photosynthetic  
3422 activity of vegetation and is an indicator of the greenness of the biomes (Robinson  
3423 et al., 2017; Tucker, 1979). NDVI is also able to offer valuable information to  
3424 monitor vegetation health, drought effects, changes in plant growth, land  
3425 degradation, deforestation, change detection/monitoring, and in relating large-  
3426 scale inter-annual variations in vegetation to climate (Smith et al., 2019).  
3427 Restrictions, however, have existed due to the effects of external factors, for  
3428 example, soil and dead material, solar and viewing geometry as well as  
3429 meteorological events, all of which pose a challenge in carrying out a proper  
3430 assessment (Zhu et al., 2012). Particularly, in drylands with generally low  
3431 vegetation canopy cover, the soil background tends to significantly influence NDVI,  
3432 leading to a need for further development of vegetation indices. The study includes  
3433 another greenness index, which is a variation of the NDVI and designed to reduce

3434 saturation issues identified with this index. The GNDVI is computed similarly to the  
 3435 NDVI, but the Green band is used instead of the Red band (Eq. 4.2) (Gitelson et al.,  
 3436 1996). Thus, GNDVI is more sensitive to chlorophyll concentration than NDVI and  
 3437 ranges from 0 to 1.0. It is related to the proportion of photosynthetically absorbed  
 3438 radiation and is linearly correlated with Leaf Area Index (LAI) and biomass (Hunt  
 3439 et al., 2008). By exploring various combinations of available spectral bands, the  
 3440 study additionally examined the sensitivity of other indices such as MSAVI, EVI to  
 3441 find the most sensitive VI to detect changes in the dryland forest. MSAVI and EVI  
 3442 were outperformed by GNDVI and thus GNDVI is presented in comparison to NDVI.  
 3443

$$\text{NDVI} = \frac{\text{NIR} - \text{Red}}{\text{NIR} + \text{Red}} \quad (\text{Eq. 4. 1})$$

$$\text{GNDVI} = \frac{\text{NIR} - \text{Green}}{\text{NIR} + \text{Green}} \quad (\text{Eq. 4. 2})$$

3444 Table 4. 1. Characteristics of the main datasets used in this study

<i>Climate Data</i>					
<i>Dataset</i>			<i>Timespan</i>	<i>Resolution</i>	<i>Source</i>
MODIS	8-day	Terra	2002-2019	500m	GEE
Surface	Reflectance	(MOD09A1.006)			
Climate Hazards Group	InfraRed Precipitation with Station Data (CHIRPS)		2002-2019	0.05 degrees	GEE
<i>MODIS vegetation Data</i>					
Terra Surface Reflectance 8-Day Global 500m			2002-2019	500m	GEE



(MOD09A1.006)			
<b><i>LANDSAT Data</i></b>			
Landsat 5 ETM sensor- Surface Reflectance	2002-2012	30m	GEE
Landsat 8 OLI sensor- Surface Reflectance	2013-2019	30m	GEE

#### 3445 4.2.5 Landsat Imagery

3446 In the Google Earth Engine platform, 2004 Landsat-5 TM (Thematic Mapper and 2019  
3447 Landsat-8 OLI (Operational Land Image) surface reflectance 30 m spatial resolution  
3448 satellite images were utilised for landcover cover classification over the study region  
3449 (Gorelick et al., 2017). For both Landsat 5 and Landsat 8 data, only optical 30 m spatial  
3450 resolution spectral bands (visible and infrared) were selected for classification. Bands 1  
3451 and 9 were not used due to strong atmospheric absorption. The study aims to use  
3452 Landsat images from 2002 for the classification, however, the year 2002 had 0 images  
3453 available for the study site, while 2003 had 5 images available for the study area, and  
3454 they only cover 1/5 of the study area. Therefore, the Landsat images for 2004 were used  
3455 because it was the closest date to 2002 with a total of 35 available images which cover  
3456 the whole study area. In 2019, a total of 84 images were available and selected for  
3457 classification.

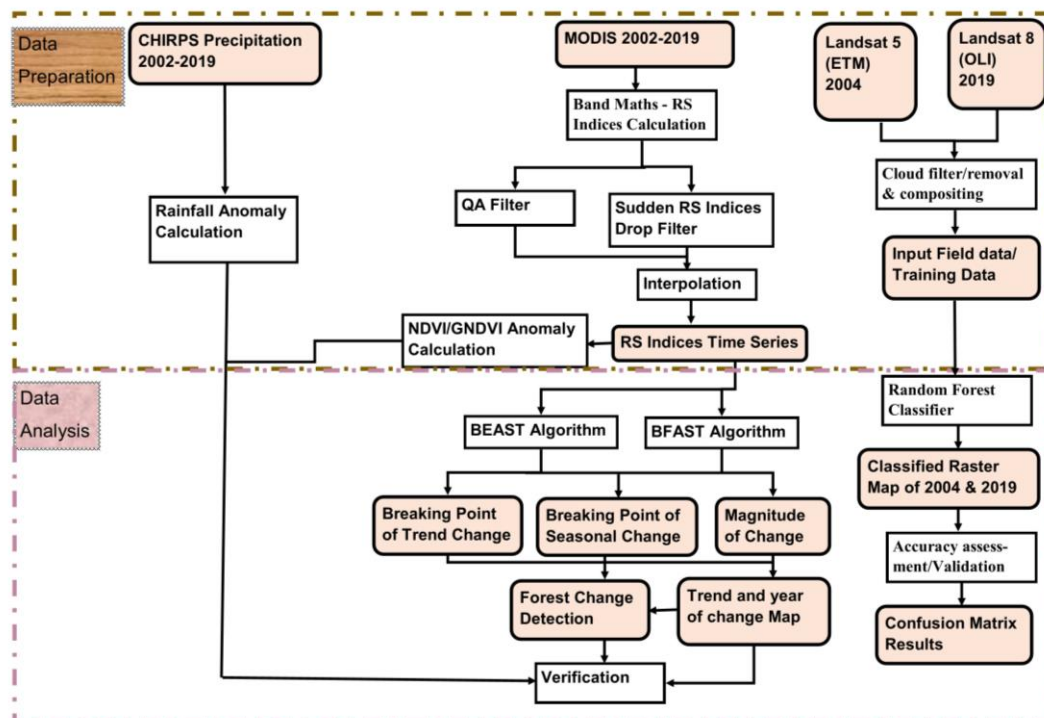
#### 3458 4.2.6 Validating data

3459 The ground field sample points were used to validate the change detected by the  
3460 algorithms. The verification was carried out quantitatively using field data  
3461 collected from the field and the classified/change maps by generating a confusion  
3462 matrix to assess the effectiveness of the land cover classification generated by the  
3463 Random Forest classification in section 4.3.5. The BFAST change detection was  
3464 validated using an area change using sample-based estimates in section 4.3.6.  
3465 Additional verification was also conducted through visual interpretation of the  
3466 Landsat surface reflectance 30 m spatial resolution satellite images  
3467 (LANDSAT/LT05/C01/T1\_SR) and (LANDSAT/LC08/C01/T1\_SR) that are  
3468 atmospherically corrected using LEDAPS and using LaSRC to ensure the data

3469 consistency and comparability (see: Table 4.1) (Claverie et al., 2015). The  
3470 acquisition date of the Landsat image in which the disturbance event was first  
3471 visible was used as a surrogate time for when the disturbance has occurred, and  
3472 such data was used to verify the detected changes of BFAST and BEAST and note  
3473 the timing of the change. This interpretation is commonly used by other  
3474 comparable studies on change detection using BFAST (Cohen et al., 2010; Dutrieux  
3475 et al., 2015). Using high resolution data, Cohen et al. (2010) used visual detection  
3476 of a large proportion of historic change processes in the forest. Their study  
3477 highlighted the importance of visual interpretation technique of change points  
3478 using high resolution images and photo interpretation because historic events can  
3479 be very difficult to ascertain. For example, DeVries et al. (2015) and Hamunyela et  
3480 al. (2016) visually examined the Landsat image time series data to validate forest  
3481 change occurred for a specific pixel detected using BFAST algorithm. Zhao et al.  
3482 (2019) developed the BEAST algorithm (also tested in this study) and visually  
3483 validated the ground-reference data on disturbances and changepoints by  
3484 interpretation of multisource imagery.

### 3485 4.3 Methods

3486 An overview of the methods for this research is shown in Fig. 4.2. The four main  
3487 steps were as follows: (1) high-quality NDVI time series data preparation. A time  
3488 series was first pre-processed to remove noise and obtain an uninterrupted data  
3489 stream. (2) Temporal and spatial analysis of climate and vegetation time series to  
3490 detect anomalies and drought impacts. (3) Trend and seasonal breakpoint  
3491 detection using BFAST and BEAST algorithms. (4) Validation of the change  
3492 detection algorithms and discussion of the potential factors driving vegetation  
3493 change.



3494

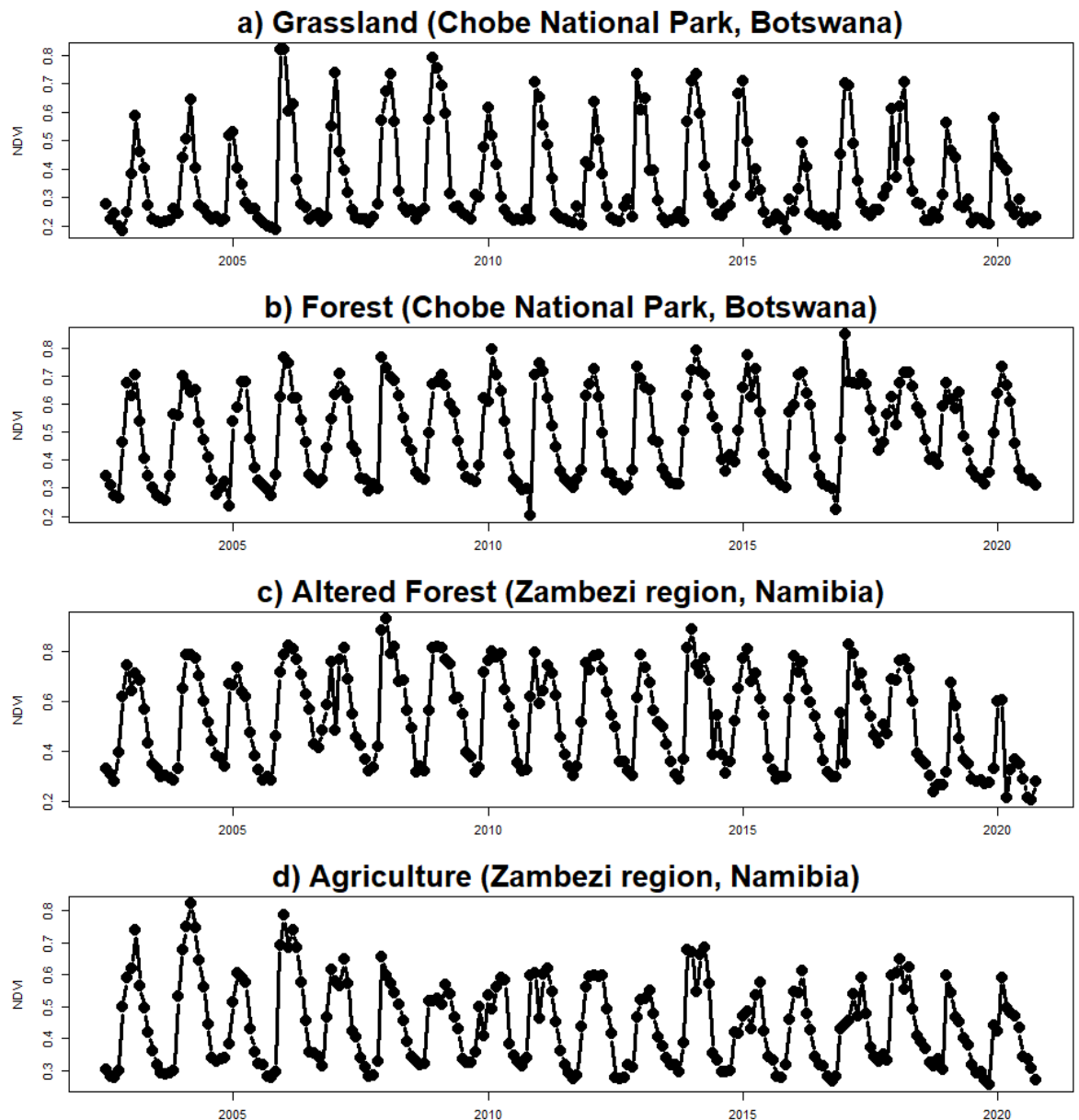
3495 Fig. 4. 2. Flow chart of data and methods.

3496 

### 4.3.1 Preparation of high-quality MODIS datasets

3497 Satellite image time series are rarely complete. Noise in a time series is brought  
3498 about by cloud contamination and other factors such as snow or device  
3499 malfunction (Vermote et al., 2002). Tropical environments such as Southern Africa  
3500 present a unique challenge for optical time series analysis, primarily owing to  
3501 fragmented data availability, persistent cloud cover, and atmospheric aerosols.  
3502 Pre-processing is necessary to reduce this noise because it may conceal actual  
3503 trends in a time series. In this study, although the monthly maximum value  
3504 composite (MVC) method has been used to decrease cloud and other atmospheric  
3505 effects in the original VIs data (Holben, 1986), residual noise resulting from poor  
3506 atmospheric conditions, cloud cover, aerosol loading and unfavourable sun sensor  
3507 surface viewing geometries remain (Huete et al., 2002). Therefore, the  
3508 corresponding MODIS quality assurance (QA) data layer was used to help identify  
3509 and remove low-quality observations, and only the time points in a time series that  
3510 are higher quality, cloud-free, and have nadir-view pixels with minimal residual  
3511 atmospheric aerosols are retained. The cloud-contaminated pixels and extreme off-  
3512 nadir sensor view angles are considered lower quality were excluded from the  
3513 composite.

3514 In addition to the QA data, to retain good quality values throughout the time series,  
3515 an assessment for data transmission errors, such as line drop out or moving from  
3516 cloudy to clear sky conditions, which can cause localised Vegetation Indices (VIs)  
3517 to increase or suddenly drop, were conducted. These fluctuations in VIs are not  
3518 compatible with the gradual process of plant regrowth. The algorithm uses a  
3519 threshold of 20% as an acceptable percentage increase in VIs for regrowth from  
3520 fire or drought for arid/semi-arid dryland grassland though to dryland forests  
3521 (Viogy et al., 1992). A low filtering threshold means that most MODIS VIs pixels  
3522 with high-frequency noise related change are included, while a high filtering  
3523 threshold produces a smoother temporal profile and can smooth out important  
3524 changes. This study used a 20% threshold to reject fluctuations attributed to data  
3525 errors. By utilising the MVC, QA data, and implementing the test for sudden drops,  
3526 the observation points contaminated by noise were detected and discarded from  
3527 the time series. The presence of contaminants such as clouds and cloud shadows,  
3528 caused anomalous values which can be detected and removed to some degree,  
3529 leaving gaps in the time series (see: Fig. B. 1). As with noise, robustness to missing  
3530 data is therefore a crucial component to evaluate when considering change  
3531 detection methods, especially when applying change detection to parts of the  
3532 world with persistent cloud such as Southern Africa. The missing values at those  
3533 points were then filled by implementing a linear average interpolation method  
3534 (see: Fig. B. 1). However, this method still requires a time series of images with low  
3535 cloud cover. The linear interpolation method has been proven to be efficient, and  
3536 most of the time it is better than non-linear interpolations for predicting missing  
3537 values in ecological phenomena time series (Gnauck, 2004). Fig. 4.3 shows the time  
3538 series of the main land cover present in the study area, including forest, grassland,  
3539 altered forest, and agricultural land.



3540

3541 Fig. 4. 3. Time series representing forest, grassland, altered forest, and agricultural land.

3542

3543 

### 4.3.2 Vegetation and precipitation time series anomaly

3544 Here, satellite data was used to first quantify the extent and severity of rainfall  
 3545 anomalies and droughts with respect to long-term patterns, with a baseline of 17  
 3546 years, and then to investigate the impacts of droughts and water stress on the  
 3547 dryland forest vegetation. The study focused on summer vegetation activity during  
 3548 the growth period. Hence the main season of interest here is January–March (JFM)  
 3549 since it is a period that contributes significantly to the summer rainy season across

3550 Southern Africa and approximately coincides with the mature phase of El Niño  
3551 (Lyon et al., 2007).

3552 For this study, to identify and map the spatial extent of drought response in  
3553 vegetation, the NDVI and GNDVI anomalies for a different season (the growing  
3554 season is presented) for the KAZA region are calculated relative to a base period of  
3555 2002–2019. The anomalies are constructed by subtracting the growing season VIs  
3556 (calculated over 2002–2019) from the long-term mean patterns for that period  
3557 (e.g., month or seasons). The departures from a base mean period are used to  
3558 detect periodic temporal patterns in VIs. This isolates the variability in the  
3559 vegetation signal and establishes a meaningful historical context to determine  
3560 relative drought severity. The NDVI and GNDVI anomaly was calculated using  
3561 MODIS data. The 2010 to 2019 period is presented because it is representative of  
3562 the record of the 21st century where drought events are extreme.

### 3563 4.3.3 Change detection algorithms

3564 Remote multispectral and hyperspectral measurements, especially in recent  
3565 years, have been an imperative source of data for drought and vegetation dynamics  
3566 assessment. Satellite remote sensing complements traditional ground-based data  
3567 collection through synoptic spatial coverage and reduced costs (Galiatsatos et al.,  
3568 2020). Numerous time-series methods have been introduced to study the temporal  
3569 trends in pixel values across remote sensing images addressing the detection of  
3570 temporal-scale changes including *seasonal, abrupt, and gradual* changes. These  
3571 methods include BFAST (Verbesselt et al., 2010a), LandTrendr (Kennedy et al.,  
3572 2010), Estimating Segments in Trend (DBEST) (Jamali et al., 2015), and BEAST  
3573 (Zhao et al., 2019). These change detection methods detect when a pixel value  
3574 drastically changes, indicating a change in surface reflectance, and thus, in land  
3575 cover or land use (Zhu, 2017).

3576 Producing forest cover change information requires approaches that also account  
3577 for intra-annual seasonal or cyclic signals to identify changes in the phenological  
3578 patterns, which indicates species' responses to environmental conditions (Menzel  
3579 et al., 1999). The study utilised BFAST and BEAST algorithms because the two  
3580 approaches use a season-trend decomposition model to take account of both inter-

3581 and intra-year variation in a time series, unlike other methods. These algorithms  
3582 consider seasonal changepoints in plant phenology caused by changes in  
3583 temperature and rainfall regimes as opposed to other trend detection methods  
3584 such as Detecting Breakpoints and Estimating Segments in Trend (DBEST) which  
3585 do not consider seasonality if any.

#### 3586 4.3.3.1 BFAST

3587 BFAST is a widely used method for detecting trends and seasonal breaks in time  
3588 series. The BFAST approach iteratively decomposes a time series to find both trend  
3589 and seasonal changes in vegetation dynamics over a univariate time-series object  
3590 (Verbesselt et al., 2010b). The function fits a model to the data by Ordinary Least  
3591 Square (OLS) fitting on a stable history period, and to check for stability of that  
3592 same model during the monitoring period. The nonlinearity in the trend  
3593 component is also simplified into a number of individual trend segments, in order  
3594 to identify sudden structural shifts. The trend is composed of segments with  
3595 gradual changes, separated from each other by relatively brief, abrupt changes  
3596 (Verbesselt et al., 2010a). The discrepancy between the model predictions and the  
3597 data during the monitoring period is estimated using a moving sum of residuals  
3598 (MOSUM) window to test whether one or more breakpoints occur. When observed  
3599 data significantly deviate from the model, a break is detected (DeVries et al., 2015).  
3600 The hypothesis of structural stability is rejected when the MOSUM  
3601 window significantly deviates from 0 and crosses a boundary defined by the  
3602 functional central limit theorem (Zeileis et al., 2005). The difference between the  
3603 intercept and slope terms of consecutive models is used to calculate change  
3604 magnitude between breakpoints (Verbesselt et al., 2010a). Having a sufficiently  
3605 long stable history period for model fitting is critical for accurate detection of  
3606 change. The history period needs to be free of disturbances and is referred to as a  
3607 'stable history'. Verbesselt et al. (2012) provide a guideline of a stable history  
3608 equal to or longer than two years for change monitoring with BFAST. Detailed  
3609 descriptions of BFAST can be found in Verbesselt et al. (2010a).

### 3610 4.3.3.2 BEAST

3611 The Bayesian estimator of abrupt change, seasonal change, and trend (BEAST) is a  
3612 recent algorithm that fits both linear and nonlinear trends and disentangles trends  
3613 from seasonality; it further pinpoints abrupt shifts in the two isolated signals  
3614 (Zhao et al., 2019). The model structure of BEAST applies a Bayesian ensemble  
3615 modeling technique to aggregate numerous competing models to reduce  
3616 uncertainty, overfitting, and model misspecification. From the numerous  
3617 competing candidate models, BEAST evaluates how probable each of them is to be  
3618 a true model and synthesises these into an average to capture multiple and subtle  
3619 phenological changes (Zhao et al., 2019). BEAST algorithm uncovers complex  
3620 nonlinear dynamics from time-series of any variables, such as LAI, climatic data, or  
3621 soil moisture. To detect the rate of change in trends, BEAST infers the sign of the  
3622 change (e.g., greening, or browning) as well as the associated error and probability  
3623 of having a phenological shift, greening or browning at any time. Time series  
3624 decomposition was performed using BFAST R package and RBEAST R package in R  
3625 version 4.0.3 (R Development Core Team, 2013). Detailed descriptions of BEAST  
3626 can be found in Zhao et al. (2019).

### 3627 4.3.4 Land cover classification

3628 Figure 4.2 presents a flow chart to classify land cover from Landsat data using  
3629 Random Forest (RF) classifier. The less-cloudy, multiple-temporal Landsat images  
3630 for the selected years (2004 and 2019), were collected and merged over the study  
3631 area. This study used Quality Assurance bands and Function of Mask (Fmask)  
3632 algorithm (Zhu and Woodcock, 2012) to mask out cloud and cloud shadows. The  
3633 Quality Assurance (QA) band sets a cloud score threshold, and any pixel scoring  
3634 higher than the threshold will be masked and merged with another image from the  
3635 same area that doesn't have any clouds. Essentially, a cloud score greater than 0.2  
3636 for a pixel shows that the pixel is a cloud (Housman et al., 2018). The composite  
3637 algorithm in Earth Engine library was also used to reduce the effect of the cloud  
3638 (Lück and van Niekerk, 2016). In the end, all imagery used for land cover detection  
3639 used in this study are free of clouds. Before land cover classification, a spatial  
3640 clipping operation was performed on images to extract the exactly defined area of  
3641 study sites within GEE.



3642 Ground surveys to collect data on forests, open forests, agriculture,  
3643 shrubs/grassland and other land cover classes were conducted in fieldwork in  
3644 Namibia in 2019, see section 4.2.2 for details on fieldwork and sampling design. A  
3645 total of 165 points were visited and collected from the field, and additional points  
3646 of 498 points were randomly added. A total of 674 points were available for the  
3647 land cover mapping. Half of the 674 points collected for training the classifiers (i.e.,  
3648 'train' points on GEE), and the other half (341 points) were used for accuracy  
3649 assessment. Additional ground truth data for land cover classification training and  
3650 verification for 2004 was also collected through Landsat, Sentinel 2, high-  
3651 resolution Google Earth, and Open Street Map using a visual interpretation. These  
3652 sources were selected because they are freely accessible, consist of high-quality  
3653 images, and this technique was also used by previous studies (Rwanga and  
3654 Ndambuki, 2017). Based on local knowledge, this study categorised land cover into  
3655 five groups, including forest, open forests/shrubs, agriculture/barren, water, and  
3656 urban areas.

3657 The classification of multi-temporal satellite imagery was performed on a per-pixel  
3658 basis using RF classification (Li et al., 2017). The classifiers are trained with the  
3659 spectral characteristics of these known areas, by assigning each pixel to the five  
3660 target classes including forest, open forests/shrubs, agriculture/barren, water, and  
3661 urban areas. RF is a popular method of classification and clustering based on an  
3662 ensemble of decision trees (DT). RF was used because it overcomes problems of  
3663 overfitting experience by other decision trees (DT) classifiers such as Classification  
3664 and Regression Tree (CART) (Cánovas-García et al., 2017). RF is a development of  
3665 the CART method by applying bagging and random feature selection to DT, which  
3666 is to randomly select several trees that have many iterations so that they resemble  
3667 forests (Breiman, 2001).

3668

### 3669 4.3.5 Accuracy assessment

3670 Once the Land cover classification is completed, the final step is to conduct an accuracy  
3671 assessment to quantitatively assess the effectiveness of the method in correctly assigning  
3672 the pixels to the proper land cover classes. Accuracy assessments are one of the most

3673 important steps of classification because it validates the output classification product as  
3674 well as the quality of the data itself, by comparing the pixels of the classified image  
3675 with ground truth data (Congalton et al., 1983). In this study, the full set of 165 training  
3676 data visited and collected in the field and 498 added training data were divided into two  
3677 subsamples, one used for algorithm training and the other used for error testing so that  
3678 the same sample is never used for both training and testing (Geiß et al., 2017). For each  
3679 classification accuracy assessment, this study used the popular measures extracted from  
3680 confusion matrix reports, such as overall accuracy (OA), producer accuracy (PA) and  
3681 user accuracy (UA) (Janssen and Vanderwel, 1994; Story and Congalton, 1986). An  
3682 error matrix is generated by comparing the Land cover types calculated by the algorithm  
3683 for a given pixel with the true Land cover class identified by the ground truth sample.  
3684 The error matrix is a simple grid that lists the target classes and their respective number  
3685 of correct and incorrect pixel classifications (Congalton et al., 1983). The uncertainty in  
3686 estimated classification accuracy depends on the uncertainty in the true accuracy of the  
3687 classifier, the number of samples and the accuracy of the observed ground truth  
3688 (Carlotto, 2009). An overall classification error including kappa coefficient,  
3689 commission and omission statistics were also calculated (Fung and LeDrew, 1988).

#### 3690 4.3.6 Validation of estimated forest changes and disturbance

3691 The BFAST change detection was conducted to provide precise estimates of changed  
3692 and unchanged forest areas. To evaluate the accuracy of the change map and validate  
3693 the estimates of the predicted change for the whole study area, the study used 341 points  
3694 in total, 165 points were visited and collected in the field and 176 points were randomly  
3695 added as detailed in the above section. A change analysis using a stratified random  
3696 sampling design was conducted to provide precise estimates of disturbances in the study  
3697 area. Stratification was on patterns of past disturbances selected according to "the risk  
3698 of disturbances". The communal areas that are unprotected were assigned "High risk",  
3699 the Zambezi State Forest that is semi-protected (red-coloured polygon) was assigned  
3700 "Medium risk" and the Mudumu National Park (Aqua-coloured polygon) that is  
3701 protected was assigned "Low risk" (see: Fig. 4.1). The accuracy of detected changes and  
3702 unchanged estimates from BFAST was independently identified using various  
3703 information sources including ground observation data collected from the field in 2019,  
3704 land cover classification and image interpretation of high spatial resolution satellite  
3705 imagery including Landsat, Google Earth images, and Sentinel 2. The study used the

3706 method of accuracy assessment as recommended by the GOFC-GOLD, 2014 guidelines  
3707 to help identify and quantify uncertainty in the level and rate of disturbances in dryland  
3708 forest areas (GOFC-GOLD, 2014). Watt et al. (2020) and Galiatsatos et al. (2020)  
3709 utilised this method to develop monitoring, reporting and verification (MRV) systems to  
3710 quantify and validate the accuracy of the change in forest cover carbon and carbon  
3711 emissions in Guyana. This study adopted this method to validate the estimated changes  
3712 because it allows the generation of detailed, consistent, transparent, and verifiable  
3713 assessment of forest area change (GFOI, 2016).

3714

3715

3716 

## 4.4 Results

3717 

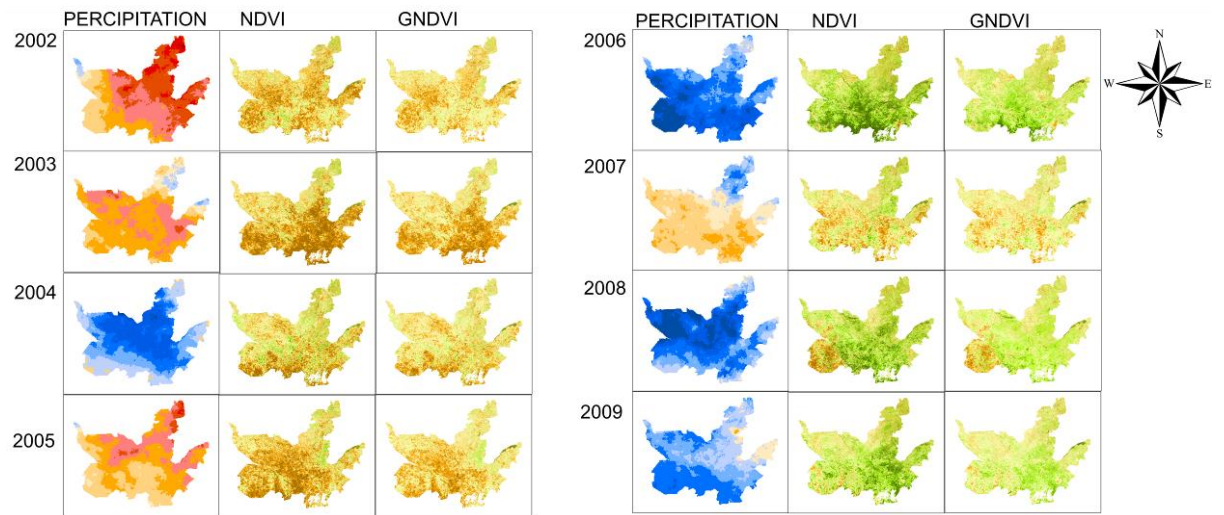
### 4.4.1 Spatial pattern of vegetation and drought stress in

  
3718 

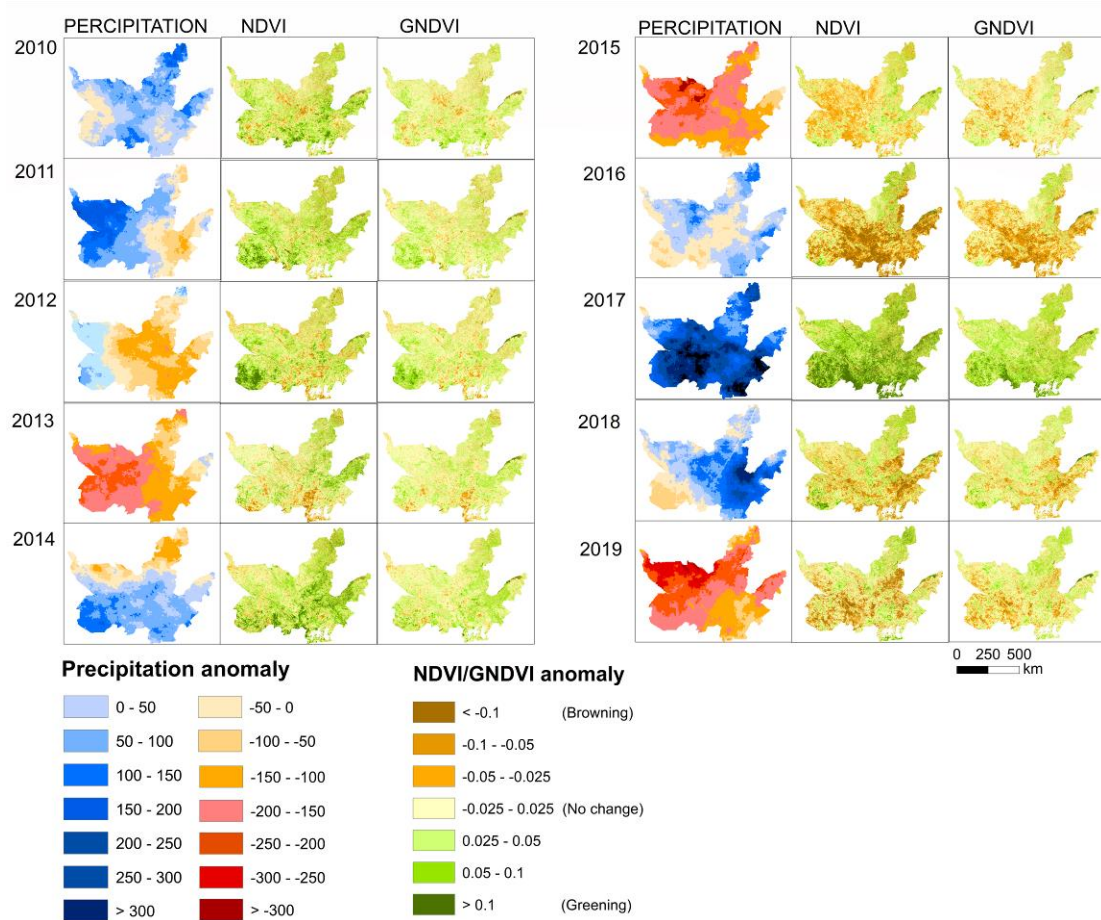
#### KAZA TFCA

3719 To provide insights into the relationship between precipitation and disturbances,  
3720 and the general vegetation dynamics response to drought, the spatial and temporal  
3721 variations of the VIs (NDVI and GNDVI) anomaly for the growing seasons of 2002  
3722 to 2019 were plotted as shown in Fig. 4.4. The spatial pattern of both NDVI and  
3723 GNDVI anomaly shows vegetation productivity increased (green to dark green  
3724 colours;  $> 0.05$ ) in 2006, 2008, and 2017 which correspond to higher than average  
3725 rainfall in these years. Regionally, negative seasonal vegetation anomalies (NDVI  
3726 and GNDVI) were mainly caused by large-scale droughts. The anomalies of  
3727 precipitation in the JFM season (see: Fig. 4.4) remained negative over the entire  
3728 KAZA region in 2002-2003, 2015-2016, and 2019 (red to dark red colours). The  
3729 centre of the maximum rainfall deficit was mostly concentrated eastward of KAZA  
3730 in 2016 and 2018. For vegetated land areas in KAZA, precipitation is a dominant  
3731 factor controlling the growing season in the region, as indicated by the anomaly in  
3732 vegetation and rainfall (see: Fig. 4.4). A close comparison indicates that the  
3733 extreme droughts in 2015 and 2019 (red to dark red colours) greatly reduced  
3734 vegetation productivity (brown colours in NDVI and GNDVI) which is coincident  
3735 with severe water stress in these years. The lag in vegetation greenness between  
3736 drought stress and browning rates extending to 2016, stands out based on the  
3737 extent of severe decrease of greenness regardless of rainfall returning to normal.

3738



3739



3740 Fig. 4. 4. Spatial pattern of ndvi and gndvi and precipitation anomalies for the 21st century  
 3741 from 2010 through 2019.

3742

3743           4.4.2 Comparison of the sensitivity of BFAST and BEAST  
3744 algorithms

3745 The study examined and compared the effectiveness of two time-series  
3746 decomposition algorithms (BFAST and BEAST) on three events to illustrate the  
3747 proposed methodology, which included: 1. Clear-cut and burnt forest, 2. Drought  
3748 impact and degradation forest, and 3. A stable, recovering forest. Table 4.2 shows  
3749 the dates of detected trend and seasonal breakpoints identified using BFAST and  
3750 BEAST algorithms for both NDVI and GNDVI time series.

3751

3752 Table 4. 2. Dates of trend and seasonal breakpoint detection relative to BFAST and BEAST  
3753 algorithms. The Bold date represents the seasonal shift with the highest probability with a  
3754 vertical dotted line.

<i><b>Clear-cut and burnt forest</b></i>			
		<i>Trend change Date</i>	<i>Seasonal change Date</i>
<i>BFAST</i>	<i>NDVI</i>	<i>2003, 2005, 2018</i>	<i>0</i>
	<i>GNDVI</i>	<i>2003, 2005, 2009, 2018</i>	<i>0</i>
<i>BEAST</i>	<i>NDVI</i>	<i>2003, 2005, 2007, 2017, 2018</i>	<i><b>2015-2017</b></i>
	<i>GNDVI</i>	<i>2003, 2005, 2006, 2007, 2009, 2017, 2018</i>	<i><b>2015-2017, 2019</b></i>
<i><b>Degrading Forest</b></i>			
<i>BFAST</i>	<i>NDVI</i>	<i>0</i>	<i>0</i>
	<i>GNDVI</i>	<i>2004, 2005, 2017</i>	<i>0</i>
<i>BEAST</i>	<i>NDVI</i>	<i>2004, 2005, 2015, 2017, 2019</i>	<i><b>2008-2009, 2012-2013</b></i>

	<i>GNDVI</i>	<i>2004, 2005, 2010, 2015, 2016, 2017, 2019</i>	<i>2008-2009, 2011-2013, 2018-2019</i>
<b><i>A stable, recovering forest</i></b>			
<i>BFAST</i>	<i>NDVI</i>	<i>0</i>	<i>0</i>
	<i>GNDVI</i>	<i>0</i>	<i>0</i>
<i>BEAST</i>	<i>NDVI</i>	<i>2017</i>	<i>2008, 2010-2011, 2015-2016</i>
	<i>GNDVI</i>	<i>2017</i>	<i>2006, 2008, 2015-2016</i>

3755

## 3756 4.4.2.1 Clearing of forest to non-forest

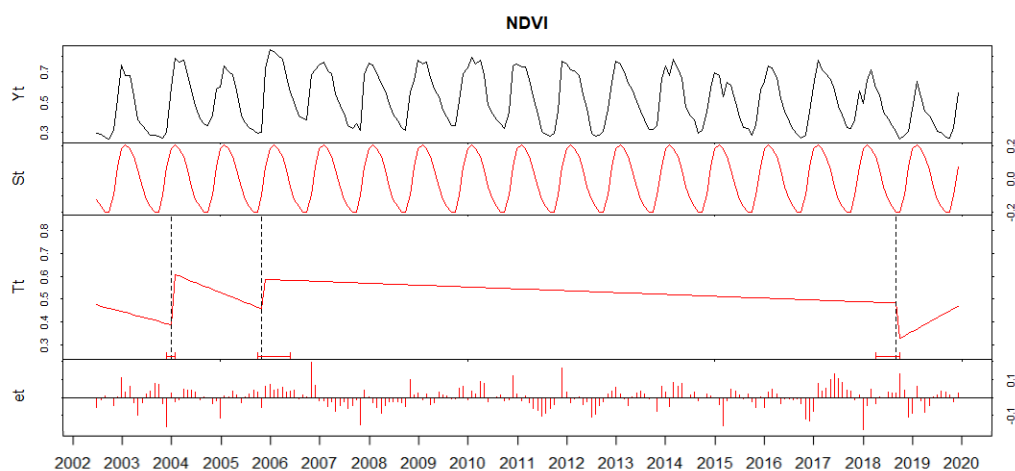
3757 Fig. 4.5 and 6 show a forest stand plot that was forest initially, however the forest  
3758 experienced a series of disturbances including a fire event around 2017 causing a  
3759 sudden loss in forest cover, and a clear-cut activity that resulted in complete forest  
3760 loss between 2018 and 2019. There were also major drought events that took  
3761 place in 2002-2003, 2005, 2015 and 2019 (see: Fig. 4.4). Photos taken in February-  
3762 May 2019 of each corresponding stand forest plot and Landsat time series images  
3763 illustrating changes are shown in the supplementary information (see: Fig. B. 1 and  
3764 B. 2).

## 3765 4.4.2.1.1 BFAST algorithm application on a Clear-cut and burnt forest:

3766 As shown in Fig 4.5, BFAST algorithm decomposed the NDVI time series and fitted  
3767 seasonal, trend, and remainder components. BFAST algorithm applied on the NDVI  
3768 time series detected three breakpoints in the trend component. BFAST predicted a  
3769 disturbance around 2003 and 2005 because of severe drought in the region, which  
3770 caused the forest to be stressed and the NDVI to decrease significantly. BFAST  
3771 algorithm run on the NDVI time series also identified the occurrence of a

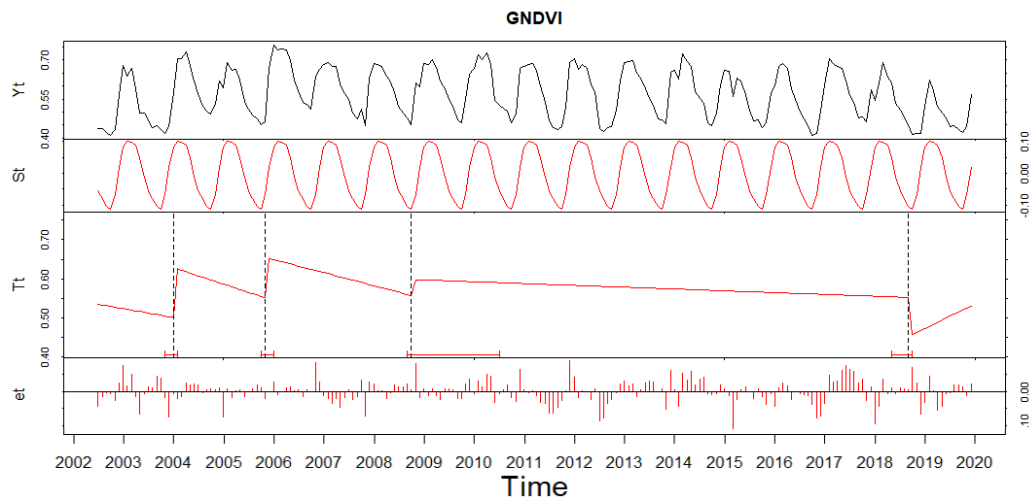
3772 breakpoint from clear-cut forest conversion to non-forest at the end of 2018.  
 3773 Around 2017 this location undergoes burning which triggered disturbance around  
 3774 the plot, however, BFAST failed to identify this trend in the NDVI trajectory.  
 3775 Furthermore, BFAST algorithm applied to the NDVI time series also failed to  
 3776 identify the disturbance in forest caused by a moderate drought event in 2007 and  
 3777 its recovery in 2009.

3778 On the other hand, BFAST algorithm run on the GNDVI time series produced four  
 3779 breakpoints in the trend component: three breakpoints in 2003, 2005 as a result of  
 3780 severe drought and deforestation towards the end of 2018. Further, using the  
 3781 GNDVI time series, BFAST identified the abrupt changes caused by vegetation  
 3782 recovery in 2009 that are not identified by the NDVI time series trajectory as  
 3783 shown in Fig 4.5. Even though using GNDVI time series, BFAST identified the  
 3784 vegetation recovery in 2009, it also failed to identify the breakpoint caused by a  
 3785 moderate drought event in 2007. BFAST algorithm did not detect abrupt changes  
 3786 in the seasonal component of NDVI and GNDVI time series (Fig. 4.5).



3787





3788

3789 Fig. 4. 5. Example of the corresponding BFAST algorithm output for NDVI and GNDVI  
 3790 extracted from a forest stand that underwent conversion from clear-cut to non-forest  
 3791 vegetation. The vertical dotted lines represent the dates of detected breakpoints, while the  
 3792 red horizontal bars represent the associated confidential intervals. The raw time series  
 3793 (Yt), the seasonal component (St), the trend component (Tt), and the noise (et)  
 3794 component, are also shown. The location of the corresponding pixels, field photo taken in  
 3795 Namibia in 2019 and Landsat time series images illustrating changes are shown in the  
 3796 supplementary information (see: Fig. B. 1 and B. 2).

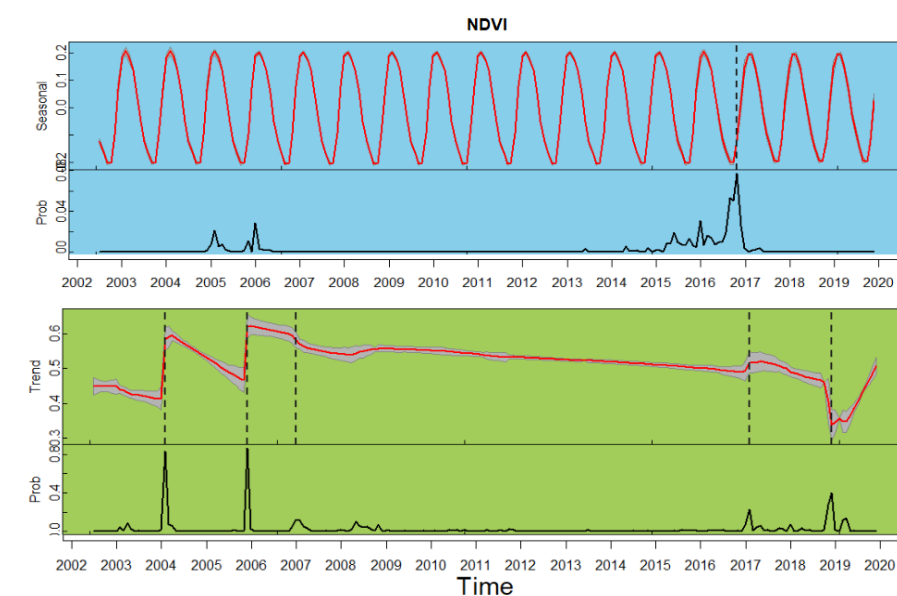
3797 4.4.2.1.2 BEAST algorithm application on a Clear-cut and burnt forest:

3798 Fig. 4.6 shows BEAST algorithm applied to the NDVI and GNDVI time series to  
 3799 detected phenological and trend changes. BEAST algorithm applied on the NDVI  
 3800 time series detected five breakpoints in the trend component. The four  
 3801 breakpoints including two breakpoints in 2003 and 2005 as a result of severe  
 3802 drought, one breakpoint in 2018 from deforestation and one abrupt change caused  
 3803 by 2009 moderate drought, similar to the changes identified by BFAST on the  
 3804 GNDVI time series in Fig. 4.5. However, the application of BEAST algorithm on the  
 3805 NDVI time series also detected one breakpoint in the trend component in 2017 as a  
 3806 result of vegetation increase (due to increase in rainfall in 2017) following the fire  
 3807 event in 2017 that neither application of BFAST was able to detect.

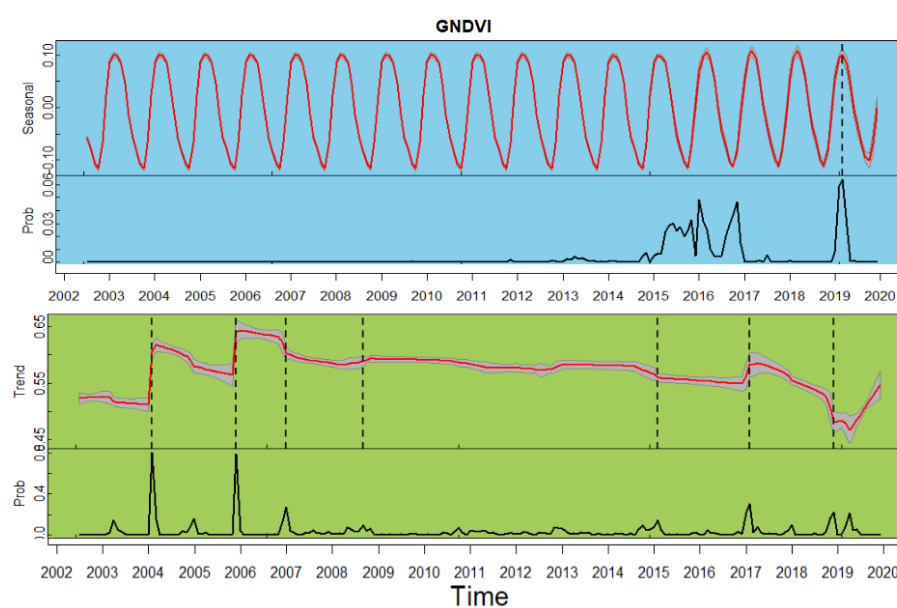
3808 The application of BEAST algorithm to the GNDVI time series detected the  
 3809 occurrence of five breakpoints, two from drought in 2003 and 2005, the fire event  
 3810 of 2017, the forest clear-cut in 2018, and vegetation increase in 2017, similar to  
 3811 exploring the NDVI signal with BEAST algorithm. However, BEAST algorithm

3812 applied to the GNDVI time series was also able to uncover the beginning of  
 3813 vegetation disturbance and the vegetation recovery, for example it captures the  
 3814 correct year of the subtle decrease in forest cover in 2007 due to 2007 drought and  
 3815 its recovery in 2009. Similarly, it detects another decrease in forest cover due to  
 3816 drought in 2015 and its recovery in 2017 that was not detected using BEAST on  
 3817 NDVI time series. For both indices, BEAST algorithm detected phenological  
 3818 changes resulting from the 2015-2016 drought. BEAST applied to the GNDVI time  
 3819 series further detected a seasonal shift associated with 2019 logging and drought  
 3820 (see: Fig. 4.6). In contrast, BFAST algorithm uncovered a stable seasonal trajectory  
 3821 (see: Fig. 4.5), suggesting no phenological change during this period (2002-2019).

3822



3823



3824 Fig. 4. 6. Example of the decomposition generated by the application of BEAST algorithm  
3825 for the NDVI and GNDVI time series extracted from a forest stand that underwent  
3826 conversion from clear-cut to non-forest vegetation. Seasonal and Trend represent the best  
3827 fitted seasonal and trend signals (red line), respectively. The vertical dotted lines  
3828 represent the dates of detected breakpoints in the trend/seasonal components, while the  
3829 black lines at the bottom panels represent the probabilities of the changepoint in the  
3830 seasonal/trend components. The location of the corresponding pixels, field photo taken in  
3831 Namibia in 2019 and Landsat time series images illustrating changes are shown in the  
3832 supplementary information (see: Fig. B. 1 and B. 2).

3833

#### 3834 4.4.2.2 Drought impact and degraded forest

3835 Fig. 4.7 and 8 show the results from modelling a forest stand plot that has  
3836 undergone multiple disturbances from drought coupled with wildlife grazing and  
3837 mega-herbivore pushovers, as a result of its location near to the Chobe river  
3838 frontage. Photos taken in February-May 2019 of each corresponding stand forest  
3839 plot and Landsat time series images, both illustrating changes are shown in the  
3840 supplementary (see: Fig. B. 3 and B. 4).

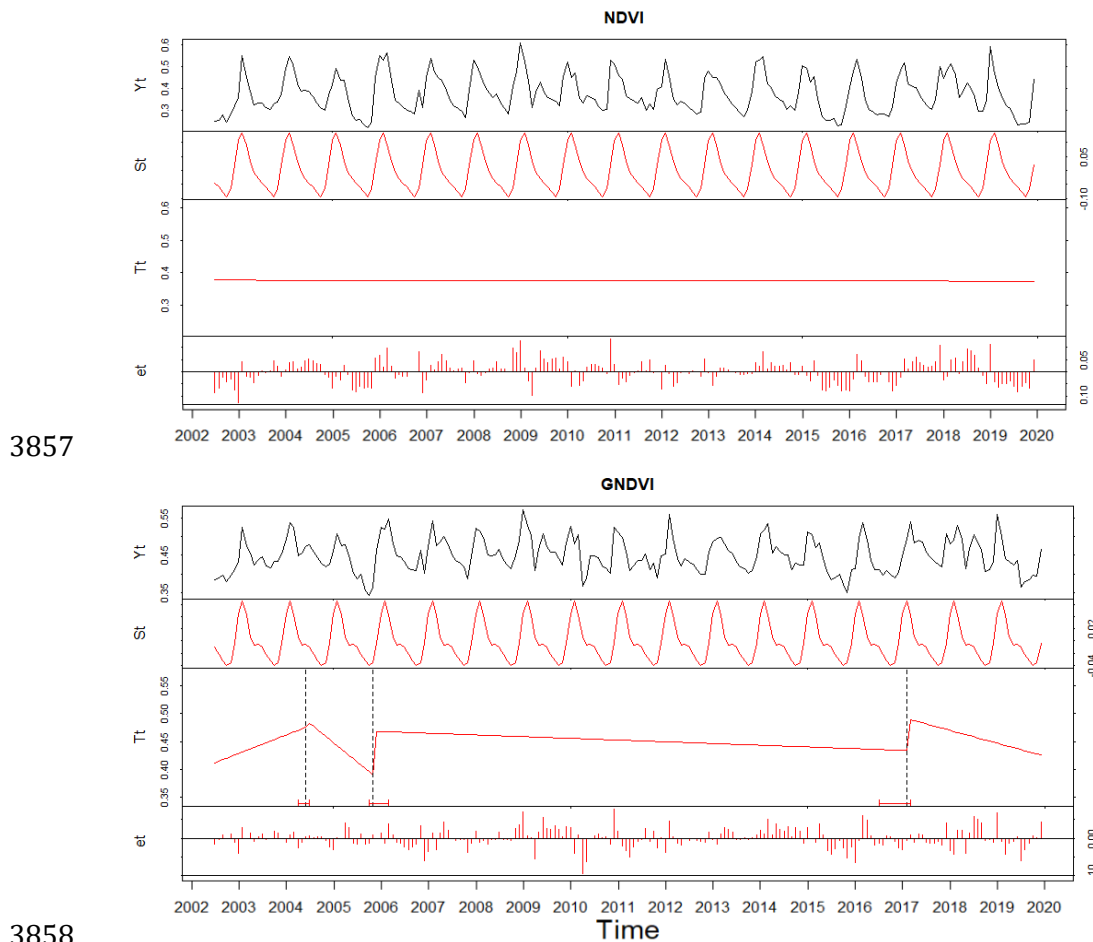
3841

##### 3842 4.4.2.2.1 BFAST algorithm application on a degraded forest:

3843 Fig. 4.7 presents BFAST algorithm decomposition of the NDVI and GNDVI time  
3844 series. BFAST was not able to capture any meaningful information relating to  
3845 disturbances to the forest from the trend and seasonal components throughout the  
3846 period of 2002 to 2019. None of the severe climatic events or moderate drought  
3847 years were identified, and the NDVI trend appeared stable when using BFAST  
3848 algorithm. This is despite the original time series showing some instances of an  
3849 NDVI drop during this period.

3850 However, using BFAST algorithm on the GNDVI time series, three breakpoints  
3851 were detected in 2004, 2005 and 2017. The two abrupt changes in 2004 and 2006,  
3852 correspond to the drought event in 2003 and 2005 (or to an increase in rainfall in  
3853 2004 and 2006 after the drought), were detected (see: Fig. 4.4 and 7). The

3854 breakpoint in 2017 represent a vegetation increase as a result of rainfall increase  
 3855 in 2017. BFAST did not detect abrupt changes in the seasonal component of NDVI  
 3856 and GNDVI time series as shown in Fig. 4.7.



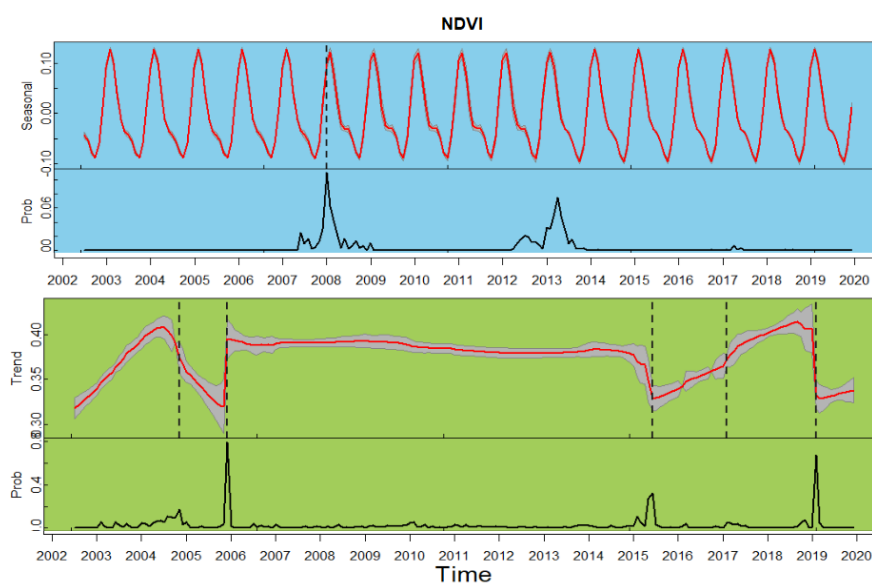
3857  
 3858  
 3859 Fig. 4. 7. Example of the corresponding BFAST for NDVI and GNDVI extracted from a forest  
 3860 stand of a degraded forest. The vertical dotted lines represent the dates of detected  
 3861 breakpoints, while the red horizontal bars represent the associated confidential intervals.  
 3862 The raw time series (Yt), the seasonal component (St), the trend component (Tt), and the  
 3863 noise (et) component, are also shown. The location of the corresponding pixels, field photo  
 3864 taken in Botswana in 2019 and Landsat time series images illustrating changes are shown  
 3865 in the supplementary information (see: Fig. B. 3 and B. 4).

3866

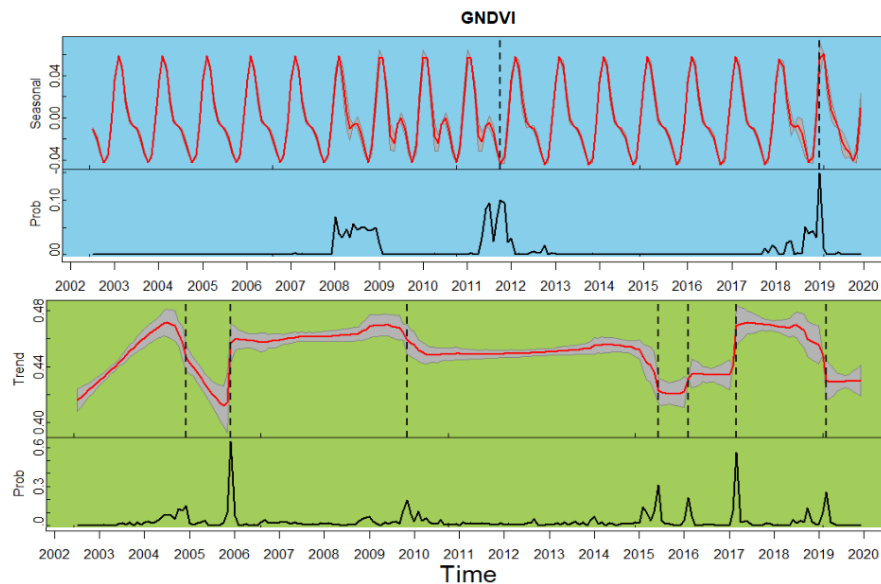
3867 4.4.2.2.2 BEAST algorithm application on a degraded forest:

3868 BEAST algorithm applied to the NDVI time series (Fig. 4.8) detected five  
 3869 breakpoints as a result of extreme effects of the 2005, 2015, 2019 droughts and the  
 3870 increase in rainfall in 2004, 2006, and 2017, which BFAST algorithm applied to the

3871 same time series did not detect, as shown in Fig. 4.7. The application of BEAST  
 3872 algorithm to the GNDVI time series was able to detect seven breakpoints, including  
 3873 the similar extreme droughts as shown with the NDVI, which were timed to similar  
 3874 dates. The increase in rainfall in 2008, and the drought stresses of 2010-2012,  
 3875 which both have a smaller magnitude of abrupt change, were also identifiable in  
 3876 the trend within the GNDVI, but not in the NDVI. BEAST algorithm was also able to  
 3877 describe the magnitude of drought impacts and recovery more clearly than when  
 3878 using BFAST. The drought impact detected by applying BEAST algorithm to the  
 3879 GNDVI time series in 2010, which is smaller in terms of the magnitude of the  
 3880 abrupt change, was not detected when using NDVI by either algorithm, as shown in  
 3881 Fig. 4.8. The Bayesian approach (BEAST) detected a phenological shift in 2008  
 3882 when applied to the NDVI time series. Three seasonal shifts resulting from changes  
 3883 in precipitation in 2008, 2010, and the 2019 drought, were noticeable in BEAST-  
 3884 derived seasonal trend of the GNDVI time series as shown in Fig. 4.8.



3885



3886

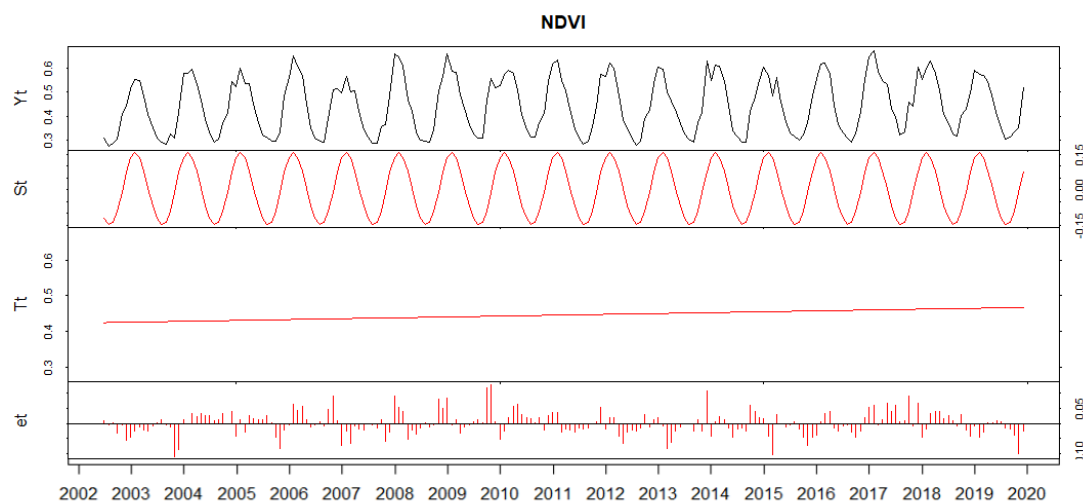
3887 Fig. 4. 8. Example of the decomposition generated by the application of BEAST algorithm  
 3888 for the NDVI and GNDVI time series extracted from a forest stand of a degraded forest.  
 3889 Seasonal and Trend represent the best fitted seasonal and trend signals (red line),  
 3890 respectively. The vertical dotted lines represent the dates of detected breakpoints in the  
 3891 trend/seasonal components, while the black lines at the bottom panels represent the  
 3892 probabilities of the changepoint in the seasonal/trend components. The location of the  
 3893 corresponding pixels, field photo taken in Botswana in 2019 and Landsat time series  
 3894 images illustrating changes are shown in the supplementary information (see: Fig. B. 3 and  
 3895 B. 4).

#### 3896 4.4.2.3 Stable forest

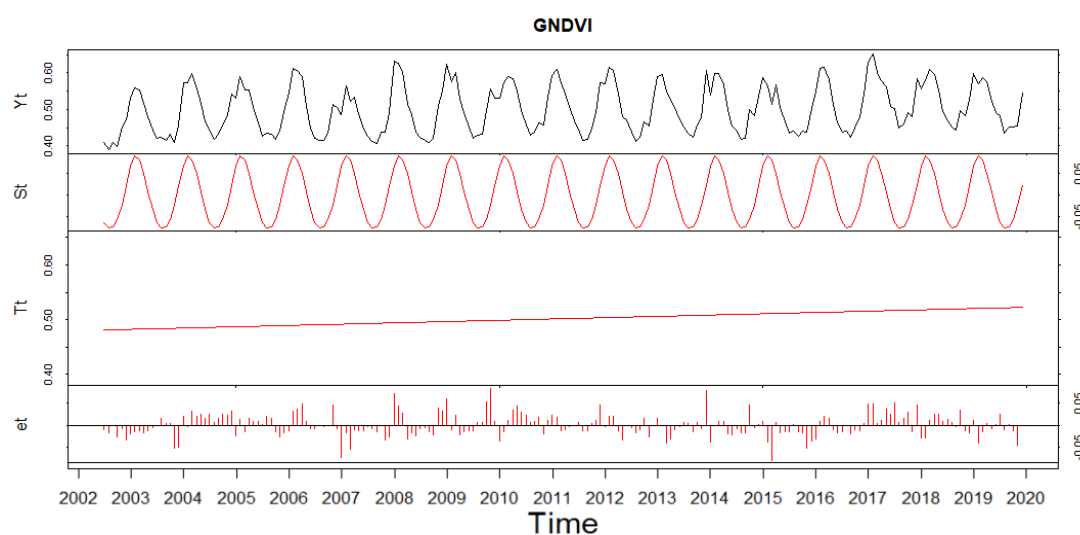
3897 Fig. 4.9 and 10 show the results from modelling a forest stand plot that has  
 3898 experienced limited human and wildlife disturbance and is considered to be stable.  
 3899 Photos taken in February-May 2019 of each corresponding stand forest plot and  
 3900 Landsat time series images, both illustrating changes are shown in the  
 3901 supplementary (see: Fig. B. 5 and B. 6).

##### 3902 4.4.2.3.1 BFAST algorithm application on a stable forest:

3903 BFAST algorithm detected no breakpoints in trend and seasonality using both the  
 3904 NDVI and GNDVI time series. Both indices show a gradual increase in the forest  
 3905 cover. In both indices, the application of BFAST failed to detect any seasonal  
 3906 change.



3907



3908

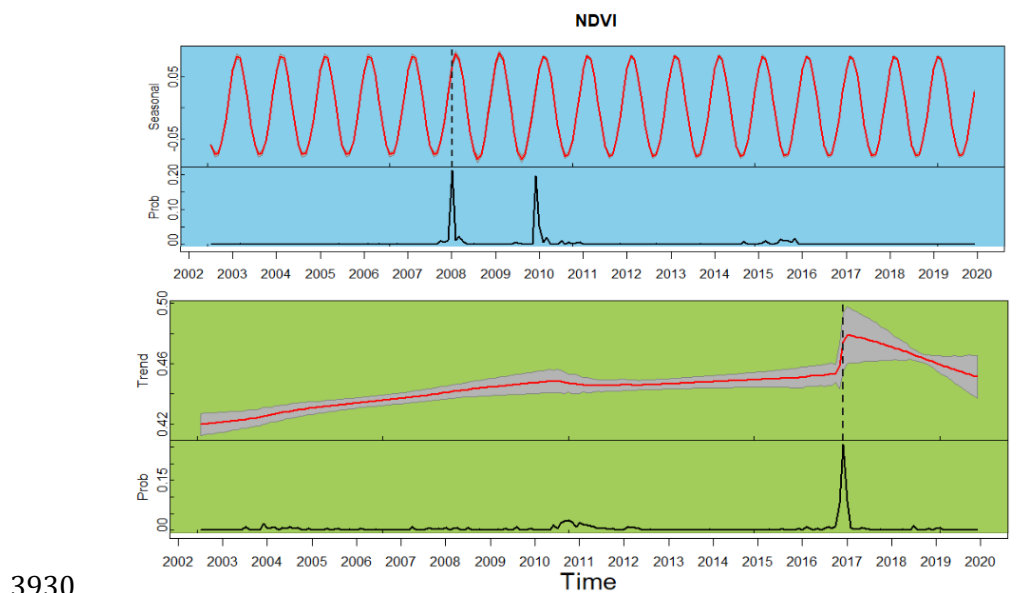
3909 Fig. 4. 9. Example of the corresponding BFAST algorithm output for NDVI and GNDVI  
 3910 extracted from a forest stand that considered stable. The vertical dotted lines represent  
 3911 the dates of detected breakpoints, while the red horizontal bars represent the associated  
 3912 confidential intervals. The raw time series ( $Y_t$ ), the seasonal component ( $S_t$ ), the trend  
 3913 component ( $T_t$ ), and the noise ( $e_t$ ) component, are also shown. The location of the  
 3914 corresponding pixels, field photo taken in Namibia in 2019 and Landsat time series images  
 3915 illustrating changes are shown in the supplementary information (see: Fig. B. 5 and 4. 6).

3916

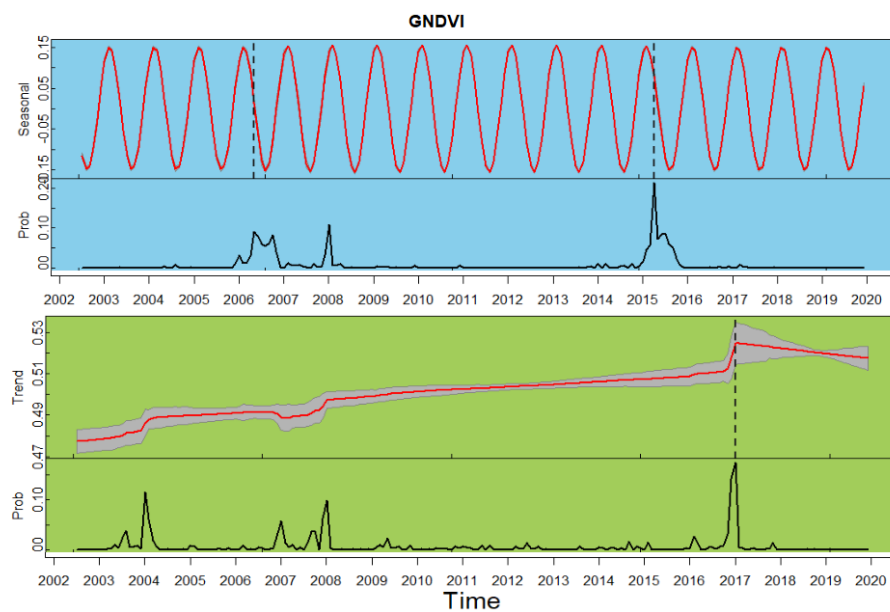
3917 4.4.2.3.2 BEAST algorithm application on a stable forest:

3918 BEAST algorithm showed a gradual increase in forest, and no abrupt trend as a  
 3919 result of a disturbance was identified in in either the NDVI or the GNDVI time

3920 series as shown in Fig. 4.10. One exception was an abrupt change as a result of  
 3921 forest cover increases was evident in 2017, as indicated by a high probability of  
 3922 this change in both indices, which was associated with plentiful rainfall in 2017. In  
 3923 terms of a seasonal signal, both indices show the phenological shifts around the  
 3924 2008 and 2015-2016 drought events, although the GNDVI time series was able to  
 3925 detect a larger number of seasonal shifts. These seasonal changes are detected in  
 3926 severe drought years that were followed by an increase in rainfall. For example,  
 3927 the seasonal shift in the 2005 drought was followed by an increase in rainfall in  
 3928 2006, and the seasonal shift in the 2015-2016 drought was followed by relatively  
 3929 high levels of precipitation in 2017, as shown in Fig. 4.4 and 4.10.



3930



3931



3932 Fig. 4. 10. Example of the decomposition generated by the application of BEAST algorithm  
 3933 for the NDVI and GNDVI time series extracted from a forest stand that considered stable.  
 3934 Seasonal and Trend represent the best fitted seasonal and trend signals (red line),  
 3935 respectively. The vertical dotted lines represent the dates of detected breakpoints in the  
 3936 trend/seasonal components, while the black lines at the bottom panels represent the  
 3937 probabilities of the changepoint in the seasonal/trend components. The location of the  
 3938 corresponding pixels, field photo taken in Namibia in 2019 and Landsat time series images  
 3939 illustrating changes are shown in the supplementary information (see: Fig. B. 5 and B. 6).

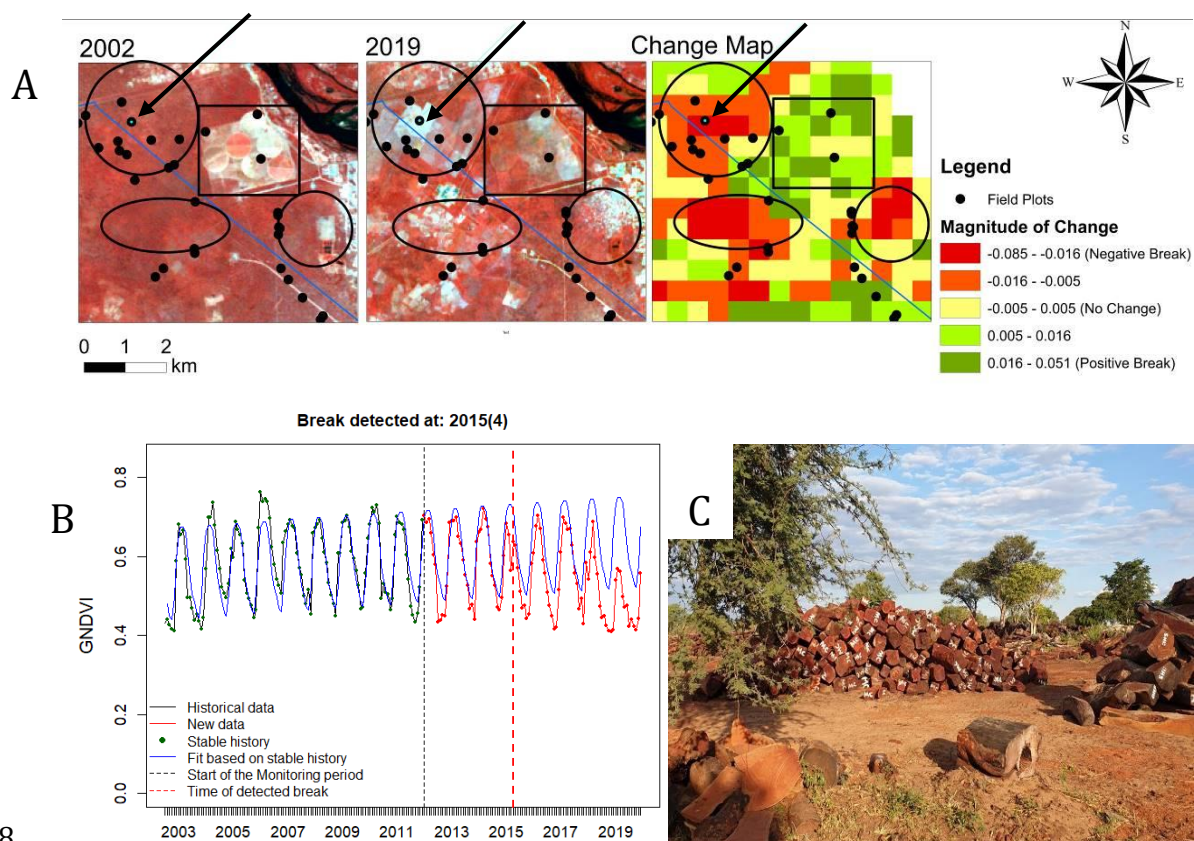
3940

#### 3941 4.4.3 Robustness of predicting forest dynamics using 3942 breakpoints and change magnitude

3943 The examples shown in Fig. 4.11 demonstrate the differences in magnitude of  
 3944 GNDVI that were commonly observed to be associated with varying degrees of  
 3945 forest cover change. The cumulative probability of each of the change classes  
 3946 (deforestation, degradation, vegetation regrowth, or no-change) detected from the  
 3947 application of BFAST algorithm using the MODIS time series from 01/01/2010 to  
 3948 31/12/2019 is shown in Fig. 4.11 and 12. The study only shows the breakpoints  
 3949 from 2010 to 2019 as these years help to highlight the impact of exceptional  
 3950 drought events (Fig. 4.4), fire, and large-scale forest clear-cutting events in the  
 3951 Mudumu NP and Zambezi ST, resulting in a negative breakpoint magnitude. Fig.  
 3952 4.11A presents 2002 Landsat 5 (LC5) ETM, 2019 Landsat 8 (LC8) OLI images, and  
 3953 the cumulative change map overlaid with field points collected with land cover and  
 3954 vegetation measurement (black-coloured circles) mapped in Zambezi ST. The  
 3955 results of the survey plot (black circle coloured blue) shown with an arrow are  
 3956 represented in Figure 4. 11 A-C. Figure 4. 11A shows the Landsat image in 2002  
 3957 and 2019 with the survey plot undisturbed (forest) in 2002, and when it is turned  
 3958 into a non-forest in 2019. A cumulative change map of MODIS produced with  
 3959 BFAST in Figure 4. 11 A shows the negative break of the same survey plot.  
 3960 Similarly, figure 4. 11 B shows the time series of the forest pixel with a negative  
 3961 break detected in April 2015, while Figure 4. 11 C represents the actual  
 3962 photograph of the survey plot with cut-down trees on the ground. This approach  
 3963 used prior knowledge of disturbances such as clearing, and BFAST allowed the

3964 most significant change event in the time series to be detected. Prior knowledge of  
3965 disturbances such as clearing was used in this approach and BFAST allowed the  
3966 most significant change event in the time-series to be detected. For mapping  
3967 cumulative change, the probability of the deforestation class increased with  
3968 decreasing change magnitude, showing a strong negative relationship with change  
3969 magnitude, whilst the probability of the degradation class showed a weak negative  
3970 relationship with change magnitude. The probability of vegetation growth class  
3971 increased with increasing change magnitude, showing a positive relationship with  
3972 change magnitude.

3973 Maps showing the time of the changepoint event and the magnitude of the GNDVI  
3974 change are displayed in Fig. 4.11 and 12. Fig. 4.11A shows the negative breakpoint  
3975 with high mean negative magnitude of change due to forest logging and clear-  
3976 cutting to almost no vegetation between 2018 and 2019 as shown by the top circle.  
3977 Other breakpoints with high mean negative magnitude due to forest clearing for  
3978 agriculture and urban areas are also observed and shown with the two bottom  
3979 circles. The breakpoint with positive mean magnitude is observed in a square  
3980 showing an agricultural area (farmland) that was abandoned and vegetation  
3981 regrowth gradually increased by 2019 (Fig. 4.11A). As shown by the plot shown by  
3982 the black arrow (see: Fig. 4.11A), the negative break in the forest pixel is detected  
3983 in April 2015 and is associated with extreme drought, as shown by the red vertical  
3984 line in the GNDVI time series in Fig. 4.11B. Another disturbance in the forest stand  
3985 plot caused a large reduction in GNDVI in 2019 as a result of forest clear-cutting  
3986 for timber, as also illustrated in the change map (Fig. 4.11A), the time series (Fig.  
3987 4.11B), and the field photo taken in 2019 (Fig. 4.11C).



3988

3989 Fig. 4. 11. A: 2002 LC5 ETM, 2019 LC8 OLI image and a map of the magnitude of change in  
 3990 the trend component from 01/01/2010 to 01/12/2019 generated by BFAST algorithm in  
 3991 and around the Zambezi ST and Mudumu NP; the colour scale represents the magnitude  
 3992 and direction of change. The circles here represent abrupt changes with a negative  
 3993 magnitude; a square represents a vegetation regrowth with a positive magnitude, and the  
 3994 arrow shows a forest stand plot for a forest disturbed by drought and subsequent forest  
 3995 canopy clearing. Fig.4.11. B: MODIS time series from 01/01/2002 to 31/12/2019 for a plot  
 3996 shown by an arrow in Fig. 4.11. A. Fig. 4.11. C: Shows the photograph of the selected plot  
 3997 (location coordinate is 17.49°S, 24.21°E) in Fig. 4.11. A, with logged for timbers  
 3998 photographed during a field campaign in Zambezi ST near the border of Namibia and  
 3999 Zambia in 2019.

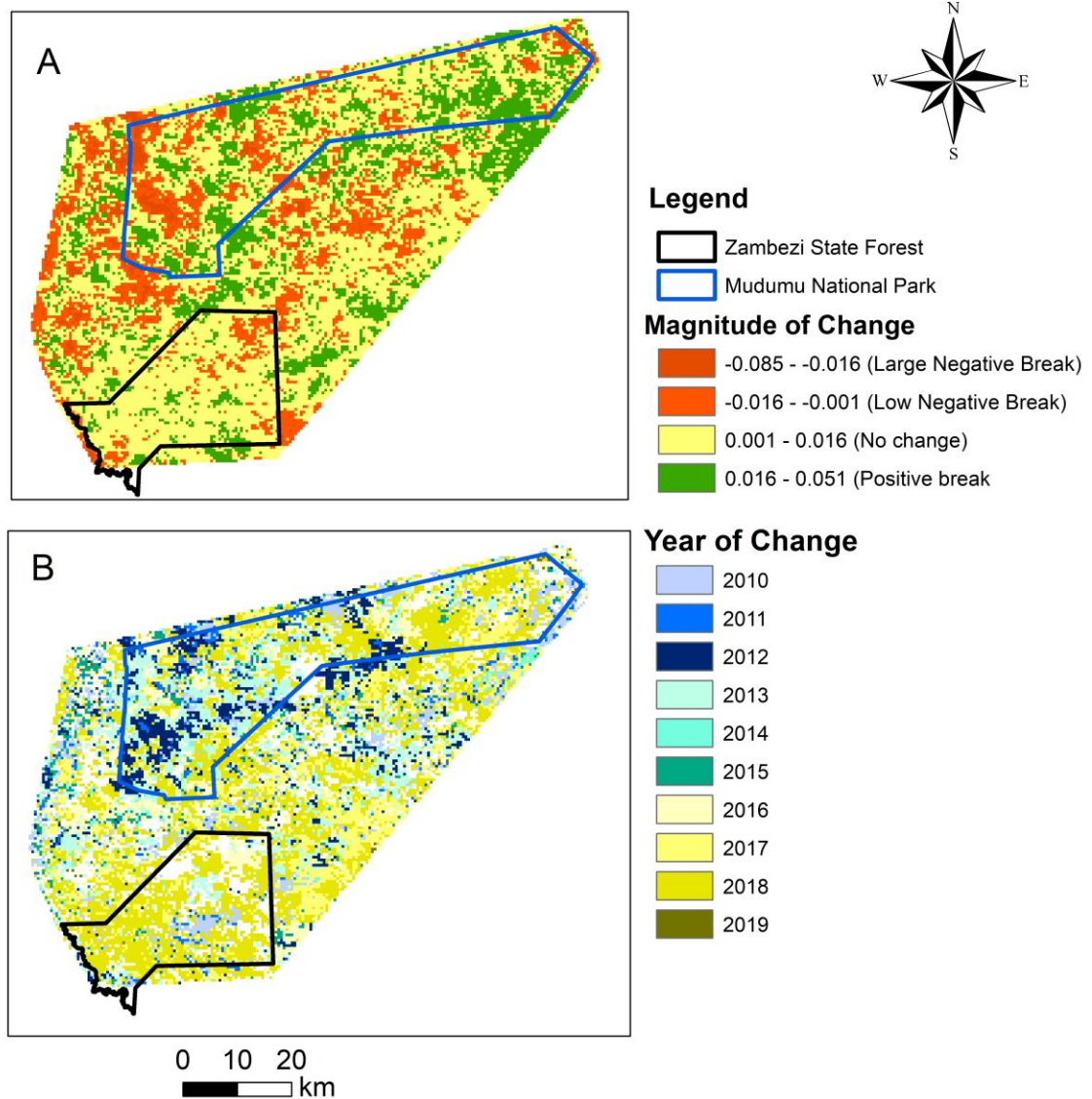
4000

#### 4001 4.4.4 Spatial pattern of predicted forest changes using 4002 breakpoints and magnitude

4003 Fig. 4.12 presents the spatial pattern of the extracted trend classification, showing  
 4004 the predicted magnitude of change in the trend component and the estimated date  
 4005 of change generated from BFAST algorithm applied to the GNDVI time series on the

4006 Zambezi region, Namibia. The final disturbance map showing disturbed versus  
4007 undisturbed areas highlights distinct spatial patterns across the study area. Fig.  
4008 4.12A shows the predicted abrupt change in the trend component. It can be seen  
4009 that the Mudumu NP remains undisturbed, although there are distinct spatial  
4010 patterns of forest degradation indicated by low magnitude negative breakpoints at  
4011 the edge of the park, around the communal villages in Sobbe conservancy.  
4012 Examining the disturbance map, forest decline from clear-cutting and forest  
4013 conversion to agricultural land were observed in Zambezi ST and in the  
4014 community conservancy and communal area surrounding the Zambezi SF and  
4015 Mudumu NP. The disturbance trends and extreme vegetation loss from  
4016 deforestation and clear-cuts are shown by extreme magnitude negative breaks and  
4017 vegetation degradation (Fig. 4.12A). Although most of the clear-cuts are associated  
4018 with an extreme magnitude negative breakpoint, some cases are associated with a  
4019 low magnitude negative/positive breakpoint. This is shown, for example, in areas  
4020 with forest clear-cuts replaced by matured shrubs in the northernmost section of  
4021 the study area (Zambezi ST) near the border between Namibia and Zambia.

4022 The map also shows continuous patches of forest showing a positive magnitude  
4023 breakpoint, which denotes a forest recovery, vegetation regrowth that follows an  
4024 earlier event, and vegetation less affected by disturbance as shown by positive  
4025 magnitude of change in Fig. 12 A. More than 50% of the breakpoint dates are in the  
4026 period between 2016 and 2019, with 2018 having the highest number of  
4027 breakpoints. The high percentage of breakpoints detected in this period, and a  
4028 negative magnitude, reflect both the impact of the 2015/2016 and 2018/2019  
4029 droughts, coupled with clear-cutting of the forest stands.



4030

4031 Fig. 4. 12. A. shows the magnitude of change in the trend component and the predicted  
 4032 time of change generated by BFAST; red colour represents negative breakpoint typically  
 4033 associated with vegetation loss. Green colour represents positive breakpoint associated  
 4034 with vegetation gain. The turquoise polygon shows Zambezi ST, and the black polygon  
 4035 shows Mudumu NP. B: shows the estimated year of change from 2010 to 2019.

4036

#### 4037 4.4.5 Validation of spatial pattern of predicted forest 4038 changes and disturbances

4039 The BFAST model was used to estimate forest disturbance for the complete study  
 4040 area (Fig. 4.12). The validation assessment used a weighted average of the within-  
 4041 stratum estimates to ensure the weights are proportional to size of high, medium

4042 and low 'risk of change' strata. The results of the comparable land cover classes for  
4043 the BFAST time series analysis and the interval-based per-pixel Random Forest  
4044 classification are shown in Tables 4.3 and 4.4. The complete tables with all the area  
4045 change classes for the two approaches are in the supplementary material (Tables  
4046 B.2, B.3 and B.4). The land cover classes for the interval-based per pixel  
4047 classification in Table B.3 were calculated based on post-classification  
4048 reorganisation of land cover area transition table (Table B. 4), where the similarly  
4049 classified class areas were summed together.

4050 The results are presented in Table 4.4 and both methods show a land transition  
4051 from forest to non-forest (deforestation) in the region. The interval-based per-  
4052 pixel classification estimated that the conversion of forest to non-forest land was  
4053 87,251 ha. The BFAST time series estimates of deforestation are corresponding to  
4054 the two-interval pixel-based classification showing an area change of 99,911 ha  
4055 (SE 9,753 ha) throughout the entire 2002–2019 period. The two-interval  
4056 classification estimated that the total unchanged forest area was 147,875 ha. These  
4057 values are higher as compared to 106,390 ha of unchanged forest land estimated  
4058 by BFAST time series analysis. The interval-based pixel-based classification which  
4059 bases the change estimates on differencing between images at only two points in  
4060 time has little capability to distinguish forest degradation, which is the progressive  
4061 reduction/losses in forest cover that do not qualify as deforestation. As a result, it  
4062 is likely that the interval-based classification does not detect forest degradation as  
4063 well as BFAST (time series) approach. The BFAST time series analysis captures the  
4064 subtle change of forest conversion to the degraded forest with an estimate of  
4065 33,131 ha (SE 6,859 ha). In addition, BFAST time series analysis found that  
4066 approximately 23,409 ha (SE 556,8 ha) of degraded forest was converted to forest  
4067 land. However, the degraded forest estimates from the BFAST time series are not  
4068 comparable with the two-based interval per pixel classification because it does not  
4069 detect degradation (see: Table 4.4). The BFAST algorithm can iteratively estimate  
4070 and characterize temporal changes (time) and characterizes the spatial change by  
4071 its magnitude and direction ("deforestation", "degradation" and "no change"). The  
4072 sample-based estimates and validation of BFAST used in this study also provide  
4073 the standard error for the continuous changes. For this study, the standard error  
4074 for the non-disturbed forest class was lower as compared to the disturbed classes

4075 (see: Table 4. 3). It is also important to note that the region has no Landsat images  
 4076 available in 2002, and few images for the year 2003, therefore the two-interval  
 4077 classification used the starting year of 2004, which can account for some difference  
 4078 in land cover class areas. In summary, BFAST (time series) approach at one level  
 4079 agrees with a two-interval traditional classification when identifying discrete  
 4080 change but it also identifies areas of more subtle change and so adds value to the  
 4081 analysis and interpretation. In broad terms, the two approaches agree where direct  
 4082 comparison is possible, but the differences also help to stimulate important  
 4083 questions about the differences.

4084

4085 Table 4. 3. Area changes of BFAST using sample-based estimates and the observed  
 4086 disturbance change rates.

<b>Change identified by BFAST</b>	<b>Area Hectares (ha)</b>	<b>Standard Error (ha)</b>	<b>2.5 % (ha)</b>	<b>97.5 % (ha)</b>
Non-disturbance (no change) <i>(Stable Forest)</i>	106,390	9,817	87,148	125,631
Non-disturbance -low negative change <i>(Stable forest to Degradation)</i>	33,132	6,859	19,688	46,576
Non-disturbance -large negative change <i>(Stable Forest to Deforestation)</i>	99,911	9,753	80,795	119,027
Low negative break -large negative change <i>(Degradation to Deforestation)</i>	59,515	8,154	43,533	75,497
Low negative changes -non-disturbance	23,409	556,8	12,497	34,322

<i>(Degradation to Stable Forest)</i>				
---------------------------------------	--	--	--	--

4087

4088 Table 4. 4. Types of changes identified by BFAST and Random Forest classification for the  
4089 period 2004 and 2019.

<b>Type of Changes</b>	<b>Two interval Classification 2004 and 2019 Area(ha)</b>	<b>BFAST Time Series analysis 2002 to 2019 Area (ha)</b>
Forest	147,875	106,390
Forest to Non-forest	87,251	99,911
Forest to Degraded Forest	-	59,515
Degraded Forest to Forest	-	33,131
Degraded Forest to Non-forest	-	23,409
Non-forest-Forest	41,447	54,517

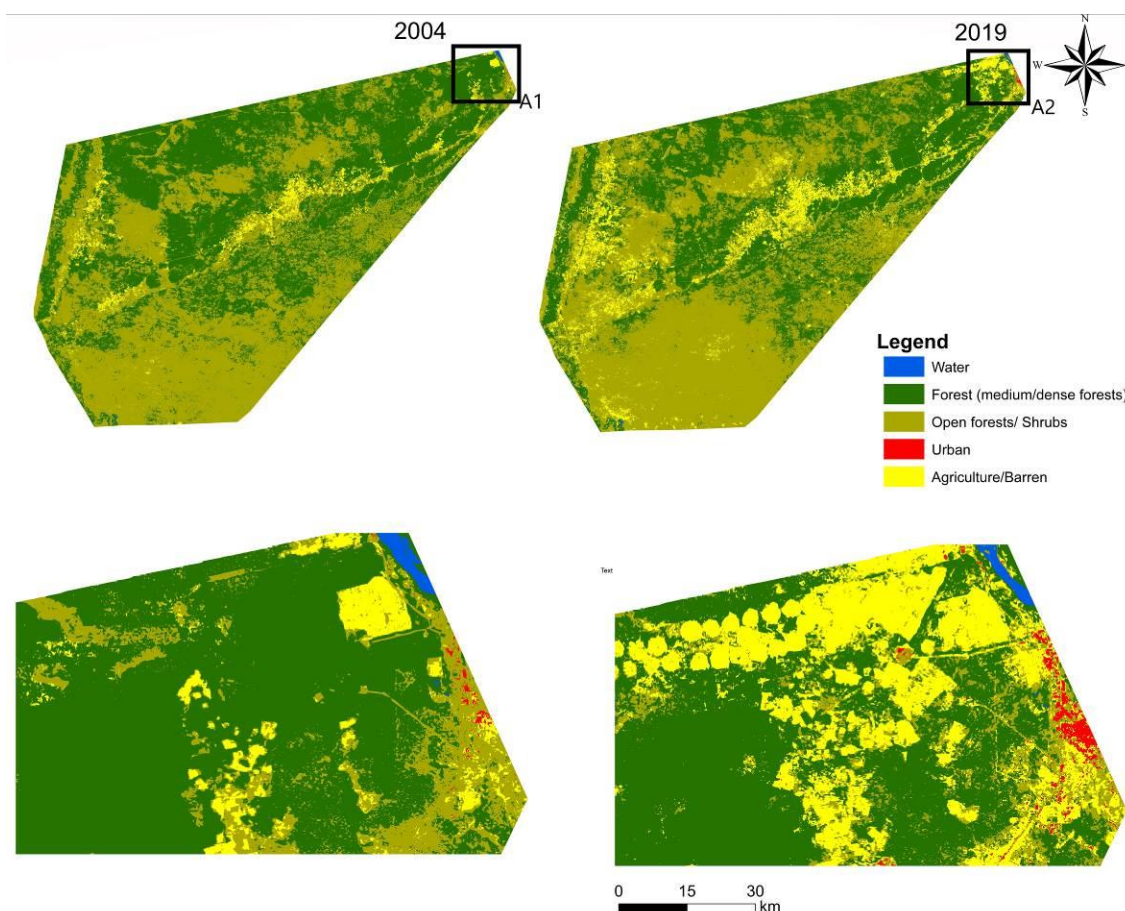
4090

#### 4091 4.4.6 Land cover classification

4092 The land cover classifications using the RF algorithm, in 2004 and 2019, are illustrated  
4093 in Fig. 4.13. To quantify the land use changes over the years, the study analysed the  
4094 error matrix which showed any classification errors that may have occurred such as a  
4095 pixel being misclassified. Table 4.6 presents the confusion matrix and accuracy  
4096 assessment for land cover classification in the years 2004 and 2019. For classification  
4097 accuracy, Landis and Koch et al (1977) suggested the Kappa result with values  $\leq 0$   
4098 indicate no agreement and 0.01–0.20 denote none to slight, 0.21–0.40 fair, 0.41– 0.60  
4099 moderate, 0.61–0.80 indicate substantial, and 0.81–1.00 as almost perfect agreement  
4100 (Sim and Wrigh, 2005). The accuracy assessment on the 2004 and 2019 classified



4101 images showed an overall classification accuracy of 82% and 88%, and an overall  
 4102 Kappa Statistic of 0.74 and 0.83, respectively. The classification results and Kappa  
 4103 statistics obtained in this study show a very good agreement between classes which is  
 4104 considered sufficient for the land cover map in the Zambezi region. The five classes that  
 4105 were used (forest, open forests/shrubs, agriculture/barren, water, and urban areas)  
 4106 resulted in 100% accuracy for the water and urban areas, and 90% for agriculture.  
 4107 However, accuracy was somewhat lower in the other two classes of forest and open  
 4108 forest/shrubs areas, with 82% and 76% accuracy, respectively (Table 4.6). The reason  
 4109 for the high accuracy of water was due to the small area comprised of water and urban  
 4110 areas. The two classes had a low number of training sample pixels because the training  
 4111 points were distributed proportionally to the study area. The classification for forests,  
 4112 open forest/shrubs and agriculture/barren exhibited low scores in both user accuracy and  
 4113 producer accuracy. The reason for the low accuracy of open forests/Shrubs was due to  
 4114 this class being often mixed with forests and agriculture/barren in this study, reducing a  
 4115 large percentage of accuracy (more than 20% reduction).



4116

4117 Fig. 4. 13. Land cover classification in 2004 and 2019; panel A1 and A2 are zoom in of land  
 4118 cover in 2004 and 2019.

4119

4120 Table 4. 5. Confusion matrix of land cover classification in 2004 and 2019 using Random

4121 Forest.

Specification	Ground Truth								
	Class Name	Water	Forest	Open Forests/ Shrubs	Urban	Agriculture	Total	User's Accuracy	Error of commission (%)
Classified Map	<b>2004</b>								
	Water	21	0	0	0	0	21	1	0
	Forest	3	111	20	0	2	154	0.82	0.16
	Open Forests/ Shrubs	1	23	101	2	6	133	0.76	0.24
	Urban	0	0	0	22	0	22	1	0
	Agriculture	0	0	1	2	26	29	0.90	0.1
	Total	25	134	122	26	34	341		
	Producer's Accuracy	0.84	0.83	0.83	0.85	0.76	<b>Overall Accuracy</b>	0.82	
	Error of omission (%)	0.16	0.17	0.17	0.15	0.24	<b>Kappa coefficient</b>	0.74	
<b>2019</b>									
Classified Map	Water	27	0	0	0	0	27	1	0
	Forest	0	40	10	0	1	51	0.78	0.21
	Open Forests/ Shrubs	0	8	109	0	9	126	0.87	0.13
	Urban	0	0	2	24	0	26	0.92	0.07

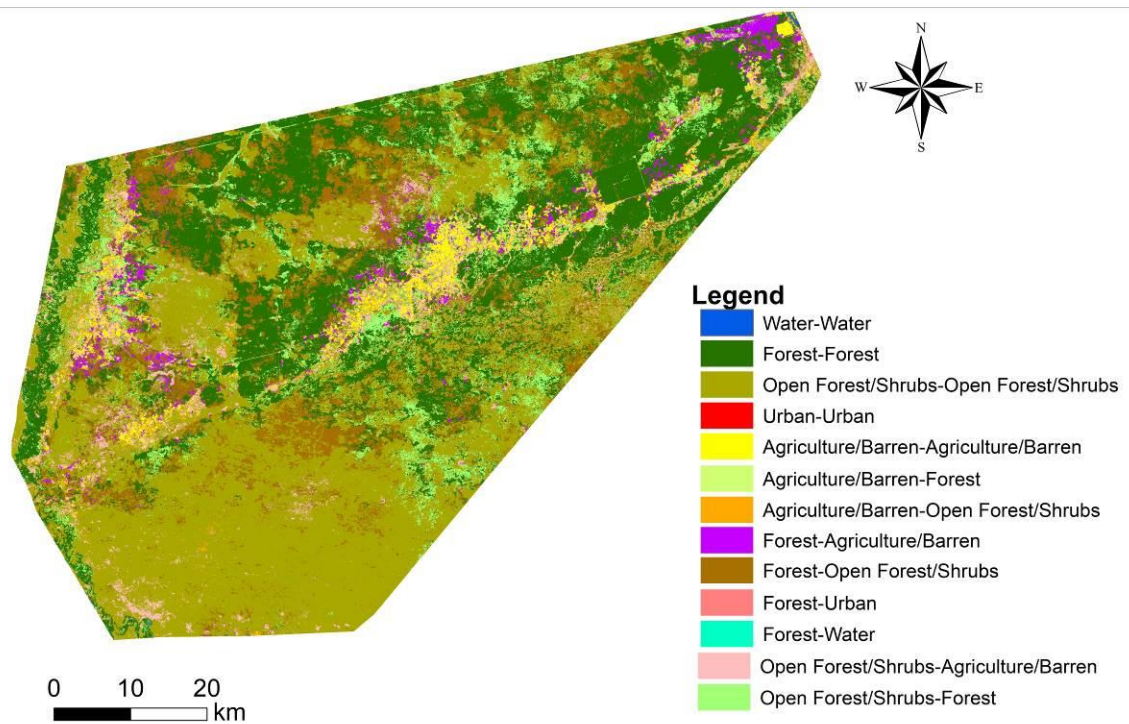
<b>Agriculture</b>	0	1	9	0	101	111	0.91	0.09
<b>Total</b>	27	49	130	24	111	341		
<b>Producer's Accuracy</b>	1	0.82	0.84	1	0.91	<b>Overall Accuracy</b>	0.88	
<b>Error of omission (%)</b>	0	0.18	0.16	0	0.09	<b>Kappa coefficient</b>	0.83	

4122

4123 

#### 4.4.7 Land cover change detection

4124 The land cover change map conversion from 2004 to 2019, is illustrated in Fig. 4.14. In  
4125 general, open forest/shrubs were the dominant land cover type followed by forests in both  
4126 years. In the northeast of the Zambezi State Forests, there was a significant change as  
4127 forested areas were replaced by barren/agricultural land as a result of forest logging. A  
4128 closer inspection of the classified maps revealed that most of the agricultural expansion  
4129 occurs primarily around the communal areas in the northern part of the study area, in  
4130 comparison to the southern part where protected areas such as Mudumu National Park  
4131 are found. The conversion from forests to open forest/shrubs was significant with  
4132 76345.98 ha (15%) and occurred mainly in the Mudumu National Park in the Southern  
4133 part and Zambezi State Forest in the northern part of the region. Table B 1 presents the  
4134 land cover change matrix between 2004 and 2019. Three major changes were an increase  
4135 in open forests/shrubs and agricultural/barren land and a reduction in forest land. In  
4136 2004, agricultural/barren land accounted for only 2.8% (143,77.87 ha) of total land. In  
4137 2019, this figure increased to 8.47% (429,36.31 ha) (see: Table B 1). On the contrary,  
4138 forest land experienced a significant decline of 9.04%, from 46.41% (235,140.91 ha) to  
4139 37.37% (189,334.60 ha) of the total area in 2004 and 2019, respectively (see: Table B 1).  
4140 The forest loss mainly was due to conversion to open forest/shrub (76,345.9), followed by  
4141 agricultural/barren land (10,634.1 ha) (see Fig. 4.14). At the same time, other land uses  
4142 are also converted to forest. For example, 40,172.9 ha of open forests/shrubs was  
4143 converted to forest, followed by agricultural/barren land (236,77.1 ha) (see Fig. 4.14).



4144

4145 Fig. 4. 14. Changed areas for the epoch (2004–2019) in the study area

4146

4147 

## 4.5 Discussion

4148 

### 4.5.1 Effectiveness of BFAST and BEAST algorithms for

  
4149 

### characterising change in dryland forests

4150 

#### 4.5.1.1 Trend

4151 Despite BFAST and BEAST algorithms being able to handle unfiltered data, the  
 4152 study found in the preliminary testing phase of the analysis that the use of filtered  
 4153 MODIS time series yields accurate results and improved forest change detection, as  
 4154 compared to the unfiltered data (see supplementary: A1). Identified changes that  
 4155 occur in the trend component indicate both gradual and abrupt changes in land  
 4156 cover, while changes occurring in the seasonal component indicate phenological  
 4157 variation. In terms of deforestation, BFAST and BEAST algorithms identify a  
 4158 consensus in time of breakpoints of larger magnitude, such as those associated  
 4159 with clear-cutting of the forest to non-forest. This agreement shows that both  
 4160 algorithms can be used to detect large-scale disturbances in the dryland forest. In

4161 terms of drought, BEAST algorithm was found to be the most successful in  
4162 identifying abrupt changes from vegetation disturbance caused by drought. BFAST  
4163 algorithm performed well in detecting abrupt changes of some known large  
4164 magnitude drought events, however, BFAST did not identify abrupt changes in  
4165 forest response for most drought and fire events, especially the lower magnitude  
4166 of change. A study by Watts et al. (2014) reported that BFAST did not detect abrupt  
4167 changes in vegetation as a result of well-known flood events. In this study, the  
4168 advantage of BEAST was the capability to detect the impact of exceptional climatic  
4169 conditions in both high and low magnitude drought years of 2002/03, 2005,  
4170 2010/11, 2015/16, and 2019 on forest stand development. Conversely, BFAST  
4171 algorithm was not able to detect such abrupt changes, as was seen in an example of  
4172 a fire event in 2017 that resulted in a known disturbance within the forest plot. In  
4173 this study, when using BFAST, sometimes 'minor changes', such as beginning or  
4174 end of periods of disturbance and recovery are not included in the identified trend,  
4175 and these breakpoints are often (incorrectly) counted as false positives. With such  
4176 limitations in the performance of BFAST algorithm, disturbance or drought events  
4177 can therefore be easily missed. A similar problem was found in a study by Wu et al.  
4178 (2020), where BFAST algorithm was applied to an NDVI time series to detect  
4179 changes within forest areas in China. They found that BFAST algorithm failed to  
4180 detect slow urban expansion which resulted in a partial forest cut within the pixel,  
4181 until the whole area of the pixel was changed.

4182 By comparing MODIS vegetation indices in detecting disturbance and trends in  
4183 dryland forests, GNDVI outperformed NDVI in both algorithms. Particularly, BEAST  
4184 algorithm generated change model using the GNDVI time series performed better  
4185 overall. Both NDVI and GNDVI predicted large-scale clear-cut deforestation events  
4186 accurately. However, GNDVI was more sensitive to detecting the abrupt changes  
4187 due to droughts, fire, and small-scale disturbances. The analysis of the NDVI time  
4188 series sometimes failed to detect abrupt changes in areas that did not undergo  
4189 complete land cover class changes. The sensitivity of NDVI to background  
4190 variations in the canopy and herbaceous layers could explain why the use of NDVI  
4191 failed to detect disturbances and drought impacts in these areas (Huete et al.,  
4192 2002). For stable or recovered forests, BFAST and BEAST algorithms performed  
4193 similarly in detecting gradual changes using NDVI and GNDVI time series. The

4194 similarity in the performance of the two indices can be attributed to the fact that  
4195 the study area is covered in trees and less of herbaceous layer (see supplementary:  
4196 D1 and D2 for field photo and LC8 time series images). The gradual increase in  
4197 forest cover of the stable forest can be a result of limited disturbance from fire,  
4198 wildlife, and logging. This suggests that the dryland forest can quickly recover from  
4199 drought in areas where multiple disturbances have not been experienced.

#### 4200 4.5.1.2 Phenology

4201 In this research study area, the dryland forests have a very pronounced seasonality  
4202 controlled mainly by humidity, with a rapid response to the onset of the rainy  
4203 season, reflected in the abrupt changes in NDVI and GNDVI responses. The  
4204 interannual variation in precipitation caused the change detection algorithms to  
4205 flag breakpoints related to dryland forest phenology (Grogan et al., 2016, Zhao et  
4206 al., 2019). BEAST algorithm detected phenological changes resulting from drought  
4207 years followed a large increase in precipitation and clear-cut deforestation in NDVI  
4208 and GNDVI time series (Table 4.2). BFAST also failed to detect any seasonal change  
4209 using both NDVI and GNDVI time series. The ability of BFAST algorithm to capture  
4210 seasonal changes triggered by interannual variations or disturbances in the  
4211 dryland biomes is limited. Studies that tested BFAST algorithm on different forest  
4212 types also reported poor performance in detecting seasonal changes. This included  
4213 limitations in identifying changes in the amplitude of the seasonal curve, or  
4214 changes in the number of seasons in which tropical dryland forests were  
4215 characterised by high inter-annual seasonal variability (Gao et al., 2021, Grogan et  
4216 al., 2016).

4217 The difference in the performance of the algorithms tested here can be attributed  
4218 to the fact that BEAST incorporates non-linear change models (Burkett et al.,  
4219 2005). BEAST not only detects the changepoints, but also quantifies their  
4220 probability of being true, providing a confidence measure to interpret the changes  
4221 in both trend and seasonality. A shortcoming of BFAST algorithm is that by relying  
4222 on linear segments to describe underlying fluctuating trends, the model assumes  
4223 vegetation trends are quasi-linear processes (i.e., regular, or stable seasonality)  
4224 (Grogan et al., 2016). Deterministic models used within BFAST algorithm often do  
4225 not therefore capture nonlinear behaviour as thresholds and complex interactions

4226 among ecosystem processes are unaccounted for (Burkett et al., 2005). For  
4227 example, Jamali et al. (2014) accounted for non-linear vegetation changes in the  
4228 Sahel using a polynomials fitting-based scheme to an annual NDVI time series and  
4229 found it to describe general non-linear change trajectories. It has been widely  
4230 observed that vegetation dynamics and land cover change can often occur in a non-  
4231 linear pattern (Lambin et al., 1997). Additionally, climatic variations and change in  
4232 moisture regimes, such as short- or long-term changes in rainfall patterns or  
4233 temperature, may also drive nonlinear progressions in vegetation cover (Foley et  
4234 al., 2003).

4235 These results demonstrate that accounting for variations at the seasonal scale  
4236 while simultaneously uncovering complex nonlinear trends in forest dynamics is  
4237 important, particularly for dryland forests where seasonality may vary  
4238 significantly in amplitude from year to year. Projected rapid climate change is of  
4239 major concern in these regions, especially when viewed with other population  
4240 stresses such as habitat conversion, the impacts of fire, and herbivores  
4241 disturbances. In KAZA, it is reported that competition between wild species occurs  
4242 when habitats become degraded, especially by elephants (FAO, 2009). These  
4243 synergistic stresses are likely to prove to be the greatest challenge to wildlife  
4244 conservation in the 21st century, hence tracking the occurrence of disturbance  
4245 events and phenological shift events as they occur is an essential task in PAs  
4246 conservation efforts.

#### 4247 4.5.2 Spectral index sensitivity in dryland forests

4248 The study found that BFAST and BEAST change models using the GNDVI time  
4249 series performed better than the more commonly used NDVI. Comparing results  
4250 from NDVI and GNDVI and related these to the precipitation anomaly shows that  
4251 the maximum differences in vegetation index performance occurred over the  
4252 dryland forest relative to the grassland, and then shrubs. There is a general  
4253 agreement between indices in areas undergoing browning and greening in the  
4254 non-forested area (see: Fig. 4.4). GNDVI had the best performance in distinguishing  
4255 browning and greening of forest from herbaceous layers affected by droughts. For  
4256 example, analysis of the NDVI was able to detect a strong greening in forest areas  
4257 in the severe droughts of 2015-2016 and 2019. These results are similar to a study

4258 by Loranty et al., (2018) that found positive decadal trends in NDVI in Siberian  
4259 forests that ranged from sparse to dense canopy cover, which correspond to  
4260 increases in understory productivity rather than an increase in forest cover. This  
4261 study results also concur with the study by Otsu et al. (2019) that found that  
4262 GNDVI performed best in distinguishing broad leaf from needle leaf forests as  
4263 compared to NDVI. Another study by Yoder et al. (1994) used the green channel in  
4264 a vegetation index and found that it had a better correlation with the  
4265 photosynthetic activity of the tree canopy in miniature Douglas-fir trees as  
4266 compared to the red channel. The main reason for the difference in the  
4267 performance of NDVI and GNDVI is likely because the former is more sensitive to  
4268 low chlorophyll concentrations, while GNDVI is more sensitive to high chlorophyll  
4269 concentrations and so is more accurate for assessing chlorophyll content at the  
4270 tree crown level (Gitelson et al., 1996). A study by Grogan et al., (2016) tested  
4271 BFAST on Land Surface Water Index (LSWI) and used NDVI on dry-deciduous and  
4272 evergreen forests and found that the LSWI time series outperformed the more  
4273 commonly used NDVI and EVI indices.

4274 In conjunction with observations from the field, these results indicate that  
4275 understory vegetation likely exerts a strong influence on NDVI. It has been shown  
4276 in other research that different plant functional types, including canopy  
4277 background variations and herbaceous vegetation, also have a pronounced  
4278 seasonal effect on the NDVI signal, while also not being directly correlated with  
4279 woody cover (Grogan et al., 2016, Prince, 1991). This is apparent in my  
4280 observations and suggests that the NDVI pattern of a higher-than-average anomaly  
4281 during the growing season of 2015 and 2019 may correspond primarily to  
4282 increases in understory productivity rather than an increase in forest cover. For  
4283 this study, a possible explanation for this is that tropical vegetation greenness can  
4284 recover rapidly soon after forest clearing as the low herbaceous cover such as  
4285 grassland and saplings grow vigorously due to increased light levels, resulting in  
4286 reduced sensitivities to detect disturbances in greenness-based indices such as  
4287 NDVI. The use of VIs for biophysical parameter retrievals is therefore a challenging  
4288 task and there remains much work in understanding VI sensitivity across and  
4289 within dryland biomes (Huete et al., 2002). Ground field validation test sites are  
4290 essential in this regard and help provide valuable insight in interpreting spatial



4291 and temporal variability in VI that arises from vegetation-related properties,  
4292 including LAI, canopy structure, and understory vegetation. Hence, both soil  
4293 characteristics and the reflectance of lower plant communities may lead to  
4294 misinterpretations of the open dry forest dynamics and an under or  
4295 overestimation of ecosystem productivity in similar semiarid environments.

#### 4296 4.5.3 Land cover classification and spatial pattern of forest 4297 changes using breakpoints and magnitude

4298 This study applied remote sensing techniques to classify satellite imagery of the  
4299 Zambezi region of Namibia in 2004 and 2019. Despite the good classification  
4300 obtained in this study, there were some general issues which may have reduced  
4301 the accuracy of the overall classification. For example, the spectral signature of  
4302 forests was mixing with the signature of open forests/shrubs, resulting in low  
4303 producer's accuracies for both classified map due to their noisy Landsat spectral  
4304 signatures and difficulty in interpreting them. A similar problem was also  
4305 encountered by Lu et al. (2003) and Zhao et al. (2016). To overcome this mixed  
4306 pixel problem, higher spatial resolution multispectral images such as SPOT images  
4307 reduced the mixed pixel problem, resulting in improved forest classification  
4308 accuracy (Lu et al., 2008). However, using higher spatial resolution with pixel-  
4309 based tree species classification approaches also increased spectral variations,  
4310 especially in savannas with open forests, because of their complex forest stand  
4311 structure and canopy shadows, resulting in poor classification accuracies (Lu and  
4312 Weng, 2005; Myeong e al., 2001; Pu et al., 2018; McElhinny et al., 2005).  
4313 Incorporation of these relatively medium spatial resolution images such as Landsat  
4314 with 30-meter spatial resolution with other data sources such as digital elevation  
4315 models (along with their derivatives such as slope and aspect), spatial texture, and  
4316 SAR can improve classification accuracy (Myeong e al., 2001).

4317 In this study, the LULC change trajectories included the conversions to-and-from  
4318 land cover classes. Unchanged areas, particularly forest land and open  
4319 forest/shrub land, are of exceptional importance for biodiversity management,  
4320 providing forest habitat and increases connectivity between forest patches for  
4321 wildlife population dynamics, and migratory species (Stoldt et al., 2020; Wegmann  
4322 et al., 2015; Wintle et al., 2019). In addition, unchanged areas provide timber and

4323 non-timber product supply, and carbon storage in the study area (David et al.,  
4324 2022a). The large areas of unchanged forest land may provide an indication of the  
4325 effectiveness of intensified efforts for forest protection and biodiversity  
4326 management such as forest fire protection programs and awareness creation on  
4327 the sustainable use of forests implemented by the Government (Russell-Smith et  
4328 al., 2017). Conversely, the large area of forest conversion to open forests/shrubs  
4329 and agricultural/Barren land could also indicate the degradation of forests from  
4330 continuous drought events and logging of forests for timbers from the Chinese  
4331 companies in the Zambezi region (Asanzi et al., 2014; Chikoore and Jury, 2021;  
4332 Weng et al., 2015). The most valuable timber tree species in Namibia include  
4333 *Pterocarpus angolensis*, *Baikiaea plurijuga*, and *Guibourtia coleosperma*. However,  
4334 the harvest of these trees has increased because of the high demand for timber  
4335 from dense tropical hardwood species from Chinese (Asanzi et al., 2014).

4336 Making full use of the opportunities that the Landsat and MODIS archive provides,  
4337 this study provides an assessment of land cover change and forest disturbances in  
4338 the KAZA region, from 2002/2004 to 2019, explored with change detection  
4339 algorithms. The main aim was to quantify and identify the Land cover change,  
4340 locations, types, and trends of the land cover during the 19-year period in  
4341 communal and protected areas of Namibia. Methodologically, this study showed  
4342 that dryland forest disturbances associated with deforestation and degradation  
4343 can be mapped reliably with both BFAST and BEAST change detection algorithms.  
4344 In terms of the performance of indices utilised, this study suggests that the GNDVI  
4345 was found to have the best performance in monitoring degradation and detecting  
4346 disturbances from droughts and fires as compared to NDVI. This study found the  
4347 NDVI is less sensitive to changes in dryland forests as compared to GNDVI, and this  
4348 result is consistent with studies that found that metrics based on the short-wave  
4349 infrared (SWIR) outperform NDVI in temperate and savanna ecosystems in the  
4350 USA (Jin and Sader, 2005, Kennedy et al., 2010, Zhu, Woodcock and Olofsson,  
4351 2012).

4352 Thematically, this study yielded three main insights. First, the study found diverse  
4353 spatial patterns of forest disturbances are more prevalent in the communal areas  
4354 and state forests such as the Zambezi ST, particularly when compared to protected  
4355 areas such as Mudumu NP. These changes are driven by different disturbance

4356 agents, including both natural processes (e.g., drought) and anthropogenic impacts  
4357 (e.g., timber logging, fire). This suggests disturbance attribution is central for  
4358 understanding the drivers and impacts of forest degradation. According to land  
4359 cover change analysis in Fig. 4.13, agricultural/barren land has increased  
4360 dramatically during 2004 to 2019. Agricultural/ barren land may be caused by (1)  
4361 cut trees for households and wood processing businesses, or (2) slash-and-burn  
4362 agricultural activities (Kamwi et al., 2017) and (3) timber trade (Asanzi et al.  
4363 2014). That unsuitable farming practice is mainly taken by local ethnic groups  
4364 living in the province, while the tree logging is due to a strong presence of logging  
4365 companies primarily from China (Nott et al, 2019). This is in agreement with  
4366 previous studies on land cover and land use analysis such as Kamwi et al. (2017)  
4367 that found agricultural expansion to be the most predominant driver in the same  
4368 study area.

4369 Second, the study found large areas of the dryland forest in the Zambezi ST have  
4370 experienced major disturbances from 2016 to 2019 from clear-cut of forests  
4371 coupled with fire, and extreme drought events, suggesting deforestation and  
4372 degradation is a widespread phenomenon in KAZA. Similar to the research  
4373 presented by Kamwi et al. (2015), the land cover analysis from this study (see: Fig.  
4374 4.13 and Fig.4.14) found that small-holder agriculture and shifting cultivation was  
4375 largely responsible for breakpoints of large magnitudes in the communal areas of  
4376 the Zambezi region detected by BFAST change detection (see: Fig 4. 12). The  
4377 BFAST change detection also detected vegetation disturbances/degradation, stable  
4378 vegetation, and vegetation regrowth, and these level of disturbances, trend and  
4379 direction of change were not detected by the bi-temporal classification. Third, a  
4380 clear association between forest disturbance and precipitation was found. Forest  
4381 disturbance was particularly widespread during severe drought years such as  
4382 2015-2016 and 2019. This study results also showed positive magnitude  
4383 breakpoints, which represented forest recovery and vegetation regrowth, which  
4384 could be attributed to increased precipitation and lack of disturbance in protected  
4385 areas such as Mudumu NP, as compared to community conservancies and the  
4386 Zambezi SF. This study disturbance maps, land cover change and field observations  
4387 suggest that drought, forest logging, agricultural expansion, large herbivore  
4388 disturbance, and increased fire may explain some of the observed pattern by the

4389 BFAST and BEAST change detection algorithms (Kamwi et al., 2017); Nott et al,  
4390 2019), (also see: Fig. B2, B3, B4 and B5). Similar patterns of increases in forest  
4391 disturbance during drought seasons were found both in the Amazon and the Gran  
4392 Chaco of Argentina (Bullock et al., 2020, De Marzo et al., 2021).

4393 Previous land cover mapping research in the KAZA region has shown contrasting  
4394 results. Kamwi et al. (2015) reported forest and woodlands are expanding in  
4395 communal land in the Zambezi region, while Meyer et al. (2021) reported that  
4396 woodland cover reduced by 2.1% within the same study area and time period of  
4397 1990 to 2010. The land cover mapping from this study shows that forests reduced  
4398 by 9% in the same region between 2004 and 2019. The deforestation and  
4399 widespread degradation identified in this study are consistent with findings by  
4400 McNicol et al. (2018) that found Southern African woodland is highly dynamic with  
4401 widespread degradation and deforestation, but also extensive vegetation  
4402 regrowth. The further step on assessing the magnitude of change reported in this  
4403 study demonstrates first that forest change occurs in an incremental manner, and  
4404 second, by making use of the magnitude parameter, that conventional bi-temporal  
4405 classification studies could further be improved and complimented by extent and  
4406 severity of forest disturbances derive here (DeVries et al., 2015). The ability to  
4407 describe these change processes with high temporal detail highlights the  
4408 advantage of a time series change detection approach used here and the additional  
4409 information they provide to conventional bi-temporal classification maps of forest  
4410 versus non-forest maps conducted in KAZA region (Kamwi et al., 2017, Meyer et  
4411 al., 2021, Fox et al., 2017).

## 4412 4.6 Conclusion

4413 This study evaluated the applicability of BFAST and BEAST algorithms to detect a  
4414 range of abrupt, gradual, and seasonal changes using MODIS vegetation index (VI)  
4415 time series data in tropical dryland forests in Southern Africa from 2002–2019.  
4416 The change detection algorithms complemented the bi-temporal Land cover  
4417 change detection in Zambezi region from 2004 and 2019. The study has shown  
4418 that analysis of monthly MODIS VI time series, climate data, and field validation  
4419 can effectively describe and help to interpret longer-term changes of vegetation

4420 dynamics. Changes occurring in the trend component identified indicate both  
4421 gradual and abrupt changes, while giving insights into the influence of drought and  
4422 phenological variation on the forest. Four main conclusions can be drawn from this  
4423 study:

4424 First, dryland forests are highly dynamic and water sensitive with high rates of  
4425 deforestation and widespread degradation, but also continuous vegetation  
4426 recovery and regrowth are identified in protected areas compared to unprotected  
4427 areas.

4428 Second, BEAST algorithm was found to give the best performance overall, correctly  
4429 identifying abrupt changes of vegetation response to fire and drought impacts.  
4430 BFAST did not perform well in identifying abrupt changes resulting from fire and  
4431 low magnitude drought events. Based on the results, the best decomposition of  
4432 trend and seasonal breakpoints were given by BEAST using the GNDVI.

4433 Third, BEAST algorithm outperformed BFAST algorithm in detecting seasonal  
4434 changes driven by climatic and clear-cutting events. BEAST algorithm detected the  
4435 abnormality of deforestation and climate-driven changes in seasonality, which  
4436 helped identify the potential drivers of these phenological shifts. However, BFAST  
4437 failed to detect any seasonal changes within the entire study period (2002-2019)  
4438 using either the NDVI or GNDVI.

4439 Fourth, conventional NDVI was highly influenced by canopy background variations  
4440 and herbaceous layers, as compared to the GNDVI. NDVI performed best in the  
4441 robust detection of areas with complete land cover class changes, while GNDVI  
4442 performed well in detecting changes within areas of partial (low magnitude  
4443 change) and complete land cover class changes. The analysis suggests that GNDVI  
4444 is more sensitive to chlorophyll concentration in vegetation when the leaf area  
4445 index is moderately high as is the case in tropical dryland forests, while NDVI is  
4446 more sensitive to forest types with low chlorophyll concentrations.

4447 Finally, the study shows that the droughts that took place in 2015 and 2019 were  
4448 longer and more extreme than the droughts in 2002-2003, 2005, 2007 and 2011-  
4449 2013. Overall, the results also show that a large part of the growing season and

4450 phenology is highly influenced by seasonal and inter-annual variations in climatic  
4451 conditions, particularly in the case of severe drought in the KAZA region.

4452 These results highlight the importance of complementing the conventional bi-  
4453 temporal classification studies on Land cover change with improved time series  
4454 change detection algorithms to detect the magnitude, extent, and severity of forest  
4455 disturbances with high temporal detail. The study also showed the importance of  
4456 considering the sensitivities of VIs used in forest monitoring when trying to  
4457 identify non-linear dynamics of dryland forests. Two extreme record droughts in  
4458 less than two years (2015-2016 and 2018-2019) are evidence of the negative  
4459 impacts of extremes of climate variability and climate change in the region.  
4460 Therefore, an in-depth assessment of the intensity, spatial coverage, and  
4461 geography of impacts of future droughts are of fundamental importance to the  
4462 region. The approach described above is transferable to other tropical forest areas  
4463 with high inter-annual variability that is influenced by seasonal climatic variations  
4464 and disturbance. These methods are subject to further tests with other datasets of  
4465 higher spatial resolution such as Landsat, Sentinel, or simulated datasets, to ensure  
4466 their efficacy.

## 4467 4.7 Acknowledgments

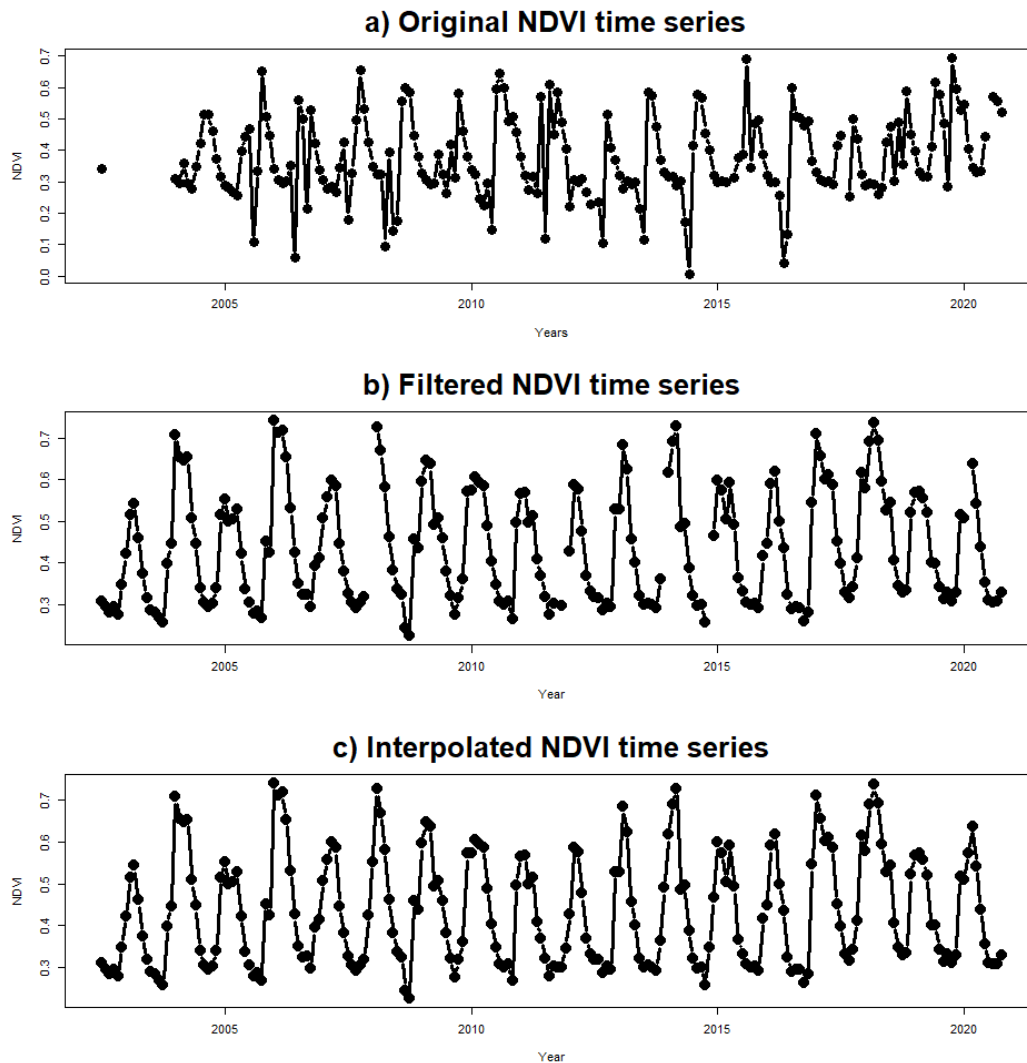
4468 This work was supported by Commonwealth Scholarship Commission PhD grant  
4469 number: NACS-2017-409 from the 2017–2021, Geography doctoral program at  
4470 Durham University. The authors acknowledge financial support from the Royal  
4471 Geographical Society (grant number: MC 08/19) and WWF Namibia Mike Knight  
4472 for travel support grant number: T225. I thank WWF KAZA TFCA Secretariat  
4473 Nyambe Nyambe, Chobe National Park Authority Michael Flyman, and University  
4474 of Namibia (Katima Branch) Dr. Ekkehard Klingelhoetter for the support during the  
4475 fieldwork. I also thank Morgan Kamwi who helped with transportation and data  
4476 collection in the field.

4477

4478

## 4479 4.8 Supplementary Information 2

## 4480 MODIS Data Processing and Filtering



4481

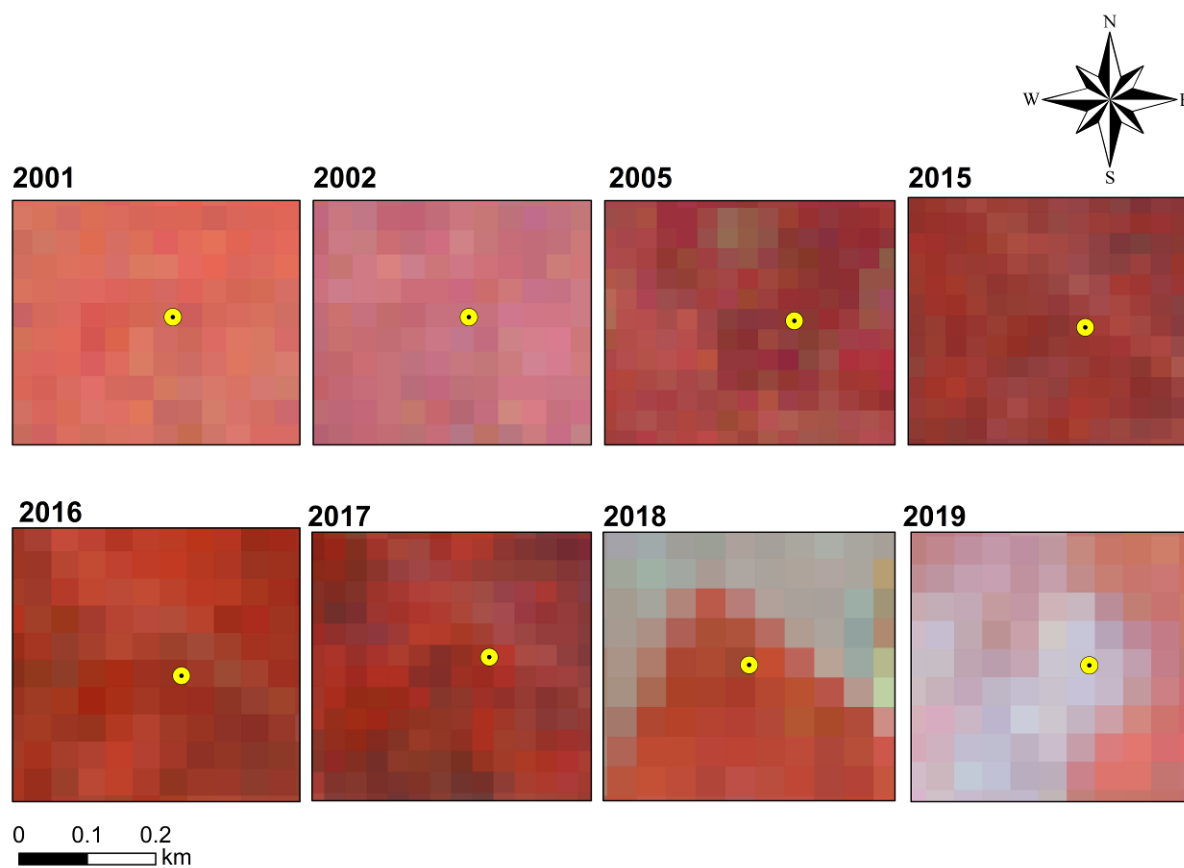
4482 Fig. B 1. Temporal profiles of raw and cleaned MODIS NDVI data for a forest plot: (a)  
 4483 original time series after MCV method; (b) time series retained after filtering, and (c) time  
 4484 series with linear interpolation on filtered points over a 17-year period.

4485

## 4486 Clear-cut and burnt forest

4487 Fig. B 2. A and B shows field photo evidence of a deforestation event in a dryland forest  
 4488 dominated by *Baikiaea plurijuga* species, the area was burned in 2017 and clear-cut for

4489 timbers in around 2018-2019. The photo location coordinate is 17.49°S, 24.21°E taken  
 4490 from ground survey in Namibia in 2019.



4491

4492 Fig. B 3. Shows the corresponding time series of Landsat images with no cloud cover in the  
 4493 pixels documenting changes in the forest (forest to shrubs) from 2015 to 2019,  
 4494 respectively. The yellow dot represents the location ID (coordinate: 17.49°S, 24.21°E). The  
 4495 year 2002 and 2005 was included because it is a drought year and 2001 was used as a  
 4496 baseline year.

4497

4498 **Drought impacts and degraded forest**

4499

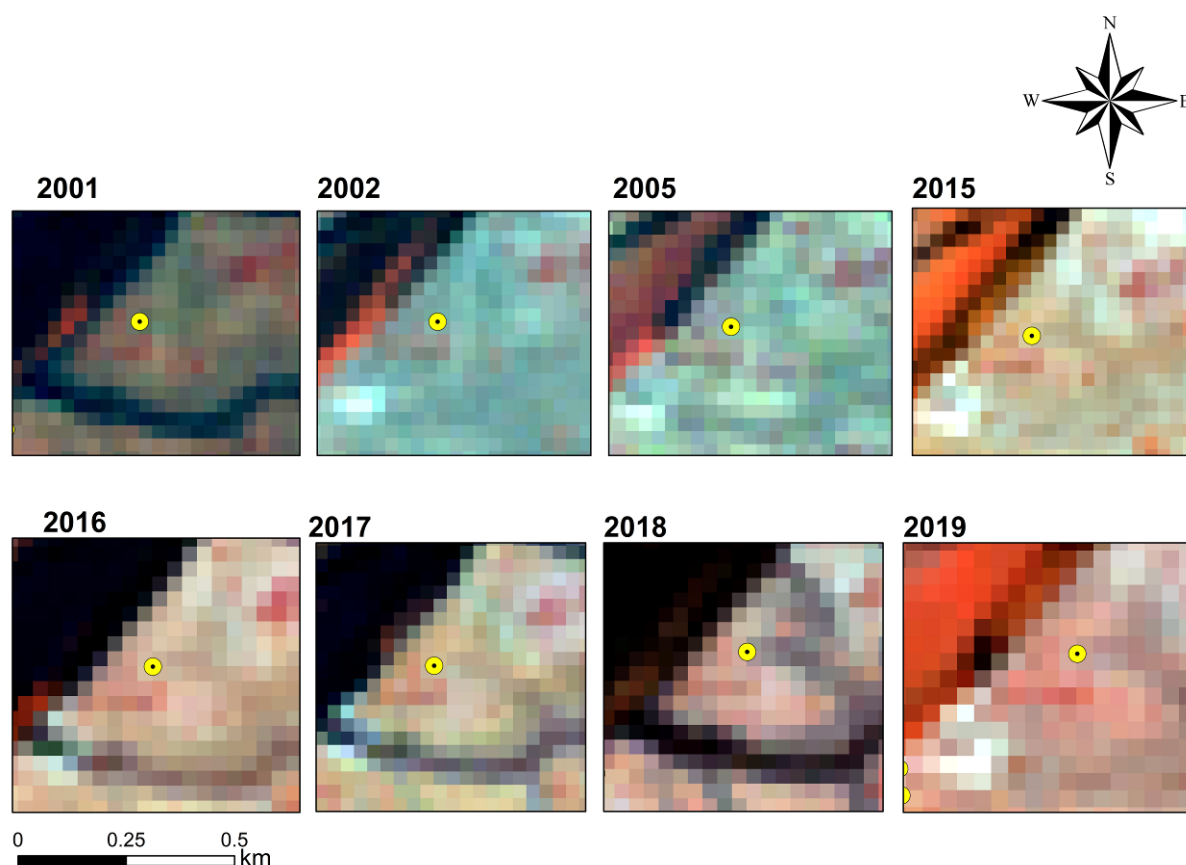




4500

4501 Fig. B 4. shows field photo evidence of a degrading forest dominated by baobabs and  
 4502 riparian woodlands species near Chobe River frontage. The photo location coordinate is  
 4503 17.80°S, 24.95°E taken from ground survey in Botswana in 2019.

4504



4505

4506

4507 Fig. B 5. shows the corresponding time series of Landsat images with no cloud cover in the  
 4508 pixels documenting changes in the plot from 2015 to 2019, respectively. The yellow dot  
 4509 represents the location ID (coordinate: 17.80°S, 24.95°E). The year 2002 and 2005 was  
 4510 included because it is a drought year and 2001 was used as a baseline year.

4511

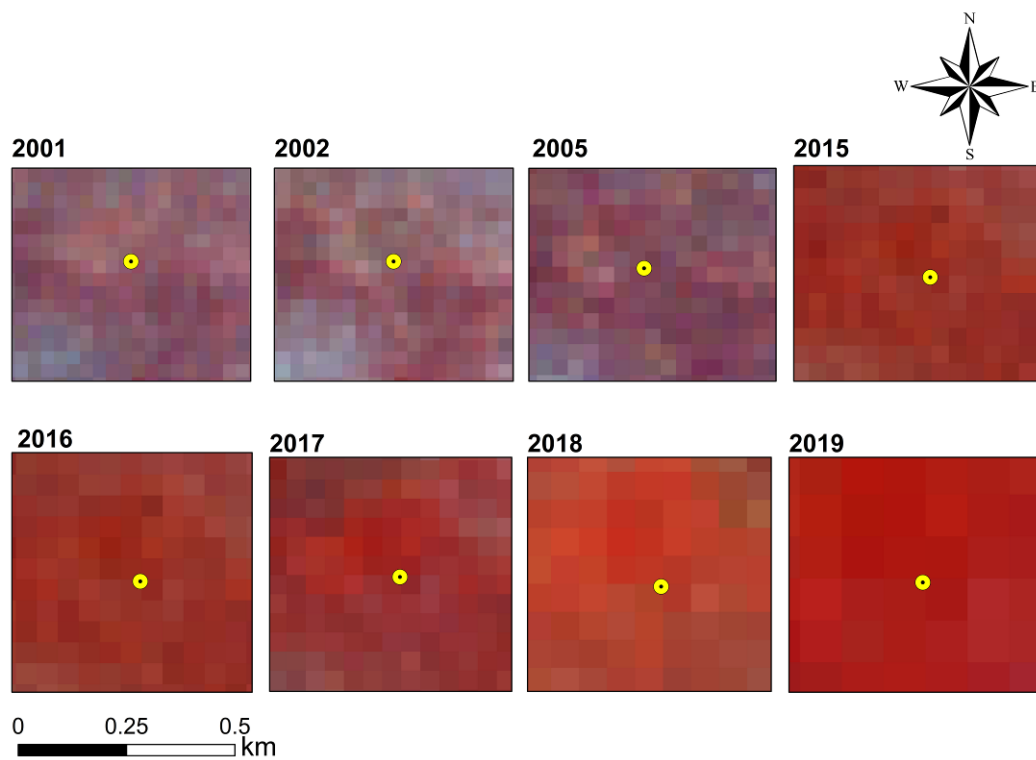
4512 A stable and recovering forest

4513



4514

4515 Fig. B 6. Shows field photo evidence of a forest that has not experienced any disturbance  
 4516 for the period of the study. The photo location coordinate is 17.57°S, 24.28°E taken from  
 4517 ground survey in Botswana in 2019.



4518

4519 Fig. B 7. shows a time series of LC8 images from 2015 to 2019 is shown below. The yellow  
 4520 dot represents the location ID (coordinate: 17.57°S, 24.28°E). The year 2002 and 2005  
 4521 was included because they are drought years and 2001 was used as a baseline year

4522 Table B. 1. Land cover areas in the study area per year (2004 and 2019) in km<sup>2</sup> and  
 4523 hectares.

Class name	2004 Area (km <sup>2</sup> )	2004 Area (ha)	2004 Area (%)	2018 Area (km <sup>2</sup> )	2018 Area (ha)	2019 Area (%)
Water	5	508	0	6	600	0
Forest	2,351	2351,411	46	1,893	189,335	34
Open forests/Shrub	2,564	256,410	51	2,735	273,512	54
Urban	3	262	0	3	318	0
Agriculture	143	14,378	3	429	42,934	8

4524

4525 Table B. 2. Area changes of BFAST (2002-2019) using sample-based estimates and the  
 4526 observed disturbance change rates in hectares.

Change identified by BFAST	Area (ha)	Standard Error (ha)	2.5 % (ha)	97.5 % (ha)
Non-disturbance (No change) <i>(Stable Forest)</i>	106,390	9,817	87,148	125,631
Low negative changes (no change) <i>(Degradation)</i>	90,929	10,636	70,083	111,776
Large negative changes (No change) <i>(Non-forest)</i>	38,873	7,162	24,836	52,910
Non-disturbance -Low negative changes <i>(Stable forest to Degradation)</i>	33,132	6,859	19,688	46,576
Non-disturbance -Large negative	99,911	9,753	80,795	119,027

changes <i>(Stable Forest to Deforestation)</i>				
Low negative changes -Large negative changes <i>(Degradation to Deforestation)</i>	59,515	8,154	43,533	75,497
Low negative changes -Non-disturbance <i>(Degradation to Stable Forest)</i>	23,409	556,8	12,497	34,322
Large negative changes -Low negative changes <i>(Deforestation to Degradation)</i>	48,537	8,353	32,167	64,908
Large negative changes -Non-disturbance <i>(Deforestation to Stable Forest)</i>	5,980	2,966	167	11,792
Total	506,676			

4527

4528 Table B. 3. Area changes for the Random Forest classification in the Zambezi region in  
4529 hectares.

<b>Change identified by two-interval classification</b>	<b>Area (ha)</b>
Forest-Forest	147,876
Non-forest-Non-forest (no change)	201,157
Forest - Non- Forest	87,251

Non-forest - Forest	41,447
Non-forest - Non-Forest (change)	28,944
Total	506,676

4530

4531 Table B. 4. Area-based transition among land cover categories for the Random Forest  
4532 classification for the period 2004–2019 in the Zambezi region in hectares.

4533

4534

Land cover class Change	Re-organisation	Area Change (ha)	Area Change (%)
Agriculture-Agriculture	Non-forest-Non-forest (no change)	8,501	2
Agriculture-Forest	Non-forest - Forest	1,109	0
Agriculture-Open forest/Shrub	Non-forest -Non-Forest (change)	4,707	1
Agriculture-Urban	Non-forest -Non-forest (change)	58	0
Agriculture-Water	Non-forest -Non-forest (change)	4	0
Forest-Agriculture	Forest to Non-forest	10,634	2
Forest-Forest	Forest-Forest	14,7876	29
Forest- Open forest/Shrub	Forest to Non-forest	76,346	15
Forest-Urban	Forest to Non-forest	16	0
Forest-Water	Forest to Non-forest	256	0
Open forest/Shrub -Agriculture	Non-forest -Non-forest (change)	23,677	5
Open forest/Shrub -Forest	Non-forest - Forest	40,173	8
Open forest/Shrub - Open Forest/Shrub	Non-forest-Non-forest (no change)	192,313	38
Open forest/Shrub -Urban	Non-forest -Non-forest (change)	205	0
Open forest/Shrub -Water	Non-forest -Non-forest (change)	34	0
Urban-Agriculture	Non-forest -Non-forest (change)	115	0
Urban-Forest	Non-forest - Forest	5	0
Urban- Open forest/Shrub	Non-forest -Non-forest (change)	101	0
Urban-Urban	Non-forest-Non-forest (no change)	39	0
Urban-Water	Non-forest -Non-forest (change)	1	0
Water-Agriculture	Non-forest -Non-forest (change)	7	0
Water-Forest	Non-forest - Forest	161	0

Water- Open forest/Shrub	Non-forest -Non-forest (change)	36	0
Water-Urban	Non-forest -Non-forest (change)	0	0
Water-Water	Non-forest-Non-forest (no change)	305	0
Total		506,676	100

4535

4536 **5 A SPATIO-TEMPORAL DROUGHT AND FIRE ANALYSIS**  
4537 **FOR SEMI-ARID DRYLAND ECOSYSTEMS IN SOUTHERN**  
4538 **AFRICA USING MODERATE RESOLUTION SATELLITE**  
4539 **IMAGERY.**

---

4540  
4541  
4542  
4543  
4544  
4545  
4546  
4547



4548

4549

4550

4551

4552 Chapter 5 Manuscript in progress: Intended for submission to *Remote Sensing in*4553 *Ecology and Conservation*.

4554

4555 **Title:** A spatio-temporal drought and fire analysis for semi-arid dryland  
4556 ecosystems in southern Africa using moderate resolution satellite imagery.

4557

4558

4559

4560

4561 **Author contributions**

4562

4563 David Ruusa- Design the research, perform the data analysis, interpret the results,  
4564 wrote the manuscript, and revised the manuscript. Nick Rosser- Contributed to the  
4565 research design, manuscript editing and supervision. Daniel Donoghue-  
4566 Contributed to the research design, conducting fieldwork, manuscript editing and  
4567 supervision.

4568

4569

4570

4571

4572

4573

4574

4575

4576

4577

4578

4579

4580

4581

4582

4583

4584

4585

4586

4587 **Abstract**

4588 The dryland ecosystem of Southern Africa is fire-prone and has a long history of  
4589 recurrent droughts that in turn, affect its ecology, structure, function and  
4590 distribution. This chapter presents a spatiotemporal analysis of drought, water  
4591 stress, fire impacts on dryland vegetation between 2002 and 2019 for the largest  
4592 conservation area: Kavango-Zambezi Transfrontier Conservation Area (KAZA). To  
4593 disentangle the relative contribution of climatic and fire regimes to dryland  
4594 vegetation, Normalised Difference Vegetation Index (NDVI), precipitation data,  
4595 temperature data, evapotranspiration, Root Soil Moisture (RSM) and Active Fire  
4596 and Burned Area data products were used. For drought condition, this study shows  
4597 most severe drought was in 2002/2003, 2005, 2015/2016 and 2018/2019. The  
4598 worst drought with the longest duration and highest magnitude was recorded in  
4599 2019. In the KAZA region, about 149,410 km<sup>2</sup> of land is burned on an annual basis  
4600 over the period 2002–2019, however significant differences were observed in the  
4601 fire patterns among the five countries of KAZA. Fire incidence was higher in Angola  
4602 and Zambia where burning is not strictly controlled; midrange fire incidences were  
4603 observed in Namibia where fire control policy and awareness programs were  
4604 introduced in 2006; and fire incidence was lower in Botswana and Zimbabwe,  
4605 where there are effective and strict fire management policies. These results reveal  
4606 that the areas with high dryland forests (or high tree cover), high rainfall, and long  
4607 dry season length coincide with areas of high fire frequency resulting in relatively  
4608 large burned areas. The combination of drought, water stress and high fire  
4609 frequency observed in this study has led to an increase in land area classified as  
4610 arid and semi-arid at the expense of dry sub-humid and humid land classes, which  
4611 were reduced by 10% in the period 2002 to 2019. These findings have important  
4612 implications on wildlife habitat management and climate change in Southern  
4613 Africa's dryland forest ecosystems.

4614 **Keywords:** Dryland vegetation, climate change, soil moisture, drought, forest fire,  
4615 Southern Africa, remote sensing

4616

## 4617 5.1 Introduction

### 4618 5.1.1 Drought stress on dryland vegetating

4619 Drought is a regular and recurrent feature of Southern African climate, and climate  
4620 change scenarios predict large-scale biogeographical shifts in vegetation in  
4621 response to the severe drought and intense moisture surplus which will be  
4622 exacerbated by higher temperatures (Diffenbaugh et al., 2017). Growing evidence  
4623 suggests that the effects of drought on vegetation under warmer conditions can be  
4624 severe, as highlighted by recent observations of regional-scale woody-plant die-off  
4625 across Southern Africa (Naidoo et al., 2013), the Sahel (Anyamba et al., 2005), and  
4626 more widely around the globe (De Jong et al., 2013). In Southern Africa's arid and  
4627 semiarid areas, droughts are a frequent occurrence and can have severe ecological  
4628 and economic consequences (Mason et al., 2000). While these events may be short  
4629 duration followed by recovery during subsequent years of higher rainfall, in some  
4630 cases droughts can trigger substantial and irreversible ecological and  
4631 socioeconomic changes (Ellis et al., 1988).

4632 The effects of drought on vegetation can vary considerably across ecosystems,  
4633 depending on plant adaptations and interactions with other ecological processes  
4634 (Engelbrecht et al., 2007). The responses of vegetation to variations in climate are  
4635 expected to be most sensitive and extreme in tropical open woodlands and forests  
4636 in arid and semi-arid ecosystems (Watson et al., 1996). Tropical open woodlands  
4637 (hereafter called "dryland forest or woodland") are forests comprising mixtures of  
4638 trees, shrubs, and grasses in which the tree canopies do not form a continuous  
4639 closed cover (Grainger, 1999). There is evidence that anomalies in tropical  
4640 vegetation greenness are linked to global inter-annual variations in sea surface  
4641 temperature (SST), land surface temperature and precipitation, as evidenced in the  
4642 dryland forests (Huang et al., 2017). The xeric areas of the dryland biome often  
4643 have unreliable rainfall and are often subject to a substantial multi-year rainfall  
4644 deficit. Furthermore, the impacts of drought tend to be aggravated by  
4645 deforestation, land degradation, growing water demand and extremes of  
4646 temperature, as a result of climate variability, anthropogenic activities and global  
4647 warming (Dale et al., 2001). For example, Chagnon et al. (2004) found a large shift  
4648 in local rainfall and seasonality with increases in deforested areas in the Amazon,

4649 associated with local atmospheric circulation that were changed by gradients in  
4650 vegetation. Monitoring drought stress in vegetation is a critical component of  
4651 proactive drought planning designed to mitigate the impact of this natural hazard.  
4652 Although it is not possible to avoid drought, its impacts can be managed through  
4653 preparedness planning. The success of drought preparedness and management  
4654 depends, among others, on how well the droughts are defined and drought  
4655 characteristics (e.g., intensity and duration) are quantified temporally and  
4656 spatially.

4657 A drought is a naturally recurring hazard and can alternatively be defined as a  
4658 temporary, recurring reduction in the precipitation in an area. Droughts have a  
4659 slow initiation and they are usually only recognised when the drought is already  
4660 well established. The deficiency in precipitation is the main causes of all drought  
4661 types, including: meteorological, agricultural, hydrological, and socioeconomic.  
4662 Meteorological drought relates to precipitation deficiencies in absolute totals for a  
4663 given period and is one of the primary causes of wider drought. On the other hand,  
4664 agricultural drought is characterised by a soil moisture deficit and changed plant  
4665 behaviours during the plant-growing period. The longer and the more spatially  
4666 extensive this deficiency, the more likely the occurrence of other types of droughts,  
4667 such as hydrological that is a reduction of streamflow, lake or reservoir storage,  
4668 and a lowering of ground-water levels. Socioeconomic drought occurs when the  
4669 demand for an economic good exceeds supply as a result of a weather-related  
4670 shortfall in water supply (Maliva et al., 2012). Drought indices derived from  
4671 meteorological data can be used to monitor not only meteorological droughts but  
4672 also agricultural and hydrological droughts, and to categorise the seriousness of  
4673 the drought, which is important for a wide range of management and planning  
4674 decisions. Drought indices commonly applied around the world are summarised by  
4675 Svoboda et al. (2016). Consequent impacts of warm droughts could include a  
4676 reduction in habitat for wildlife, enhanced opportunities for invasion by exotic  
4677 species, formation of novel communal areas, imbalances in the hydrologic cycle,  
4678 and temporal disruptions to ecosystem goods and services (Rands et al., 2010).

## 4679            5.1.2 Fire impacts on dryland vegetation

4680    In addition to drought, within the forest-dryland mosaics other natural  
4681    disturbances that affect forests include large pulses of forest disturbances from  
4682    agents such large mammalian herbivore damage, insect outbreaks, strong winds  
4683    and wildfires (Geist et al., 2004). Fire is considered a major determinant of the  
4684    ecology and distribution of Africa's dryland forests and the frequency and severity  
4685    of large wildfires has increased during some extremely dry years in past decades  
4686    (Archibald et al., 2018). The burning of natural vegetation is common and  
4687    widespread throughout the tropics and is considered to be a significant source of  
4688    aerosol, trace gas and particles to the global atmosphere (Frost, 1999). Within the  
4689    tropical landscape, 42% of CO<sub>2</sub> emissions are estimated to come from Africa, 29%  
4690    from Asia, 23% from South America, and 6% from Oceania (Andreae et al., 1998).  
4691    In Africa, fire is generally viewed as key to ecosystem structure and function. For  
4692    example fire is used to maintain grasslands by suppressing bush encroachment  
4693    (Chidumayo, 1997). In Southern Africa, fire is started either by people or by  
4694    lightning, and is intensified by a prolonged annual dry season combined with  
4695    relatively rapid rates of fuel accumulation. Often, fires originate outside of  
4696    protected areas but later burn uncontrolled into protected areas. Uncontrolled  
4697    wildland fires can destroy extensive landscapes, posing a major threat to the  
4698    survival of dryland tree species, human life and property, encouraging society and  
4699    policy makers to take measures that mitigate its effects (Turner et al., 1999).

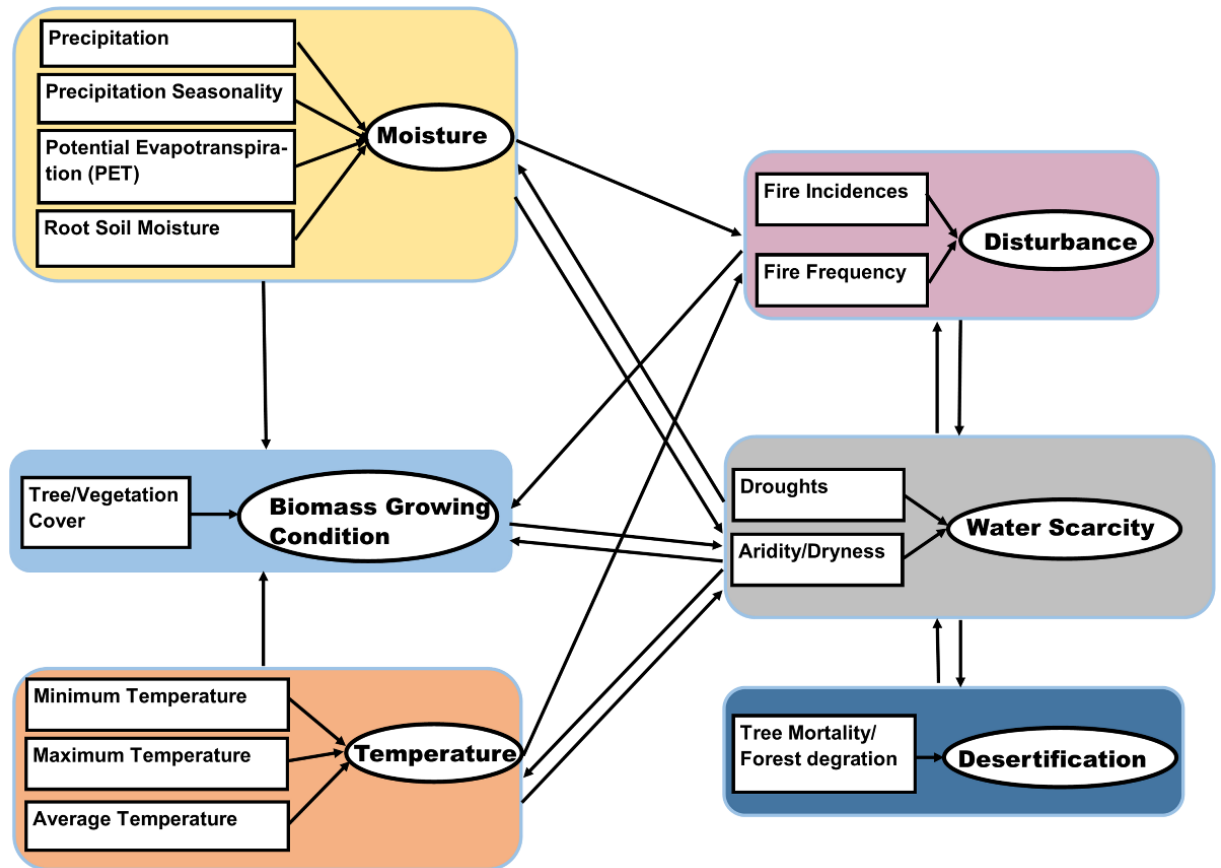
4700    The fire regime of an area is defined by several variables, including the patterns of  
4701    frequency, season, type, severity and extent. All of these characteristics are  
4702    intricately linked to ecosystem structure and function, and are highly dependent  
4703    on weather and climate oscillations (Archibald et al., 2009; Gill, 1975). Reliable  
4704    observed data on fire frequency (or, alternately, the reciprocal of the fire return  
4705    time) for calculating biomass burned at regional scales are fundamentally  
4706    important (Frost, 1999). This is partly because biome characteristics, mainly  
4707    biomass loads and moisture levels, determine fire behaviour, but also fire alters  
4708    vegetation structure, composition and development (Bond et al., 2005; Hantson et  
4709    al., 2016). On the other hand, climate affects fire occurrence through temperature  
4710    and precipitation cycles, but climate is also affected by fire through by gaseous

4711 emissions (Bojinski et al., 2014). These mutual influences between vegetation,  
4712 climate and fire highlight the importance of having long-term burned area (BA)  
4713 and climate information that serves as an input for a holistic vegetation analysis.  
4714 Therefore, better fire observations and improved estimates of fire impacts will  
4715 reduce uncertainty and improve prediction for future ecosystem feedbacks on  
4716 atmosphere interactions.

4717 Recent research has also pointed out a decline of forest resilience to wildfires  
4718 because of an intensification of the interactions between extreme droughts and fire  
4719 (Brando et al., 2019). Fire and grazing regimes, in conjunction with changes in  
4720 climate characteristics affecting soil moisture status, relative humidity, or drought  
4721 stress, will have the greatest influence on grassland-woody species boundaries  
4722 (Barros et al., 2018). A drying climate, in combination with non-adapted and  
4723 unsustainable land-use therefore increases the risk of desertification (Geist et al.,  
4724 2004). Intensifying disturbance regimes are thus expected to be among the most  
4725 severe impacts of climate change on forest ecosystems and can bring forests to a  
4726 threshold for massive die-off (Turner, 2010). The killing of plants causes  
4727 substantial vegetation change and limits productivity, thereby causing shifts in  
4728 plant communities resulting in species loss (Williams et al., 2013). Such forest  
4729 disturbances significantly affect the global carbon cycle by, for example, vegetation  
4730 loss or changing forest phenology. This is raising concerns that disturbances to  
4731 dryland natural resources in these areas might increasingly interfere with  
4732 sustainable provision of ecosystem services and wildlife habitat management in  
4733 the tropics (Scholes et al., 2004).

4734 A drying climate, in combination with unsustainable land use practises, in already  
4735 water-scarce regions, increases the risk of drying conditions (Reynolds et al.,  
4736 2007). Desertification is a complex phenomenon, driven by socio-economic and  
4737 climate-related processes, such as increasing aridity and more frequent and/or  
4738 severe droughts (Reynolds et al., 2007) (Fig. 5.1). Desertification is not confined to  
4739 drylands, however, they are some of the most vulnerable regions to land  
4740 degradation processes due to the delicate balance between natural resources (e.g.,  
4741 limited rainfall, low soil moisture, high temperature, low vegetation productivity)  
4742 (Vogt et al., 2011) (Fig. 5.1). Consequently, an important contribution in the fight  
4743 against desertification is to quantify whether the extent of drylands has changed

4744 and, if this process has taken place, where and to what degree it has occurred  
 4745 (UNCCD, 1994). In addition, this knowledge would allow natural resource  
 4746 managers to implement best management practices under drought conditions and  
 4747 other decision makers to better target assistance and response activities (e.g., early  
 4748 detection of hot spots for wildfires) in a timely manner.



4749

4750

4751 Fig. 5. 1. Conceptual model depicting theoretical relationships among moisture availability,  
 4752 temperature, plant growing conditions, and disturbance (fire frequency), water scarcity  
 4753 (droughts) and their effects on dryland vegetation cover directly or indirectly as it  
 4754 characterises desertification.

4755

4756

4757 The interrelations between dryland fire regimes and vegetation dynamics are  
 4758 indeed complex; they are conditioned by various climatic, biotic and anthropogenic  
 4759 factors involving different feedbacks. Although many studies have been

4760 undertaken in southern Africa (see (Chidumayo, 1997; Korontzi et al., 2003), very  
4761 few of these have investigated the combined effects of all these on dryland  
4762 vegetation cover. The majority of research on the potential impacts on fire regimes  
4763 and climate change on drylands has focused on the Amazon and West Africa (e.g.,  
4764 Sahel) (Aragão et al., 2007; Herrmann et al., 2005; Samanta et al., 2011). By  
4765 contrast, the regional studies that analyse the impacts of climate and fire on  
4766 dryland forests and vegetation in many parts of Southern Africa have been more  
4767 sparse (Blackie et al., 2014). There is, to my knowledge, no study that has  
4768 investigated drought and fire impacts on dryland vegetation cover across the KAZA  
4769 region over a long-term basis. A study published by Pricope et al. (2012), did  
4770 consider fire frequency from 2000 to 2010 in KAZA region, but only focused on the  
4771 central part, while Mpakairi et al. (2019) only focused on Zimbabwean component  
4772 of KAZA. Neither study considered the whole region and were solely based on fire  
4773 analysis without incorporating vegetation information.

4774 This chapter analyses trends of fire regimes of all the five of the national  
4775 constituents of KAZA, noting that each country manages fire differently. Some aim  
4776 to prevent fires, others legislate for seasonal prescribed burns, and others witness  
4777 more uncontrolled fires in protected and unprotected areas. To investigate the  
4778 drivers underlying the observed long-term vegetation cover change in the KAZA  
4779 region, a conceptual model was constructed (see: Fig. 5.1) based on the knowledge  
4780 that there are direct and indirect effects of climate, soil moisture, and fire on  
4781 woody vegetation cover. Fire disturbance and soil moisture were included in the  
4782 climate-vegetation analyses because they are considered an Essential Climate  
4783 Variable (ECV) by the Global Climate Observing System (GCOS) program, which  
4784 encourages the generation of long-term time series of ECVs to better understand  
4785 climate trends (Bojinski et al., 2014; Mason et al., 2009). The present study was  
4786 designed to investigate the relationship between moisture availability as a function  
4787 of effective rainfall, rainfall seasonality, evapotranspiration, and root soil moisture,  
4788 temperature, fire incidence and frequency, drought and vegetation index. This was  
4789 used to characterise spatiotemporal changes in aridity in the KAZA region using  
4790 long-term time series from both ground and satellite observations from 2002 to  
4791 2019.



## 4792 5.2 Aims and Objectives

### 4793 Aims

4794 The aims of this study are to investigate the relationship between fire and different  
4795 climate effects on vegetation spectral characteristics at the regional scale of KAZA.

### 4796 Objectives

4797 ○ To characterise drought conditions using climatic data (SPEI, root-soil  
4798 moisture, temperature, and precipitation) and explore the variability of  
4799 drought using monitoring indicators (i.e., the drought duration, severity and  
4800 magnitude)

4801 ○ To characterise the frequency, seasonality, and extent of fires through time  
4802 on different land use management in KAZA region

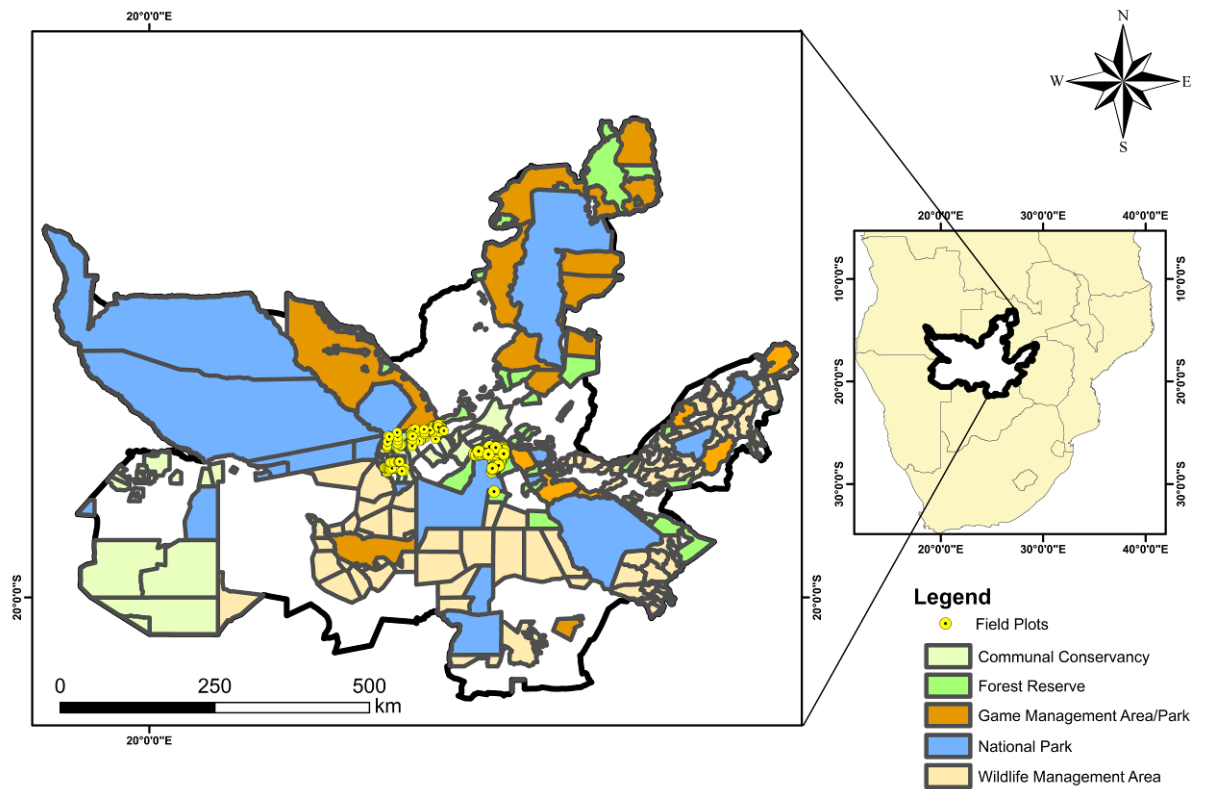
4803 ○ To investigate the spatiotemporal changes in aridity in KAZA region from  
4804 2002 to 2010 and 2011 to 2019

4805

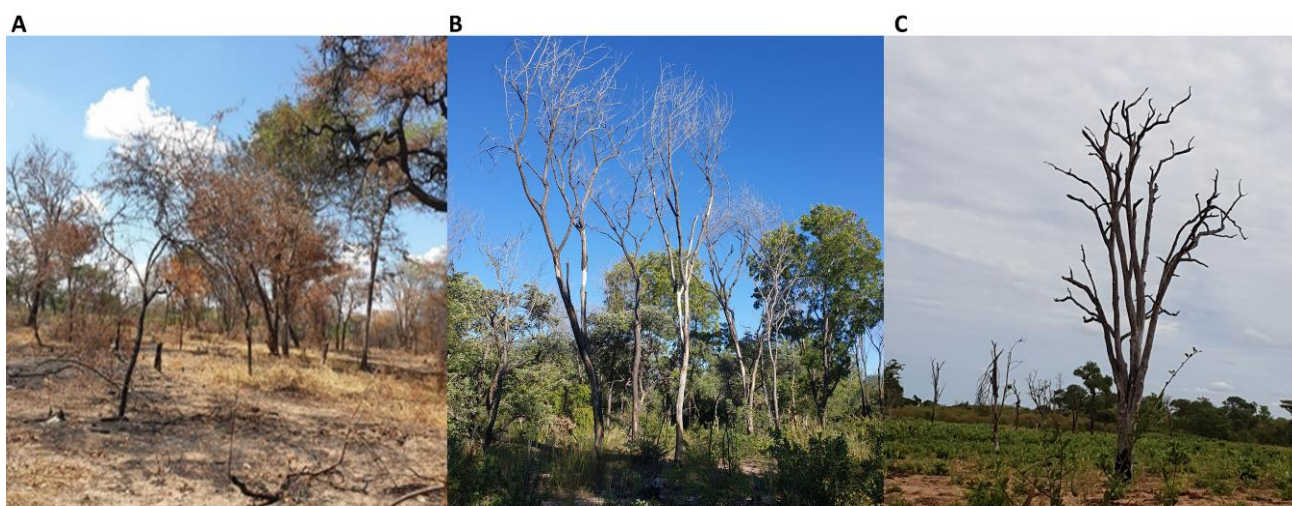
## 4806 5.3 Materials and methods

### 4807 5.3.1 Study Area

4808 The Kavango Zambezi Transfrontier Conservation Area (KAZA TFCA) (18.00°S  
4809 23.00°E) in Southern Africa, is a large multi-nationally managed network of  
4810 national parks (NP), wildlife and game management areas, forests reserves and  
4811 communal. The KAZA TFCA is the largest transfrontier conservation area in the  
4812 world, and encompasses an area of approximately almost 520 000 km<sup>2</sup> shared by  
4813 Botswana, Namibia, Zambia, Zimbabwe, and Angola (KAZA, 2014). The KAZA was  
4814 established to improve the cooperative management of shared resources, to  
4815 improve links between wildlife habitats, to create economic development to the  
4816 local communities adjacent to protected areas through tourism. KAZA was also  
4817 intended as a means to contribute to peace and friendly relationships between  
4818 participating countries through cooperation in nature protection and development  
4819 (Stoldt et al., 2020). The region hosts the largest elephant population (*Loxodonta*  
4820 *africana*) in the world and it is characterised by large-scale migrations of  
4821 megafauna such as buffalo (*Syncerus caffer*), leopard (*Panthera pardus*), zebra  
4822 (*Equus quagga*). The region is home to numerous red-listed tree species, and  
4823 contains the world-heritage listed Okavango Delta (Matswiri, 2017; Naidoo et al.,  
4824 2012). The largest portion of KAZA is generally water- and nutrient-poor due to its  
4825 location in the Kalahari Basin, and has a climate that is characterised by a single  
4826 rainy season and a long dry season (see: Fig. 5.4), with an annual rainfall average  
4827 of 300–950 mm from 1983 to 2019 (see: Fig. 5.3). During the dry season, as most  
4828 natural pans dry up, water is mostly available at a large number of artificial  
4829 waterholes across parts of the landscape and most animals migrate between  
4830 seasons to other parts of KAZA converging to rivers such as Zambezi and Chobe  
4831 Rivers in northern Botswana, and Gwaii river in Zimbabwe (Cumming, 1981;  
4832 Tshipa et al., 2017). This rainfall seasonality provides a fire-prone climate such  
4833 that the drylands of Africa are thought to experience the most extensive biomass  
4834 burning in the world (Lehmann et al., 2014).



4835



4836

4837 Fig. 5. 2. Location of the study area in KAZA Conservation Area Southern Africa, showing  
 4838 the yellow circles representing the sampling sites, protected areas and land management  
 4839 classes as designated by the World Database on Protected Areas (WDPA). Examples of  
 4840 sample plots representing degradation from fire captured during a field campaign in 2019  
 4841 are shown, A) Burned Forest for cultivation near the protected area of Mudumu NP,  
 4842 Namibia, B) Forest scorched by wildfire with dead trees that could not recover in the  
 4843 Zambezi state forests (ST) C) forest or woodland burned down to create a field.

## 4844 5.3.2 Fieldwork and Sampling Design

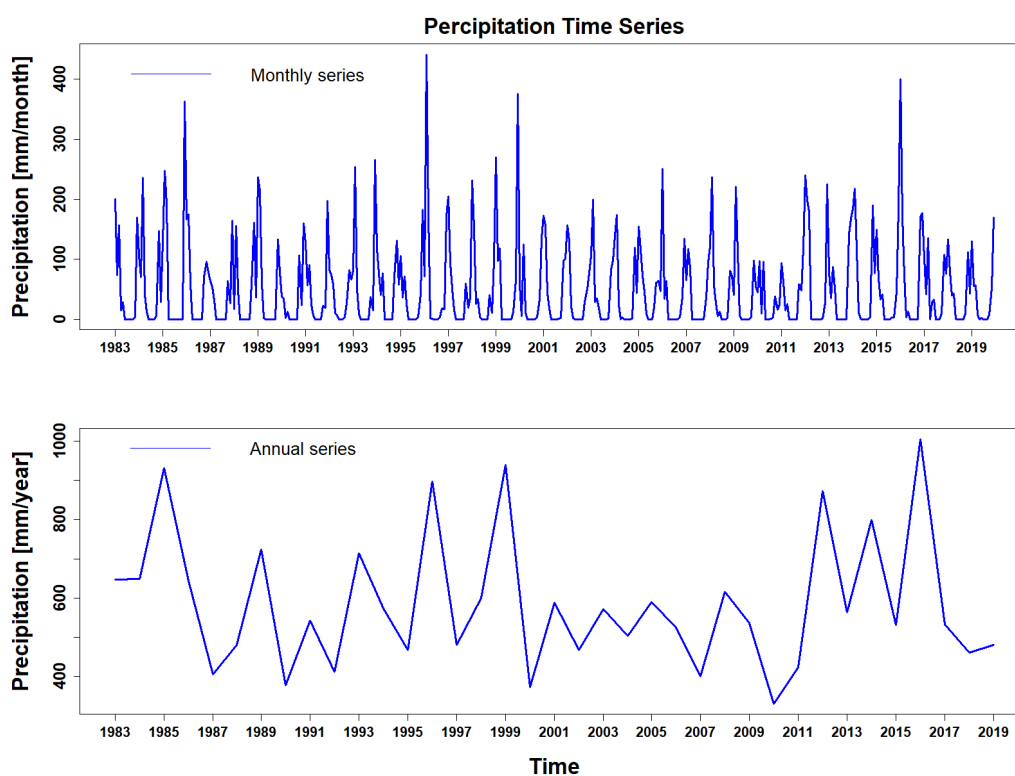
4845 Field work was undertaken to measure forest stand characteristics from three  
4846 locations with different land cover characteristics to provide ground validation in  
4847 the KAZA region. The 2019 was one of the most severe droughts this century,  
4848 which caused major impacts on vegetation and generated an economic shock felt  
4849 throughout the region. Measurements were made in forests and woodlands,  
4850 shrubland areas, and grassland agricultural land. One was located in Botswana,  
4851 which is within the Chobe NP (18.7°S, 24.5°E). The other two sites were located in  
4852 Namibia, Mudumu NP and Zambezi ST (17.8° S, 23.9° E) (Fig. 5.2). These sites were  
4853 chosen because dryland forests within and around the protected area have been  
4854 particularly susceptible to disturbance and drought during the 21st century, with  
4855 severe events in 2015 and 2019, warranting particular attention. For this reason,  
4856 survey fieldwork was undertaken to record forest tree stand characteristics, and to  
4857 observe the different land cover types present in the study area during the  
4858 growing season (1st February - 30th May 2019). The 2019 was one of the most  
4859 severe droughts this century, which caused major impacts on vegetation and  
4860 generated an economic shock felt throughout the region. At each sample plot, and  
4861 before the biophysical measurements, plot information such as land use, land  
4862 cover, vegetation type, soil, and disturbance history (e.g., evidence of fire) was  
4863 recorded (Fig 5.2). Also, information about regeneration, deadwood, and stumps  
4864 was collected. Field sites were chosen to cover a range of landscapes given the  
4865 constraints of road accessibility, wildlife danger, and public access restrictions  
4866 allowed. Measurements were collected from a total of 250 individual sample plots.  
4867 Field surveys of woody plants were conducted on sites where damage was  
4868 specifically observed to identify sites where drought had an obvious impact. These  
4869 sites can be used for further long-term monitoring.

## 4870 5.3.3 Ground-based Climate Data

### 4871 5.3.3.1 Rainfall Data

4872 The climate in the region is considered subtropical with an annual rainfall of about  
4873 600-700 mm, dry winters, and hot, wet summers (Fig. 5.3 and 4). The daily and  
4874 monthly rainfall data values recorded at Kasane and Kavimba have been used in

4875 this study (Table 5.1). The data set spans a period of 60 years from 1960 to  
 4876 2019/20 from Kasane meteorological gauging station, and a period of 46 years  
 4877 from 1971 to 2017 for Kavimba meteorological police gauging station. The Kasane  
 4878 meteorological station data have a consistent and longer record and so was used in  
 4879 this study. All the rainfall observation data were from the Botswana Department of  
 4880 Meteorological Service (BDMS) Data Network.



4881

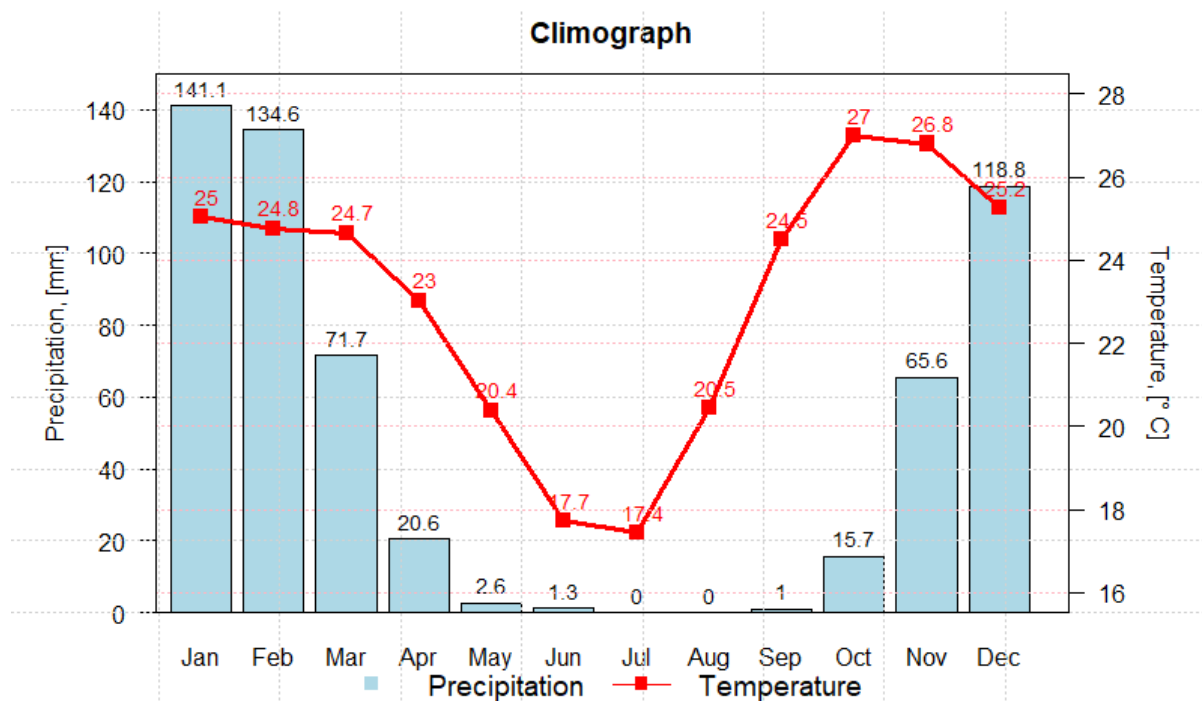
4882 Fig. 5. 3. Monthly (top) and annual (bottom) precipitation (mm) for the period 1983 to  
 4883 2019 using data obtained from Kasane meteorological station in Botswana.

4884

### 4885 5.3.3.2 Temperature Data

4886 Monthly meteorological data (minimum and maximum temperature) were  
 4887 acquired from BDMS. A long record of temperature data was obtained from Kasane  
 4888 and Pandamatenga meteorological stations. The temperature data from the Kasane  
 4889 meteorological station is used in this study because it has a longer timespan  
 4890 covering 38 years from 1982/3 to 2019/20, compared to Pandamatenga  
 4891 meteorological station which is continuous only since 1989 (Table 5.1).

4892 The climograph in Fig. 5.4 shows that rains in the region are expected in  
 4893 November, peaking in January and February and ending around March. These are  
 4894 warm summer months, with temperatures and humidity high. January averages  
 4895 the highest amount of precipitation and October observes the highest temperature.



4896

4897 Fig. 5. 4. Climograph of average monthly precipitation and temperature from 1983 to 2019  
 4898 using data obtained from Kasane meteorological station in Botswana.

4899

4900 Table 5. 1. Weather stations in the study area.

Station Name	Data Type	Data Span	Data length
Kasane	Precipitation	1960 to 2019/20	60
Kavimba	Precipitation	1971 to 2017	46
Kasane	Max and Min Temperature	1982/3-2019/20	38
Pandamatenga	Max and Min Temperature	1989-2020	31

4901

4902

### 4903 5.3.4 Remote sensing based rainfall - Climate Hazards Group 4904 Infrared Precipitation with Station Data (CHIRPS)

4905 The characteristics of the main satellite-based data used in this study is shown in  
4906 Table 5.2. Drought monitoring has been historically carried out using ground-  
4907 based observations (Chen et al., 2002). However, many regions do not have  
4908 adequate gauge instruments, particularly in Africa (e.g., remote regions or  
4909 agricultural areas) to obtain detailed precipitation, temperature, relative humidity  
4910 and wind speed data, necessary for accurate assessment of drought (Washington-  
4911 Allen et al., 2006). Furthermore, gauge (point) data do not capture the spatial  
4912 variability of drought events. Satellite measurements overcome the limitations of  
4913 gauge-based meteorological observation through continuous spatial observation  
4914 that allows drought conditions to be determined where gauge sampling is  
4915 otherwise unavailable. Often satellite-only rainfall estimates are merged with  
4916 gauge-based observations for calibration and validation. This results in merged  
4917 data sets, which exploit the strengths of each of the data source, and so improve  
4918 the overall quality of key environmental variables (Xie et al., 1995).

4919 Climate Hazards Group Infrared Precipitation (CHIRP) with Station Data (CHIRPS)  
4920 is a recently-developed, high-resolution, daily, pentadal, decadal, and monthly  
4921 precipitation dataset, from 1981 to near present. It was created by the US  
4922 Geological Survey (USGS) Earth Resources Observation and Science (EROS) Centre,  
4923 with collaborators at the University of California, Santa Barbara, Climate Hazards  
4924 Group (Funk et al., 2015a). It was developed for drought early warning and  
4925 environmental monitoring to support the Famine Early Warning Systems Network  
4926 (FEWS-NET). It was produced by blending a set of satellite-only precipitation  
4927 estimates with monthly and pentadal station observations. The CHIRP is based on  
4928 infrared cold cloud duration (CCD) estimates calibrated with the Tropical Rainfall  
4929 Measuring Mission Multi-Satellite Precipitation Analysis v.7 (TMPA 3B42 v.7) and  
4930 the Climate Hazards Group Precipitation Climatology (CHPclim). The estimates are  
4931 available at a resolution of  $0.05^\circ \times 0.05^\circ$  resolution, or at a coarser resolution of  
4932  $0.25^\circ \times 0.25^\circ$  (Funk et al., 2015). The fine resolution  $0.05^\circ \times 0.05^\circ$  dataset was used  
4933 in this study.

4934

### 4935 5.3.5 Root Soil Moisture (GLEAM)

4936 GLEAM stands for Global Land Evaporation Amsterdam Model, and is designed to  
4937 estimate land surface evaporation and root-zone soil moisture from satellite  
4938 observations and re-analysis data (Miralles et al., 2011). The potential evaporation  
4939 is computed from surface net radiation and near-surface air temperature data  
4940 using a Priestley & Taylor equation. The root-zone soil moisture (SMroot) is  
4941 calculated using a multi-layer running water balance model, which combines  
4942 observed precipitation and soil moisture observations (Martens et al., 2017).  
4943 GLEAM v3.3b provides global monthly potential and actual evaporation,  
4944 evaporative stress conditions and root zone soil moisture spanning the  
4945 approximately 18-year period between 2003–2020 at a spatial resolution of 0.25°.  
4946 The vegetation fractional cover in v3.5b comes from MOD44B and uses the latest  
4947 version of CERES radiation (v4.1), AIRS temperature (v7.0), MSWEP precipitation  
4948 (v2.8), and ESA-CCI soil moisture (v5.3) (Martens et al., 2017). GLEAM datasets  
4949 have already been comprehensively evaluated and used for multiple drought  
4950 analysis and monitoring applications (Peng et al., 2019; Vicente-Serrano et al.,  
4951 2018). For this study, the GLEAM root zone soil moisture was used. GLEAM  
4952 datasets are openly available globally at daily temporal resolution and 0.25° spatial  
4953 resolution for 1980–2019 (<https://www.gleam.eu/#downloads/> (accessed 10 July  
4954 2020).

### 4955 5.3.6 Vegetation Indices from Remote Sensing Imagery

4956 Vegetation indices uses vegetation reflectance in the near and shortwave infrared  
4957 regions for reducing the effects of irradiance and exposure, and enhancing the  
4958 contrast between vegetation and the ground (Xue et al., 2017). NDVI has been  
4959 widely used in many studies to monitor drought impacts on vegetation and forests,  
4960 predict agricultural production, assist in hazardous fire zone prediction, and to  
4961 map desert encroachment which defines the vegetation growth status (Anyamba et  
4962 al., 2005; Myneni et al., 1997; Xulu et al., 2018). The NDVI was used in this study  
4963 because it is a biophysical parameter that correlates with the photosynthetic  
4964 activity of vegetation and is an indicator of the greenness of the biomes (Robinson  
4965 et al., 2017; Tucker, 1979). NDVI is also able to offer valuable information to  
4966 monitor vegetation health, drought effects, changes in plant growth, land



4967 degradation, deforestation, change detection/monitoring, and in relating large-  
 4968 scale inter-annual variations in vegetation to climate (Smith et al., 2019). As  
 4969 shown in Eq. 5.1, vegetation reflectance is at a minimum in the visible (red) part of  
 4970 the electromagnetic spectrum due to absorption of radiation by chlorophyll  
 4971 pigments, whereas maximum reflection is in the Near Infra-Red (NIR) spectral  
 4972 region owing to refraction of radiation by leaf cellular structure. The NDVI index  
 4973 outputs values range between -1.0 and 1.0, and has been shown to correlate well  
 4974 with leaf area index (LAI), and fraction of photosynthetically active radiation  
 4975 absorbed by vegetation (fAPAR) (Fensholt et al., 2004; Tucker, 1979). Negative  
 4976 values are mostly due to clouds, snow, water, and values near zero are generally  
 4977 generated from rock and bare soil. Lower NDVI values often correspond to  
 4978 stressed or sparse vegetation. Shrubs and grasslands have moderate values (0.2 to  
 4979 0.5) and high values (0.5 to 0.8) are typical of healthy vegetation with different  
 4980 densities. I analysed the NDVI patterns during the growing season (January –  
 4981 March) using 2002 to 2019 time series data from the MODIS (MYD09A1.006) 8-  
 4982 day product, with a 500 m spatial resolution.

$$\text{NDVI} = \frac{\text{NIR} - \text{Red}}{\text{NIR} + \text{Red}} \quad (\text{Eq. 5. 1})$$

4983 where NIR is the near infrared range of the electromagnetic spectrum (841–876  
 4984 nm) and RED is the red spectrum of the electromagnetic spectrum (620–670 nm),  
 4985 respectively, as measured by the MODIS sensor.

### 4986 5.3.7 Product of burnt area MODIS MCD64A1

4987 Satellite-based strategies for large-area burn assessment may rely on two types of  
 4988 remote sensing data including postfire reflectance images and active fires and can  
 4989 be used in combination or separately (Fraser et al. 2000). So, this study used  
 4990 Burned Area Products of 500 m spatial resolution for analysing spatial dynamics of  
 4991 burned areas and FIRMS Active Fire Products was used for seasonal temporal  
 4992 variations. This is because Active Fire Products are unable to estimate burned  
 4993 areas with an acceptable degree of accuracy due to coarse resolution of 1 km

4994 spatial resolution, and untrivial spatial and temporal sampling issues as stated by  
4995 Giglio et al. (2006b). The burnt area data were obtained from the MODIS burnt  
4996 area sensor monthly product MCD64A1 v.6, and was accessed via Google Earth  
4997 Engine (GEE). MCD64 (Giglio et al., 2009) is the latest product from the MODIS  
4998 Burnt Area product, and was updated as reported in Giglio et al., (2018). This is a  
4999 global grid-level 3 product at 500 m spatial resolution containing per-pixel burnt-  
5000 area and quality information. It is based on an automated hybrid approach that  
5001 employs 500 m surface reflectance imagery coupled with 1 km MODIS active fire  
5002 observations. The algorithm applies dynamic thresholds to composite images  
5003 generated from a burn sensitive vegetation index, which in turn are derived from  
5004 MODIS shortwave infrared surface reflectance band 5 and 7, and a measure of  
5005 temporal texture (Giglio et al., 2016). Data layers include a recording of burn date,  
5006 data uncertainty, quality assurance and the first and last day of reliable change in  
5007 the year. The date on which the burn occurred with values assigned to unburnt  
5008 land pixels is encoded in a single data layer as the ordinal day of the calendar year.  
5009 The data layer also contains additional values reserved for missing data and water  
5010 grid cells. Overall, the MCD64A1 has improved the detection of burnt areas,  
5011 provides better detection of small fires and has proven adaptability to different  
5012 regional conditions in multiple ecosystems.

### 5013 5.3.8 MODIS MCD14ML Active Fire Product

5014 Fire point location were obtained from the Aqua & Terra MODIS wildland fire data,  
5015 with a spatial resolution of 1 km, Collection 6, from January 2002 to December  
5016 2019, available from the NASA Fire Information for Resource Management System  
5017 (FIRMS) at <https://firms.modaps.eosdis.nasa.gov/download/> (accessed 21 March  
5018 2020). The data have a 1-day temporal resolution, and the location of the fire  
5019 nominally corresponds to the centre of a 1x1 km pixel, signalled by the algorithm  
5020 as containing one or more fires within that pixel. A full description of the  
5021 algorithms used to acquire the data can be found in Davies et al. (2008). FIRMS  
5022 was developed to provide a simpler and faster means to obtain MODIS active fire  
5023 locations and expand the distribution of MODIS fire data to a broader range of fire  
5024 and forest monitoring organisations around the world. In this study, active fire  
5025 products were used to determine fire seasons by determining the months when

5026 fire activity is very high. The fire seasons were determined from the cumulative  
 5027 ratio of active fires on a regional scale detected during each month across the  
 5028 seventeen years of observation (2002-2019) and the proportion of this number to  
 5029 the overall number of fires. FIRMS is an extension to the MODIS Rapid Response  
 5030 (MRR) system for near-real-time active fire information in a format that is easy to  
 5031 use, and for users that could not handle image files (Ilavajhala et al., 2014).

5032 Table 5. 2. Characteristics of the main datasets used in this study.

<i>Dataset</i>	<i>Timespan</i>	<i>Resolution</i>	<i>Source</i>
<b><i>Climate Data</i></b>			
<i>Climate Hazards Group InfraRed Precipitation with Station Data (CHIRPS)</i>	2002-2019	0.05 degrees	GEE
<i>High resolution Standardised Precipitation Evapotranspiration Index (SPEI) dataset for Africa</i>	2002-2016	5 km	CHIRPS and GLEAM
<i>The Global Land Evaporation Amsterdam Model (GLEAM v3.3b)</i>	2003-2019	0.25° x 0.25°	GLEAM
<i>Rainfall Data</i>	1975-2020	-	Botswana department of Meteorological Service (BDMS)
<i>Minimum and Maximum Temperature Data</i>	1983-2020	-	Botswana department of Meteorological Service (BDMS)
<b><i>Vegetation Data</i></b>			
<i>MODIS 8-day time series (MOD13Q1)</i>	2002-2020	250m	GEE (MODIS09, 2020).
<i>MODIS Terra Surface Reflectance 8-Day Global 500m (MOD09A1.006) and (MYD09A1.006)</i>	2002-2019	500m	GEE (MODIS09, 2020).
<b><i>Fire Data</i></b>			

<i>MODIS burnt area (MCD64A1)</i>	<i>2002-2019</i>	<i>500m</i>	<i>GEE (MODIS09, 2020).</i>
<i>MODIS wildland fire point data</i>	<i>2002-2019</i>	<i>500m</i>	<i>FIRMS</i>

5033

5034

5035

5036 

## 5.4 Methods

5037 

### 5.4.1 Calculating the standardised precipitation

  
5038 

### evapotranspiration index (SPEI) from ground observation

5039 Satellite-based drought indices are capable of characterising spatial and temporal  
5040 variability of drought based on the magnitude, duration, and intensity, and so they  
5041 represent promising tools for monitoring drought at regional scales, which is  
5042 important for developing a drought watch system for an area. A variety of drought  
5043 indices have been developed to quantify whether or not a region is experiencing a  
5044 drought, and to categorise the seriousness of that drought. Dryness severity was  
5045 quantified using the multiscalar Standardised Precipitation Evapotranspiration  
5046 Index (SPEI), calculated from ground meteorological data (rainfall and  
5047 precipitation) from the Kasane meteorological station. Drought severity is  
5048 predominantly caused by either precipitation decreases or increases in  
5049 temperature induced evapotranspiration. Hence, precipitation does not represent  
5050 the only control on ecologically and socially relevant water resources, such as  
5051 stream flow, reservoir storage, and soil moisture (Cook et al. 2004). SPEI is used to  
5052 measure environmental water stress by combining information from both  
5053 evaporation and precipitation. The SPEI is a drought indicator that determines  
5054 deviations from a location's average water balance (the ratio of temperature and  
5055 precipitation) over a specified timeframe which is then fitted to a statistical  
5056 distribution (Vicente-Serrano et al. 2012). The SPEI was quantified based on the  
5057 Hargreaves equation (Hargreaves, 1994) using the 'SPEI' package (Bergueria et al.,  
5058 2014) in the R software package. Due to the complex computation of Potential  
5059 Evapotranspiration (PET), which involves several variables, including surface  
5060 temperature, air humidity, soil, incoming radiation, water vapour pressure, and  
5061 ground-atmosphere latent and sensible heat fluxes, this study made use of  
5062 Hargreaves' and Samani's temperature-based method for PET estimation. The  
5063 Hargreaves approach has the advantage of only requiring data on monthly mean  
5064 minimum and maximum temperatures.

5065

5066 The SPEI was chosen over the commonly used Standardised Precipitation Index  
5067 (SPI) because it includes PET as well as precipitation (Stagge et al. 2014). PET is  
5068 the amount of evapotranspiration that could occur if enough water were available  
5069 (Oudin et al. 2005). For example, Dutrieux et al., (2015) used SPI and they found it  
5070 to perform poorly in tropical dry forest and concluded SPI was not the ideal way to  
5071 include moisture conditions in the dryland environment. Limitations of SPI, which  
5072 considers rainfall anomalies alone without including evaporative demand have  
5073 also been discussed by Trenberth et al. (2014). The SPEI is calculated based on the  
5074 accumulated difference between precipitation (P) and temperature used to  
5075 compute potential evapotranspiration (PET). The SPEI can comprehensively  
5076 reflect the change in surface water balance, hence automatically capturing the  
5077 well-known temporal lag of vegetation response to rainfall (Stagge et al. 2014;  
5078 Potop et al., 2014). Since SPEI is a standardised variable it can be used to compare  
5079 droughts over different spatial and temporal scales. SPEI produces a graph with  
5080 values ranging from 2 to -2 (Table 5.3).

5081 This study places emphasis on moderate to extreme droughts and the SPEI index  
5082 scale is given as: extreme drought ( $\leq -2$ ); severe drought ( $-2$  to  $-1.5$ ); and,  
5083 moderate drought ( $-1.5$  to  $-1$ ). A continuously negative SPEI generally implies an  
5084 abnormally drier climate/drought period based on intensity, severity, magnitude,  
5085 and duration, while positive values correspond to abnormally wet periods. It  
5086 should be noted that drought ends when the SPI/SPEI approaches zero and  
5087 progresses to a positive value. For this study, the duration of the drought is  
5088 considered as the number of months for which the drought has occurred, whilst  
5089 the magnitude of the indices indicates the severity of the drought. Vegetation has  
5090 been found predominantly responsive to short-term drought time scales, hence 1,  
5091 3 and 12 months were determined as an appropriate time scales for  
5092 contextualizing meteorological, vegetation/crop and hydrological drought on  
5093 vegetation (Vicente-Serrano et al. 2012). Two data periods were used in the SPEI  
5094 analysis. The 1983–2019 period was used as the baseline period based on  
5095 availability of the high-quality observed data for temperature and rainfall. The  
5096 2002–2019 time period was used in SPEI analysis to investigate sensitivity of the  
5097 vegetation to drought events.

5098 Table 5. 3. Categories of dry and wet conditions indicated by SPEI values.

SPEI	Category
2 and above	Extremely wet
1.5 to 1.99	Very wet
1.0 to 1.49	Moderately wet
−0.99 to 0.99	Near Normal
−1.0 to −1.49	Moderately dry
−1.5 to −1.99	Severely dry
−2 and less	Extremely dry

5099

5100

5101 

### 5.4.2 Calculation of the satellite-based aridity index (AI)

5102 The degree of dryness is not determined by precipitation alone. If the temperature  
5103 is high/low, evaporation is either large or small. Therefore, the degree of dryness  
5104 is normally expressed as the ratio of PET and precipitation, giving the aridity  
5105 index, which is an important indicator of regional climate. The study adopted the  
5106 aridity index (AI) recommended by the United Nations Educational, Scientific and  
5107 Cultural Organisation (UNESCO), the Global Environment Monitoring System  
5108 (GEMS), the Global Resource Information Database (GRID), and the Desert Cure  
5109 and Prevention Activity Centre (DC/PAS), to reflect the aridity changes of the KAZA  
5110 region. The AI was calculated using the following form (Eq. 5.2).

$$AI = \frac{PRE}{PET} \quad (\text{Eq. 5. 2})$$

5111 where PET is the Potential Evapotranspiration (in mm) and PRE is the  
5112 precipitation (in mm). The aridity index (AI) has been widely used to divide  
5113 climate zones and to assess changes in aridity trends. Under this quantitative  
5114 indicator, drylands are defined as regions with  $AI < 0.65$  and are further divided  
5115 into subtypes of: hyper-arid ( $AI < 0.03$ ); arid ( $0.03 \leq AI < 0.2$ ); semiarid ( $0.2 \leq AI <$   
5116  $0.5$ ); dry subhumid ( $0.5 \leq AI < 0.65$ ); and, humid ( $AI > 0.65$ ) regions, as shown in  
5117 Table 5.4 (Middleton et al., 1997).

5118

5119 AI was calculated using the MODIS data products MOD16A2 v.6  
 5120 Evapotranspiration/Latent Heat Flux product, which is an 8-day composite  
 5121 product produced at 500 m resolution. The algorithm used for the MOD16A2  
 5122 product is based on the logic of the Penman-Monteith equation, which includes  
 5123 inputs of daily meteorological reanalysis data along with MODIS data on vegetation  
 5124 property dynamics, albedo, and land cover. The pixel values for the PET layer are  
 5125 the sum of all values in the 8 days within the composite period.

5126 Table 5. 4. UNESCO (1979) aridity classification and bioclimatic index thresholds

<i>Threshold</i>	$0.03 \leq AI < 0.2$	$0.2 \leq AI < 0.5$	$0.5 \leq AI < 0.65$	$AI > 0.65$	$AI > 0.75$
<i>Arid conditions</i>	<i>Arid</i>	<i>Semi-arid</i>	<i>Dry sub-humid</i>	<i>Humid</i>	
<i>Desertification risk</i>	<i>Risk</i>				<i>No risk</i>

5127

### 5128 5.4.3 Evaluation Criteria

5129 Most of the currently employed indexes in climate and drought regionalisation  
 5130 reflect meteorological variables, without taking the diversity of landscape (such as  
 5131 soil condition) into consideration. Therefore, a single index is insufficient for a  
 5132 nationwide drought regionalisation program. In this respect, the regionalisation  
 5133 indexes presented above that can be used to reflect climate wetness and assess  
 5134 agricultural and plant droughts were developed. The SPEI at fine spatial resolution  
 5135 based on CHIRPS and GLEAM v3 (root zone soil moisture) is compared temporally  
 5136 and spatially to the CHIRPS precipitation dataset. In addition, the NDVI can also  
 5137 serve as an indicator for drought and vegetation health and was used to assess the  
 5138 performance of drought indices (Vicente-Serrano et al., 2013; Aadhar and Mishra,  
 5139 2017). Furthermore, root zone soil moisture is an ideal hydrological variable for  
 5140 plant (soil moisture) drought monitoring.

5141



5142 A critical issue for identifying and quantifying droughts is the local historic  
 5143 climatic distribution (i.e., what is “normal”?). The sample size must be large  
 5144 enough to guarantee that sample statistics are reasonable approximations of the  
 5145 corresponding population parameter (Maliva et al., 2012). For a region to receive  
 5146 its long-term average annual precipitation in a year should be a rare event; most  
 5147 years will be either wetter or drier than the mean or median. To facilitate direct  
 5148 comparison between SPEI, precipitation, NDVI and RSM, both precipitation, NDVI  
 5149 and RSM are standardised by subtracting their corresponding (2002–2019) mean  
 5150 and are expressed as the resulting anomalies in terms of numbers of standard  
 5151 deviations (Eq. 5.3). The monthly and seasonal standardised anomalies (*std.*  
 5152 *anomaly*) for vegetation and climate parameters were computed using Eq. 5.3,  
 5153 below

$$\text{std.anomaly} = \frac{x_i - \bar{x}}{\delta} \quad (\text{Eq. 5. 3})$$

5154 where  $x_i$  is the value of NDVI/climate at a particular time (month/season),  $\bar{x}$  and  
 5155  $\delta$  are the average (monthly/seasonal) and standard deviation (monthly/seasonal),  
 5156 respectively, over the study time period, 2002-2019. This standardisation has been  
 5157 applied by many studies to evaluate drought indices (e.g., Anderson et al., 2011;  
 5158 Mu et al., 2013; Zhao et al., 2017).

5159

5160

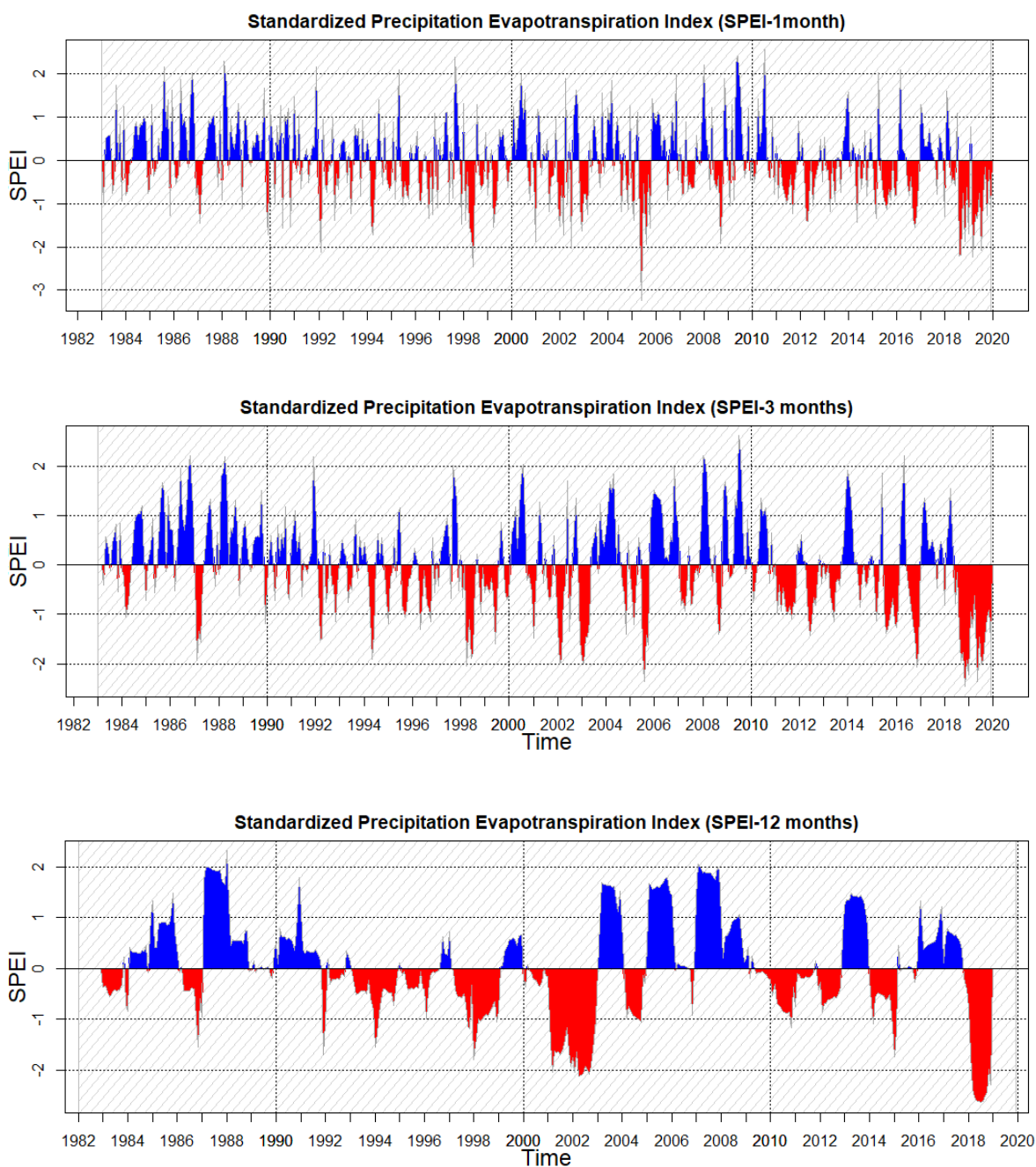
## 5161 5.5 Results

### 5162 5.5.1 Temporal analyses drought and water stress

#### 5163 5.5.1.1 Drought index at different scales

5164 To demonstrate the temporal variation of drought at different time scales (1, 3 and  
5165 12 months) for the study period (1982–2019) in the KAZA region, the SPEIs were  
5166 generated and presented in Fig. 5.5. All three timescales had SPEI values close to  
5167 the extreme drought level of -2 for the entire hydrological year of 2019. In general,  
5168 the index data show the same pattern of variability for each timescale, with  
5169 different durations and magnitudes of drought. Also, the frequency of occurrence  
5170 of droughts was higher for the shorter, compared to the longer timescales; hence,  
5171 the meteorological droughts (1-month) show the highest frequency of occurrence,  
5172 followed by agricultural droughts (3-months), and lastly the hydrological droughts  
5173 (12-months). The number of drought events observed at the 3- and 12-month time  
5174 scales were 77, compared to 80 in the 1-month time scale (Supplementary, Table C  
5175 1). It takes a shorter time (at most 1-month) of prevailing water deficiency for a  
5176 meteorological drought to develop, hence the high variability of droughts.  
5177 However, at the longer timescales the drought lasts longer and the SPEI magnitude  
5178 increases. The variability shows that at the 12-month timescale, SPEI was found to  
5179 be of greater severity and magnitude compared to the 1- and 3-month timescales.  
5180 The SPEI event with the greatest magnitude at the 12-month scale was found in  
5181 2019 with the SPEI value  $>2.5$  (Fig. 5.5).

5182



5183

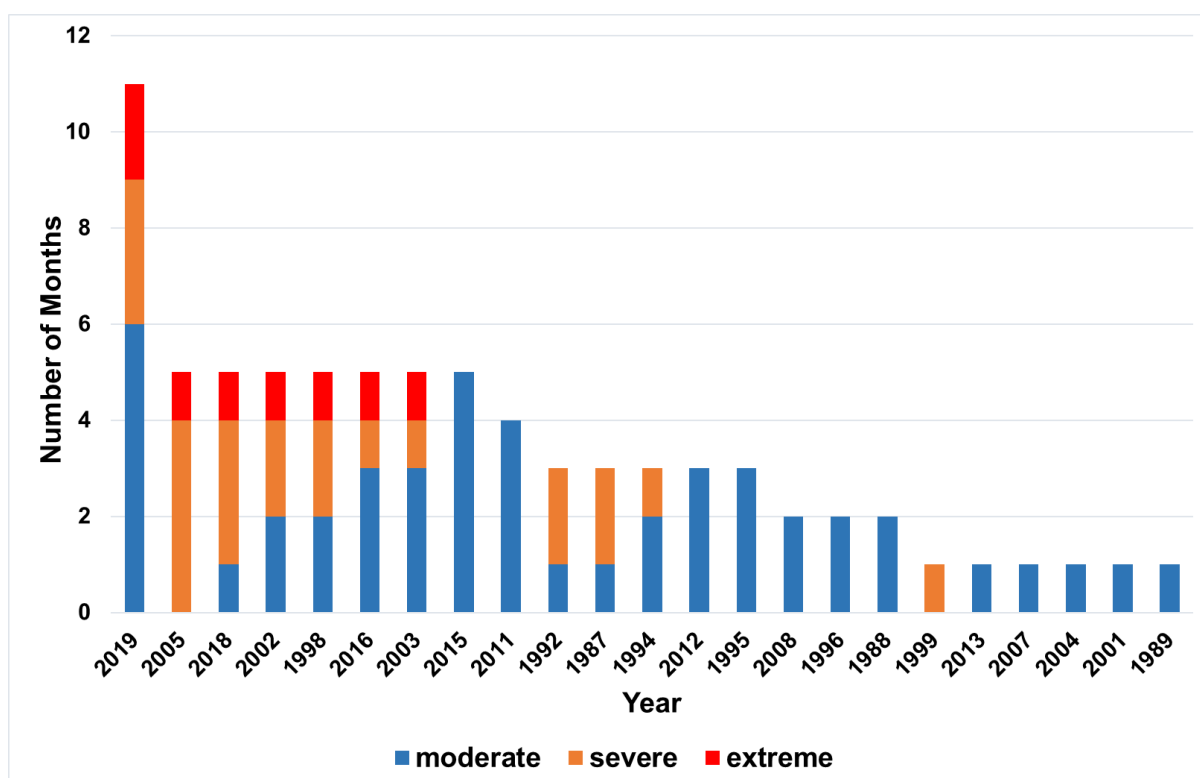
5184

5185 Fig. 5. 5. SPEI for 37 years calculated from ground precipitation and temperature at  
 5186 different timescales. SPEI index scale is given as, extreme drought ( $\leq -2$ ), severe drought  
 5187 ( $-2$  to  $-1.5$ ) and moderate drought ( $-1.5$  to  $-1$ ).

5188

5189 Given that it takes up to 3 months for most vegetation to be fully developed, a  
 5190 water deficiency accumulation of at least 3 months during the growing season will  
 5191 adversely impact vegetation and crop yields, thus quickly developing into an  
 5192 agricultural drought. On the other hand, a longer period of water deficit

5193 accumulation or depletion of water storage in rivers and reservoirs is required for  
 5194 a hydrological drought to occur. Fig. 5.6 shows the number of droughts per year at  
 5195 a time scale of 3 months, including the drought categories. For the period under  
 5196 observation (1983–2019), drought was more extreme in 1998/1999, 2002/2003,  
 5197 2005, 2015/2016 and 2018/2019. Severe drought was also observed in 1987,  
 5198 1992, 1994, and 1999. The SPEIs calculated for 2019 show the worst drought and  
 5199 accompanying effects on crops and vegetation ever recorded over the Southern  
 5200 African region.



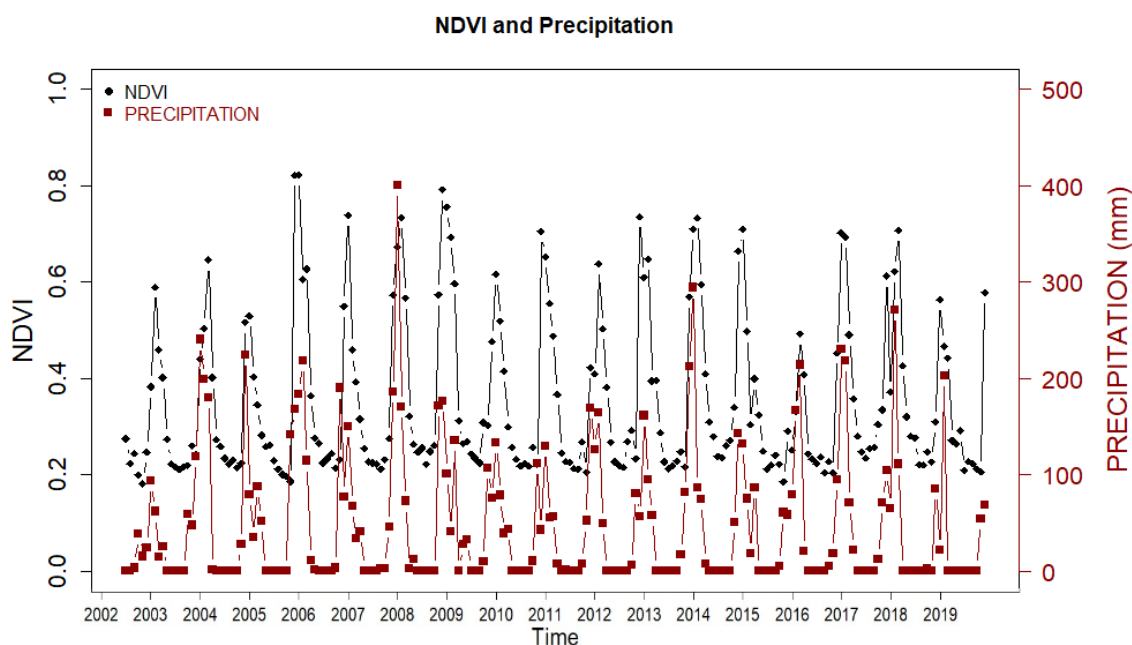
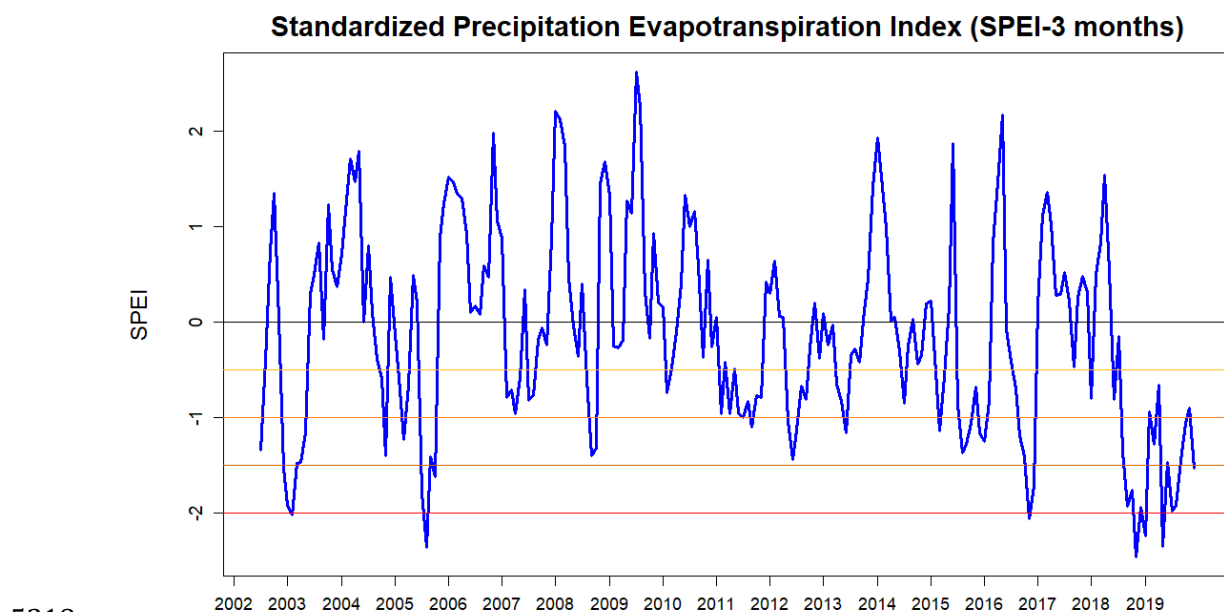
5201

5202 Fig. 5. 6. Number of drought events for the years that experienced droughts in the period  
 5203 of 1983 to 2019 using a 3-month time scale, ranked by number of drought months.

### 5204 5.5.1.2 Drought index, precipitation and vegetation relationship

5205 To contextualise the drought impacts on vegetation, the 3-month SPEI,  
 5206 precipitation from the ground station, and monthly NDVI values of a forested area  
 5207 between 2002 and 2019 were plotted to determine the interplay between  
 5208 vegetation and climate variability. Monthly NDVI varied closely as a function of  
 5209 rainfall distribution, as shown in Fig. 5.7. Low NDVI values appear to coincide with  
 5210 large drops in SPEI and these correspond to abnormally dry years as shown in the  
 5211 graph of precipitation. The lowest NDVI range was recorded in 2002-2003, 2005,

5212 2010/2012, 2015/2016, and 2019, corresponding to the low rainfall values and  
 5213 drought years, visible in the SPEI data. Similarly, the highest NDVI was observed in  
 5214 2004, 2006, 2008 /2009, and 2017, which are associated with good rainfall in the  
 5215 growing season. The SPEI values show that 2019 experienced extreme drought  
 5216 with a negative anomaly from the mean conditions reaching the level of -2, and this  
 5217 corresponds with reduced NDVI and rainfall levels.



5221 Fig. 5. 7. Top: SPEI from 2002 through 2019 calculated from ground precipitation and  
 5222 temperature at 3 months timescales. SPEI index scale is given as, extreme drought ( $\leq -2$ ),

5223 severe drought ( $-2$  to  $-1.5$ ), and moderate drought ( $-1.5$  to  $-1$ ). The different vertical line  
5224 colours represent the drought scale (yellow colour shows mild drought and red colour  
5225 shows extreme drought). Bottom: Temporal variation of the NDVI (black circles) and  
5226 inverted monthly precipitation from ground station data (red squares) from 2002 through  
5227 2019.

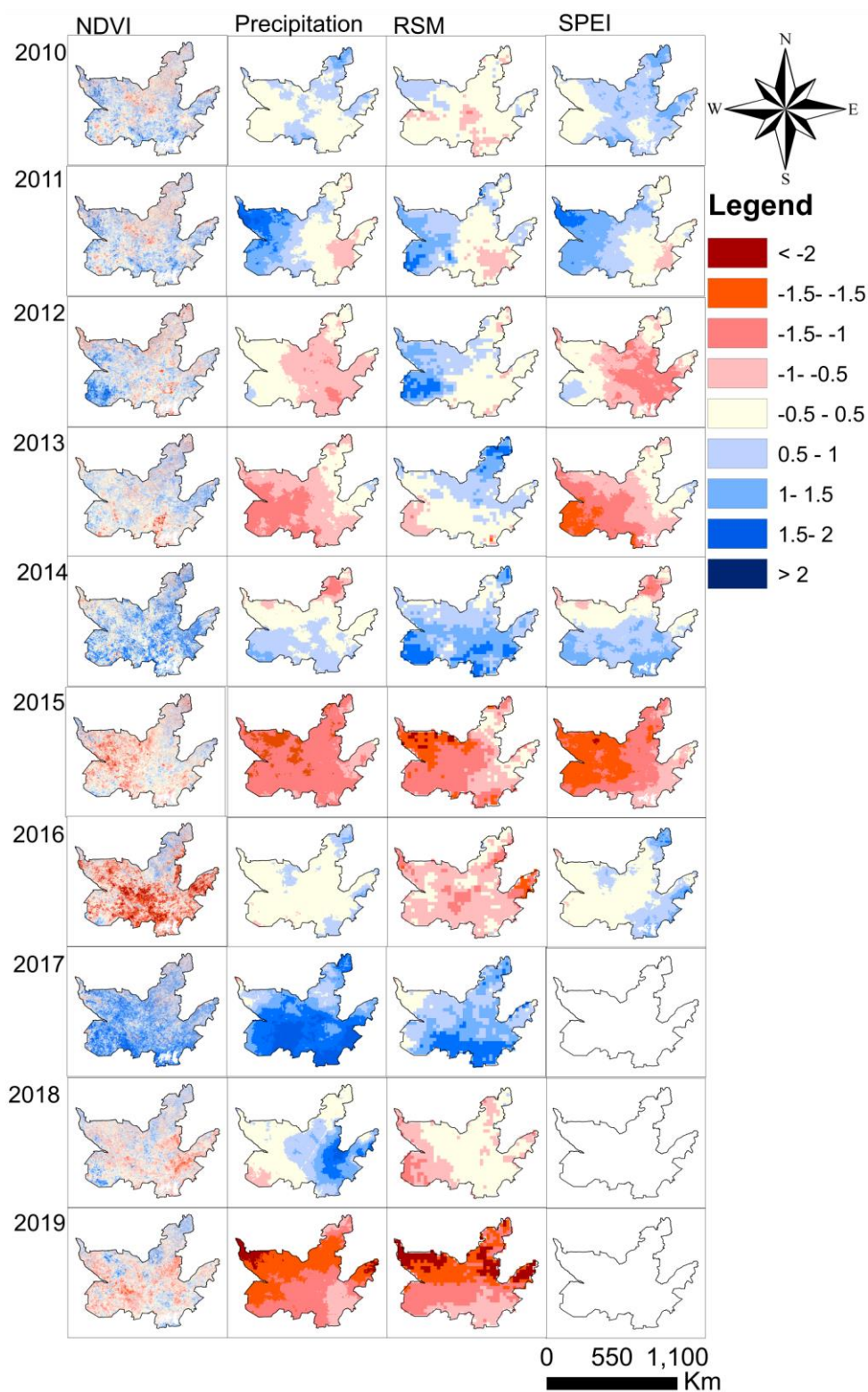
5228

## 5229 5.5.2 Spatial analyses of drought and water stress on 5230 vegetation

5231 The precipitation, SPEI and RSM dataset are compared with NDVI to gain more  
5232 insight into their significance, and to assess which climatic variables explain spatial  
5233 patterns of forest and vegetation in this region. Fig. 5.8 shows the results of the  
5234 spatial and temporal comparison from 2010 to 2019 for NDVI, precipitation, and  
5235 RSM. Note that SPEI maps end in 2016 due to lack of data availability. In general,  
5236 these four variables reflect a progressive dry-out during the events from 2010-  
5237 2019. The period between 2010 to 2019 was chosen because it is the period with  
5238 more years experiencing severe drought events. For example, a severe drought is  
5239 revealed by the SPEI in 2012, with values  $< -1$ , mostly in the west of the KAZA  
5240 region, coinciding with a decline in NDVI in this area. The drought of 2012 in  
5241 western KAZA could be exacerbated by low rainfall values in 2011 which lead to a  
5242 considerable decrease in RSM and SPEI values. However, in 2012, the eastern part  
5243 of KAZA experienced an increase in vegetation cover, despite receiving less than  
5244 average rainfall. The high NDVI in eastern KAZA corresponds to high RSM with  
5245 values  $>1.5$  in the same area, which can be attributed to high rainfall, wet  
5246 conditions, as reflected in the in SPEI and high RSM values from 2011 in the  
5247 eastern KAZA. In 2013, extremely low rainfall was recorded which is reflected by a  
5248 severe drought in SPEI with values  $<-1.5$  over almost the whole of the KAZA region.  
5249 This drought resulted in a decreased vegetation productivity, although not as  
5250 severely as the RSM which was still high for most parts of KAZA. In 2015, the entire  
5251 KAZA region experienced extremely low precipitation, with a value  $<-1$ . This  
5252 resulted in a strong and extreme drought, as shown by the SPEI and RSM, with  
5253 extremely low values  $<-1.5$  across  $>80\%$  of KAZA. The 2015 drought event  
5254 impacted vegetation in the region severely, with an NDVI value  $<-1$  in  $>50\%$  of  
5255 KAZA. Precipitation returned to normal in 2016, which corresponds to the SPEI

5256 data, as there was no drought or dry condition experienced in 2016. However, the  
5257 NDVI progressively declined through 2016, which is explained by RSM values  $<-1$   
5258 across the whole of KAZA, despite precipitation and SPEI showing a different  
5259 pattern.

5260 The slight increase in NDVI values in northern KAZA corresponds to the very few  
5261 areas with average RSM in 2016. The RSM reflected the main drought conditions  
5262 that are shown also by negative values in NDVI, rather than rainfall or SPEI. The  
5263 extreme drought of 2015-2016 is followed by a high level of precipitation in 2017  
5264 over almost the entirety of KAZA region, showing wet condition values of  $>1.5$ .  
5265 This corresponds to an increase in NDVI and RSM over most of the region,  
5266 although most dryland forest in northern and central KAZA remained negative. In  
5267 2019, the whole of the region received extremely low precipitation with values  
5268  $<1.5$ . This resulted in a distressing drought with extremely low RSM values  
5269 coinciding with a decline in NDVI. The location of the maximum precipitation and  
5270 RSM deficit is concentrated in the north and east of KAZA in both 2015 and 2019.  
5271 While the wetter conditions were mostly concentrated in south of KAZA, where it  
5272 is more arid with less dryland forest such as in 2014 and 2017. RSM was useful in  
5273 explaining the spatial-temporal patterns of vegetation lag effects and revealing the  
5274 cumulative effect of climate anomalies on vegetation conditions, that were not  
5275 explained by precipitation or SPEI.



5276

5277 Fig. 5. 8. Spatial distribution of PRECIPITATION, NDVI, SPEI and RSM anomalies expressed  
 5278 as numbers of standard deviations sampled from the monthly data in the growing season  
 5279 from 2010 to 2019. Extreme droughts ( $\leq -2$ ), severe drought ( $-2$  to  $-1.5$ ) and moderate  
 5280 drought ( $-1.5$  to  $-1$ ), mild droughts ( $-1$  to  $-0.5$ ) and no drought ( $-0.5$  to  $0.5$ ). The map  
 5281 shows the whole of KAZA region as represented by the study area in Fig. 5.2.



5282 Comparisons of climate variables against the NDVI values show that reduced NDVI  
5283 uniformly coincide with extremely high temperatures and with low precipitation.  
5284 Similarly, low SPEI values ( $< -0.5$ ) moisture coincides with low NDVI values  
5285 (Fig. 5.9). SPEI values indicate that the drought event of 2019 was the worst with  
5286 SPEI values falling below  $-1$ , followed by the drought event of 2015. The root soil  
5287 moisture shows that the dry forest vegetation corresponds strongly to the drought  
5288 events of 2019 and 2015, with both years experiencing the lowest root-soil  
5289 moisture resulting in low NDVI values. In contrast, high NDVI values are captured  
5290 for the year 2017 strongly responding to the high moisture availability as  
5291 illustrated by the high value of precipitation, root soil moisture, and SPEI. The max  
5292 and average temperature also show a sharp contrast of the drought years (2015  
5293 and 2019) and the wet years (2017 and 2014). The drought year (2019 and 2015)  
5294 has the highest average and maximum temperatures, with low NDVI values  
5295 coinciding with extremely high temperatures. On the other hand, the high NDVI  
5296 values of wet years (2017 and 2014) correspond with the lowest average and  
5297 maximum temperature. There is a lag observed in dryland vegetation productivity  
5298 in some years following drought events such as 2016 and 2013, in which the NDVI  
5299 remain very low despite an increase in precipitation and positive values in SPEI.  
5300 The min temperature does not uniformly coincide with the NDVI deviation, with  
5301 low NDVI values weakly responding to both low and high min temperatures  
5302 (Fig. 5.9).

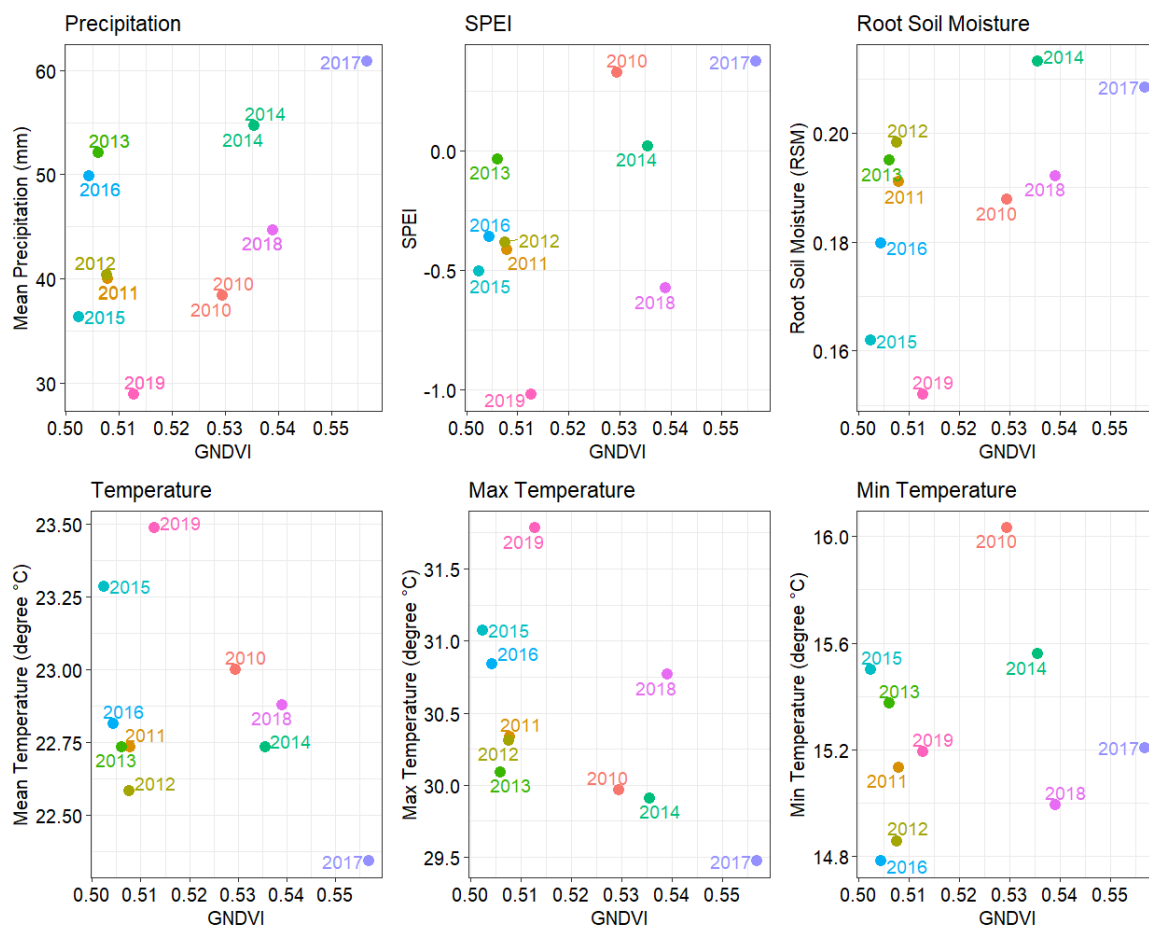
5303

5304

5305

5306

5307

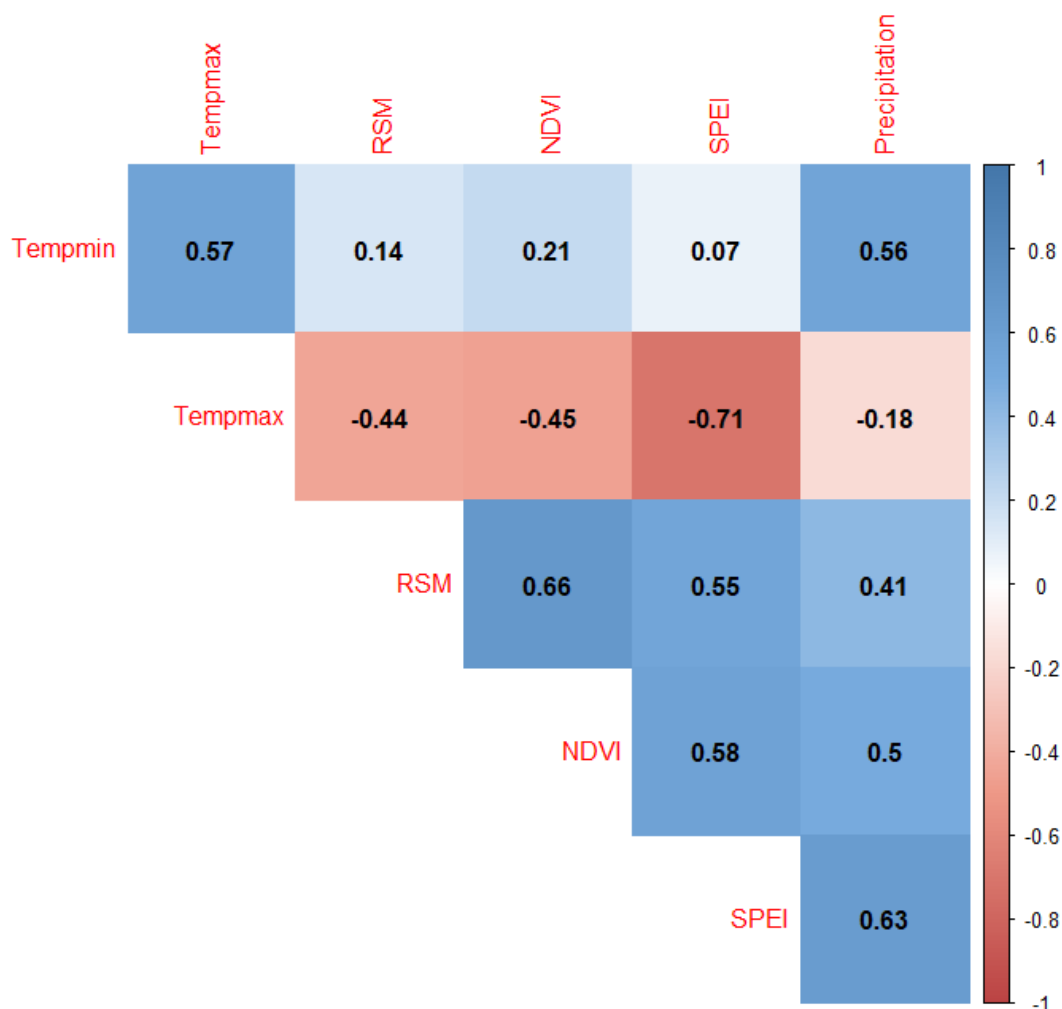


5308

5309 Fig. 5. 9. Association between climate variables and NDVI from the Kavango Zambezi  
 5310 region. The average daily mean, maximum temperatures, precipitation, SPEI and Root Soil  
 5311 Moisture were calculated from the monthly data in the growing season from 2010 to 2019.

5312

5313 The correlations of NDVI, precipitation, SPEI, root soil moisture, minimum  
 5314 temperature and maximum temperature are presented in Fig. 5.10. The NDVI  
 5315 shows a strong correlation with the root soil moisture ( $r = 0.66$ ), highlighting the  
 5316 constraints imposed by root soil moisture deficit on dryland vegetation. The  
 5317 results also indicate a higher correlation between NDVI and SPEI ( $r = 0.58$ ), as well  
 5318 as the NDVI and precipitation ( $r = 0.50$ ), reaffirming the consistent mechanism of  
 5319 influence of drier conditions. The NDVI - maximum temperature correlation ( $r = -$   
 5320  $0.45$ ) was also notable. The SPEI index showed a strong negative correlation with  
 5321 maximum temperature ( $r = -0.71$ ), and a positive correlation with precipitation  
 5322 ( $r = 0.63$ ).



5323

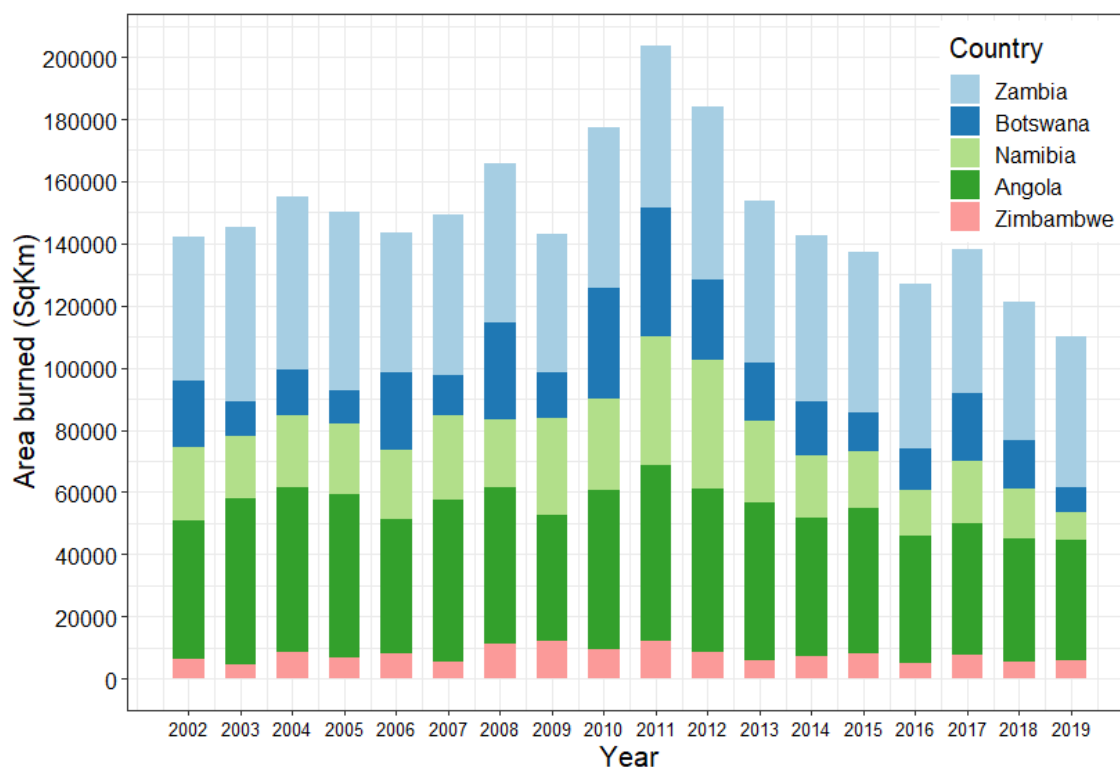
5324 Fig. 5. 10. Pearson's correlation of the NDVI, precipitation, SPEI, root soil moisture,  
5325 minimum temperature and maximum temperature.

### 5326 5.5.3 Temporal analyses of fire

#### 5327 5.5.3.1 Fire seasonality and extent

5328 Fig. 5.11 shows the area burnt for each country in the KAZA region. Every year,  
5329 between 110,173 km<sup>2</sup> (21%) and 203,849 km<sup>2</sup> (39%) of the land area in the KAZA  
5330 region were burnt on an annual basis in the period 2002 to 2019. The year 2011  
5331 experienced the highest degree of burning with 203,849 km<sup>2</sup> (39%), followed by  
5332 2010 and 2012 with 177,493 km<sup>2</sup> (34%) and 184,186 km<sup>2</sup> (36%), respectively.  
5333 The year 2019 experienced the lowest burning with only 110,173 km<sup>2</sup> (21%). In  
5334 KAZA region, a mean 149,410 km<sup>2</sup> of land is burnt on an annual basis in the period  
5335 2002–2019. Most of this burnt area is situated in Angola and Zambia, with an  
5336 average of 47,492 km<sup>2</sup> (32%; Angola) to 50,935 km<sup>2</sup> (35%; Zambia), respectively,

5337 of the land area burnt on an annual basis between 2002 and 2019 respectively. The  
 5338 average area burnt annually in Namibia, Botswana, and Zimbabwe was lower,  
 5339 varying between 23,806 km<sup>2</sup> (16%; Namibia), 19,554 km<sup>2</sup> (13%; Botswana) and  
 5340 7,623 km<sup>2</sup> (5%; Zimbabwe), respectively (see supplementary: Fig. C. 1 and Table C  
 5341 1).

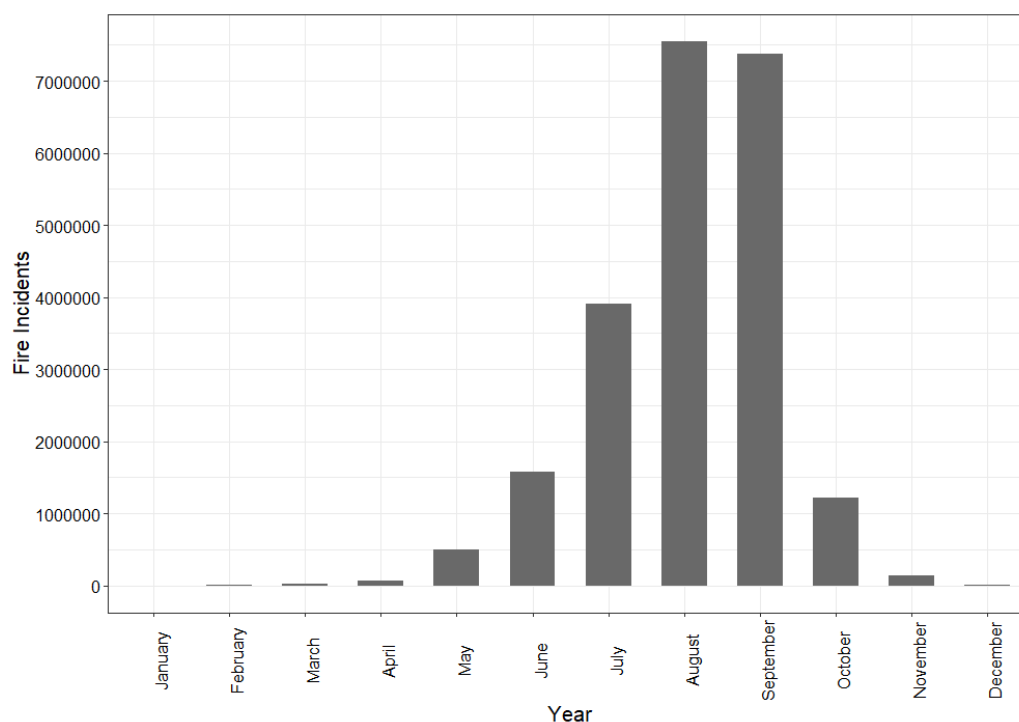


5342

5343 Fig. 5. 11. Total area burnt annually for each country of KAZA from 2002 to 2019 in  
 5344 km<sup>2</sup> based on the MODIS Burnt Area product data.

5345 Fig. 5.12 shows the cumulative monthly seasonal distribution of fires in KAZA  
 5346 between 2002 to 2019, as determined from an analysis of the 1 km FIRMS fire  
 5347 activity data. The FIRMS data are reported to have considerable amount of  
 5348 uncertainty on individual fire number/size distribution. Therefore, FIRMS point  
 5349 data were used as complementary to MODIS burned data (Mouillot et al., 2014).  
 5350 Vegetation burning in the KAZA region occurs mainly in the dryland forests during  
 5351 the dry season between May to October each year. The highest degree of burning is  
 5352 experienced during the late dry season, with the months of August and September  
 5353 representing the peak months for fire incidences. More than 96% of the incidences  
 5354 are due to dry season fires from May to October. There is a relatively low level of  
 5355 fire incidences in the months of November, December, January, February, March

5356 and April (Fig. 5.12). Looking at burning incidences per individual country,  
 5357 Namibia, Botswana and Zimbabwe have the highest levels in September, while  
 5358 Zambia and Angola have the highest levels in August (see supplementary, Fig. C .  
 5359 2). On a regional scale, August shows the highest burning rate followed by  
 5360 September because Zambia and Angola experience the highest burning incidences  
 5361 on an individual basis in comparison to the other three countries (Botswana,  
 5362 Namibia and Zimbabwe) combined, as shown below (Fig. 5.12).



5363

5364 Fig. 5. 12. Cumulative monthly fire incidences for the whole of KAZA from 2002 to 2019  
 5365 using FIRMS fire activity data.

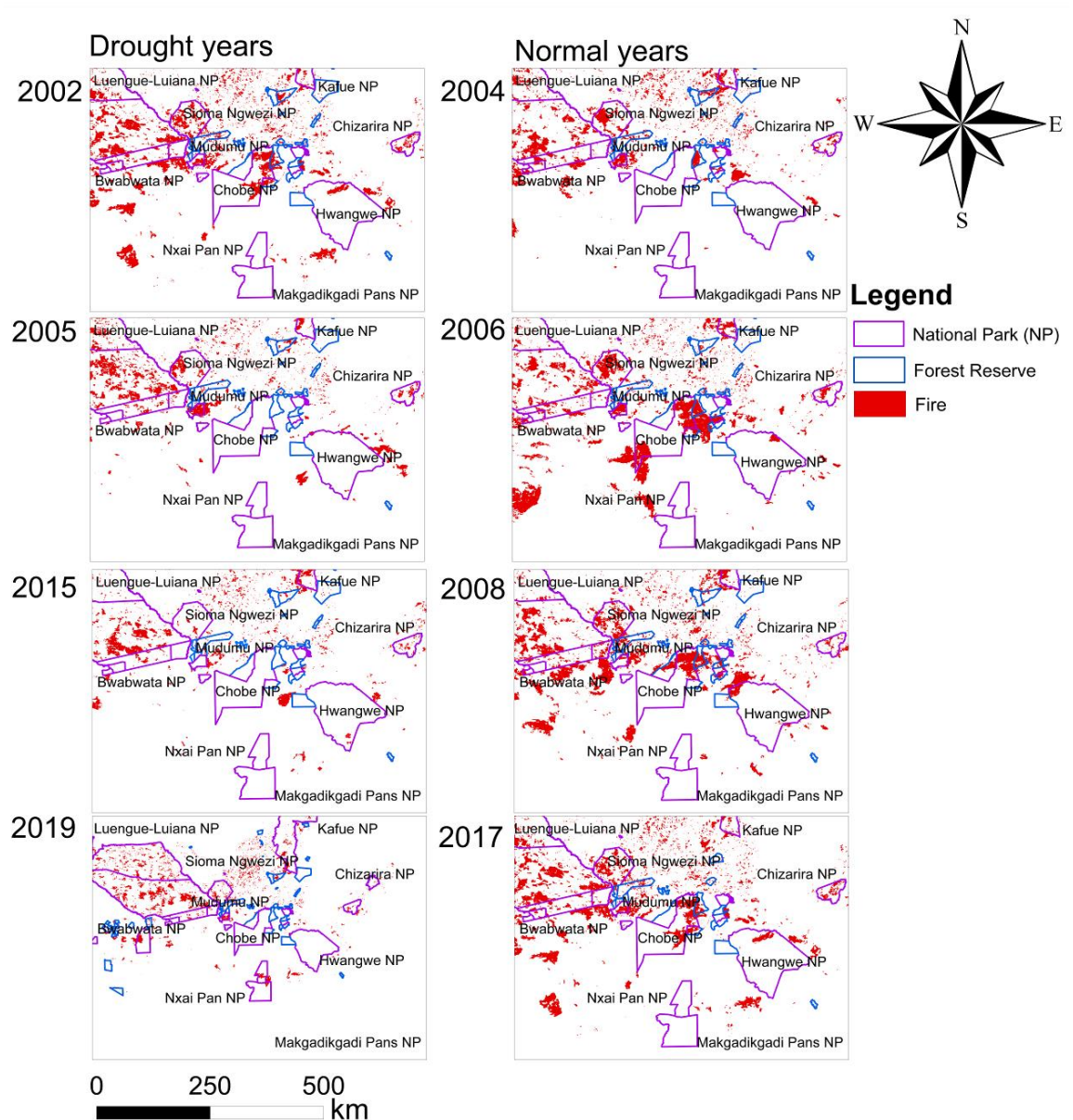
5366

#### 5367 5.5.4 Spatial analyses of fire seasonality and extent

5368

5369 Fig. 5.13 shows comparison between the fires burnt in September in drought and  
 5370 wet years. Data from the month of September are used because it represents the  
 5371 peak month for fire incidences in most of the KAZA countries. Spatial analysis  
 5372 indicates that the years with extreme drought, including 2002, 2005, 2015 and  
 5373 2019, experience the lowest extent of area burnt as compared to normal and wet  
 5374 and less drought affected years. The burnt area was greatest in the wet years of  
 5375 2004, 2006, 2008-2010 and 2017, and in the very low drought years (2011 to

5376 2013) for all the five countries in the study area, and most of the burnt area is  
5377 situated within National Parks. As shown in Fig. 5.13, the Chobe NP has no fire  
5378 incidences during the drought years, but fire intensified in the normal/wet years. It  
5379 can be noted that the northeastern section of Chobe NP (near Kasane Forest  
5380 Reserve) is more prone to fire than the north and southern part of the park. The  
5381 national parks including Chobe NP, Mudumu NP, Sioma Ngwesi NP and Luengue-  
5382 Luiana NP and Kafue NP are more vulnerable to fires in wet years as compared to  
5383 drought years. The Nxai Pan NP and Makgaikgadi Pans NP of Botswana and  
5384 Hangwe NP of Zimbabwe has little to no fire incidence in most years. The  
5385 National Parks in Angola, Zambia, and Namibia including Sioma Ngwesi NP and  
5386 Luengue-Luiana NP, Kafue NP and Mudumu NP experience severe burning in both  
5387 dry and wet years, even though the national parks are more vulnerable to fire in  
5388 wet years as compared to drought years.



5389

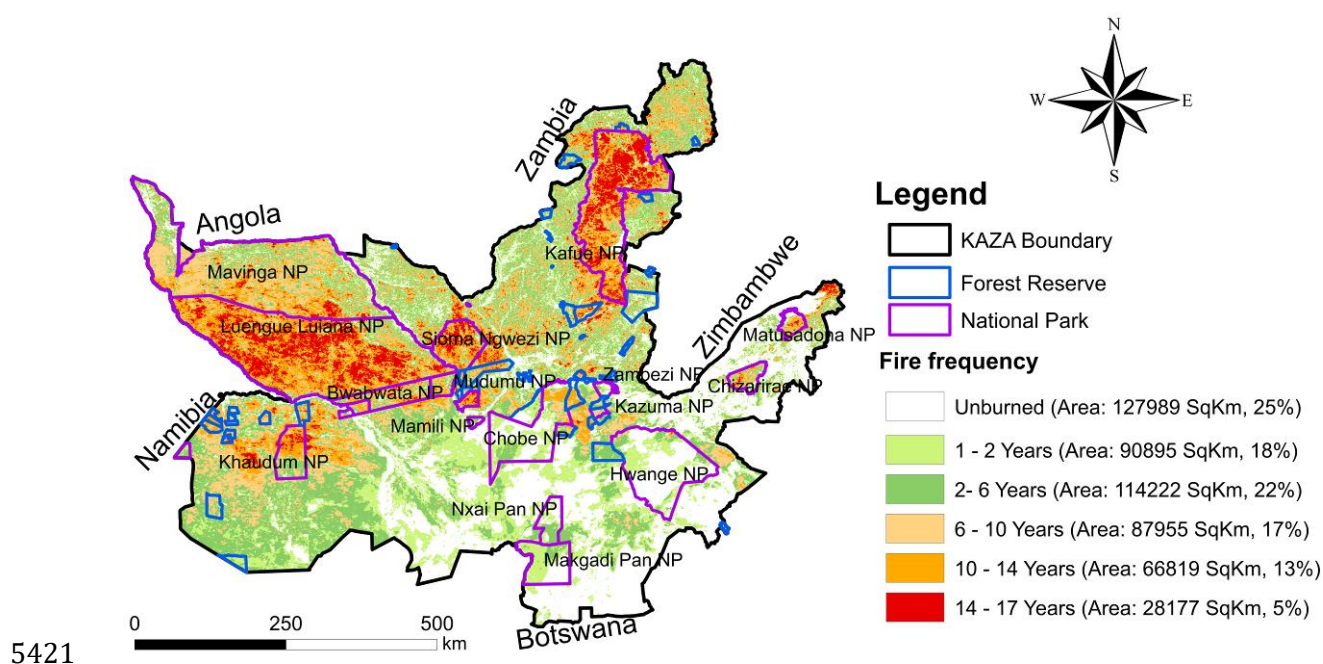
5390 Fig. 5. 13. Burnt area derived from the September month of MODIS MCD64A1 product for  
 5391 selected drought years (2002, 2005, 2015 and 2019) and wet years (2004, 2006, 2008 and  
 5392 2017) based on SPEI data.

5393

5394 **5.5.5 Fire frequency index**

5395 Fire-affected pixels were considered as those area that burnt at least once in the  
 5396 17-year monitoring period. As shown in Fig. 5.14, between 2002 and 2019, about  
 5397 390,678 km<sup>2</sup> (75%) of the land area is classified as fire-affected at least once, and  
 5398 127,989 km<sup>2</sup> (25%) of the area is not affected by fire (Fig. 5.14). Of the 390,678  
 5399 km<sup>2</sup> (75%) of fire-affected area, 90,895 km<sup>2</sup> (18%) of the area burnt only once or

5400 twice during the 17 years, indicating a low overall fire frequency overall. The  
 5401 majority of the area, 114,222 km<sup>2</sup> (22%), burnt 2-6 times, while 87,955 km<sup>2</sup> (17%)  
 5402 burnt 6-10 times over the same period. About 28,177 km<sup>2</sup> (13%) burnt frequently,  
 5403 >10-14 times, and 28,177 km<sup>2</sup> (5%) burnt every in >14 of the 17 years indicating a  
 5404 high frequency overall (Table C 2). The national parks are affected by higher levels  
 5405 of fire occurrence than other protected areas such as forest reserves. The fire  
 5406 frequency map shows that Zambia including Sioma Ngwezi NP and Luengue-  
 5407 Luiana NP, Kafue NP experienced high rates of fire return with many of the same  
 5408 areas burning every year, during the monitoring period, with very large areas  
 5409 burnt in >14 out of 17 years. In Namibia, Mudumu, Bwabwata and Khaudum NPs  
 5410 also experienced very high rates of fire return for the majority of their total area  
 5411 ranging returning in 10 to 17 years. In Botswana and Zimbabwe, fire return is  
 5412 generally <6 years, with the exception of the Northeasten Chobe NP, Chizarirae NP  
 5413 and Matusadona NP, which had a fire return of between 6 to 14 years. Hwange NP  
 5414 in Zimbabwe experienced a fire return >6 years for a very small proportion of the  
 5415 northeast area adjacent but outside Hwange NP, and the two parks at the  
 5416 southernmost tip of Botswana (Makgadimkadi Pan NP, and Nzai Pan NP) have the  
 5417 lowest fire reoccurrence of <6 times out of the 17 monitored years. A large portion  
 5418 of the 25% of unburnt pixels were recorded south of Zambezi River in Botswana  
 5419 and Zimbabwe. By comparison, the fire return and incidence of burning are higher  
 5420 in Botswana than in Zimbabwe.





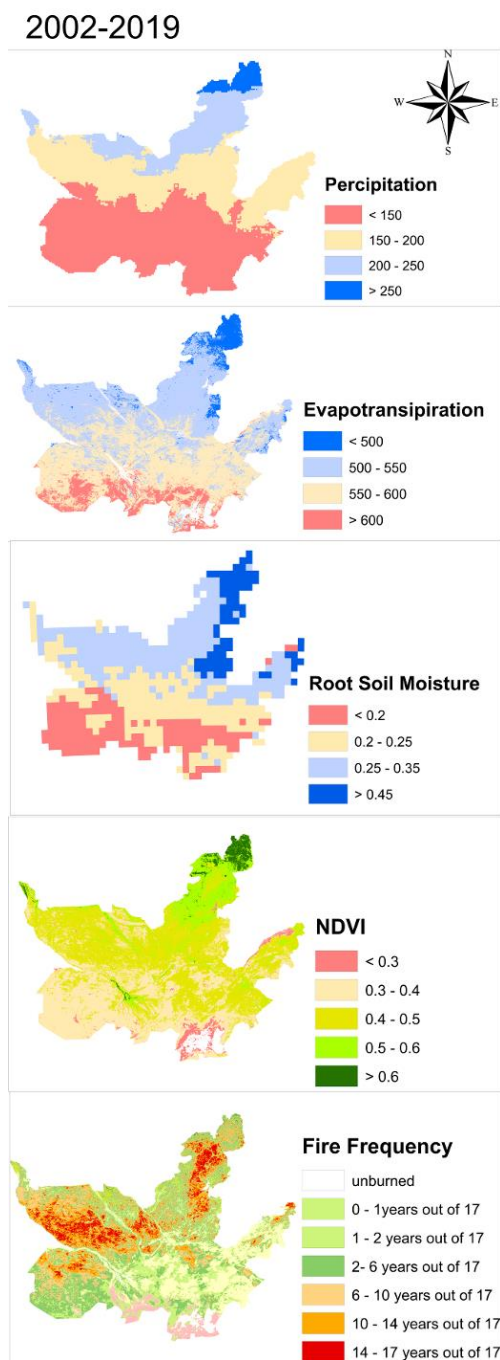
5422 Fig. 5. 14. The area affected by fire determined from monthly using MODIS Burnt Area data  
5423 from 2002 to 2019 for different land categories in the region. Colours indicate the number  
5424 of times pixels were classified as burnt. White areas represent pixels that were classified  
5425 as unburnt over the time period.

5426 Fig. 5.15 shows climate, fire and vegetation indices data from 2002 to 2019. Very  
5427 high and extremely low burnt areas coincide with a certain combination of climatic  
5428 factors. A comparison of the distribution of these climatic data and burnt areas,  
5429 with the spatial distribution of NDVI values, an index of 'greenness' of the  
5430 vegetation also derived from the MODIS sensor, shows that burning is closely  
5431 related to areas with proportions of high dryland forests. The areas with high  
5432 dryland forests (or high tree cover), high rainfall, and dry season length  
5433 correspond to areas with high fire frequency and large burnt areas (Fig. 5.15). For  
5434 example, areas with high dryland tree cover and vegetation with NDVI >0.4  
5435 receiving mean annual precipitation >150 mm were burnt in approximately 6 to  
5436 17 out of the 17 monitored years, here it was common that the same areas burned  
5437 frequently and recurrently. The areas with low tree cover and vegetation with  
5438 NDVI <0.4 receiving mean annual precipitation <150 mm were burnt 1 to 6 times  
5439 out of 17 years. The very dry areas, such as the succulent deserts, burnt once and,  
5440 in most cases, remained unburnt in the 17 years. The precipitation variations  
5441 corresponded with the highest degree of spatial similarity to the root soil moisture,  
5442 and with consistent high rainfall in northern part of KAZA, and the extremely low  
5443 rainfall (<150 mm) in the southern part of the region.

5444 In contrast, the potential evapotranspiration has the lowest variation in the  
5445 northern part of the study area (>550 mm) and highest variations in the south  
5446 (<5500 mm). This is consistent with the root soil moisture, which have high  
5447 variations (>0.25) in the northern part of the region in comparison to the northern  
5448 side with very low soil moisture (<0.25). The northern part of the region is  
5449 situated in the countries with the largest dryland forest cover, Angola and Zambia,  
5450 which is consistent with high NDVI (light and dark green colours in Fig. 5.15).  
5451 However, these areas also have a very high rate of burning in consecutive years,  
5452 with a fire return of between 14 to 17 years within 17 years, as shown by the fire  
5453 frequency index. The high fire return rate is also prevalent in other areas with  
5454 dryland forests, such as the forest reserves and national parks in Namibia and

5455 Botswana (e.g., Mudumu, Chobe NP, Zambezi ST and Kasane forest reserves),  
 5456 which display a fire return of between 6 to 14 in 17 years, with proportions of  
 5457 their areas experiencing fire recurrences in more than 14 years. The south of  
 5458 Zambezi River shows a very low fire frequency and a large portion of the 25% of  
 5459 unburnt pixels from 2002 to 2019 are recorded here (see supplementary: Table C  
 5460 2).

5461

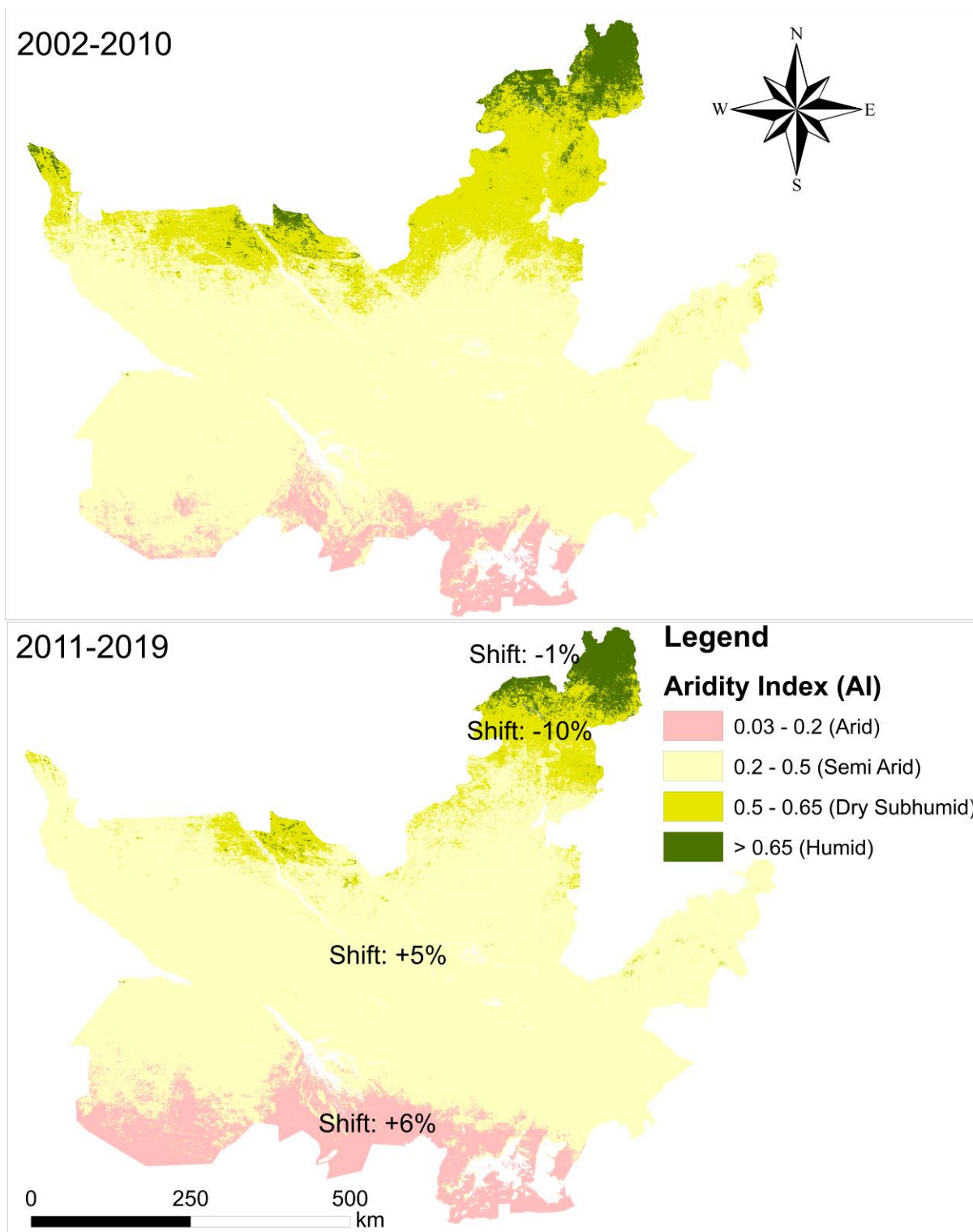


5462

5463 Fig. 5. 15. Areas where the fire frequency is under varying degrees of climatic condition  
5464 (precipitation, potential evapotranspiration, root soil moisture), and NDVI sampled from  
5465 the averaged monthly-mean of the growing season of 2002 to 2019.

### 5466 5.5.6 Spatiotemporal changes in the Aridity Index

5467 Fig. 5.16 presents the spatiotemporal aridity changes in the whole of the KAZA  
5468 region to explore whether frequent drought and fire dynamics in recent years have  
5469 led to increased dryness, and subsequent vegetation change. A subset of the AI  
5470 data over the last 9 years of the period (2011–2019) is compared with the first 9  
5471 years (2002 - 2010) to highlight these temporal changes. The temporal changes of  
5472 AI showed a significant increasing dryness since 2002. Observed areal changes  
5473 (Fig. 5.16) are apparent, with the change to drier subtypes being dominant and  
5474 mainly located in southern side of the region as compared to the northern side in  
5475 the period of 2002-2010, as compared to 2011-2019. An increase in the drying  
5476 variations and changes in the aridity index were observed in transition zones  
5477 between arid, semi-arid, and sub-humid regions between 2011 and 2019. The arid  
5478 and semi-arid regions have increased at the expense of neighbouring dry sub-  
5479 humid areas, and represented 5.56% and 4.84%, respectively. The sub-humid  
5480 areas experienced a significant decrease of approximately 10% of the KAZA land  
5481 area. The largest expansion of drylands occurs in semiarid regions, which account  
5482 for nearly half of the total dryland expansion and cover >70% of the region (Table  
5483 C 3). The AI indicator detected areas with increasing aridity to be mainly in  
5484 southern KAZA, and these areas are shifting towards more arid and hotter classes,  
5485 while northern the KAZA areas with semi humid regions are shifting into semi-arid  
5486 regions and, therefore, increasing climatological drying risk.



5487

5488 Fig. 5. 16. Spatial distribution of averaged aridity over KAZA region for 2002-2010 and  
 5489 2011-2019.

5490

## 5491 5.6 Discussion

### 5492 5.6.1 Drought impacts on vegetation

5493 Temporal analysis of the SPEI index, precipitation and soil moisture anomalies all  
5494 reveal that the 2019 drought event surpasses the severity of events in 2002, 2005,  
5495 2010, and 2015, which were all considered severe drought events. The results  
5496 show that the dryland vegetation in the region has a strong correlation with  
5497 precipitation and closely responds to variability in precipitation and drought (see:  
5498 Fig. 5.7). A study by Caylor et al. (2005) showed that vegetation in the Kalahari  
5499 region depends on the stochastic distribution of rainfall events and interannual  
5500 variation in rainfall that can induce shifts in vegetation structure with prolonged  
5501 periods of wet (or dry) regime. Comparing the satellite-based rainfall anomalies  
5502 (CHIRPS) with ground-based rainfall observations also indicates that the results  
5503 are not sensitive to the precipitation data used in this analysis. The multi-year  
5504 spatial patterns of change in climate, soil moisture and vegetation were  
5505 categorised from 2002 through 2019 (see: Fig 5.8). Fig 5.8 shows the results of  
5506 2010 to 2019 as this period was more affected by drought impacts as compared to  
5507 the period 2002-2009. As shown in Fig. 5.8, the severity and extensiveness of the  
5508 2015 and 2019 drought resulted in considerable precipitation and soil water  
5509 deficit, which caused a significant change in dryland forest vegetation. A similar  
5510 pattern was seen by Liu et al. (2013) who found climate variability to be extreme  
5511 in dryland trees and grassland in the KAZA region. The browning hotspots are  
5512 concentrated in unprotected woodland and grassland, although significant  
5513 browning patterns were also observed in protected national parks (e.g., Chobe NP  
5514 and Kafue NP). On the one hand, some large-scale browning patterns are not  
5515 corresponding to the low precipitation values and drought years, which implies  
5516 that they could not be directly associated with climate change (see: Fig. 5.8).  
5517 Agricultural expansion, deforestation, and frequent fire burning could be  
5518 associated with these changes, particularly in Namibia and Zambia.

5519 The lag in greening rate in dryland biomes can be seen in some years following  
5520 drought (e.g., 2016), with most dryland trees suffering drastically reduced growth  
5521 rates despite an increase in rainfall and a subsequent lack of a dry spell, as shown  
5522 in the SPEI of 2016 (see: Fig. 5.8 and 5.9). The root soil moisture data explained the

5523 consistent decrease in vegetation productivity in 2016, despite precipitation and  
5524 the SPEI showing a positive trend, indicating that RSM root soil moisture is one of  
5525 the major controlling factors that helps to explain changes in vegetation cover  
5526 across the KAZA region, as indicated by Caylor et al. (2005). Sporadic, erratic and  
5527 extremely poor rainfall accompanied by high temperatures in preceding years,  
5528 seems to have resulted in an absence of soil water storage with root soil moisture  
5529 levels becoming very low, resulting in potential carry-over effects on plants.  
5530 Although SPEI considers the effects of both temperature and precipitation, and has  
5531 been very useful in detecting vegetation drought in many studies (Marumbwa et  
5532 al., 2020; Vicente-Serrano et al., 2015), the RSM showed a better performance in  
5533 explaining the climatic relationship with vegetation vulnerability to prolonged  
5534 drought resulting in lack of moisture in plant roots (see: Fig. 5.8 and 9). This  
5535 finding is similar to Anderegg et al. (2013) and Case et al. (2019) who also  
5536 observed lag-effect patterns between drought stress and extended multiyear tree  
5537 disturbances in 2015-2016 in temperate forests in North America and dryland  
5538 woodland in Kruger NP. These results confirm that MODIS-derived VIs time series  
5539 coupled with climatic variables, soil moisture and ground measurements of forest  
5540 stands can provide insights into the influence of water stress on dryland biomes.

## 5541 5.6.2 Fire

5542 Changes in fire regime were analysed in conjunction with climate data as the  
5543 climate variability and change also modify the risks of fires, pest and pathogen  
5544 outbreaks, which each negatively affect vegetation (IPCC, 2014). The data show  
5545 that every year, between 110173 km<sup>2</sup> (21%) and 203849 km<sup>2</sup> (39%) of the land  
5546 area in the KAZA region were burned in the period 2002 to 2019. The year 2011  
5547 experienced the highest amount of burning with 203849 km<sup>2</sup> (39%), and 2019  
5548 experienced the lowest burning with only 110173 km<sup>2</sup> (21%). The results show an  
5549 increase in annual precipitation in the study region has led to a potential increase  
5550 in fire incidence, and the reoccurrence of drought events have exacerbated fire  
5551 incidences in the wet years. During wet years (2004, 2006, 2008-2009 and 2017)  
5552 and less drought prone years (2011 to 2013), fire incidence in the KAZA was  
5553 greatest across protected areas. By comparison, dry years of 2002-2003, 2005,  
5554 2015-2016 and 2018-2019 show unusually low fire incidence and notably, 2019

5555 which experienced extreme drought conditions also experienced the lowest  
5556 number of fire incidences (see: Fig. 5.11 and 13). The findings of this study are in  
5557 agreement with Fox et al. (2017) who analysed fire incidences in Chobe NP from  
5558 2001 to 2013, and found more active fires recorded in years with higher rainfall. In  
5559 addition, during wet seasons or low drought years, fire is also used to remove  
5560 biomass from land being cleared for agriculture, shifting cultivation, weed and  
5561 disease control, or, afterwards, for removal of the previous-year's agricultural  
5562 waste (Eriksen, 2007; Frost, 1999). However, inverse results were found in the  
5563 Amazon, where many studies demonstrate that fire incidence and extent increases  
5564 in drought years (Aragão et al., 2007; Nobre et al., 2009)..

5565 One explanation for the high incidence of fire in wet years is that in the KAZA  
5566 region, more than 90% of fire incidences are due to dry season fires in June to  
5567 October, the highest number of burning incidences occur in the late dry season  
5568 between August and September (see Fig. 5.12), and the end of dry season affects  
5569 the amount of fuel available in wet years (see: Fig 5.4). During the dry season, the  
5570 herbaceous vegetation is either dry/dead (annual grasslands), and deciduous trees  
5571 have shed their leaves, thereby contributing to the build-up on the surface of  
5572 ignition sources after only a few weeks of dry weather (Higgins et al., 2000;  
5573 Lehmann et al., 2014). This evidence suggests that most fires in the region are set  
5574 by people, because there are few thunderstorms in the late dry season months that  
5575 might naturally trigger fires. The late dry seasons are normally hot, windy with  
5576 extremely dry conditions, which means the fires can spread easily and are difficult  
5577 to control, and subsequently burn large areas (Archibald et al., 2010). On the other  
5578 hand, severe drought conditions with very low rainfall does not permit the  
5579 accumulation of sufficient fuel to become a source of ignition and then to sustain  
5580 extensive fires (Stott, 2000). The fieldwork of 2019 revealed that a frequent late  
5581 dry season fire transforms woodland into open, tall grass savanna with only  
5582 isolated fire-tolerant canopy trees. This suppresses the regrowth of woody plants  
5583 resulting in scattered understorey trees and shrubs. Similarly, in the Amazon, huge  
5584 and successive fires have substantially increased forest disturbances and favoured  
5585 the occurrence of short-life-cycle pioneer species (Nobre et al., 2016).

5586 Between 2002 and 2019, about 390678 km<sup>2</sup> (75%) of the land area was classified  
5587 as fire-affected at least once, and 127989 km<sup>2</sup> (25%) of the area was not affected

5588 by fire (see: Fig. 5.14). Even though all of the KAZA member countries have fire  
5589 suppression policies that largely date back to colonial days, the striking difference  
5590 in fire incidence and extent of area burnt is due to the different types of fire laws,  
5591 and the enforcement of these laws. The national parks are more affected by high  
5592 fire occurrence as compared to other protected areas, such as forest reserves,  
5593 game reserves and wildlife management areas. The fire frequency map shows that  
5594 a large portion of the 75% burned pixels were located in the Zambian and Angolan  
5595 areas of KAZA. The two countries experienced high rates of fire return, with many  
5596 of the same areas burning every year, in the last two decades, with very large areas  
5597 burned in 14 to 17 years out of 17 years. Within Angola, anthropogenic fire is  
5598 thought to be a significant cause of deforestation and the fire incidence rate is  
5599 significantly higher during the dry season, which has a negative impact on forest  
5600 resources and biodiversity in Kuando-Kubango Province (the Angolan component  
5601 in KAZA), as recorded by United States Forest Service report (Zweede et al., 2006).  
5602 Although there is legislation and regulation on fire control in Angola, these are  
5603 rarely enforced, and so uncontrolled dry-season burning for clearing land and to  
5604 flush animals for hunting are common practices (USAID, 2013). In Zambia, fire is  
5605 perceived as an important land management tool in agricultural and caterpillar  
5606 breeding. The Zambian State Forestry Department and local NGOs encourage  
5607 burning earlier in the dry season to enable fire suppression in the late dry season  
5608 across most national parks and other protected areas. Even though there is  
5609 existing state law on fire regimes in Zambia, these laws are not strictly followed,  
5610 again due to the difficulty of enforcement, and potentially a lack of understanding  
5611 of the laws in many remote rural areas (Eriksen, 2007). A separate study by  
5612 Archibald et al. (2010) also reported similar results, whereby Angola and Zambia  
5613 have the highest burnt areas amongst Southern African countries, with much of  
5614 their area burned >4 in the 8-year period monitored.

5615 In Namibia, fire return periods for most of areas are midrange compared to other  
5616 areas of KAZA (e.g., Mudumu, Bwabwata and Khaudum NP experienced high rates  
5617 of fire return for most of its total area ranging from 10 to 17 years out of the 17  
5618 years). In Namibia, a fire management project that includes the establishment of a  
5619 community fire break, and the implementation of awareness programs on fire, to  
5620 manage and reduce wildfires was established in 1996 through the Namibia-



5621 Finland Forestry Programme (NFFP) (Verlinden et al., 2006). In addition, an  
5622 innovative integrated fire management program (Integrated Rural Development  
5623 and Nature Conservation Caprivi Program) was implemented between 2006 and  
5624 2010 to support national parks and forestry agencies via decentralization of fire  
5625 management decision-making to include community members in decision-making  
5626 (Russell-Smith et al., 2017). Fire management in the Namibian section of the  
5627 Wildlife Dispersal Area (WDA) has progressed significantly through collaborative  
5628 efforts between the Directorate of Forestry, NGOs and local communities (KAZA,  
5629 2014). According to Verlinden et al. (2006), the implementation of fire  
5630 management into schools and community meetings, through awareness raising  
5631 interventions in Namibian were very effective and the results appear to show a  
5632 significant decrease in burned area in comparison to the prior era.

5633 A large portion of the 25% of unburned pixels from 2002 to 2019 are recorded in  
5634 Zimbabwe and south of Zambezi River around the Makgadikgadi Pans National  
5635 Park and Nxai Pan National Park in Botswana. This is due to the generally drier  
5636 environment with low precipitation and low tree cover as both Makgadikgadi Pans  
5637 National Park and Nxai Pan National Park are physically and ecologically part of  
5638 the “Kalahari Desert,” and possibly due to better controlled fire regimes in these  
5639 areas (Chinamatira et al., 2016; EMA, 2007). The incidence of burning is lower in  
5640 Botswana than in Zimbabwe, despite the higher human population density in the  
5641 latter. In the two countries, the fire return is generally low with <6 years  
5642 experiencing burning from 17, with the exception of northeast of Chobe NP, the  
5643 northeast of Hwange NP, Chizarirae NP and Matusadona NP, which have a fire  
5644 return of between 6 and 14 years. This is in line with the findings by Mpakairi et al.  
5645 (2019) who reported fire hotspots in Chizarira, Matusadona NP and northeast of  
5646 Hwange NP. Botswana has a fire suppression management strategy through the  
5647 use of fire breaks and firefighting crews including the military, police and  
5648 volunteer members of the general public, mobilised through the District  
5649 Commissioner (Dube, 2013). The Zimbabwean component have strict laws on fire  
5650 management and control in place, dating back to colonial days bolstered by recent  
5651 laws passed in 1998 (Zweede et al., 2006). The Zimbabwean Environmental  
5652 Management Authority passed regulations on fire suppression in 2007, such that  
5653 anyone caught setting a wildfire outside a residential or commercial premises

5654 during the dry summer period from 31 July to 31 October of each year are  
5655 arrested, face expulsion from the area, or can be fined by decree (Chinamatira et  
5656 al., 2016; EMA, 2007).

### 5657 5.6.3 Changes in aridity

5658 Understanding the long-term areal change in the aridity is essential for taking  
5659 early action to prevent the aggravation of drying conditions. The results shown in  
5660 Fig. 5.16 confirm that the KAZA region is becoming drier in the 20th century, and  
5661 there is an increased risk of arid conditions as result of enhanced warming,  
5662 wildfires and the rapidly growing human population in the drylands of KAZA  
5663 region. Such an expansion of arid areas detected in this study is in agreement with  
5664 the projection by IPCC (2007) that by 2020, most African countries are projected  
5665 to be exposed to increased water stress due to climate change and this would lead  
5666 to reduced carbon sequestration and enhanced regional warming, resulting in  
5667 increased warming trends over the drylands. In the scientific literature, there are  
5668 many publications dealing with aridity changes, but as there is no study of aridity  
5669 change at a regional scale across KAZA, it is difficult to make detailed comparisons.  
5670 At regional scale, climate shifts can be notably different to those observed at global  
5671 scale. The most relevant precursor to this study aridity maps can be the global  
5672 maps produced by Huang et al. (2017). Huang et al. (2017) compared aridity data  
5673 over 10 years, from 1996 to 2005, to a 10 year period between 1948 to 1957. Their  
5674 study found that most vegetation change from dry sub-humid to semi-arid  
5675 occurred in the area of the KAZA region in Southern Africa. In comparison to this  
5676 study, an increase in the drying variations and changes in the aridity index were  
5677 observed in the arid and semi-arid regions represented by 5.56% and 4.84%  
5678 between 2002 to 2019 (this study), as compared to 1.16% and 2.32% in the arid  
5679 and semi-arid regions between 1948 to 1957 observed in Huang et al. (2017).

5680 Another global study by Spinoni et al. (2015) compared AI from 1951 to 2010  
5681 using FAO AI and the KG climate classification. Their study found that the extent of  
5682 arid lands increased in Africa by 1.95%, followed by Asia (0.55%) and decreased in  
5683 the North and South Americas by -0.47 and -70%, respectively. Their study found  
5684 that that the arid lands in Southern Africa are larger by the end of the period 1981  
5685 to 2010, as compared to the period 1951-1980, and the largest increase in arid

5686 regions of Southern Africa were located in the KAZA region (Southern Zambia,  
5687 Zambezi region of Namibia and western Zimbabwe) as compared to any other part  
5688 of Southern Africa. These findings more or less agree with the results presented  
5689 here, with one exception: the shifts identified in this study were found to be larger  
5690 in dry-sub-humid and humid area, with 10.40% of the regional land area becoming  
5691 arid compared to the previously published 1.95% at a continental scale. The  
5692 difference could be attributed to the difference in data, as this study used high-  
5693 resolution precipitation and PET data at a much smaller scale, while the global  
5694 studies used a more coarser resolution Global Precipitation Climatology Centre  
5695 (GPCC) and the Climatic Research Unit (CRU) for precipitation and PET. This  
5696 difference could also be due to the fact that the thesis considered data up to 2019,  
5697 and the 21st century recorded the worst drought periods, notably in 2012-2013,  
5698 2015-2016 and 2018-2019.

5699 As a result of the multiple effects of consecutive droughts, many countries such as  
5700 Namibia and Angola, declared a state of emergency in response to drought 3 times  
5701 in a period of 6 years, with the drought of 2019 declared as the worst in the last 90  
5702 years (Shikangalah, 2020). In addition, projected aridification-prone areas overlap  
5703 with regions at risk of severe drought, marked soil moisture depletion, and shifts  
5704 in potential vegetation distributions. This suggests that, compared with globally  
5705 averaged aridity changes, the KAZA region show a much drier climate than most  
5706 regions in Africa, and globally. The results shows that if future precipitation  
5707 extremes become more severe, this region is likely to have vegetation that is more  
5708 unstable or may even to experience extreme vegetation shifts that will be hard to  
5709 adapt to, as predicted by (IPCC, 2014). Therefore, being able to understand areas at  
5710 risk of risk of drying conditions through drought indices should give land  
5711 managers information that may allow the implementation of mitigation or  
5712 adaptation measures, which can be fundamental in terms of dryland vegetation  
5713 sustainability.

5714

## 5715 5.7 Conclusion

5716 This study detected spatial and temporal patterns of climate, burnt areas and  
5717 dryland vegetation across KAZA, using a combination of ground-data and remote  
5718 sensing imagery to understand the ecological effects of climate and fire. The long-  
5719 term climate, fire, and vegetation data analysis led to the following conclusions:

5720 First, the extreme droughts of 2015 and 2019 resulted in considerable  
5721 precipitation and soil water deficits. Dryland forest vegetation is to be more  
5722 susceptible to changes in soil moisture trends, as opposed to changes in rainfall  
5723 and drought index.

5724 Second, at decadal time scales, interannual variability in fire frequency and burnt  
5725 area is likely to be driven largely by variation in rainfall, vegetation distribution  
5726 and dry season length. The areas with high tree cover, high rainfall, and less severe  
5727 drought season coincide with areas of high fire frequency and large burned areas,  
5728 while low tree cover (e.g., succulent deserts), low rainfall and extended severe  
5729 drought conditions correspond to areas with low fire frequency.

5730 Finally, the detected aridification-prone areas overlap with regions at risk of  
5731 severe drought, marked soil moisture depletion, and shifts in potential vegetation  
5732 distribution. The KAZA region has become drier due to aridification in the period  
5733 between 2002 to 2019 as a consequence of both drought and wildfire, which  
5734 critically affect agriculture, water quality, vegetation productivity, and biodiversity.

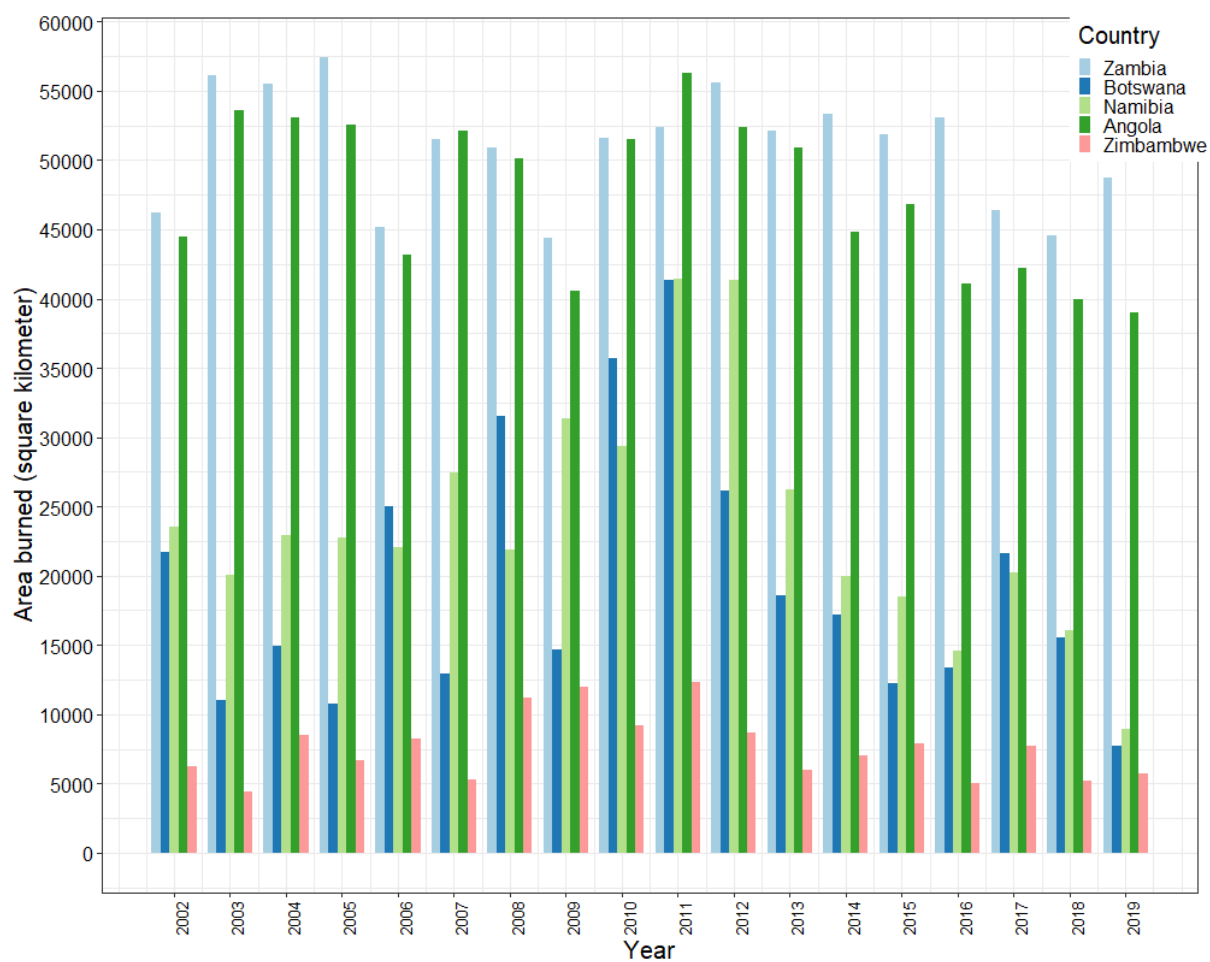
5735 The identification of the areas with significant trends of change is extremely  
5736 important in tropical dryland areas where low levels of field data are available and  
5737 limited financial resources can be invested in monitoring and assessment, as is the  
5738 case in much of the KAZA region. The detailed relationship between remotely  
5739 sensed drought/fire indicators and vegetation stress at the regional scale shown  
5740 here allow us to make several suggestions to move towards a more impact-  
5741 oriented drought and fire monitoring approach, with the potential to provide early  
5742 warnings in to devise more practical measures to control aridity in vulnerable  
5743 areas.

5744

5745

## 5746 5.8 Supplementary Information 3

5747 Temporal analyses: burned area

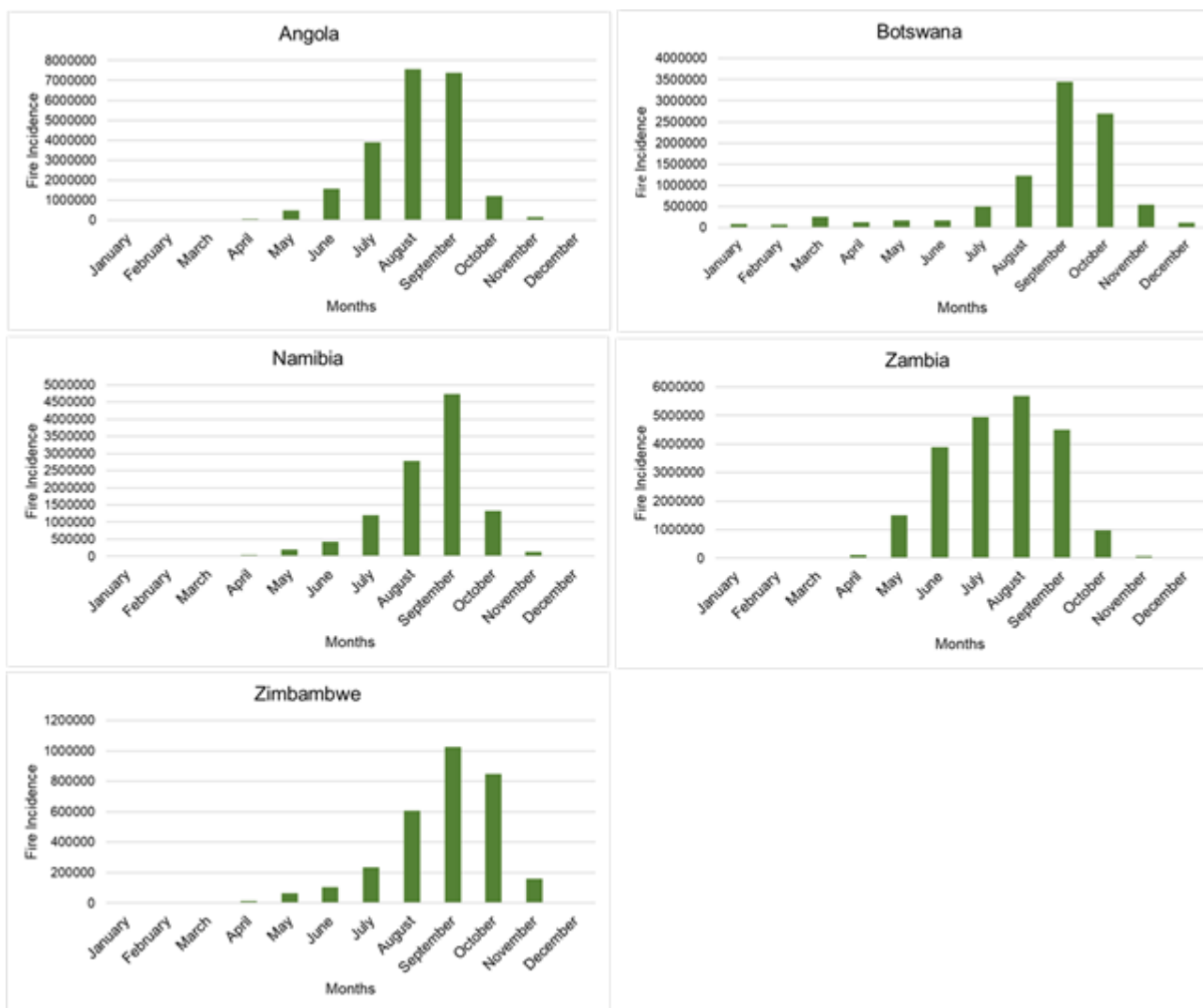


5748

5749 Fig C 1. Total area burned annually for each country of KAZA from 2002 to 2019 in  
 5750 km<sup>2</sup> based on the MODIS Burned Area product data.

5751

5752



5753

5754 Fig C 2. Cumulative monthly fire frequency for all the countries from 2009 to 2019 using  
5755 MODIS Active Fire product.

5756 Spatial analyses: burned area

5757 Table C 1. Estimates of the total area of burnt and unburnt areas in km<sup>2</sup> and their % from  
5758 2002 to 2017 in KAZA region

Year	Burnt area(km <sup>2</sup> )	Burnt (%)	Unburnt (km <sup>2</sup> )	Unburnt (%)
2002	142235	27	376463	73
2003	145168	28	373530	72
2004	154911	30	363783	70
2005	1501678	29	368530	71

<b>2006</b>	143703	28	374995	72
<b>2007</b>	149365	29	369333	71
<b>2008</b>	165706	32	352991	68
<b>2009</b>	142975	28	375723	72
<b>2010</b>	177493	34	341205	66
<b>2011</b>	203849	39	314849	61
<b>2012</b>	184186	36	334511	64
<b>2013</b>	153835	30	364863	70
<b>2014</b>	142463	27	376234	73
<b>2015</b>	137259	26	381439	74
<b>2016</b>	127181	25	391516	75
<b>2017</b>	138072	27	380626	73
<b>2018</b>	121363	23	397335	77
<b>2019</b>	110173	21	408525	79

5759

5760 Table C 2. Recorded areal fire frequencies of burnt and unburnt areas in km<sup>2</sup> and their %

5761 from 2002 to 2017 in KAZA region

<b>Year</b>	<b>Area (km<sup>2</sup>)</b>	<b>Area (%)</b>
<b>Unburnt</b>	127989	25
<b>1-2</b>	90895	18
<b>2-6</b>	114222	22
<b>6-10</b>	87955	17

<b>10-14</b>	66819	13
<b>14-17</b>	28177	5

5762

5763 Table C 3. KAZA shifts of AI per class from 2001-2010 to 2011-2020

<b>Class (SbAI)</b>	<b>2001-2010 (km<sup>2</sup>)</b>	<b>2001-2010 (%)</b>	<b>2011-2020 (km<sup>2</sup>)</b>	<b>2011-2010 (%)</b>	<b>Shift %</b>
<b>Arid</b>	33957	6.75	61897	12.31	5.56%
<b>Semi-Arid</b>	368016	73.13	392072	77.97	4.84%
<b>Dry Sub-humid</b>	82464	16.39	35369	7.03	-9.36%
<b>Humid</b>	18769	3.73	13503	2.7	-1.04%

5764 Drought

5765 Table C 4. Drought years and drought categories of SPEI at different time scales

<b>Year</b>	<b>SPEI1</b>				<b>SPEI3</b>				<b>spei2</b>			
	<b>moderate</b>	<b>severe</b>	<b>extreme</b>	<b>Σ</b>	<b>moderate</b>	<b>severe</b>	<b>extreme</b>	<b>Σ</b>	<b>moderate</b>	<b>severe</b>	<b>extreme</b>	<b>Σ</b>
1983	2	-	-	2	-	-	-	-	-	-	-	-
1984	-	-	-	-	1	-	-	1	1	-	-	1
1985	1	-	-	1	-	-	-	-	-	-	-	-
1986	-	-	-	-	-	-	-	-	-	-	-	-
1987	1	-	-	1	1	2	-	3	3	1	-	4
1988	-	-	-	-	2	-	-	2	-	-	-	-
1989	-	1	-	1	1	-	-	1	1	-	-	1
1990	2	2	-	4	-	-	-	-	-	-	-	-
1991	-	-	-	-	-	-	-	-	-	-	-	-
1992	2	-	1	3	1	2	-	3	2	1	-	3
1993	1	-	-	1	-	-	-	-	-	-	-	-
1994	1	1	-	2	2	1	-	3	2	1	-	3
1995	2	-	-	2	3	-	-	3	1	-	-	1
1996	5	-	-	5	2	-	-	2	3	-	-	3



1997	2	-	-	2	-	-	-	-	-	-	-	-
1998	1	2	1	4	2	2	1	5	5	-	1	6
1999	1	1		2	-	1	-	1	2	-	-	2
2000	1	-	-	1	-	-	-	-	-	-	-	-
2001	2	1		3	1	-	-	1	1		-	1
2002	2	4	1	7	2	2	1	5	4	2	1	7
2003	1	-	-	1	3	1	1	5	4	3	1	8
2004	2	-	-	2	1	-	-	1	1			1
2005	2	2	1	5	-	4	1	5	-	3	1	4
2006	1	-	-	1	-	-	-	-	-	-	-	-
2007	-	-	-	-	1	-	-	1	1		-	1
2008	1	-	-	1	2	-	-	2	-	-	-	-
2009	2	-	-	2		-	-	-	-	-	-	-
2010	-	-	-	-	-	-	-	-	-	-	-	-
2011	2	-	-	2	4		-	4	3	-	-	3
2012	3	-	-	3	3		-	3	2	-	-	2
2013	2	-	-	2	1		-	1	1	-	-	1
2014	1	-	-	1	-	-	-	-	-	-	-	-
2015	5	-	-	5	5		-	5	4	-	-	4
2016	2		1	3	3	1	1	4	3	1	1	5
2017		-	-	-	-	-	-	-	-	-	-	-
2018	1	1	2	4	1	3	1	5	2		2	4
2019	4	1	2	7	6	3	2	11	4	6	2	12
<b>Σ</b>	55	16	9	80	47	22	8	77	50	18	9	77

5766

5767 **6 DISCUSSION**

---

5768

5769

5770 

## 6.1 Introduction

5771 Changes in climate, land-cover, and land-use intensification have contributed to  
5772 land degradation and desertification in tropical forest ecosystems (Allen et al.,  
5773 2010; Brink et al., 2014; Brown et al., 2002). Extreme climate events and human-  
5774 induced environmental changes such as deforestation can act synergistically (Le  
5775 Houérou, 1996). In tropical dryland ecosystems, deforested and degraded areas  
5776 can affect regional climate, and the regional climate, in turn, can amplify  
5777 deforestation and forest degradation (Chagnon et al., 2004; Huang et al., 2017).  
5778 Climate change and anthropogenic processes appear to amplify fire occurrence  
5779 and spreading, and land degradation in dryland tropical forest ecosystems (Fox et  
5780 al., 2017).

5781 As a consequence forests, plant species, and biomass have experienced changes in  
5782 their species range, abundances, and shifts in their seasonality, resulting in an  
5783 impacts on biodiversity and forest ecosystem services (Desanker et al., 2001).  
5784 Severe dry forest biome shifts and land degradation as a result of climate change  
5785 are predicted to be most severe in Southern Africa (IPCC, 2014; King, 2014).  
5786 Already deforestation in Southern African countries is high, with about 1.4 million  
5787 ha net forest loss annually (Darkoh, 2009; Lesolle, 2012). In Southern Africa, a  
5788 range of policy options have been advocated to reduce the continuing loss and  
5789 degradation of dryland forests, including expansion of protected area networks,  
5790 improving governance and better management of dryland forests (Cumming,  
5791 2008; Hanks, 2003; KAZA, 2014). However, high-quality, long-term, and reliable  
5792 information on dryland forests and ecosystems over large areas are needed to  
5793 estimate and manage the impacts of forest changes on biodiversity, biomass  
5794 carbon stocks and dryland ecosystem functions accurately.

5795 There are significant advantages to forest analysis, such as remote sensing to  
5796 better improve estimates of forest changes and biomass, characterise forest  
5797 structures, and to understand the dynamics of tropical dryland forests in the  
5798 context of climate changes (Andela et al., 2013; Donoghue, 2002; Lu, 2006).

5799 However, such approaches that integrate forest studies and remote sensing need  
5800 to be replicated and tested across different regions, geographic scales, and over  
5801 relevant time periods to change (decades) (Lehmann et al., 2015; Mitchard et al.,  
5802 2013). Existing literature shows limitations in terms of methodological  
5803 inconsistency and generalisation, and constraints on the spatial and temporal  
5804 scales of investigation which limits the actual effectiveness of integrating remote  
5805 sensing into the tropical dryland forest assessment (Foody et al., 2001; Woodcock  
5806 et al., 2001).

5807 Given these challenges, this thesis set out to overcome such limitations to  
5808 contribute to the ability to characterise above ground biomass, forest structural  
5809 parameters, land cover change, and disturbances in the context of climate change  
5810 in the dryland forests of the Kavango Zambezi Transfrontier Conservation Area  
5811 (KAZA TFCA) of Southern Africa. KAZA is a conservation area with over thirty-six  
5812 protected areas including national parks, game reserves, community conservancies  
5813 and game management areas. It established to merge fragmented wildlife habitats  
5814 into an interconnected mosaic of protected areas and transboundary wildlife  
5815 corridors, to enhance the free movement of animals across international  
5816 boundaries and to create economic development in the region (Cumming, 2008;  
5817 Stoldt et al., 2020). However, the region is experiencing large-scale shifts in  
5818 vegetation cover, biomass degradation and increased vulnerability to climate  
5819 change, manifesting through altered disturbance regimes which hold significant  
5820 implications for forest biodiversity and ecosystem function of this region. By  
5821 addressing the above limitations, the thesis explored the use of novel application of  
5822 improved satellite remote sensing approaches and datasets including optical and  
5823 SAR, and their combination, that can in principle improve estimates of forest  
5824 biomass and structural parameters, disturbances, and climatic impacts at a  
5825 regional scale.

5826 The research presented here was structured around three research priorities  
5827 identified in a systematic review (chapter 2, David et al., 2022a). Specifically, the  
5828 review identified a need to address (i) the feasibility of combining SAR, optical  
5829 remote sensing data and ground measurements to estimate the forest stand  
5830 parameters, (ii) vegetation dynamics, and spatially detailed patterns of change  
5831 using different remote sensing proxies, (iii) characterisation of spatiotemporal

5832 changes in climate and fire using different climatic and vegetation time series data  
5833 at regional scale. By combining improvements across each of the three research  
5834 priorities, this thesis aims to combine ground measurements and multiple remote  
5835 sensing including climate, fire, and vegetation data to enable estimates of forest  
5836 biomass, and changes in dryland forests, across different spatial and temporal  
5837 scales.

## 5838 6.2 Suitability of remote sensing data

### 5839 6.2.1 Combining sensors

5840 Remote sensing techniques can be applied to detect changes, estimate forest  
5841 structural parameters including biomass, and to monitor the extent in tropical  
5842 dryland forest cover at different spatial scales, from individual trees, large blocks  
5843 of the unbroken canopy, to regional and pantropical or even global extents (Baccini  
5844 et al., 2004). However, there are large discrepancies in the methodologies used to  
5845 quantify forest structural changes in tropical dryland forests, including attempts to  
5846 relate forest cover and biomass to optical remote sensing measurements (Mitchell  
5847 et al., 2017; Sexton et al., 2016). In the research presented in this thesis, the use of  
5848 the medium to coarse resolution optical data, such as NASA's MODIS sensor,  
5849 demonstrate an approach to monitoring forest cover change and degradation due  
5850 to clear-cutting, fire, and drought (chapter 4 & 5), but also showed that certain  
5851 types of change remain difficult to detect. The quantitative assessment of the  
5852 ability of sensors with different spatial resolutions, and the integration of multiple  
5853 datasets from optical and SAR sensors, to improve estimates of forest biomass and  
5854 structures in the dryland ecosystems are limited and have not been carried out in  
5855 Southern Africa (Chapter 2, David et al., 2022a). Consequently, there is an  
5856 opportunity to exploit the benefits of different remote sensing in this context,  
5857 alongside a need to consider the trade-offs between spectral and spatial resolution,  
5858 and geographic coverage, when estimating biomass and forest structural  
5859 parameters in dryland forests ecosystems (chapter 2, David et al., 2022a).

5860 This thesis combined freely available Sentinel 1 (S1) SAR, Sentinel 2 (S2) and  
5861 Landsat 8 (LC8) multispectral imagery to estimate biomass at regional level and  
5862 the relatively fine resolution of S2 (10 m pixels) which reduced the mixed pixel

5863 problem observed in medium spatial resolution data (30 m pixels; e.g. LC8), and  
5864 led to an increase in the precision of biomass estimation compared to using single  
5865 sensors alone (Chapter 3, David et al., 2022b). In this research, AGB is more  
5866 accurately estimated when adding Sentinel 1 SAR and Sentinel 2 to a Random  
5867 Forest algorithm (instead of using multispectral or SAR on its own). For example,  
5868 this research found that SAR data was better at detecting aggregations of  
5869 individual trees in the dryland landscape than optical data. But this research also  
5870 found that SAR data alone overestimated AGB in the dryland area (Fig 3.7, Chapter  
5871 3, David et al., 2022b). A similar problem of SAR overestimating AGB was noted by  
5872 other studies such as Zhang et al. (2019), and this problem was overcome by fusing  
5873 SAR and multispectral data in this thesis (Fig 3.7, Chapter 3, David et al., 2022b).  
5874 The comparison of recently published pan-tropical AGB datasets (Avitabile et al.,  
5875 2016; Baccini et al., 2017; Bouvet et al., 2018) with the regional scale maps  
5876 produced in this thesis, using a combination of optical and SAR datasets with DBH  
5877 and tree height measurement of more than 4300 tree ground-validation, resolves  
5878 realistic spatial patterns in estimated biomass for the study area (Fig. 3.5, chapter  
5879 3, David et al., 2022b). Here, S1 SAR and S2 data were combined to show in fine  
5880 detail AGB ranges, including a mix of very low biomass (due to different degrees of  
5881 degradation) to intermediate biomass for certain areas with very large but  
5882 scattered trees, through to higher biomass areas in high-density forests (Fig.3.7,  
5883 chapter 3, David et al., 2022b).

5884 Partly, this study has improved biomass estimation by investigating the  
5885 capabilities and correlation of AGB with diverse spectral bands from Sentinel 2,  
5886 Landsat 8, and radar backscatter polarisation from Sentinel 1 SAR data. For optical  
5887 data, although NDVI and EVI remain two of the most widely used vegetation  
5888 indices, they were outperformed by the red edge index (NDRE1) and the green  
5889 channel index (GNDVI) in estimating AGB for dryland forests (Table 3.3, Chapter 3,  
5890 David et al., 2022b). NDVI is utilised in biomass mapping by different studies such  
5891 as (Cunliffe et al., 2020; Gizachew et al., 2020), however this study detected  
5892 saturation in NDVI when the spectral values remain insensitive to increases in  
5893 forest AGB value beyond 80 Mg/ha (Fig. 3.7, Chapter 3, David et al., 2022b).  
5894 Gitelson et al., 1996 found the green channel index to be much more sensitive to  
5895 the Chlorophyll concentration and enabled precise estimation of pigment

5896 concentration than the original "red" NDVI. The red edge-based indices were found  
5897 to have a better correlation with the photosynthetic activity of the tree canopy and  
5898 leaf cell structure reflection (Cho et al., 2008; Mutanga and Skidmore, 2004).

5899 There has been concern that structural variation and understory herbaceous cover  
5900 reduce measurement precision when mapping from remotely sensed estimates in  
5901 semi-arid savanna and dryland forests (Baccini et al., 2004; Santos et al., 2002).  
5902 Combining information from optical sensors that describe photosynthetic activity  
5903 (e.g., through various vegetation indices) with SAR-derived information on forest  
5904 structure and biomass in winter months, brings the benefits of higher spectral  
5905 resolution, and compensates for the shortcomings of using single data products  
5906 alone that are commonly subject to saturation, temporal gaps, and clouds cover  
5907 (chapter 3, David et al., 2022b). Comparing the performance of ML and RF  
5908 regression algorithm and considering the collinearity between predictor variables  
5909 also improved biomass mapping and reduced uncertainty in the models. ML  
5910 regression overestimated low values, and underestimated high biomass values,  
5911 which is also common in previous studies using ML (Fuchs et al., 2009; Zheng et al.,  
5912 2007). RF had a positive impact on the biomass estimation accuracy, and  
5913 performed better than ML regression, reducing the RMSE for the estimation  
5914 models by almost 50%. Therefore, it is important to assess the ability of combining  
5915 improved methods and freely available optical and SAR data with sample plot  
5916 survey data/forest inventory to characterise large-area biomass distributions to  
5917 provide regional estimates of forest carbon stocks. Although this study has  
5918 improved AGB estimation in dryland forests, there is room for improvement, for  
5919 example RF regression model estimated medium and high-density forests with  
5920 good accuracy but showed variation in low-density forests that include  
5921 understoreys and low herbaceous cover such as grassland often with relatively low  
5922 canopy density. This study did not consider multitemporal seasonal time series  
5923 data and texture information from images in AGB modelling which provides  
5924 additional information on seasonal variations and reduce the impacts of  
5925 heterogeneity as suggested by studies in temperate and evergreen broad leaf  
5926 forests (Sarker and Nichol, 2011; Zhu and Liu, 2015). Incorporation seasonal time  
5927 series and textural information in AGB modelling in dryland forests could improve  
5928 biomass modelling and is a topic for future research. Despite these limitations, this

5929 study aimed to improve the performance of the regional forest biomass model and  
5930 can provide a reference and support for future plans of relevant forestry  
5931 departments.

## 5932 6.2.2 Spatial scale

5933 In sensor integration, issues of scale are critical for biomass and habitat mapping,  
5934 where the adequacy of spatial resolution to the problem in hand is key. Pan-  
5935 tropical and global maps derived from satellite imagery can show large uncertainty  
5936 in the extent and distribution of tropical dryland forest recorded, and typically  
5937 underestimate the extent of forest cover and biomass in dryland areas (Bastin et  
5938 al., 2017). This is illustrated by the substantial spatial disagreements between  
5939 recent satellite-based global (Giri et al., 2005) and pantropical forest maps  
5940 (Mitchard et al. (2013), and is further hindered by the relative scarcity of large-  
5941 scale studies assessing forest cover in dryland biomes (Chapter 2; David et al.,  
5942 2022a). The distribution of AGB and precision varied between this study and  
5943 pantropical maps (Fig. 3.9, Chapter 3 David et al., 2022b). The observed  
5944 discrepancies may have arisen due to satellite data characteristics (such as spatial  
5945 resolution), unavailability of cloud-free images, availability of ground-truth  
5946 information, and forest definitions (such as tree cover thresholds) used in the  
5947 analyses (De Sy et al., 2012). In the research presented in this thesis, comparing  
5948 three recent pan-tropical forest maps to estimate above ground biomass (AGB)  
5949 revealed important differences: 0-30 Mg/ha using the pan-tropical AGB map (1 km  
5950 resolution), 0-50 Mg/ha using Landsat (30 m), 0-70 Mg/ha using ALOS PALSAR  
5951 (25 m); and 0-145 Mg/ha from this study using combined optical and SAR (10 m)  
5952 (Fig. 3.8, Chapter 3, David et al., 2022b). This research has a high mean estimate of  
5953 biomass of 51 mg/ha in comparison to Bouvet et al. (2018) using radar data, that  
5954 estimated mean biomass of 26.7 Mg/ha which is 50 % less compared to this study  
5955 mean biomass (Fig. 3.9, Chapter 3, David et al., 2022b). Avitabile et al. (2016) only  
5956 estimated the mean biomass of 5.92 Mg/ha for the study area and predicted AGB  
5957 values in the 0 to 30 Mg/ha range.

5958 In this research, biomass mapping at a regional scale using SAR backscatter in  
5959 conjunction with the strategically positioned optical bands (red edge wavebands)  
5960 improved estimation at high AGB values and allowing the identification of small-



5961 scale degradation patterns of biomass such as roads compared to either sensor  
5962 alone (Fig. 3.11, chapter 3, David et al., 2022b). In addition, the AGB model from  
5963 this study showed that biomass for dryland forests exceeds estimates derived from  
5964 pan-tropical products which underestimate biomass and forests in dryland  
5965 ecosystems of less-studied areas such as the KAZA region, which are often  
5966 neglected in this type of analysis (Chapter2; David et al., 2022).

5967 However, the advent of free Landsat data combined with improving computational  
5968 and data storage capabilities mean that large area Landsat land cover products are  
5969 increasingly being generated. In this study, a large volume of Landsat data using  
5970 high quality training data derived from the field survey was demonstrated using  
5971 Google Earth Engine and Random Forest classifier (Fig. 4.13-4.14, Chapter 4). A 30  
5972 m Landsat land cover map was generated and was able to detect large scale  
5973 deforestation and changes with an acceptable classification accuracy >80%  
5974 (Chapter 4). This study used medium spatial resolution Landsat data because land  
5975 cover maps based on coarse spatial resolution imagery (nominally at 500 or 250  
5976 m) limits the ability for detecting changes and provide a highly generalised  
5977 representation of land cover and ultimately land cover change, over large areas  
5978 (Hamunyela et al., 2020; Zhu and Woodcock, 2014). Using a two point in time  
5979 classification is useful to detect changes in land cover, however such bi-temporal  
5980 change detection approach can have some limitation of potentially masking  
5981 considerable within-year vegetation dynamic and variations (Chapter 2; David et  
5982 al., 2022a). For example, this type of change estimates risks interpreting natural  
5983 phenological change as actual changes in the land cover (DeVries et al., 2015).  
5984 Therefore, this study has moved from a relatively static, bi-temporal view of  
5985 change toward a more continuous mapping of vegetation dynamics to improve the  
5986 detection of disturbance's spatiotemporal patterns using change detection  
5987 algorithms of BFAST and BEAST (Chapter 4). These change detections algorithms  
5988 were useful in assessing small scale deforestation, degradation, and regrowth by  
5989 capturing vegetation changes during the year and over longer time-periods at the  
5990 regional scales (Chapter 3, David et al., 2022b). Such large area analyses on change  
5991 detection conducted in this research can be used to adjust and update global land  
5992 cover and biomass estimates. The pan-tropical and global maps are limited in their  
5993 spatial resolution and temporal coverage, and most of them provide inadequate

5994 information for policymaker regarding restoration intervention efforts that are  
5995 needed for regional- or local-scale restoration projects (Abbas et al., 2020). At  
5996 regional-to-national scales, the adoption and application of satellite technology is  
5997 highly variable across countries in the tropics. For example, many countries across  
5998 Southern African are faced with scarcities of technology, finances, and computer  
5999 time limitations, preventing the use of conventional downloaded high-resolution  
6000 satellite data (chapter 2, David et al., 2022a). To overcome these limitations, the  
6001 thesis utilised the recent developments in cloud computing platforms, such as  
6002 Google Earth Engine (GEE), which have greatly increased access to pre-processed  
6003 optical, SAR, and climatic datasets, enabling a comprehensive analysis of multiple  
6004 threats including deforestation, and degradation from fire and climatic impacts on  
6005 vegetation at regional scale (chapter 3, 4 & 5).

### 6006 6.2.3 Temporal scale

6007 To characterise vegetation and climate interactions, changes in forest cover must  
6008 be quantified over different temporal scales, to capture both short term and  
6009 gradual changes experienced by dryland ecosystems (chapter 2, David et al.,  
6010 2022a). The study has shown that the impact of degradation varies from fine-scale  
6011 structural changes in canopy, to broad-scale rapid loss of biomass (chapter 3 David  
6012 et al., 2022b). Several methods and techniques are proposed in the literature to  
6013 address land cover characterisation and forest cover change. Mapping changes  
6014 through comparing images at two different times, based on discrete classification,  
6015 are one of the most common forms of remote sensing change detection utilised  
6016 (Jensen, 1996). This is despite change detection between two dates (pre-and post-  
6017 disturbance imagery) is generally limited to the detection of broad-scale changes  
6018 (chapter 2, David et al., 2022a).

6019 Change detection is more powerful, however, when the signal is analysed over a  
6020 long time period (decadal, or longer) in a continuous and consistent manner,  
6021 providing an improved signal-to-noise ratio, detection of subtle/transient changes  
6022 in forest cover or phenology and condition (Huang et al., 2009; Verbesselt et al.,  
6023 2012). Here, the ability to make precise estimates of change in dryland forest  
6024 distribution was improved by combining a long high frequency time-series of  
6025 MODIS data with pixel-based break detection (chapter 4). The abrupt changes (e.g.,

6026 deforestation), gradual change (e.g., forest degradation), and other slow processes  
6027 (e.g., seasonal changes) in response to wildfire, disease, and climate variability  
6028 were each detected effectively (chapter 4). In the research presented in this thesis,  
6029 the fire estimates in the KAZA region reveal that between 2002 and 2019, about  
6030 390,678 km<sup>2</sup> (75%) of the landmass is classified as fire-affected for at least one  
6031 time in the monitored period, leaving 127,989 km<sup>2</sup> (25%) of the area not affected  
6032 by fire. This showed that national parks are more affected by high fire occurrence  
6033 than other protected areas (chapter 5). As shown in this thesis, the failure of  
6034 vegetation to recover and browning intensification following drought years  
6035 reaffirm the consistent multiple threats from severe drought, soil moisture deficit,  
6036 and high fire reoccurrence on dryland vegetation responses (chapter 4 & 5).  
6037 Consequently, this combined approach to change assessment using long term  
6038 monitoring (> decadal), as used here, allows spatiotemporal aridity information to  
6039 be extracted, thereby enabling quantification of vegetation shifts and increased  
6040 risks of land degradation and drying risk that cumulatively occur over many years  
6041 in the dryland forest ecosystems (chapter 4 & 5). In addition to visual detection  
6042 validation of historic change using high resolution data proposed by Cohen et al.  
6043 (2010), this study demonstrated that the change estimates and precision from  
6044 BFAST can be validated and improve using a stratum-based estimate of variance  
6045 that will be more precise than using simple random sampling (Stehman and  
6046 Czaplewski, 1998; Stehman, 2009; Potapov *et al.*, 2014). As shown in this study  
6047 (Chapter 4), the large-scale changes such as clear felling of woodland for  
6048 agriculture are comparable while more subtle changes such as land degradation  
6049 were detected by BFAST better than interval-based per-pixel classification. Since  
6050 this study used a rather small sample size (341 points), the change estimates need  
6051 to be tested with training data of a larger sample size to be conclusive. In addition,  
6052 the research conducted here can be improved with recently developed new  
6053 algorithm such as Continuous Change Detection and Classification (CCDC) that  
6054 make better use of the temporal domain of Landsat data to improve both  
6055 continuous change detection and land cover classification at medium spatial  
6056 resolution and high temporal frequency (Zhu and Woodcock, 2014) . CCDC use all  
6057 available Landsat clear observation data to classify land cover from multiple time  
6058 period. In addition to land cover classification from any time period in history, it  
6059 can monitor large scale deforestation and small-scale changes such as degradation

6060 in near real time as the algorithms updates the time series model every time new  
6061 observations are available (Arévalo et al., 2020).

#### 6062 6.2.4 Ecological relevance of mapping changes

6063 There are two parts to the problem that this research has addressed; one was to  
6064 show changes within the forest ecosystems (deforestation and degradation) and  
6065 the other was to characterise forest structural parameters and to estimate biomass  
6066 distribution in the forest. In both situations, methodologically consistent  
6067 approaches were identified as one of the important needs to improve upon current  
6068 monitoring of dryland forests (Mitchell et al., 2017); (chapter 2, David et al.,  
6069 2022a). At the regional scale, monitoring poses a number of methodological  
6070 challenges including the lack of quantitative, spatially explicit, and statistically  
6071 representative methods, which have previously resulted in simplistic  
6072 representations (Coppin et al., 2004). Therefore, as shown in this thesis, testing  
6073 different models and their suitability to characterise trends and phenological  
6074 patterns can reveal suitable algorithms for estimating dryland forest covers  
6075 (chapter 4). Furthermore, Foody et al. (2003) and Woodcock et al. (2001) have  
6076 pointed out concerns of generalising or transferring methods derived from  
6077 remotely sensed imagery over both space and time, based on lessons learned in far  
6078 better-studied ecosystems. Generalisation also limits the interpretation of change  
6079 patterns and the impacts that these changes will have on the biodiversity of  
6080 forests, conservation of wildlife habitats conservation, and dryland ecological  
6081 function (chapter 2, David et al., 2022a).

6082 Whilst models based on remote sensing data can show promising results in  
6083 different ecosystems (e.g., rain forests), it can fail to detect non-linear vegetation  
6084 patterns (e.g., degraded areas) in largely climate and fire-driven ecosystems, such  
6085 as drylands, as shown here (chapter 4). This observation justifies the importance  
6086 of testing and utilising a range of sensors and vegetation indices for forest  
6087 structure parameter and change detection estimation. The results in this thesis,  
6088 reveals that spectral indices based on the red edge spectral region and green  
6089 normalised vegetation index (GNDVI) have a stronger relationship skill in  
6090 describing dryland forests than conventional NDVI (chapter 3 & 4). Consequently,  
6091 there is good reason to believe that NDVI is not an ideal indicator of stress

6092 response in dryland forests despite the widespread use of this index in studies of  
6093 forest health decline. In the research presented in this thesis, indices based on fire,  
6094 such as the fire frequency index, and several climatological indices, such as SPEI  
6095 and the aridity index, were tested in dryland forest cover to assess vegetation  
6096 response to environmental change over large areas (chapter 5). This was  
6097 undertaken because testing different algorithm and sensor combinations can help  
6098 detect specific strengths and limitations for a dryland ecosystem, particularly  
6099 where climate change and variability negatively affecting dryland vegetation and  
6100 biomass (chapter 3, 4 & 5).

6101 Oliveira et al. (2021), working in Brazil, modelled biomass in tropical dryland  
6102 forests using linear regression, and recommended testing the ability of non-  
6103 parametric machine learning algorithms over linear regression analysis in dryland  
6104 forests. Some image classification algorithms and traditional statistical approaches  
6105 make unrealistic assumptions about the distributional properties of forests, and  
6106 are unable to describe underlying fluctuating trends as these models assume  
6107 vegetation trends to be quasi-linear (i.e., regular, or stable seasonality) (Grogan et  
6108 al., 2016). In this research, multivariate machine learning models, integrated with  
6109 stepwise-regression methods, enabled better adjustment and fit to ground  
6110 measurement, which was tested against more than 4300 individual trees (Chapter  
6111 3, David et al., 2022b). This approach enabled both the interpretation and  
6112 validation of remotely sensed forest structure and biomass estimates, providing a  
6113 very high  $R^2$  of 0.95 and a low RMSE error of 0.25 Mg/ha (Chapter 3, David et al.,  
6114 2022b).

6115 Despite prior concerns raised over the need to use ground truth verification for  
6116 estimating biomass and changes in forest mapping (Grainger, 2008), there are few  
6117 vegetation-related studies that link vegetation estimates to field measurements  
6118 and forest inventory data (Chapter 2, David et al., 2022a). As shown in this thesis,  
6119 obtaining field data for validation of remote sensing data in dryland ecosystems of  
6120 protected areas, such as National parks, can be challenging because many areas are  
6121 very remote and often dangerous to visit due to hazardous, and if present and in  
6122 some cases unexploded landmines (chapter 3, David et al., 2022b). Consequently,  
6123 most detected changes in the spectral signature that occur due to an increase in  
6124 woody biomass, deforestation and forest degradation in the dryland ecosystems of

6125 Southern Africa have not been validated (chapter 2, David et al., 2022a). The  
6126 optical sensors at 250 m-1 km resolution (e.g., MODIS) used here make consistent  
6127 and frequent measurements over large areas building a long time series, which  
6128 helps identify locations of active forest change ('hotspots') with good precision and  
6129 that was validated against ground-truth data (chapter 4). However, where  
6130 possible, important areas of change and in particular for key forest structural  
6131 parameters, such as AGB that are needed for baseline carbon stock maps, there are  
6132 benefits to further ground measurement for validation and finer spatial resolution  
6133 data. Maps of AGB, if sufficiently detailed, can assist conservation managers,  
6134 practitioners, and policymakers to formulate specific interventions (e.g., corridor  
6135 planning, tree thinning, fire control, biodiversity surveys) that are appropriate to  
6136 support the conservation of forest habitats and their management.

### 6137 6.3 Recommendation for policy and practice

6138 Dryland forests in protected areas such as KAZA face an increasing number of  
6139 threats ranging from those originating from climate change and competing  
6140 economic pressures, especially when they span international borders. Learning  
6141 from this research and past experience on dryland forests in KAZA (Cumming,  
6142 2008; WWF, 2016), there are often conflicting views related to the amount of  
6143 biomass and changes in forest cover in dryland ecosystems. These differences are  
6144 however not confined to science only, but also between the understanding of  
6145 dryland monitoring programmes and policies (Appendix A: N8 AgriFood policy  
6146 brief). These challenges present also an opportunity for a mutual benefit; with  
6147 more freely accessible data, such as that explored in this thesis, scientists and  
6148 policy makers may now refine their focus to share knowledge on the management  
6149 of forestry, and the interface with land uses, including wildlife management and  
6150 ecosystem function (Sexton et al., 2016). Based on the findings of this research,  
6151 along with the challenges and lessons learnt throughout, there are three  
6152 recommendations that can be made for policy and practice, which can  
6153 subsequently be used in decision making of the KAZA region, and beyond, in  
6154 Southern Africa more widely.

6155 First, a large part of the knowledge base for dryland forest landscapes in Southern  
6156 Africa is derived from research generated outside of Africa (chapter 2, David et al.,  
6157 2022a), and so there is an opportunity to change academic narratives by working  
6158 in partnership with local organisations to foreground local research and  
6159 knowledge. Given the growing technical capacity for monitoring, reporting and  
6160 verification, there is a need to shift the focus to producing and sharing transparent  
6161 research maps with resource managers. Technology platforms such as the cloud-  
6162 based image-analysis pipeline using freely available remote sensing imagery, as  
6163 used here, is an opportunity to overcome the limitations previously enforced by  
6164 data scarcity, volumes and costs, and can enhance substantially the collective  
6165 knowledge of dryland forest environments (chapter 3, 4 &5). Sharing of research  
6166 outputs and often captivating satellite imagery with the news media to inform  
6167 citizens and to create awareness about the extent and location of deforestation  
6168 hotspots is a potentially important component of the KAZA monitoring  
6169 programme. If such information can influence local practitioners and public  
6170 opinion, it can exert pressure on policymakers in democratic societies to  
6171 strengthen enforcement and to tighten regulations around forest management and  
6172 protection. Improved monitoring of forest cover itself is unlikely to produce any  
6173 change in behaviour unless it is linked to research, forest management and  
6174 practice, and all key stakeholders in these regions (Olsson et al., 2019).

6175 Second, the process of monitoring dryland forests could be enhanced through the  
6176 greater involvement of stakeholders in the modelling process itself. Building on the  
6177 existing regional networks in the KAZA region, workshops could be facilitated  
6178 between academic scientists, decision makers and practitioners to identify current  
6179 gaps in knowledge, data requirements and training needs. Most studies in KAZA  
6180 region on drought, fire and vegetation analyses are done at local level (e.g., within  
6181 a single community) and others cover only a part of the KAZA region (Mpakairi et  
6182 al., 2019; Pricope et al., 2012), making it impossible to compare to a regional  
6183 perspective. Similar research studies on tropical dryland forest change analyses at  
6184 large(r) scales (chapter 3, 4 & 5) are needed, ideally retaining fine spatial  
6185 resolutions and a longer temporal duration. A significant proportion of studies in  
6186 Southern Africa have been undertaken in Kruger National Park, leaving many other  
6187 national parks and protected areas in KAZA relatively understudied. Furthermore,

6188 future efforts to estimate changes in important variables such as forest cover and  
6189 biomass, need not be restricted by country boundaries but can extend across the  
6190 less well studied private and international protected areas (chapter 2, David et al.,  
6191 2022a). Such workshops would allow stakeholders and other users to have an  
6192 opportunity to present their work, examine the research outputs in their area of  
6193 interest with reference to existing or predicted scenarios of future change.  
6194 Consequently, such structures can harness a wealth of existing research and  
6195 expertise and help to provide a support network to stimulate high quality  
6196 published outputs from scientists, and to facilitate input from local experts and  
6197 practitioners (Appendix A: N8 AgriFood policy brief).

6198 Lastly, the KAZA region concept recognises that borders are political rather than  
6199 ecological and aims to ensure that key ecological processes continue to function  
6200 where borders have previously divided ecosystems and/or wildlife migration  
6201 corridors. Based on my own engagement with stakeholders such as WWF Namibia  
6202 and the KAZA secretariat, Botswana, there is a willingness to work together and  
6203 support research, across KAZA region to ensure such information will continue to  
6204 support future conservation efforts and economic development in countries such  
6205 as Angola, Botswana, Namibia, Zambia, and Zimbabwe. Such interdisciplinary  
6206 knowledge and evidence-based policy, generated through partnership and data  
6207 sharing, is urgently needed. In this region, climate change will cause large-scale  
6208 shifts in vegetation cover and biomass degradation resulting in increases in the  
6209 vulnerability of ecosystems across large areas of dryland forest in Southern Africa,  
6210 which represents risks faced by all stakeholders.

## 6211 6.4 Future work

6212 The work presented in this thesis offers a platform to improve the understanding  
6213 of biomass, disturbance patterns, and climate change relationships in dryland  
6214 forest ecosystems. The thesis considered the factors that cause changes in forest,  
6215 biodiversity, and ecological function. Numerous spectral indices have been  
6216 developed to assess vegetation cover and growth dynamics, which provide useful  
6217 insights for applications in forestry, biodiversity conservation, agriculture, and  
6218 other related fields. However, most of these indices are derived from a limited



6219 selection of species and are typically developed in often quite different regions and  
6220 ecosystems. The research presented in this thesis tested optimum spectral indices  
6221 from multispectral data in dryland forests that improve the ability to effectively  
6222 estimate forest stand characteristics (chapter 3, David et al., 2022b), identify shifts  
6223 in vegetation dynamics and the timing of key phenological events (chapter 4), and  
6224 helps us to assess forest health and vulnerability to different stressors, including  
6225 fire and climate change (chapter 5).

6226 One potential future avenue for research is different sensors. For example,  
6227 airborne imaging spectroscopy can provide up to 2000 contiguous narrow-band  
6228 spectral information across the solar spectrum, often at fine spatial resolution  
6229 (Morley et al., 2020). Asner et al. (2016) used airborne imaging spectroscopy and  
6230 satellite data trained on spectroscopy data to estimate water lost from California's  
6231 forest ecosystems over the drought years between 2011 and 2015. To detect a  
6232 decline in forest cover and shifts in the timing of phenological events requires  
6233 spectral indices that are sufficiently sensitive to chlorophyll content, and in  
6234 particular to capture the response of trees to a stress event. Therefore, further  
6235 research could explore the potential to relate dryland forest cover to hyperspectral  
6236 data, to identify more sensitive spectral bands corresponding to different  
6237 vegetation species, and to identify the most important wavelength regions for  
6238 predicting drought and fire-sensitive species.

6239 Optical sensors have recently been presented as a viable alternative for estimating  
6240 biomass and carbon stock in tropical forests, due to their global coverage,  
6241 frequency of capture, and cost-effectiveness (Kumar et al., 2015). Furthering the  
6242 research presented in this thesis, the primary challenge of MODIS data, despite its  
6243 high temporal resolution, is the large spatial resolution of between 250 m and 500  
6244 m. The temporal resolution of Landsat (16-days, and now 8 days with the recent  
6245 launch of Landsat 9), which is often occluded by cloud cover can be a major  
6246 obstacle, despite the relatively fine spatial resolution of 30 m. The integration of  
6247 MODIS with Landsat to combine fine spatial and temporal resolutions could  
6248 therefore be used in future to improve the mapping of forests patterns of changes  
6249 and disturbances.

6250 On the other hand, there is a need to incorporate satellite imagery with a fine  
6251 spatial resolution information for estimating biomass and carbon stock. For  
6252 example, the thesis has shown that Sentinel-2 data show a better ability to improve  
6253 the estimation of above ground biomass and forest structure in tropical dryland  
6254 forests as compared to Landsat-8 (Chapter 3, David et al., 2022b). Despite  
6255 improvements in the spatial precision of optical data, such as Sentinel-2, improved  
6256 characterisation of forest structure may not be possible using multispectral  
6257 imagery alone due to the spectral similarities between structural classes.  
6258 Furthering the research presented in this thesis by improving the characterisation  
6259 of forest structure using a fusion of data such as that from airborne light detection  
6260 and ranging (LiDAR), collected from airborne platforms, SAR, and/or other forms  
6261 of optical data, could further advance the understanding of the detailed structural  
6262 information and accurate vertical distribution of canopy in tropical dryland forests.  
6263 Li et al. (2017) highlighted that metrics derived from a LiDAR point cloud led to  
6264 improved biomass estimates at nearly all resolutions in comparison to raster-  
6265 derived metrics in the drylands of the US. Despite these benefits, LiDAR data are  
6266 not widely available in many dryland ecosystems, particularly in developing  
6267 countries, and the acquisition of new data sets can be prohibitively expensive.  
6268 However, new satellites such as the Global Ecosystems Dynamics Investigation  
6269 (GEDI) LiDAR and the Multi-footprint Observation Lidar and Imager (MOLI)  
6270 promise space-borne imaging with laser altimetry, which can contribute to the  
6271 development biomass, forest distribution, and its relationship with climate in  
6272 tropical dryland forests (Coyle et al., 2015; Kimura et al., 2017). MOLI includes  
6273 LIDAR to measure canopy height, vegetation phenology, vegetation indices, and an  
6274 optical imager to measure the position of the canopy for improving biomass  
6275 estimation (Sakaizawa et al., 2018). GEDI estimates mean aboveground biomass  
6276 density at 1 km grid and provides metrics of tree height and canopy cover at a  
6277 footprint of 25 m (Dubayah et al., 2020), and can be used in fusion with other  
6278 existing radar data such as Sentinel-1, ALOS PALSAR, along with other optical data  
6279 sets such as from Landsat and Sentinel-2. The successful unification of forested  
6280 vegetation monitoring data with detailed information on three-dimensional (3-D)  
6281 structure would represent a significant improvement in the capacity of ecologists  
6282 and decision makers to estimate the impacts of forest cover change on

6283 biodiversity, wildlife habitat, and forest management approaches more widely, and  
6284 should be a core focus of future research.

6285

## 6286 6.5 Conclusion

6287 In this thesis, the close integration of field data, Sentinel-1 SAR, Landsat-8 and  
6288 Sentinel-2, regional climate and MODIS time-series data, has enabled a more  
6289 precise estimation of biomass and forest stand structural parameters, which has  
6290 enabled the quantification of changes in vegetation patterns. The long-term  
6291 changes and trends identified enabled the characterisation of various influences,  
6292 from climate, fire and animals to be assessed in terms of their impact on forest  
6293 biodiversity and dryland ecosystem function. The KAZA region has the highest  
6294 population of elephants in Africa, which have a destructive influence on forest  
6295 diversity and density, forest structure, and the wider landscape. The increasing  
6296 human population, occurrence of wildfires, and changing climate variability, set in  
6297 a wider context of limited levels of development, are aggravating forest and  
6298 vegetation decline. Such declines risk the loss of dryland tree species, wildlife, and  
6299 pose a significant threat to dryland biodiversity. Ongoing monitoring of changes  
6300 within dryland forest ecosystems integrating open-access Earth observation data  
6301 alongside improved methods of analysis is vital in the context of future climate  
6302 change, and the expected impacts of this on dryland forest areas. The key findings  
6303 of the research are therefore summarised as follow: The thesis has demonstrated  
6304 that using a combination of radar backscatter in conjunction with strategically  
6305 selected multispectral optical imagery at fine resolution (10 m pixels) significantly  
6306 improved above ground biomass and forest stand structural parameter  
6307 estimations, and reduced saturation effects in areas of high biomass, across large  
6308 areas with mixed forest stands compared to using single sensors alone. This part of  
6309 the thesis highlighted the importance of considering spatial scale when mapping  
6310 forest characteristics that are relevant to management of biodiversity and wildlife  
6311 in dryland forests, which can help improve the wider understanding of these  
6312 habitats. The study demonstrated that long-term monthly time-series analysis in  
6313 combination with change detection models (Breaks for Additive Seasonal and

6314 Trend (BFAST) and the Bayesian analysis (BEAST)) can identify abrupt and  
6315 gradual changes associated with fire, drought and seasonality driven by climate  
6316 changes and clear-cutting. Critically, the results emphasised the importance of  
6317 considering the sensitivity of the chosen vegetation indices, and the need to adopt  
6318 advanced change detection methods, such as BEAST algorithm, that can fully  
6319 characterise the complex non-linear dynamics of dryland forest ecosystems. This  
6320 research has demonstrated that an analysis of long-continuous time series data  
6321 describing drought, water stress and fire impacts across large spatial scales can  
6322 reveal regional trends in vegetation change, drying patterns, and the expansion of  
6323 drylands (arid and semi-arid). These findings highlighted the importance of a  
6324 precise and timely assessment of the intensity and geography of impacts of  
6325 droughts within and across conservation areas, both at present and into the future.  
6326 This approach therefore creates a valuable evidence base for understanding the  
6327 multiple and interacting impacts on forest biodiversity, wildlife and ecosystem  
6328 function at a regional-scale, which has hitherto not been possible, and which is  
6329 essential for more effective management of these critical ecosystems.

6330

## References

- Abbas, S., Wong, M.S., Wu, J., Shahzad, N. and Muhammad Irteza, S., 2020. Approaches of Satellite Remote Sensing for the Assessment of Above-Ground Biomass across Tropical Forests: Pan-tropical to National Scales. *Remote Sensing*, 12(20), p.3351.
- Adam, E., Mutanga, O., Abdel-Rahman, E.M. and Ismail, R., 2014. Estimating standing biomass in papyrus (*Cyperus papyrus* L.) swamp: exploratory of in situ hyperspectral indices and random forest regression. *International Journal of Remote Sensing*, 35(2), 693-714.
- Adelabu, S., Mutanga, O., Adam, E.E. and Cho, M.A., 2013. Exploiting machine learning algorithms for tree species classification in a semiarid woodland using RapidEye image. *Journal of Applied Remote Sensing*, 7(1), p.073480.
- Adjorlolo, C. and Mutanga, O., 2013. Integrating remote sensing and geostatistics to estimate woody vegetation in an African savanna. *Journal of Spatial Science*, 58(2), pp.305-322.
- Agbaje, G.I., 2010. Nigeria in space—an impetus for rapid mapping of the country for sustainable development planning. A report prepared for FIG Congress 2010 Facing the Challenges Building the Capacity Sydney, Australia. [https://www.fig.net/resources/proceedings/fig\\_proceedings/fig2010/papers/ts03h/ts03h\\_agbaje\\_4621.pdf/](https://www.fig.net/resources/proceedings/fig_proceedings/fig2010/papers/ts03h/ts03h_agbaje_4621.pdf/)(accessed 20 January 2021).
- Aggarwal, S., 2004. Principles of remote sensing. Satellite remote sensing and GIS applications in agricultural meteorology, 23(2), pp.23-28.
- Aguilar, M.A., Saldaña, M.M. and Aguilar, F.J., 2013. GeoEye-1 and WorldView-2 pan-sharpened imagery for object-based classification in urban environments. *International Journal of Remote Sensing*, 34(7), pp.2583-2606.
- Ahlström, A., Raupach, M. R., Schurgers, G., Smith, B., Arneth, A., Jung, M., Reichstein, M., Canadell, J.G., P. Friedlingstein, P., Jain, A.K., Kato, E., Poulter, B., Sitch, S., Stocker, B.D., Viovy, Y.P., Wang, A., Wiltshire, A., Zaehle, S., Zeng, N., 2015. The dominant role of semi-arid ecosystems in the trend and variability of the land CO<sub>2</sub> sink. *Science*, 348(6237), 895-899.
- Aide, T.M., Clark, M.L., Grau, H.R., López-Carr, D., Levy, M.A., Redo, D., Bonilla-Moheno, M., Riner, G., Andrade-Núñez, M.J. and Muñiz, M. (2013). Deforestation and Reforestation of Latin America and the Caribbean (2001–2010). *Biotropica*, 45(2), pp.262-271.
- Akinyemi, F.O. and Kgomo, M.O., 2019. Vegetation dynamics in African drylands: an assessment based on the Vegetation Degradation Index in an agro-pastoral region of Botswana. *Regional Environmental Change*, 19(7), pp.2027-2039.
- Alcañiz, I. and Gutierrez, R.A. (2020). Between the global commodity boom and subnational state capacities: payment for environmental services to fight deforestation in Argentina. *Global Environmental Politics*, 20(1), pp.38-59.
- Aleman, J.C., Jarzyna, M.A. and Staver, A.C. (2018). Forest extent and deforestation in tropical Africa since 1900. *Nature ecology & evolution*, 2(1), pp.26-33.
- Ali, I., Greifeneder, F., Stamenkovic, J., Neumann, M. and Notarnicola, C. (2015). Review of machine learning approaches for biomass and soil moisture retrievals from remote sensing data. *Remote Sensing*, 7(12), pp.16398-16421.

- Alleaume, S., Hely, C., Le Roux, J., Korontzi, S., Swap, R.J., Shugart, H.H. and Justice, C.O., 2005. Using MODIS to evaluate heterogeneity of biomass burning in southern African savannahs: a case study in Etosha. *International Journal of Remote Sensing*, 26(19), pp.4219-4237.
- Allen, C.D., Macalady, A.K., Chenchouni, H., Bachelet, D., McDowell, N., Vennetier, M., Kitzberger, T., Rigling, A., Breshears, D.D., Hogg, E.T. and Gonzalez, P., 2010. A global overview of drought and heat-induced tree mortality reveals emerging climate change risks for forests. *Forest ecology and management*, 259(4), pp.660-684.
- Alvarez-Añorve, M.Y., Quesada, M., Sánchez-Azofeifa, G.A., Avila-Cabadilla, L.D. and Gamon, J.A. (2012). Functional regeneration and spectral reflectance of trees during succession in a highly diverse tropical dry forest ecosystem. *American journal of botany*, 99(5), pp.816-826.
- Andela, N., Liu, Y.Y., Van Dijk, A.I.J.M., De Jeu, R.A.M. and McVicar, T.R., 2013. Global changes in dryland vegetation dynamics (1988–2008) assessed by satellite remote sensing: comparing a new passive microwave vegetation density record with reflective greenness data. *Biogeosciences*, 10(10), pp.6657-6676.
- Anderegg, W.R., Plavcová, L., Anderegg, L.D., Hacke, U.G., Berry, J.A. and Field, C.B., 2013. Drought's legacy: multiyear hydraulic deterioration underlies widespread aspen forest die-off and portends increased future risk. *Global change biology*, 19(4), pp.1188-1196.
- Andreae, M., Andreae, T.W., Annegarn, H., Beer, J., Cachier, H., Le Canut, P., Elbert, W., Maenhaut, W., Salma, I., Wienhold, F.G. and Zenker, T., 1998. Airborne studies of aerosol emissions from savanna fires in southern Africa: 2. Aerosol chemical composition. *Journal of Geophysical Research: Atmospheres*, 103(D24), pp.32119-32128.
- Anyamba, A. and Tucker, C.J., 2005. Analysis of Sahelian vegetation dynamics using NOAA-AVHRR NDVI data from 1981–2003. *Journal of arid environments*, 63(3), pp.596-614.
- Anyamba, A., Tucker, C.J. and Mahoney, R., 2002. From El Niño to La Niña: Vegetation response patterns over east and southern Africa during the 1997–2000 period. *Journal of climate*, 15(21), pp.3096-3103.
- Aragão, L.E.O., Malhi, Y., Roman-Cuesta, R.M., Saatchi, S., Anderson, L.O. and Shimabukuro, Y.E., 2007. Spatial patterns and fire response of recent Amazonian droughts. *Geophysical Research Letters*, 34(7).
- Archibald, S. and Scholes, R.J., 2007. Leaf green-up in a semi-arid African savanna-separating tree and grass responses to environmental cues. *Journal of Vegetation Science*, 18(4), pp.583-594.
- Archibald, S., Lehmann, C.E., Belcher, C.M., Bond, W.J., Bradstock, R.A., Daniau, A.L., Dexter, K.G., Forrestel, E.J., Greve, M., He, T. and Higgins, S.I., 2018. Biological and geophysical feedbacks with fire in the Earth system. *Environmental Research Letters*, 13(3), p.033003.
- Archibald, S., Roy, D.P., van Wilgen, B.W. and Scholes, R.J., 2009. What limits fire? An examination of drivers of burnt area in Southern Africa. *Global Change Biology*, 15(3), pp.613-630.
- Archibald, S., Scholes, R.J., Roy, D.P., Roberts, G. and Boschetti, L., 2010. Southern African fire regimes as revealed by remote sensing. *International Journal of Wildland Fire*, 19(7), pp.861-878.
- Arévalo, P., Olofsson, P. and Woodcock, C.E., 2020. Continuous monitoring of land change activities and post-disturbance dynamics from Landsat time series: A test methodology for REDD+ reporting. *Remote Sensing of Environment*, 238, p.111051.

- Arino, O., Leroy, M., Ranera, F., Gross, D., Bicheron, P., Nino, F., Brockman, C., Defourny, P., Vancutsem, C., Achard, F. and Durieux, L., 2007, April. Globcover-a global land cover service with MERIS. In *Proceedings of the ENVISAT Symposium* (pp. 23-27).
- Armston, J.D., Denham, R.J., Danaher, T.J., Scarth, P.F. and Moffiet, T.N., 2009. Prediction and validation of foliage projective cover from Landsat-5 TM and Landsat-7 ETM+ imagery. *Journal of Applied Remote Sensing*, 3(1), p.033540.
- Asanzi, P., Putzel, L., Gumbo, D. and Mupeta, M., 2014. Rural livelihoods and the Chinese timber trade in Zambia's Western Province. *International Forestry Review*, 16(4), pp.447-458.
- Asner, G. P., Hughes, R. F., Varga, T. A., Knapp, D. E., Kennedy-Bowdoin, T., 2009. Environmental and biotic controls over aboveground biomass throughout a tropical rain forest. *Ecosystems*, 12(2), 261-278.
- Asner, G.P., Brodrick, P.G., Anderson, C.B., Vaughn, N., Knapp, D.E. and Martin, R.E., 2016. Progressive forest canopy water loss during the 2012–2015 California drought. *Proceedings of the National Academy of Sciences*, 113(2), pp.E249-E255.
- Asner, G.P., Hughes, R.F., Varga, T.A., Knapp, D.E. and Kennedy-Bowdoin, T., 2009. Environmental and biotic controls over aboveground biomass throughout a tropical rain forest. *Ecosystems*, 12(2), pp.261-278.
- Assessment & Ecosystems Protection) Regulations, 2007. <http://www.fao.org/faolex/results/details/en/c/LEX-FAOC181644/> (accessed 21 July 2019).
- Avitabile, V., Herold, M., Heuvelink, G.B.M., Lewis, S.L., Phillips, O.L., Asner, G.P., Armston, J., Ashton, P.S., Banin, L., Bayol, N., Berry, N.J., Boeckx, P., de Jong, B.H.J., DeVries, B., Girardin, C.A.J., Kearsley, E., Lindsell, J.A., Lopez-Gonzalez, G., Lucas, R., Malhi, Y., Morel, A., Mitchard, E.T.A., Nagy, L., Qie, L., Quinones, M.J., Ryan, C.M., Ferry, S.J.W., Sunderland, T., Laurin, G.V., Gatti, R.C., Valentini, R., Verbeeck, H., Wijaya, A., Willcock, S., 2016. An integrated pan-tropical biomass map using multiple reference datasets. *Global Change Biology*, 22(4), 1406-1420.
- Avitabile, V., Baccini, A., Friedl, M.A. and Schmullius, C., 2012. Capabilities and limitations of Landsat and land cover data for aboveground woody biomass estimation of Uganda. *Remote Sensing of Environment*, 117, pp.366-380.
- Baccini, A., Friedl, M. A., Woodcock, C. E., Warbington, R., 2004. Forest biomass estimation over regional scales using multisource data. *Geophysical Research Letters*, 31(10).
- Baccini, A., Goetz, S. J., Walker, W. S., Laporte, N. T., Sun, M., Sulla-Menashe, D., Hackler, J., Beck, P. S. A., Dubayah, R., Friedl, M. A., Samanta, S., Houghton, R. A., 2012. Estimated carbon dioxide emissions from tropical deforestation improved by carbon-density maps. *Nature Climate Change*, 2(3), 182-185.
- Baccini, A., Walker, W., Carvalho, L., Farina, M., Sulla-Menashe, D. and Houghton, R.A., 2017. Tropical forests are a net carbon source based on aboveground measurements of gain and loss. *Science*, 358(6360), pp.230-234.
- Baker, T. R., Phillips, O. L., Malhi, Y., Almeida, S., Arroyo, L., Di Fiore, A., Erwin, T., Higuchi, N., Killeen, T.J., Laurance, S. G., Laurance, W.F., Lewis, S.L., Monteagudo, A., Neill, D.A., Nunez Vargas, P., Pitman, N.C.A., Silva, J.N.M., Vasquez Martinez, R., 2004. Increasing biomass in Amazonian forest plots. *Philosophical Transactions of the Royal Society of London. Series B: Biological Sciences*, 359(1443), 353-365.

- Balint, P.J. and Mashinya, J., 2006. The decline of a model community-based conservation project: Governance, capacity, and devolution in Mahenye, Zimbabwe. *Geoforum*, 37(5), pp.805-815.
- Balzter, H., 2001. Forest mapping and monitoring with interferometric synthetic aperture radar (InSAR). *Progress in physical geography*, 25(2), pp.159-177.
- Barbosa, J.M., Broadbent, E.N. and Bitencourt, M.D., 2014. Remote sensing of aboveground biomass in tropical secondary forests: A review. *International Journal of Forestry Research*, 2014.
- Barros, C., Thuiller, W. and Münkemüller, T., 2018. Drought effects on the stability of forest-grassland ecotones under gradual climate change. *PloS one*, 13(10), p.e0206138.
- Bartholome, E. and Belward, A.S., 2005. GLC2000: a new approach to global land cover mapping from Earth observation data. *International Journal of Remote Sensing*, 26(9), 1959-1977.
- Bastin, J.F., Mollicone, D., Grainger, A., Sparrow, B., Picard, N., Lowe, A. and Castro, R., 2017. Response to Comment on “The extent of forest in dryland biomes”. *Science*, 358(6362).
- Bastin, J.F., Rutishauser, E., Kellner, J.R., Saatchi, S., Péliissier, R., Herault, B., Slik, F., Bogaert, J., De Cannière, C., Marshall, A.R. and Poulsen, J., 2018. Pan-tropical prediction of forest structure from the largest trees. *Global Ecology and Biogeography*, 27(11), pp.1366-1383
- Basuki, T.M., Skidmore, A.K., Hussin, Y.A. and Van Duren, I., 2013. Estimating tropical forest biomass more accurately by integrating ALOS PALSAR and Landsat-7 ETM+ data. *International journal of remote sensing*, 34(13), pp.4871-4888.
- Becker, F. and Choudhury, B.J. (1988). Relative sensitivity of normalized difference vegetation index (NDVI) and microwave polarization difference index (MPDI) for vegetation and desertification monitoring. *Remote sensing of environment*, 24(2), pp.297-311.
- Belgiu, M. and Drăguț, L., 2016. Random forest in remote sensing: A review of applications and future directions. *ISPRS journal of photogrammetry and remote sensing*, 114, 24-31.
- Ben-Shahar, R., 1996. Do elephants over-utilize mopane woodlands in northern Botswana? *Journal of Tropical Ecology*, 12(4), 505-515.
- Berger, C., Werner, S., Wigley-Coetsee, C., Smit, I. and Schmutlius, C., 2019, July. Multi-temporal sentinel-1 data for wall-to-wall herbaceous biomass mapping in Kruger National Park, South Africa—first results. In *IGARSS 2019-2019 IEEE International Geoscience and Remote Sensing Symposium* (pp. 7358-7360). IEEE.
- Berninger, A., Lohberger, S., Zhang, D., & Siegert, F., 2019. Canopy height and above-ground biomass retrieval in tropical forests using multi-pass X-and C-band Pol-InSAR data. *Remote Sensing*, 11(18), 2105.
- Biggs, R., Simons, H., Bakkenes, M., Scholes, R.J., Eickhout, B., van Vuuren, D. and Alkemade, R., 2008. Scenarios of biodiversity loss in southern Africa in the 21st century. *Global Environmental Change*, 18(2), pp.296-309.
- Blackburn, G.A., 2007. Hyperspectral remote sensing of plant pigments. *Journal of experimental botany*, 58(4), pp.855-867.
- Blackie, R., Baldauf, C., Gautier, D., Gumbo, D., Kassa, H., Parthasarathy, N., Paumgarten, F., Sola, P., Pulla, S., Waeber, P. and Sunderland, T., 2014. *Tropical dry forests: The state of global knowledge and recommendations for future research* (Vol. 2). Cifor.



- Bollig, M. and Vehrs, H.P., 2021. The making of a conservation landscape: the emergence of a conservationist environmental infrastructure along the Kwando River in Namibia's Zambezi region. *Africa*, 91(2), pp.270-295.
- Bodart, C., Brink, A.B., Donnay, F., Lupi, A., Mayaux, P. and Achard, F., 2013. Continental estimates of forest cover and forest cover changes in the dry ecosystems of Africa between 1990 and 2000. *Journal of biogeography*, 40(6), pp.1036-1047.
- Boggs, G.S., 2010. Assessment of SPOT 5 and QuickBird remotely sensed imagery for mapping tree cover in savannas. *International journal of applied earth observation and geoinformation*, 12(4), pp.217-224.
- Boisvenue, C. and White, J.C., 2019. Information needs of next-generation forest carbon models: opportunities for remote sensing science. *Remote Sensing*, 11(4), 463.
- Bojinski, S., Verstraete, M., Peterson, T. C., Richter, C., Simmons, A., Zemp, M., 2014. The concept of essential climate variables in support of climate research, applications, and policy. *Bulletin of the American Meteorological Society*, 95(9), 1431-1443.
- Bollig, M. and Vehrs, H.P., 2021. The making of a conservation landscape: the emergence of a conservationist environmental infrastructure along the Kwando River in Namibia's Zambezi region. *Africa*, 91(2), pp.270-295.
- Bond, W.J. and Keeley, J.E., 2005. Fire as a global 'herbivore': the ecology and evolution of flammable ecosystems. *Trends in ecology & evolution*, 20(7), pp.387-394.
- Bouvet, A., Mermoz, S., Le Toan, T., Villard, L., Mathieu, R., Naidoo, L. and Asner, G.P., 2018. An above-ground biomass map of African savannahs and woodlands at 25 m resolution derived from ALOS PALSAR. *Remote sensing of environment*, 206, pp.156-173.
- Boyd, D.S. and Danson, F.M., 2005. Satellite remote sensing of forest resources: three decades of research development. *Progress in Physical Geography*, 29(1), pp.1-26.
- Bozdogan, H., 1987. Model selection and Akaike's information criterion (AIC): The general theory and its analytical extensions. *Psychometrika*, 52(3), 345-370.
- Božić, M., Čavlović, J., Lukić, N., Teslak, K., Kos, D., 2005. Efficiency of ultrasonic Vertex III hypsometer compared to the most commonly used hypsometers in Croatian forestry. *Croatian Journal of Forest Engineering: Journal for Theory and Application of Forestry Engineering*, 26(2), 91-99.
- Brando, P.M., Paolucci, L., Ummenhofer, C.C., Ordway, E.M., Hartmann, H., Cattau, M.E., Rattis, L., Medjibe, V., Coe, M.T. and Balch, J., 2019. Droughts, wildfires, and forest carbon cycling: A pantropical synthesis. *Annual Review of Earth and Planetary Sciences*, 47, pp.555-581.
- Brandt, M., Hiernaux, P., Rasmussen, K., Mbow, C., Kergoat, L., Tagesson, T., Ibrahim, Y.Z., Wélé, A., Tucker, C.J. and Fensholt, R. (2016). Assessing woody vegetation trends in Sahelian drylands using MODIS based seasonal metrics. *Remote Sensing of Environment*, 183, pp.215-225.
- Brandt, M., Rasmussen, K., Hiernaux, P., Herrmann, S., Tucker, C.J., Tong, X., Tian, F., Mertz, O., Kergoat, L., Mbow, C. and David, J.L. (2018a). Reduction of tree cover in West African woodlands and promotion in semi-arid farmlands. *Nature Geoscience*, 11(5), pp.328-333
- Brandt, M., Wigneron, J.P., Chave, J., Tagesson, T., Penuelas, J., Ciais, P., Rasmussen, K., Tian, F., Mbow, C., Al-Yaari, A. and Rodriguez-Fernandez, N., 2018b. Satellite passive microwaves

reveal recent climate-induced carbon losses in African drylands. *Nature ecology & evolution*, 2(5), pp.827-835.

Breiman, L. (2001), Random forests. *Machine Learning*, 45(1), 5-32.

Brink, A.B. and Eva, H.D., 2009. Monitoring 25 years of land cover change dynamics in Africa: A sample based remote sensing approach. *Applied geography*, 29(4), pp.501-512.

Brink, A.B., Bodart, C., Brodsky, L., Defourney, P., Ernst, C., Donney, F., Lupi, A. and Tuckova, K., 2014. Anthropogenic pressure in East Africa—Monitoring 20 years of land cover changes by means of medium resolution satellite data. *International Journal of Applied Earth Observation and Geoinformation*, 28, pp.60-69.

Broge, N.H. and Leblanc, E., 2001. Comparing prediction power and stability of broadband and hyperspectral vegetation indices for estimation of green leaf area index and canopy chlorophyll density. *Remote sensing of environment*, 76(2), pp.156-172.

Brown, S., Lugo, A. E., 1982. The storage and production of organic matter in tropical forests and their role in the global carbon cycle. *Biotropica*, 161-187.

Brown, S., Lugo, A. E., 1982. The storage and production of organic matter in tropical forests and their role in the global carbon cycle. *Biotropica*, 161-187.

Brown, S., Swingland, I.R., Hanbury-Tenison, R., Prance, G.T. and Myers, N., 2002. Changes in the use and management of forests for abating carbon emissions: issues and challenges under the Kyoto Protocol. *Philosophical Transactions of the Royal Society of London. Series A: Mathematical, Physical and Engineering Sciences*, 360(1797), pp.1593-1605.

Bucini, G., Hanan, N.P., Boone, R.B., Smit, I.P., Saatchi, S.S., Lefsky, M.A. and Asner, G.P., 2010. Woody fractional cover in Kruger National Park, South Africa: remote sensing-based maps and ecological insights. In *Ecosystem function in savannas: measurement and modeling at landscape to global scales* (pp. 219-237). *CRC Press*.

Bucini, G., Saatchi, S., Hanan, N., Boone, R.B. and Smit, I., 2009, July. Woody cover and heterogeneity in the savannas of the Kruger National Park, South Africa. In *2009 IEEE International Geoscience and Remote Sensing Symposium* (Vol. 4, pp. IV-334). *IEEE*.

Buhne, H. S. T., Pettorelli, N., 2018. Better together: Integrating and fusing multispectral and radar satellite imagery to inform biodiversity monitoring, ecological research and conservation science. *Methods in Ecology and Evolution*, 9(4), pp. 849-865.

Bullock, E.L., Woodcock, C.E., Souza Jr, C. and Olofsson, P., 2020. Satellite-based estimates reveal widespread forest degradation in the Amazon. *Global Change Biology*, 26(5), pp.2956-2969.

Bullock, S.H., Mooney, H.A. and Medina, E. eds., 1995. *Seasonally dry tropical forests*. Cambridge University Press.

Bunting, E.L., Southworth, J., Herrero, H., Ryan, S.J. and Waylen, P., 2018. Understanding Long-Term Savanna Vegetation Persistence across Three Drainage Basins in Southern Africa. *Remote Sensing*, 10(7), p.1013.

Bunyavechewin, S., Baker, P.J. and Davies, S.J., 2011. Seasonally dry tropical forests in continental Southeast Asia: structure, composition and dynamics. In *The ecology and conservation of seasonally dry forests in Asia* (pp. 9-35). Smithsonian Institution Scholarly Press.

- Burkett, V.R., Wilcox, D.A., Stottlemeyer, R., Barrow, W., Fagre, D., Baron, J., Price, J., Nielsen, J.L., Allen, C.D., Peterson, D.L. and Ruggerson, G., 2005. Nonlinear dynamics in ecosystem response to climatic change: case studies and policy implications. *Ecological complexity*, 2(4), pp.357-394
- Cabral, A.I.R., Vasconcelos, M.J., Oom, D. and Sardinha, R. (2011). Spatial dynamics and quantification of deforestation in the central-plateau woodlands of Angola (1990–2009). *Applied Geography*, 31(3), pp.1185-1193.
- Cáceres, A., Melo, M., Barlow, J., Cardoso, P., Maiato, F. and Mills, M.S., 2015. Threatened birds of the Angolan Central Escarpment: distribution and response to habitat change at Kumbira Forest. *Oryx*, 49(4), pp.727-734.
- Campo-Bescós, M.A., Muñoz-Carpena, R., Southworth, J., Zhu, L., Waylen, P.R. and Bunting, E., 2013. Combined spatial and temporal effects of environmental controls on long-term monthly NDVI in the southern Africa Savanna. *Remote Sensing*, 5(12), pp.6513-6538.
- Cánovas-García, F., Alonso-Sarría, F., Gomariz-Castillo, F. and Oñate-Valdivieso, F., 2017. Modification of the random forest algorithm to avoid statistical dependence problems when classifying remote sensing imagery. *Computers & Geosciences*, 103, pp.1-11.
- Carlotto, M.J., 2009. Effect of errors in ground truth on classification accuracy. *International Journal of Remote Sensing*, 30(18), pp.4831-4849.
- Carreiras, J., Melo, J.B. and Vasconcelos, M.J., 2013. Estimating the above-ground biomass in miombo savanna woodlands (Mozambique, East Africa) using L-band synthetic aperture radar data. *Remote Sensing*, 5(4), pp.1524-1548.
- Carter, G.A., 1993. Responses of leaf spectral reflectance to plant stress. *American journal of botany*, 80(3), pp.239-243.
- Case, M.F., Wigley-Coetsee, C., Nzima, N., Scogings, P.F. and Staver, A.C., 2019. Severe drought limits trees in a semi-arid savanna. *Ecology*, 100(11), p.e02842.
- Castillo, A., Magaña, A., Pujadas, A., Martínez, L. and Godínez, C. (2005). Understanding the interaction of rural people with ecosystems: a case study in a tropical dry forest of Mexico. *Ecosystems*, 8(6), pp.630-643.
- Castro, K.L., Sanchez-Azofeifa, G.A. and Rivard, B., 2003. Monitoring secondary tropical forests using space-borne data: implications for Central America. *International Journal of Remote Sensing*, 24(9), pp.1853-1894.
- Castro, S.M., Sanchez-Azofeifa, G.A. and Sato, H. 2018. Effect of drought on productivity in a Costa Rican tropical dry forest. *Environmental Research Letters*, 13(4), p.045001.
- Catarino, S., Romeiras, M.M., Figueira, R., Aubard, V., Silva, J. and Pereira, J., 2020. Spatial and temporal trends of burnt area in Angola: implications for natural vegetation and protected area management. *Diversity*, 12(8), p.307.
- Caylor, K.K., Shugart, H.H. and Rodriguez-Iturbe, I., 2005. Tree canopy effects on simulated water stress in southern African savannas. *Ecosystems*, 8(1), pp.17-32.
- Chadwick, R., Good, P., Martin, G. and Rowell, D.P., 2016. Large rainfall changes consistently projected over substantial areas of tropical land. *Nature Climate Change*, 6(2), pp.177-181.

- Chagnon, F.J.F., Bras, R.L. and Wang, J., 2004. Climatic shift in patterns of shallow clouds over the Amazon. *Geophysical Research Letters*, 31(24).
- Chagumaira, C., Rurinda, J., Nezomba, H., Mtambanengwe, F. and Mapfumo, P., 2016. Use patterns of natural resources supporting livelihoods of smallholder communities and implications for climate change adaptation in Zimbabwe. *Environment, development and sustainability*, 18(1), pp.237-255.
- Chambers, J.Q., Asner, G.P., Morton, D.C., Anderson, L.O., Saatchi, S.S., Espirito-Santo, F.D., Palace, M. and Souza Jr, C., 2007. Regional ecosystem structure and function: ecological insights from remote sensing of tropical forests. *Trends in Ecology & Evolution*, 22(8), pp.414-423.
- Chapungu, L., Nhamo, L., Gatti, R.C. and Chitakira, M., 2020. Quantifying changes in plant species diversity in a savanna ecosystem through observed and remotely sensed data. *Sustainability*, 12(6), p.2345.
- Charles-Dominique, T., Staver, A.C., Midgley, G.F. and Bond, W.J., 2015. Functional differentiation of biomes in an African savanna/forest mosaic. *South African Journal of Botany*, 101, pp.82-90.
- Chave, J., Andalo, C., Brown, S., Cairns, M.A., Chambers, J.Q., Eamus, D., Fölster, H., Fromard, F., Higuchi, N., Kira, T. and Lescure, J.P., 2005. Tree allometry and improved estimation of carbon stocks and balance in tropical forests. *Oecologia*, 145(1), pp.87-99.
- Chazdon, R.L., Brancalion, P.H., Laestadius, L., Bennett-Curry, A., Buckingham, K., Kumar, C., Moll-Rocek, J., Vieira, I.C.G. and Wilson, S.J., 2016. When is a forest a forest? Forest concepts and definitions in the era of forest and landscape restoration. *Ambio*, 45(5), pp.538-550.
- Chazdon, R.L., Broadbent, E.N., Rozendaal, D.M., Bongers, F., Zambrano, A.M.A., Aide, T.M., Balvanera, P., Becknell, J.M., Boukili, V., Brancalion, P.H. and Craven, D. (2016). Carbon sequestration potential of second-growth forest regeneration in the Latin American tropics. *Science Advances*, 2(5), p.e1501639.
- Chen, M., Xie, P., Janowiak, J.E. and Arkin, P.A., 2002. Global land precipitation: A 50-yr monthly analysis based on gauge observations. *Journal of Hydrometeorology*, 3(3), pp.249-266.
- Chidumayo, E.N. 2013. Forest degradation and recovery in a miombo woodland landscape in Zambia: 22 years of observations on permanent sample plots. *Forest Ecology and Management*, 291, pp.154-161.
- Chidumayo, E.N. and Gumbo, D.J. eds., 2010. *The dry forests and woodlands of Africa: managing for products and services*. Earthscan.
- Chidumayo, E.N., 1997. Annual and spatial variation in herbaceous biomass production in a Zambian dry miombo woodland. *South African Journal of Botany*, 63(2), pp.74-81.
- Chidumayo, E.N., 2001. Climate and phenology of savanna vegetation in southern Africa. *Journal of Vegetation Science*, pp.347-354.
- Chidumayo, E.N., 2013. Forest degradation and recovery in a miombo woodland landscape in Zambia: 22 years of observations on permanent sample plots. *Forest Ecology and Management*, 291, pp.154-161.
- Chikoore, H. and Jury, M.R., 2021. South African drought, deconstructed. *Weather and Climate Extremes*, 33, 100334.

- Child, B.A., Musengezi, J., Parent, G.D. and Child, G.F. (2012). The economics and institutional economics of wildlife on private land in Africa. *Pastoralism: Research, Policy and Practice*, 2(1), pp.1-32.
- Chinamatira, L., Mtetwa, S. and Nyamadzawo, G., 2016. Causes of wildland fires, associated socio-economic impacts and challenges with policing, in chakari resettlement area, kadoma, zimbabwe. *Fire Science Reviews*, 5(1), pp.1-11.
- Chiteculo, V., Abdollahnejad, A., Panagiotidis, D., Surový, P. and Sharma, R.P., 2019. Defining deforestation patterns using satellite images from 2000 and 2017: Assessment of forest management in miombo forests—A case study of Huambo Province in Angola. *Sustainability*, 11(1), p.98.
- Cho, M.A., Debba, P., Mutanga, O., Dudeni-Tlhone, N., Magadla, T. and Khuluse, S.A., 2012. Potential utility of the spectral red-edge region of SumbandilaSat imagery for assessing indigenous forest structure and health. *International journal of applied earth observation and Geoinformation*, 16, pp.85-93.
- Cho, M.A., Malahlela, O. and Ramoelo, A., 2015. Assessing the utility WorldView-2 imagery for tree species mapping in South African subtropical humid forest and the conservation implications: Dukuduku forest patch as case study. *International Journal of Applied Earth Observation and Geoinformation*, 38, pp.349-357.
- Cho, M.A., Ramoelo, A., Debba, P., Mutanga, O., Mathieu, R., Van Deventer, H. and Ndlovu, N., 2013. Assessing the effects of subtropical forest fragmentation on leaf nitrogen distribution using remote sensing data. *Landscape ecology*, 28(8), pp.1479-1491.
- Cho, M.A., Skidmore, A., Corsi, F., Van Wieren, S.E. and Sobhan, I., 2007. Estimation of green grass/herb biomass from airborne hyperspectral imagery using spectral indices and partial least squares regression. *International journal of applied Earth observation and geoinformation*, 9(4), pp.414-424.
- Cho, M.A., Skidmore, A.K. and Atzberger, C., 2008. Towards red-edge positions less sensitive to canopy biophysical parameters for leaf chlorophyll estimation using properties optique spectrales des feuilles (PROSPECT) and scattering by arbitrarily inclined leaves (SAILH) simulated data. *International Journal of Remote Sensing*, 29(8), pp.2241-2255.
- Chongo, D., Nagasawa, R., Ahmed, A.O.C. and Perveen, M.F., 2007. Fire monitoring in savanna ecosystems using MODIS data: a case study of Kruger National Park, South Africa. *Landscape and Ecological Engineering*, 3(1), pp.79-88.
- Clark, S., Bolt, K. and Campbell, A., 2008. Protected areas: an effective tool to reduce emissions from deforestation and forest degradation in developing countries. *UNEP-WCMC*, Cambridge, UK.
- Claverie, M., Vermote, E.F., Franch, B. and Masek, J.G., 2015. Evaluation of the Landsat-5 TM and Landsat-7 ETM+ surface reflectance products. *Remote Sensing of Environment*, 169, pp.390-403.
- Coetzer-Hanack, K.L., Witkowski, E.T.F. and Erasmus, B.F., 2016. Thresholds of change in a multi-use conservation landscape of South Africa: historical land-cover, future transformation and consequences for environmental decision-making. *Environmental Conservation*, 43(3), pp.253-262.

- Cohen, W.B., Yang, Z. and Kennedy, R., 2010. Detecting trends in forest disturbance and recovery using yearly Landsat time series: 2. TimeSync—Tools for calibration and validation. *Remote Sensing of Environment*, 114(12), pp.2911-2924.
- Collaboration for Environmental Evidence. (2013). Guidelines for systematic review and evidence synthesis in environmental management. *Environmental Evidence*.
- Congalton, R.G. (1988). A comparison of sampling schemes used in generating error matrices for assessing the accuracy of maps generated from remotely sensed data. *Photogrammetric engineering and remote sensing*.
- Congalton, R.G. and Green, K., 2019. Assessing the accuracy of remotely sensed data: principles and practices. *CRC press*.
- Congalton, R.G., 2018. Landsat's enduring legacy: pioneering global land observations from space. *Photogrammetric Engineering & Remote Sensing*, 84(1), pp.9-10
- Congalton, R.G., Oderwald, R.G. and Mead, R.A., 1983. Assessing Landsat classification accuracy using discrete multivariate analysis statistical techniques. *Photogrammetric engineering and remote sensing*, 49(12), pp.1671-1678.
- Cook, C., Reason, C.J. and Hewitson, B.C., 2004. Wet and dry spells within particularly wet and dry summers in the South African summer rainfall region. *Climate Research*, 26(1), pp.17-31.
- Coppin, P., Jonckheere, I., Nackaerts, K., Muys, B. and Lambin, E., 2004. Review Article Digital change detection methods in ecosystem monitoring: a review. *International journal of remote sensing*, 25(9), pp.1565-1596.
- Coyle, D.B., Stysley, P.R., Poullos, D., Clarke, G.B. and Kay, R.B., 2015, September. Laser transmitter development for NASA's Global Ecosystem Dynamics Investigation (GEDI) lidar. In *Lidar Remote Sensing for Environmental Monitoring XV* (Vol. 9612, p. 961208). International Society for Optics and Photonics.
- Cui, Q., Shi, J., Du, J., Zhao, T. and Xiong, C. (2015). An approach for monitoring global vegetation based on multiangular observations from SMOS. *IEEE Journal of Selected Topics in Applied Earth Observations and Remote Sensing*, 8(2), pp.604-616.
- Cumming, D. H. M., 2008. Large scale conservation planning and priorities for the Kavango-Zambezi transfrontier conservation area. A report prepared for Conservation International. [http://www.wcs-ahead.org/kaza/kaza\\_tfca\\_large\\_scale\\_planning\\_final\\_7nov08\\_logo.pdf/](http://www.wcs-ahead.org/kaza/kaza_tfca_large_scale_planning_final_7nov08_logo.pdf/) (accessed 24 May 2021).
- Cumming, D.H.M., 1981. The management of elephant and other large mammals in Zimbabwe. In "Problems in Management of Locally Abundant Wild Mammals"(P. Jewell and S. Holt, Eds.) pp. 91-118.
- Cunliffe, A.M., Assmann, J.J., Daskalova, G.N., Kerby, J.T. and Myers-Smith, I.H., 2020. Aboveground biomass corresponds strongly with drone-derived canopy height but weakly with greenness (NDVI) in a shrub tundra landscape. *Environmental Research Letters*, 15(12), p.125004.
- Curran, P., 1980. Multispectral remote sensing of vegetation amount. *Progress in physical geography*, 4(3), pp.315-341.

- Curry, T.R. (2020). Mexico's Tropical Dry Forests. In Shobert, A.L. and Maguire, R.O. Reference Module in Earth Systems and Environmental Science.
- Cutler, M.E.J., Boyd, D.S., Foody, G.M. and Vetrivel, A., 2012. Estimating tropical forest biomass with a combination of SAR image texture and Landsat TM data: An assessment of predictions between regions. *ISPRS Journal of Photogrammetry and Remote Sensing*, 70, pp.66-77.
- Dai, A., 2013. Increasing drought under global warming in observations and models. *Nature climate change*, 3(1), pp.52-58.
- Dale, V.H., Joyce, L.A., McNulty, S., Neilson, R.P., Ayres, M.P., Flannigan, M.D., Hanson, P.J., Irland, L.C., Lugo, A.E., Peterson, C.J. and Simberloff, D., 2001. Climate change and forest disturbances: climate change can affect forests by altering the frequency, intensity, duration, and timing of fire, drought, introduced species, insect and pathogen outbreaks, hurricanes, windstorms, ice storms, or landslides. *BioScience*, 51(9), pp.723-734.
- Darkoh, M.B.K., 2009. An overview of environmental issues in Southern Africa. *African Journal of Ecology*, 47, pp.93-98.
- Daskin, J.H., Stalmans, M. and Pringle, R.M., 2016. Ecological legacies of civil war: 35-year increase in savanna tree cover following wholesale large-mammal declines. *Journal of Ecology*, 104(1), pp.79-89.
- David, R.M., Rosser, N.J. and Donoghue, D.N., 2022b. Improving above ground biomass estimates of Southern Africa dryland forests by combining Sentinel-1 SAR and Sentinel-2 multispectral imagery. *Remote Sensing of Environment*, 282, p.113232.
- David, R.M., Rosser, N.J. and Donoghue, D.N., 2022a. Remote sensing for monitoring tropical dryland forests: a review of current research, knowledge gaps and future directions for Southern Africa. *Environmental Research Communications*, 4(4), 042001.
- Davies, D.K., Ilavajhala, S., Wong, M.M. and Justice, C.O., 2008. Fire information for resource management system: archiving and distributing MODIS active fire data. *IEEE Transactions on Geoscience and Remote Sensing*, 47(1), pp.72-79.
- Davis, C.L., Hoffman, M.T. and Roberts, W., 2017. Long-term trends in vegetation phenology and productivity over Namaqualand using the GIMMS AVHRR NDVI3g data from 1982 to 2011. *South African Journal of Botany*, 111, pp.76-85.
- Dawson, T.P., Cutler, M.E.J. and Brown, C., 2016. The role of remote sensing in the development of SMART indicators for ecosystem services assessment. *Biodiversity*, 17(4), pp.136-148.
- Day, M., Baldauf, C., Rutishauser, E., Sunderland, T. C., 2014. Relationships between tree species diversity and above-ground biomass in Central African rainforests: implications for REDD. *Environmental Conservation*, 41(1), 64-72.
- de Araujo Barbosa, C.C., Atkinson, P.M. and Dearing, J.A., 2015. Remote sensing of ecosystem services: A systematic review. *Ecological Indicators*, 52, pp.430-443.
- De Jong, R., Verbesselt, J., Zeileis, A. and Schaepman, M.E., 2013. Shifts in global vegetation activity trends. *Remote Sensing*, 5(3), pp.1117-1133.
- De Marzo, T., Pflugmacher, D., Baumann, M., Lambin, E.F., Gasparri, I. and Kuemmerle, T., 2021. Characterizing forest disturbances across the Argentine Dry Chaco based on Landsat time series. *International Journal of Applied Earth Observation and Geoinformation*, 98, p.102310.

- de Oliveira, W.N., Miziara, F. and Ferreira, N.C., 2019. Mapeamento do Uso e Cobertura do Solo de Moçambique Utilizando a Plataforma Google Earth Engine. *Anuário do Instituto de Geociências*, 42(1), pp.336-345.
- De Sy, V., Herold, M., Achard, F., Asner, G.P., Held, A., Kelndorfer, J. and Verbesselt, J., 2012. Synergies of multiple remote sensing data sources for REDD+ monitoring. *Current Opinion in Environmental Sustainability*, 4(6), pp.696-706.
- Desanker, P.V. and Justice, C.O., 2001. Africa and global climate change: critical issues and suggestions for further research and integrated assessment modeling. *Climate Research*, 17(2), pp.93-103.
- DeVries, B., Decuyper, M., Verbesselt, J., Zeileis, A., Herold, M. and Joseph, S., 2015. Tracking disturbance-regrowth dynamics in tropical forests using structural change detection and Landsat time series. *Remote Sensing of Environment*, 169, pp.320-334.
- DeVries, B., Verbesselt, J., Kooistra, L. and Herold, M., 2015. Robust monitoring of small-scale forest disturbances in a tropical montane forest using Landsat time series. *Remote Sensing of Environment*, 161, pp.107-121.
- Deweese, P.A. (1994). Social and economic aspects of miombo woodland management in southern Africa: options and opportunities for research. *CIFOR Occasional paper*, (2).
- Dexter, K.G., Smart, B., Baldauf, C., Baker, T.R., Balinga, M.P., Brienen, R.J.W., Fauset, S., Feldpausch, T.R., Silva, L., Muledi, J.I. and Lewis, S.L., 2015. Floristics and biogeography of vegetation in seasonally dry tropical regions. *International Forestry Review*, 17(2), pp.10-32.
- Diffenbaugh, N.S., Singh, D., Mankin, J.S., Horton, D.E., Swain, D.L., Touma, D., Charland, A., Liu, Y., Haugen, M., Tsiang, M. and Rajaratnam, B., 2017. Quantifying the influence of global warming on unprecedented extreme climate events. *Proceedings of the National Academy of Sciences*, 114(19), pp.4881-4886.
- Djouidi, H., Vergles, E., Blackie, R.R., Koame, C.K. and Gautier, D., 2015. Dry forests, livelihoods and poverty alleviation: understanding current trends. *International Forestry Review*, 17(2), pp.54-69.
- Dlamini, W.M., 2017. Mapping forest and woodland loss in Swaziland: 1990–2015. *Remote Sensing Applications: Society and Environment*, 5, pp.45-53.
- do Espírito-Santo, M.M., Rocha, A.M., Leite, M.E., Silva, J.O., da Silva, L.P. and Sanchez-Azofeifa, G.A. (2020). Biophysical and socioeconomic factors associated to deforestation and forest recovery in Brazilian tropical dry forests. *Frontiers in Forests and Global Change*, 3, p.141.
- Dogru, A.O., Goksel, C., David, R.M., Tolunay, D., Sözen, S. and Orhon, D., 2020. Detrimental environmental impact of large scale land use through deforestation and deterioration of carbon balance in Istanbul Northern Forest Area. *Environmental Earth Sciences*, 79, pp.1-13.
- Dong, J., Kaufmann, R.K., Myneni, R.B., Tucker, C.J., Kauppi, P.E., Liski, J., Buermann, W., Alexeyev, V. and Hughes, M.K., 2003. Remote sensing estimates of boreal and temperate forest woody biomass: carbon pools, sources, and sinks. *Remote sensing of Environment*, 84(3), pp.393-410.
- Donoghue, D. N., 2002. Remote sensing: environmental change. *Progress in Physical Geography*, 26(1), pp.144-151.



- Donoghue, D.N., 2000. Remote sensing: sensors and applications. *Progress in Physical Geography*, 24(3), pp.407-414.
- Dubayah, R., Blair, J.B., Goetz, S., Fatoyinbo, L., Hansen, M., Healey, S., Hofton, M., Hurtt, G., Kellner, J., Luthcke, S. and Armston, J., 2020. The Global Ecosystem Dynamics Investigation: High-resolution laser ranging of the Earth's forests and topography. *Science of remote sensing*, 1, p.100002.
- Dube, O. P, 2013. Challenges of wildland fire management in Botswana: Towards a community inclusive fire management approach. *Weather and Climate Extremes*, 1, 26-41.
- Dube, T., Gara, T.W., Mutanga, O., Sibanda, M., Shoko, C., Murwira, A., Masocha, M., Ndaimani, H. and Hatendi, C.M., 2018. Estimating forest standing biomass in savanna woodlands as an indicator of forest productivity using the new generation WorldView-2 sensor. *Geocarto International*, 33(2), pp.178-188.
- Dube, T., Mutanga, O., Adam, E. and Ismail, R., 2014. Intra-and-inter species biomass prediction in a plantation forest: testing the utility of high spatial resolution spaceborne multispectral rapideye sensor and advanced machine learning algorithms. *Sensors*, 14(8), pp.15348-15370.
- Ducheyne, E., Mweempwa, C., De Pus, C., Vernieuwe, H., De Deken, R., Hendrickx, G. and Van den Bossche, P., 2009. The impact of habitat fragmentation on tsetse abundance on the plateau of eastern Zambia. *Preventive veterinary medicine*, 91(1), pp.11-18.
- Dupuis, C., Lejeune, P., Michez, A. and Fayolle, A., 2020. How can remote sensing help monitor tropical moist forest degradation?—a systematic review. *Remote Sensing*, 12(7), p.1087.
- Durant, S.M., Petteorelli, N., Bashir, S., Woodroffe, R., Wachter, T., De Ornellas, P., Ransom, C., Abáigar, T., Abdelgadir, M., El Alqamy, H. and Beddiaf, M., 2012. Forgotten biodiversity in desert ecosystems. *Science*, 336(6087), pp.1379-1380.
- Durden, S.L., Van Zyl, J.J. and Zebker, H.A., 1989. Modeling and observation of the radar polarization signature of forested areas. *IEEE Transactions on Geoscience and Remote Sensing*, 27(3), pp.290-301.
- Dutrieux, L.P., Verbesselt, J., Kooistra, L. and Herold, M., 2015. Monitoring forest cover loss using multiple data streams, a case study of a tropical dry forest in Bolivia. *ISPRS Journal of Photogrammetry and Remote Sensing*, 107, pp.112-125.
- Eitel, J.U., Vierling, L.A., Litvak, M.E., Long, D.S., Schulthess, U., Ager, A.A., Krofcheck, D.J. and Stoscheck, L., 2011. Broadband, red-edge information from satellites improves early stress detection in a New Mexico conifer woodland. *Remote Sensing of Environment*, 115(12), 3640-3646.
- Ellis, J.E. and Swift, D.M., 1988. Stability of African pastoral ecosystems: alternate paradigms and implications for development. *Rangeland Ecology & Management/Journal of Range Management Archives*, 41(6), pp.450-459.
- EMA., 2007. Chapter 20:27 Environment Management Act (Environmental Impact
- Engelbrecht, B.M., Comita, L.S., Condit, R., Kursar, T.A., Tyree, M.T., Turner, B.L. and Hubbell, S.P., 2007. Drought sensitivity shapes species distribution patterns in tropical forests. *Nature*, 447(7140), pp.80-82.
- Eriksen, C., 2007. Why do they burn the 'bush'? Fire, rural livelihoods, and conservation in Zambia. *Geographical Journal*, 173(3), pp.242-256.

- Erkkilä, A. and Löfman, S., 1999. Forest cover change in the Ohangwena region, northern Namibia: A case study based on multitemporal Landsat images and aerial photography. *Southern African Forestry Journal*, 184(1), pp.25-32.
- ESA, 2014. Global land cover map for the epoch 2005. Available at: <http://www.esa-landcover-cci.org/> (accessed 9 July 2015)
- ESA, 2020. Level-1. <https://earth.esa.int/web/sentinel/user-guides/sentinel-1-sar/product-types-processing-levels/level-1/> (accessed 19 November 2020).
- ESA. 2013. SENTINEL-2 User Handbook. [https://sentinel.esa.int/documents/247904/685211/Sentinel-2 User Handbook/](https://sentinel.esa.int/documents/247904/685211/Sentinel-2_User_Handbook/) (accessed 19 March 2021).
- Estes, L., Elsen, P.R., Treuer, T., Ahmed, L., Caylor, K., Chang, J., Choi, J.J. and Ellis, E.C., 2018. The spatial and temporal domains of modern ecology. *Nature ecology & evolution*, 2(5), pp.819-826.
- Eva, H.D., Brink, A. and Simonetti, D., 2006. Monitoring land cover dynamics in sub-Saharan Africa. *Institute for Environmental and Sustainability, Tech. Rep. EUR, 22498*.
- Fajardo, L., Gonzalez, V., Nassar, J.M., Lacabana, P., Portillo Q, C.A., Carrasquel, F. and Rodriguez, J.P. (2005). Tropical Dry Forests of Venezuela: Characterization and Current Conservation Status 1. *Biotropica: The Journal of Biology and Conservation*, 37(4), pp.531-546.
- Falkowski, M.J., Smith, A.M., Gessler, P.E., Hudak, A.T., Vierling, L.A. and Evans, J.S., 2008. The influence of conifer forest canopy cover on the accuracy of two individual tree measurement algorithms using lidar data. *Canadian Journal of Remote Sensing*, 34(sup2), pp. S338-S350
- FAO, 2011 FAO Global Forest Resources Assessment 2010. Rome, Italy (2011)
- FAO. (1999). Tropical forest management techniques: a review of the sustainability of forest management practices in tropical countries, from <https://www.fao.org/documents/card/en/c/10c5f896-03f8-536d-b253-aebb36dd2cef/> , accessed 24 March 2021)
- AO. 2000. FRA 2000: On Definitions of Forest and Forest Change. Forest Resources Assessment.
- FAO., 2001. FRA 2000: Global Ecological Zoning for the Global Forest Resources Assessment 2000, Final Report, Food and Agriculture Organization of the United Nations. Forestry Department, Rome. <http://www.fao.org/3/ad652e/ad652e00.htm/> (accessed 19 March 2021).
- FAO., 2009. Human-wildlife conflict in Africa: causes, consequences and management strategies: Food and Agriculture Organization of the United Nations (FAO).
- FAO., 2010. Assessing forest degradation-towards the development of globally applicable guidelines. Forest Resources Assessment Working Paper, 177.
- Fassnacht, F.E., Hartig, F., Latifi, H., Berger, C., Hernández, J., Corvalán, P. and Koch, B., 2014. Importance of sample size, data type and prediction method for remote sensing-based estimations of aboveground forest biomass. *Remote Sensing of Environment*, 154, 102-114.

- Feng, S. and Fu, Q., 2013. Expansion of global drylands under a warming climate. *Atmospheric Chemistry and Physics*, 13(19), pp.10081-10094.
- Fensham, R.J. and Fairfax, R.J. 2002. Aerial photography for assessing vegetation change: a review of applications and the relevance of findings for Australian vegetation history. *Australian Journal of Botany*, 50(4), pp.415-429.
- Fensholt, R., Sandholt, I. and Rasmussen, M.S., 2004. Evaluation of MODIS LAI, fAPAR and the relation between fAPAR and NDVI in a semi-arid environment using in situ measurements. *Remote sensing of Environment*, 91(3-4), pp.490-507.
- Fidzani, N., 2014. The Management of Forest Reserves in Botswana, in Rietbergen-McCracken, J., Abaza, H. (Eds.), *Economic Instruments for Environmental Management: A Worldwide Compendium of Case Studies*. *Routledge*, pp. 39-46.
- Field, C.B., Randerson, J.T. and Malmström, C.M., 1995. Global net primary production: combining ecology and remote sensing. *Remote sensing of Environment*, 51(1), pp.74-88.
- Foley, J.A., Coe, M.T., Scheffer, M. and Wang, G., 2003. Regime shifts in the Sahara and Sahel: interactions between ecological and climatic systems in Northern Africa. *Ecosystems*, 6(6), pp.524-532.
- Foody, G.M., 2003. Remote sensing of tropical forest environments: towards the monitoring of environmental resources for sustainable development. *International journal of remote sensing*, 24(20), pp.4035-4046.
- Foody, G.M., Boyd, D.S. and Cutler, M.E., 2003. Predictive relations of tropical forest biomass from Landsat TM data and their transferability between regions. *Remote sensing of environment*, 85(4), pp.463-474.
- Foody, G.M., Cutler, M.E., McMorrow, J., Pelz, D., Tangki, H., Boyd, D.S. and Douglas, I.A.N., 2001. Mapping the biomass of Bornean tropical rain forest from remotely sensed data. *Global Ecology and Biogeography*, 10(4), pp.379-387.
- Forkuor, G., Dimobe, K., Serme, I. and Tondoh, J.E., 2018. Landsat-8 vs. Sentinel-2: examining the added value of sentinel-2's red-edge bands to land-use and land-cover mapping in Burkina Faso. *GIScience & remote sensing*, 55(3), 331-354.
- Forkuor, G., Zoungrana, J.-B. B., Dimobe, K., Ouattara, B., Vadrevu, K. P., Tondoh, J. E., 2020. Above-ground biomass mapping in West African dryland forest using Sentinel-1 and 2 datasets-A case study. *Remote Sensing of Environment*, 236, 111496.
- Fox, J., 2015. *Applied regression analysis and generalized linear models*. Sage Publications.
- Fox, J.T., Vandewalle, M.E. and Alexander, K.A., 2017. Land cover change in northern botswana: the influence of climate, fire, and elephants on semi-arid dryland woodlands. *Land*, 6(4), p.73.
- Frankie, G.W., Mata, A. and Vinson, S.B. eds. (2004). *Biodiversity conservation in Costa Rica: Learning the lessons in a seasonal dry forest*. *Univ of California Press*.
- Frost17, P.G., 1999. Fire in southern African woodlands: origins, impacts, effects and control. *Carbon*, 8(7,000), p.181.

- Fuchs, H., Magdon, P., Kleinn, C. and Flessa, H., 2009. Estimating aboveground carbon in a catchment of the Siberian forest tundra: Combining satellite imagery and field inventory. *Remote Sensing of Environment*, 113(3), pp.518-531.
- Fullman, T. J., 2009. Spatial dynamics of elephant impacts on trees in Chobe National Park, Botswana. MS Thesis. University of Florida, Gainesville (USA).
- Fullman, T. J., Child, B., 2013. Water distribution at local and landscape scales affects tree utilization by elephants in Chobe National Park, Botswana. *African Journal of Ecology*, 51(2), 235-243.
- Fullman, T.J. and Bunting, E.L., 2014. Analyzing vegetation change in an elephant-impacted landscape using the moving standard deviation index. *Land*, 3(1), pp.74-104.
- Fung, T. and LeDrew, E., 1988. For change detection using various accuracy. *Photogrammetric engineering and remote sensing*, 54(10), pp.1449-1454.
- Funk, C., Peterson, P., Landsfeld, M., Pedreros, D., Verdin, J., Shukla, S., Husak, G., Rowland, J., Harrison, L., Hoell, A. and Michaelsen, J., 2015. The climate hazards infrared precipitation with stations—a new environmental record for monitoring extremes. *Scientific data*, 2(1), pp.1-21.
- Gallego, F.J., 2000. Double sampling for area estimation and map accuracy assessment. *Quantifying Spatial Uncertainty in Natural Resources: Theory and Applications from GIS and Remote Sensing*, pp.65-77.
- Galiatsatos, N., Donoghue, D.N., Watt, P., Bholanath, P., Pickering, J., Hansen, M.C. and Mahmood, A.R., 2020. An assessment of global forest change datasets for national forest monitoring and reporting. *Remote Sensing*, 12(11), p.1790.
- Gao, Y., Solórzano, J.V., Quevedo, A. and Loya-Carrillo, J.O., 2021. How BFAST Trend and Seasonal Model Components Affect Disturbance Detection in Tropical Dry Forest and Temperate Forest. *Remote Sensing*, 13(11), p.2033.
- Gara, T.W., Murwira, A. and Ndaimani, H., 2016. Predicting forest carbon stocks from high resolution satellite data in dry forests of Zimbabwe: exploring the effect of the red-edge band in forest carbon stocks estimation. *Geocarto international*, 31(2), pp.176-192.
- Gara, T.W., Murwira, A., Dube, T., Sibanda, M., Rwasoka, D.T., Ndaimani, H., Chivhenge, E. and Hatendi, C.M., 2017. Estimating forest carbon stocks in tropical dry forests of Zimbabwe: exploring the performance of high and medium spatial-resolution multispectral sensors. *Southern Forests: a Journal of Forest Science*, 79(1), pp.31-40.
- Gasparri, N.I. and Grau, H.R., 2009. Deforestation and fragmentation of Chaco dry forest in NW Argentina (1972–2007). *Forest ecology and Management*, 258(6), pp.913-921.
- Gasparri, N.I., Parmuchi, M.G., Bono, J., Karszenbaum, H. and Montenegro, C.L., 2010. Assessing multi-temporal Landsat 7 ETM+ images for estimating above-ground biomass in subtropical dry forests of Argentina. *Journal of Arid Environments*, 74(10), pp.1262-1270.
- Geiß, C., Pelizari, P.A., Schrade, H., Brenning, A. and Taubenböck, H., 2017. On the effect of spatially non-disjoint training and test samples on estimated model generalization capabilities in supervised classification with spatial features. *IEEE Geoscience and Remote Sensing Letters*, 14(11), pp.2008-2012.
- Geist, H.J. and Lambin, E.F., 2004. Dynamic causal patterns of desertification. *Bioscience*, 54(9), pp.817-829.

- Geist, H.J., 2002. Causes and Pathways of Land Change in Southern Africa during the Past 300 Years: Moving from Simplifications to Generality and Complexity (Ursachen-und Verlaufsanalyse von terrestrischem Wandel im südlichen Afrika (1700–1990). Generalisierung und Komplexität statt Vereinfachung). *Erdkunde*, pp.144-156.
- Gessner, U., Machwitz, M., Conrad, C. and Dech, S., 2013. Estimating the fractional cover of growth forms and bare surface in savannas. A multi-resolution approach based on regression tree ensembles. *Remote Sensing of Environment*, 129, pp.90-102.
- GFOI, 2016. Integration of remote-sensing and ground-based observations for estimation of emissions and removals of greenhouse gases in forests: Methods and Guidance from the Global Forest Observations Initiative (GFOI), Edition 2.0. UN Food and Agriculture Organization.
- Gibbs, H.K., Brown, S., Niles, J.O. and Foley, J.A., 2007. Monitoring and estimating tropical forest carbon stocks: making REDD a reality. *Environmental research letters*, 2(4), p.045023.
- Gibson, L.A., Jarman, C., Su, Z. and Eckardt, F.E., 2013. Estimating evapotranspiration using remote sensing and the Surface Energy Balance System—A South African perspective. *Water Sa*, 39(4), pp.477-484.
- Giglio, L., Boschetti, L., Roy, D., Hoffmann, A.A., Humber, M. and Hall, J.V., 2016. Collection 6 modis burned area product user's guide version 1.0. *NASA EOSDIS Land Processes DAAC: Sioux Falls, SD, USA*.
- Giglio, L., Boschetti, L., Roy, D.P., Humber, M.L. and Justice, C.O., 2018. The Collection 6 MODIS burned area mapping algorithm and product. *Remote sensing of environment*, 217, pp.72-85.
- Giglio, L., Loboda, T., Roy, D.P., Quayle, B. and Justice, C.O., 2009. An active-fire based burned area mapping algorithm for the MODIS sensor. *Remote sensing of environment*, 113(2), pp.408-420.
- Gill, A.M., 1975. Fire and the Australian flora: a review. *Australian forestry*, 38(1), pp.4-25.
- Gillespie, T.W., Grijalva, A. and Farris, C.N., 2000. Diversity, composition, and structure of tropical dry forests in Central America. *Plant ecology*, 147(1), pp.37-47.
- Giri, C., Zhu, Z. and Reed, B., 2005. A comparative analysis of the Global Land Cover 2000 and MODIS land cover data sets. *Remote sensing of environment*, 94(1), pp.123-132.
- Gitelson, A.A., Kaufman, Y.J. and Merzlyak, M.N., 1996. Use of a green channel in remote sensing of global vegetation from EOS-MODIS. *Remote sensing of Environment*, 58(3), pp.289-298.
- Gizachew, B., Astrup, R., Vedeld, P., Zahabu, E.M. and Duguma, L.A., 2017, May. REDD+ in Africa: contexts and challenges. In *Natural Resources Forum* (Vol. 41, No. 2, pp. 92-104). Oxford, UK: Blackwell Publishing Ltd.
- Gizachew, B., Solberg, S., Næsset, E., Gobakken, T., Bollandsås, O.M., Breidenbach, J., Zahabu, E. and Mauya, E.W., 2016. Mapping and estimating the total living biomass and carbon in low-biomass woodlands using Landsat 8 CDR data. *Carbon balance and management*, 11(1), pp.1-14.
- Glick, H.B., Bettigole, C., Maynard, D.S., Covey, K.R., Smith, J.R. and Crowther, T.W., 2016. Spatially-explicit models of global tree density. *Scientific data*, 3(1), pp.1-11.

- Gnauck, A., 2004. Interpolation and approximation of water quality time series and process identification. *Analytical and bioanalytical chemistry*, 380(3), pp.484-492.
- GOFC-GOLD., 2014. A sourcebook of methods and procedures for monitoring and reporting anthropogenic greenhouse gas emissions and removals associated with deforestation, gains and losses of carbon stocks in forests remaining forests, and forestation (No. COP20-1). GOFC-GOLD. Land Cover Project Office, Wageningen University, The Netherlands).
- Göksel, Ç., David, R.M. and Dogru, A.O., 2018. Environmental monitoring of spatio-temporal changes in northern Istanbul using remote sensing and GIS. *International Journal of Environment and Geoinformatics*, 5(1), pp.94-103.
- González-M, R., Posada, J.M., Carmona, C.P., Garzón, F., Salinas, V., Idárraga-Piedrahita, Á., Pizano, C., Avella, A., López-Camacho, R., Norden, N. and Nieto, J. (2021). Diverging functional strategies but high sensitivity to an extreme drought in tropical dry forests. *Ecology Letters*, 24(3), pp.451-463.
- Google. 2020, Google Earth Engine. <https://developers.google.com/earth-engine/sentinel1/> (accessed 26 November 2020).
- Gorelick, N., Hancher, M., Dixon, M., Ilyushchenko, S., Thau, D. and Moore, R., 2017. Google Earth Engine: Planetary-scale geospatial analysis for everyone. *Remote sensing of Environment*, 202, pp.18-27.
- Grainger, A., 1999. Constraints on modelling the deforestation and degradation of tropical open woodlands. *Global Ecology and Biogeography*, 8(3-4), pp.179-190.
- Grainger, A., 2008. Difficulties in tracking the long-term global trend in tropical forest area. *Proceedings of the National Academy of Sciences*, 105(2), pp.818-823.
- Grogan, K., Pflugmacher, D., Hostert, P., Verbesselt, J. and Fensholt, R., 2016. Mapping clearances in tropical dry forests using breakpoints, trend, and seasonal components from MODIS time series: does forest type matter?. *Remote Sensing*, 8(8), p.657.
- Guirado, E., Alcaraz-Segura, D., Cabello, J., Puertas-Ruíz, S., Herrera, F. and Tabik, S., 2020. Tree cover estimation in global drylands from space using deep learning. *Remote Sensing*, 12(3), p.343.
- Guyon, I. and Elisseeff, A., 2003. An introduction to variable and feature selection. *Journal of machine learning research*, 3(Mar), 1157-1182.
- Halperin, J., LeMay, V., Chidumayo, E., Verchot, L. and Marshall, P., 2016. Model-based estimation of above-ground biomass in the miombo ecoregion of Zambia. *Forest Ecosystems*, 3(1), pp.1-17.
- Hamunyela, E., Brandt, P., Shirima, D., Do, H.T.T., Herold, M. and Roman-Cuesta, R.M., 2020. Space-time detection of deforestation, forest degradation and regeneration in montane forests of Eastern Tanzania. *International Journal of Applied Earth Observation and Geoinformation*, 88, p.102063.
- Hamunyela, E., Verbesselt, J. and Herold, M., 2016. Using spatial context to improve early detection of deforestation from Landsat time series. *Remote Sensing of Environment*, 172, pp.126-138.
- Hanks, J., 2003. Transfrontier Conservation Areas (TFCAs) in Southern Africa: their role in conserving biodiversity, socioeconomic development and promoting a culture of peace. *Journal of Sustainable Forestry*, 17(1-2), pp.127-148.

- Hansen, M.C. and Loveland, T.R., 2012. A review of large area monitoring of land cover change using Landsat data. *Remote sensing of Environment*, 122, pp.66-74.
- Hansen, M.C., Potapov, P.V., Moore, R., Hancher, M., Turubanova, S.A., Tyukavina, A., Thau, D., Stehman, S.V., Goetz, S.J., Loveland, T.R. and Kommareddy, A., 2013. High-resolution global maps of 21st-century forest cover change. *science*, 342(6160), pp.850-853.
- Hantson, S., Pueyo, S. and Chuvieco, E., 2016. Global fire size distribution: from power law to log-normal. *International journal of wildland fire*, 25(4), pp.403-412.
- Harris, A., Carr, A.S. and Dash, J., 2014. Remote sensing of vegetation cover dynamics and resilience across southern Africa. *International Journal of Applied Earth Observation and Geoinformation*, 28, pp.131-139.
- Harris, N.L., Brown, S., Hagen, S.C., Saatchi, S.S., Petrova, S., Salas, W., Hansen, M.C., Potapov, P.V. and Lotsch, A., 2012. Baseline map of carbon emissions from deforestation in tropical regions. *Science*, 336(6088), 1573-1576.
- Hastie, T., Tibshirani, R., Friedman, J., 2009. The elements of statistical learning: data mining, inference, and prediction, *Springer*, New York.
- Hawryło, P., Bednarz, B., Wężyk, P., Szostak, M., 2018. Estimating defoliation of Scots pine stands using machine learning methods and vegetation indices of Sentinel-2. *European Journal of Remote Sensing*, 51(1), 194-204.
- Hayward, R.M., Banin, L.F., Burslem, D.F., Chapman, D.S., Philipson, C.D., Cutler, M.E., Reynolds, G., Nilus, R. and Dent, D.H., 2021. Three decades of post-logging tree community recovery in naturally regenerating and actively restored dipterocarp forest in Borneo. *Forest Ecology and Management*, 488, p.119036.
- Heckel, K., Urban, M., Schratz, P., Mahecha, M.D. and Schmullius, C., 2020. Predicting forest cover in distinct ecosystems: The potential of multi-source Sentinel-1 and-2 data fusion. *Remote Sensing*, 12(2), p.302.
- Herold, M., Mayaux, P., Woodcock, C.E., Baccini, A. and Schmullius, C., 2008. Some challenges in global land cover mapping: An assessment of agreement and accuracy in existing 1 km datasets. *Remote Sensing of Environment*, 112(5), pp.2538-2556.
- Herrero, H., Southworth, J., Muir, C., Khatami, R., Bunting, E. and Child, B., 2020. An Evaluation of Vegetation Health in and around Southern African National Parks during the 21st Century (2000–2016). *Applied Sciences*, 10(7), p.2366.
- Herrmann, S.M., Anyamba, A. and Tucker, C.J., 2005. Recent trends in vegetation dynamics in the African Sahel and their relationship to climate. *Global Environmental Change*, 15(4), pp.394-404.
- Higginbottom, T.P., Symeonakis, E., Meyer, H. and van der Linden, S., 2018. Mapping fractional woody cover in semi-arid savannahs using multi-seasonal composites from Landsat data. *ISPRS Journal of Photogrammetry and Remote Sensing*, 139, pp.88-102.
- Higgins, S.I., Bond, W.J. and Trollope, W.S., 2000. Fire, resprouting and variability: a recipe for grass–tree coexistence in savanna. *Journal of Ecology*, 88(2), pp.213-229.
- Higgins, S.I., Delgado-Cartay, M.D., February, E.C. and Combrink, H.J., 2011. Is there a temporal niche separation in the leaf phenology of savanna trees and grasses?. *Journal of Biogeography*, 38(11), pp.2165-2175.

- Hoffman, M.T. and Todd, S., 2000. A national review of land degradation in South Africa: the influence of biophysical and socio-economic factors. *Journal of Southern African Studies*, 26(4), pp.743-758.
- Holben, B.N., 1986. Characteristics of maximum-value composite images from temporal AVHRR data. *International journal of remote sensing*, 7(11), pp.1417-1434.
- Holloway, J. and Mengersen, K., 2018. Statistical machine learning methods and remote sensing for sustainable development goals: a review. *Remote Sensing*, 10(9), p.1365.
- Horion, S., Fensholt, R., Tagesson, T. and Ehammer, A. (2014). Using earth observation-based dry season NDVI trends for assessment of changes in tree cover in the Sahel. *International Journal of Remote Sensing*, 35(7), pp.2493-2515.
- Houghton, R.A., Hall, F. and Goetz, S.J., 2009. Importance of biomass in the global carbon cycle. *Journal of Geophysical Research: Biogeosciences*, 114(G2).
- Housman, I.W., Chastain, R.A. and Finco, M.V., 2018. An evaluation of forest health insect and disease survey data and satellite-based remote sensing forest change detection methods: Case studies in the United States. *Remote Sensing*, 10(8), p.1184.
- Huang, C., Goward, S.N., Schleeweis, K., Thomas, N., Masek, J.G. and Zhu, Z., 2009. Dynamics of national forests assessed using the Landsat record: Case studies in eastern United States. *Remote sensing of Environment*, 113(7), pp.1430-1442.
- Huang, J., Li, Y., Fu, C., Chen, F., Fu, Q., Dai, A., Shinoda, M., Ma, Z., Guo, W., Li, Z. and Zhang, L., 2017. Dryland climate change: Recent progress and challenges. *Reviews of Geophysics*, 55(3), pp.719-778.
- Huang, J., Yu, H., Guan, X., Wang, G. and Guo, R., 2016. Accelerated dryland expansion under climate change. *Nature Climate Change*, 6(2), pp.166-171.
- Huang, W., Sun, G., Ni, W., Zhang, Z. and Dubayah, R., 2015. Sensitivity of multi-source SAR backscatter to changes in forest aboveground biomass. *Remote Sensing*, 7(8), pp.9587-9609.
- Huemmerich, K.F., Privette, J.L., Mukelabai, M., Myneni, R.B. and Knyazikhin, Y., 2005. Time-series validation of MODIS land biophysical products in a Kalahari woodland, Africa. *International Journal of Remote Sensing*, 26(19), pp.4381-4398.
- Huete, A., Didan, K., Miura, T., Rodriguez, E.P., Gao, X. and Ferreira, L.G., 2002. Overview of the radiometric and biophysical performance of the MODIS vegetation indices. *Remote sensing of environment*, 83(1-2), pp.195-213.
- Huete, A., Justice, C. and Van Leeuwen, W., 1999. MODIS vegetation index (MOD13). *Algorithm theoretical basis document*, 3(213), pp.295-309.
- Hunt, E.R., Hively, W.D., Daughtry, C.S., McCarty, G.W., Fujikawa, S.J., Ng, T.L., Tranchitella, M., Linden, D.S. and Yoel, D.W., 2008, November. Remote sensing of crop leaf area index using unmanned airborne vehicles. In *Proceedings of the Pecora* (Vol. 17, pp. 18-20).
- Hüttich, C., Gessner, U., Herold, M., Strohbach, B.J., Schmidt, M., Keil, M. and Dech, S., 2009. On the suitability of MODIS time series metrics to map vegetation types in dry savanna ecosystems: A case study in the Kalahari of NE Namibia. *Remote sensing*, 1(4), pp.620-643.
- Hüttich, C., Herold, M., Strohbach, B.J. and Dech, S., 2011. Integrating in-situ, Landsat, and MODIS data for mapping in Southern African savannas: experiences of LCCS-based land-cover



- mapping in the Kalahari in Namibia. *Environmental monitoring and assessment*, 176(1), pp.531-547.
- Hyde, P., Dubayah, R., Walker, W., Blair, J.B., Hofton, M. and Hunsaker, C., 2006. Mapping forest structure for wildlife habitat analysis using multi-sensor (LiDAR, SAR/InSAR, ETM+, Quickbird) synergy. *Remote Sensing of Environment*, 102(1-2), pp.63-73.
- Ibrahim, S.A., Balzter, H., Tansey, K., Tsutsumida, N. and Mathieu, R., 2018. Estimating fractional cover of plant functional types in African savannah from harmonic analysis of MODIS time-series data. *International Journal of Remote Sensing*, 39(9), pp.2718-2745.
- Ilavajhala, S., Davies, D., Schmaltz, J.E. and Murphy, K.J., 2014, December. Early warning of active fire hotspots through NASA FIRMS fire information system. In *2014 AGU Fall Meeting*. AGU.
- Immitzer, M., Böck, S., Einzmann, K., Vuolo, F., Pinnel, N., Wallner, A. and Atzberger, C., 2018. Fractional cover mapping of spruce and pine at 1 ha resolution combining very high and medium spatial resolution satellite imagery. *Remote sensing of environment*, 204, pp.690-703.
- IPCC, 2014. Climate change 2014–Impacts, adaptation and vulnerability: Regional aspects. Cambridge: Cambridge University Press.
- IPCC. (2007). Climate Change 2007 : An Assessment of the Intergovernmental Panel on Climate Change'. Cambridge: Cambridge University Press.
- IPCC. (2014). Climate change 2014–Impacts, adaptation and vulnerability: Regional aspects. Niang, I., O.C. Ruppel, M.A. Abdrabo, A. Essel, C. Lennard, J. Padgham, and P. Urquhart, 2014: Africa. In: Climate Change 2014: Impacts, Adaptation, and Vulnerability. Part B: Regional Aspects. Contribution of Working Group II to the Fifth Assessment Report of the Intergovernmental Panel on Climate Change [Barros, V.R., C.B. Field, D.J. Dokken, M.D. Mastrandrea, K.J. Mach, T.E. Bilir, M. Chatterjee, K.L. Ebi, Y.O. Estrada, R.C. Genova, B. Girma, E.S. Kissel, A.N. Levy, S. MacCracken, P.R. Mastrandrea, and L.L. White (eds.)]. Cambridge University Press, Cambridge, United Kingdom and New York, NY, USA, pp. 1199-1265
- IPCC. 2003. Definitions and Methodological Options to Inventory Emissions from Direct Human induced Degradation of Forests and Devegetation of Other Vegetation Types. Penman, J., Gytarsky, M., Krug, T., Kruger, D., Pipatti, R., Buendia, L., Miwa, K., Ngara, T., Tanabe, K. and Wagner, F. (eds.), IPCC-IGES, Kanagawa. IPCC National Greenhouse Gas Inventories Programme, Japan. [http://www.ipcc-nggip.iges.or.jp/public/gpplulucf/degradation\\_contents.htm](http://www.ipcc-nggip.iges.or.jp/public/gpplulucf/degradation_contents.htm)
- IPCC., 2007. Climate Change 2007 : An Assessment of the Intergovernmental Panel on Climate Change'. Cambridge: Cambridge University Press.
- IPCC., 2014. Climate change 2014–Impacts, adaptation and vulnerability: Regional aspects. Cambridge: Cambridge University Press.
- ITTO. 2002. Guidelines for the restoration, management and rehabilitation of degraded and secondary tropical forests (No. 13). International Tropical Timber Organization (ITTO).
- IUCN. (2020). The IUCN Red List of Threatened Species. [www.iucnredlist.org/species/](http://www.iucnredlist.org/species/). (accessed 21 February 2020).
- Jamali, S., Jönsson, P., Eklundh, L., Ardö, J. and Seaquist, J., 2015. Detecting changes in vegetation trends using time series segmentation. *Remote Sensing of Environment*, 156, pp.182-195.

- Jamali, S., Seaquist, J., Eklundh, L. and Ardö, J., 2014. Automated mapping of vegetation trends with polynomials using NDVI imagery over the Sahel. *Remote Sensing of Environment*, 141, pp.79-89.
- James, G., Witten, D., Hastie, T. and Tibshirani, R., 2013. An introduction to statistical learning (Vol. 112, 101). New York: springer.
- Janssen, L.L. and Vanderwel, F.J., 1994. Accuracy assessment of satellite derived land-cover data: a review. *Photogrammetric engineering and remote sensing;(United States)*, 60(4).
- Janzen, D. H., 1988. Tropical dry forests. *Biodiversity*, 130-137.
- Jensen, J.R., 2005. Digital image processing: a remote sensing perspective. *Upper Saddle River, NJ: sPrentice Hall*.
- Jin, S. and Sader, S.A., 2005. Comparison of time series tasseled cap wetness and the normalized difference moisture index in detecting forest disturbances. *Remote sensing of Environment*, 94(3), pp.364-372.
- Jolly, W.M. and Running, S.W., 2004. Effects of precipitation and soil water potential on drought deciduous phenology in the Kalahari. *Global Change Biology*, 10(3), pp.303-308.
- Jones, M.O., Jones, L.A., Kimball, J.S. and McDonald, K.C. (2011). Satellite passive microwave remote sensing for monitoring global land surface phenology. *Remote Sensing of Environment*, 115(4), pp.1102-1114.
- Joshi, N., Baumann, M., Ehammer, A., Fensholt, R., Grogan, K., Hostert, P., Jepsen, M.R., Kuemmerle, T., Meyfroidt, P., Mitchard, E.T. and Reiche, J., 2016. A review of the application of optical and radar remote sensing data fusion to land use mapping and monitoring. *Remote Sensing*, 8(1), p.70.
- Junker, J., 2009. An analysis of numerical trends in African elephant populations (Doctoral dissertation, *University of Pretoria*).
- Kajisa, T., Murakami, T., Mizoue, N., Top, N. and Yoshida, S., 2009. Object-based forest biomass estimation using Landsat ETM+ in Kampong Thom Province, Cambodia. *Journal of Forest Research*, 14(4), pp.203-211.
- Kamwi, J.M. and Mbidzo, M., 2020. Impact of land use and land cover changes on landscape structure in the dry lands of Southern Africa: a case of the Zambezi Region, Namibia. *GeoJournal*, pp.1-12.
- Kamwi, J.M., Chirwa, P.W., Manda, S.O., Graz, P.F. and Kätsch, C., 2015. Livelihoods, land use and land cover change in the Zambezi Region, Namibia. *Population and Environment*, 37(2), pp.207-230.
- Kamwi, J.M., Kaetsch, C., Graz, F.P., Chirwa, P. and Manda, S., 2017. Trends in land use and land cover change in the protected and communal areas of the Zambezi Region, Namibia. *Environmental monitoring and assessment*, 189(5), p.242.
- Karidozo, M., La Grange, M. and Osborn, F.V., 2016. Assessment of the human wildlife conflict mitigation measures being implemented by the Kavango-Zambezi Transfrontier Conservation Area (KAZA TFCA) partner countries. Report to the KAZA TFCA Secretariat. *Report to the KAZA TFCA Secretariat (BMZ No.: 2009 66 788 and BMZ No.: 2006 65 646)*.

- Kasischke, E.S., Melack, J.M. and Dobson, M.C., 1997. The use of imaging radars for ecological applications—A review. *Remote sensing of environment*, 59(2), pp.141-156.
- Kattenborn, T., Leitloff, J., Schiefer, F. and Hinz, S. (2021). Review on Convolutional Neural Networks (CNN) in vegetation remote sensing. *ISPRS Journal of Photogrammetry and Remote Sensing*, 173, pp.24-49.
- KAZA., 2014., Kavango-Zambezi Transfrontier Conservation Area, Master Integrated Development Plan 2015-2020.
- Kellndorfer, J.M., Walker, W.S., LaPoint, E., Kirsch, K., Bishop, J. and Fiske, G., 2010. Statistical fusion of Lidar, InSAR, and optical remote sensing data for forest stand height characterization: A regional-scale method based on LVIS, SRTM, Landsat ETM+, and ancillary data sets. *Journal of Geophysical Research: Biogeosciences*, 115(G2).
- Kennedy, R.E., Andréfouët, S., Cohen, W.B., Gómez, C., Griffiths, P., Hais, M., Healey, S.P., Helmer, E.H., Hostert, P., Lyons, M.B. and Meigs, G.W., 2014. Bringing an ecological view of change to Landsat-based remote sensing. *Frontiers in Ecology and the Environment*, 12(6), pp.339-346.
- Kennedy, R.E., Yang, Z. and Cohen, W.B., 2010. Detecting trends in forest disturbance and recovery using yearly Landsat time series: 1. LandTrendr—Temporal segmentation algorithms. *Remote Sensing of Environment*, 114(12), pp.2897-2910.
- Kimura, T., Imai, T., Sakaizawa, D., Murooka, J. and Mitsunashi, R., 2017, July. The overview and status of vegetation Lidar mission, MOLI. In *2017 IEEE International Geoscience and Remote Sensing Symposium (IGARSS)* (pp. 4228-4230). IEEE.
- King, E. (2014). Southern Africa's Dryland Forests and Climate Change Adaptation. A policy briefing prepared for Governance of Africa's Resources Programme. [https://media.africaportal.org/documents/saia\\_spb\\_91\\_king\\_20140702.pdf/](https://media.africaportal.org/documents/saia_spb_91_king_20140702.pdf/) (accessed 23 August 2020).
- Klogo, G.S., Gasonoo, A. and Ampomah, I.K., 2013. On the Performance of Filters for Reduction of Speckle Noise in SAR Images off the Coast of the Gulf of Guinea. *arXiv preprint arXiv:1312.2383*.
- Koch, B., 2010. Status and future of laser scanning, synthetic aperture radar and hyperspectral remote sensing data for forest biomass assessment. *ISPRS Journal of Photogrammetry and Remote Sensing*, 65(6), 581-590.
- Korontzi, S., Justice, C.O. and Scholes, R.J., 2003. Influence of timing and spatial extent of savanna fires in southern Africa on atmospheric emissions. *Journal of Arid Environments*, 54(2), pp.395-404.
- Kuenzer, C., Bluemel, A., Gebhardt, S., Quoc, T.V. and Dech, S., 2011. Remote sensing of mangrove ecosystems: A review. *Remote Sensing*, 3(5), pp.878-928.
- Kuplich, T.M., Moreira, A. and Fontana, D.C., 2013. Série temporal de índice de vegetação sobre diferentes tipologias vegetais no Rio Grande do Sul. *Revista Brasileira de Engenharia Agrícola e Ambiental*, 17, pp.1116-1123.
- Kussul, N., Lavreniuk, M., Skakun, S. and Shelestov, A. (2017). Deep learning classification of land cover and crop types using remote sensing data. *IEEE Geoscience and Remote Sensing Letters*, 14(5), pp.778-782.

- Lambin, E.F. and Ehrlich, D., 1997. Land-cover changes in sub-Saharan Africa (1982–1991): Application of a change index based on remotely sensed surface temperature and vegetation indices at a continental scale. *Remote sensing of environment*, 61(2), pp.181-200.
- Lambin, E.F. and Meyfroidt, P., 2010. Land use transitions: Socio-ecological feedback versus socio-economic change. *Land use policy*, 27(2), pp.108-118.
- Lambin, E.F., Geist, H.J. and Lepers, E., 2003. Dynamics of land-use and land-cover change in tropical regions. *Annual review of environment and resources*, 28(1), pp.205-241.
- Latifi, H., Nothdurft, A. and Koch, B., 2010. Non-parametric prediction and mapping of standing timber volume and biomass in a temperate forest: application of multiple optical/LiDAR-derived predictors. *Forestry*, 83(4), pp.395-407.
- Laurin, G.V., Puletti, N., Hawthorne, W., Liesenberg, V., Corona, P., Papale, D., Chen, Q. and Valentini, R., 2016. Discrimination of tropical forest types, dominant species, and mapping of functional guilds by hyperspectral and simulated multispectral Sentinel-2 data. *Remote Sensing of Environment*, 176, 163-176.
- Lawal, S., Lennard, C., Jack, C., Wolski, P., Hewitson, B. and Abiodun, B., 2019. The observed and model-simulated response of southern African vegetation to drought. *Agricultural and Forest Meteorology*, 279, p.107698.
- Lawley, V., Lewis, M., Clarke, K. and Ostendorf, B. (2016). Site-based and remote sensing methods for monitoring indicators of vegetation condition: An Australian review. *Ecological Indicators*, 60, pp.1273-1283.
- Le Canut, P., Andreae, M.O., Harris, G.W., Wienhold, F.G. and Zenker, T., 1996. Airborne studies of emissions from savanna fires in southern Africa: 1. Aerosol emissions measured with a laser optical particle counter. *Journal of Geophysical Research: Atmospheres*, 101(D19), pp.23615-23630.
- Le Houérou, H.N., 1996. Climate change, drought and desertification. *Journal of arid Environments*, 34(2), pp.133-185.
- Lehmann, C.E., Anderson, T.M., Sankaran, M., Higgins, S.I., Archibald, S., Hoffmann, W.A., Hanan, N.P., Williams, R.J., Fensham, R.J., Felfili, J. and Hutley, L.B., 2014. Savanna vegetation-fire-climate relationships differ among continents. *Science*, 343(6170), pp.548-552.
- Lehmann, E.A., Caccetta, P., Lowell, K., Mitchell, A., Zhou, Z.S., Held, A., Milne, T. and Tapley, I., 2015. SAR and optical remote sensing: Assessment of complementarity and interoperability in the context of a large-scale operational forest monitoring system. *Remote Sensing of Environment*, 156, pp.335-348.
- Leite, A., Cáceres, A., Melo, M., Mills, M.S. and Monteiro, A.T., 2018. Reducing emissions from Deforestation and forest Degradation in Angola: Insights from the scarp forest conservation 'hotspot'. *Land Degradation & Development*, 29(12), pp.4291-4300.
- Lesolle, D., 2012. SADC Policy Paper on Climate Change: Assessing the Policy Options for SADC Member States; SADC Secretariat, Policy, Planning. *Resource Mobilisation Directorate: Gaborone, Botswana*.
- Lewis, S.L., Sonké, B., Sunderland, T., Begne, S.K., Lopez-Gonzalez, G., Van Der Heijden, G.M., Phillips, O.L., Affum-Baffoe, K., Baker, T.R., Banin, L. and Bastin, J.F., 2013. Above-ground biomass and structure of 260 African tropical forests. *Philosophical Transactions of the Royal Society B: Biological Sciences*, 368(1625), p.20120295.

- Li, A., Dhakal, S., Glenn, N.F., Spaete, L.P., Shinneman, D.J., Pilliod, D.S., Arkle, R.S. and McIlroy, S.K., 2017. Lidar aboveground vegetation biomass estimates in shrublands: Prediction, uncertainties and application to coarser scales. *Remote Sensing*, 9(9), p.903.
- Li, C., Gong, P., Wang, J., Zhu, Z., Biging, G.S., Yuan, C., Hu, T., Zhang, H., Wang, Q., Li, X. and Liu, X., 2017. The first all-season sample set for mapping global land cover with Landsat-8 data. *Science Bulletin*, 62(7), pp.508-515.
- Li, C., Zhou, L. and Xu, W., 2021. Estimating aboveground biomass using Sentinel-2 MSI data and ensemble algorithms for grassland in the Shengjin Lake Wetland, China. *Remote Sensing*, 13(8), 1595
- Liao, W., Van Coillie, F., Gao, L., Li, L., Zhang, B. and Chanussot, J. (2018). Deep learning for fusion of APEX hyperspectral and full-waveform LiDAR remote sensing data for tree species mapping. *IEEE Access*, 6, pp.68716-68729.
- Liaw, A., Wiener, M., 2002. Classification and regression by randomForest. *R news*, 2(3), 18-22.
- Liaw, A., Wiener, M., 2002. Classification and regression by randomForest. *R news*, 2(3), 18-22.
- Linares-Palomino, R., Oliveira-Filho, A.T. and Pennington, R.T., 2011. Neotropical seasonally dry forests: diversity, endemism, and biogeography of woody plants. In *Seasonally dry tropical forests* (pp. 3-21). *Island Press*, Washington, DC.
- Liu, G., Liu, H. and Yin, Y., 2013. Global patterns of NDVI-indicated vegetation extremes and their sensitivity to climate extremes. *Environmental Research Letters*, 8(2), p.025009.
- Liu, X. and Zhou, J., 2021. Assessment of the Continuous Extreme Drought Events in Namibia during the last decade. *Water*, 13(20), 2942.
- Liu, X., Wigneron, J.P., Fan, L., Frappart, F., Ciais, P., Baghdadi, N., Zribi, M., Jagdhuber, T., Li, X., Wang, M. and Bai, X. (2021). ASCAT IB: A radar-based vegetation optical depth retrieved from the ASCAT scatterometer satellite. *Remote Sensing of Environment*, 264, p.112587.
- Liu, Y. A., Gong, W. S., Xing, Y. Q., Hu, X. Y., ong, J. Y., 2019. Estimation of the forest stand mean height and aboveground biomass in Northeast China using SAR Sentinel-1B, multispectral Sentinel-2A, and DEM imagery. *ISPRS Journal of Photogrammetry and Remote Sensing*, 151, 277-289.
- Liu, Y.Y., De Jeu, R.A., McCabe, M.F., Evans, J.P. and Van Dijk, A.I. (2011). Global long-term passive microwave satellite-based retrievals of vegetation optical depth. *Geophysical Research Letters*, 38(18).
- Liu, Y.Y., Van Dijk, A.I., De Jeu, R.A., Canadell, J.G., McCabe, M.F., Evans, J.P. and Wang, G. (2015). Recent reversal in loss of global terrestrial biomass. *Nature Climate Change*, 5(5), pp.470-474.
- Liu, Z., Wimberly, M.C. and Dwomoh, F.K., 2017. Vegetation dynamics in the upper guinean forest region of West Africa from 2001 to 2015. *Remote Sensing*, 9(1), p.5.
- Lu, D. and Weng, Q., 2005. Urban classification using full spectral information of Landsat ETM+ imagery in Marion County, Indiana. *Photogrammetric Engineering & Remote Sensing*, 71(11), pp.1275-1284.
- Lu, D., 2006. The potential and challenge of remote sensing-based biomass estimation. *International journal of remote sensing*, 27(7), pp.1297-1328.

- Lu, D., Batistella, M., Moran, E. and de Miranda, E.E., 2008. A comparative study of Landsat TM and SPOT HRG images for vegetation classification in the Brazilian Amazon. *Photogrammetric Engineering & Remote Sensing*, 74(3), pp.311-321.
- Lu, D., Chen, Q., Wang, G., Liu, L., Li, G., Moran, E., 2016. A survey of remote sensing-based aboveground biomass estimation methods in forest ecosystems. *International Journal of Digital Earth*, 9(1), 63-105.
- Lu, D., Chen, Q., Wang, G., Moran, E., Batistella, M., Zhang, M., Vaglio Laurin, G. and Saah, D., 2012. Aboveground forest biomass estimation with Landsat and LiDAR data and uncertainty analysis of the estimates. *International Journal of Forestry Research*, 2012.
- Lu, D., Mausel, P., Brondizio, E., Moran, E., 2004. Relationships between forest stand parameters and Landsat TM spectral responses in the Brazilian Amazon Basin. *Forest Ecology and Management*, 198(1-3), 149-167.
- Lu, D., Moran, E. and Batistella, M., 2003. Linear mixture model applied to Amazonian vegetation classification. *Remote sensing of environment*, 87(4), pp.456-469.
- Lucas, R., Accad, A., Randall, L., Bunting, P., Armston, J., 2008. Assessing Human Impacts on Australian Forests through Integration of Remote Sensing Data, in Laforzezza, R., Chen, J., Sanesi, G., Crow, Th.R. (Eds.), *Patterns and Processes in Forest Landscapes*, Springer, Dordrecht, pp. 213-239.
- Lucas, R.M., Cronin, N., Lee, A., Moghaddam, M., Witte, C. and Tickle, P., 2006. Empirical relationships between AIRSAR backscatter and LiDAR-derived forest biomass, Queensland, Australia. *Remote Sensing of Environment*, 100(3), 407-425.
- Lucas, R.M., Mitchell, A.L. and Armston, J., 2015. Measurement of forest above-ground biomass using active and passive remote sensing at large (subnational to global) scales. *Current Forestry Reports*, 1(3), pp.162-177.
- Lück, W. and Van Niekerk, A., 2016. Evaluation of a rule-based compositing technique for Landsat-5 TM and Landsat-7 ETM+ images. *International Journal of Applied Earth Observation and Geoinformation*, 47, pp.1-14
- Lund, H.G., 2009. What is a degraded forest. Gainesville, VA. USA: Forest Information Services.
- Lyon, B. and Mason, S.J., 2007. The 1997–98 summer rainfall season in southern Africa. Part I: Observations. *Journal of Climate*, 20(20), pp.5134-5148.
- Madonsela, S., Cho, M.A., Ramoelo, A., Mutanga, O. and Naidoo, L., 2018. Estimating tree species diversity in the savannah using NDVI and woody canopy cover. *International journal of applied earth observation and geoinformation*, 66, pp.106-115.
- Maglione, P., 2016. Very high resolution optical satellites: An overview of the most commonly used. *American Journal of Applied Sciences*, 13(1), p.91.
- Maliva, R. and Missimer, T., 2012. Aridity and drought. In *Arid lands water evaluation and management* (pp. 21-39). Springer, Berlin, Heidelberg.
- Manatsha, B. T., Malebang, G. G., 2016. The Botswana-Japan Diplomatic Relations, 1966-2016. *Botswana Notes and Records*, 48, 97-108.

- Mapfumo, R.B., Murwira, A., Masocha, M. and Andriani, R., 2016. The relationship between satellite-derived indices and species diversity across African savanna ecosystems. *International journal of applied earth observation and geoinformation*, 52, pp.306-317.
- Mareya, H.T., Tagwireyi, P., Ndaimani, H., Gara, T.W. and Gwenzi, D., 2018. Estimating tree crown area and aboveground biomass in miombo woodlands from high-resolution RGB-only imagery. *IEEE Journal of selected topics in applied earth observations and remote sensing*, 11(3), pp.868-875.
- Marín-Spiotta, E., Cusack, D.F., Ostertag, R. and Silver, W.L. (2008). Trends in above and belowground carbon with forest regrowth after agricultural abandonment in the neotropics. In *Post-agricultural succession in the neotropics* (pp. 22-72). Springer, New York, NY.
- Marston, C.G., Wilkinson, D.M., Sponheimer, M., Codron, D., Codron, J. and O'Regan, H.J., 2020. 'Remote' behavioural ecology: do megaherbivores consume vegetation in proportion to its presence in the landscape?. *PeerJ*, 8, p.e8622.
- Marta, S., 2018. Planet Imagery Product Specifications. *Planet Labs: San Francisco, CA, USA*, p.91.
- Martens, B., Miralles, D.G., Lievens, H., Van Der Schalie, R., De Jeu, R.A., Fernández-Prieto, D., Beck, H.E., Dorigo, W.A. and Verhoest, N.E., 2017. GLEAM v3: Satellite-based land evaporation and root-zone soil moisture. *Geoscientific Model Development*, 10(5), pp.1903-1925.
- Marumbwa, F.M., Cho, M.A. and Chirwa, P.W., 2020. An assessment of remote sensing-based drought index over different land cover types in southern Africa. *International Journal of Remote Sensing*, 41(19), pp.7368-7382.
- Marumbwa, F.M., Cho, M.A. and Chirwa, P.W., 2021. Geospatial analysis of meteorological drought impact on Southern Africa biomes. *International Journal of Remote Sensing*, 42(6), pp.2155-2173.
- Masiello, G., Cersosimo, A., Mastro, P., Serio, C., Venafra, S. and Pasquariello, P., 2020, September. Emissivity-based vegetation indices to monitor deforestation and forest degradation in the Congo basin rainforest. In *Remote Sensing for Agriculture, Ecosystems, and Hydrology XXII* (Vol. 11528, p. 115280L). *International Society for Optics and Photonics*.
- Mason, P.J., Zillman, J.W., Simmons, A., Lindstrom, E.J., Harrison, D.E., Dolman, H., Bojinski, S., Fischer, A., Latham, J., Rasmussen, J. and Arkin, P., 2009, December. Implementation plan for the global observing system for climate in support of the UNFCCC (2010 Update). In *Proceedings of the Conference of the Parties (COP), Copenhagen, Denmark* (pp. 7-18).
- Mason, S.J. and Tyson, P., 2000. The occurrence and predictability of droughts over southern Africa, *Routledge*. <https://doi.org/10.4324/9781315830896/> (accessed 04 August 2021).
- Matavire, M. M., Sibanda, M., & Dube, T. (2015). Assessing the aftermath of the fast track land reform programme in Zimbabwe on land-use and land-cover changes. *Transactions of the Royal Society of South Africa*, 70(2), pp.181-186.
- Mathieu, R., Main, R., Roy, D.P., Naidoo, L. and Yang, H., 2019. The Effect of Surface Fire in Savannah Systems in the Kruger National Park (KNP), South Africa, on the Backscatter of C-Band Sentinel-1 Images. *Fire*, 2(3), p.37.
- Mathieu, R., Naidoo, L., Cho, M.A., Leblon, B., Main, R., Wessels, K., Asner, G.P., Buckley, J., Van Aardt, J., Erasmus, B.F. and Smit, I.P., 2013. Toward structural assessment of semi-arid

African savannahs and woodlands: The potential of multitemporal polarimetric RADARSAT-2 fine beam images. *Remote Sensing of Environment*, 138, pp.215-231.

Matswiri, G.M., 2017. Two in one: explaining the management of the Okavango Delta World Heritage Site, Botswana (*Master's thesis, University of Cape Town*).

Mayes, M., Mustard, J., Melillo, J., Neill, C. and Nyadzi, G., 2017. Going beyond the green: senesced vegetation material predicts basal area and biomass in remote sensing of tree cover conditions in an African tropical dry forest (miombo woodland) landscape. *Environmental Research Letters*, 12(8), p.085004.

Mayr, M.J., Vanselow, K.A. and Samimi, C., 2018. Fire regimes at the arid fringe: A 16-year remote sensing perspective (2000–2016) on the controls of fire activity in Namibia from spatial predictive models. *Ecological Indicators*, 91, pp.324-337.

Mbow, C., Brandt, M., Ouedraogo, I., De Leeuw, J. and Marshall, M., 2015. What four decades of earth observation tell us about land degradation in the Sahel?. *Remote Sensing*, 7(4), pp.4048-4067.

McCarthy, J., Gumbricht, T. and McCarthy, T.S., 2005. Ecoregion classification in the Okavango Delta, Botswana from multitemporal remote sensing. *International Journal of Remote Sensing*, 26(19), pp.4339-4357.

McClean, C.J., Lovett, J.C., Küper, W., Hannah, L., Sommer, J.H., Barthlott, W., Termansen, M., Smith, G.F., Tokumine, S. and Taplin, J.R., 2005. African plant diversity and climate change. *Annals of the Missouri Botanical Garden*, pp.139-152.

McElhinny, C., Gibbons, P., Brack, C. and Bauhus, J., 2005. Forest and woodland stand structural complexity: its definition and measurement. *Forest Ecology and Management*, 218(1-3), pp.1-24.

McGann, J., 2004. The current status of unfccc article 6 work program implementation in Namibia. *In African Workshop on Article*, vol. 6, pp. 28-30.

McIntyre, C., 2010. Botswana: Okavango Delta-Chobe-Northern Kalahari: *Bradt Travel Guides*, pp. 197-214.

McKenzie, J.E., Brennan, S.E., Ryan, R.E., Thomson, H.J., Johnston, R.V. and Thomas, J., 2019. Defining the criteria for including studies and how they will be grouped for the synthesis. *Cochrane handbook for systematic reviews of interventions*, pp.33-65.

McNicol, I.M., Ryan, C.M. and Mitchard, E.T., 2018. Carbon losses from deforestation and widespread degradation offset by extensive growth in African woodlands. *Nature communications*, 9(1), pp.1-11.

Meadows, M.E., 2006. Global change and southern Africa. *Geographical Research*, 44(2), pp.135-145.

Melton, D.A., 1985. The status of elephants in northern Botswana. *Biological Conservation*, 31(4), 317-333.

Méndez, V.E., Gliessman, S.R. and Gilbert, G.S. (2007). Tree biodiversity in farmer cooperatives of a shade coffee landscape in western El Salvador. *Agriculture, Ecosystems & Environment*, 119(1-2), pp.145-159.



- Mendivelso, H.A., Camarero, J.J., Gutiérrez, E. and Zuidema, P.A. (2014). Time-dependent effects of climate and drought on tree growth in a Neotropical dry forest: Short-term tolerance vs. long-term sensitivity. *Agricultural and Forest Meteorology*, 188, pp.13-23
- Menzel, A. and Fabian, P., 1999. Growing season extended in Europe. *Nature*, 397(6721), pp.659-659.
- Metternicht, G., Zinck, J.A., Blanco, P.D. and del Valle, H.F. (2010). Remote sensing of land degradation: Experiences from Latin America and the Caribbean. *Journal of environmental quality*, 39(1), pp.42-61.
- Meyer, M., Klingelhoefter, E., Naidoo, R., Wingate, V. and Börner, J., 2021. Tourism opportunities drive woodland and wildlife conservation outcomes of community-based conservation in Namibia's Zambezi region. *Ecological Economics*, 180, p.106863.
- Meyer, T., D'Odorico, P., Okin, G.S., Shugart, H.H., Caylor, K.K., O'Donnell, F.C., Bhattachan, A. and Dintwe, K., 2014. An analysis of structure: biomass structure relationships for characteristic species of the western Kalahari, Botswana. *African journal of ecology*, 52(1), pp.20-29.
- Michelakis, D., Stuart, N., Lopez, G., Linares, V. and Woodhouse, I.H., 2014. Local-scale mapping of biomass in tropical lowland pine savannas using ALOS PALSAR. *Forests*, 5(9), pp.2377-2399.
- Middleton, N. and Thomas, D., 1997. World atlas of desertification.. ed. 2. Edward Arnold, London. (pp. 66).
- Midgley, G.F. and Thuiller, W., 2011. Potential responses of terrestrial biodiversity in Southern Africa to anthropogenic climate change. *Regional Environmental Change*, 11(1), pp.127-135.
- Miles, L., Newton, A. C., DeFries, R. S., Ravilious, C., May, I., Blyth, S., Kapos, V., Gordon, J. E., 2006. A global overview of the conservation status of tropical dry forests. *Journal of Biogeography*, 33(3), 491-505.
- Mitchard, E. T., Saatchi, S. S., Baccini, A., Asner, G. P., Goetz, S. J., Harris, N. L., Brown, S., 2013. Uncertainty in the spatial distribution of tropical forest biomass: a comparison of pan-tropical maps. *Carbon Balance and Management*, 8(1), 1-13.
- Mitchard, E.T. and Flintrop, C.M. (2013). Woody encroachment and forest degradation in sub-Saharan Africa's woodlands and savannas 1982–2006. *Philosophical Transactions of the Royal Society B: Biological Sciences*, 368(1625), p.20120406.
- Mitchard, E.T., Saatchi, S.S., Lewis, S.L., Feldpausch, T.R., Woodhouse, I.H., Sonké, B., Rowland, C. and Meir, P., 2011. Measuring biomass changes due to woody encroachment and deforestation/degradation in a forest–savanna boundary region of central Africa using multi-temporal L-band radar backscatter. *Remote Sensing of Environment*, 115(11), 2861-2873.
- Mitchard, E.T., Saatchi, S.S., Woodhouse, I.H., Nangendo, G., Ribeiro, N.S., Williams, M., Ryan, C.M., Lewis, S.L., Feldpausch, T.R. and Meir, P., 2009. Using satellite radar backscatter to predict above-ground woody biomass: A consistent relationship across four different African landscapes. *Geophysical Research Letters*, 36(23).
- Mitchell, A.L., Rosenqvist, A. and Mora, B., 2017. Current remote sensing approaches to monitoring forest degradation in support of countries measurement, reporting and verification (MRV) systems for REDD+. *Carbon balance and management*, 12(1), pp.1-22.

- Moher, D., Liberati, A., Tetzlaff, J., Altman, D.G. and Prisma Group, 2009. Preferred reporting items for systematic reviews and meta-analyses: the PRISMA statement. *PLoS medicine*, 6(7), p.e1000097.
- Mooney, H. A., Bullock, S. H., and Medina, E., 1995. Introduction. In: Bullock SH, Mooney HA, Medina E (eds) Seasonally dry tropical forests. *Cambridge: Cambridge University Press*.
- Moore, C.E., Brown, T., Keenan, T.F., Duursma, R.A., Van Dijk, A.I., Beringer, J., Culvenor, D., Evans, B., Huete, A., Hutley, L.B. and Maier, S. (2016). Reviews and syntheses: Australian vegetation phenology: new insights from satellite remote sensing and digital repeat photography. *Biogeosciences*, 13(17), pp.5085-5102.
- Morley, P.J., Donoghue, D.N., Chen, J.C. and Jump, A.S., 2019. Quantifying structural diversity to better estimate change at mountain forest margins. *Remote Sensing of Environment*, 223, pp.291-306.
- Morley, P.J., Jump, A.S., West, M.D. and Donoghue, D.N., 2020. Spectral response of chlorophyll content during leaf senescence in European beech trees. *Environmental Research Communications*, 2(7), p.071002.
- Mosugelo, D. K., Moe, S. R., Ringrose, S., Nellemann, C., 2002. Vegetation changes during a 36-year period in northern Chobe National Park, Botswana. *African Journal of Ecology*, 40(3), 232-240.
- Mouillot, F., Schultz, M.G., Yue, C., Cadule, P., Tansey, K., Ciais, P. and Chuvieco, E., 2014. Ten years of global burned area products from spaceborne remote sensing—A review: Analysis of user needs and recommendations for future developments. *International Journal of Applied Earth Observation and Geoinformation*, 26, pp.64-79.
- Mpakairi, K.S., Tagwireyi, P., Ndaimani, H. and Madiri, H.T., 2019. Distribution of wildland fires and possible hotspots for the Zimbabwean component of Kavango-Zambezi Transfrontier Conservation Area. *South African Geographical Journal= Suid-Afrikaanse Geografiese Tydskrif*, 101(1), pp.110-120.
- Muraoka, H. and Koizumi, H., 2009. Satellite Ecology (SATECO)—linking ecology, remote sensing and micrometeorology, from plot to regional scale, for the study of ecosystem structure and function. *Journal of plant research*, 122(1), pp.3-20.
- Murphy, C.A., 2008. Living in a Global Commons—the case of residents of a national park in the Kavango-Zambezi Transfrontier Conservation Area (KaZa TFCA), southern Africa.
- Murphy, P.G. and Lugo, A.E., 1986. Ecology of tropical dry forest. *Annual review of ecology and systematics*, 17(1), pp.67-88.
- Mutanga, O. and Rugege, D., 2006. Integrating remote sensing and spatial statistics to model herbaceous biomass distribution in a tropical savanna. *International Journal of Remote Sensing*, 27(16), pp.3499-3514.
- Mutanga, O. and Skidmore, A.K., 2004. Narrow band vegetation indices overcome the saturation problem in biomass estimation. *International journal of remote sensing*, 25(19), pp.3999-4014.
- Mutanga, O., Adam, E. and Cho, M.A., 2012. High density biomass estimation for wetland vegetation using WorldView-2 imagery and random forest regression algorithm. *International Journal of Applied Earth Observation and Geoinformation*, 18, 399-406.

- Mutanga, O., Dube, T. and Ahmed, F., 2016. Progress in remote sensing: vegetation monitoring in South Africa. *South African Geographical Journal*, 98(3), pp.461-471.
- Mutanga, O., Van Aardt, J. and Kumar, L., 2009. Imaging spectroscopy (hyperspectral remote sensing) in southern Africa: an overview. *South African Journal of Science*, 105(5), pp.193-198.
- Myeong, S., Nowak, D.J., Hopkins, P.F. and Brock, R.H., 2001. Urban cover mapping using digital, high-spatial resolution aerial imagery. *Urban ecosystems*, 5(4), pp.243-256.
- Myneni, R.B., Keeling, C.D., Tucker, C.J., Asrar, G. and Nemani, R.R., 1997. Increased plant growth in the northern high latitudes from 1981 to 1991. *Nature*, 386(6626), pp.698-702.
- NACSO. (2014). The state of community conservation in Namibia. A review of communal conservancies, community forests and other CBNRM initiatives. *Windhoek, NASCO*.
- Næsset, E., McRoberts, R.E., Pekkarinen, A., Saatchi, S., Santoro, M., Trier, Ø.D., Zahabu, E. and Gobakken, T., 2020. Use of local and global maps of forest canopy height and aboveground biomass to enhance local estimates of biomass in miombo woodlands in Tanzania. *International Journal of Applied Earth Observation and Geoinformation*, 93, 102138.
- Naidoo, L., Mathieu, R., Main, R., Wessels, K. and Asner, G.P., 2016. L-band Synthetic Aperture Radar imagery performs better than optical datasets at retrieving woody fractional cover in deciduous, dry savannahs. *International journal of applied earth observation and geoinformation*, 52, pp.54-64.
- Naidoo, R., Chase, M.J., Beytell, P., Du Preez, P., Landen, K., Stuart-Hill, G. and Taylor, R., 2016. A newly discovered wildlife migration in Namibia and Botswana is the longest in Africa. *Oryx*, 50(1), pp.138-146.
- Naidoo, R., Du Preez, P., Stuart-Hill, G., Jago, M. and Wegmann, M., 2012. Home on the range: factors explaining partial migration of African buffalo in a tropical environment. *PLoS one*, 7(5), p.e36527.
- Naidoo, S., Davis, C. and Van Garderen, E.A., 2013. Forests, rangelands and climate change in southern Africa. *Forests and climate change working paper*, 12.
- Naik, M., 2015. Modeling the potential impacts of vegetation change on the future climate of Southern Africa (*Master's thesis, University of Cape Town*).
- Nandy, S., Singh, R., Ghosh, S., Watham, T., Kushwaha, S.P.S., Kumar, A.S. and Dadhwal, V.K., 2017. Neural network-based modelling for forest biomass assessment. *Carbon Management*, 8(4), 305-317.
- Nanni, A.S., Sloan, S., Aide, T.M., Graesser, J., Edwards, D. and Grau, H.R. (2019). The neotropical reforestation hotspots: A biophysical and socioeconomic typology of contemporary forest expansion. *Global environmental change*, 54, pp.148-159.
- Narine, L.L., Popescu, S.C. and Malambo, L. (2019). Synergy of ICESat-2 and Landsat for mapping forest aboveground biomass with deep learning. *Remote Sensing*, 11(12), p.1503.
- Nemani, R.R., Keeling, C.D., Hashimoto, H., Jolly, W.M., Piper, S.C., Tucker, C.J., Myneni, R.B. and Running, S.W., 2003. Climate-driven increases in global terrestrial net primary production from 1982 to 1999. *science*, 300(5625), pp.1560-1563.
- Niang, I., Ruppel, O. C., Abdrabo, M. A., Essel, A., Lennard, C., Padgham, J., and Urquhart, P., 2014. Climate Change 2014: Impacts, Adaptation and Vulnerability - Contributions of the

Working Group II to the Fifth Assessment Report of the Intergovernmental Panel on Climate Change., (pp. 1199–1265).

- Nichols, C., Vandewalle, M., Alexander, K., 2017. Emerging threats to dryland forest resources: elephants and fire are only part of the story. *Forestry: An International Journal of Forest Research*, 90(4), 473-484.
- Nicholson, S.E., 2011. Dryland climatology.
- Nizalapur, V., Jha, C.S. and Madugundu, R., 2010. Estimation of above ground biomass in Indian tropical forested area using multi-frequency DLR-ESAR data. *International Journal of Geomatics and Geosciences*, 1(2), 167.
- Nobre, C.A. and Borma, L.D.S., 2009. 'Tipping points' for the Amazon forest. *Current Opinion in Environmental Sustainability*, 1(1), pp.28-36.
- Nobre, C.A., Sampaio, G., Borma, L.S., Castilla-Rubio, J.C., Silva, J.S. and Cardoso, M., 2016. Land-use and climate change risks in the Amazon and the need of a novel sustainable development paradigm. *Proceedings of the National Academy of Sciences*, 113(39), pp.10759-10768.
- Nott, K., Nott, A. and Newton, D., 2020. NAMIBIAN INDIGENOUS FOREST/TIMBER INDUSTRY.
- O'Brien, R.M., 2007. A caution regarding rules of thumb for variance inflation factors. *Quality & quantity*, 41(5), 673-690.
- O'Connell-Rodwell, C.E., Rodwell, T., Rice, M. and Hart, L.A., 2000. Living with the modern conservation paradigm: can agricultural communities co-exist with elephants? A five-year case study in East Caprivi, Namibia. *Biological conservation*, 93(3), pp.381-391.
- Olander, L.P., Gibbs, H.K., Steininger, M., Swenson, J.J. and Murray, B.C., 2008. Reference scenarios for deforestation and forest degradation in support of REDD: a review of data and methods. *Environmental Research Letters*, 3(2), p.025011.
- Oliveira, C.P.D., Ferreira, R.L.C., da Silva, J.A.A., Lima, R.B.D., Silva, E.A., Silva, A.F.D., Lucena, J.D.S.D., dos Santos, N.A.T., Lopes, I.J.C., Pessoa, M.M.D.L. and Melo, C.L.S.M.S.D., 2021. Modeling and Spatialization of Biomass and Carbon Stock Using LiDAR Metrics in Tropical Dry Forest, Brazil. *Forests*, 12(4), p.473.
- Olson, D. M., Dinerstein, E., 2002. The Global 200: Priority ecoregions for global conservation. *Annals of the Missouri Botanical Garden*, 199-224.
- Olson, D.M., Dinerstein, E., Wikramanayake, E.D., Burgess, N.D., Powell, G.V., Underwood, E.C., D'amico, J.A., Itoua, I., Strand, H.E., Morrison, J.C. and Loucks, C.J. (2001). Terrestrial Ecoregions of the World: A New Map of Life on Earth A new global map of terrestrial ecoregions provides an innovative tool for conserving biodiversity. *BioScience*, 51(11), pp.933-938.
- Olsson, L., Barbosa, H., Bhadwal, S., Cowie, A., Delusca, K., Flores-Renteria, D., Hermans, K., Jobbagy, E., Kurz, W., Li, D. and Sonwa, D.J., 2019. Land degradation: IPCC special report on climate change, desertification, land 5 degradation, sustainable land management, food security, and 6 greenhouse gas fluxes in terrestrial ecosystems. In *IPCC Special Report on Climate Change, Desertification, Land 5 Degradation, Sustainable Land Management, Food Security, and 6 Greenhouse gas fluxes in Terrestrial Ecosystems* (p. 1). Intergovernmental Panel on Climate Change (IPCC).

- Olsson, L., Eklundh, L. and Ardö, J. (2005). A recent greening of the Sahel—trends, patterns and potential causes. *Journal of Arid Environments*, 63(3), pp.556-566.
- Omar, H., Misman, M. A., Kassim, A., 2017. Synergetic of PALSAR-2 and Sentinel-1A SAR Polarimetry for Retrieving Aboveground Biomass in Dipterocarp Forest of Malaysia. *Applied Sciences*, 7(7), 675.
- Omphile, U.J. and Powell, J., 2002. Large ungulate habitat preference in Chobe National Park, Botswana. *Rangeland Ecology & Management/Journal of Range Management Archives*, 55(4), pp.341-349.
- Otsu, K., Pla, M., Duane, A., Cardil, A. and Brotons, L., 2019. Estimating the threshold of detection on tree crown defoliation using vegetation indices from UAS multispectral imagery. *Drones*, 3(4), p.80.
- Ouaadi, N., Jarlan, L., Ezzahar, J., Zribi, M., Khabba, S., Bouras, E., Bousbih, S. and Frison, P.L., 2020. Monitoring of wheat crops using the backscattering coefficient and the interferometric coherence derived from Sentinel-1 in semi-arid areas. *Remote Sensing of Environment*, 251, 112050.
- Owe, M., Van de Griend, A.A. and Chang, A.T.C. (1992). Surface moisture and satellite microwave observations in semiarid southern Africa. *Water Resources Research*, 28(3), pp.829-839.
- Paradzayi, C. and Annegarn, H.J., 2012. Estimating potential woody biomass in communal savanna woodlands from synthetic aperture radar (SAR). *International Journal of Applied Geospatial Research (IJAGR)*, 3(1), pp.53-62.
- Paruelo, J.M., Texeira, M., Staiano, L., Mastrángelo, M., Amdan, L. and Gallego, F. (2016). An integrative index of Ecosystem Services provision based on remotely sensed data. *Ecological Indicators*, 71, pp.145-154.
- Pause, M., Schweitzer, C., Rosenthal, M., Keuck, V., Bumberger, J., Dietrich, P., Heurich, M., Jung, A. and Lausch, A., 2016. In situ/remote sensing integration to assess forest health—A review. *Remote Sensing*, 8(6), p.471.
- Pearse, G.D., Watt, M.S., Dash, J.P., Stone, C. and Caccamo, G., 2019. Comparison of models describing forest inventory attributes using standard and voxel-based lidar predictors across a range of pulse densities. *International Journal of Applied Earth Observation and Geoinformation*, 78, 341-351.
- Peng, J., Dadson, S., Leng, G., Duan, Z., Jagdhuber, T., Guo, W. and Ludwig, R., 2019. The impact of the Madden-Julian Oscillation on hydrological extremes. *Journal of Hydrology*, 571, pp.142-149.
- Pennington, R.T., Lehmann, C.E. and Rowland, L.M., 2018. Tropical savannas and dry forests. *Current Biology*, 28(9), pp.R541-R545.
- Pereira Júnior, A.C., Oliveira, S.L., Pereira, J.M. and Turkman, M.A.A. (2014). Modelling fire frequency in a Cerrado savanna protected area. *PLoS one*, 9(7), p.e102380.
- Petheram, L., Campbell, B.M., Marunda, C.T., Tiveau, D. and Shackleton, S., 2006. The wealth of the dry forests: can sound forest management contribute to the millennium development goals in Sub-Saharan Africa?
- Pettorelli, N., Vik, J.O., Mysterud, A., Gaillard, J.M., Tucker, C.J. and Stenseth, N.C., 2005. Using the satellite-derived NDVI to assess ecological responses to environmental change. *Trends in ecology & evolution*, 20(9), pp.503-510.

- Pham, M.H., Do, T.H., Pham, V.M. and Bui, Q.T., 2020. Mangrove forest classification and aboveground biomass estimation using an atom search algorithm and adaptive neuro-fuzzy inference system. *Plos one*, 15(5), e0233110.
- Pirotti, F., 2011. Analysis of full-waveform LiDAR data for forestry applications: a review of investigations and methods. *iForest-Biogeosciences and Forestry*, 4(3), p.100.
- Popescu, S.C., 2007. Estimating biomass of individual pine trees using airborne lidar. *Biomass and Bioenergy*, 31(9), 646-655.
- Portillo, C. 2010. Assessing the Conservation status of Neotropical Dry forests using Geographic Information Systems and Optical Remote Sensing.
- Portillo-Quintero, C.A., Sanchez, A.M., Valbuena, C.A., Gonzalez, Y.Y. and Larreal, J.T. (2012). Forest cover and deforestation patterns in the Northern Andes (Lake Maracaibo Basin): a synoptic assessment using MODIS and Landsat imagery. *Applied Geography*, 35(1-2), pp.152-163.
- Potapov, P.V., Dempewolf, J., Talero, Y., Hansen, M.C., Stehman, S.V., Vargas, C., Rojas, E.J., Castillo, D., Mendoza, E., Calderón, A. and Giudice, R., 2014. National satellite-based humid tropical forest change assessment in Peru in support of REDD+ implementation. *Environmental Research Letters*, 9(12), p.124012.
- Poulter, B., Frank, D., Ciais, P., Myneni, R.B., Andela, N., Bi, J., Broquet, G., Canadell, J.G., Chevallier, F., Liu, Y.Y., Running, S.W., 2014. Contribution of semi-arid ecosystems to interannual variability of the global carbon cycle. *Nature*, 509(7502), 600-603.
- Powell, S.L., Cohen, W.B., Healey, S.P., Kennedy, R.E., Moisen, G.G., Pierce, K.B. and Ohmann, J.L., 2010. Quantification of live aboveground forest biomass dynamics with Landsat time-series and field inventory data: A comparison of empirical modeling approaches. *Remote Sensing of Environment*, 114(5), pp.1053-1068.
- Prado, D., Pennington, R. and Pendry, C. (2000). Neotropical seasonally dry forests and Quaternary vegetation changes. *Journal of Biogeography*, 27, pp.261-273.
- Pricope, N.G. and Binford, M.W., 2012. A spatio-temporal analysis of fire recurrence and extent for semi-arid savanna ecosystems in southern Africa using moderate-resolution satellite imagery. *Journal of environmental management*, 100, pp.72-85.
- Pricope, N.G., Gaughan, A.E., All, J.D., Binford, M.W. and Rutina, L.P., 2015. Spatio-temporal analysis of vegetation dynamics in relation to shifting inundation and fire regimes: disentangling environmental variability from land management decisions in a Southern African Transboundary Watershed. *Land*, 4(3), pp.627-655.
- Prince, S. D., 2012. Mapping desertification in southern Africa. In *Land Change Science* (pp. 163-184): *Springer*.
- Prince, S.D., 1991. Satellite remote sensing of primary production: comparison of results for Sahelian grasslands 1981-1988. *International Journal of remote sensing*, 12(6), pp.1301-1311.
- Privette, J.L. and Roy, D.P., 2005. Southern Africa as a remote sensing test bed: The SAFARI 2000 Special Issue overview. *International journal of remote sensing*, 26(19), pp.4141-4158.

- Propastin, P., 2012. Modifying geographically weighted regression for estimating aboveground biomass in tropical rainforests by multispectral remote sensing data. *International Journal of Applied Earth Observation and Geoinformation*, 18, 82-90.
- Pu, R., Landry, S. and Yu, Q., 2018. Assessing the potential of multi-seasonal high resolution Pléiades satellite imagery for mapping urban tree species. *International Journal of Applied Earth Observation and Geoinformation*, 71, pp.144-158.
- Puhr, C.B. and Donoghue, D.N.M., 2000. Remote sensing of upland conifer plantations using Landsat TM data: a case study from Galloway, south-west Scotland. *International Journal of Remote Sensing*, 21(4), pp.633-646.
- Putz, F.E. and Redford, K.H., 2010. The importance of defining 'forest': Tropical forest degradation, deforestation, long-term phase shifts, and further transitions. *Biotropica*, 42(1), pp.10-20.
- Quijas, S., Romero-Duque, L.P., Trilleras, J.M., Conti, G., Kolb, M., Brignone, E. and Dellafiore, C. (2019). Linking biodiversity, ecosystem services, and beneficiaries of tropical dry forests of Latin America: Review and new perspectives. *Ecosystem services*, 36, p.100909.
- R CORE TEAM, 2013. R: A language and environment for statistical computing. <https://www.R-project.org/>
- Visscher, D., 2006. GPS measurement error and resource selection functions in a fragmented landscape. *Ecography*, 29(3), pp.458-464.
- Rahmoune, R., Ferrazzoli, P., Kerr, Y.H. and Richaume, P. (2013). SMOS level 2 retrieval algorithm over forests: Description and generation of global maps. *IEEE Journal of Selected Topics in Applied Earth Observations and Remote Sensing*, 6(3), pp.1430-1439.
- Ramoelo, A., Cho, M.A., Mathieu, R., Madonsela, S., Van De Kerchove, R., Kaszta, Z. and Wolff, E., 2015. Monitoring grass nutrients and biomass as indicators of rangeland quality and quantity using random forest modelling and WorldView-2 data. *International journal of applied earth observation and geoinformation*, 43, 43-54.
- Rampheri, M., Dube, T. and Dhau, I., 2020. Use of remotely sensed data to estimate tree species diversity as an indicator of biodiversity in Blouberg Nature Reserve, South Africa. *Geocarto International*, pp.1-17.
- Rands, M.R., Adams, W.M., Bennun, L., Butchart, S.H., Clements, A., Coomes, D., Entwistle, A., Hodge, I., Kapos, V., Scharlemann, J.P. and Sutherland, W.J., 2010. Biodiversity conservation: challenges beyond 2010. *science*, 329(5997), pp.1298-1303.
- Ranjan, R., Chopra, U.K., Sahoo, R.N., Singh, A.K. and Pradhan, S., 2012. Assessment of plant nitrogen stress in wheat (*Triticum aestivum* L.) through hyperspectral indices. *International Journal of Remote Sensing*, 33(20), pp.6342-6360.
- Reiche, J., Lucas, R., Mitchell, A.L., Verbesselt, J., Hoekman, D.H., Haarpaintner, J., Kellndorfer, J.M., Rosenqvist, A., Lehmann, E.A., Woodcock, C.E. and Seifert, F.M., 2016. Combining satellite data for better tropical forest monitoring. *Nature Climate Change*, 6(2), pp.120-122.
- Reynolds, J., Wesson, K., Desbiez, A.L., Ochoa-Quintero, J.M. and Leimgruber, P. (2016). Using remote sensing and random forest to assess the conservation status of critical Cerrado habitats in Mato Grosso do Sul, Brazil. *Land*, 5(2), p.12.
- Reynolds, J.F., Smith, D.M.S., Lambin, E.F., Turner, B.L., Mortimore, M., Batterbury, S.P., Downing, T.E., Dowlatabadi, H., Fernández, R.J., Herrick, J.E. and Huber-Sannwald, E., 2007. Global

- desertification: building a science for dryland development. *science*, 316(5826), pp.847-851.
- Ringrose, S., Chipanshi, A.C., Matheson, W., Chanda, R., Motoma, L., Magole, I. and Jellema, A., 2002. Climate-and human-induced woody vegetation changes in Botswana and their implications for human adaptation. *Environmental management*, 30(1), pp.98-109.
- Ringrose, S., Matheson, W., Matlala, C.J.S.S., O'Neill, T. and Werner, P.A., 1994. Vegetation spectral reflectance along a north-south vegetation gradient in northern Australia. *Journal of Biogeography*, pp.33-47.
- Rodríguez, J.P., Nassar, J.M., Rodríguez-Clark, K.M., Zager, I., Portillo-Quintero, C.A., Carrasquel, F. and Zambrano, S. (2008). Tropical dry forests in Venezuela: assessing status, threats and future prospects. *Environmental Conservation*, 35(4), pp.311-318.
- Rouse, J.W., 1974. Monitoring the vernal advancement of retrogradation of natural vegetation. NASA/GSFC, type III, *final report, greenbelt*, MD, 371.
- Rumiano, F., Wielgus, E., Miguel, E., Chamailé-Jammes, S., Valls-Fox, H., Cornélis, D., Garine-Wichatitsky, M.D., Fritz, H., Caron, A. and Tran, A., 2020. Remote sensing of environmental drivers influencing the movement ecology of sympatric wild and domestic ungulates in semi-arid savannas, a review. *Remote Sensing*, 12(19), p.3218.
- Russell-Smith, J., Monagle, C., Jacobsohn, M., Beatty, R.L., Bilbao, B., Millán, A., Vessuri, H. and Sánchez-Rose, I., 2017. Can savanna burning projects deliver measurable greenhouse emissions reductions and sustainable livelihood opportunities in fire-prone settings?. *Climatic Change*, 140(1), pp.47-61.
- Rwanga, S.S. and Ndambuki, J.M., 2017. Accuracy assessment of land use/land cover classification using remote sensing and GIS. *International Journal of Geosciences*, 8(04), p.611.
- Saatchi, S.S., Harris, N.L., Brown, S., Lefsky, M., Mitchard, E.T., Salas, W., Zutta, B.R., Buermann, W., Lewis, S.L., Hagen, S., Petrova, S., 2011. Benchmark map of forest carbon stocks in tropical regions across three continents. *Proceedings of the National Academy of Sciences*, 108(24), 9899-9904.
- Sader, S.A., Waide, R.B., Lawrence, W.T. and Joyce, A.T., 1989. Tropical forest biomass and successional age class relationships to a vegetation index derived from Landsat TM data. *Remote Sensing of Environment*, 28, pp.143-198.
- Safriel, U., Adeel, Z., Niemeijer, D., Puigdefabregas, J., White, R., Lal, R., Winslow, M., Ziedler, J., Prince, S., Archer, E. and King, C., 2005. Dryland systems. In *Ecosystems and Human Well-being: Current State and Trends.: Findings of the Condition and Trends Working Group* (pp. 623-662). Island Press.
- Sakaizawa, D., MITSUHAHI, R., MUROOKA, J., Tadashi, I.M.A.I., Kimura, T. and Kazuhiro, A.S.A.I., 2018, July. Current status of the ISS-vegetation lidar Mission-MOLI. In *IGARSS 2018-2018 IEEE International Geoscience and Remote Sensing Symposium* (pp. 1861-1864). IEEE.
- Salajanu, D. and Olson, C.E., 2001. The significance of spatial resolution: Identifying forest cover from satellite data. *Journal of forestry*, 99(6), pp.32-38.
- Salis, S. M., Assis, M. A., Mattos, P. P., & Pião, A. C., 2006. Estimating the aboveground biomass and wood volume of savanna woodlands in Brazil's Pantanal wetlands based on allometric correlations. *Forest Ecology and Management*, 228(1-3), 61-68.



- Samanta, A., Ganguly, S. and Myneni, R.B., 2011. MODIS enhanced vegetation index data do not show greening of Amazon forests during the 2005 drought. *The New Phytologist*, 189(1), pp.11-15.
- Sanchez-Azofeifa, A., Portillo-Quintero, C., Wilson-Fernandes, G., Stoner, K. and Shimizu, T. (2013). The policy process for land use/cover change and forest degradation in the semi-arid Latin American/Caribbean region: perspectives and opportunities. A literature review prepared for the Inter-American Development Bank. A literature review prepared for the Inter-American Development Bank.
- Sánchez-Azofeifa, G.A., Castro, K.L., Rivard, B., Kalascka, M.R. and Harriss, R.C. (2003). Remote sensing research priorities in tropical dry forest environments. *Biotropica*, 35(2), pp.134-142.
- Sánchez-Azofeifa, G.A., Quesada, M., Rodríguez, J.P., Nassar, J.M., Stoner, K.E., Castillo, A., Garvin, T., Zent, E.L., Calvo-Alvarado, J.C., Kalacska, M.E. and Fajardo, L., 2005. Research priorities for Neotropical dry forests 1. *Biotropica: The Journal of Biology and Conservation*, 37(4), pp.477-485
- Santoro, M., Beer, C., Cartus, O., Schmullius, C., Shvidenko, A., McCallum, I., Wegmüller, U. and Wiesmann, A., 2011. Retrieval of growing stock volume in boreal forest using hyper-temporal series of Envisat ASAR ScanSAR backscatter measurements. *Remote Sensing of Environment*, 115(2), pp.490-507.
- Santos, J.R., Lacruz, M.P., Araujo, L.S. and Keil, M., 2002. Savanna and tropical rainforest biomass estimation and spatialization using JERS-1 data. *International Journal of Remote Sensing*, 23(7), pp.1217-1229
- Sarker, L.R. and Nichol, J.E., 2011. Improved forest biomass estimates using ALOS AVNIR-2 texture indices. *Remote Sensing of Environment*, 115(4), pp.968-977.
- Schimel, D., Pavlick, R., Fisher, J.B., Asner, G.P., Saatchi, S., Townsend, P., Miller, C., Frankenberg, C., Hibbard, K. and Cox, P., 2015. Observing terrestrial ecosystems and the carbon cycle from space. *Global Change Biology*, 21(5), 1762-1776.
- Scholes, R.J. and Biggs, R.A., 2004. *Ecosystem services in Southern Africa a regional assessment* (No. 33355 Caja (533)). CSIR.
- Scholes, R.J., Frost, P.G. and Tian, Y., 2004. Canopy structure in savannas along a moisture gradient on Kalahari sands. *Global Change Biology*, 10(3), pp.292-302.
- Scholes, R.J., Montanarella, L., Brainich, E., Barger, N., Ten Brink, B., Cantele, M., Erasmus, B., Fisher, J., Gardner, T., Holland, T.G. and Kohler, F., 2018. IPBES (2018): Summary for policymakers of the assessment report on land degradation and restoration of the Intergovernmental Science-Policy Platform on Biodiversity and Ecosystem Services.
- Schröder, J.M., Rodriguez, L.P.A. and Günter, S., 2021. Research trends: Tropical dry forests: The neglected research agenda?. *Forest Policy and Economics*, 122, p.102333.
- Schulte to Bühne, H. and Pettorelli, N., 2018. Better together: Integrating and fusing multispectral and radar satellite imagery to inform biodiversity monitoring, ecological research and conservation science. *Methods in Ecology and Evolution*, 9(4), pp.849-865.
- Schultz, M., Shapiro, A., Clevers, J.G., Beech, C. and Herold, M., 2018. Forest cover and vegetation degradation detection in the Kavango Zambezi Transfrontier Conservation area using BFAST monitor. *Remote Sensing*, 10(11), p.1850.

- Senf, C., Pflugmacher, D., Hostert, P. and Seidl, R., 2017. Using Landsat time series for characterizing forest disturbance dynamics in the coupled human and natural systems of Central Europe. *ISPRS Journal of Photogrammetry and Remote Sensing*, 130, pp.453-463.
- Sexton, J.O., Noojipady, P., Song, X.P., Feng, M., Song, D.X., Kim, D.H., Anand, A., Huang, C., Channan, S., Pimm, S.L. and Townshend, J.R., 2016. Conservation policy and the measurement of forests. *Nature Climate Change*, 6(2), pp.192-196.
- Sexton, J.O., Song, X.P., Feng, M., Noojipady, P., Anand, A., Huang, C., Kim, D.H., Collins, K.M., Channan, S., DiMiceli, C. and Townshend, J.R., 2013. Global, 30-m resolution continuous fields of tree cover: Landsat-based rescaling of MODIS vegetation continuous fields with lidar-based estimates of error. *International Journal of Digital Earth*, 6(5), pp.427-448.
- Shackleton, C., Shackleton, S.E., Gambiza, J., Nel, E., Rowntree, K., Urquhart, P., Fabricius, C. and Ainslie, A., 2010. *Livelihoods and vulnerability in the arid and semi-arid lands of southern Africa: exploring the links between ecosystem services and poverty alleviation*. Nova Publishers.
- Shannon, G., Thaker, M., Vanak, A. T., Page, B. R., Grant, R., Slotow, R., 2011. Relative impacts of elephant and fire on large trees in a savanna ecosystem. *Ecosystems*, 14(8), 1372-1381.
- Shao, Z., Zhang, L. and Wang, L. (2017). Stacked sparse autoencoder modeling using the synergy of airborne LiDAR and satellite optical and SAR data to map forest above-ground biomass. *IEEE Journal of Selected Topics in Applied Earth Observations and Remote Sensing*, 10(12), pp.5569-5582.
- Sheffield, J. and Wood, E.F., 2008. Projected changes in drought occurrence under future global warming from multi-model, multi-scenario, IPCC AR4 simulations. *Climate dynamics*, 31(1), pp.79-105.
- Shelestov, A., Lavreniuk, M., Kussul, N., Novikov, A. and Skakun, S., 2017. Exploring Google Earth Engine platform for big data processing: Classification of multi-temporal satellite imagery for crop mapping. *frontiers in Earth Science*, 5, p.17.
- Shi, J., Jackson, T., Tao, J., Du, J., Bindlish, R., Lu, L. and Chen, K.S. (2008). Microwave vegetation indices for short vegetation covers from satellite passive microwave sensor AMSR-E. *Remote sensing of environment*, 112(12), pp.4285-4300.
- Shikangalah, R.N., 2020. The 2019 drought in Namibia: an overview. *J. Namibian Stud*, 27, pp.37-58.
- Shimada, M., 2018. *Imaging from spaceborne and airborne SARs, calibration, and applications*. CRC Press.
- Sibanda, M., Mutanga, O. and Rouget, M., 2016. Discriminating rangeland management practices using simulated hyspIRI, landsat 8 OLI, sentinel 2 MSI, and VENUS spectral data. *IEEE Journal of Selected Topics in Applied Earth Observations and Remote Sensing*, 9(9), 3957-3969.
- Silva, J.M., Pereira, J.M., Cabral, A.I., Sá, A.C., Vasconcelos, M.J., Mota, B. and Grégoire, J.M., 2003. An estimate of the area burned in southern Africa during the 2000 dry season using SPOT-VEGETATION satellite data. *Journal of Geophysical Research: Atmospheres*, 108(D13).
- Silvy, N.J. ed., 2020. *The Wildlife Techniques Manual: Volume 1: Research. Volume 2: Management*. JHU Press.

- Simard, M., Pinto, N., Fisher, J.B. and Baccini, A., 2011. Mapping forest canopy height globally with spaceborne lidar. *Journal of Geophysical Research: Biogeosciences*, 116(G4).
- Simula, M., 2009. Towards defining forest degradation: comparative analysis of existing definitions. *Forest Resources Assessment Working Paper*, 154, p.59.
- Smith, W.K., Dannenberg, M.P., Yan, D., Herrmann, S., Barnes, M.L., Barron-Gafford, G.A., Biederman, J.A., Ferrenberg, S., Fox, A.M., Hudson, A. and Knowles, J.F., 2019. Remote sensing of dryland ecosystem structure and function: Progress, challenges, and opportunities. *Remote Sensing of Environment*, 233, p.111401.
- Spinoni, J., Vogt, J., Naumann, G., Carrao, H. and Barbosa, P., 2015. Towards identifying areas at climatological risk of desertification using the Köppen–Geiger classification and FAO aridity index. *International Journal of Climatology*, 35(9), pp.2210-2222.
- Stan, K. and Sanchez-Azofeifa, A. (2019). Tropical dry forest diversity, climatic response, and resilience in a changing climate. *Forests*, 10(5), p.443.
- Staver, A.C., Archibald, S. and Levin, S.A. (2011). The global extent and determinants of savanna and forest as alternative biome states. *science*, 334(6053), pp.230-232.
- Steininger, M.K., 2000. Satellite estimation of tropical secondary forest above-ground biomass: data from Brazil and Bolivia. *International journal of remote sensing*, 21(6-7), 1139-1157.
- Stehman, S.V. and Czaplewski, R.L., 1998. Design and analysis for thematic map accuracy assessment: fundamental principles. *Remote sensing of environment*, 64(3), pp.331-344.
- Stehman, S.V., 2009. Sampling designs for accuracy assessment of land cover. *International Journal of Remote Sensing*, 30(20), pp.5243-5272.
- Stehman, S.V., 2009. Sampling designs for accuracy assessment of land cover. *International Journal of Remote Sensing*, 30(20), pp.5243-5272.
- Stoldt, M., Göttert, T., Mann, C. and Zeller, U., 2020. Transfrontier conservation areas and human-wildlife conflict: the case of the Namibian component of the Kavango-Zambezi (KAZA) TFCA. *Scientific reports*, 10(1), pp.1-16.
- Stoner, K.E., Timm, R.M., Frankie, G.W., Mata, A. and Vinson, S.B. (2004). Tropical dry-forest mammals of Palo Verde. *Biodiversity conservation in Costa Rica. Learning the lessons in a seasonal dry forest. University of California Press. Berkeley, Los Angeles*, pp.48-66.
- Story, M. and Congalton, R.G., 1986. Accuracy assessment: a user's perspective. *Photogrammetric Engineering and remote sensing*, 52(3), pp.397-399.
- Stott, P., 2000. Combustion in tropical biomass fires: a critical review. *Progress in Physical Geography*, 24(3), pp.355-377.
- Stratoulas, D., Balzter, H., Sykioti, O., Zlinszky, A. and Tóth, V.R., 2015. Evaluating sentinel-2 for lakeshore habitat mapping based on airborne hyperspectral data. *Sensors*, 15(9), pp.22956-22969.
- Sunderland, T., Apgaua, D., Baldauf, C., Blackie, R., Colfer, C., Cunningham, A.B., Dexter, K., Djoudi, H., Gautier, D., Gumbo, D. and Ickowitz, A., 2015. Global dry forests: a prologue. *International Forestry Review*, 17(2), pp.1-9.

- Suresh, H.S., Dattaraja, H.S., Mondal, N. and Sukumar, R., 2011. Seasonally dry tropical forests in Southern India. An analysis of floristic composition, structure, and dynamics in Mudumalai Wildlife Sanctuary. *The ecology and conservation of seasonally dry forests in Asia*, pp.37-58.
- Svoboda, M. and Fuchs, B.A., 2016. Handbook of drought indicators and indices. Integrated drought management programme (IDMP), integrated drought management tools and guidelines series 2. *World meteorological organization and global water partnership, Geneva, Switzerland*, 52.
- Symeonakis, E., Higginbottom, T.P., Petroulaki, K. and Rabe, A., 2018. Optimisation of savannah land cover characterisation with optical and SAR data. *Remote Sensing*, 10(4), p.499.
- Symeonakis, E., Korkofigkas, A., Vamvoukakis, G., Stamou, G. and Arnau-Rosalen, E. (2020). Deep Learning Monitoring of Woody Vegetation Density in a South African Savannah Region. *International Archives of the Photogrammetry, Remote Sensing and Spatial Information Sciences-ISPRS Archives*, 43, pp.1645-1649.
- Thompson, I.D., Guariguata, M.R., Okabe, K., Bahamondez, C., Nasi, R., Heymell, V. and Sabogal, C., 2013. An operational framework for defining and monitoring forest degradation. *Ecology and Society*, 18(2).
- Tian, F., Brandt, M., Liu, Y.Y., Rasmussen, K. and Fensholt, R. (2017). Mapping gains and losses in woody vegetation across global tropical drylands. *Global change biology*, 23(4), pp.1748-1760.
- Timothy, D., Onisimo, M. and Riyad, I., 2016. Quantifying aboveground biomass in African environments: A review of the trade-offs between sensor estimation accuracy and costs. *Tropical Ecology*, 57(3), pp.393-405.
- Toth, C. and Józków, G. (2016). Remote sensing platforms and sensors: A survey. *ISPRS Journal of Photogrammetry and Remote Sensing*, 115, pp.22-36.
- Townsend, P. A, 2002. Estimating forest structure in wetlands using multitemporal SAR. *Remote Sensing of Environment*, 79(2-3), 288-304.
- Trejo, I. and Dirzo, R. (2000). Deforestation of seasonally dry tropical forest: a national and local analysis in Mexico. *Biological conservation*, 94(2), pp.133-142.
- Treuhaft, R. N., Law, B. E., Asner, G. P., 2004. Forest attributes from radar interferometric structure and its fusion with optical remote sensing. *BioScience*, 54(6), 561-571.
- Trier, Ø.D., Salberg, A.B., Kermit, M., Rudjord, Ø., Gobakken, T., Næsset, E. and Aarsten, D. (2018). Tree species classification in Norway from airborne hyperspectral and airborne laser scanning data. *European Journal of Remote Sensing*, 51(1), pp.336-351
- Trollope, W.S.W., 1984. Fire in savanna. In *Ecological effects of fire in South African ecosystems* (pp. 149-175). Springer, Berlin, Heidelberg.
- Tsalyuk, M., Kelly, M. and Getz, W.M., 2017. Improving the prediction of African savanna vegetation variables using time series of MODIS products. *ISPRS Journal of Photogrammetry and Remote Sensing*, 131, pp.77-91.
- Tshipa, A., Valls-Fox, H., Fritz, H., Collins, K., Sebele, L., Mundy, P. and Chamailé-Jammes, S., 2017. Partial migration links local surface-water management to large-scale elephant conservation in the world's largest transfrontier conservation area. *Biological Conservation*, 215, pp.46-50.

- Tu, M.C., Smith, P. and Filippi, A.M., 2018. Hybrid forward-selection method-based water-quality estimation via combining Landsat TM, ETM+, and OLI/TIRS images and ancillary environmental data. *Plos one*, 13(7), e0201255.
- Tucker, C.J., 1979. Red and photographic infrared linear combinations for monitoring vegetation. *Remote sensing of Environment*, 8(2), pp.127-150.
- Turner, D.P., Cohen, W.B., Kennedy, R.E., Fassnacht, K.S. and Briggs, J.M., 1999. Relationships between leaf area index and Landsat TM spectral vegetation indices across three temperate zone sites. *Remote sensing of environment*, 70(1), pp.52-68.
- Turner, M.G., 2010. Disturbance and landscape dynamics in a changing world. *Ecology*, 91(10), pp.2833-2849.
- UN., 2011. Global drylands: a UN system-wide response. Environment Management Group of the United Nations Geneva. [http://www.unccd.int/Lists/SiteDocumentLibrary/Publications/Global\\_Drylands\\_Full\\_Report.pdf/](http://www.unccd.int/Lists/SiteDocumentLibrary/Publications/Global_Drylands_Full_Report.pdf/) (accessed 19 July 2021).
- UN., 2015. Transforming our world: the 2030 Agenda for Sustainable Development. *United Nations: New York, NY, USA*.
- UNCCD., 1994. United Nations: Convention to combat desertification in those countries experiencing serious drought and/or desertification, particularly in Africa. *Int. Legal Mater*, 33, pp.1328-1382.
- UNCCD., 2009. United Nations Convention to Combat Desertification: Climate Change in the African Drylands. Options and Opportunities for Adaptation and Mitigation. In: UNDP and UNEP Nairobi.
- UNCCD., 2015. United Nations Convention to Combat Desertification (UNCCD), UNCCD's support for the New Partnership for Africa's Development (NEPAD). <http://www.un.org/en/africa/osaa/pdf/unsystemfolder/2016/unccd2016.pdf/> (accessed 01 July 2021).
- UNFCCC., 2009. Methodological guidance for activities relating to reducing emissions from deforestation and forest degradation and the role of conservation, sustainable management of forests and enhancement of forest carbon stocks in developing countries. In. Decision 4/CP.15. *United Nations Framework Convention on Climate Change, Bonn*.
- Unger, D.R., Hung, I.K., Brooks, R. and Williams, H., 2014. Estimating number of trees, tree height and crown width using Lidar data. *GIScience & remote sensing*, 51(3), pp.227-238.
- Urban, M., Berger, C., Mudau, T.E., Heckel, K., Truckenbrodt, J., Onyango Odipo, V., Smit, I.P. and Schmullius, C., 2018. Surface moisture and vegetation cover analysis for drought monitoring in the Southern Kruger National Park using sentinel-1, sentinel-2, and landsat-8. *Remote Sensing*, 10(9), p.1482.
- USAID., 2010. USAID/NAMIBIA Environmental Threats and opportunities assessment with an emphasis on tropical forestry and biodiversity conservation. Prepared by the International Resource Group (IRG) for the United States Agency for International Development (USAID). *Washington, DC, USA*.
- USAID., 2013. ANGOLA BIODIVERSITY AND TROPICAL FORESTS: 118/119 ASSESSMENT. <https://usaidgems.org/Documents/FAA&Regs/FAA118119/Angola2013.pdf/> (accessed 14 March 2021).

- Valentini, R., Arneth, A., Bombelli, A., Castaldi, S., Cazzolla Gatti, R., Chevallier, F., Ciais, P., Grieco, E., Hartmann, J., Henry, M. and Houghton, R.A., 2014. A full greenhouse gases budget of Africa: synthesis, uncertainties, and vulnerabilities. *Biogeosciences*, 11(2), pp.381-407.
- van Bommel, F.P., Heitkönig, I.M., Epema, G.F., Ringrose, S., Bonyongo, C. and Veenendaal, E.M., 2006. Remotely sensed habitat indicators for predicting distribution of impala (*Aepyceros melampus*) in the Okavango Delta, Botswana. *Journal of tropical ecology*, 22(1), pp.101-110.
- van der Sande, M.T., Peña-Claros, M., Ascarrunz, N., Arets, E.J., Licona, J.C., Toledo, M. and Poorter, L., 2017. Abiotic and biotic drivers of biomass change in a Neotropical forest. *Journal of Ecology*, 105(5), pp.1223-1234.
- van der Werf, G.R., Randerson, J.T., Giglio, L., Collatz, G.J., Kasibhatla, P.S. and Arellano Jr, A.F., 2006. Interannual variability in global biomass burning emissions from 1997 to 2004. *Atmospheric Chemistry and Physics*, 6(11), pp.3423-3441.
- Van Marle, M.J.E., Van Der Werf, G.R., De Jeu, R.A.M. and Liu, Y.Y. (2016). Annual South American forest loss estimates based on passive microwave remote sensing (1990–2010). *Biogeosciences*, 13(2), pp.609-624.
- Van Wilgen, B.W., Govender, N. and Biggs, H.C., 2007. The contribution of fire research to fire management: a critical review of a long-term experiment in the Kruger National Park, South Africa. *International Journal of Wildland Fire*, 16(5), pp.519-530.
- Veldkamp, A. and Lambin, E. F., 2001. Predicting land-use change. *Agriculture, Ecosystems & Environment*, 85(1-3), pp. 1-6.
- Venter, Z.S., Scott, S.L., Desmet, P.G. and Hoffman, M.T., 2020. Application of Landsat-derived vegetation trends over South Africa: Potential for monitoring land degradation and restoration. *Ecological Indicators*, 113, p.106206.
- Verbesselt, J., Hyndman, R., Newnham, G. and Culvenor, D., 2010a. Detecting trend and seasonal changes in satellite image time series. *Remote sensing of Environment*, 114(1), pp.106-115.
- Verbesselt, J., Hyndman, R., Zeileis, A. and Culvenor, D., 2010b. Phenological change detection while accounting for abrupt and gradual trends in satellite image time series. *Remote Sensing of Environment*, 114(12), pp.2970-2980.
- Verbesselt, J., Somers, B., Lhermitte, S., Jonckheere, I., van Aardt, J., and Coppin, P., 2007. Monitoring herbaceous fuel moisture content with SPOT VEGETATION time-series for fire risk prediction in savanna ecosystems. *Remote Sensing of Environment*, 108(4), pp.357-368.
- Verbesselt, J., Somers, B., van Aardt, J., Jonckheere, I., and Coppin, P., 2006. Monitoring herbaceous biomass and water content with SPOT VEGETATION time-series to improve fire risk assessment in savanna ecosystems. *Remote Sensing of Environment*, 101(3), pp.399-414.
- Verbesselt, J., Zeileis, A. and Herold, M., 2012. Near real-time disturbance detection using satellite image time series. *Remote Sensing of Environment*, 123, pp.98-108.
- Verlinden, A. and Laamanen, R., 2006a. Long term fire scar monitoring with remote sensing in northern Namibia: Relations between fire frequency, rainfall, land cover, fire management and trees. *Environmental Monitoring and Assessment*, 112(1-3), pp.231-253.
- Verlinden, A. and Laamanen, R., 2006b. Modeling woody vegetation resources using Landsat TM imagery in northern Namibia. *Southern African Forestry Journal*, 207(1), pp.27-39.

- Vermote, E.F., El Saleous, N.Z. and Justice, C.O., 2002. Atmospheric correction of MODIS data in the visible to middle infrared: first results. *Remote Sensing of Environment*, 83(1-2), pp.97-111.
- Vicente-Serrano, S.M., Cabello, D., Tomás-Burguera, M., Martín-Hernández, N., Beguería, S., Azorin-Molina, C. and Kenawy, A.E., 2015. Drought variability and land degradation in semiarid regions: Assessment using remote sensing data and drought indices (1982–2011). *Remote Sensing*, 7(4), pp.4391-4423.
- Vicente-Serrano, S.M., Miralles, D.G., Domínguez-Castro, F., Azorin-Molina, C., El Kenawy, A., McVicar, T.R., Tomás-Burguera, M., Beguería, S., Maneta, M. and Peña-Gallardo, M., 2018. Global assessment of the Standardized Evapotranspiration Deficit Index (SEDI) for drought analysis and monitoring. *Journal of Climate*, 31(14), pp.5371-5393.
- Viovy, N., Arino, O. and Belward, A.S., 1992. The Best Index Slope Extraction (BISE): A method for reducing noise in NDVI time-series. *International Journal of remote sensing*, 13(8), pp.1585-1590.
- Vogt, J.V., Safriel, U., Von Maltitz, G., Sokona, Y., Zougmore, R., Bastin, G. and Hill, J., 2011. Monitoring and assessment of land degradation and desertification: towards new conceptual and integrated approaches. *Land Degradation & Development*, 22(2), pp.150-165.
- Wagenseil, H. and Samimi, C., 2006. Assessing spatio-temporal variations in plant phenology using Fourier analysis on NDVI time series: results from a dry savannah environment in Namibia. *International Journal of Remote Sensing*, 27(16), pp.3455-3471.
- Walter, H. and Burnett, J.H., 1971. *Ecology of tropical and subtropical vegetation* (Vol. 539). Edinburgh: Oliver and Boyd.
- Wang, F. M., Huang, J. F., Tang, Y. L., Wang, X. Z., 2007. New vegetation index and its application in estimating leaf area index of rice. *Rice Science*, 14(3), 195-203.
- Wang, L., Jia, M., Yin, D., and Tian, J., 2019. A review of remote sensing for mangrove forests: 1956–2018. *Remote Sensing of Environment*, 231, 111223.
- Wang, Y., Day, J. L., and Davis, F. W., 1998. Sensitivity of modeled C- and L-band radar backscatter to ground surface parameters in loblolly pine forest. *Remote Sensing of Environment*, 66(3), pp. 331-342.
- Warren, M.S., Brumby, S.P., Skillman, S.W., Kelton, T., Wohlberg, B., Mathis, M., Chartrand, R., Keisler, R. and Johnson, M., 2015, October. Seeing the Earth in the Cloud: Processing one petabyte of satellite imagery in one day. In *2015 IEEE Applied Imagery Pattern Recognition Workshop (AIPR)* (pp. 1-12). IEEE.
- Washington-Allen, R.A., Ramsey, R.D., West, N.E. and Norton, B.E., 2008. Quantification of the ecological resilience of drylands using digital remote sensing. *Ecology and Society*, 13(1).
- Washington-Allen, R.A., West, N.E., Ramsey, R.D. and Efroymson, R.A., 2006. A protocol for retrospective remote sensing-based ecological monitoring of rangelands. *Rangeland Ecology & Management*, 59(1), pp.19-29.
- Watson, R.T., Zinyowera, M.C. and Moss, R.H., 1996. Climate change 1995. Impacts, adaptations and mitigation of climate change: scientific-technical analyses. *Cambridge: Cambridge University Press*. <http://www.repositorio.cenpatconicet.gob.ar/bitstream/handle/123456789/577/climateChange1995ImpactsAdpatationsMitigation.pdf?sequence=1> (accessed 25 August 2021).

- Watt, P., Bholanath, P., Dewnath, N., Smartt, T., Chan, C. and Donoghue, D., 2020. INTEROPERABILITY OF VARIOUS DATA STREAMS WITHIN GUYANA'S MRV SYSTEM. *International Archives of the Photogrammetry, Remote Sensing and Spatial Information Sciences*, 42(3/W11).
- Watts, L.M. and Laffan, S.W., 2014. Effectiveness of the BFAST algorithm for detecting vegetation response patterns in a semi-arid region. *Remote Sensing of Environment*, 154, pp.234-245.
- Wegmann, M., Santini, L., Leutner, B., Safi, K., Rocchini, D., Bevanda, M., Latifi, H., Dech, S. and Rondinini, C., 2014. Role of African protected areas in maintaining connectivity for large mammals. *Philosophical Transactions of the Royal Society B: Biological Sciences*, 369(1643), p.20130193
- Weng, X., Dong, Z., Wu, Q. and Qin, Y., 2015. China's path to a green economy. *Decoding China's green economy concepts and policies. Country report. IEED, London.*
- Wessels, K.J., Prince, S.D., Zambatis, N., MacFadyen, S., Frost, P.E. and Van Zyl, D., 2006. Relationship between herbaceous biomass and 1-km<sup>2</sup> Advanced Very High Resolution Radiometer (AVHRR) NDVI in Kruger National Park, South Africa. *International Journal of Remote Sensing*, 27(05), pp.951-973.
- Westinga, E., Beltran, A.P.R., De Bie, C.A. and van Gils, H.A., 2020. A novel approach to optimize hierarchical vegetation mapping from hyper-temporal NDVI imagery, demonstrated at national level for Namibia. *International Journal of Applied Earth Observation and Geoinformation*, 91, p.102152
- White, B.L.A. (2019). Satellite detection of wildland fires in South America. *Floresta*, 49(4), pp.851-858.
- Whitecross, M.A., Witkowski, E.T. and Archibald, S., 2017. Assessing the frequency and drivers of early-greening in broad-leaved woodlands along a latitudinal gradient in southern Africa. *Austral ecology*, 42(3), pp.341-353.
- Wiens, J., Sutter, R., Anderson, M., Blanchard, J., Barnett, A., Aguilar-Amuchastegui, N., Avery, C. and Laine, S., 2009. Selecting and conserving lands for biodiversity: The role of remote sensing. *Remote sensing of Environment*, 113(7), pp.1370-1381.
- Wijaya, A., Liesenberg, V., Susanti, A., Karyanto, O. and Verchot, L.V., 2015. Estimation of Biomass Carbon Stocks over Peat Swamp Forests using Multi-Temporal and Multi-Polarizations SAR Data. *Int. Arch. Photogramm. Remote Sens. Spat. Inf. Sci*, 551-556
- Wilcox, B.P., Sorice, M.G. and Young, M.H., 2011. Dryland ecohydrology in the anthropocene: Taking stock of human-ecological interactions. *Geography Compass*, 5(3), pp.112-127.
- Williams, A.P., Allen, C.D., Macalady, A.K., Griffin, D., Woodhouse, C.A., Meko, D.M., Swetnam, T.W., Rauscher, S.A., Seager, R., Grissino-Mayer, H.D. and Dean, J.S., 2013. Temperature as a potent driver of regional forest drought stress and tree mortality. *Nature climate change*, 3(3), pp.292-297.
- Williams, M. R. C. M., Ryan, C. M., Rees, R. M., Sambane, E., Fernando, J., & Grace, J., 2008. Carbon sequestration and biodiversity of re-growing miombo woodlands in Mozambique. *Forest Ecology and management*, 254(2), 145-155.
- Williams, M., Hill, T.C. and Ryan, C.M., 2013. Using biomass distributions to determine probability and intensity of tropical forest disturbance. *Plant Ecology & Diversity*, 6(1), pp.87-99.



- Wingate, V.R., Phinn, S.R., Kuhn, N. and Scarth, P., 2018. Estimating aboveground woody biomass change in Kalahari woodland: combining field, radar, and optical data sets. *International Journal of Remote Sensing*, 39(2), pp.577-606.
- Wintle, B.A., Kujala, H., Whitehead, A., Cameron, A., Veloz, S., Kukkala, A., Moilanen, A., Gordon, A., Lentini, P.E., Cadenhead, N.C. and Bekessy, S.A., 2019. Global synthesis of conservation studies reveals the importance of small habitat patches for biodiversity. *Proceedings of the National Academy of Sciences*, 116(3), pp.909-914.
- Wood, E.M., Pidgeon, A.M., Radeloff, V.C. and Keuler, N.S., 2012. Image texture as a remotely sensed measure of vegetation structure. *Remote Sensing of Environment*, 121, pp.516-526.
- Woodcock, C.E., Macomber, S.A., Pax-Lenney, M. and Cohen, W.B., 2001. Monitoring large areas for forest change using Landsat: Generalization across space, time and Landsat sensors. *Remote sensing of environment*, 78(1-2), pp.194-203.
- Worldagroforestry, 2019. Worldwide open access tree functional attributes and ecological database. [http://db.worldagroforestry.org//species/properties/Baikiaea\\_plurijuga/](http://db.worldagroforestry.org//species/properties/Baikiaea_plurijuga/) (accessed 12 December 2019).
- Wu, C., Shen, H., Shen, A., Deng, J., Gan, M., Zhu, J., Xu, H. and Wang, K., 2016. Comparison of machine-learning methods for above-ground biomass estimation based on Landsat imagery. *Journal of Applied Remote Sensing*, 10(3), 035010.
- Wu, L., Li, Z., Liu, X., Zhu, L., Tang, Y., Zhang, B., Xu, B., Liu, M., Meng, Y. and Liu, B., 2020. Multi-type forest change detection using BFAST and monthly landsat time series for monitoring spatiotemporal dynamics of forests in subtropical wetland. *Remote Sensing*, 12(2), p.341
- Wulder, M.A., Hall, R.J., Coops, N.C. and Franklin, S.E., 2004. High spatial resolution remotely sensed data for ecosystem characterization. *BioScience*, 54(6), pp.511-521.
- Wulder, M.A., White, J.C., Nelson, R.F., Næsset, E., Ørka, H.O., Coops, N.C., Hilker, T., Bater, C.W. Gobakken, T., 2012. Lidar sampling for large-area forest characterization: A review. *Remote Sensing of Environment*, 121, 196-209.
- WWF., 2016. Five countries work toward a common goal in southern Africa, *Magazine Articles, WWF. World Wildlife Fund*. <https://www.worldwildlife.org/magazine/issues/spring-2016/articles/five-countries-work-toward-a-common-goal-in-southern-africa/> (accessed 01 July 2021).
- Xie, H., Zhang, Y., Wu, Z. and Lv, T., 2020. A bibliometric analysis on land degradation: Current status, development, and future directions. *Land*, 9(1), p.28.
- Xie, P. and Arkin, P.A., 1995. An intercomparison of gauge observations and satellite estimates of monthly precipitation. *Journal of Applied Meteorology and Climatology*, 34(5), pp.1143-1160.
- Xu, K., Zhang, Z., Yu, W., Zhao, P., Yue, J., Deng, Y. and Geng, J., 2021. How spatial resolution affects forest phenology and tree-species classification based on satellite and up-scaled time-series images. *Remote Sensing*, 13(14), p.2716.
- Xue, J. and Su, B., 2017. Significant remote sensing vegetation indices: A review of developments and applications. *Journal of sensors*, 2017.
- Xulu, S., Peerbhay, K., Gebreslasie, M. and Ismail, R., 2018. Drought influence on forest plantations in Zululand, South Africa, using MODIS time series and climate data. *Forests*, 9(9), p.528.

- Yang, J. and Prince, S.D., 2000. Remote sensing of savanna vegetation changes in Eastern Zambia 1972-1989. *International Journal of Remote Sensing*, 21(2), pp.301-322.
- Yang, J., Weisberg, P.J. and Bristow, N.A., 2012. Landsat remote sensing approaches for monitoring long-term tree cover dynamics in semi-arid woodlands: Comparison of vegetation indices and spectral mixture analysis. *Remote sensing of environment*, 119, 62-71.
- Yengoh, G.T., Dent, D., Olsson, L., Tengberg, A.E. and Tucker III, C.J., 2015. Use of the Normalized Difference Vegetation Index (NDVI) to assess Land degradation at multiple scales: current status, future trends, and practical considerations. *Springer*.
- Yoder, B.J. and Waring, R.H., 1994. The normalized difference vegetation index of small Douglas-fir canopies with varying chlorophyll concentrations. *Remote Sensing of Environment*, 49(1), pp.81-91.
- Zeileis, A., Leisch, F., Kleiber, C. and Hornik, K., 2005. Monitoring structural change in dynamic econometric models. *Journal of Applied Econometrics*, 20(1), pp.99-121.
- Zhang, W., Brandt, M., Wang, Q., Prishchepov, A.V., Tucker, C.J., Li, Y., Lyu, H., Fensholt, R., 2019.. From woody cover to woody canopies: How Sentinel-1 and Sentinel-2 data advance the mapping of woody plants in savannas. *Remote Sensing of Environment*, 234, 111465.
- Zhang, X., Kondragunta, S. and Quayle, B., 2011. Estimation of biomass burned areas using multiple-satellite-observed active fires. *IEEE Transactions on Geoscience and Remote Sensing*, 49(11), pp.4469-4482.
- Zhao, K., Wulder, M.A., Hu, T., Bright, R., Wu, Q., Qin, H., Li, Y., Toman, E., Mallick, B., Zhang, X. and Brown, M., 2019. Detecting change-point, trend, and seasonality in satellite time series data to track abrupt changes and nonlinear dynamics: A Bayesian ensemble algorithm. *Remote sensing of Environment*, 232, p.111181.
- Zhao, P., Lu, D., Wang, G., Wu, C., Huang, Y., Yu, S., 2016. Examining spectral reflectance saturation in Landsat imagery and corresponding solutions to improve forest aboveground biomass estimation. *Remote Sensing*, 8(6), 469.
- Zhao, Z., Li, W., Ciais, P., Santoro, M., Cartus, O., Peng, S., Yin, Y., Yue, C., Yang, H., Yu, L. and Zhu, L., 2021. Fire enhances forest degradation within forest edge zones in Africa. *Nature Geoscience*, 14(7), pp.479-483.
- Zheng, G., Chen, J.M., Tian, Q.J., Ju, W.M. and Xia, X.Q., 2007. Combining remote sensing imagery and forest age inventory for biomass mapping. *Journal of Environmental Management*, 85(3), pp.616-623.
- Zhou, B., Okin, G.S. and Zhang, J., 2020. Leveraging Google Earth Engine (GEE) and machine learning algorithms to incorporate in situ measurement from different times for rangelands monitoring. *Remote Sensing of Environment*, 236, p.111521
- Zhu, X. and Liu, D., 2015. Improving forest aboveground biomass estimation using seasonal Landsat NDVI time-series. *ISPRS Journal of Photogrammetry and Remote Sensing*, 102, pp.222-231.
- Zhu, X.X., Tuia, D., Mou, L., Xia, G.S., Zhang, L., Xu, F. and Fraundorfer, F. (2017). Deep learning in remote sensing: A comprehensive review and list of resources. *IEEE Geoscience and Remote Sensing Magazine*, 5(4), pp.8-36.
- Zhu, Z. and Woodcock, C.E., 2012. Object-based cloud and cloud shadow detection in Landsat imagery. *Remote sensing of environment*, 118, pp.83-94.

- Zhu, Z. and Woodcock, C.E., 2014. Continuous change detection and classification of land cover using all available Landsat data. *Remote sensing of Environment*, 144, pp.152-171.
- Zhu, Z., 2017. Change detection using landsat time series: A review of frequencies, preprocessing, algorithms, and applications. *ISPRS Journal of Photogrammetry and Remote Sensing*, 130, pp.370-384.
- Zhu, Z., Woodcock, C.E. and Olofsson, P., 2012. Continuous monitoring of forest disturbance using all available Landsat imagery. *Remote sensing of environment*, 122, pp.75-91.
- Zweede, M., Safford, H. and Juergens, G., 2006. USDA Forest Service Forest Resource Assessment Trip Kuando Kubango Province, Angola. support of the USAID Southern Africa's Okavango Integrated River Basin and the Angolan Ministry of Agriculture and Rural Development's National Institute for Forestry Development and Management Project, May 16 – June 1, 2006. *US-AID, Washington D.C., USA*.

# Appendix A

A policy brief published with N8 AgriFood at <https://policyhub.n8agrifood.ac.uk/>



## Remote sensing could enable more evidence-based policy to monitor and manage tropical dryland forests

### Key Messages

- Remote sensing and Earth Observation technologies help to assess and monitor forest ecosystems and provide spatially explicit, operational, and long-term data to assist the sustainable use of tropical environment landscapes.
- However, few studies assess carbon storage or biomass, and there is little research on EO methods for assessing REDD+ initiatives in dryland forests in most Southern African countries.
- Africa has the potential to emulate other continents, such as Latin America, that have made notable progress in employing freely available remote sensing data to monitor tropical dryland forest area change and biomass on a large scale.
- Greater use of a wider range of EO products could enable more evidence-based policy to prioritise sustainable use of forests, enabling the policy community to learn what works to reduce deforestation and forest degradation, to improve livelihoods in a changing climate.

### The Research

Researchers have assessed the evidence base for a number of tropical dryland forests-remote sensing options, asking how remote sensing technology was used to monitor and estimate changes in dryland forests in southern Africa. The researchers considering evidence from over 130 peer-reviewed papers including research on land-use/land-cover, forest cover/types, biomass, forest structure, biodiversity/habitats, phenology, plant traits, and disturbances from drought and fire. It considered publication trends over time, study location, remote sensing sensor/platform used, spatial and temporal coverage, remote sensing product (e.g., biophysical indices) used, and application areas of the study (e.g., land cover, forest biomass).

### Key findings and evidence

Publication trends	Although the volume of scientific literature has demonstrated a sharp increase, the use of remote sensing is still limited, and up until 2013, the number of publications on tropical dryland forests was relatively small.
Time scales	Time series analysis on dryland forests, which enables tracking changes is scarce, only 22 (16%) out of 137 studies feature time series lengths that exceed 15 years and only 11 (8%) studies that cover more than 20 years. Longer time series of remote sensing data afford the ability to assess the dynamics of forest structures, biodiversity, degradation, disturbance from climatic extremes, and change in phenology, in which a gap still exists.

Spatial scales	Despite new sensor and EO data availability, it is clear that a systematic and consistent regional monitoring of dryland forests is not yet fully exploited and is still in its infancy in Southern Africa. In fact, the majority of publications 88 (64%) concentrated their research efforts on local scale investigations. To fully assess regional and long-term implications for tropical dryland forest change studies, analyses on large(r) scales are needed, ideally with higher spatial resolutions and longer temporal duration.
Geographical focus	The Republic of South Africa is, by far the most studied nation across all categories in Southern Africa and the dryland forests of Angola, Mozambique, Lesotho, Swaziland, and Zambia are noticeably very poorly studied. In terms of National Parks, a large proportion of studies were undertaken in the Kruger National Park, leaving many other private and international protected areas relatively understudied. Future efforts to estimate important variables such as forest cover and biomass need not be restricted by country boundaries.
Research categories	Most studies focused on forest cover/types 41 (26%) and land cover/land use 36 (23%) categories while there is limited research on forest biomass and structures, disturbances from drought, phenology, plant traits, and biodiversity/habitats.
Vegetation indices	More than half of the studies, 84 (54%) of papers utilised the normalized difference vegetation index (NDVI), and few studies used other vegetation indices. Testing other vegetation indices beyond NDVI such as the Sentinel-2 red-edge related indices is needed in tropical dryland forests.
Remote sensing sensors	Imagery from optical sensors is most commonly used, out of all sensor types. More than 90% of papers investigated used optical sensors, 6% used SAR data and only 4% used a combination of SAR and Optical sensors. Further improvements should focus on extensive combination and fusion of SAR and optical data.
Validation and accuracy assessments	Our results show there is limited information on sources of error and uncertainty levels of the estimates provided by most studies, with only 54 (39%) of the studies appearing to have performed some form of accuracy assessment. Evidence indicates a need for more frequent use of field observation and inventory data, a greater use of validation/accuracy assessments.
Use of innovative remote sensing platforms	Only nine papers (6%) out of 137 used cloud-based geospatial analysis platforms such as Google Earth Engine (GEE) to access or analyse remote sensing data. The web-based platforms that reduce the need for costly local infrastructure (e.g., GEE), is an opportunity to overcome the limitations previously enforced by data scarcity, large volumes of data, and the scale of analysis.

## Limitations

- There is limited information on sources of error and uncertainty levels of the estimates provided by most studies assessed. As a result, for some interventions, there is not sufficient evidence to determine whether the number of studies done equates to research quality, which remains difficult to articulate from a review of this nature.
- One major problem encountered is that commonly used vegetation indices and classification schemes are generalised from better-studied ecosystems, such as temperate and rain forests and this has led to poor accuracy results when extrapolated to, for example, tropical dryland forests, making it difficult to create robust syntheses for decision-makers in policy and practice.

## Find out more

For more information, please contact:  
 Ruusa-Magano David  
 Email: [ruusa-magano.david@durham.ac.uk](mailto:ruusa-magano.david@durham.ac.uk)  
 Department of Geography, University of Durham

**Policy Brief:** [doi.org/10.5281/zenodo.5566493](https://doi.org/10.5281/zenodo.5566493)

**N8 AgriFood Food Systems Policy Hub**

Email: [policy@n8agrifood.ac.uk](mailto:policy@n8agrifood.ac.uk)

Website: <https://policyhub.n8agrifood.ac.uk>

*This brief is one of a collection produced by participants on the Rapid Evidence Synthesis Training (REST) programme. REST was delivered through a collaboration between the University of Leeds, Newcastle University and the N8 AgriFood Programme, supported by Research England QR-SPF funds from the University of Leeds and the University of York.*

## Appendix B

The analytical codes used in this thesis have been written in R and Google Earth Engine developed by Ruusa David. The substantial code will be uploaded in GitHub.

### CHAPTER 2

#### 2A. R CODE FOR ANALYSING AND PLOTTING DATA

This part of the R code is for analysing data for the systematic review

*Number of papers integrating remote sensing and dryland forests in Southern Africa.*

*# Install needed packages through the pkgTest which is a helper function to load packages and install packages only when they are not installed yet.*

```
pkgTest <- function(x)
{
  if (x %in% rownames(installed.packages()) == FALSE) {
    install.packages(x, dependencies= TRUE)
  }
  library(x, character.only = TRUE)
}
neededPackages <- c("sp", "zoo", "ggplot2", "dplyr")
for (package in neededPackages){pkgTest(package)}
```

*#Load the library*

```
library(ggplot2)
library(dplyr)
library(tidyverse)
library(sf)
```

```
library(scales)
library(ggrepel)
```

### **#path to data**

```
path=("C:/ ")
```

### **#Read the data**

```
No_study_SA <-read.csv(paste(path,"File.csv",sep="",collapse=""))
```

### **#Create the chart**

```
No_study_SA_plot1<- ggplot(No_study_SA, aes(y = NoPublication, x = Year,
width=.60)) + geom_col(fill = "aquamarine4", colour = "grey38", width=.85)
```

```
No_study_SA_plot2<- No_study_SA _plot1 + labs(x = "Year", y = "Number of
publications")+scale_x_continuous(breaks=seq(1997,2020,2))+scale_y_continuous
(breaks = breaks_width(2))+theme_bw()+geom_smooth(method = "lm",
colour="red", linetype="dashed", size=1.5,se=FALSE)
```

```
No_study_SA_plot2<- No_study_R_topic_country_plot2 +
theme(text=element_text(family="Tahoma",colour="black", size = 15),
axis.text.x=element_text(colour="black", size =12),
axis.text.y=element_text(colour="black", size = 12))
```

### **#run lm to get the intercept and slope**

```
lm(formula = NoPublication ~Year, data = No_study_SA_plot2)
```

### **#plot a trend line on the line graph**

```
No_study_SA_plot2<- No_study_SA _plot2 + geom_abline(intercept = -1100.7132 ,
slope = 0.5509 , colour="red", linetype="dashed", size=1.5)
```

### **#Plot the Chart**

```
No_study_SA_plot2
```

*Number of papers by research institutions.*

### **#Read the data**



```
No_study_Inst <-read.csv(paste(path," File.csv ",sep="",collapse=""))
```

### **#Create the Chart**

```
No_study_Inst_plot1<- ggplot(No_study_Inst (x = NoPublication, y  
=Institution.Category, fill = Institution.Type)) + geom_col()
```

```
No_study_Inst_plot2<- No_study_R_topic_country_plot1 + labs(x = "Published  
papers", y = "1st author Country")+ scale_fill_brewer(palette = "Dark2")  
+theme_bw()
```

```
No_study_Inst_plot2<- No_study_R_topic_country_plot2 +  
theme(text=element_text(family="Tahoma",colour="black", size = 15),  
axis.text.x=element_text(colour="black", size = 12),  
axis.text.y=element_text(colour="black", size = 12))
```

```
No_study_Inst_plot2<- No_study_Inst_plot2 +  
guides(fill=guide_legend(title="Institution category"))
```

### **#Plot the Chart**

```
No_study_Inst_plot2
```

## **Spatial extent of studies.**

### **#Read the data**

```
No_study_S_extent <-read.csv(paste(path," File.csv ",sep="",collapse=""))
```

### **#Create the chart**

```
No_study_S_extent_plot1<- ggplot(No_study_S_extent, aes(x =Scale, y  
=NumberofPublication, fill = fct_inorder(Scale))) +  
geom_col(colour = "grey50",width=0.9)
```

```
No_study_S_extent_plot2<- No_study_R_topic_country_plot1 + labs(x = "Spatial  
extent", y = "Number of publications")+ scale_colour_brewer()  
+scale_y_continuous(breaks = breaks_width(4))+ theme_bw()
```

```
No_study_S_extent_plot2<- No_study_S_extent_plot2 +  
theme(text=element_text(family="Tahoma",colour="black", size = 15),  
axis.text.x=element_text(colour="black", size =12),  
axis.text.y=element_text(colour="black", size = 12))
```

```
No_study_S_extent_plot2<- No_study_S_extent_plot2 +  
guides(fill=guide_legend(title="Spatial scale"))
```

### **#Plot the Chart**

```
No_study_S_extent_plot2
```

## **Temporal duration of studies.**

### **#Read the data**

```
No_study_T_extent <-read.csv(paste(path," File.csv ",sep="",collapse=""))
```

### **#Create the chart**

```
No_study_T_extent_plot1<- ggplot(No_study_T_extent, aes(x = Year, y  
=NoPublication, fill = TemporalResolution, width=.85)) +  
geom_col(colour="grey39", size=0.60)
```

```
No_study_T_extent_plot2<- No_study_T_extent_plot1 + labs(x = "Temporal extent  
(years)", y = "Number of publications")+ scale_fill_brewer(palette = "Set1")  
+scale_x_continuous(labels = 1:34, breaks = 1:34)+scale_y_continuous(breaks =  
breaks_width(4))+ theme_bw()
```

```
No_study_T_extent_plot2<- No_study_T_extent_plot2 +  
theme(text=element_text(family="Tahoma",colour="black", size = 15),  
axis.text.x=element_text(colour="black", size =10),  
axis.text.y=element_text(colour="black", size = 12))
```

```
No_study_T_extent_plot2<- No_study_T_extent_plot2  
+guides(fill=guide_legend(title="Temporal resolution"))
```

### **#Plot the Data**

```
No_study_T_extent_plot2
```

## **Research topic categories**

### **#Read the data**

```
No_study_R_topic <-read.csv(paste(path," File.csv.csv",sep="",collapse=""))
```

### **# Add label position #Note, calculate this before adding % sign to the number of publication**

```
No_study_R_topic <- No_study_R_topic %>%
```

```
arrange(desc(Research.focus)) %>% mutate(midpoint =
cumsum(Number.of.Publication) - 0.5*Number.of.Publication)
```

```
mycols <- c("#0073C2FF", "#EFC000FF", "#868686FF",
"#CD984CFF", "#007672FF", "#EFC000CC", "#896686FF", "#CD529CFF")
```

```
ggplot(No_study_R_topic, aes(x = "", y = Number.of.Publication, fill =
Research.focus)) +
```

```
geom_bar(width = 1, stat = "identity", colour = "white") + coord_polar("y", start =
0)+
```

```
geom_text(aes(y = midpoint, label = Number.of.Publication), colour = "white")+
```

```
scale_fill_manual(values = mycols) + theme_void()
```

### **#add columns for percentage**

```
No_study_R_topic <- No_study_R_topic %>%
```

```
mutate(Research.focus = factor(Research.focus,
```

```
levels = Research.focus[length(Research.focus):1]),
```

```
cumulative = cumsum(Number.of.Publication),
```

```
midpoint = cumulative - Number.of.Publication / 2,
```

```
labels = paste0(round((Number.of.Publication/ sum(Number.of.Publication))
* 100, 0), "%", " (", Number.of.Publication, ") ")
```

### **# Get the Pie Chart positions**

```
No_study_R_topic <- No_study_R_topic %>% mutate(csum =
rev(cumsum(rev(Number.of.Publication))),
```

```
pos = Number.of.Publication/2 + lead(csum, 1),
```

```
pos = if_else(is.na(pos), Number.of.Publication/2, pos))
```

### **#Plot the chart**

```
ggplot(No_study_R_topic, aes(x = "", y = Number.of.Publication, fill =
fct_inorder(Research.focus))) +
```

```
geom_col(width = 1, colour = 1) +
```

```
coord_polar(theta = "y") +
```

```
scale_fill_brewer(palette = "Set3") +
```

```
geom_label_repel(data = No_study_R_topic,
  aes(y = pos, label =labels),
  size = 4.5, nudge_x = 0.14, show.legend = FALSE) +
guides(fill = guide_legend(title = "Resesarch topic")) +
theme_void()
```

### *Number of studies based upon platform and sensor type.*

#### **#Read the data**

```
No_study_R_sensor <-read.csv(paste(path," File.csv ",sep="",collapse=""))
```

#### **#Create the chart**

```
No_study_R_sensor_plot1<- ggplot(No_study_R_sensor, aes(x =InstrumentName, y =
=NumberofPublication, fill = Sensor.Type,width=.60)) +
```

```
geom_col()
```

```
No_study_R_sensor_plot2<- No_study_R_sensor_plot1 + labs(x = "Platform", y =
"Number of publications")+ scale_colour_brewer(palette = "Greens")
+scale_y_continuous(breaks = breaks_width(10))+ theme_bw()+theme(axis.text.x
= element_text(angle = 90))
```

```
No_study_R_sensor_plot2<- No_study_R_sensor_plot2 +
theme(text=element_text(family="Tahoma",colour="black", size = 15),
```

```
axis.text.x=element_text(colour="black", size =12),
```

```
axis.text.y=element_text(colour="black", size = 12))
```

```
No_study_R_sensor_plot2<- No_study_R_sensor_plot2 +
guides(fill=guide_legend(title="Sensor Type"))
```

#### **#Plot the Chart**

```
No_study_R_sensor_plot2
```

### *Research topic by country*

#### **#Read the data**

```
No_study_R_topic_country<-read.csv(paste(path,"Article
Assessment_reseracharea_bycountry_2.csv",sep="",collapse=""))
```

#### **#Create the chart**

```
No_study_R_topic_country_plot1<- ggplot(No_study_R_topic_country, aes(x =
Country, y =Publications, fill = Research.Topic,width=.60)) + geom_col()
```

```
No_study_R_topic_country_plot2<- No_study_R_topic_country_plot1 + labs(x =
"Country", y = "Number of publications")+ scale_fill_brewer(palette =
```

```
"Set2")+theme_bw()+scale_y_continuous(breaks =  
breaks_width(5))+theme(axis.text.x = element_text(angle = 90))  
No_study_R_topic_country_plot2<- No_study_R_topic_country_plot2 +  
theme(text=element_text(family="Tahoma",colour="black", size = 15),  
axis.text.x=element_text(colour="black", size =12),  
axis.text.y=element_text(colour="black", size = 12))
```

### ***#Plot the Chart***

```
No_study_R_topic_country_plot2
```

## **CHAPTER 3**

### **3A. GOOGLE EARTH ENGINE CODE FOR DOWNLOADING IMAGES, CLASSIFICATION AND CHANGE DETECTION**

Google Earth Engine Code for downloading Landsat, Sentinel 1 and 2  
images, satellite image classification and change detection

#### ***Image classification for Landsat 2004***

<https://code.earthengine.google.com/5f543641fb703ab0bbf23ea869e3d4a8?noload=1>

#### ***Image classification for 2018 code***

<https://code.earthengine.google.com/57348f290a26907372d530f21762c718?noload=1>

#### ***Perform a Change detection***

<https://code.earthengine.google.com/d7618eedeaf46fcf53a7de56df0af330?noload=1>

#### ***Landsat image code***

<https://code.earthengine.google.com/421117de52df03e0fabf48edac554aae?noload=1>

## Sentinel image code

<https://code.earthengine.google.com/33b7477b23ad3a8bf1f220486c283da1?noload=1>

### 3B. R CODE FOR ESTIMATING FOREST STAND PARAMETERS

This part of the R code is for estimating forest stand parameters

*Estimates for forest stand parameters using Chave et al., 2005 allometric Equation*

#### **ESTIMATES FOREST STAND PARAMETERS**

##### **# Install needed packages through the pkgTest**

```
pkgTest <- function(x)
{
  if (x %in% rownames(installed.packages()) == FALSE) {
    install.packages(x, dependencies= TRUE)
  }
  library(x, character.only = TRUE)
}
neededPackages <- c("rgeos "," raster ", "ggplot2", "dplyr")
for (package in neededPackages){pkgTest(package)}
```

##### **#Load the library**

```
library(rgdal)
library(raster)
library(rgeos)
library(ggplot2)
library(rcompanion) #for transforming
library(Hmisc) # compute significance levels for pearson
library(dplyr) # to use select
library(ggpubr) #for ggscatterForest
library(ggpmisc)
library(corrplot) #Forest correlation
library(MASS) #for BOXCOS Transformation
library(devtools)
library(ithir) #To check regression prediction
library(MASS)
library(car)#for vif to test multicollinearity
```

```

library(performance) #To test model performance
library(randomForest)
library(DAAG) #for k fold validation in linear regression
to test multicollinearity
library(performance)

```

**#Apply the allometric equation from Chave et al., 2005 for dry forest**

```

ForestPlots <- plotdata %>%
  mutate(BasalArea_m2 = 0.0001*pi*(DBH/2)^2,
         standBasalArea_m2=0.0001*pi*(DBH/2)^2/0.05*20,
         WoodDensity = 0.79,

```

**#Estimate DBH**

```

AGB_kg_Chave_DBH = WoodDensity*exp(-
0.667+(1.784*log(DBH))+(0.207*(log(DBH))^2)-(0.0281*(log(DBH))^3))

```

**#Estimate with DBH and total tree height (H)**

```

AGB_kg_Chave_H_DBH = exp(-2.187+(0.916*log(WoodDensity*DBH^2*Height))),

```

**CALCULATE/ ESTIMATES OF STAND LEVEL PARAMETERS**

**(including DBH, Basal Area, Height, AGB, Carbon etc)**

```

StandPhysicalParams <- Plotmeta %>%
  group_by(ForestID) %>%
  mutate(PlotArea_m2 = pi * PlotSize^2,
         scalingFactor = 10000/PlotArea_m2) #convert to hectare

```

```

StandForestParams <- ForestPlots %>%
  group_by(ForestID) %>%
  summarise(DBH_mean = mean(DBH, na.rm = T),
            DBH_sd = sd(DBH, na.rm = T),
            DBH_median= median(DBH, na.rm = T),
            BA_mean = mean(BasalArea_m2, na.rm = T),
            BA_sum = sum(BasalArea_m2, na.rm = T),
            BA_sd = sd(BasalArea_m2, na.rm = T),

```

```

standBA_sum=sum(standBasalArea_m2, na.rm = T),
standBA_mean=mean(standBasalArea_m2, na.rm = T),
Height_mean = mean(Height, na.rm = T),
Height_median = median(Height, na.rm = T),
Height_sd = sd(Height, na.rm = T),
Tree_Density = n(),
AGB_kg_sum_Chav_Height_DBH = sum(AGB_kg_Chave_H_DBH, na.rm = T),
AGB_kg_sum_Chav_DBH =sum(AGB_kg_Chave_DBH, na.rm = T))
standParams <- left_join(StandPhysicalParams,StandForestParams, by =
"ForestID") %>%
mutate(Tree_DensityHa = Tree_Density*scalingFactor,
BA_m2Ha = BA_sum*scalingFactor,
AGB_kgHa_Chav_H = AGB_kg_sum_Chav_Height_DBH*scalingFactor,
AGB_tHa_Chav_H = AGB_kgHa_Chav_H/1000,
AGB_tCHa_Chav_H = AGB_tHa_Chav_H*0.5,

AGB_kgHa_Chav_DBH = AGB_kg_sum_Chav_DBH*scalingFactor,
AGB_tHa_Chav_DBH = AGB_kgHa_Chav_DBH/1000,
AGB_tCHa_Chav_DBH = AGB_tHa_Chav_DBH*0.5)

```

### **# Plots of forest stand parameters**

```
library (cowplot)
```

```
library(ggpubr)
```

### ***#Stand forest DBH***

```
Stand_DBH <-
```

```
ggplot(aes(ForestID, DBH_mean),
```

```
data = standParams[1:78,]) +
```

```
geom_col(aes()) +
```

```
theme_bw() +
```

```
theme(panel.grid.major.x = element_blank(),
```

```
text = element_text(size=12),
```

```
axis.text.x = element_text(angle = 55, hjust = 1)) +
```



```
labs(x = "Plot ID", y = "Mean DBH (cm)") +
geom_errorbar(aes(ymin=DBH_mean-DBH_sd, ymax=DBH_mean+DBH_sd),
              width=.5)
```

### ***# Stand forest Basal Area***

```
Stand_BA <-
ggplot(aes(ForestID, BA_mean),
       data = standParams[1:78,]) +
geom_col(aes()) +
theme_bw() +
theme(panel.grid.major.x = element_blank(),
       text = element_text(size=12),
       axis.text.x = element_text(angle = 55, hjust = 1)) +
labs(x = "Plot ID", y = "Mean Basal Area (m2)") +
geom_errorbar(aes(ymin=BA_mean-BA_sd, ymax=BA_mean+BA_sd),
              width=.5)
```

### ***# Stand forest Height***

```
Stand_Height <-
ggplot(aes(ForestID, Height_mean),
       data = standParams[1:78,]) +
geom_col(aes()) +
theme_bw() +
theme(panel.grid.major.x = element_blank(),
       text = element_text(size=12),
       axis.text.x = element_text(angle = 55, hjust = 1)) +
labs(x = "Plot ID", y = "Mean Tree Height (m)") +
geom_errorbar(aes(ymin=Height_mean-Height_sd, ymax=Height_mean+Height_sd),
              width=.5)
```

### ***# Stand forest Tree Density***

```
Stand_Density <-
```

```

ggplot(aes(ForestID, Tree_DensityHa),
  data = standParams[1:78,]) +
geom_col(aes()) +
theme_bw() +
theme(panel.grid.major.x = element_blank(),
  text = element_text(size=12),
  axis.text.x = element_text(angle = 55, hjust = 1)) +
labs(x = "Plot ID", y = "Tree Density (Trees ha-1)")

```

### ***# Above Ground Biomass using DBH for CHAVE***

```

Stand_AGB_tha_DBH_Chav <-
ggplot(aes(ForestID, AGB_tHa_Chav_DBH),
  data = standParams[1:78,]) +
geom_col(aes()) +
theme_bw() +
theme(panel.grid.major.x = element_blank(),
  text = element_text(size=12),
  axis.text.x = element_text(angle = 55, hjust = 1)) +
labs(x = "Plot ID", y = "AGB with DBH; (t ha-1)")

```

```

Stand_AGB_tCha_DBH_Chav <-
ggplot(aes(ForestID, AGB_tCha_Chav_DBH),
  data = standParams[1:78,]) +
geom_col(aes()) +
theme_bw() +
theme(panel.grid.major.x = element_blank(),
  text = element_text(size=12),
  axis.text.x = element_text(angle = 55, hjust = 1)) +
labs(x = "Plot ID", y = "Total Carbon with DBH; (t C ha-1)")

```

### ***# Stand forest AGB with Height***

```

Stand_AGB_tha_H_Chav <-
  ggplot(aes(ForestID, AGB_tHa_Chav_H),
    data = standParams[1:78,]) +
  geom_col(aes()) +
  theme_bw() +
  theme(panel.grid.major.x = element_blank(),
    text = element_text(size=16),
    axis.text.x = element_text(angle = 55, hjust = 1)) +
  labs(x = "Plot ID", y = "AGB (Mg/ha)")

```

```

Stand_AGB_tCha_H_Chav <-
  ggplot(aes(ForestID, AGB_tCHa_Chav_H),
    data = standParams[1:78,]) +
  geom_col(aes()) +
  theme_bw() +
  theme(panel.grid.major.x = element_blank(),
    text = element_text(size=16),
    axis.text.x = element_text(angle = 55, hjust = 1)) +
  labs(x = "Plot ID", y = "Total Carbon (Mg/ha)")

```

**#Plot the forest stand parameters Individually**

```

plot_grid(Stand_DBH)
plot_grid(Stand_BA)
plot_grid(Stand_Height)
plot_grid(Stand_Density)
plot_grid(Stand_AGB_tha_H_Chav)
plot_grid(Stand_AGB_tCha_H_Chav, labels = "auto",
  label_size = 18,
  align = "v")
plot_grid(Stand_AGB_tha_DBH_Chav)
plot_grid(Stand_AGB_tCha_DBH_Chav)

```

**#Plot the forest stand parameters in one Figure**

```
StandFigure <- hist(Stand_AGB_tha_H_Chav,Stand_AGB_tCha_H_Chav,  
  ncol = 1, nrow = 2, align = "v", axis = "r",labels="auto", label_size = 18)  
StandFigure
```

**PLOT THE DENSITY AND HISTOGRAM PLOTS FOR AGB AND CARBON**

**3.1 Create density and histogram plots for Aboveground biomass (AGB)of each field plot with woodland trees.**

```
AGB<-ggplot(standParams[1:78,], aes(x=AGB_tHa_Chav_H)) +  
  geom_histogram(aes(y =..density..),  
    breaks=seq(2, 170, by = 10),  
    col="Black",  
    fill="#FF6666", alpha = .1 ) + theme_bw()+  
  geom_density(alpha=.2, fill="black") +  
  # labs(title="AGB (Mg/ha)") +  
  labs(x="AGB (Mg/ha)", y="Count") +  
  theme(axis.line = element_line(size=1, colour = "black"),  
    panel.grid.major = element_blank(),  
    panel.grid.minor = element_blank(),  
    panel.border = element_blank(),  
    panel.background = element_blank(),  
    plot.title=element_text(size = 20,face="bold"),  
    text=element_text(size = 16),  
    axis.text.x=element_text(colour="black", size = 14,face="bold"),  
    axis.text.y=element_text(colour="black", size = 14,face="bold"),  
    axis.title.x = element_text(colour="black", size=16, face="bold"),  
    axis.title.y = element_text(colour="black", size=16, face="bold"),  
    axis.text=element_text(colour="black", size=14))
```

**3.2 CARBON: Create density and histogram plots Carbon stock (Mg/ha) of each field plot with woodland trees.**

```

carbon<-ggplot(standParams[1:78,], aes(x=AGB_tCHa_Chav_H)) +
  geom_histogram(aes(y =..density..),
    breaks=seq(1.03, 84, by = 10),
    col="black",
    fill="#FF6666", alpha = .1
  ) + theme_bw()+
  geom_density(alpha=.2, fill="black") +
  # labs(title="AGB (Mg/ha)") +
  labs(x="Total Carbon (Mg/ha)", y="") +
  theme(axis.line = element_line(size=1, colour = "black"),
    panel.grid.major = element_blank(),
    panel.grid.minor = element_blank(),
    panel.border = element_blank(),
    panel.background = element_blank(),
    plot.title=element_text(size = 20,face="bold"),
    text=element_text(size = 16),
    axis.text.x=element_text(colour="black", size = 14,face="bold"),
    axis.text.y=element_text(colour="black", size = 14,face="bold"),
    axis.title.x = element_text(colour="black", size=16, face="bold"),
    axis.title.y = element_text(colour="black", size=16, face="bold"),
    axis.text=element_text(colour="black", size=14))

```

### **# Plot the density and histogram plot for carbon**

```
carbon
```

### **#Combine all the plots**

```
ggarrange(AGB, carbon,
```

```

  labels = c("A", "B"),common.legend=TRUE,legend = "top",# specify the legend
  position and specify whether they should share the common legend or not.

```

```

  ncol = 2, nrow = 2) # column and row numbers

```

## **2. Estimates the AGB using Linear Model (Raster data)**

### **#Read the csv data**

```
S2chobezam_wo.num<-read.csv(paste(path,"File.csv",sep="",collapse=""))
```

### **#Transform the data for normality**

```
S2chobezam_wo.num$AGBL<-log(S2chobezam_wo.num$AGB_tHa_Chav_H)
```

### **#display histogram for transformed AGB**

```
hist(S2chobezam_wo.num$AGBL)
```

### **#choose variables to work (Sentinel 1, Sentinel 2 and Landsat 8 bands and indices)**

```
S2chobezam_wo.num=dplyr::select(S2chobezam_wo.num,AGBL,B2,B3,B4,B5,B6,B7,B8,B8A,B11,B12,S1_VH,S1_VV,ndvi,grvi,evi,savi,msav,nbr,nbr2,gndvi,nR1,nR2,nR3,nR4,ndi45,ireci,srtm)
```

### **#read in Raster data-sentinel**

### **# NB: Load Sentinel 1, Sentinel 2, and Landsat 8 tif files. Below is an example of Sentinel 2 data loaded in r**

```
S2_chobe<-list.files ("Path/", pattern = ".tif$", full.names = TRUE)
```

### **#stack all bands**

### **#covariates are of the same scale in terms of resolution and extent.**

```
S2_03_chobe<- stack(S2_chobe[])
```

### **# Linear Model prediction**

```
hv.MLR.rh <-lm(AGBL~B3+B5+S1_VH+S1_VV, data =S2chobezam_wo.num)
```

```
vif(hv.MLR.rh)
```

```
summary(hv.MLR.rh)
```

### **#Estimate AGB using Linear Model**

### **#predict from raster data**

```
map.MLR1<- exp(predict(S2_03_chobe,hv.MLR.rh,format = "GTiff", datatype = "FLT4S", overwrite = TRUE)) # backtransform the log data to original
```

```
plot(map.MLR1, main = "S2 Biomass prediction with linear model")
```

**# including all bands and indices, and choose the right variables**

```
tempD <- data.frame(cellNos = seq(1:ncell(S2_03_chobe)))  
vals <- as.data.frame(getValues(S2_03_chobe))  
tempD <- cbind(tempD, vals)  
tempD <- tempD[complete.cases(tempD), ]  
cellNos <- c(tempD$cellNos)  
gXY <- data.frame(xyFromCell(S2_03_chobe, cellNos, spatial = FALSE))  
tempD <- cbind(gXY, tempD)  
str(tempD)
```

**# backtransform the log data to original scale with exp**

```
map.MLR <- exp(predict(hv.MLR.rh, newdata = tempD))  
map.MLR <- cbind(data.frame(tempD[, c("x", "y")]), map.MLR) #include x and y  
coordinates
```

**#rasterise the predictions for mapping**

```
map.MLR.r <- rasterFromXYZ(as.data.frame(map.MLR[, 1:3])) #include the cell  
numbers  
plot(map.MLR.r, main = "S2 Biomass prediction with glm forest")
```

**Validate the AGB using Linear Model**

**# validate the Linear model**

**#split the data 70 and 30% for validation**

```
set.seed(123)  
training <- sample(nrow(S2chobezam_wo.num), 0.7 *  
nrow(S2chobezam_wo.num))
```

**#display the calibration data**

```
training
```

**#fit the model**

```
hv.MLR.rh <-lm(AGBL~B3+B5+S1_VH+S1_VV+gndvi+ndi45, data
=S2chobezam_wo.num,y=TRUE, x=TRUE)
```

```
AGB.pred.F <- predict(hv.MLR.rh, S2chobezam_wo.num)
```

#### **#Evaluate the model with goof:**

```
goof(observed = S2chobezam_wo.num$AGBL, predicted= AGB.pred.F,plot.it =
TRUE)
```

#### **#Check model performance**

```
model_performance(hv.MLR.rh)
```

#### **#Evaluate the calibration model**

```
AGB.pred.C <- predict(hv.MLR.rh, S2chobezam_wo.num[training, ])
```

```
goof(observed = S2chobezam_wo.num$AGBL[training], predicted
= AGB.pred.C,plot.it = TRUE)
```

#### **#Evaluate the validation model**

```
AGB.pred.V <- predict(hv.MLR.rh, S2chobezam_wo.num[-training, ])
```

```
goof(observed = S2chobezam_wo.num$AGBL[-training], predicted
= AGB.pred.V,plot.it = TRUE)
```

#### **# set the CRS to +zone=35 +south +datum=WGS84**

```
crs(map.MLR.r) <- "+proj=utm +zone=35 +south +datum=WGS84 +units=m
+no_defs +ellps=WGS84 +towgs84=0,0,0"
```

#### **#Export the map**

```
writeRaster(map.MLR.r, filename="Path", datatype = "FLT4S", overwrite = TRUE)
```

#### **Estimated AGB vs Field-based AGB for Linear Models (Calibration Data: 70%)**

#### **#Plot the predicted vs the observed for Linear Model**

#### **#fit the model**

```
chobe.MLR<-lm(AGBL~B3+B5+S1_VV, data =S2chobezam_wo.num)
```

```
summary(chobe.MLR)
```



```
predicted AGB <- predict(chobe.MLR, S2chobezam_wo.num)
goof(observed = S2chobezam_wo.num$AGBL, predicted= predicted_AGB)
```

### **#plot the model**

```
gg0 <- ggplot(S2chobezam_wo.num,aes(
AGBL,predicted_AGB))+geom_point(aes()) #colour by forest types
gg0<-gg0+geom_point( size=4)
gg1 <- gg0 + geom_smooth(method="lm",se=FALSE,
colour="black")#+geom_abline(linetype="dashed",col="red")
gg1
glm1<- gg1+stat_regline_equation (aes(label = paste(..adj.rr.label., sep =
"~~~~")), label.x.npc = "left", label.y.npc = 0.95,hjust=0,size=5.5,face="bold")
#include Y
```

### **# Calculate RMSE**

```
chobe.MLR1 <-lm(AGBL~predicted_AGB, data =S2chobezam_wo.num)
rmse <- round(sqrt(mean(resid(chobe.MLR1 )^2)), 2)
```

### **#plot the rmse**

```
gg<-glm1 + geom_text(aes(x=0.5, y=4.8,size=30, label= paste("RMSE= ", rmse,
"Mg/ha"), hjust=0))
gg<-gg+theme_bw()
gg<-gg + labs(y="Predicted AGB (Mg/ha)", x = "Observed AGB (Mg/ha)", title = "(a)
MLR AGB Model")
rmse_xy<-gg + theme(
plot.title = element_text(colour="black", size=20, face="bold.italic"),
axis.title.x = element_text(colour="black", size=20, face="bold"),
axis.title.y = element_text(colour="black", size=20, face="bold"),
axis.text=element_text(colour="black", size=20, face="bold")
)
rmse_xy
```

### **#Calculate the residuals**

```

chobe.MLR <-lm(AGBL~B3+B5+S1_VV, data =S2chobezam_wo.num)

predicted_AGB <- predict(chobe.MLR, S2chobezam_wo.num)

err<-predicted_AGB- S2chobezam_wo.num$AGBL

df<-data.frame(residuals=err, fitted.values=predicted_AGB )

df2<-df[order(df$fitted.values),]

plot(residuals~fitted.values, data=df2, ylab="Residuals", xlab="AGB (Mg/ha)",
      main="(a MLR AGB residuals ", cex.lab=2.0, cex.main=2.0,
      cex.axis=2.0,pch=19,cex=1.4, font = 2, font.lab=2,font.main=4) +abline(0,0,
      col="black")

```

*Estimated AGB vs Field-based AGB for Linear Models (Validation Data: 30%)*

**#Plot the predicted vs the observed for Linear Model**

**#fit the model**

```

chobe.MLR<-lm(AGBL~B3+B5+S1_VV, data =S2chobezam_wo.num)
summary(chobe.MLR)
predicted_AGB <- predict(chobe.MLR, S2chobezam_wo.num)
goof(observed = S2chobezam_wo.num$AGBL, predicted= predicted_AGB)

```

**#plot the model**

```

gg0 <- ggplot(S2chobezam_wo.num,aes(
AGBL,predicted_AGB))+geom_point(aes()) #colour by forest types
gg1 <- gg0 + geom_smooth(method="lm",se=FALSE,
colour="black")#+geom_abline(linetype="dashed",col="red")

gg1

glm1<- gg1+stat_regline_equation (aes(label = paste(..adj.rr.label., sep =
"~~~~")), label.x.npc = "left", label.y.npc = 0.95,hjust=0,face="bold") #include Y

```

**# Calculate RMSE**

```
chobe.MLR1 <-lm(AGBL~predicted_AGB, data =S2chobezam_wo.num)
rmse <- round(sqrt(mean(resid(chobe.MLR1 )^2)), 2)
```

### **#plot the rmse**

```
gg<-glm1 + geom_text(aes(x=0.5, y=4.8, label= paste("RMSE= ", rmse, "Mg/ha"),
hjust=0))
```

```
gg<-gg+theme_bw()
```

```
gg<-gg + labs(y="Predicted AGB (Mg/ha)", x = "Observed AGB (Mg/ha)", title =
"AGB Model (a) Linear regression")
```

```
gg
```

```
rmse_xy<-gg + theme(
  plot.title = element_text(colour="black", size=20, face="bold.italic"),
  axis.title.x = element_text(colour="black", size=16, face="bold"),
  axis.title.y = element_text(colour="black", size=16, face="bold"),
  axis.text=element_text(colour="black", size=14)
)
rmse_xy
```

### **#Calculate the residuals**

```
chobe.MLR <-lm(AGBL~B3+B5+S1_VV, data =S2chobezam_wo.num)
predicted_AGB <- predict(chobe.MLR, S2chobezam_wo.num)
err<-predicted_AGB- S2chobezam_wo.num$AGBL
df<-data.frame(residuals=err, fitted.values=predicted_AGB )
df2<-df[order(df$fitted.values),]
```

### **#Plot the residuals**

```
plot(residuals~fitted.values, data=df2, ylab="Residuals", xlab="AGB (Mg/ha)",
  main="AGB residuals (a) Linear regression ", cex.lab=1.5, cex.main=1.5,
  cex.axis=1.5) +
  abline(0,0, col="black")
```

## Validate Estimated AGB vs Field-based AGB for Linear Models

### **#split the data 70 and 30% for validation**

```
training <- sample(nrow(S2chobezam_wo.num), 0.7 *  
nrow(S2chobezam_wo.num))
```

### **#fit the model**

```
chobe.MLR <- lm(AGBL~B3+B5+S1_VV, data =S2chobezam_wo.num[-training,])
```

```
summary(chobe.MLR)
```

```
predicted_AGB <- predict(chobe.MLR, S2chobezam_wo.num[-training,])
```

```
goof(observed = S2chobezam_wo.num[-training,]$AGBL, predicted=  
predicted_AGB)
```

```
RF.pred.C <- predict(chobe.MLR, newdata =S2chobezam_wo.num[training, ])
```

### **#calibration**

```
goof(observed = S2chobezam_wo.num$AGBL[training], predicted = RF.pred.C,  
plot.it=TRUE)
```

### **#Validation**

```
MLR.pred.V <- predict(chobe.MLR, newdata = S2chobezam_wo.num[-training, ])
```

```
goof(observed = S2chobezam_wo.num$AGBL[-training], predicted  
=MLR.pred.V,plot.it = TRUE)
```

## Estimates the AGB using Random Forest Model (Raster data)

### **#Split the data into calibration and validation dataset**

```
set.seed(123)
```

```
training <- sample(nrow(S2chobezam_wo.num), 0.7 *  
nrow(S2chobezam_wo.num))
```

### **#fit the RF model**

```
chobe.rf.mod <- randomForest(AGBL~B3+B5+S1_VV, data  
=S2chobezam_wo.num,mtry=3,importance=TRUE,ntree=1000)
```

```
print(chobe.rf.mod)
```

### **#Plot variable importance**

```
varImpPlot(chobe.rf.mod)
```

### **#check the model residuals**

```
S2chobezam_wo.num$residual <- S2chobezam_wo.num$AGBL-  
predict(chobe.rf.mod,  
newdata = S2chobezam_wo.num, plot.it=True)  
hist(S2chobezam_wo.num$residual)  
mean(S2chobezam_wo.num$residual)
```

### **# backtransform the log data to original**

```
map.RF.r1 <- exp(predict(S2_03_chobe, chobe.rf.mod, "Chobe Biomass_RF.tif",  
format = "GTiff", datatype = "FLT4S", overwrite = TRUE))
```

### **#Plot the data**

```
plot(map.RF.r1 , main = "Random Forest model predicted Biomass")
```

## **Estimated AGB vs Field-based AGB for Random Forest Model (Calibration Data: 70%)**

### **#Plot the predicted vs the observed**

#### **#fit the model**

```
chobe.rf.mod <- randomForest(AGBL~B3+B5+S1_VV, data  
=S2chobezam_wo.num,mtry=3,importance=TRUE,ntree=1000, trace=true)  
print(chobe.rf.mod)  
predicted_AGB <- predict(chobe.rf.mod, S2chobezam_wo.num)  
goof(observed = S2chobezam_wo.num$AGBL, predicted= predicted_AGB)
```

#### **#plot the model**

```
gg0 <- ggplot(S2chobezam_wo.num,aes(  
AGBL,predicted_AGB))+geom_point(aes()) #colour by forest types  
gg0<-gg0+geom_point( size=4)
```

```
gg1 <- gg0 + geom_smooth(method="randomForest",
  colour="black")+geom_abline(linetype="dashed",col="red")
gg1<-gg1+geom_abline(intercept = 0,slope=1,col="black")
glm1<- gg1+stat_regline_equation (aes(label = paste(..adj.rr.label., sep =
"~~~~")), label.x.npc = "left", label.y.npc = 0.9,hjust=0,size=5.5,face="bold")
#include Y
```

### **# Calculate RMSE**

```
chobe.rf.mod1 <-randomForest(AGBL~predicted_AGB, data
=S2chobezam_wo.num,importance=TRUE,ntree=1000)
rmse_function<-function(pred,actual){
  sqrt(sum(pred-actual)^2)
}
rmse<-round(rmse_function( predicted_AGB,S2chobezam_wo.num$AGB),2)
rmse
```

### **#plot the rmse**

```
gg<-glm1 + geom_text(aes(x=0.5, y=4.3,size=30,face="bold", label= paste("RMSE=
", rmse, "Mg/ha"), hjust=0))
gg<-gg+theme_bw()
gg<-gg + labs(y="Predicted AGB (Mg/ha)", x = "Observed AGB (Mg/ha)", title = "(b)
RFR AGB Model")
```

```
gg
rmse_xy<-gg + theme(
  plot.title = element_text(colour="black", size=20, face="bold.italic"),
  axis.title.x = element_text(colour="black", size=20, face="bold"),
  axis.title.y = element_text(colour="black", size=20, face="bold"),
  axis.text=element_text(colour="black", size=20, face="bold")
)
rmse_xy
```

### **#Calculate the residuals**

```
chobe.rf.mod <-randomForest(AGBL~B3+B5+S1_VV, data
=S2chobezam_wo.num,mtry=3, importance=TRUE,ntree=1000)
```

```

print(chobe.rf.mod)
predicted_AGB <- predict(chobe.rf.mod, S2chobezam_wo.num)
err<-predicted_AGB- S2chobezam_wo.num$AGBL
df<-data.frame(residuals=err, fitted.values=predicted_AGB )
df2<-df[order(df$fitted.values),]

```

### **#Plot the residuals**

```

plot(residuals~fitted.values, data=df2, ylab="Residuals", xlab="AGB (Mg/ha)",
     main="(b) RFR AGB residuals ", cex.lab=2.0, cex.main=2.0,
     cex.axis=2.0,pch=19,cex=1.4, font = 2, font.lab=2,font.main=4) +
     abline(0,0, col="black",lwd=2.5)

```

## **Validate Estimated AGB vs Field-based AGB for Random Forest Model**

### **#split the data 70 and 30% for validation**

```

training <- sample(nrow(S2chobezam_wo.num), 0.7 *
nrow(S2chobezam_wo.num))

```

### **#fit the model**

```

chobe.rf.mod <-randomForest(AGBL~B3+B5+S1_VV, data
=S2chobezam_wo.num,mtry=3,importance=TRUE,ntree=1000)
print(chobe.rf.mod)
predicted_AGB <- predict(chobe.rf.mod, S2chobezam_wo.num)
goof(observed = S2chobezam_wo.num$AGBL, predicted= predicted_AGB)

```

### **# Internal validation**

```

RF.pred.C <- predict(chobe.rf.mod, newdata =S2chobezam_wo.num[training, ])
goof(observed = S2chobezam_wo.num$AGBL[training], predicted = RF.pred.C,
plot.it=TRUE)

```

### **#External validation**

```

RF.pred.V <- predict(chobe.rf.mod, newdata = S2chobezam_wo.num[-training, ])

```

```
goof(observed = S2chobezam_wo.num$AGBL[-training], predicted =  
RF.pred.V,plot.it = TRUE)
```

### Computing variables correlation

#### (i) PEARSON CORRELATION WITH S2 BANDS

##### #Read the csv data

```
S2chobezam_wo.num<-read.csv(paste(path," File.csv ",sep="",collapse=""))
```

##### #Choose the variable (Sentinel 1, Sentinel 2 and Landsat 8 bands and indices)

```
S2chobezam_wo.num2=dplyr::select(S2chobezam_wo.num,AGBL,  
B2,B3,B4,B5,B6,B7,B8,B8A,B11,B12,S1_VH,S1_VV,ndvi,grvi,evi,savi,msav,nbr,nbr2,  
gndvi,nR1,nR2,nR3,nR4,ndi45,ireci,srtm, HeightL, DenHAL)
```

##### compute the correlation matrix

```
cor2<-rcorr((as.matrix(S2chobezam_wo.num2)))
```

##### # compute variable p-values

```
cor2$P
```

#### (ii) CREATE A SCATTER PLOTS FOR CORRELATION

##### #SAR sentinel 1 scatterplot

##### #Plot S1 VV and AGB

```
S1_VV <- ggplot(data = S2chobezam_wo.num, aes(x=S1_VV, y = AGBL))+  
geom_point(aes())  
S1_VV<-S1_VV+geom_point( size=4)  
S1_VV<-S1_VV+geom_smooth(method = "lm", se=FALSE, colour="black", formula =  
y ~ x) #to exclude the line in the middle set (se=FALSE),
```

##### # Get equation and r-squared as string

##### #make a function to plot the equation

```
lm_eqn <- function(S2chobezam_wo.num){  
  m <- lm(AGBL~S1_VV, S2chobezam_wo.num);  
  eq <- substitute(italic(y) == a + b %.% italic(x)*" ~ ~italic(r)^2 ~ "=" ~r2,  
    list(a = format(unname(coef(m)[1]), digits = 2),  
      b = format(unname(coef(m)[2]), digits = 2),  
      r2 = format(summary(m)$r.squared, digits = 2)))  
  as.character(as.expression(eq));}  
S1_VV_eq <- S1_VV + geom_text(x = -15.0, y = 4.8, size=5.5,label =  
lm_eqn(S2chobezam_wo.num), parse = TRUE)  
S1_VV_eq
```



### **# Calculate RMSE**

```
S1_VV_model<-lm(AGBL~S1_VV, data=S2chobezam_wo.num)
rmse <- round(sqrt(mean(resid(S1_VV_model)^2)), 2)
```

### **# Plot RMSE**

```
S1_VV_rmse<-S1_VV_eq + geom_text(aes(x=-16.0, y=4.5, size=35,label=
paste("RMSE= ", rmse, "Mg/ha"), hjust=0))+theme_bw()
S1_VV_rmse_xy <- S1_VV_rmse + labs(y="AGB (Mg/ha)", x="S1 VV
Polarisation",title="(a) Sentinel-1 Backscatter Value on VV")
S1_VV_rmse_xy<-S1_VV_rmse_xy + theme(text = element_text(size = 14))
S1_VH_rmse_xy
```

### **#Sentinel 2 scatterplot**

#### **#Plot Sentinel 2 variable ands AGB**

```
B2 <- ggplot(data = S2chobezam_wo.num, aes(x =B2, y = AGBL))+
geom_point(aes())
```

```
B2<-B2+geom_smooth(method = "lm", colour="black", formula = y ~ x) #to
exclude the line in the middle set (se=FALSE),
```

### **#Get equation and r-squared as string**

#### **#make a function to plot the equation**

```
lm_eqn <- function(S2chobezam_wo.num){
  m <- lm(AGBL~B2, S2chobezam_wo.num);
  eq <- substitute(italic(y) == a + b %.% italic(x)*", "~italic(r)^2~"="~r2,
    list(a = format(unname(coef(m)[1]), digits = 2),
          b = format(unname(coef(m)[2]), digits = 2),
          r2 = format(summary(m)$r.squared, digits = 2)))
  as.character(as.expression(eq));
}
```

```
B2_eq <- B2 + geom_text(x = 0.06, y = 2, label = lm_eqn(S2chobezam_wo.num),
parse = TRUE)
```

### **# Calculate RMSE**

```
B2_model<-lm(AGBL~B2, data=S2chobezam_wo.num)
rmse <- round(sqrt(mean(resid(B2_model)^2)), 2)
```

### **# Plot RMSE**

```
B2_rmse<-B2_eq + geom_text(aes(x=0.05, y=1.5, label= paste("RMSE= ", rmse,
"mg/ha"), hjust=0))+theme_bw()
B2_rmse
B2_rmse_xy <- B2_rmse + labs(y="AGB (Mg/ha)", x="Reflectance in
B2",title="Sentinel 2")
B2_rmse_xy<-B2_rmse_xy + theme(text = element_text(size = 14))
```

## Simple and Multivariate regression models

**CREATE THE SIMPLE MODEL FOR AGB USING SAR S1, S2 SPECTRAL BANDS, S2 INDICES.** NB: Only showed certain models, the rest of the models can be provided upon request

### **#B3**

```
B2_lm <-lm(AGBL~B2, data =S2chobezam_wo.num)
summary(B2_lm)
r2(B2_lm)
model_performance(B2_lm)
```

### **#B3**

```
B3_lm <-lm(AGBL~B3, data =S2chobezam_wo.num)
summary(B3_lm)
r2(B3_lm)
model_performance(B3_lm)
```

### **#B5**

```
B5_lm <-lm(AGBL~B5, data =S2chobezam_wo.num)
summary(B5_lm)
r2(B5_lm)
model_performance(B5_lm)
```

### **#NDVI**

```
ndvi_m <-lm(AGBL~ndvi, data =S2chobezam_wo.num)
summary(ndvi_lm)
r2(ndvi_m)
model_performance(ndvi_m)
```

### **#GRVI**

```
grvi_m <-lm(AGBL~grvi, data =S2chobezam_wo.num)
summary(grvi_lm)
```

```
r2(grvi_m)
model_performance(grvi_m)
```

### **#S1 VV**

```
S1_VV_lm <-lm(AGBL~S1_VV, data =S2chobezam_wo.num)
summary(S1_VV_lm)
r2(S1_VV_lm)
model_performance(S1_VV_lm)
```

### **#S1 VH**

```
S1_VH_lm <-lm(AGBL~S1_VH, data =S2chobezam_wo.num)
summary(S1_VH_lm)
r2(S1_VH_lm)
model_performance(S1_VH_lm)
```

**#CREATE THE MULTIVARIATE MODEL AND PREDICTION FOR ABOVE  
GROUND BIOMASS USING SAR S1, S2 SPECTRAL BANDS, S2 INDICES  
COMBINATIONS.** *NB: Only showed certain models, the rest of the models can be provided  
upon request*

### **# a)model SAR S1**

```
sar.model<-lm(AGBL~S1_VH+S1_VV, data=S2chobezam_wo.num)
summary(sar.model)
r2(sar.model)
model_performance(sar.model)
vif(sar.model)
```

### **# b)Sentinel 2 bands**

```
sentinel2.model<-lm(AGBL~B3+B5+B4+B5+B6+B7+B8+B8A+B11+B12,  
data=S2chobezam_wo.num)
```

```
summary(sentinel2.model)
r2(sentinel2.model)
model_performance(sentinel2.model)
vif(sentinel2.model)
```

### **# c) Sentinel 2 and Sentinel 1 bands**

```
sentinel2SAR.model<-
lm(AGBL~B3+B5+B4+B5+B6+B7+B8+B8A+B11+B12+S1_VV+S1_VH,
data=S2chobezam_wo.num)
summary(sentinel2SAR.model)
r2(sentinel2SAR.model)
model_performance(sentinel2SAR.model)
vif(sentinel2SAR.model)
```

### **# d) S2 indices only**

```
S2ind.model<-
lm(AGBL~ndvi+grvi+evi+savi+msav+nbr+nbr2+gndvi+nR1+nR2+nR3+nR4+ndi4
5+ireci, data=S2chobezam_wo.num)
summary(S2ind.model)
r2(S2ind.model)
model_performance(S2ind.model)
vif(S2ind.model)
```

## CHAPTER 4

### GOOGLE EARTH ENGINE CODE FOR THE VEGETATION INDICES

Google Earth Engine Code for the vegetation Indices time series time series

<https://code.earthengine.google.com/fe5b816a2cde4a03c63183cb3f1b2cfb?noload=1/>\*/

Code generated for calculating different vegetation Indices using 8 day MODIS at 500m, developed by-Ruusa David August 2020

\*/

**//add the shapefile to the map**

```
Map.addLayer(Chobe, ndviVis,'NDVI 8 days')
```

```
Map.addLayer(Chobe, ndviVis,'NDVI 8 days')
```

**// mask out cloud and bad pixels**

```
var maskclouds = function(image) {  
  return image.updateMask(image.select("SummaryQA").eq(0));  
};
```

```
var maskcloudsQC = function(image) {  
  var QA = image.select('StateQA')  
  var bitMask = 1 << 10;  
  return image.updateMask(QA.bitwiseAnd(bitMask).eq(0))  
}
```

**// Load MODIS image collection**

```
var MODIS = ee.ImageCollection("MODIS/006/MOD09A1")  
.filterDate('2019-12-01', '2019-12-31')  
.map(maskcloudsQC).max().clip(Chobe);
```

**//create a function to calculate NDVI**

```
var addNDVI = function(image){  
  var newImg = image.normalisedDifference(['sur_refl_b02',  
    'sur_refl_b01']).double()  
  .rename('ndvi');  
  return newImg.  
  set({  
    'system:index' : image.get('system:index'),  
    'system:time_start' : image.get('system:time_start')  
  });  
};  
var ndvi =addNDVI(MODIS);
```

**//Define visualisation parameters**

```
var ndviVis = {  
  min: 0.0,  
  max: 1.0,  
  palette: [  
    'FFFFFF', 'CE7E45', 'DF923D', 'F1B555', 'FCD163', '99B718', '74A901',  
    '66A000', '529400', '3E8601', '207401', '056201', '004C00', '023B01',  
    '001E01', '011D01', '011301'  
  ], };  
Map.addLayer(ndvi, ndviVis, 'NDVI 8 days')
```

**//create EVI function**

```
var addEVI = function(image) {  
  return image.expression(  
    '(NIR-RED) / (NIR + 6*RED - 7.5*BLUE + 1)',  
    {  
      'NIR': image.select('sur_refl_b02'),
```

```

    'RED': image.select('sur_refl_b01'),
    'BLUE': image.select('sur_refl_b03')
  }
).rename('evi') }
var evi = addEVI(MODIS)
Map.addLayer(evi,ndviVis,'EVI 16 days')

```

**//create a function to calculate GNDVI**

```

var addGNDVI = function(image){
  var newImg = image.normalisedDifference(['sur_refl_b02',
'sur_refl_b04']).double()
  .rename('gndvi');
  return newImg.
  set({
    'system:index' : image.get('system:index'),
    'system:time_start' : image.get('system:time_start')
  }); };
var gndvi =addGNDVI(MODIS);
Map.addLayer(gndvi, ndviVis,'GNDVI 16 days')

```

**//Export the NDVI data**

```

Export.image.toDrive({
  image:ndvi ,
  folder: 'ChobeMODIS_1',
  fileNamePrefix: 'ND_12_2020',
  description:"Modis_ndvi_8_days_02_500m",
  region: Chobe,
  crs:"EPSG:32735 ",
  scale: 500,
  maxPixels:1e13
});

```

**//Export the EVI data**

```
Export.image.toDrive({  
  image: evi,  
  folder: 'ChobeMODIS_1',  
  fileNamePrefix: 'EV_12_2020',  
  description:"Modis_evi_8_days_02_500m",  
  region: Chobe,  
  crs:"EPSG:32735 ",  
  scale: 500,  
  maxPixels:1e13  
});
```

**//Export the GNDVI data**

```
Export.image.toDrive({  
  image: gndvi,  
  folder: 'ChobeMODIS_1',  
  fileNamePrefix: 'GN_12_2020',  
  description:"Modis_gndvi_8_days_02_500m",  
  region: Chobe,  
  crs:"EPSG:32735 ",  
  scale: 500,  
  maxPixels:1e13  
});
```

**R CODE FOR ANALYSING TIME SERIES OF DIFFERENT  
VEGETATION INDICES, AND CLIMATE DATA**

This part of the R code is for analysing time series of different  
vegetation indices, climate data with change detection algorithms

*Script for gap filling Vegetation Index e.g. NDVI values derived  
from MODIS composites.*



**# Script for gap filling site level NDVI values derived from MODIS composites.**

**# Install needed packages through the pkgTest**

```
pkgTest <- function(x)
{
  if (x %in% rownames(installed.packages()) == FALSE) {
    install.packages(x, dependencies= TRUE)
  }
  library(x, character.only = TRUE)
}
neededPackages <- c("r imputeTS "," (lubridate )
for (package in neededPackages){pkgTest(package)}
```

**# load Libraries**

```
library(tidyverse)
library(imputeTS)
library(lubridate)
```

**#Read the data**

```
MODIS<-read.csv(paste("File.csv",sep="",collapse=""))
```

**# Convert date to Date format**

```
MODIS$Date <- as.Date(MODIS$Date, "%d.%m.%Y")
```

**# Plot all the land cover types (forest, grassland, water etc) to analyse the data**

```
ggplot(MODIS %>% filter(NDVI > -1)) +
  geom_point(aes(Date, NDVI, col = PlotType)) +
  facet_wrap(~PlotType, ncol = 1)
```

**# Plot one land cover types (forest, grassland, water etc) for all the 12 months to see data distribution**

```
ggplot(MODIS %>% filter(NDVI > -1) %>% filter(PlotType == "grass")) +
  geom_point(aes(Date, NDVI, col = PlotType)) +
```

```
facet_wrap(~month)
```

```
# In this section, remove the lowest 1% of values in each month
```

```
# this method assumes low values are contamination and not real change so use with caution
```

```
# 1% could be changed to 5% by swapping 'probs=0:100/100' for 'probs=0:20/20' or by selecting
```

```
MODISa <- MODIS %>%  
  filter(NDVI > -1) %>%  
  group_by(PlotType,month) %>%  
  mutate(quantile = as.integer(cut(NDVI, quantile(NDVI, probs=0:100/100),  
include.lowest=TRUE)),  
         NDVI=replace(NDVI, quantile==1, NA)) %>%  
  drop_na(NDVI) %>%  
  ungroup() %>%  
  select(!c(Year,month))
```

```
# Reformat data in preparation for gap filling
```

```
## Expand data frame to include all date values for every site id
```

```
MODISb <- MODISa %>%  
  complete(Date = seq(floor_date(min(MODISa$Date),unit = "month"),  
                     floor_date(max(MODISa$Date), unit = "month"), by = "month"),  
           nesting(ForestID,PlotType))  
ggplot(MODISb) +  
  geom_point(aes(Date, NDVI, col = PlotType)) +  
  facet_wrap(~PlotType, ncol = 1)
```

```
# Reformat data and fill missing metadata values
```

```
MODISb <- MODISb %>%  
  mutate(DATE = as.Date(Date,"%Y-%m-%d"),  
         DOY = lubridate::yday(DATE)) %>%  
  separate(Date, into = c("YEAR","MONTH","DAY"), sep = "([-])")
```

```
MODISb <- MODISb %>%  
  group_by(ForestID) %>%  
  fill(PlotType, .direction = "updown")
```

**# check how many na values are there in the NDVI series?**

```
sum(is.na(MODISb$NDVI))
```

**# Gap fill missing NDVI data**

**# This first stage will only be carried out where there is 1 missing value. if there are 2 or more**

**# consecutive missing values then this first step will not fill the gap**

```
MODISb <- MODISb %>%  
  arrange(DATE) %>%  
  group_by(ForestID) %>%  
  mutate(GapFill1 = na_interpolation(NDVI, option = "stine", maxgap = 1))
```

**#check how many na values are there in the NDVI series?**

```
sum(is.na(MODISb$GapFill1)) # in this dataset we have no filled all of the missing data
```

**# If there are still missing values then we can fill gaps based on the next nearest matching month from a different year**

**# using the linear interpolation between the values in**

```
MODISb <- MODISb %>%  
  arrange(DATE) %>%  
  group_by(ForestID, MONTH) %>%  
  mutate(GapFill2 = na_interpolation(GapFill1, option = "linear"))
```

**# check how many na values are there in the NDVI series?**

```
sum(is.na(MODISb$GapFill2))
```

**# Plot restulant data**

```
ggplot(MODISb) +  
  geom_point(aes(DATE, GapFill2, col = PlotType)) +  
  facet_wrap(~PlotType, ncol = 1)
```

**# investigate difference in Gapfill 1(filled from the month immediately adjacent to missing value)**

**# and 2(filled from nearest matching month)**

```
ggplot(MODISb %>% filter(ForestID == "STATE128")) +  
  geom_point(aes(DATE, GapFill2), col = "red") +  
  geom_point(aes(DATE, GapFill1), col = "blue") +  
  geom_point(aes(DATE, NDVI), col = "black") +  
  ylab("NDVI")
```

**# Write csv for future use**

```
write_csv(MODISb, "modis_ndvi_2000_2020_Gapfilled.csv" )
```

**Script for BFAST and BEAST algorithm on time series data**

**# load Libraries**

```
library(tidyverse)  
library(imputeTS)  
library(lubridate)  
library(zoo)  
library(bfast)  
library(strucchange)  
library(ggplot2)  
library(tidyverse)  
library(Rbeast)  
library(sp)  
library(stringr)
```

```
library(raster)
library(devtools)
library(bfastSpatial)
library(rgdal)
```

### **# Read MODIS and climate monthly data**

```
modisall<-read.csv(paste("File.csv",sep="",collapse=""))
str(modisall)
```

### **#convert the date from factor to DATE format**

```
modisall$DATE=as.Date(modisall$DATE, "%d/%m/%Y")
```

### **#convert the csv to a dataframe**

```
modisall.df<-as.data.frame(modisall)
```

### **# aggregate the data and calculate average based on plottype and location(e.g., Namibia and Botswana)**

```
mean<-aggregate(modisall.df[,13:18],
list(PlotType=modisall.df$PlotType,Location=modisall.df$Location,
Date=modisall.df$DATE ), mean)
```

### **#Plot Different types of land cover/ forest types**

#### **# create the time series for mediumforest**

```
NDVI_QA_zammedium.ts <- ts(
  data = meanmedium.zam$NDVI_QA,
  start = c(2002, as.numeric(format(meanmedium.zam$NDVI_QA[1], 07))),
  end = c(2020,as.numeric(format(meanmedium.zam$NDVI_QA[1], 10))),
  frequency = 12 #number of observations per year)
plot(NDVI_QA_zammedium.ts ,type='b', ylab="NDVI",xlab="Year", main =" Average
of mediumforest plots (n=48)",cex=2.0,lwd = 3.5, pch=16,cex.main =
2.0,cex.lab=3.5)
```

#### **# create the time series for closedforest**

```

NDVI_QA_zamclosed.ts <- ts(
  data = meanclosed.zam$NDVI_QA,
  start = c(2002, as.numeric(format(meanclosed.zam$NDVI_QA[1], 07))),
  end = c(2020,as.numeric(format(meanclosed.zam$NDVI_QA[1], 10))),
  frequency = 12 # number of observations per year

plot(NDVI_QA_zamclosed.ts ,type='b',ylab="NDVI",xlab="Year", main =" Average of
closedforest plots (n=16), Zambezi Namibia",cex=2.0,lwd = 3.5, pch=16,cex.main =
2.0,cex.lab=3.5)

```

**#create the time series for agriculture**

```

NDVI_QA_zamagri.ts <- ts(
  data = meanagri.zam$NDVI_QA,
  start = c(2002, as.numeric(format(meanagri.zam$NDVI_QA[1], 07))),
  end = c(2020,as.numeric(format(meanagri.zam$NDVI_QA[1], 10))),
  frequency = 12 # number of observations per year)

plot(NDVI_QA_zamagri.ts ,type='b', ylab="NDVI",xlab="Date", main =" Average of
agricultural plots (n=7)",cex=2.0,lwd = 3.5, pch=16,cex.main = 2.0,cex.lab=3.5)

```

**#Alternatively choose a single plot type**

```

mean_Chobe001<-mean%>% dplyr::filter(
  ForestID=="STATE035")

```

**#create the NDVI time series for the chosen plot**

```

NDVI_Chobe001.ts <- ts(
  data = mean_Chobe001$NDVI,
  start = c(2002, 7),
  end = c(2019,12),
  frequency = 12 # number of observations per year)

plot(MSAVI_Chobe001.ts ,type='b', ylab="MSAVI",xlab="Year", main =" Disturbed
forest plot",cex=2.0,lwd = 3.5, pch=16,cex.main = 2.0,cex.lab=3.5)

#axis(side=1, at=c(2002:2020))

axis(side=1, at=seq(2002, 2019, by=1))

#box()

```

**#create the GNDVI time series for the chosen plot**

```
GNDVI_Chobe001.ts <- ts(  
  data = mean_Chobe001$GNDVI,  
  start = c(2002,7),  
  end = c(2019,12),  
  frequency = 12 #number of observations per year)  
plot(MSAVI_Chobe001.ts ,type='b', ylab="MSAVI",xlab="Year", main =" Disturbed  
forest plot",cex=2.0,lwd = 3.5, pch=16,cex.main = 2.0,cex.lab=3.5)  
#axis(side=1, at=c(2002:2020))  
axis(side=1, at=seq(2002, 2019, by=1))  
#box()
```

**#create the EVI time series for the chosen plot**

```
EVI_Chobe001.ts <- ts(  
  data = mean_Chobe001$EVI,  
  start = c(2002, 7),  
  end = c(2020,6),  
  frequency = 12 # number of observations per year)  
plot(EVI_Chobe001.ts ,type='b', ylab="EVI",xlab="Year", main =" Disturbed forest  
plot",cex=2.0,lwd = 3.5, pch=16,cex.main = 2.0,cex.lab=3.5)
```

**#Run BFAST algorithm on NDVI**

**# define the ratio of distance between breaks (time steps) and length of the time series**

```
rdist <- 15/length(NDVI_Chobe001.ts)  
fit <- bfast(NDVI_Chobe001.ts, h=rdist,  
  season="harmonic", max.iter=1)  
plot(fit, xlab="DATE", main="NDVI",axes=F)
```

**#Run BEAST algorithm on NDVI**

```
fit <- beast(NDVI_Chobe001.ts,12)
```

```
plot(fit,xlab="", main="NDVI",axes=FALSE,labels=F)
```

### **#Run BFAST algorithm on GNDVI**

```
rdist <- 15/length(GNDVI_Chobe001.ts) #I tried 25 , but 15 work best  
fit <- bfast(GNDVI_Chobe001.ts, h=rdist,  
            season="harmonic", max.iter=1)  
plot(fit, main="GNDVI")
```

### **#Run BEAST algorithm on GNDVI**

```
fit <- beast(GNDVI_Chobe001.ts,12)  
plot(fit,main="GNDVI")
```

## **Script for SPATIAL ANALYSIS OF BFAST ALGORITHM (RASTER ANALYSES)**

### **PREPROCESS and ANALYSE THE RASTER DATA WITH BFAST**

#### **# Define path to files**

```
VlpathGNDVI <- "Path/"
```

#### **# Load list of raster file names**

```
MODIS8GNDVI.fileList <- list.files(VlpathGNDVI , pattern = "*.tif")
```

#### **# load individual files into a raster brick**

```
MODIS8dayGNDVI <-  
do.call("brick",lapply(paste0(VlpathGNDVI,"/",MODIS8GNDVI.fileList[1:216]),  
                      FUN = function(x){  
                        r <- raster(x)  
                      })
```

#### **#project the raster**



```
crs(MODIS8dayGNDVI)
```

**#rename the files**

```
names(MODIS8dayGNDVI) <- MODIS8GNDVI.fileList
```

**# create object for original names**

```
MODISnamesGNDVI <- names(MODIS8dayGNDVI)
```

```
# Create object for each part of the required name
```

```
band <- str_sub(MODISnamesGNDVI, 1,2)
```

```
month <- str_sub(MODISnamesGNDVI, 4,5)
```

```
year <- str_sub(MODISnamesGNDVI, 7,10)
```

**# create a new object with the new layernames**

```
MODISnamesGNDVI.new <- paste(band,month,year,sep = ".")
```

**# relabel modis data with new names**

```
names(MODIS8dayGNDVI) <- MODISnamesGNDVI.new
```

**# reorder the raster brick according to new names**

```
MODIS8dayGNDVI.reordered <- subset(MODIS8dayGNDVI,  
order(MODISnamesGNDVI.new))
```

```
names(MODIS8dayGNDVI.reordered)
```

**# Save the stacked image data in a single file, .grd with ENVI header file  
preserves the layer names**

```
MODISStackGNDVI <-
```

```
writeRaster(MODIS8dayGNDVI.reordered,paste0(VIpathGNDVI,"/MODIS_NDVIsta  
ck.grd"), format="raster",overwrite=TRUE)
```

```
s<-hdr(MODISStack, format = "ENVI")
```

```
par(mar=c(1,2,2,1))
```

**#assign dates from 2002 to 2019**

```
dtGNDVI<-c('2002-01-01','2003-01-01','2004-01-01','2005-01-01','2006-01-01',
```

'2007-01-01','2008-01-01','2009-01-01','2010-01-01','2011-01-01','2012-01-01',  
'2013-01-01','2014-01-01','2015-01-01','2016-01-01','2017-01-01','2018-01-01',  
'2019-01-01','2002-02-01','2003-02-01','2004-02-01',  
'2005-02-01','2006-02-01','2007-02-01','2008-02-01','2009-02-01','2010-02-01',  
'2011-02-01','2012-02-01','2013-02-01','2014-02-01','2015-02-01','2016-02-01',  
'2017-02-01','2018-02-01','2019-02-01',  
'2002-03-01','2003-03-01','2004-03-01','2005-03-01','2006-03-01','2007-03-01',  
'2008-03-01','2009-03-01','2010-03-01','2011-03-01','2012-03-01','2013-03-01',  
'2014-03-01','2015-03-01','2016-03-01','2017-03-01','2018-03-01','2019-03-01',  
'2002-04-01','2003-04-01','2004-04-01',  
'2005-04-01','2006-04-01','2007-04-01','2008-04-01','2009-04-01','2010-04-01',  
'2011-04-01','2012-04-01','2013-04-01','2014-04-01','2015-04-01','2016-04-01',  
'2017-04-01','2018-04-01','2019-04-01',  
'2002-05-01','2003-05-01','2004-05-01','2005-05-01','2006-05-01','2007-05-01',  
'2008-05-01','2009-05-01','2010-05-01','2011-05-01','2012-05-01','2013-05-01',  
'2014-05-01','2015-05-01','2016-05-01','2017-05-01','2018-05-01','2019-05-01',  
'2002-06-01','2003-06-01','2004-06-01',  
'2005-06-01','2006-06-01','2007-06-01','2008-06-01','2009-06-01','2010-06-01',  
'2011-06-01','2012-06-01','2013-06-01','2014-06-01','2015-06-01','2016-06-01',  
'2017-06-01','2018-06-01','2019-06-01',  
'2002-07-01','2003-07-01','2004-07-01','2005-07-01','2006-07-01','2007-07-01',

```

'2008-07-01','2009-07-01','2010-07-01','2011-07-01','2012-07-01','2013-
07-01',
'2014-07-01','2015-07-01','2016-07-01','2017-07-01','2018-07-01','2019-
07-01',
'2002-08-01','2003-08-01','2004-08-01',
'2005-08-01','2006-08-01','2007-08-01','2008-08-01','2009-08-01','2010-
08-01',
'2011-08-01','2012-08-01','2013-08-01','2014-08-01','2015-08-01','2016-
08-01',
'2017-08-01','2018-08-01','2019-08-01',
'2002-09-01','2003-09-01','2004-09-01','2005-09-01','2006-09-01','2007-
09-01',
'2008-09-01','2009-09-01','2010-09-01','2011-09-01','2012-09-01','2013-
09-01',
'2014-09-01','2015-09-01','2016-09-01','2017-09-01','2018-09-01','2019-
09-01',
'2002-10-01','2003-10-01','2004-10-01',
'2005-10-01','2006-10-01','2007-10-01','2008-10-01','2009-10-01','2010-
10-01',
'2011-10-01','2012-10-01','2013-10-01','2014-10-01','2015-10-01','2016-
10-01',
'2017-10-01','2018-10-01','2019-10-01',
'2002-11-01','2003-11-01','2004-11-01','2005-11-01','2006-11-01','2007-
11-01',
'2008-11-01','2009-11-01','2010-11-01','2011-11-01','2012-11-01','2013-
11-01',
'2014-11-01','2015-11-01','2016-11-01','2017-11-01','2018-11-01','2019-
11-01',
'2002-12-01','2003-12-01','2004-12-01','2005-12-01',
'2006-12-01','2007-12-01','2008-12-01','2009-12-01','2010-12-01','2011-
12-01',
'2012-12-01','2013-12-01','2014-12-01','2015-12-01','2016-12-01','2017-
12-01',
'2018-12-01','2019-12-01')# corresponding dates to all rasters
my_datesGNDVI <- as.Date(dtGNDVI, format = "%Y-%m-%d")

```

**# define the function that will be applied across the brick using the calc function**

```
bfmRaster = function(pixels)
{
  tspx <- timeser(pixels, my_datesGNDVI) # create a timeseries of all pixels
  bfm <- bfastmonitor(tspx, response ~ trend + harmon, order = 3, start =
c(2014,1)) # run bfast on all pixels
  return(c(bfm$breakpoint, bfm$magnitude))
}
```

**# calc function**

```
bfmRGNDVI <- calc(MODIS8dayGNDVI.reordered, bfmRaster)
names(bfmRGNDVI ) <- c('time of break', 'magnitude of change')
plot(bfmRGNDVI ) # resulting time and magnitude of change
```

**# Ensure the raster images have correct number of rows and columns**

```
rGNDVI<- raster(ncol= 210, nrow=166)
sGNDVI <- stack(lapply(1:216, function(x) setValues(rGNDVI,
runif(ncell(rGNDVI))))))
MODIS8dayGNDVI.reordereds <- setZ(MODIS8dayGNDVI.reordered,
my_datesGNDVI)
MODIS8dayGNDVI.reordereds
getZ(MODIS8dayGNDVI.reordereds)
plot(MODIS8dayGNDVI.reordereds[[1]])
```

**# Define path to files to export**

```
VlpathGNDVI_out <- "path/"
```

**#Define output path**

```
outsGNDVI <- file.path(VlpathGNDVI_out ,
"bfmSpatial_start2010,1_gndvi_until2019.tif")
```

**#Run the bfmSpatial on raster data starting 2010**

```
bfmSpatial(MODIS8dayGNDVI.reordereds, start = c(2010, 1),formula =
response~harmon,order = 1, filename = outsGNDVI)
```

**PREPARE THE RASTER DATA AND EXTRACT THE  
MAGNITUDE**

**#Read in the data**

```
gndvistate2010_ha1 <- brick("File.tif")
plot(gndvistate2010_ha1,1, main="Monitoring period 2013-2020, gndvi ")
```

**# extract change raster**

```
change_gndvistate2010_ha1 <- raster(gndvistate2010_ha1, 1)
# extract magn raster
magn_gndvistate2010_ha1 <- raster(gndvistate2010_ha1, 2)
# make a version showing only breakpoing pixels
magn_bkpgndvistate2010_ha1 <- magn_gndvistate2010_ha1
magn_bkpgndvistate2010_ha1[is.na(change_gndvistate2010_ha1)] <- NA
op <- par(mfrow=c(1, 3))
plot(magn_bkpgndvistate2010_ha1, main="Magnitude: breakpoints")
plot(magn_gndvistate2010_ha1, main="Magnitude: all pixels")
```

**# extract and rescale magnitude and apply a threshold**

```
magn09thresh_gndvistate2010_ha1 <- magn_gndvistate2010_ha1
magn09thresh_gndvistate2010_ha1 [magn_gndvistate2010_ha1 > 0.00] <- NA
```

**# compare all magn rasters**

```
op <- par(mfrow=c(2, 2))
plot(magn09thresh_gndvistate2010_ha1, main="magnitude")
plot(magn09_sieve_gndvistate2010_ha1, main="pixel sieve")
plot(magn09_areasieve_gndvistate2010_ha1, main="0.5ha sieve")
plot(magn09_as_rook_gndvistate2010_ha1, main="0.5ha sieve, rook's case")
```

```
changeSize_queengndvistate2010_ha1 <-
clumpSize(magn09_areasieve_gndvistate2010_ha1)
```

```
changeSize_rookgndvistate2010_ha1 <-  
clumpSize(magn09_areasievegndvistate2010_ha1, directions=4)
```

### **#Calculate the change size**

```
op <- par(mfrow=c(1, 2))
```

```
plot(changeSize_queengndvistate2010_ha1, col=bpy.colours(50), main="Clump  
size: Queen's case")
```

```
plot(changeSize_rookgndvistate2010_ha1, col=bpy.colours(50), main="Clump size:  
Rook's case")
```

```
changeSize <- clumpSize(magn09_areasievegndvistate2010_ha1,  
f=250000/10000)
```

```
plot(changeSize, col=bpy.colours(50), main="Pixel size gndvi (hectares)")
```

### **#export path**

```
writeFormats()
```

```
GNDVI_VIpath <- "path/"
```

### **#Write the year of change and magnitude of change raster and export it out for further analysis in ArcGIS**

```
MODISStack <- writeRaster(changegndvistate2010_ha1,paste0(File.tif"), format =  
"GTiff",overwrite=TRUE)
```

```
MODISStack <- writeRaster(magngndvistate2010_ha1,paste0(File.tif"), format =  
"GTiff",overwrite=TRUE)
```

## **CHAPTER 5**

### **GOOGLE EARTH ENGINE CODE FOR FIRE**

Google Earth Engine Code for the fire time series

<https://code.earthengine.google.com/7a868676bc7ac534247a19d7cdc6b150?noload=1>

```
/*////////////////////////////////////
```

```
Code geerated for MODIS Burned Area Monthly at 500m, developed by-Ruusa  
David August 2020
```

```

*////////////////////////////////////
//This is a code to get the monthly Burned pixels
//Get list of images
var MODISBurn_Image = ee.ImageCollection(MonthlyBurnedArea)
  .filterDate('2019-09-01', '2019-09-30') //define the month, change this to the
month of your choice
  .filterBounds(kaza).mean().clip(kaza); //get the mean and clip the data

//Get the burn date
var MODISBurn_Image = MODISBurn_Image.select('BurnDate');
var firesVis = {
  min: 325.0,
  max: 400.0,
  palette: ['red', 'orange', 'yellow'],};

//Display on the map
Map.addLayer(MODISBurn_Image, firesVis, 'Fires');
print(MODISBurn_Image)
print('ImageList')

//export the burned data out
Export.image.toDrive({
  image: MODISBurn_Image,
  folder: 'MCD64A1_fireUncertainty_2019',
  description:"MCD64A1_fire_2019_12_500m",
  region: kaza.geometry().bounds(),
  crs:"EPSG:32735 ",
  scale: 500,
  maxPixels:210984237950});

//This is a code to get the uncertainty of the Burned pixels

```

**// Get list of images to test**

```
var MODISUncertainty_Image = ee.ImageCollection(MonthlyBurnedArea)
  .filterDate('2019-12-01', '2019-12-30')
  .filterBounds(kaza).mean().clip(kaza);
```

**//Get the uncertainty burn date**

```
var MODISUncertainty_Image = MODISUncertainty_Image.select('Uncertainty');
var firesVis = {
  min: 325.0,
  max: 400.0,
  palette: ['red', 'orange', 'yellow'],};
```

**//Display on the map**

```
Map.addLayer(MODISUncertainty_Image, firesVis, 'Fires');
print(MODISUncertainty_Image)
print('ImageList')
```

```
//export the uncertainty out
```

```
Export.image.toDrive({
  image: MODISUncertainty_Image,
  folder: 'MCD64A1_fireUncertainty_2019',
  description:"MCD64A1_fireUncertainty_2019_12_500m",
  region: kaza.geometry().bounds(),
  crs:"EPSG:32735 ",
  scale: 500,
  maxPixels:210984237950});
```

## **GOOGLE EARTH ENGINE CODE FOR THE CLIMATE DATA**

Google Earth Engine Code for the climate time series



<https://code.earthengine.google.com/93b50f3bd714cb527ce6573fbd1f23dc?noload=1>

```
/*////////////////////////////////////////////////////////////////////////////////////////////////////
```

Code generated for comparing Ground precipitation and satellite based precipitation, developed by-Ruusa David June 2019

```
*////////////////////////////////////////////////////////////////////////////////////////////////////
```

**//Add the ground precipitation on the map**

```
Map.addLayer(gpcc1981)
```

```
Map.addLayer(gpcc2016)
```

**//extract all the climate data**

```
var collections = [ {
```

```
  name: 'CHIRPS', scale: 5000,
```

```
  collection: ee.ImageCollection('UCSB-CHG/CHIRPS/PENTAD')
```

```
},
```

```
{
```

```
  name: 'gpcc', scale: 3000,
```

```
  collection: ee.ImageCollection('users/ruusadavid2/gpccCollection_1891')
```

```
},
```

```
{
```

```
  name: 'cru', scale: 3000,
```

```
  collection: ee.ImageCollection('users/ruusadavid2/cruCollection')
```

```
},
```

```
{
```

```
  name: 'CFSV2', scale: 5000,
```

```
  collection: ee.ImageCollection('NOAA/CFSV2/FOR6H')
```

```
  .select('Precipitation_rate_surface_6_Hour_Average')
```

```
  .map(function(i) {
```

```
    return i.multiply(60 * 60 * 6) // convert to mm by 6 since it is in mm/second and is a 6 hour basis
```

```
    .copyProperties(i, ['system:time_start'])
```

```
  }) }];
```

**//create a function to define the the range of date to be mapped through**

```
function getDates(start, stop, step) {  
  return ee.List.sequence(start, stop).map(function(year) {  
    return ee.List.sequence(1, 12, step).map(function(month) {  
      return ee.Date.fromYMD(year, month, 1)  
    })  
  }).flatten()  
}
```

**//create a function to compute the sum and mean through all precipitation bands in all images**

```
function compute(start, stop, step) {  
  var dates = getDates(start, stop, step)  
  var features = collections.map(function(c) {  
    return dates.map(function(d) {  
      var p = c.collection  
        .filterDate(d, ee.Date(d).advance(step, 'month'))  
        .sum()  
        .reduceRegion(ee.Reducer.mean(), southAfrica, c.scale).values().get(0)  
      return ee.Feature(null)  
        .set('system:time_start', ee.Date(d).millis())  
        .set(c.name, p)  
    })  
  })  
  return ee.FeatureCollection(ee.List(features).flatten())  
}
```

**//define the the time period to be computed on**

```
var monthly = compute(1981, 2016, 1)
```

```
var annual = compute(1981, 2016, 12)
```

**//set a function to define the chart titles, x and y axis titles**

```
function chart(features, title) {  
  var chart = ui.Chart.feature.byFeature(features, 'system:time_start')  
  chart.setOptions({  
    vAxis: { title: 'Precipitation [mm]' },  
    title: title  
  })  
  print(chart)  
}
```

**//create the charts**

```
chart(monthly, 'Monthly precipitation in Southern Africa Subcontinent (2001-  
2015)')  
  
chart(annual, 'Raingauge and satellite-based annual precipitation in Central  
Angola, coordinates[18.71,-11.00](1981-2016)')
```

## **R CODE FOR ANALYSING TIME SERIES OF VEGETATION DATA AND CLIMATE DATA**

This part of the R code is for analysing time series of Vegetation Data and Climate Data

### **ANALYSE AND PLOT THE GROUND RAINFALL AND TEMPERATURE**

**#Load the Library**

```
library(corr)  
library(dplyr)  
library(tidyverse)  
library(igraph)  
library(ggraph)
```

```
library(Hmisc )
library(corrplot)
library(sp)
library(zoo)
library(xts)
library(hydroTSM)
library(ggplot2)
library(dplyr)
```

### **#Import the data**

```
precip8<-read.csv(paste("File.csv",sep="",collapse=""))
```

### **#prepare the data**

#### **#convert to data frame**

```
x<-as.data.frame(precip8)
```

#### **# Convert date to Date format**

```
x$Dates=as.Date(x$Date, "%d.%m.%Y")
```

```
#anyDuplicated(x$Dates)
```

```
#duplicated(x$Dates) | duplicated(x$Dates, fromLast = TRUE)
```

#### **#create a zoo object for time series**

```
x<- zoo(x$Rainfall,x$Dates)
```

#### **#plot rainfall**

```
plot(x, main="rainfall", ylab="precipitation (mm)", xlab="Time")
```

#### **#find the number of years**

```
( nyears <- yip(from=start(x), to=end(x), out.type="nubr" ) )
```

#### **#plot the prepared data with hydroplot**

```
hydroplot(x, var.type="Precipitation", main="at Chobe National Park",
```

```
pfreq = "dm", from="1975-01-01")  
dwi(x)
```

### **#Analyse the rainfall time series data**

#### **#Monthly analysis**

```
monthlyfunction(x, FUN=median, na.rm=TRUE)  
cmonth <- format(time(x), "%b")  
months <- factor(cmonth, levels=unique(cmonth), ordered=TRUE)
```

#### **#Boxplot of the monthly values**

```
boxplot( coredata(x) ~ months, col="lightblue", main="Monthly Precipitation",  
        ylab="Precipitation, [mm]", xlab="Month")
```

#### **#Average seasonal values of precipitation**

```
seasonalfunction(x, FUN=sum, na.rm=TRUE) / nyears
```

#### **#Extracting the seasonal values for each year**

```
m<-monthlyfunction(x, FUN=sum, na.rm=TRUE)  
( DJF <- dm2seasonal(x, season="DJF", FUN=sum) )  
( MAM <- dm2seasonal(x, season="MAM", FUN=sum) )  
( JJA <- dm2seasonal(x, season="JJA", FUN=sum) )  
( SON <- dm2seasonal(x, season="SON", FUN=sum) )
```

#### **#Extract the seasonal values for each year**

```
hydroplot(x, pfreq="seasonal", FUN=sum, stype="default",ylab="Precipitation  
(mm)",lwd=2)
```

#### **# Mean winter (DJF) values of streamflow for each year of 'x'**

```
dm2seasonal(x, FUN=sum, season="DJF")  
dm2seasonal(x, FUN=sum, season="MAM")  
dm2seasonal(x, FUN=sum, season="JJA")
```

```
dm2seasonal(x, FUN=sum, season="SON")
```

### **# Selecting only a three-year time slice for the analysis**

```
x <- window(x, start=as.Date("1975-01-01"))
```

```
#Plotting the selected time series
```

```
hydroplot(x, FUN=sum, ptype="ts", pfreq="ma",  
var.unit="mm",ylab="Precipitation",lwd=1.8)
```

### **Create the Climograph from the rainfall and temperature data**

#### **#Read the Precipitation and Temperature data**

```
preciptemp<-read.csv(paste("File.csv",sep="",collapse=""))
```

#### **#convert to data frame**

```
y<-as.data.frame( preciptemp)
```

#### **# Convert date to Date format**

```
Dates=as.Date(y$Date, "%d.%m.%Y")
```

#### **#create a zoo for time series**

```
z <- zoo(y[, 2:4], as.Date(as.character(y[, 1]), format="%d.%m.%Y"))
```

```
colnames(z) <- c("Precipitation", "Max Temperature", "Min Temperature")
```

#### **# extracting individual ts of precipitation, maximum and minimum temperature**

```
pcp <-z[,1]
```

```
tmx <- z[,2]
```

```
tmn <-z[, 3]
```

#### **# Plotting the climograph**

```
m <- climograph(pcp=pcp, tmx=tmx, tmn=tmn, na.rm=TRUE, main="Monthly  
Precipitation, Min and Max Temperature")
```

```
plot(z, main = "Monthly Rainfall, Maximum and Minimum  
Temperature",xlab="Years", lwd=2, col=c("blue", "red","black"),cex.axis  
=1.5,cex.main = 2)
```

**CALCULATING SPEI FROM GROUND RAINFALL AND TEMPERATURE**

**#Calculating SPEI using Ground rainfall and temperature from Kasane Chobe Botswana**

**#Read the data**

```
raintemp<-read.csv(paste("File.csv",sep="",collapse="")) #with all data and outliers removed
```

**#convert points into dataframe**

```
raintemp<-data.frame(raintemp)  
str(raintemp)
```

**#calculate potential evapotranspiration**

```
raintemp$PET<-hargreaves(Tmin=raintemp$Tempmin,  
Tmax=raintemp$Tempmax, lat =-17.82947 )  
raintemp$PET
```

**#calculate climatic water balance**

```
raintemp$CIWaBAL<-raintemp$Precip-raintemp$PET  
raintemp$CIWaBAL  
CIWaBAL<-raintemp$Precip-raintemp$PET
```

**#calculate standardised precipitation evapotranspiration index, and define the scale by 1 moth or two months or 12 etc**

```
SPEI1<-spei(raintemp$CIWaBAL,1) #for 1 month  
raintemp$SPEI1.dataframe=as.data.frame(fitted(SPEI1)) #convert to dataframe  
par(mar=c(5, 4, 4, 6) + 0.1)
```

**#calculate SPEI for 1 month**

```
plot.spei(spei(ts(raintemp$CIWaBAL,  
freq=12,start=c(1983,1)),1,ref.start=c(1983,1),ref.end=c(2020,10)),main  
="Standardised Precipitation Evapotranspiration Index (SPEI-1 months)",textSize  
= 8 )
```

```
mtext(side=1, line=2, "Time", font=2,cex=1.2)
```

### **#calculate SPEI for 2 month**

```
plot.spei(spei(ts(raintemp$CIWaBAL,  
freq=12,start=c(1983,1)),2,ref.start=c(1983,1),ref.end=c(2020,10)),main  
="Standardised Precipitation Evapotranspiration Index (SPEI-2 months)",textSize  
= 8 )
```

```
mtext(side=1, line=2, "Time", font=2,cex=1.2)
```

### **#calculate SPEI for 12 month**

```
plot.spei(spei(ts(raintemp$CIWaBAL,  
freq=12,start=c(1983,1)),12,ref.start=c(1983,1),ref.end=c(2020,10)),main  
="Standardised Precipitation Evapotranspiration Index (SPEI-12 months)",textSize  
= 8 )
```

```
mtext(side=1, line=2, "Time", font=2,cex=1.2)
```

### **#Plot all three SPEI timescale (1,3,12 months) in one plot**

```
par(mar=c(5, 4, 5, 6) + 0.1)
```

```
par(mfrow=c(1,1))
```

### **#Plot first plot for 1 month**

```
plot.spei(spei(ts(raintemp$CIWaBAL,  
freq=12,start=c(2002,7)),1,ref.start=c(2002,7),ref.end=c(2019,12)),main  
="Standardised Precipitation Evapotranspiration Index (SPEI-1month)",textSize  
=12, xlab="", ylab="", axes=FALSE, )
```

```
#mtext(side=1, line=2, "Time", cex=1.5)
```

```
mtext(side=2, line=2, "SPEI", cex=1.5)
```

```
axis(side=1, at=seq(2002, 2019, by=1),cex.axis = 1.0, cex.lab = 1)
```

```
box()
```

### **#Plot second plot for 2 months**

```
plot.spei(spei(ts(raintemp$CIWaBAL,  
freq=12,start=c(1983,1)),3,ref.start=c(1983,1),ref.end=c(2019,12)),main  
="Standardised Precipitation Evapotranspiration Index (SPEI-3 months)",textSize  
=12, xlab="", ylab="", axes=FALSE, )
```



```

mtext(side=1, line=2, "Time", cex=1.5)
mtext(side=2, line=2, "SPEI", cex=1.5)
axis(side=1, at=seq(1982, 2019, by=1),cex.axis = 1.0, cex.lab = 1)
box()

```

### **#Plot second plot for 22 months**

```

plot.spei(spei(ts(raintemp$CIWaBAL,
freq=12,start=c(1982,1)),12,ref.start=c(1982,1),ref.end=c(2019,12)),main
="Standardised Precipitation Evapotranspiration Index (SPEI-12 months)",textSize
=12, xlab="", ylab="", axes=FALSE, )
mtext(side=1, line=2, "Time", cex=1.5)
mtext(side=2, line=2, "SPEI", cex=1.5)
axis(side=1, at=seq(1982, 2019, by=1),cex.axis = 1.0, cex.lab = 1)
box()

```

## **ANALYSE THE CLIMATE DATA AND VEGETATION DATA (NDVI)**

### **#Plotting climate and NDVI**

#### **#Read the data**

```

preciptemp<-read.csv(paste("File.csv",sep="",collapse=""))
head( preciptemp)

```

#### **#Covert the data to a dataframe**

```

y<-as.data.frame( preciptemp)

```

#### **#Covertto the Date understood by r**

```

y$Dates=as.Date(y$Date, "%d.%m.%Y")
tail( preciptemp)

```

#### **# Plot first set of data (NDVI in this case) and draw its axis**

```

plot(y$Dates, y$NDVI, pch=16, axes=TRUE, ylim=c(0,1), xlab="", ylab="",
      cex.axis = 1.3, cex.lab = 2, type="b",col="black", main="NDVI and Precipitation")
#axis(2, ylim=c(0,1),col="black",las=1) # las=1 makes horizontal labels

```

```
mtext("NDVI",side=2,line=2.5, cex=1.5)
```

```
box()
```

### **# Allow a second plot on the same graph**

```
par(new=TRUE)
```

### **# Plot the second plot (precipitation) and put axis scale on right**

```
plot(y$Dates, y$Precip, pch=15, xlab="", ylab="", ylim=c(0,500), axes=FALSE,  
type="b", col="dark red", )
```

### **# add labels**

```
mtext("PRECIPITATION",side=4,col="dark red",line=4, cex=1.5)
```

```
axis(4, ylim=c(500), col="dark red",col.axis="dark red",las=1,cex.axis = 1.3, cex.lab  
= 2)
```

### **# Draw the time axis**

```
mtext("Time",side=1,col="black",line=2.5, cex= 1.8)
```

### **# Add Legend**

```
legend("topleft",legend=c("NDVI","PRECIPITATION"),bty = "n",  
text.col=c("black","dark red"),pch=c(16,15), col=c("black","dark red"))
```

## **ANALYSE THE RELATIONSHIP BETWEEN CLIMATE DATA (SOIL MOISTURE, SPEI, RSM, PRECIPITATION, TEMPERATURE) AND VEGETATION DATA**

### **#Read the data**

```
modis8<-read.csv(paste("XFile.csv",sep="",collapse=""))
```

### **#Create a function to plot**

```
flattenCorrMatrix <- function(cormat, pmat) {  
  ut <- upper.tri(cormat)  
  data.frame(  
    row = rownames(cormat)[row(cormat)[ut]],  
    column = rownames(cormat)[col(cormat)[ut]],
```

```

cor =(cormat)[ut],
p = pmat[ut]
)
}
s2corAll3<-rcorr(as.matrix(modis8.num[]))
flattenCorrMatrix(s2corAll3$r,s2corAll3$P)

```

**# Mark the insignificant coefficients according to the specified p-value significance level**

```

cor_5 <- rcorr(as.matrix(modis8.num))
M <- cor_5$r
p_mat <- cor_5$P
col <- colourRampPalette(c("#BB4444", "#EE9988", "#FFFFFF", "#77AADD",
"#4477AA"))
corrplot(M, method = "colour", col = col(200),
type = "upper", order = "hclust",
addCoef.col = "black", # Add coefficient of correlation
# Combine with significance level
p.mat = p_mat, sig.level = 0.01,
# hide correlation coefficient on the principal diagonal
diag = FALSE )

```